059

ISSN 0386-5878
Technical Memorandum
of PWRI No. 3276

RECENT SELECTED PUBLICATIONS AT EARTHQUAKE ENGINEERING DIVISION, PUBLIC WORKS RESEARCH INSTITUTE (No. 3)

March, 1994

Earthquake Engineering Division
Public Works Research Institute
Ministry of Construction
Tsukuba Science City, Ibaraki-ken, 305, Japan

Copyright ©1994 by P.W.R.I.

All rights reserved. No part of this book may be reproduced by any means, nor translated into a machine language without the written permission of the Director General of P.W.R.I.

この報告書は，土木研究所長の承認を得て刊行したものである。したがって，本報告書の全部又は一部の転載，複製は，土木研究所長の文書による承認を得ずしてこれを行ってはならない。

Technical Memorandum
of PWRI No. 3276

RECENT SELECTED PUBLICATIONS AT EARTHQUAKE ENGINEERING DIVISION, PUBLIC WORKS RESEARCH INSTITUTE

by

Kazuhiko Kawashima,
Head, Earthquake Engineering Division

Synopsis:

At the Earthquake Engineering Division of the Public Works Research Institute, various researches for aiming to develop rational seismic design methods of bridges and underground structures, seismic evaluation and strengthening methods of existing structures, passive, active and hybrid control, loss estimation caused by earthquake are being made.

This reports presents some of the selected publications in the research on earthquake damage investigation, seismic design, seismic evaluation and strengthening of highway bridges, dynamic strength and ductility of structural components, structural response of menshin bridges (seismic isolated bridges), hybrid control, and seismic response of embedded pipes. They were presented at international conferences and workshops held in the last one years.

Key word: EARTHQUAKE DAMAGE, SEISMIC DESIGN, SEISMIC INSPECTION, SEISMIC STRENGTHENING, SEISMIC RETROFIT, BASE ISOLATION, MENSHIN DESIGN, DUCTILITY, DYNAMIC STRENGTHENING, SHIELD TUNNEL, EMBEDDED PIPE, BRIDGE, BRIDGE PIER, SEISMIC RESPONSE CONTROL.

TABLE OF CONTENTS

1. Evaluation of Modal Damping Ratio of Bridges Based on Strain Energy Proportional Method: Kazuhiko KAWASHIMA, Hiroyuki NAGASHIMA and Hideaki IWASAKI (9th U.S.-Japan Bridge Workshop, Tsukuba, Japan, May, 1993) 1

2. Dynamic Strength and Ductility Characteristics of Steel Bridge Piers: Kazuhiko KAWASHIMA, Hideki SUGITA and Tomoru NAKAJIMA (9th U.S.-Japan Bridge Workshop, Tsukuba, Japan, May, 1993) 19

3. Seismic Response of Reinforced Concrete Bridge Piers Subjected to Eccentric Loading: Kazuhiko KAWASHIMA, Shigeki UNJOH and Hidetoshi MUKAI (9th U.S.-Japan Bridge Workshop, Tsukuba, Japan, May, 1993) 41

4. Comparison of the Seismic Design of Highway Bridges In California and In Japan: Mohsen SULTAN and Kazuhiko KAWASHIMA (9th U.S.-Japan Bridge Workshop, Tsukuba, Japan, May, 1993) 59

5. Guidelines for Disaster Information Systems for Important Infra-Structures: Kazuhiko KAWASHIMA, Ken-ichi TOKIDA, Hideki SUGITA, Tomoru NAKAJIMA and Hideo MATSUMOTO (25th Joint Meeting of The U.S.-Japan Cooperative Program In Natural Resources, Panel on Wind and Seismic Effects, Tsukuba, Japan, May, 1993) 77

6. Seismic Response Control of Highway Bridges by Variable Damper: Kazuhiko KAWASHIMA, Shigeki UNJOH and Hidetoshi MUKAI (25th Joint Meeting of The U.S.-Japan Cooperative Program In Natural Resources, Panel on Wind and Seismic Effects, Tsukuba, Japan, May, 1993) 91

7. Infrastructures Damage by Cairo, Egypt, Earthquake of October 1992 and Flores Island, Indonesia, Earthquake of December 1991: Tomomitsu FUJII and Kazuhiko KAWASHIMA (25th Joint Meeting of The U.S.-Japan Cooperative Program In Natural Resources, Panel on Wind and Seismic Effects, Tsukuba, Japan, May, 1993) 113

8. Variable Dampers and Variable Stiffness for Seismic Control of Bridges: Kazuhiko KAWASHIMA and Shigeki UNJOH (International Workshop on Structural Control, Hawaii, U.S.A., August, 1993) 137

9. Seismic Isolation of Bridges In Japan: Kazuhiko KAWASHIMA, Shigeki UNJOH and Hidetoshi MUKAI (First Egyptian Conference on Earthquake Engineering, August, 1993) .. 155

10. Seismic Design Method of Underground Structures: Kazuhiko KAWASHIMA, Hideki SUGITA and Tomoru NAKAJIMA (First Egyptian Conference on Earthquake Engineering, August, 1993) 167

11. Seismic Design of Highway Bridges In Japan: Kazuhiko KAWASHIMA and Shigeki UNJOH (First Egyptian Conference on Eearthquake Engineering, August, 1993) 179

12. Seismic Strengthening of Highway Bridges: Kazuhiko KAWASHIMA, Shigeki UNJOH and Hidetoshi MUKAI (2nd U.S.-Japan Workshop on Seismic Retrofit of Bridges, Berkeley, U.S.A., January, 1994) 191

13. Damage of Bridges by Kushiro-oki Earthquake, January 1993, and Hokkaido Nansei-oki Earthquake, July 1993: Kazuhiko KAWASHIMA, Shigeki UNJOH, Tomoru NAKAJIMA and Jun-ichi HOSHIKUMA (2nd U.S.-Japan Workshop on Seismic Retrofit of Bridges, Berkeley, U.S.A., January, 1994) 229

14. Damage Analysis of Reinforced Concrete Bridge Piers by Kushiro-oki Earthquake, January, 1993 and Hokkaido Nansei-oki Earthquake, July, 1993: Kazuhiko KAWASHIMA, Jun-ichi HOSHIKUMA and Shigeki UNJOH (2nd U.S.-Japan Workshop on Seismic Retrofit of Bridges, Berkeley, U.S.A., January, 1994) 257

15. A Stress-Strain Model for Reinforced Concrete Bridge Piers Confined by Hoop Reinforcement: Jun-ichi HOSHIKUMA, Kazuhiko KAWASHIMA and Kazuhiro NAGAYA (2nd U.S.-Japan Workshop on Seismic Retrofit of Bridges, Berkeley, U.S.A., January, 1994) 283

16. Seismic Response of Reinforced Concrete Bridge Piers Subjected to Eccentric Loading: Kazuhiko KAWASHIMA, Shigeki UNJOH and Hidetoshi MUKAI (2nd U.S.-Japan Workshop on Seismic Retrofit of Bridges, Berkeley, U.S.A., January, 1994) 311

17. Menshin Design of Highway Bridges in Japan: Kazuhiko KAWASHIMA and Shigeki UNJOH (3rd U.S.-Japan Workshop on Earthquake Protective Systems for Bridges, Berkeley, U.S.A., January, 1994) 327

18. Seismic Response Control of Highway Bridges by Variable Stiffness Control: Kazuhiko KAWASHIMA, Shigeki UNJOH and Hidetoshi MUKAI (3rd U.S.-Japan Workshop on Earthquake Protective Systems for Bridges, Berkeley, U.S.A., January, 1994) 359

19. Application of Electro-Rheological Fluid for Variable Damper: Kazuhiko KAWASHIMA, Shigeki UNJOH, Shigenobu SUZUKI and Shigeki ENDOH (3rd U.S.-Japan Workshop on Earthquake Protective Systems for Bridgtes, Berkeley, U.S.A., January, 1994) 373

20. Response of On-netoh Bridge During Kushiro-oki Earthquake of January 1993: Masashi SATO, Hiroaki NISHI, Kazuhiko KAWASHIMA and Shigeki UNJOH (3rd U.S.-Japan Workshop on Earthquake Protective Systems for Bridges, Berkeley, U.S.A., January, 1994) 383

21. Menshin Design Example of Highway Bridge: Kazuhiko KAWASHIMA, Shigeki UNJOH, Tsuneo UZUKA, Kazuhiko KAWAKAMI, Kazuomi KUMAKURA and Hideo TANI (3rd U.S.-Japan Workshop on Earthquake Protective Systems for Bridges, Berkeley, U.S.A., January, 1994) 401

22. Response Analysis of Miyagawa Bridge Based on A Measured Acceleration Record: Kazuhiko KAWASHIMA, Hiroyuki NAGASHIMA, Shinji MASUMOTO and Kohji HARA (Journal of Structural Engineering, JSCE, Vol.40A, Tokyo, Japan, March, 1994) 427

23. Evaluation of Modal Damping Ratio Based on Strain Energy Proportional Damping Method: Kazuhiko KAWASHIMA, Hiroyuki NAGASHIMA and Hideaki IWASAKI (Journal of Structural Engineering, JSCE, Vol.40A, Tokyo, Japan, March, 1994) 439

24. Development of Variable Damper for Reducing Seismic Response of Highway Bridges: Kazuhiko KAWASHIMA, Shigeki UNJOH and Hidetoshi MUKAI (Journal of Structural Engineering, JSCE, Vol.40A, Tokyo, Japan, March, 1994) 455

25. Seismic Behavior of Buried Pipelines Through Field Observation: Kazuhiko KAWASHIMA, Hideki SUGITA and Tomoru NAKAJIMA (Journal of Structural Engineering, JSCE, Vol.40A, Tokyo, Japan, March, 1994) 467

26. Seismic Response Control of Highway Bridges by Variable Damper: Kazuhiko KAWASHIMA, Shigeki UNJOH and Hidetoshi MUKAI (5th U.S. National Conference on Earthquake Engineering, EERI, Chicago, U.S.A., July, 1994) 479

27. Seismic Response of Reinforced Concrete Bridge Piers Subjected to Eccentric Loading: Kazuhiko KAWASHIMA, Shigeki UNJOH and Hidetoshi MUKAI (5th U.S. National Conference on Earthquake Engineering, EERI, Chicago, U.S.A., July, 1994) 491

Evaluation of Modal Damping Ratio of Bridges Based on Strain Energy Proportional Method

Kazuhiko KAWASHIMA
Hiroyuki NAGASHIMA
and
Hideaki IWASAKI

9th U.S.–Japan Bridge Workshop
Tsukuba, Japan
May, 1993

EVALUATION OF MODAL DAMPING RATIO OF BRIDGES BASED ON STRAIN ENERGY PROPORTIONAL METHOD

by

Kazuhiko KAWASHIMA[1], Hiroyuki NAGASHIMA[2] and Hideaki IWASAKI[3]

1) Head, Earthquake Engineering Division, Earthquake Disaster Prevention Department, Public Works Research Institute
2) Former Research Engineer, ditto
3) Research Engineer, Ground Vibration Division, ditto

ABSTRACT

Presented in this paper is a model free oscillation test and an analysis for clarifying the strain energy proportional damping method which is widely adopted for evaluating modal damping ratio of structures. Because damping ratio of structural components is sometimes different even in the same structure, it is required in the modal dynamic response analysis to evaluate the damping ratio for each mode. In this paper it is presented from the experiment and analysis that the strain energy proportional method is quite accurate for evaluating the modal damping ratio of structures for seismic analysis.

Key Words : Seismic Design, Damping Ratio, Energy Dissipation, Bridges

INTRODUCTION

Damping ratio is an important parameter for evaluating seismic response of structures. Although the mass and stiffness can be accurately computed from mass and stiffness distribution of structures, the damping ratio can not be evaluated in the similar manner because prediction of energy dissipation in structures is very complex. Therefore instead of directly evaluating energy dissipation in structures it is generally adopted to evaluate the energy dissipation of structures in terms of damping ratio. The damping ratio is an appropriate parameter for assigning the damping characteristics of structures. But it should be keep in mind that the damping ratio can be defined only for a single-degree-of-freedom oscillator. From the analogy of the orthogonal condition of modal matrix with respect to stiffness and mass matrix, the damping ratio has been assumed for seismic analysis of structures.

Damping ratio is sometimes different depending on structural components even in the same structure. Therefore it is required to evaluate the modal damping ratio based on the different damping ratio assigned for each structural component. The strain energy proportional method has been

widely used for such purpose[1]. Because most of energy dissipation is developed due to deformation of structures, it has been considered reasonable to assume this method. But theoretical verification was not yet fully made.

This paper attempts to verify the strain energy proportional method for application to seismic design of structures. Based on a model oscillation test which is carefully made for evaluating energy dissipation of structural components as well as whole structure, accuracy and application of the strain energy proportional method is clarified. A bridges is considered for analysis.

ENERGY PROPORTIONAL DAMPING

For a linear discrete structure, the equations of motion may be written as

$$M\ddot{u} + C\dot{u} + Ku = M\{1, 0, 0, \cdots 1, 0, 0\}^{T}\ddot{z}_{gx} \tag{1}$$

where

M : mass matrix
C : damping matrix
K : stiffness matrix
$\ddot{u}$, $\dot{u}$, u : displacement, velocity and acceleration vector
$\ddot{z}_{gx}$: ground acceleration in x axis

Denoting ω_i and ϕ_i as the undamped angular natural frequency and mode shapes for i-th mode, $\ddot{u}$, $\dot{u}$, u may be expressed as

$$\left.\begin{aligned} \ddot{u} &= \sum_{i=1}^{K} \phi_i \ddot{q}_i(t) \\ \dot{u} &= \sum_{i=1}^{K} \phi_i \dot{q}_i(t) \\ u &= \sum_{i=1}^{K} \phi_i q_i(t) \end{aligned}\right\} \tag{2}$$

in which q_i represents the generalized coordinate for i-th mode and K represents number of freedom.

From the orthogonal condition, the stiffness matrix K and mass matrix M become as

$$\left.\begin{aligned} \phi_m^{T} K \phi_n &= 0 \\ \phi_m^{T} M \phi_n &= 0 \end{aligned}\right\} \quad (m \neq n) \tag{3}$$

Assuming that the damping matrix C can be also orthogonalized as

$$\phi_m{}^T C \phi_n = 0 \tag{4}$$

one can have k sets of uncoupled equation of motion as

$$\ddot{q}_i + 2 h_i \omega_i \dot{q}_i + \omega_i{}^2 q_i = -\Gamma_{ix} \ddot{Z}_{gx} \tag{5}$$

in which h_i and Γ_{ix} represent the modal damping ratio and mode participation factor for i-th mode, respectively.

It is important to note here that the modal damping ratio h_i which is defined only for a single degree of freedom oscillator has been adopted in a dynamic response analysis of multi-degree-of-freedom system in the form of Eq. (5) because there is not a practical definition for energy dissipation for multi-degree-of-freedom system.

It is then required to evaluate the modal damping ratio of Eq. (5) based on the energy dissipation mechanism of the structure. For such purpose it is assumed to divide a structure into several structural segments in which energy dissipation has the same mechanism as shown in Fig. 1[2)3)]. The segment is designated hereinafter as a substructure. The substructure may be a deck, a pier and a foundation as shown in Fig. 2 in the analysis of a bridge.

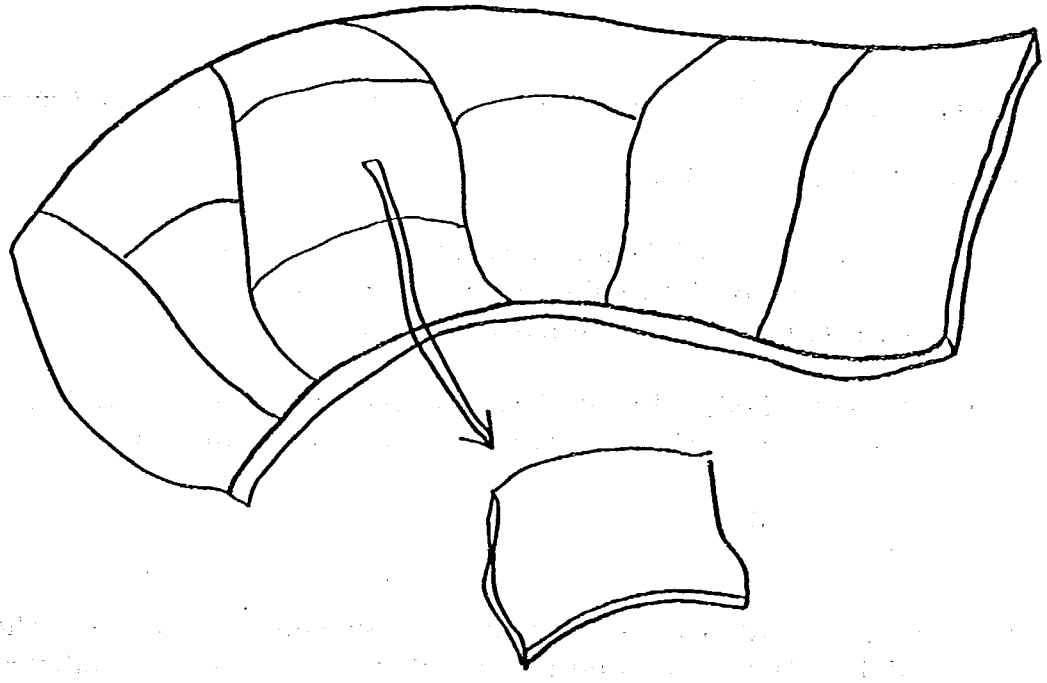


Fig.1 Substructures

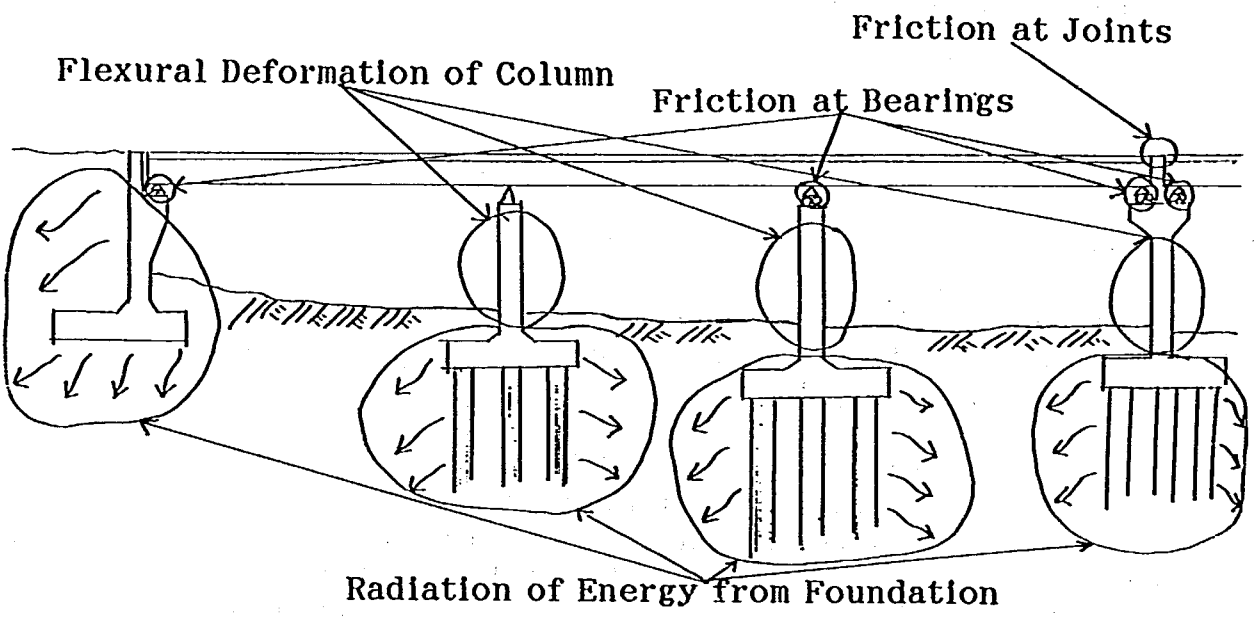


Fig.2 Substructures for Bridges

Strain energy in j-th substructure for i-th mode may be evaluated as

$$E_{ij} = \Sigma \ \phi_{ij}^{T} \cdot k_j \cdot \phi_{ij} \qquad (6)$$

where

E_{ij} : strain energy of j-th substructure for i-th mode
ϕ_{ij} : mode shape of j-th substructure for i-th mode
k_j : stiffness matrix of j-th substructure

Denoting the energy dissipation in j-th substructure for i-th mode as ΔE_{ij}, the damping ratio of the j-th substructure may be evaluated as

$$h_{ij} = \frac{1}{2\pi} \frac{\Delta E_{ij}}{E_{ij}} \qquad (7)$$

Because the damping ratio of substructures depends on the mode shape and boundary condition, it needs to be the one developed when the substructures deform as a part of the structure in the i-th mode shape.

Then the strain energy and energy dissipation of the whole structure for i-th mode can be evaluated as

$$E_i = \sum_{j=1}^{n} E_{ij}$$

$$\Delta E_i = \sum_{j=1}^{n} \Delta E_{ij} \tag{8}$$

in which n represents number of substructures. The damping ratio of whole structure (modal damping ratio) for i-th mode may be written from Eq. (8) as

$$h_i = \frac{1}{2\pi} \frac{\Delta E_i}{E_i} \tag{9}$$

Substituting Eqs. (7) and (8) into Eq. (9), one obtains an equation for evaluating the modal damping ratio as

$$h_i = \frac{\sum_{j=1}^{n} E_{ij} h_{ij}}{\sum_{j=1}^{n} E_{ij}} \tag{10}$$

Eq. (10) is called as the strain energy proportional damping because the averaged damping ratio over each substructure is taken with the strain energy of the substructure being the weighting function. Substituting Eq. (6) into Eq. (10), Eq. (10) can be modified in the form which is more appropriate for computation

$$h_i = \frac{\sum_{j=1}^{n} \phi_{ij}^{T} \cdot h_{ij} \cdot k_j \cdot \phi_{ij}}{\sum_{j=1}^{n} \phi_{ij}^{T} \cdot k_j \cdot \phi_{ij}} \tag{11}$$

MODEL FREE OSCILLATION TEST

Fig. 3 shows the model bridge studied for verifying the effectiveness of the strain energy proportional damping method. Photos 1 and 2 show the bridge model and the bearing. The girder is of a rigid steel plate so that energy dissipation during excitation is negligibly small. The girder has the span length of 2.1 m and the weight of 611.7 kgf. Each column with the height of 95 cm is of four steel plates with the top of each two plates being rigidly connected. The bottom of the columns are rigidly connected to base frame for preventing energy dissipation at the bottom.

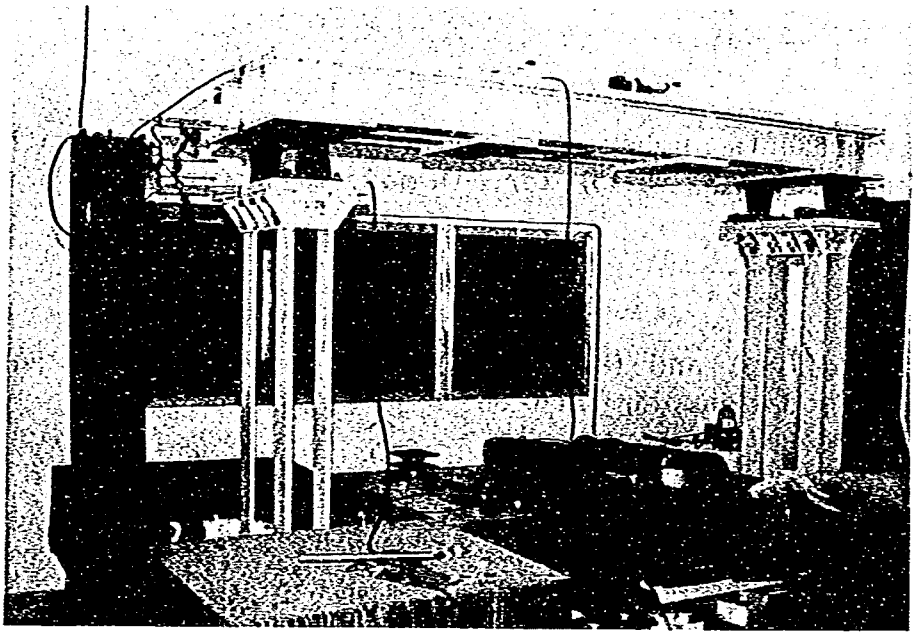


Photo 1 Bridge Model

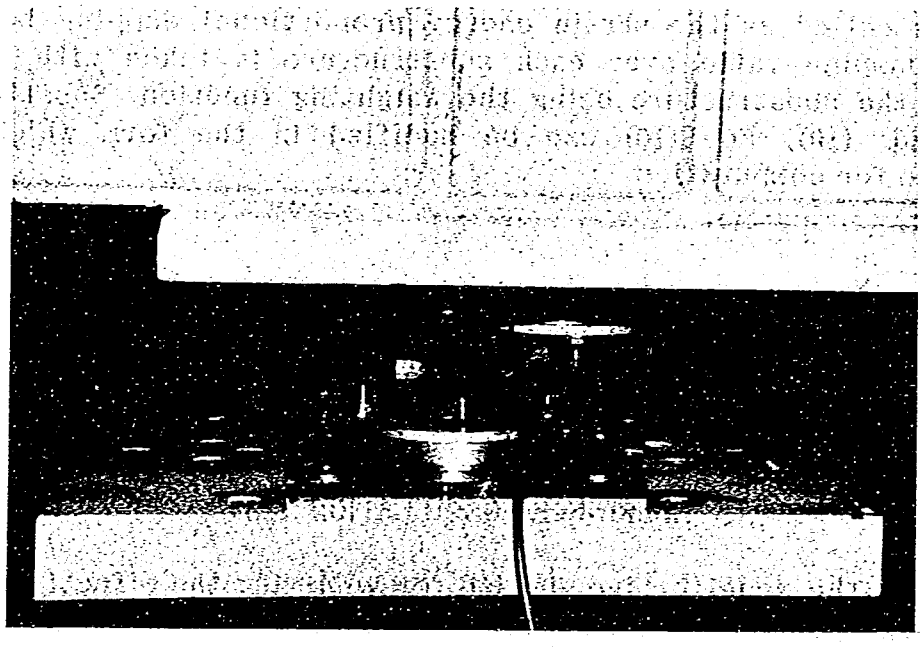


Photo 2 Bearings

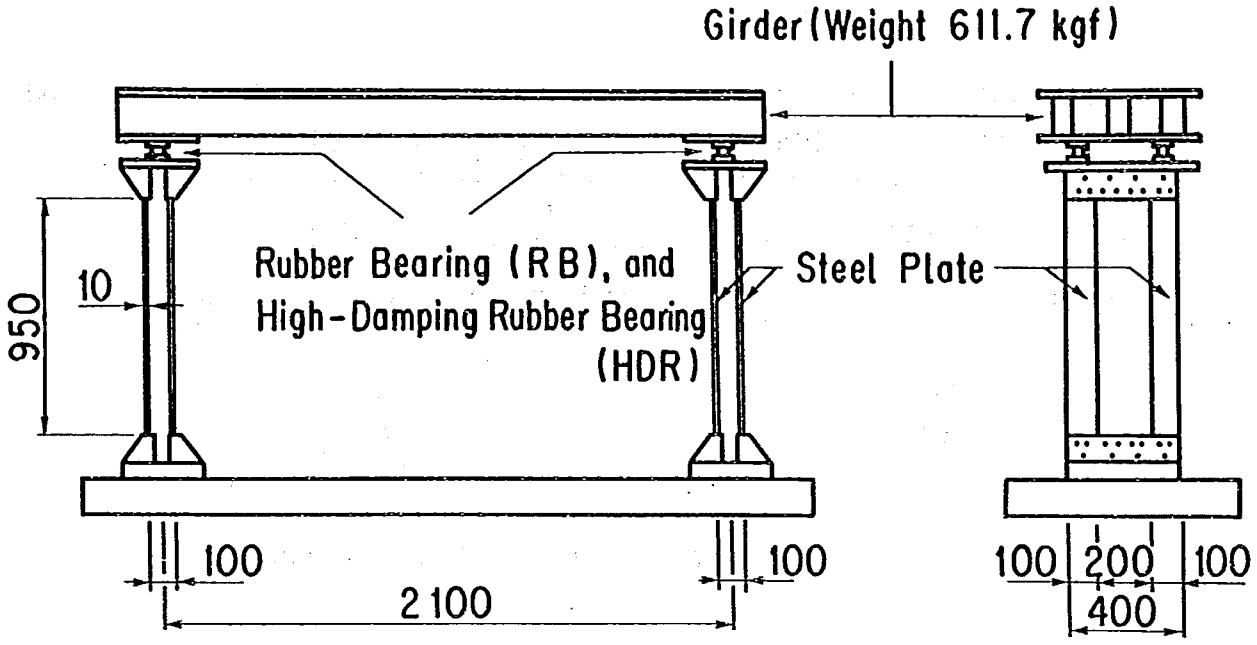


Fig.3 Model Bridge used for Free Oscillation Test

Four bearings were used for supporting the deck. Two types of bearings as shown in Fig. 4 were adopted for the test. One is the laminated natural rubber bearing, which is called hereinafter as RB. This was made by laminating 25 natural rubber plates with thickness of 0.9 mm and 24 steel plates with thickness of 0.3 mm. Total thickness of rubber is 22.5 mm. It has elastic restoring force characteristics. The other is the laminated high damping rubber bearing, which is called as HDR in this paper. This was made by laminating 37 high energy absorbing rubber plates with thickness of 0.5 mm and 36 steel plates with thickness of 0.3 mm. Total thickness of high energy absorbing rubber is 18.5 mm.

In the model bridge, energy dissipation is developed at bearings and columns. Therefore, bearings and columns are regarded as the substructures for evaluating modal damping ratio of the model bridge by Eq. (11). Because little energy dissipation is developed at the rigid deck, it is disregarded in the analysis. The modal damping ratio only for 1st mode is evaluated in the test for making the excitation simple and easy.

For evaluating the damping ratio of each substructure, free oscillation test was made for two types of bearings (RB and HDR) and two columns (Column A and B). Free oscillation test of the model bridge was also made for evaluating the modal damping ratio of whole structure.

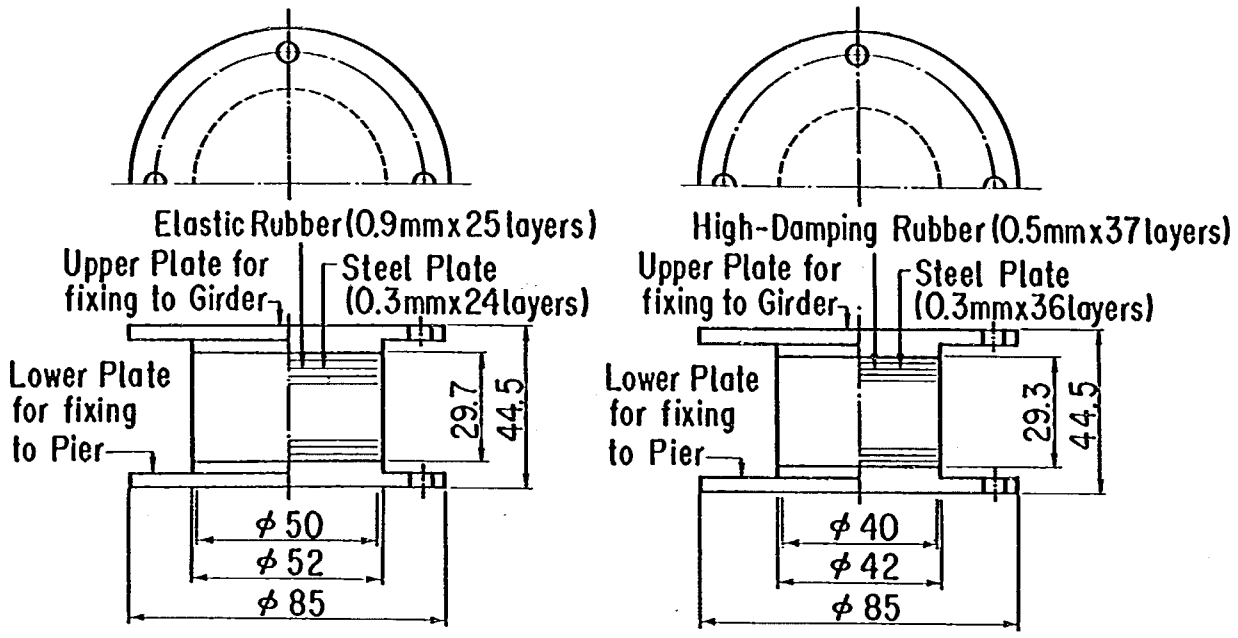


Fig.4 Model Bearings for Free Oscillation Test

In the free oscillation test of the model bridge, the deck was displaced in longitudinal direction, and by releasing it from the displaced position, free oscillation was developed. The 1st mode shape of the model bridge in longitudinal direction is of lateral movement of the deck with flexural deformation of cantilevered columns. Similarly the free oscillation test was made separately for the column A and B. In the free oscillation test of the bearings, four sets of bearings were directly placed on a rigid steel frame and the deck was placed on them. Then the deck was displaced laterally and released smoothly so that shear deformation was developed in the four bearings. Because the steel frame and deck are rigid, energy dissipation developed in this test represents that developed in the bearings. The test was made separately for RB and HDR.

Because the stiffness of the bearing depends on temperature, the tests were made in a room with the constant temperature with 20 ℃. Displacement of the deck and columns was measured. Acceleration was measured so that the inertia force of the deck be evaluated. It will be used to evaluate the stiffness of bearings. Each test was made twice to verify the stableness of the test results.

FREE OSCILLATION OF MODEL BRIDGE

Fig. 5 shows the decay of free oscillation of the bridge model. It is apparent that the free oscillation decays much faster in the model supported by HDR than the model supported by RB. Logarithmic damping ratio δ can be evaluated from the free oscillation as

$$\delta = \log_e (a_m / a_{m+1}) \qquad (12)$$

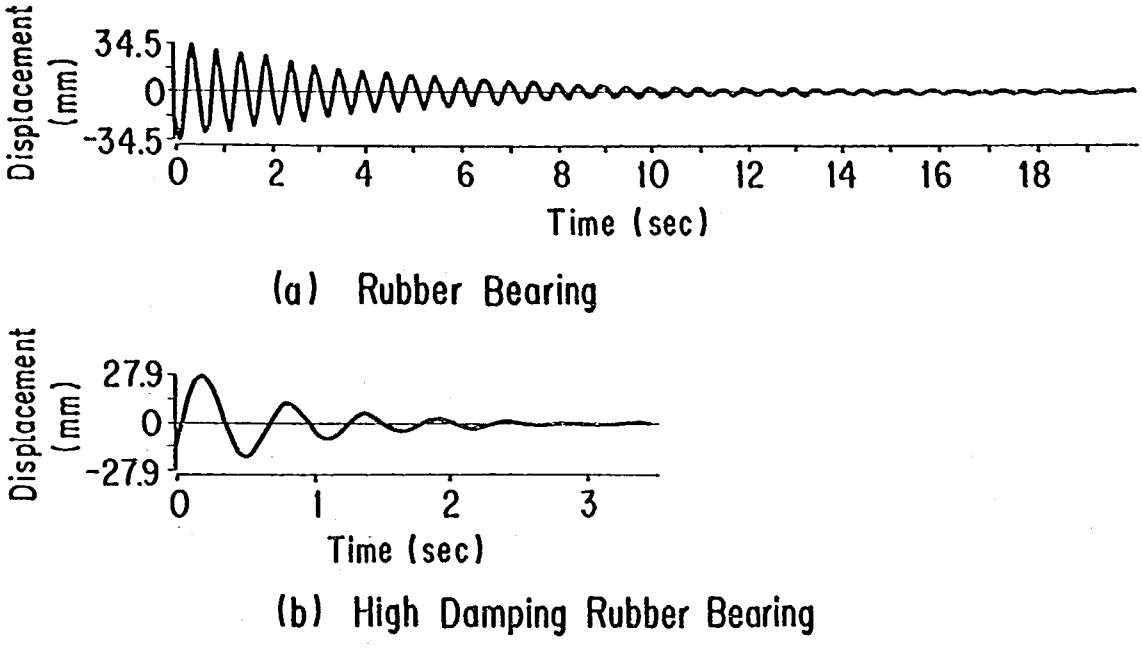


Fig.5 Decay of Free Oscillation of Deck Displacement Amplitude of Bridge Model

where

δ : logarithmic damping ratio

a_m : displacement amplitude of m-th peak of free oscillation

Damping ratio h may be evaluated from the logarithmic damping ratio as

$$\delta = 2\pi h / \sqrt{1-h^2} \tag{13}$$

Fig. 6 shows the dependence of the 1st mode damping ratio of the model bridge thus evaluated on the displacement amplitude of the deck. Some scatter is seen at small displacement in the bridge model supported by HDR. HDR shows low damping ratio at small displacement. Therefore disregarding such part, damping ratio was evaluated for the displacement range of 6.3 mm - 27.9 mm in the model supported by HDR and 23.8 mm - 33.0 mm in the model supported by RB. The averaged damping ratio over this range is 11.4 % in the model supported by HDR and 1.69 % in the model supported by RB.

Fig 7 compares the decay of free oscillation of RB and HDR. It is apparent that the oscillation decreases faster in HDR than RB. Fig. 8 shows the dependence of damping ratio of RB and HDR on the lateral displacement developed in the bearings. Decrease of damping ratio at small displacement is seen, especially in HDR. This is the reason for causing the decrease of the damping ratio of the bridge model as shown in Fig. 6. The damping ratio of both RB and HDR has less displacement dependency. The averaged damping ratio over the displacement range developed during the above described free oscillation test of the whole model bridge is 3.27 % in RB and 25.4 % in HDR.

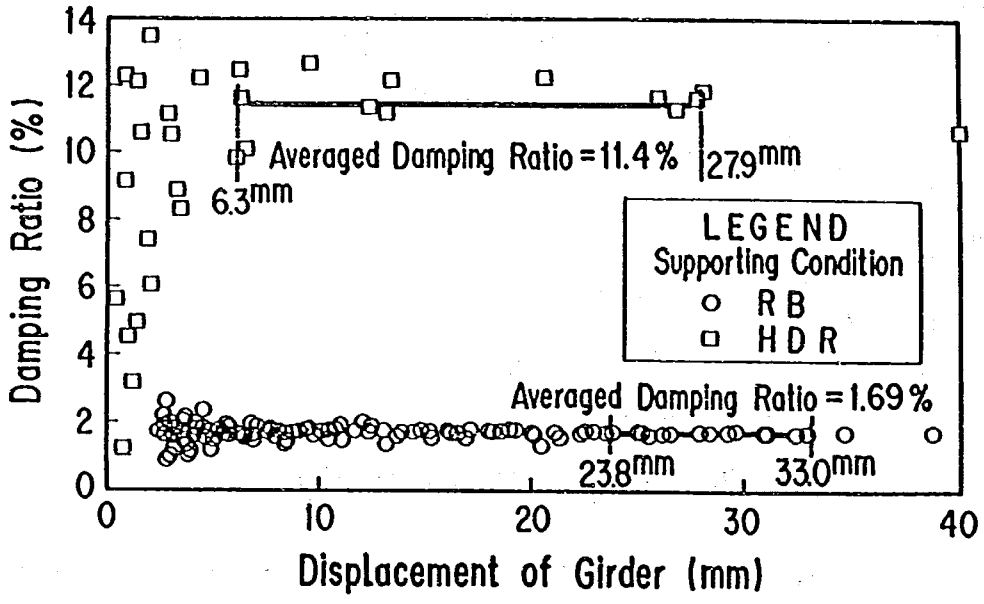


Fig.6 Damping Ratio of Model Bridge vs. Oscillation Amplitude

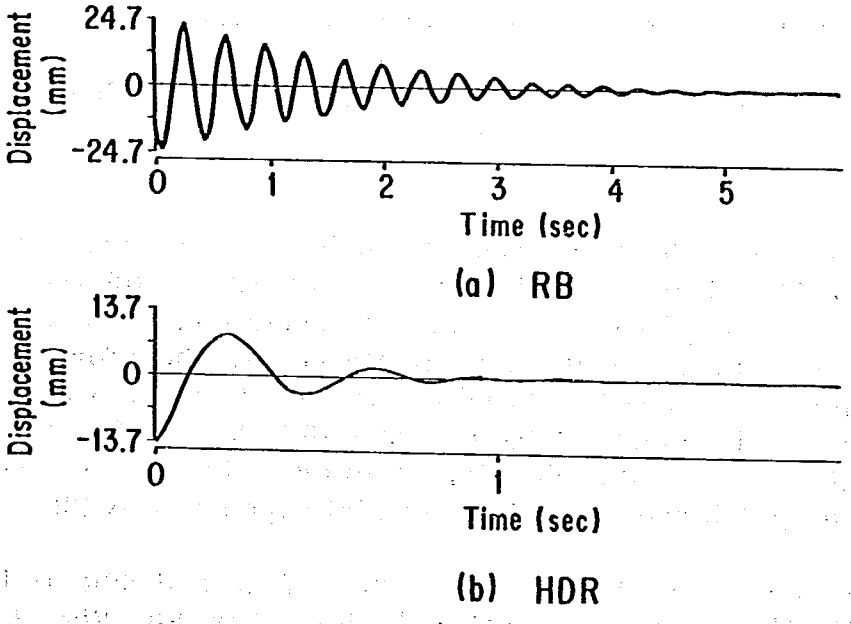


Fig.7 Decay of Free Oscillation of Bearing Displacement

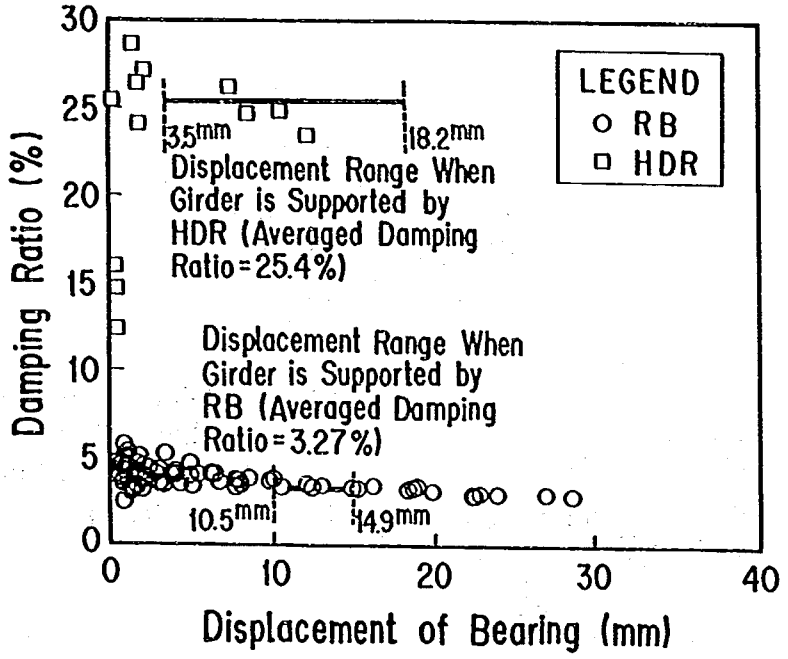


Fig.8 Damping Ratio of Bearing vs. Shear Displacement

Fig. 9 shows the decay of free oscillation at the top of of a column. Fig. 10 shows the displacement dependence of the damping ratio thus evaluated. Because the displacement amplitude developed at the column top during the free oscillation test of the whole bridge model is 13.4 - 18.2 when the deck is supported by RB and 3.0 - 10.9 when the deck is supported by HDR, the damping ratio of the columns A and B is 0.708 % and 0.954 % for RB and 0.459 % and 0.544 % for HDR.

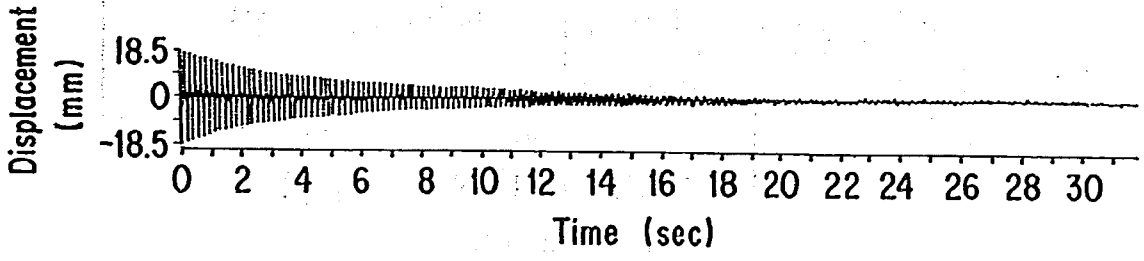
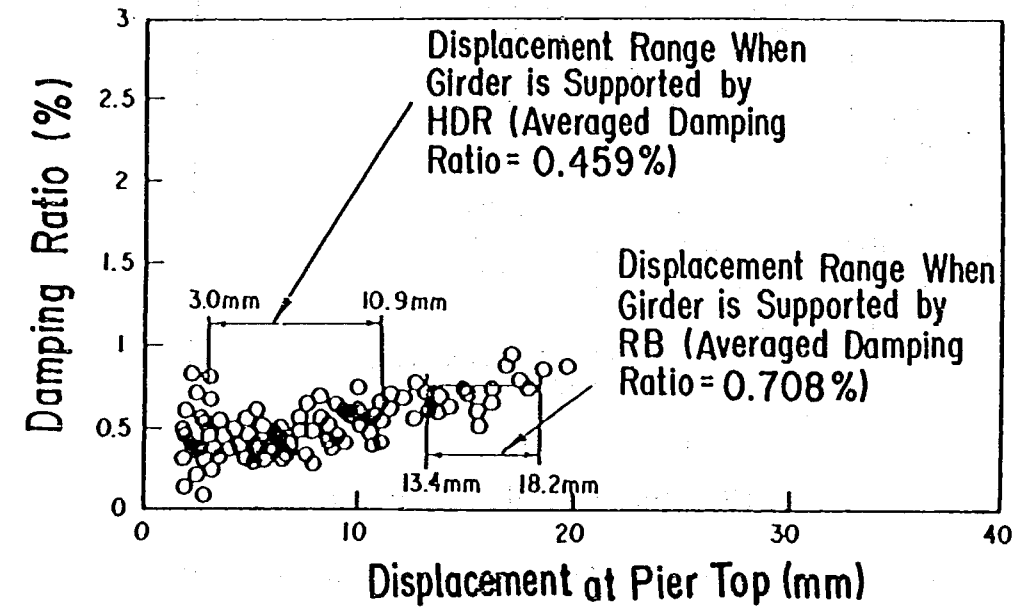
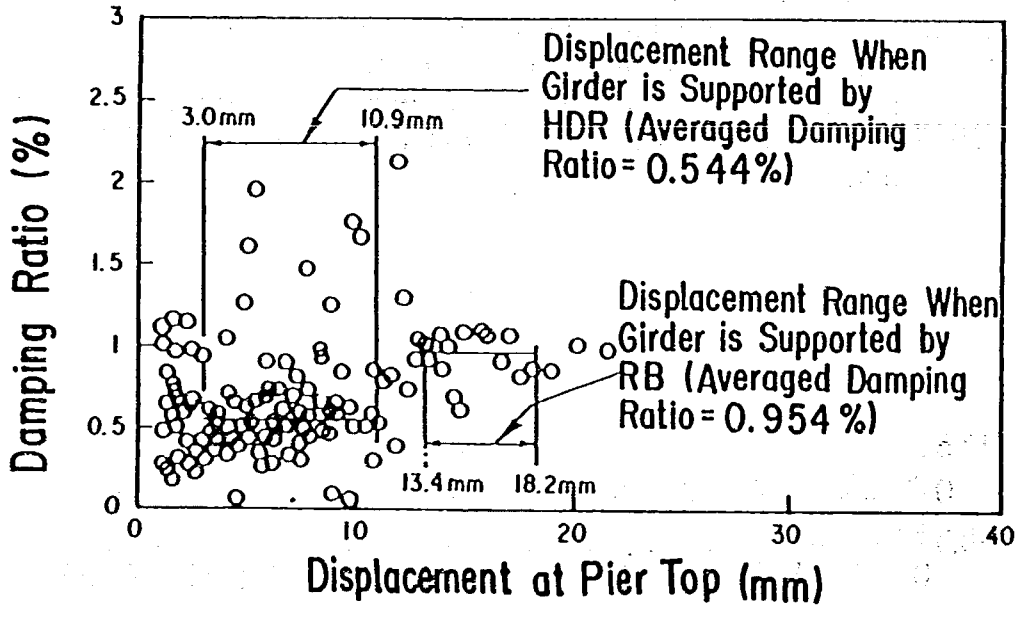


Fig.9 Decay of Free Oscillation of Column



(a) Column A



(b) Column B

Fig.10 Damping Ratio of Column vs. Oscillation Amplitude

ACCURACY OF STRAIN ENERGY PROPORTIONAL METHOD

Because the damping ratio of each substructure was evaluated, the damping ratio h_1 of the the whole bridge model for 1st mode may be evaluated from Eq. (10) as

$$h_1 = \frac{E_{1cA}h_{1cA} + E_{1cB}h_{1cB} + E_{b1}h_{1b}}{E_{1cA} + E_{1cB} + E_{1b}} \tag{14}$$

where

E_{1cA}, E_{1cB} : strain energy of column A and B for 1st mode
E_{1b} : strain energy of bearings for 1st mode
h_{1cA}, h_{1cB} : damping ratio of column A and B
h_{1b} : damping ratio of bearings

Because the damping ratio of the whole bridge model was obtained from the test, accuracy of Eq. (10) is clarified by comparing the damping ratio predicted by Eq. (14) with the one evaluated from the test.

Strain energy of the columns and bearings may be evaluated as

$$E_{1cN} = \frac{1}{2} k_{cN} u_{cN}^2 \quad (N=A, B) \tag{15}$$

$$E_{1b} = \frac{1}{2} k_b u_b^2 \tag{16}$$

where

E_{1cA}, E_{1cB} : strain energy of column A and B for 1st mode
E_{1b} : strain energy of bearings for 1st mode
k_{cA}, k_{cB} : stiffness of column A and B
k_b : stiffness of bearings
u_{cA}, u_{cB} : lateral displacement at top of column A and B
u_b : shear displacement of bearings

The stiffness of the columns k_{cA} and k_{cB} can be evaluated based on the dimension of the columns and elastic modulus. The stiffness of the bearings was evaluated from the hysteresis loop of the force vs. displacement relation as the equivalent stiffness. Fig. 11 shows the stiffness of the bearings thus evaluated vs. shear displacement relation. Because the stiffness of the bearings has some displacement dependency, it was approximated as

$$k_b = 22.7 - 0.2u_b \quad \text{(RB)} \tag{17}$$
$$k_b = 8.0 - 0.2u_b \quad \text{(HDR)}$$

In the free oscillation test of the whole bridge model, the deck displacement can be evaluated as

$$u_d = u_p + u_b \tag{18}$$

where

u_d : deck displacement

u_p : displacement at column top

u_b : shear displacement of bearings

Because u_d and u_p were measured during the test, u_b can be computed from Eq. (18). Then the stiffness of the bearings can be estimated by Eq. (17).

Thus the damping ratio of the model bridge was evaluated from Eq. (14) for several peaks of free oscillations as shown in Table 1. Fig. 12 compares the predicted and measured damping ratio of the bridge model. The predicted values are very close with the measured ones. They are within ± 20 % of the measured damping ratio.

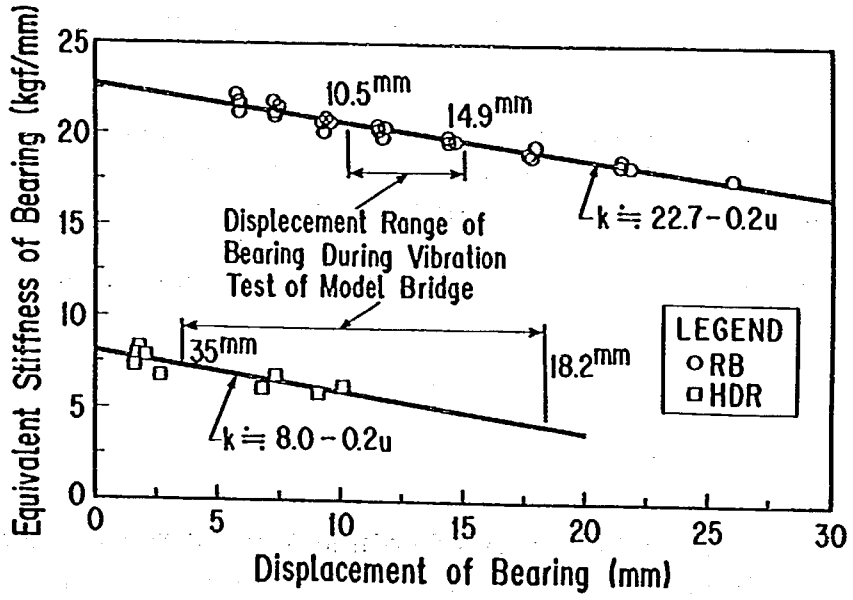


Fig.11 Displacement Dependence of Stiffness of Bearings

Table 1 Comparison of Predicted and Measured Damping Ratio of Model Bridge

Type of Bearing	Number of Free Oscillation	Displacement of Bridge Model			Damping Ratio and Strain Energy of Structural Members						Modal Damping of Bridge	
		Displacement at Girder d_d (mm)	Displacement at Pier Top d_p (mm)	Displacement at Bearing d_b (mm)	Pier A		Pier B		Bearing		Estimated by Eq.(11) h_A	Measured h_E
					h_{pA}(%)	E_{pA}	h_{pB}(%)	E_{pB}	h_b (%)	E_b		
Rubber Bearing (RB)	1	33.0	18.2	14.9	0.708	1.437	0.954	1.424	3.273	2.192	1.890	1.690
	2	29.6	16.5	13.3	0.708	1.181	0.954	1.170	3.273	1.775	1.881	1.690
	3	26.5	14.8	11.8	0.708	0.950	0.954	0.944	3.273	1.418	1.877	1.690
	4	23.8	13.4	10.5	0.708	0.779	0.954	0.772	3.273	1.137	1.864	1.690
High-Damping Rubber Bearing (HDR)	1	27.9	10.9	18.2	0.459	0.516	0.544	0.511	25.4	0.710	10.7	11.4
	2	13.4	5.7	8.2	0.459	0.141	0.544	0.140	25.4	0.213	11.2	11.4
	3	6.3	3.0	3.5	0.459	0.039	0.544	0.039	25.4	0.045	9.6	11.4

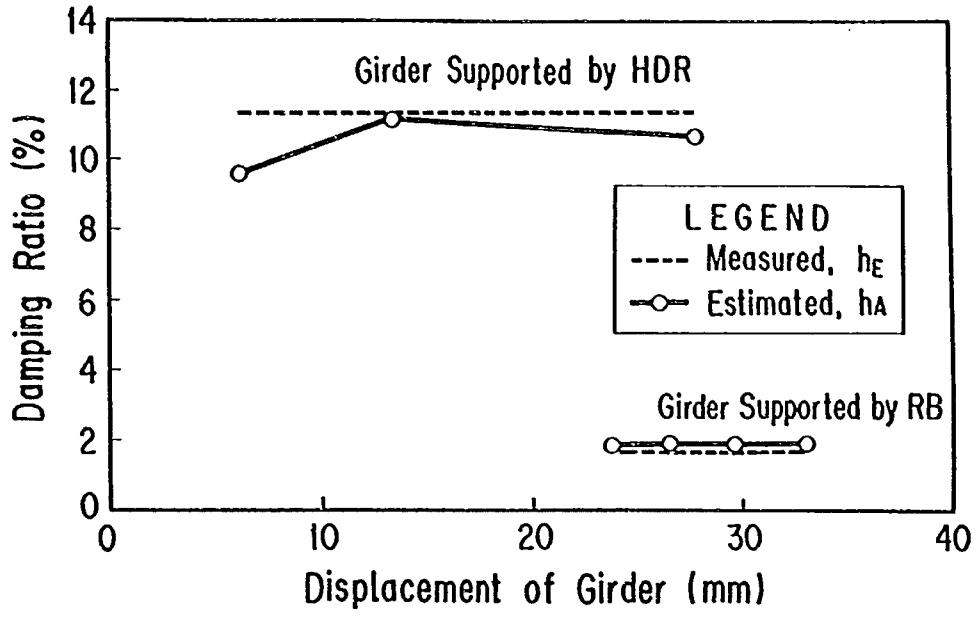


Fig.12 Accuracy of Predicted Damping Ratio

CONCLUSIONS

The effectiveness of the strain energy proportional damping method was verified through the free oscillation test of a model bridge. Damping ratio only for 1st mode was analyzed because of simplicity of the free oscillation test. It became apparent that the damping ratio of the bridge can be predicted by the strain energy proportional method with enough accuracy when the damping ratio of substructures is correctly evaluated.

REFERENCES

1) Japan Road Association : Part V Seismic Design, Design Specification of Road Bridges, February 1990
2) Kawashima, K., Unjoh, S. and Tsunomoto, M. : Damping Characteristics of Cable Stayed Bridges for Seismic Design, Journal of Research, Vol. 27, Public Works research Institute, December 1991
3) Kawashima, K., Unjoh, S. and Tsunomoto, M. : Estimation of Damping Ratio of Cable Stayed Bridges for Seismic Design, Journal of Structural Engineering, Vol. 119, No. 4, April 1993

Dynamic Strength and Ductility Characteristics of Steel Bridge Piers

Kazuhiko KAWASHIMA
Hideki SUGITA
and
Tomoru NAKAJIMA

9th U.S.–Japan Bridge Workshop
Tsukuba, Japan
May, 1993

DYNAMIC STRENGTH AND DUCTILITY CHARACTERISTICS OF STEEL BRIDGE PIERS

Kazuhiko KAWASHIMA1), Hideki SUGITA2) and Tomoru NAKAJIMA2)

ABSTRACT

This paper presents a series of loading test results of steel bridge piers constructing for highway bridges. Even for a significant earthquake, the bridge has to avoid critical failure. Because the steel pier is the most important member for preventing critical failure of bridge, it is desirable to check bearing capacity for lateral load to prevent brittle failure. Failure mechanism and effect of longitudinal stiffeners on strength and ductility of steel bridge piers are presented.

INTRODUCTION

Steel bridge piers, constructed by the welding together of thin plate, have been used over past 30 years for constructing highway bridges. Because the section size of steel piers is significantly less than that of reinforced concrete piers, it is ideal to use in city locations where there are various restrictions derived from land use and construction space.

In the 1990 JRA specification for seismic design of highway bridges, ductility check for the design of reinforced concrete piers was introduced in addition to the standard design force requirements. In this check, it is required that reinforced concrete piers be able to resist a level of earthquake acceleration which is significantly greater than the level of standard earthquake acceleration by a combination of strength and ductility.

The steel pier is the most important member for preventing critical failure of bridge. It is desirable to check bearing capacity for the acceleration of significant earthquake. Because actual damage has not been observed in recent earthquakes and few tests for earthquake resistance have been carried out, strength and ductility of steel bridge piers are still unknown.

For aiming to study the strength and ductility of steel bridge piers, a series of loading tests was made. This paper presents the effect of longitudinal stiffeners on strength and ductility of steel piers through the loading tests.

DYNAMIC LOADING TESTS OF STEEL BRIDGE PIERS

Test Specimens

As shown in Fig.1 and Table 1, 3 types of specimens of steel bridge piers were used in the dynamic loading tests. Specimen number presented show those used to identify specimens in a series of dynamic loading tests conducted at Public Works Research Institute. Scale of specimens used in this tests was assumed approximately 1/3 in length to typical highway bridge piers. The dimension of the cross section is 80.0cm × 81.6cm. The height of specimens is 7.1m including a footing of 0.7m height at the bottom of the column. Diaphram and rib are used as lateral stiffeners alternatively in longitudinal direction. 3 plates of ribs for each flange and web are used as longitudinal stiffeners.

Spacing of lateral stiffeners, size and plate thickness of longitudinal stiffeners are different in each type of specimens. Spacing between lateral stiffeners is 35cm for specimen S-23 and S-24, and 60cm for specimen S-28. Spacing between longitudinal stiffeners is 20cm for all specimens. Plate thickness of flange, web and lateral stiffeners are 8mm, 8mm and 4.5mm alternatively. Section size of longitudinal stiffeners are 6 × 64mm for specimen S-23, 10 × 64mm for specimen S-24 and 6 × 59mm for specimen S-28. SM490A steel material is used for all flange, web and stiffeners. Average yield strength and strain derived from tests of materials are shown in Table 2.

Panel and stiffener were designed according to the Design Specification for Highway Bridges-part II Steel Bridge(JRA). The stiffness of longitudinal stiffeners must be sufficient to ensure that wall buckling does not prematurely decrease the strength of piers. In the specification, both sectional area and sectional second moment of a longitudinal stiffener should be satisfy the certain values given in equation (1) and (2).

$$I_l \geqq \frac{bt^3}{11} \cdot \gamma_{l \cdot req} \qquad (1)$$

$$A_l \geqq \frac{bt}{10n} \qquad (2)$$

where

b: the width of the section(mm)
t: plate thickness(mm)
n: number of panels divided by longitudinal stiffeners
$\gamma_{l \cdot req}$: relative stiffness required

Relative stiffness of longitudinal stiffeners γ_l presents the ratio of sectional second moment between a longitudinal stiffener and a panel. γ

$\ell \cdot req$ means the minimum γ_ℓ required not to develop overall wall buckling but local panel buckling which is, as shown in Fig.2, local buckling of each panel between the longitudinal stiffeners. Whether the buckling mode of panel is overall wall buckling and local panel buckling can be estimated by the gamma ratio($\gamma_\ell / \gamma_{\ell \cdot req}$). In the case if gamma ratio is greater than 1.0 then buckling mode would be expected to be local buckling. In the case if gamma ratio is less than 1.0 then overall wall buckling is expected. Because gamma ratios of specimen S-23, S-24 and S-28 are calculated as 4.1, 6.0 and 1.1 respectively, the buckling mode of all specimens is expected as local panel buckling.

The box shaped section consists of 4 major plates to which stiffeners and diaphrams are welded from the inside. Fig.3 shows the weld way between each materials. Weld between web and flange was carried out by a combination of fillet weld with leg length of 6mm and V-shape weld with leg length of 5mm. Longitudinal stiffeners were welded onto both web and flange by fillet weld with leg length of 3mm. Although there are various way to connect both web and flange with upper base plate, in these specimens both web and flange go through upper base plate and are welded onto lower base plate which is the way adopted in piers of Metropolitan Expressway Publish Corporation. Weld between upper base plate and both web and flange was carried out by butt-weld.

Dynamic Loading Test

Fig.4 shows the experimental set-up of specimen. Specimens were fixed on the steel footing which was attached on the reaction wall with bolts. The dynamic actuator installed on the reaction wall was set at the crest of specimens. 10% of yield load associate with dead weight was applied in the axial direction with use of static actuator. Dynamic loading test was carried out by controlling the lateral displacement of the dynamic actuator.

Fig.5 shows the loading hysteresis loop of specimens. Because the reaction wall and steel footing are not completely rigid, it is desirable to estimate the lateral displacement developed at the crest of specimens due to their deformation. So, in the first, to determine the loading displacement δ, 75% yield load which was calculated from the result of material test was statically applied to the specimen. Against the yield load, Lateral displacement developed at the crest can be estimated in equation(3).

$$\delta_D = \delta_y + \delta_E \qquad (3)$$

where

δ_y: yield displacement, is defined as the displacement at which yielding first occurs in the extreme fiber of the section(cm)

δ_E: lateral displacement developed at the crest due to deformation of

reaction wall and steel footing(cm)

δ_O: loading displacement at the crest(cm)

Because δ_E is in proportion to the lateral load, δ_E can be calculated in equation(3). Loading displacement δ_O which is desirable for applying lateral displacement $1\delta_y$ to the specimen can be also calculated in equation(3) with use of δ_E. But, because δ_E becomes larger according with the increment of lateral load, loading displacement for applying over $2\delta_y$($2\delta_y, 3\delta_y \cdots$) can not be determined. In this study, loading displacement $n\delta_O$ for applying $n\delta_y$ is calculated in equation(4) based on an assumption that lateral load does not increase after yielding of specimen.

$$n\delta_O = n\delta_{py} + \delta_E (n=1,2,3\cdots) \quad (4)$$

where

$n\delta_O$: standard loading displacement at the crest(cm)

δ_{py}: calculated yield displacement of specimen(cm)

δ_E : lateral displacement developed at the crest due to deformation of reaction wall and steel footing(cm)

Calculated yield displacement δ_{py} are 56mm, 57mm and 53mm for specimen S-23, S-24 and S-28 respectively. δ_E is 19mm for both specimen S-23 and S-24, and 22mm for specimen S-28.

As shown in Fig.5, loading displacement was increased by $1\delta_y$ step. Although the number of cyclic loading for each δ_y($1\delta_y, 2\delta_y, 3\delta_y, \cdots$) should effect on the deformation characteristics of steel piers, 10 times cyclic loading which is the way adopted in the past loading tests at PWRI was carried out. Lateral displacement was increased up to the ultimate displacement that was defined as the displacement at which maximum load become smaller than yield load. Because the effect of loading speed on the deformation characteristics seemed to be small enough, an unified 0.04Hz loading was carried out for every specimens.

PROGRESS OF FAILURE

3 types of specimens commonly deformed up to $1\delta_y$ lateral displacement loading. Lateral thin lines which means the yielding of material were developed on the flange plates. The lines were developed at the section between upper base plate and neighboring diaphram, which section is designated hereinafter as the panel. The 4 panels of each specimen is designated hereinafter as shown in Fig.6. After $2\delta_y$ lateral displacement loading, deformation characteristics and progress of failure of each specimens were as follows.

Specimen S-23 (gamma ratio of 4)

Fig.7 shows the failure mode after $2\delta_y$ lateral displacement loading. Out-of-plane residual deformation was developed. The residual deformation was extremely large at the section of 20cm from the upper base plate. Typical point was the buckling mode at the section between 2 longitudinal stiffeners, i.e., concave deformation and convex deformation developed alternatively at each 2 sections neighboring a lateral stiffener. The deformation mode seemed similar to the local panel buckling mode. Also, concave deformation and convex deformation generally developed alternatively at each 2 sections neighboring a longitudinal stiffener. Although residual deformation was larger at the section between longitudinal stiffeners, deformation of 2~3mm was developed at longitudinal stiffeners. The amount of residual deformation was about 30mm toward outside of specimen and about 25mm toward inside of specimen. According to the residual deformation at the panel, 8mm decreace of specimen height was developed.

Fig.8 shows the failure mode after $3\delta_y$ lateral displacement loading. Typical point on this stage was the transition of the deformation mode. According to the deformation of longitudinal stiffeners, overall wall buckling turned from local panel buckling was developed. Overall wall buckling was developed on 3 panels of specimen. Picture 1 and Picture 2 show the residual deformation of face-2 and face-4 at which local panel buckling and overall wall buckling were developed alternatively. Picture 3 shows the residual deformation of longitudinal stiffeners welded on face-2. Large deformation of longitudinal stiffeners was developed at the section at which large deformation of panel was developed. Maximum amount of residual deformation was about 70mm toward outside of specimen and about 85mm toward inside of specimen.

Most important point on this stage was the fracture of panels. Fracture of panels was developed at the following section.
(1) Welded section at which large difference of deformation between web and flange was developed due to the difference of each out-of-plane deformation. (Fig.8 ①④⑥)
(2) Knuckle section of buckling mode on which longitudinal stiffener was welded. (Fig.8 ②③)
(3) Crest section of buckling mode (Fig.8 ④⑥)
In these sections fracture of panel was developed by the alternative tension and compression according with the cyclic lateral displacement loading.

Specimen S-24 (gamma ratio of 6)

Fig. 9 shows the failure mode after $2\delta_y$ lateral displacement loading.

Amount of residual out-of-plane deformation developed at face-4 was about 20mm toward outside of specimen and about 12mm toward inside of specimen. On the other panel, amount of residual deformation was about 5~6mm toward both outside and inside of specimen. So, amount of residual deformation developed at specimen S-24 seems smaller than that of specimen S-23. Although local panel buckling between 2 longitudinal stiffeners could be seen, local panel buckling of sections neighboring longitudinal stiffener which was shown on specimen S-23 on this stage could not be seen. Because the stiffness of longitudinal stiffeners are larger than that of specimen S-23, local panel buckling knuckled by longitudinal stiffeners could hardly be developed rather than overall wall buckling. decreace of specimen height was much smaller than that of specimen S-23.

Fig.10 shows the failure mode after $3\delta_y$ lateral displacement loading. Residual deformation toward outside of specimen was developed at almost all panels excepting small part of face-2 and face-4. Residual deformation was developed in the overall wall buckling mode. As shown in Picture 4, according to the large deformation of panel, fracture of weld between panel and longitudinal stiffeners was developed. There were few sections where fracture at weld between longitudinal stiffeners and upper base plate was developed. Maximum amount of residual deformation was about 60mm toward outside and about 35mm toward inside of specimen. Fractures at weld between web and flange developed on the 4 corners of specimen could almost progress up to the lowest lateral stiffener. Decreace of specimen height was 44mm, which was about 40% smaller than that of specimen S-23.

Specimen S-28 (gamma ratio of 1)

Fig.11 shows the failure mode after $2\delta_y$ lateral displacement loading. Residual out-of-plane deformation was developed at the lower panel which was about 60cm height section from upper base plate. Amount of residual deformation developed at face-1 was about 32mm toward outside and about 40mm toward inside of specimen. Residual deformation was much larger than that of the other specimens. Major buckling mode was overall wall buckling. In the small section of face-1 and face-3, local panel buckling at sections neighboring with lateral stiffener could be seen. Because the stiffness of longitudinal stiffener was smaller than that of the other specimens, local panel buckling knuckling by longitudinal stiffeners could not hardly be developed.

Fig.12 shows the failure mode after $3\delta_y$ lateral displacement loading. All of the residual deformation was developed in overall wall buckling mode. Almost all of the residual deformation was developed toward inside of specimen excepting small part of face-1 and face-3. Maximum amount of residual deformation was about 85mm toward outside and about 110mm toward

inside of specimen.

Picture 5 shows the fracture at weld between web and flange. The fracture at weld was developed at 4 corners with fracture length of 10～40cm. Fracture of panel at the crest of buckling mode was also developed with fracture length of 3～5cm.

STRENGTH AND DEFORMATION CHARACTERISTICS

Fig.13 shows the comparison of loading hysteresis loops among 3 specimens. First hysteresis loop for each loading displacement($1\delta_y$,$2\delta_y$,$3\delta_y$) are presented. Because of the large stiffness of longitudinal stiffeners, maximum strength for each loading displacement is larger in the order as $1\delta_y$,$2\delta_y$,$3\delta_y$. But any difference among 3 specimens can not be seen on the shape of the loading hysteresis loop.

Fig.14 shows the decline of strength due to the 10 times cyclic loadings for each specimen. The characteristics of decline of strength for each specimen was as follows.

Specimen S-23 (gamma ratio of 4)

Maximum strength P_{max} of 61.2tf was shown in the first hysteresis loop for loading displacement of $2\delta_y$. Because any decline of strength due to cyclic loadings could not be seen for loading displacement of $1\delta_y$, it should be pointed out that specimen deformed elastically in this stage. For loading displacement of $2\delta_y$, remarkable decline of strength occurred after third cyclic loadings. The reason why should be the residual out-of-plane deformation developed at lowest panel as was mentioned above. The maximum strength of 61.2tf for the first cyclic loading was about 30% decreased to 43.0tf after 10 times cyclic loadings.

Specimen S-24 (gamma ratio of 6)

The hysteresis loop for loading displacement of $1\delta_y$ was similar with that of specimen S-23. Maximum strength of 67.3tf was shown in the first hysteresis loop for loading displacement of $2\delta_y$. In this stage, maximum strength of 67.3tf was about 10% decreased to 60.4tf after 10 times cyclic loadings. The extent of decrease was about 20% smaller than that of specimen S-23. The reason why should be the large stiffness of stiffeners, i.e., large stiffness of stiffeners could prevent the residual out-of-plane deformation to be developed, and could reduce the decrease of strength due to cyclic loadings. But for the loading displacement of $3\delta_y$, decrease of strength due to cyclic loadings had become larger. The maximum strength of 57.8tf for the first cyclic loading was about 85% decreased to 8.7tf after 10 times cyclic

loadings. The extent of decrease was rather larger than that of specimen S-23. In this stage, large stiffness of stiffeners caused concentration of stress onto the weld between web and flange, and caused fracture at this section.

Specimen S-28 (gamma ratio of 1)

The hysteresis loop for loading displacement of $1\delta_y$ was similar with that of both specimen S-23 and S-24. Maximum strength of 51.8tf was shown in the first hysteresis loop for loading displacement of $2\delta_y$. In this stage, maximum strength of 51.8tf was about 76% decreased to 12.5tf after 10 times cyclic loadings. The extent of decrease was the largest of all specimens. The reason why should be the smallest stiffness of stiffeners, i.e., the smallest stiffness of stiffeners caused the overall wall buckling to be developed at the panel, and caused the largest residual out-of-plane deformation.

Table 3 shows the comparison of strength and ductility for each specimens. The extent of strength increase after yielding (maximum load P_{max}/ yield load P_y), which is 1.34 for specimen S-23, 1.38 for specimen S-24 and 1.18 for specimen S-28, is smallest on specimen S-28. The reason why is related with the smallest section area of longitudinal stiffeners on specimen S-28. Because the maximum strength of specimen would be developed just after complete yielding of longitudinal stiffeners, smaller the section area of longitudinal stiffeners are, smaller the energy absorbed due to yielding becomes. For developing the extent of strength increase after yielding, it seems important to study the section shape of longitudinal stiffeners for developing energy absorbed due to yielding.

The ductility (yield displacement δ_y/ maximum displacement δ_u) is 2.35 for specimen S-23, 2.71 for specimen S-24 and 1.90 for specimen S-28, respectively. The ductility of specimen becomes small according to the decrease of gamma ratio. The reason why seems to be related with both maximum strength and the extent of strength decrease due to panel buckling. Smaller the gamma ratio is, both smaller the maximum strength and larger the extent of strength decrease would be developed. So, it should be noted that increase of gamma ratio is quite effective to increase the ductility of steel piers.

CONCLUDING REMARKS

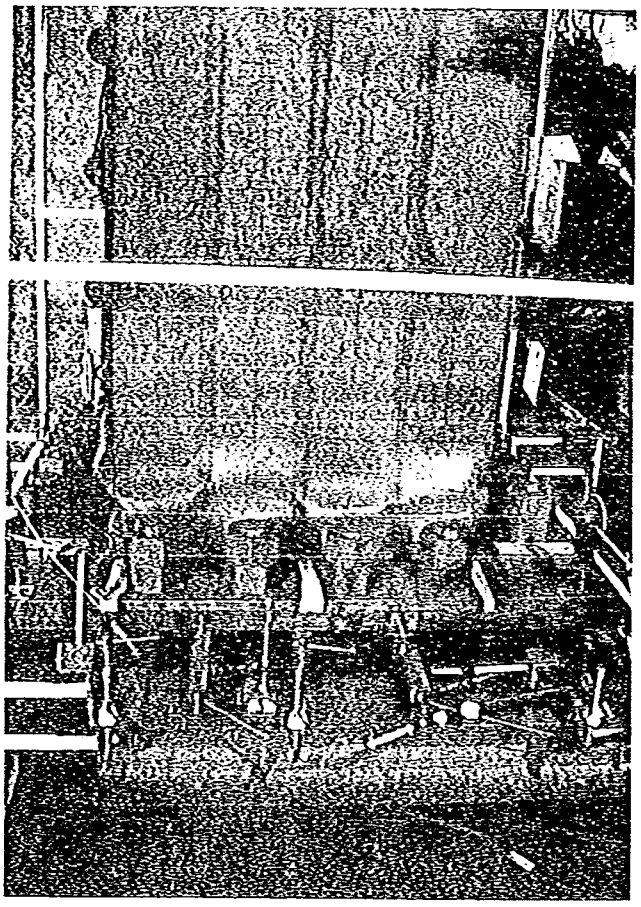
Dynamic loading tests were made on 3 types of steel pier models to study the effect of longitudinal stiffeners on strength and ductility of steel bridge pier. From the results presented, following conclusions may be deduced.

(1) Residual out-of-plane deformation of panels were developed at the

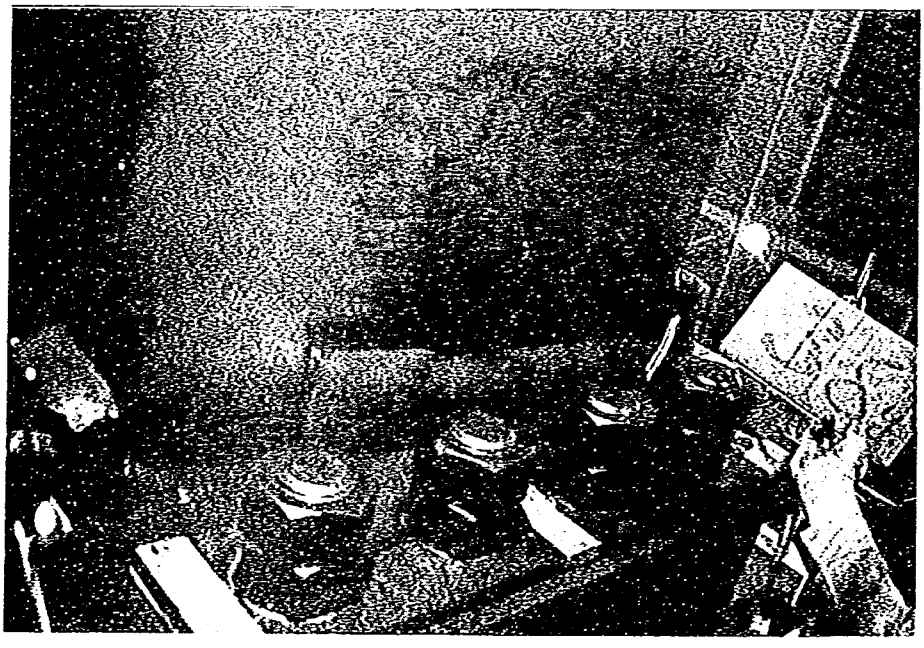
section between upper base plate and lowest diaphram. The buckling mode was local panel buckling for specimen with gamma ratio of 4, and overall wall buckling for specimens with gamma ratio of 6 and 1.
(2) Major failure of specimen was fracture at weld. Major fracture was developed at weld between web and flange. Fracture of panels at the crest and knuckle part of the buckling mode were also developed.
(3) According to the development of panel buckling and fracture at weld, decline of maximum strength due to the cyclic loadings was increased.
(4) As the gamma ratio became larger, the extent of strength after yielding was increased. And as the gamma ratio became larger, the decrease of strength according to the cyclic loadings was reduced. For these reasons, the ductility of specimen was increased as the gamma ratio became larger.

REFERENCES

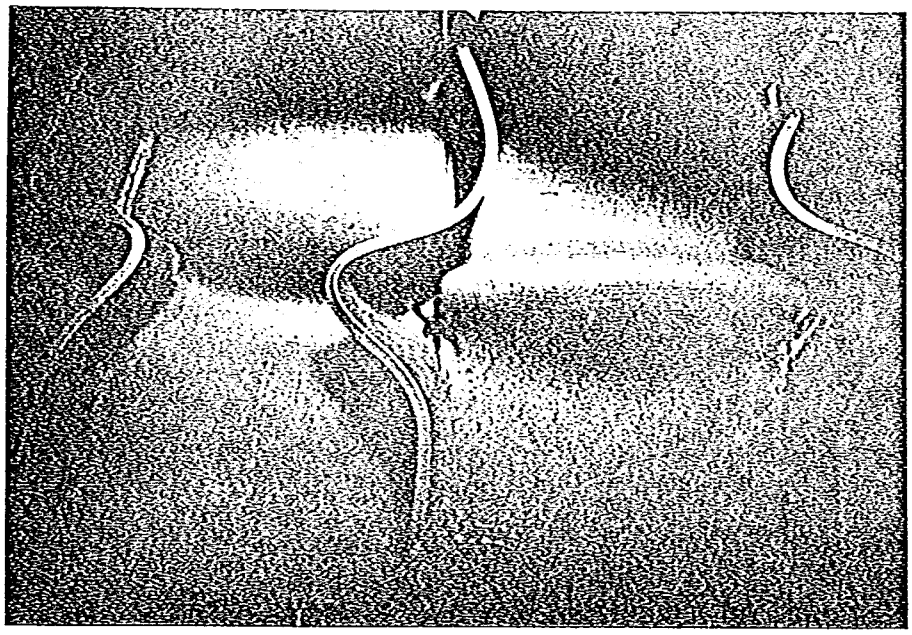
(1) Japan Road Association: Design Specifications for Highway Bridges, Part II Steel Bridges, English Edition, 1987
(2) Subcommittee on Stability Design: Guidelines for the stability of Steel Structures, Japan Society of Civil Engineering, 1987
(3) K.KAWASHIMA, G.A.MacRae and K.HASEGAWA: The Strength and Ductility of Steel Bridge Piers Based on Loading Tests, PWRI Journal of Research, Vol.29, March 1992



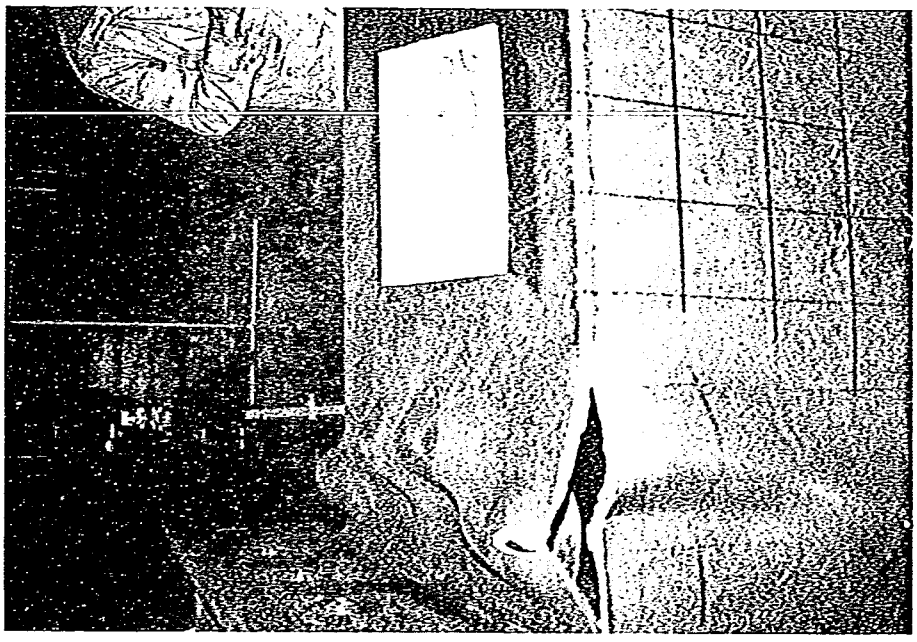
Picture 1 Failure Mode of Specimen with Gamma Ratio of 4 (Face-2)



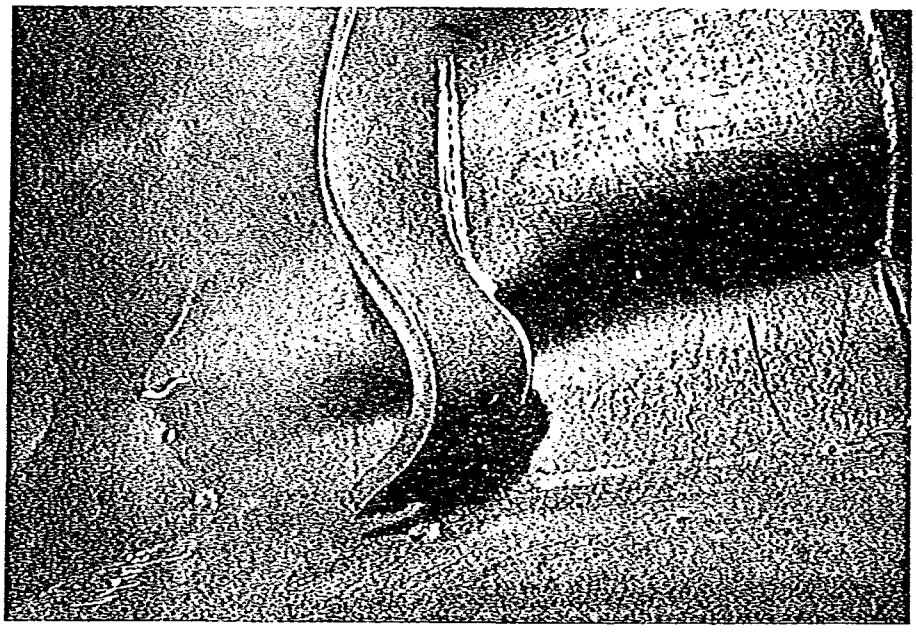
Picture 2 Failure Mode of Specimen with Gamma Ratio of 4 (Face-4)



Picture 3 Residual Deformation of Longitudinal Stiffeners



Picture 4 Fracture at Weld Between Web and Flange (Specimen S-24, Gamma Ratio of 6)



Picture 5 Fracture between Panel and Longitudinal Stiffeners (Specimen S-24, Gamma Ratio of 6)

Table 1 Characteristics of Specimens

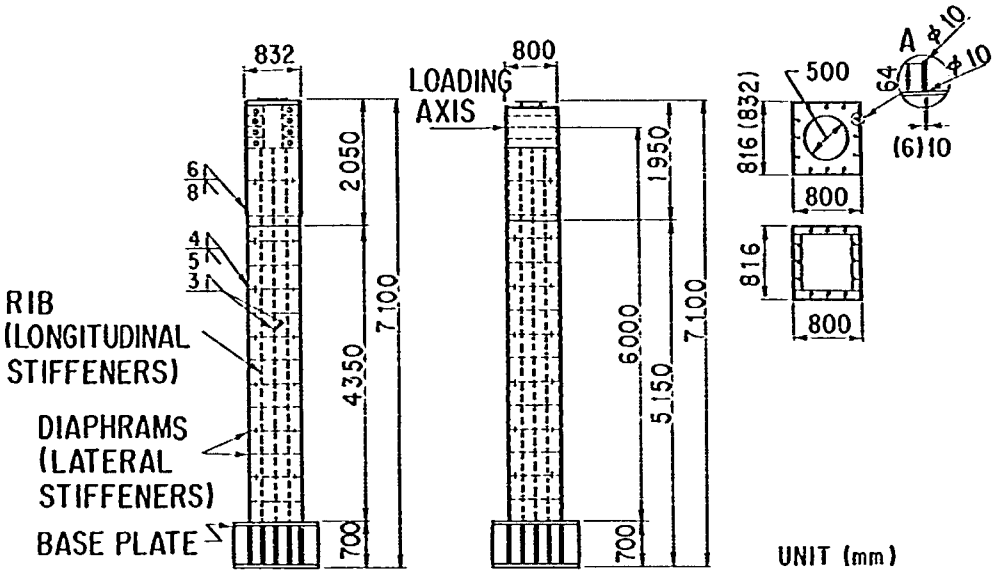
SPECIMEN		S-24	S-23	S-28
LONGITUDINAL STIFFENER	SECTION SIZE (mm)	10 x 64	6 x 64	6 x 59
	NUMBER OF PANEL	4		
LATERAL STIFFENER	PLATE THICK (mm)	4.5		
	SPACING (mm)	350		600
RERATIVE STIFFNESS γ_ℓ		23.46	14.08	11.03
RERATIVE STIFFNESS $\gamma_{\ell\cdot req}$		3.94	3.45	10.38
GAMMA RATIO $\gamma_\ell / \gamma_{\ell\cdot req}$		5.95 ≒ 6	4.08 ≒ 4	1.06 ≒ 1

Table 2 Average Yield Strength and Strain

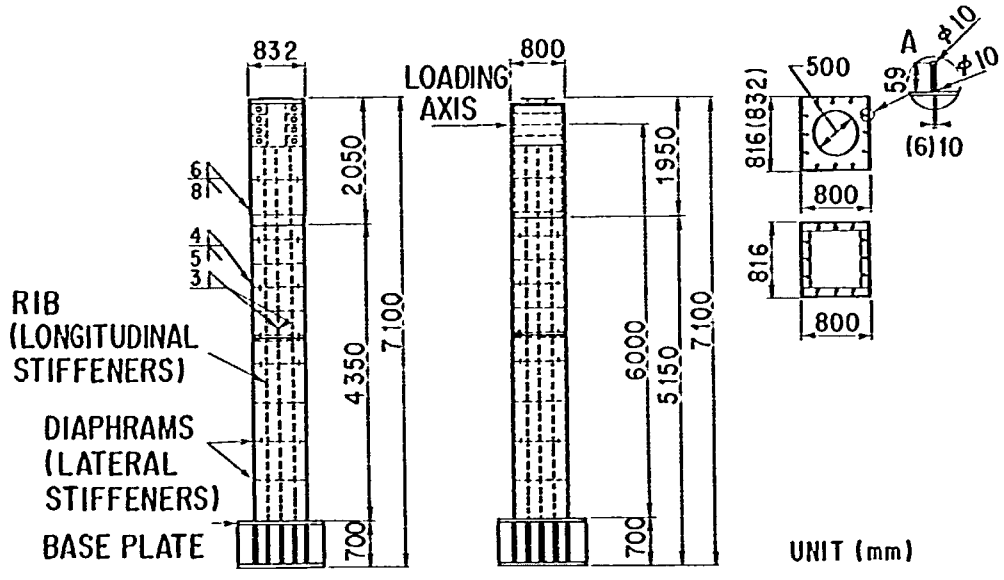
	LONGITUDINAL STIFFENERS		WEB AND FLANGE	
THICKNESS (mm)	10	6	8	
STANDARD	SM490A			
YIELD STRENGTH (kgf/cm^2)	3872	4021	3920	3946
YIELD STRAIN(μ)	1850	1920	1870	1880

Table 3 Strength and Ductility of Specimen

SPECIMEN	S-24	S-23	S-28
GAMMA RATIO $\gamma_l / \gamma_{l \cdot req}$	6	4	1
YIELD LOAD P_y (tf)	48.8	45.6	43.8
MAXIMUM LOAD P_{max} (tf)	67.3	61.2	51.8
P_{max} / P_y	1.38	1.34	1.18
YIELD DISPLACEMENT δ_y (mm)	65.0	66.0	75.1
MAXIMUM DISPLACEMENT δ_u (mm)	176.3	155.3	143.0
DUCTILITY δ_u / δ_y	2.71	2.35	1.90

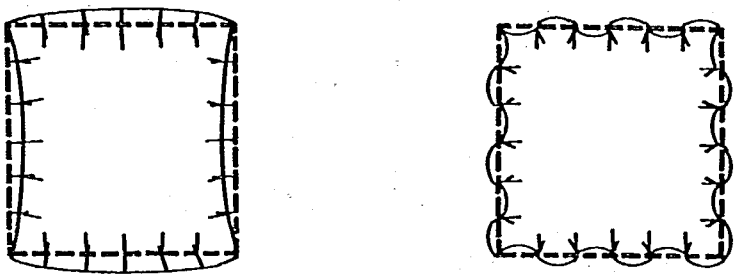


(a) Specimen S-23 and S-24



(b) Specimen S-28

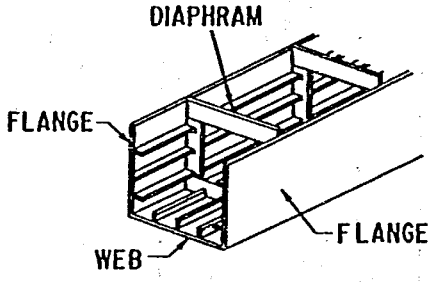
Fig.1 Specimens



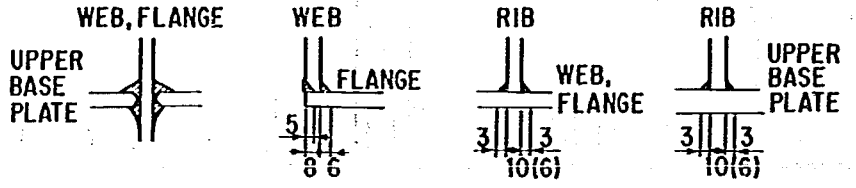
(a) Overall Wall Buckling ($\gamma_\ell / \gamma_{\ell \cdot req} < 1.0$)

(b) Local Panel Buckling ($\gamma_\ell / \gamma_{\ell \cdot req} \geqq 1.0$)

Fig.2 Buckling mode of Box-shaped Section



(a) Method of Construction



(b) Method of Welding

Fig.3 Method of Construction and Welding

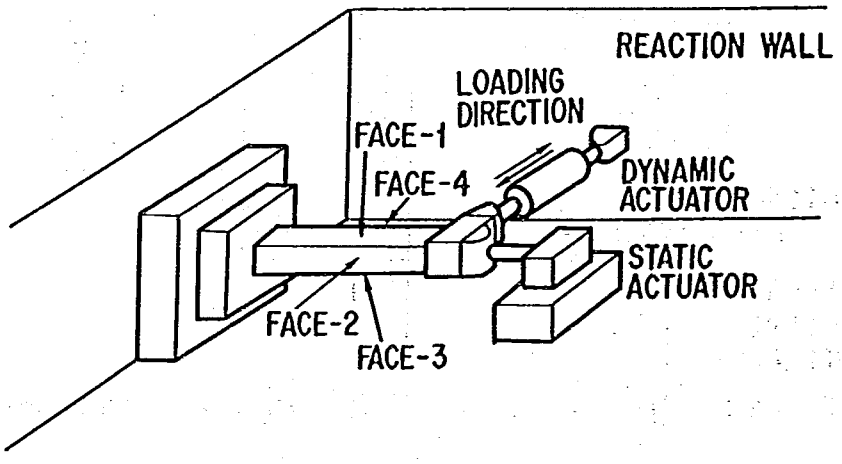


Fig.4 Experimental Set-up of Specimen

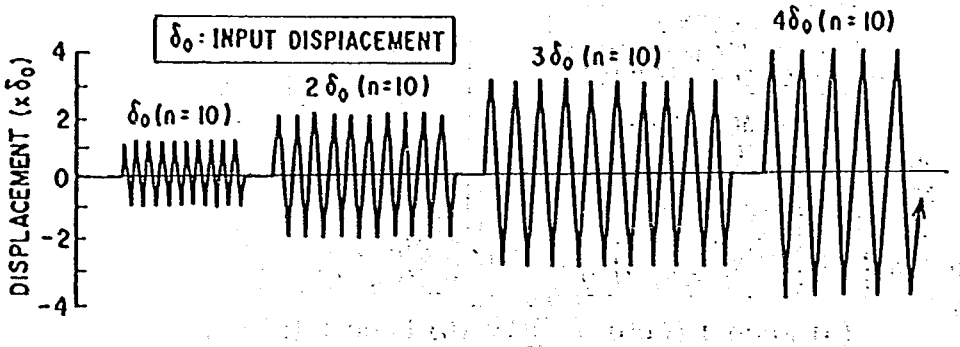


Fig.5 Loading Hysteresis Loop

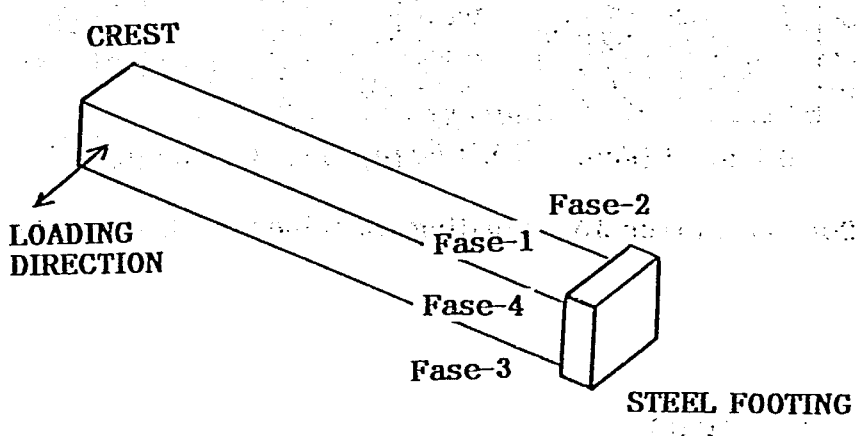


Fig.6 4 Panels of Specimen

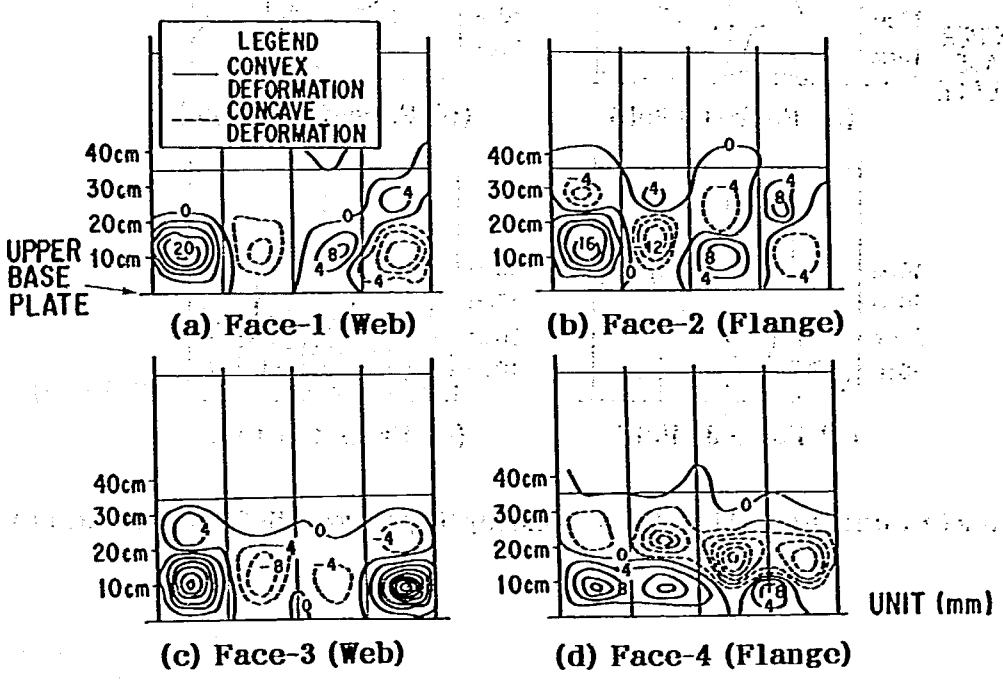


Fig.7 Buckle Contours after 2δ y Loading (Specimen S-23, Gamma Ratio of 4)

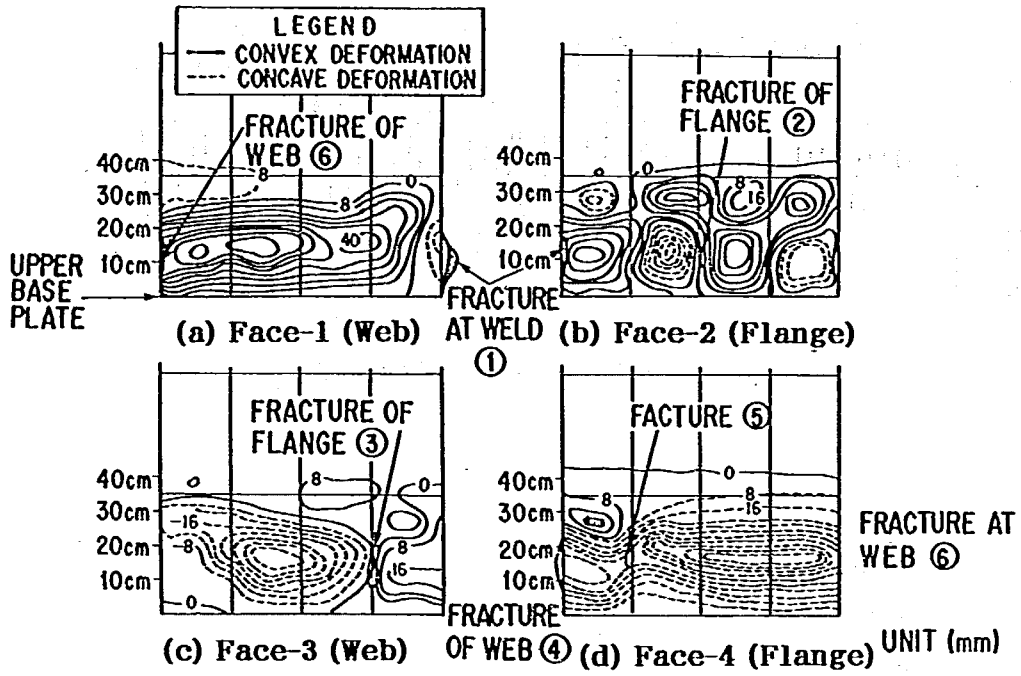


Fig.8 Buckle Contours after 3δ y Loading (Specimen S-23, Gamma Ratio of 4)

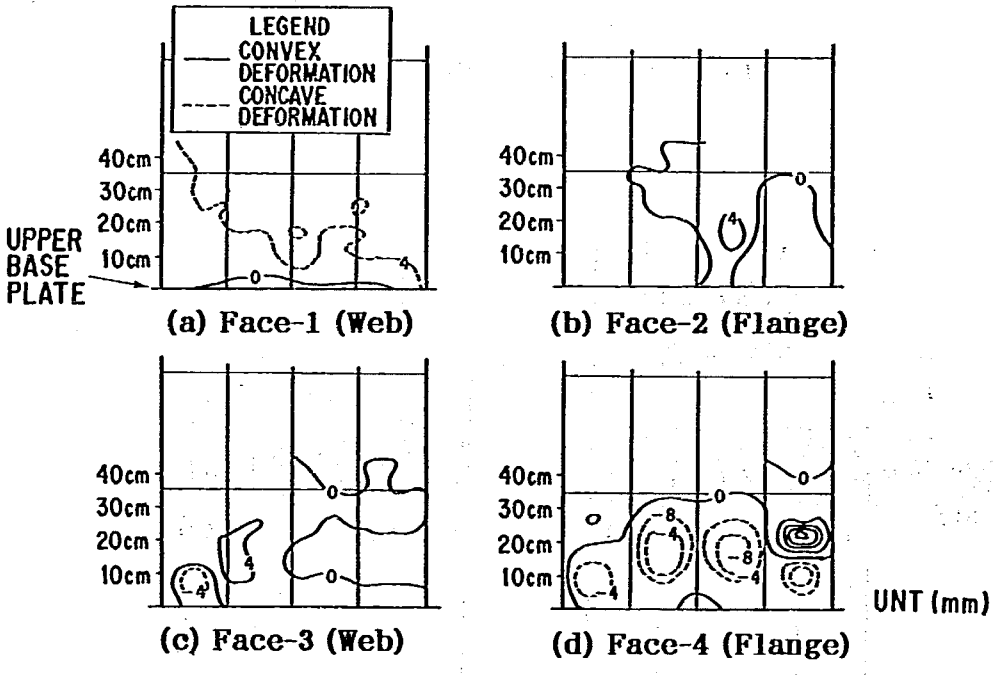


Fig.9 Buckle Contours after 2δ y Loading (Specimen S-24, Gamma Ratio of 6)

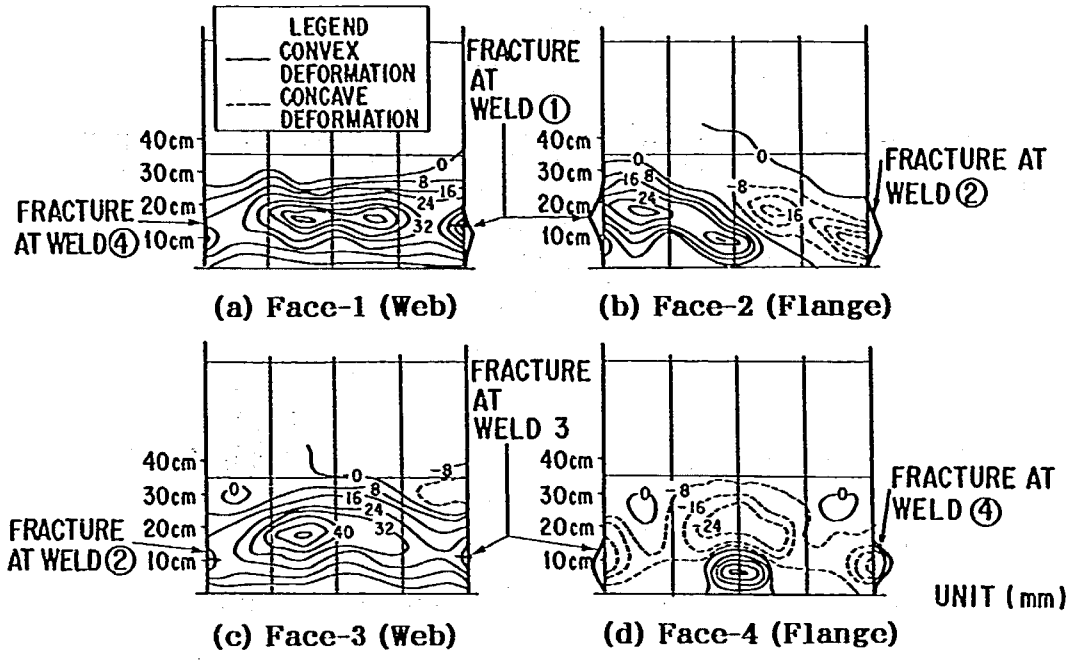


Fig.10 Buckle Contours after 3δ y Loading (Specimen S-24, Gamma Ratio of 6)

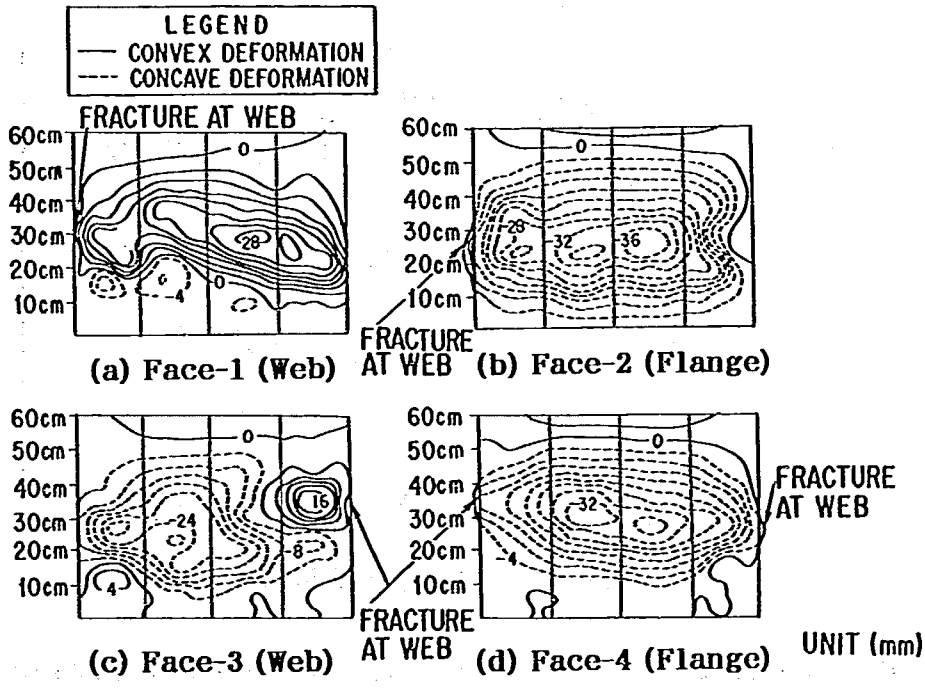


Fig.11 Buckle Contours after 2δ y Loading (Specimen S-28, Gamma Ratio of 1)

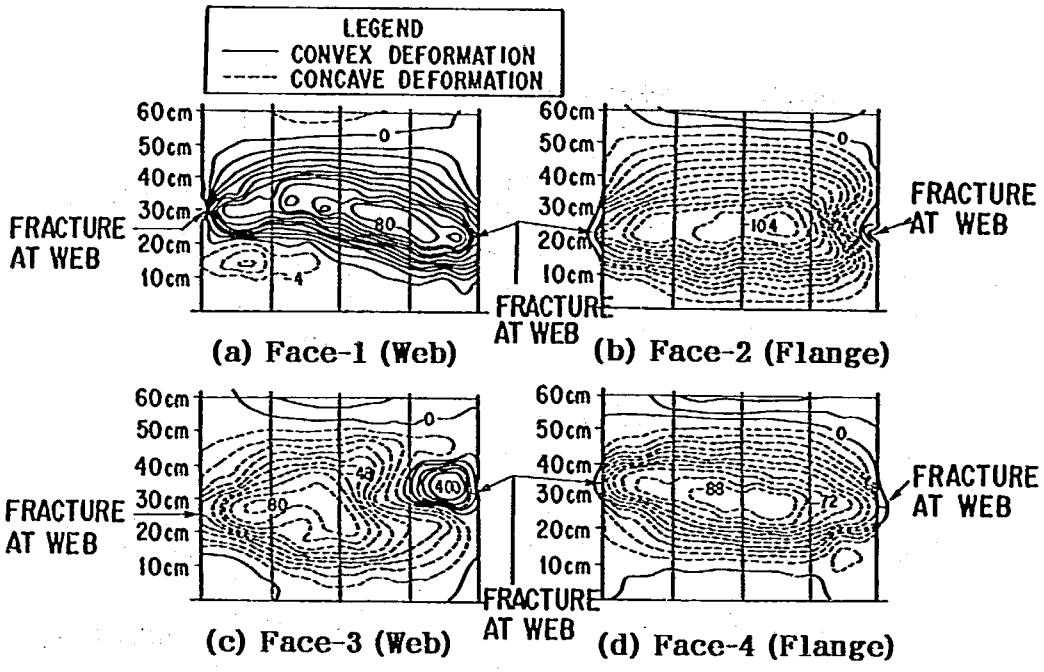


Fig.12 Buckle Contours after 3δy Loading (Specimen S-28, Gamma Ratio of 1)

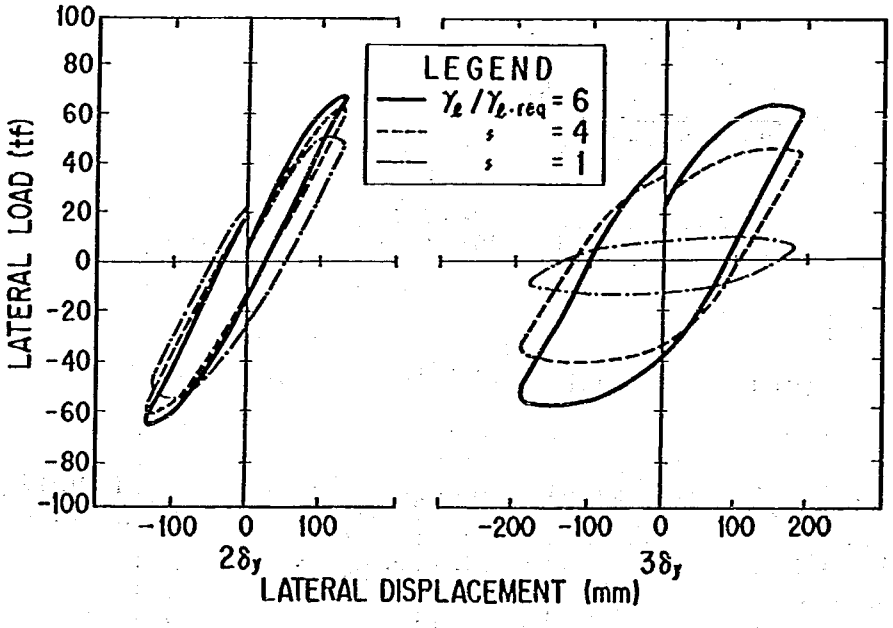
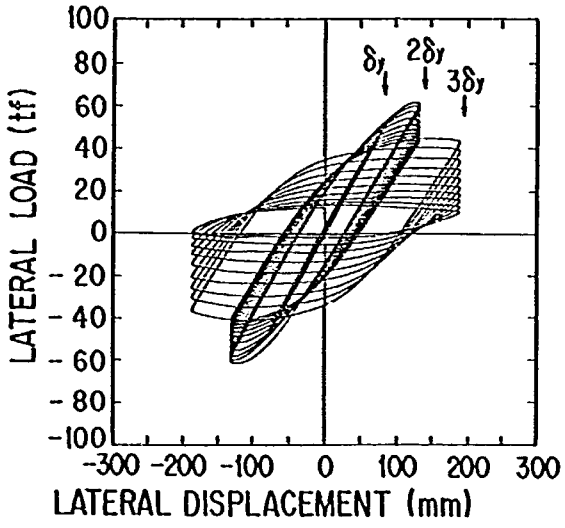
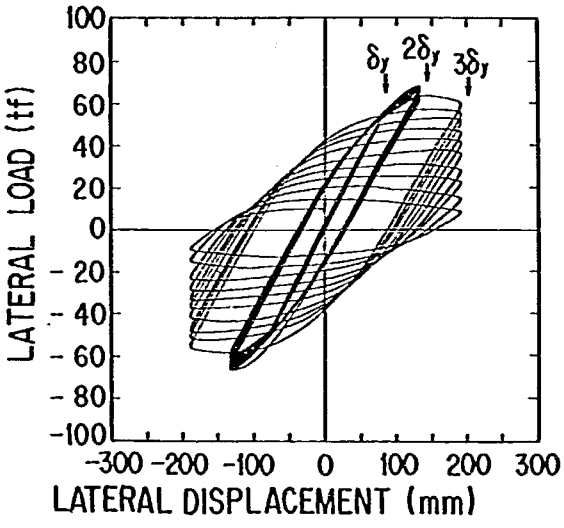


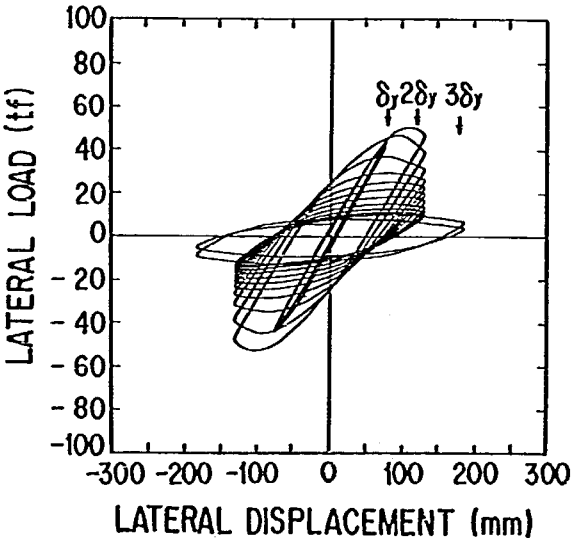
Fig.13 Comparison of Loading Hysteresis Loop among 3 Types of Specimens



(a) Specimen S-23 with Gamma Ratio of 4



(b) Specimen S-24 with Gamma Ratio of 6



(c) Specimen S-28 with Gamma Ratio of 1

Fig.14 Loading hysteresis Loop of Specimen

Seismic Response of Reinforced Concrete Bridge Piers Subjected to Eccentric Loading

Kazuhiko KAWASHIMA
Shigeki UNJOH
and
Hidetoshi MUKAI

9th U.S.–Japan Bridge Workshop
Tsukuba, Japan
May, 1993

SEISMIC RESPONSE OF REINFORCED CONCRETE BRIDGE PIERS SUBJECTED TO ECCENTRIC LOADING

by

Kazuhiko KAWASHIMA[1] Shigeki UNJOH[2] and Hideki MUKAI[3]

1) Head, Earthquake Engineering Division, Earthquake Disaster Prevention Department, Public Works Research Institute, Ministry of Construction, Tsukuba Science City, Japan 305
2) Senior Research Engineer, ditto
3) Assistant Research Engineer, ditto

ABSTRACT

Presented are the seismic response characteristics of C-shaped reinforced concrete bridge piers which is subjected to eccentric loading by the dead weights of superstructure and cantilevered beam. The shaking table test and dynamic loading tests of model piers were made to investigate the seismic response characteristics. It is found that the response of pier increases only in one direction in which the bending moment increases and that the excessive residual displacement was developed. It is also found that the ductility significantly decreases with increase of bending moment by the eccentric loading.

1. INTRODUCTION

Recently, new types of structures have been constructed in urban areas by land use restriction and other construction conditions. A C-shaped reinforced concrete (RC) bridge pier as shown in Fig.1 is one of the typical examples. However, the seismic response characteristics of this type of RC piers have not yet been studied. The C-Shaped RC piers is subjected to eccentric loading by the dead weights of superstructure and cantilevered beam to support the superstructure. Therefore, since it is anticipated that the seismic response increases only in one direction during a severe earthquake, it is an important subject to investigate the strength and ductility characteristics and to develop the seismic design method against large-scale earthquakes.

This paper presents the seismic response characteristics of C-shaped reinforced concrete bridge piers through the shake table test and dynamic loading tests of model piers.

2. DEFINITION OF ECCENTRIC LOADING

When RC piers are C-shaped and subjected to eccentric loading in the transverse direction to the bridge axis, the load-displacement relation of RC piers may be illustrated as shown in Fig.2, in which load-displacement relation is assumed as tri-linear. In case in which dead weights of superstructure is concentrically loaded, displacement by seismic loading is developed from the

origin. The pier is deformed in nonlinear region as crack and yielding and ultimate stages with increase of the seismic loading. However, when the dead weights of superstructure is loaded eccentrically, the pier is initially deformed and the origin of displacement developed by the seismic loading is shifted. Therefore, it is anticipated that the seismic response increases only in one direction during a severe earthquake.

In order to define the amount of the eccentric loading, bending moment ratio is assumed as

$$r_M = \frac{M_E}{M_D + M_E} \quad (1)$$

where

r_M : bending moment ratio

M_E : bending moment by design seismic load, and

M_D : bending moment by eccentric loading of superstructure and cantilevered beam

Eq.(1) shows that when the eccentric loading increases r_M deceases, on the other hand, when the eccentric loading decreases r_M increases. r_M = 1 means concentric loading.

Fig.3 shows distribution of the bending moment ratio r_M based on the survey of 45 existing C-shaped RC bridge piers in Metropolitan area, bending moment ratio r_M is in the range of 0.4 - 0.9. Averaged bending moment ratio r_M is 0.55.

3. SEISMIC RESPONSE CHARACTERISTICS OF C-SHAPED RC PIER BASED ON SHAKING TABLE TESTS

3.1 Bridge Pier Model Studied

In order to investigate the seismic response characteristics of a C-shaped RC pier, shaking table test was made at the Public Works Research Institute. Objective of the shaking table test is to investigate how the C-shaped pier responds and behaves in the transverse direction to a bridge axis during an actual earthquake.

Fig.4 shows a C-shaped bridge pier model used for the shaking table test. Details of the pier model was determined based on the actual bridge pier. The actual pier with average bending moment ratio, r_M, of 0.55 was selected as a prototype. The height of pier is 10.2m and the height of girder is 1.5m. The similarity ratio of the pier model with the prototype pier was assumed as 1/4.6.

The specimen has an effective height, h, of 2.55m and cross section of 52cm × 42cm (width in bridge axis : 52cm). The shear span ratio h/d, which is defined as the effective height divided by the effective depth, d, of the cross section of 37cm, is 6.9. Longitudinal reinforcing bars are arranged by 5 reinforcing bars with diameter of 16mm (D16) in the initial compression side by the eccentric loading, 5 reinforcing bars with that of 22mm (D22) in the tension side, and 3 reinforcing bars with that of 16mm (D16) in the other sides. The reinforcement ratio is 0.45, 1.06 and 0.27, respectively. Tie reinforcement was arranged by 17.3cm pitch by reinforcing bars with diameter of 10mm (D10). Tie reinforcement ratio is 0.16. Averaged yielding stress of the longitudinal and tie reinforcement was 3,608kgf/cm^2 for D16, 3,500kgf/cm^2 for D22 and 3,552kgf/cm^2 for D10. Averaged compression strength of the concrete was 335kgf/cm^2. It

should be noted here that since weight of the superstructure supported by the pier model is 40.1tf, seismic coefficient of the pier model can be regarded as 0.27. Axial stress by the dead weight of superstructure was 9.2kgf/cm^2. Computed yield displacement, δ_y, corresponding to one displacement ductility factor and yield strength of the pier in the direction in which the bending moment increases are 7.7tf and 20.5mm computed from the shifted origin. On the other hand, in the direction in which the bending moment decreases they are 11.8tf and 91.3mm, respectively.

3.2 Shaking Table Test

Photo 1 shows the set up of shaking table test. A pier model is fixed at the center of the shaking table and two spans of simply supported girders with total weights of 40.1tf and length of 15m were placed on the pier model. Because two ends of the girder could not be supported by the shaking table, they are supported by the two steel frames placed outside of the table. The pier model and girders were connected by fixed bearings. The steel frames and girder were connected by movable roller bearings so that inertia force developed at the girder during excitation be directly applied to the pier model. It should be noted here that although the direction of the eccentric loading is assumed to be transverse direction, the girder axis was set up in parallel direction with transverse direction of the pier model. However, since the two girders was to load the weight of superstructure and to simulate the inertia force, the direction of the girders is not important.

The shaking table was excited along transverse direction to bridge axis (direction to the girder axis of model bridge). An acceleration record triggered at the Hachirogata during the Nihon-kai-chubu, Japan, Earthquake of 1983 was used as an input motion by reducing the time axis one half so that the predominant frequency of the record matches with the fundamental natural frequency of the pier model. Intensity of the record was assumed as 3.5 times the original.

Extensive instrumentations were made to measure basic parameters including accelerations at the foot of pier and at the girder as well as relative displacement of the girder with reference to shaking table. Inertia force of the superstructure was computed by multiplying the acceleration developed at the girder by the mass of girder.

3.3 Seismic Response Characteristics

Fig.5 shows acceleration of shaking table, response acceleration and displacement of girder. Although measured peak acceleration of shaking table is 812cm/s^2, this is spike-like response and effective seismic intensity to excite the pier model is about 0.35G as assumed. The pier model developed residual lateral displacement with an amount of 16cm at the pier crest in the direction in which eccentric weight is loaded. However, the stopper for preventing falling-off of girders worked at this moment. If the stopper was not installed the larger residual displacement would be developed. Such a permanent displacement is clearly observed in Fig.5 from biased inelastic response displacement. The drift of response displacement was developed at time 12sec when the first large excitation, which exceeded the yielding displacement, loaded. However, after the excitation with larger displacement at time 17sec, the residual displacement reached to about 16cm. Therefore, accumulation of

drifting of response displacement after the first large excitation seems to be less significant. It should be noted here that although the residual displacement was developed in the shaking table test of RC pier model subjected to concentric loading, the amount was much smaller than that mentioned above. Photo 2 shows the residual deformation of the pier model after excitation.

Fig.6 and Photo 3 show the failure mode of the pier model after the excitation by shaking table. Compression failure was found in the compression side by the eccentric loading. Only horizontal tension crack was found in the tension side.

Fig.7 shows the hysteresis loop of the load-displacement relation obtained through the shaking table test. The biased displacement response was clearly developed after the first significant excitation with larger displacement exceeding the yield displacement. The degradation of the stiffness in accordance with nonlinear response can be clearly observed.

4. DYNAMIC LOADING TEST OF RC PIER MODELS

4.2 Bridge Pier Models Studied

In order to investigate the strength and ductility characteristics of C-shaped RC pier, dynamic loading tests were made. Fig.8 shows a C-shaped bridge pier model used for the dynamic loading test. The pier models are basically the same as the shaking table test as mentioned in the above. Five pier models in total were tested, in which bending moment ratio, r_{M}, and loading direction was varied as a parameters to be investigated.

All pier models have a loading effective height, h, of 2.55m and cross section of 52cm × 42cm (width in bridge axis : 52cm). The shear span ratio, h/d, is 6.9. The bending moment ratio, r_{M}, was assumed as 0.69 (P-60; small eccentric loading), 0.55 (P-62; medium eccentric loading) and 0.51 (P-64; large eccentric loading), in which the specimen number is the serial number of pier models tested at the Public Works Research Institute. P-62 has the same condition as one used for the shaking table test. More two piers (P-65 and P-66) are for the purpose to investigate the effect of longitudinal loading. The detail of the piers is the same as P-62. Eccentric weight in transverse direction was not loaded for P-65. Axial loading was assumed as 20tf which is the same as the shaking table test. Therefore, axial stress by the axial loading is 9.2kgf/cm^2. It should be noted here that the axial force to P-60 was assumed as 13tf (axial stress is 6.0kgf/cm^2) because of limitation of loading apparatus.

4.2 Dynamic Loading Test

Photo 4 shows the set up of the pier model for the dynamic loading tests. The pier model was anchored to the reaction wall with bolts. The large-stroke dynamic actuator, which was installed to the reaction wall in such a manner, was fixed to the head of the pier model. Also, axial loading apparatus was fixed to the head of the pier models so that the necessary eccentric loading be applied. At the pier crest the steel-made apparatus was set for the purpose to eccentrically impose the axial force.

Fig.9 shows the pattern of loading displacement for dynamic loading tests. The yield displacement corresponding to one ductility factor was assumed as an

unit loading displacement. However, the pier models subjected to eccentric loading is initially displaced by displacement of δ_0. Therefore, unit loading displacement, $\delta 1$, was assumed with the assumption of that the origin is shifted to the initial point as

$$\delta 1 = \delta_y - \delta_0 \qquad (2)$$

where

$\delta 1$: unit loading displacement
δ_y : yielding displacement
δ_0 : initial displacement by eccentric loading

The pier models were subjected to a series of step-wise increasing symmetric displacement cycles as shown in Fig.9. At each step, 10 cycles of loading with the same displacement amplitude was carried out. It should be noted here that the yield displacement was determined by computation with the strain of main reinforcement at the base. The loading velocity was assumed as 1cm/s. The loading direction was assumed as transverse and longitudinal directions depending on the test objectives.

4.3 Failure Mode of Pier Models

Fig.10 and Photo 5 show the failure mode of P-62 (r_M = 0.55; medium eccentric loading). Damage of a side parallel to the loading direction is shown. During δ_1 to δ_2 loading cycles, only small horizontal cracks were found on the concrete surface. This is by the loading in the plus side (the loading in which bending moment increases, this side is referred to A-side), no cracks was found at the minus side (the loading in which bending moment decreases, this side is referred to B-side). After δ_3 loading cycles the cracks was initiated to be developed in B-side. During δ_4 loading cycles, diagonal cracks were developed from the bottom of A-side to B-side. With increase of loading cycles, the significant cracks were developed at the bottom of B-side and cover concrete was spalled-off. During δ_6 loading cycles, concrete of the bottom of pier was failed with a triangular wedge shape and 2 reinforcing bars were fractured in the B-side. During δ_7 loading cycles, deformation of pier was significantly extended at the base and the pier was inclined. It should be noted here that comparing of the failure mode with the shaking table test result, the failure mode was significantly different between two tests. Although the diagonal crack was developed in the dynamic loading test, such diagonal crack was not developed during the shaking table test. This is because that although displacement in the minus side was forced to be loaded to the pier in the dynamic loading test, displacement during shaking table test was developed in one direction in which the bending moment increases.

Figs.11 and 12 show the failure modes of P-60 (r_M = 0.69; small eccentric loading) and P-64 (r_M; large eccentric loading). In case of P-60, from δ_1 loading cycles, crack was developed also in the B-side. Then the crack increased in both A-side and B-side. During δ_6 loading cycles, cover concrete was spalled-off in the both sides of the bottom. During δ_7 loading cycles, 3 longitudinal reinforcing bars were fractured. The difference in the failure mode between P-62 and P-60 is that the damage was developed in both sides and the progress of the damage of P-60 with loading cycles became slower than that of P-62.

On the other hand, in case of P-64 (r_M = 0.51; large eccentric loading), during δ_3 loading cycles the diagonal crack was developed. The cover concrete in the B-side of the bottom was spalled-off during δ_4 loading cycles. During δ_5, concrete at the bottom of B-side was failed by compression and one longitudinal reinforcing bar was fractured. Comparing with the failure mode of P-62, the progress of damage of P-64 became faster than P-62.

Figs.13 and 14 show the failure modes of the P-65 (no eccentric loading, longitudinal loading) and P-66 (eccentric loading). The compression side by the eccentric loading was shown. During δ_5 and δ_6 loading cycles cover concrete was spalled-off. Then during δ_8 loading cycles, 5 reinforcing bars in total were fracture in the both sides for two model piers. The slight difference between two pier models was found in the failure mode. In P-66 in which eccentric loading was applied, the diagonal crack was found more remarkably than P-65 with no eccentric loading.

4.4 Strength and Ductility Characteristics

Fig.15 shows the effect of bending moment ratio, r_M, on load-displacement relation. In the plus side in which the bending moment increases, the displacement range in which load reaches to peak and the displacement increase stably was shorter as the bending moment ratio is smaller. Therefore, the bending moment ratio is smaller, the ductility becomes smaller.

Fig.16 shows the effect of longitudinal loading on the load-displacement relation. The load-displacement relations of two piers are almost the same even if the eccentric loading was applied. Therefore, there is small effect of eccentric loading when seismic load was applied in the longitudinal direction.

Fig.17 shows the comparison of load-displacement relation between shaking table test and dynamic loading test results. The load-displacement relation was the almost close. However, in the shaking table test, the load did not decrease suddenly with increase of displacement. This is because of the difference of loading methods. In the dynamic loading test, forced displacement was applied by the 10 cycles loading.

Table 1 shows the strength and ductility of the tested pier models. The ductility was almost same when r_M is 0.69 and 0.55, but when the r_M is 0.51 the ductility decreases to one of half of those. The ratio of peak strength by yield strength of the P-64 decreases by 10% than P-60 and P-62.

5. CONCLUDING REMARKS

In order to investigate the seismic response characteristics of C-shaped reinforced concrete bridge piers which is subjected to eccentric loading in the transverse direction to bridge axis by the dead weights of superstructure and lateral beam, the shaking table test and dynamic loading tests of model piers were made to investigate the seismic response characteristics.

According to the above results the following conclusions may be deduced:

(1) When the pier model subjected to eccentric loading, the displacement was developed only in one direction in which the bending moment increases. The large amount of residual displacement was finally developed.

(2) When the bending moment ratio is 0.51, the ductility decreases to one half that greater than 0.55. Therefore, the bending moment ratio is smaller, ductility becomes smaller.

REFERENCES

1. Kawashima, K., Hasegawa, K., Koyama, T. and Yoshida, T. : Hysteretic Behavior of Reinforced Concrete Bridge Piers by Dynamic Loading Tests and Shaking Table Tests, Ninth World Conference on Earthquake Engineering, Tokyo-Kyoto, Japan, August 2 - 9, 1988
2. Kawashima, K., Hasegawa, K., Koyama, K. and Yoshida, T. : Experimental Investigation on Dynamic Strength and Ductility of Reinforced Concrete Bridge Piers, (Part.1), Technical Memorandum of PWRI, No.2232, 1985
3. Kawashima, K., Hasegawa, K., Koyama, K. and Yoshida, T. : Experimental Investigation on Dynamic Strength and Ductility of Reinforced Concrete Bridge Piers, (Part.3), Technical Memorandum of PWRI, No.2504, 1987
4. Iwasaki, T., Kawashima, K., Hasegawa, K., Koyama, T. and Yoshida, T. : Effect of Number of Loading Cycles and Loading Velocity of Reinforced Concrete Bridge Piers, 19th Joint Meeting, Wind and Seismic Effects, UJNR, Tsukuba, Japan, 1987
5. Iwasaki, T., Kawashima, K., Hasegawa, K. and Yoshida, T. : Dynamic Strength and Ductility of Reinforced Concrete Bridge Piers, 20th Joint Meeting, Wind and Seismic Effects, UJNR, 1988
6. Iwasaki, T., Ueda, O., Kawashima, K., Hasegawa, K. and Yoshida, T. : Inelastic Behavior of Reinforced Concrete Bridge Pier, -Effect of Bilateral Loading and Circular Hollow Section-, 21st Joint Meeting, Wind and Seismic Effects, UJNR, Tsukuba, Japan, 1989
7. Kawashima, K., and Koyama, T. : Effect of Number of Loading Cycles on Dynamic Characteristics of Reinforced Concrete Bridge Pier Columns, Structural Eng./Earthquake Eng., Proc. JSCE, Vol.5, No.1, pp.183-191, 1988.4
8. Kawashima, K., and Koyama, T. : Effect of Cyclic Loading Hysteresis on Dynamic Behavior of Reinforced Concrete Bridge Pier, Structural Eng./Earthquake Eng., Proc. JSCE, Vol.5, No.2, pp.343-350, 1988.10

Table 1 Strength and Ductility of Pier Models

	P-60	P-62	P-64	P-65	P-66
Loading Direction	Trans.	Trans.	Trans.	Longi.	Longi.
Bending Moment Ratio r_M (Eccentric Loading)	0.69 Small	0.55 Medium	0.51 Large	0 --	0.55 Medium
Yield Strength Py (tf)	12.7	15.0	22.8	17.2	16.0
Peak Strength Pmax (tf)	14.8	18.3	24.3	21.3	20.1
Pmax/Py	1.17	1.22	1.07	1.24	1.26
Yield Displacement δ y(cm)	1.6	1.3	2.0	1.6	1.8
Ultimate Displacement δ y(cm)	8.8	7.3	5.4	7.3	7.9
Ductility Factor δ y/δ u	5.5	5.6	2.7	4.6	4.4

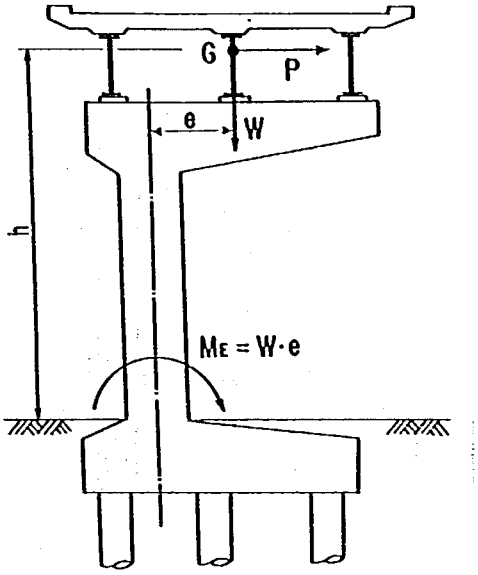


Fig.1 C-Shaped Reinforced Concrete Bridge Pier Subjected to Eccentric Loading

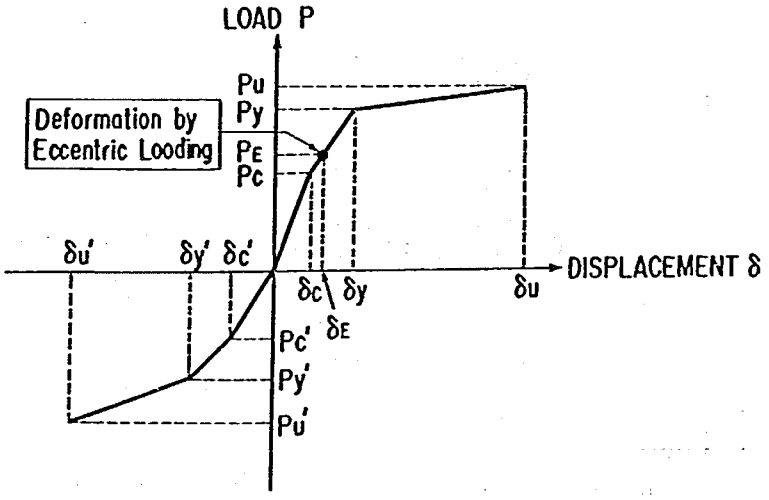


Fig.2 Effect of Eccentric Loading on Load-Displacement Relation

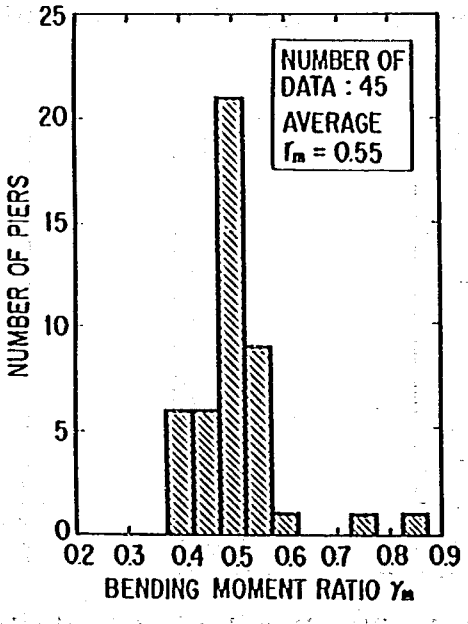


Fig.3 Distribution of Bending Moment Ratio of Actual Bridge Piers Surveyed

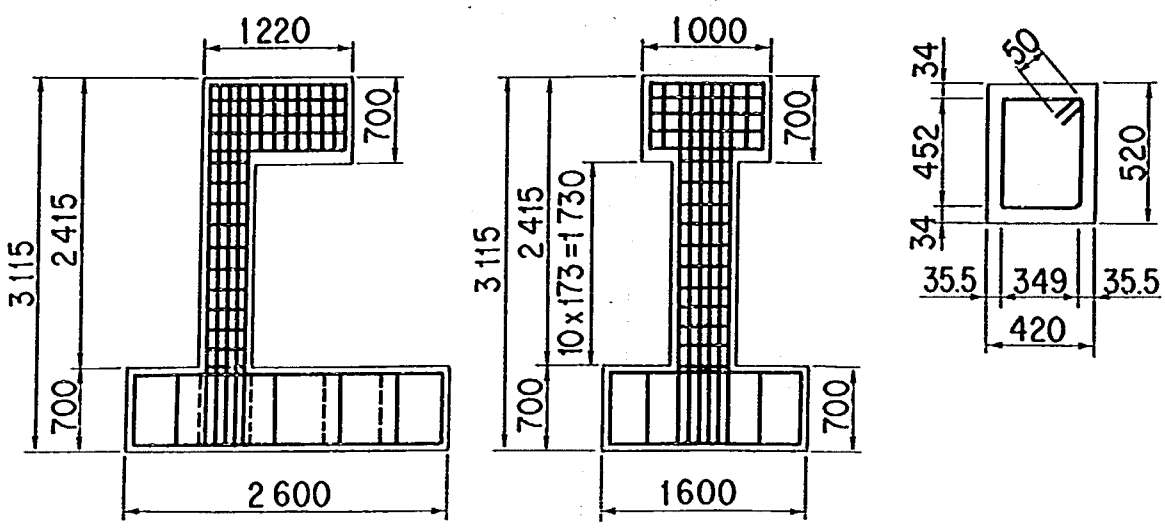


Fig.4 C-Shaped Bridge Pier Model for Shaking Table Test

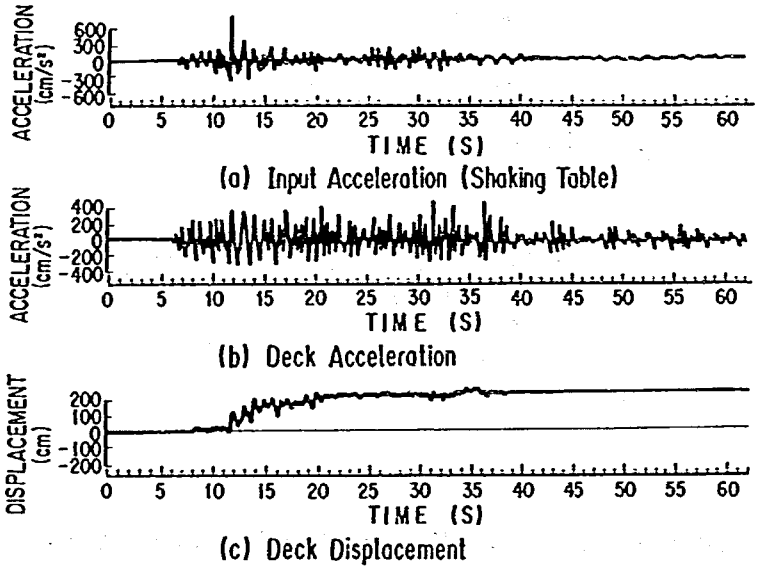


Fig.5 Response Accelerations and Displacement

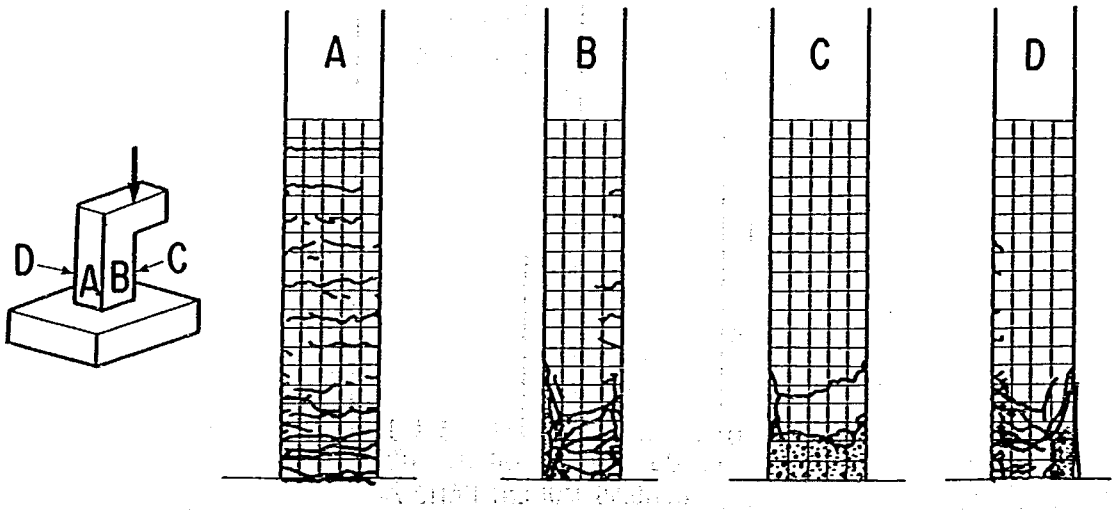


Fig.6 Failure Mode of the Pier Model after Excitaion by Shaking Table

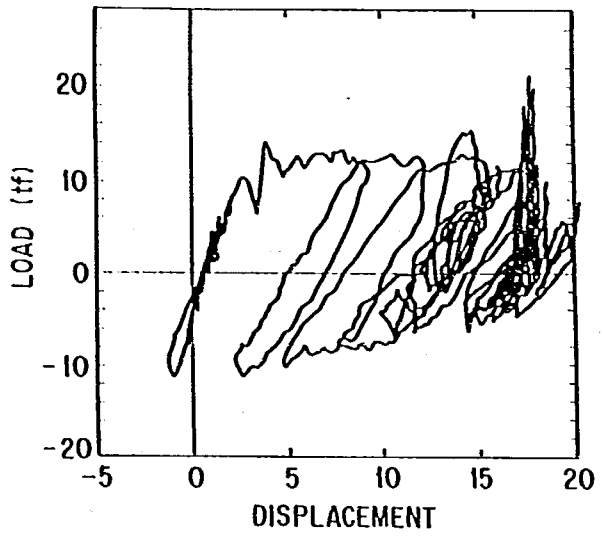


Fig.7 Hysteresis Loop of load-displacement relation obtained through Shaking Table Test

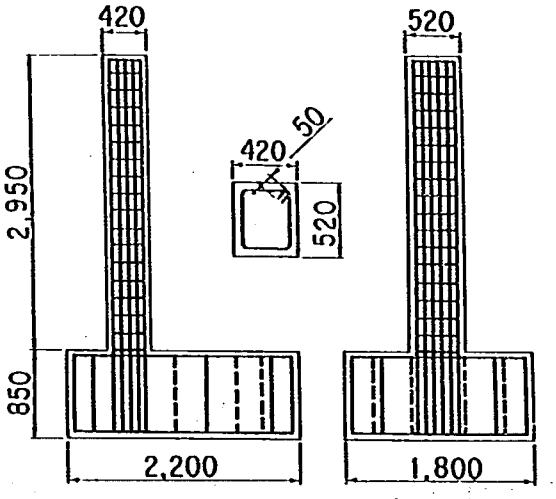


Fig.8 C-Shaped Bridge Pier Model for Dynamic Loading Tests

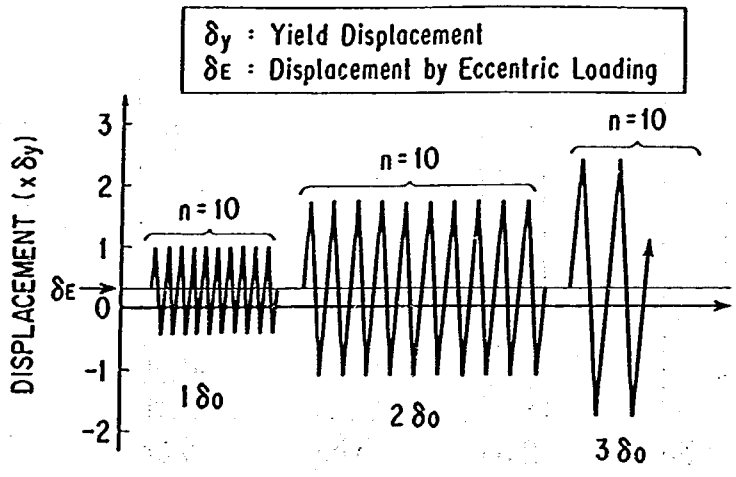


Fig.9 Loading Pattern of Displacement for Dynamic Loading Tests

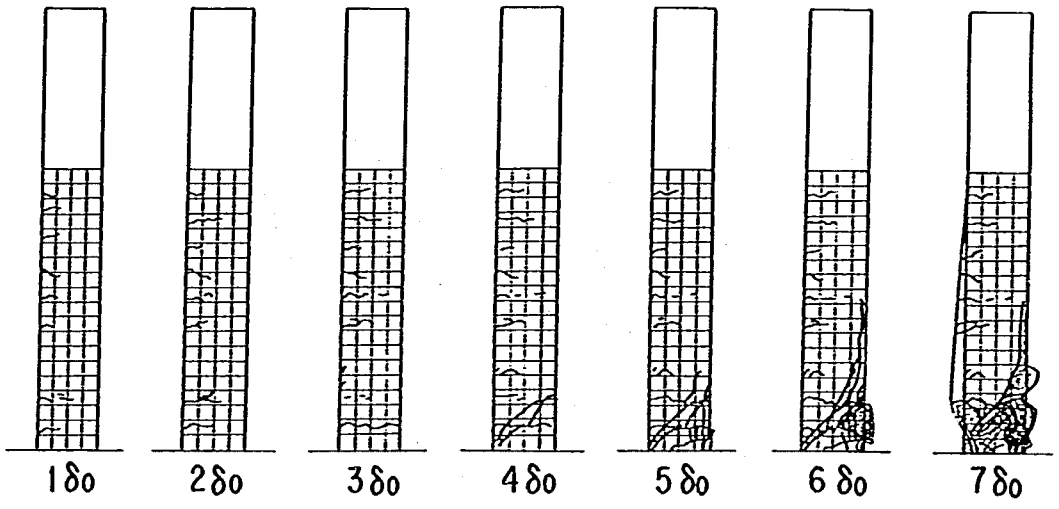


Fig.10 Failure Mode of P-62 (r_M = 0.55)

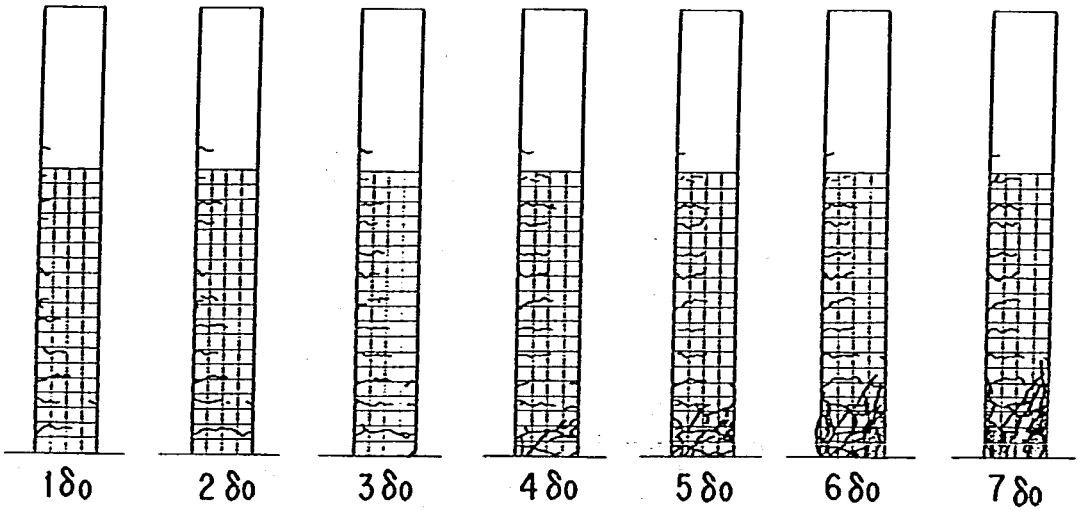


Fig.11 Failure Mode of P-60 (r_M = 0.69)

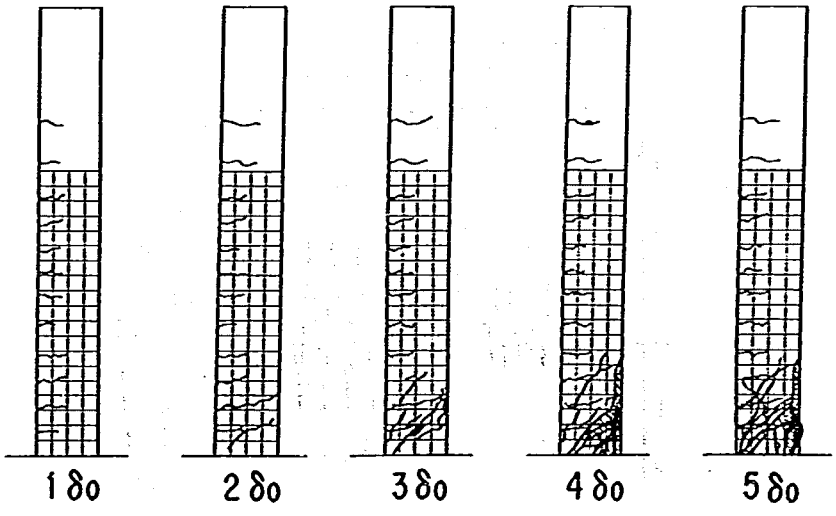


Fig.12 Failure Mode of P-64 (r_M = 0.51)

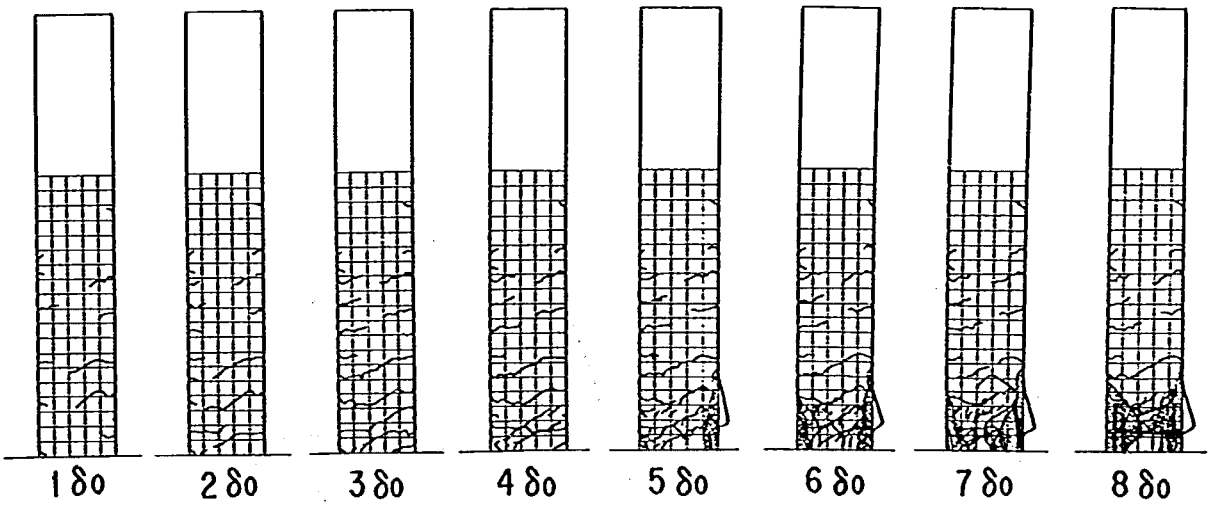


Fig.13 Failure Mode of P-65 (No Eccentric Loading, Longitudinal Loading)

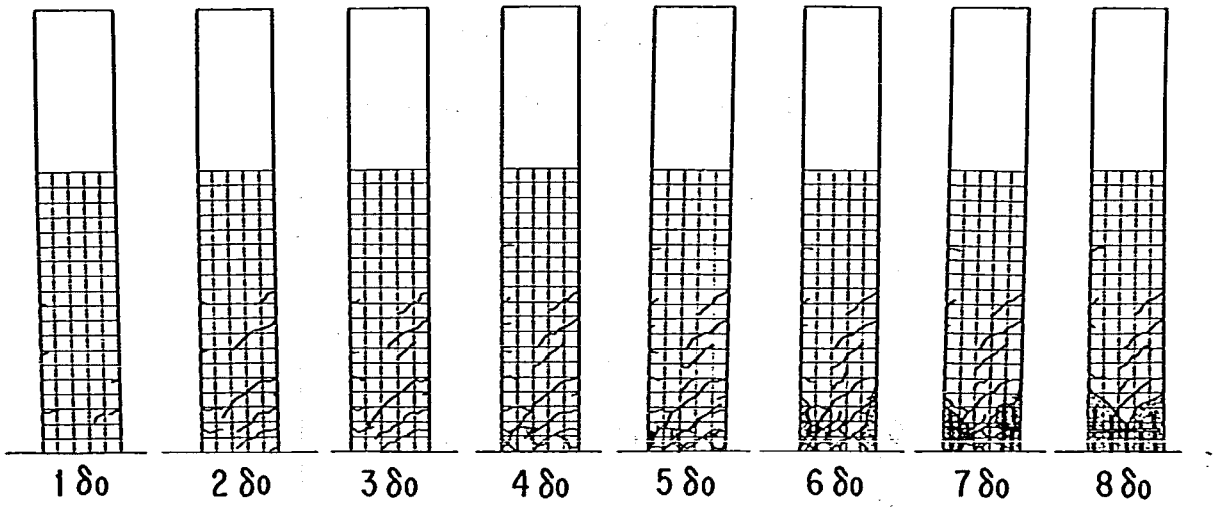


Fig.14 Failure Mode of P-65 (Longitudinal Loading)

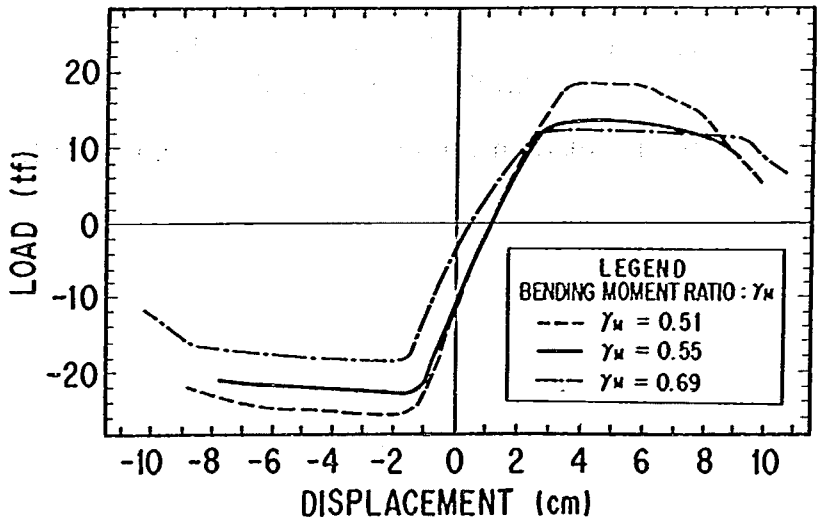


Fig.15 Effect of Bending Moment Ratio r_M on Load-Displacement Relation

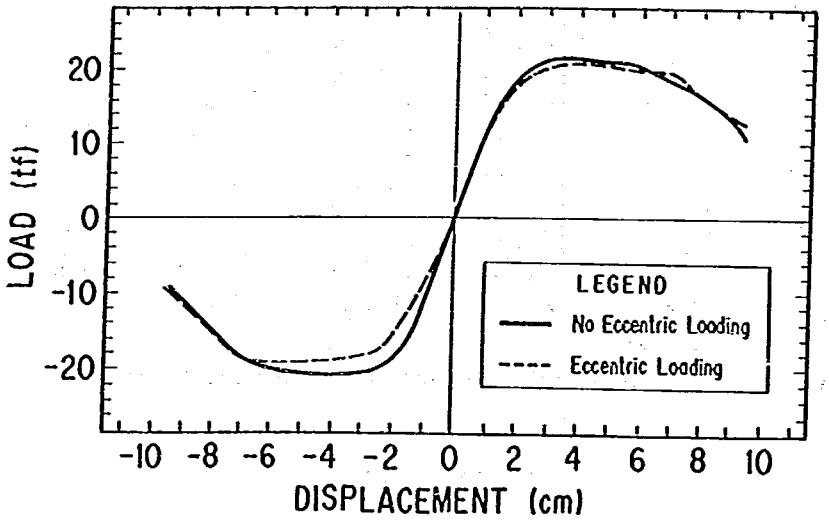


Fig.16 Effect of Loading Direction

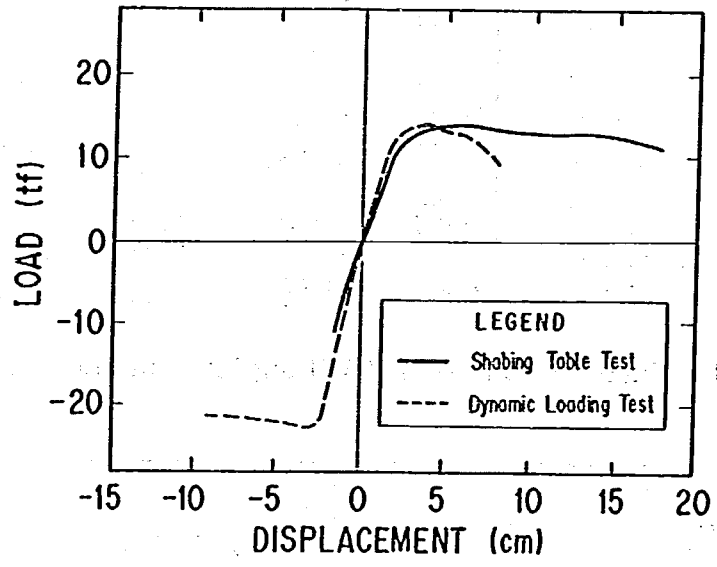


Fig.17 Comparison between Shaking Table Test and Loading Test

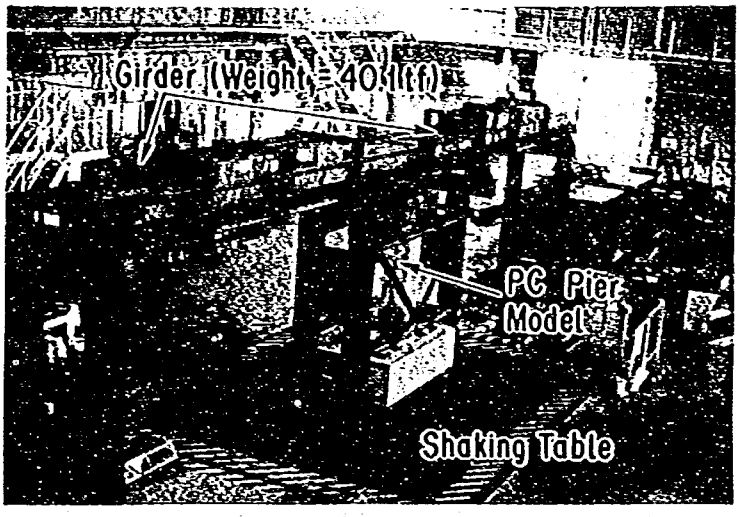


Photo 1 Set up of Shaking Table Test

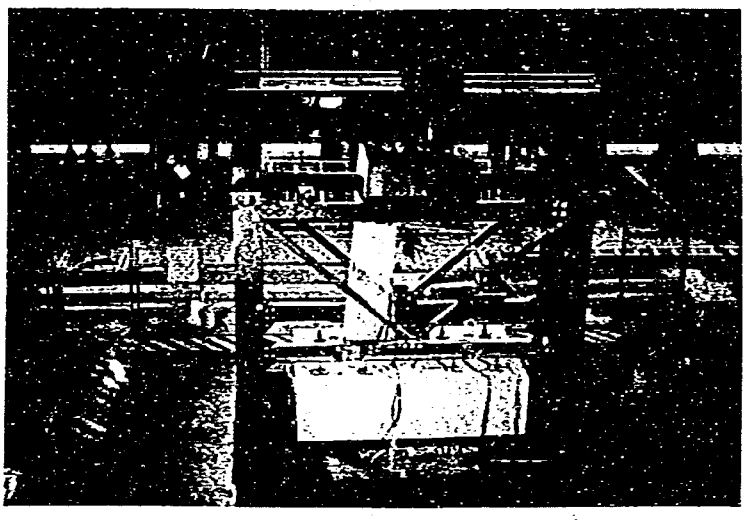


Photo 2 Residual Deformation of the Pier Model

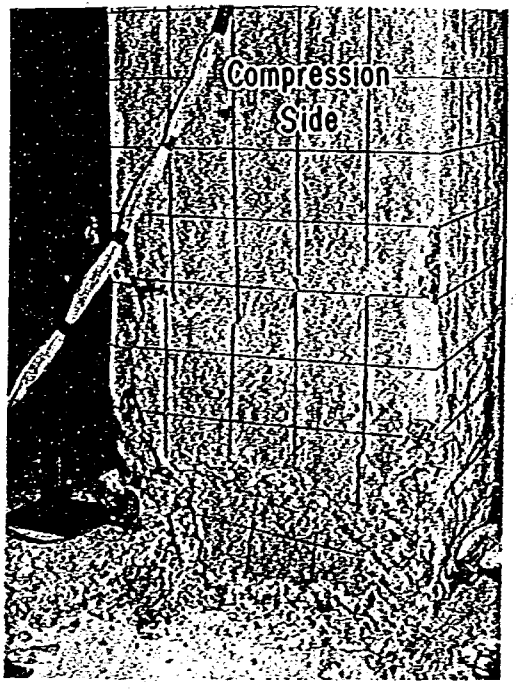


Photo 3 Failure Mode of the Pier Model

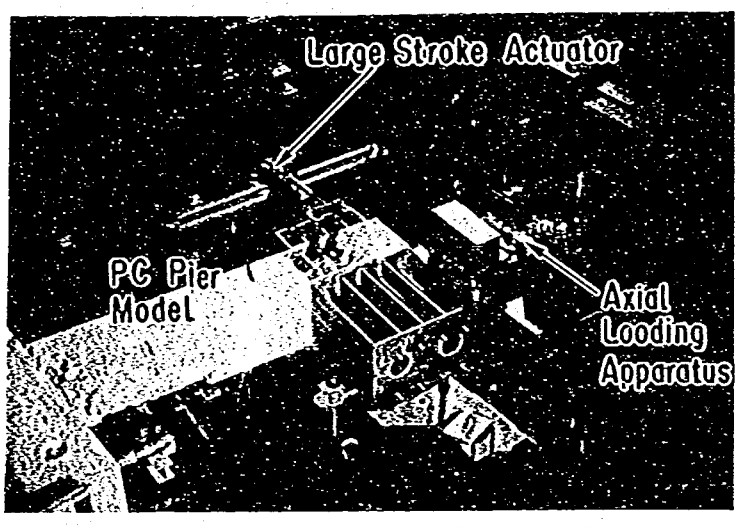


Photo 4 Set up of Dynamic Loading tests

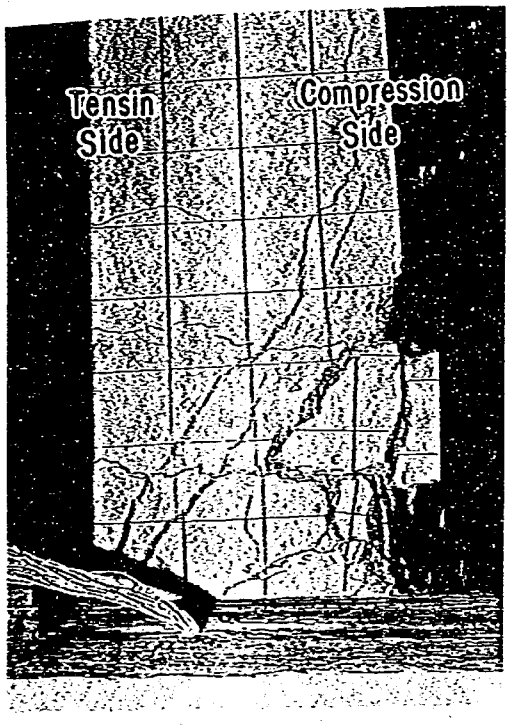


Photo 5 Failure Mode of the Pier Model

Comparison of the Seismic Design of Highway Bridges In California and In Japan

Mohsen SULTAN
and
Kazuhiko KAWASHIMA

9th U.S.–Japan Bridge Workshop
Tsukuba, Japan
May, 1993

COMPARISON OF THE SEISMIC DESIGN OF HIGHWAY BRIDGES IN CALIFORNIA AND IN JAPAN

By

Mohsen Sultan, P.E.
Senior Bridge Engineer
Division of Structures
California Dept. of Transportation
Sacramento, California, U.S.A

and

Kazuhiko Kawashima, D. Eng.
Head, Earthquake Engineering Division
Public Works Research Institute
Tsukuba Science City, Japan

1. INTRODUCTION

This paper presents preliminary results of a study on the comparative seismic design of highway bridges designed using both the California Department of Transportation (Caltrans) and Japanese seismic design specifications. Such comparison is aimed at providing a better understanding of the two seismic design methods and structural differences. The research project this paper is based on included two bridge design examples. A typical California highway bridge was designed using the Caltrans Bridge Design Specifications (BDS), and keeping the superstructure unchanged, it was redesigned using the Japanese specifications. Similarly, a typical Japanese bridge was first designed using the Japanese specifications, then was redesigned using the California method. Where appropriate, this paper highlights basic seismic design considerations and differences between the two design methods. In this paper, an emphasis on the Caltrans design details and seismic loading is provided.

2. GENERAL ASSUMPTIONS

Differences in the seismic design approach for highway bridges, between California and Japan, include the predominant structure type, the design method and seismic force levels. California bridges typically consist of a moment resisting frame system with monolithic joints connecting the superstructure to the substructure, whereas, in Japan, bearing type supports are typically used for those connections. Load factor (ultimate strength) design with force reduction, based on displacement or curvature ductility and risk factor, is the California approach. In Japan, the seismic force coefficient method based on allowable stresses is utilized. The ultimate capacity check of reinforced concrete piers or columns is performed using a ductility approach, where force levels of up to 1.0 g are applied to vertical support members.

In the process of redesigning the U.S. bridge using the Japanese method, the superstructure is kept unchanged, whereas, substructure components can be different, i.e. column or pier size, and their reinforcement, footings, number of piles, including size and capacity, and abutments are all permissible changes. The focus is to narrow the differences down to a minimum and concentrate on the seismic approach of both Japan and California. The maximum traditional design seismic force in both places is assumed, i.e. ground acceleration of 0.7 g in California, and force coefficient k = 0.3 in Japan.

3. BRIDGE DESCRIPTION

The California bridge as shown in Fig. 1, referred to in this paper as the U.S. bridge, is assumed to be a freeway connector having straight alignment and the following span configuration: 130 ft, 3 spans at 175 ft, 130 ft. It consists of a five span continuous, prestressed concrete box girder with single column bents. The girder is 7'-0" (2.13 m) deep and 42'-6" (12.95 m) wide as shown in Fig. 2.

Columns are fixed-fixed (top-bot) and are 65 feet long (to C.G.) supported on pile footings. Abutments are "seat type" supported on pile caps. As for foundations, driven piles with 100 ton service load capacity (Caltrans Class 100) for the bents and 70 ton capacity (Class 70) for the abutments were assumed, although the size in the equivalent Japanese bridge may differ. Only vertical piles are used, as battered piles are rare in Japan.

Soil type, as shown in Fig. 3, used in the design was based on soil conditions found in the vicinity of the Los Angeles area. It consists of a mixture of sand and silt slightly compact to dense with unit weight of 115-125 pcf. Standard penetration index ranges from 11 to 70. The internal friction angle is 25-35 degrees, cohesion is 0 - 1000 psf and the shear strength is 2.0 - 2.9 tsf. The predominant period of vibration of the ground is 0.35 second and the depth to rock like material is greater than 300 feet.

To increase the ultimate moment capacity of the box girder, the typical section is flared over a distance of 20 ft (6.10 m) to reach its maximum at the face of supports. This is done only at the bents not the abutments, since seat type abutments do not resist moments. Table 1 below shows the section properties at those locations. Fig. 4 shows the global axis designation.

Table 1- TYPICAL SECTION PROPERTIES

Location	Area (ft^2)	IZZ (ft^4)	IYY (ft^4)
At Supports	83.77	634.93	10086.61
Minimum Section	74.69	554.79	9449.00

Columns are round 8 feet in diameter, with the area A= 50.27 ft^2 and Izz=Iyy= 201.06 ft^4. Since column size is a permissible change in the redesign, the Japanese version utilizes a 9'- 2" by 19'- 7" (2.8X6 m) rectangular cross section with an area A= 180.74 ft^2 (16.8 m^2).

Table 2 lists dead load reactions. Trial (0) refers to the dead load portion present at time of prestressing, trial (1) refers to added dead load, such as overlay and barrier rail. These numbers do not include the bent cap portion that is not necessarily modeled in the static model. The Caltrans terminology utilizes the terms "column" and "bent" where the Japanese version refers to the same thing as "Pier". The term "Pier" has a specific definition according to Caltrans and therefore will only be used where appropriate.

Table 2- Dead Load Reactions* (Kips)

Loading	Abut 1	Bent 2	Bent 3	Bent 4	Bent 5	Abut 6
Trial (0) Top	566	2058	2138	2138	2058	566
Trial (0) Bot	-	2548	2629	2629	2548	-
Column Weight	-	490	490	490	490	-
Trial (1)	64	229	238	238	229	64

(*) Does not include additional dead load due to bent cap weight at the bents.

4. SEISMIC LOADING

In designing the column (Fig. 5), all load cases prescribed by the specifications are analyzed at all critical locations. The loading at the top of column did control the Caltrans design with the maximum longitudinal seismic load case being the controlling group (Grp. VII case 2). A summary of seismic load input is presented in Table 3.

Table 3- SEISMIC LOADING

(a) Top of Column

	ARS UNREDUCED FORCES	
	CASE 1	CASE 2
MY trans	116257	34877
MX Long	28339	94465
P Axial	104	347

P/S Moment = 3325 k-ft, P (DL)= 2589 k

(b) Bottom of Column

	ARS UNREDUCED FORCES	
	CASE 1	CASE 2
MY trans	61520	18456
MX Long	27423	91432
P Axial	104	347

P/S Moment = 4472 k-ft, P (DL)= 3079 k

Earthquake forces were reduced by the ductility and risk factor Z=5.30. Applied factored moments (reduced) and axial loads are summarized in Table 4.

Table 4- Applied Earthquake Loads

Grp	My	Mx	Comb M	P	Mu	Mu/M
VII-I	21935	8974	23700	2693	24603	1.04
VII-2	6581	21451	22437	2936	24942	1.11

Boundary conditions are essential to the modal behavior of the structure. In the Caltrans design for the subject bridge, all column connections are modeled as fixed top (to the

superstructure) and bottom (to the footings). Abutments possess transverse fixity which means they are restricted only in the transverse direction. However, soil stiffnesses in the longitudinal and transverse directions are used to model the embankment behind the abutment wall.

5. RESPONSE SPECTRUM ANALYSIS RESULTS

Generally, Caltrans utilizes a linear multi-modal dynamic analysis method in calculating maximum forces and displacements, where, an appropriate ARS curve is selected depending on the foundation conditions at the proposed site. The designer may choose the number of vibration modes to be utilized in combining modal maxima and thus computing maximum displacements and forces. The Caltrans analysis is based on the Complete Quadratic Combination (CQC) method as reported by the program "SEISAB". The U.S. bridge dynamic results are concluded from 15 modes of vibration. The Japanese bridge results are reported as 15 modes in the longitudinal direction and 15 modes in the transverse direction. Table 5 summarizes the modal response of the U.S. bridge.

Table 5- Bridge Modal Response (Caltrans Method)

MODE	PERIOD (sec)	SPECTRAL VALUE (g)	DIRECTION
1	1.344	0.84	Transverse
2	1.014	0.93	Longitudinal
3	0.737	1.01	N.P.
4	0.547	1.08	Vertical
5	0.463	1.08	Longitudinal
6	0.400	1.07	Transverse
7	0.382	1.06	Vertical
8	0.301	1.01	Longitudinal
9	0.296	1.01	Vertical
10	0.247	0.96	N.P.
11	0.167	0.88	Longitudinal
12	0.166	0.88	Transverse
13	0.166	0.88	Vertical
14	0.151	0.86	Vertical
15	0.137	0.85	Longitudinal

Table 6 lists the maximum displacements (in feet) at various locations of the structure using the Caltrans method. Design displacements are derived from this list and combined in accordance with the loading combination criteria.

Table 6- DISPLACEMENTS (CALTRANS METHOD)

Direction	Abut 1	Bent 2	Bent 3	Bent 4	Bent 5	Abut 6
Max Lng	0.791	0.788	0.786	0.786	0.788	0.791
Max Tra.	0.019	0.811	1.521	1.521	0.811	0.019

Table 7 shows the natural period and mass participation factors of the Japanese design.

Table 7- BRIDGE MODAL RESPONSE (JAPAN METHOD)

A- LONGITUDINAL DIRECTION

MODE	PERIOD (sec)	Ratio of Mass Participation
1	0.685	76.14
2	0.452	0.00
3	0.424	0.20
4	0.396	0.00
5	0.300	0.00
6	0.298	2.21
7	0.178	0.00
8	0.127	0.45
9	0.123	0.00
10	0.113	9.70
11	0.108	0.00
12	0.079	0.03
13	0.056	0.00
14	0.044	0.01
15	0.040	0.00

B-TRANSVERSE DIRECTION

MODE	PERIOD (sec)	Ratio of Mass Participation
1	0.661	64.25
2	0.539	0.00
3	0.370	7.54
4	0.254	0.00
5	0.173	3.73
6	0.140	0.00
7	0.121	2.18
8	0.108	0.00
9	0.097	2.14
10	0.080	7.37
11	0.080	0.00
12	0.069	0.00
13	0.066	1.85
14	0.059	0.00
15	0.059	1.78

Design of the footings by the Caltrans method was controlled by the probable plastic moment (Mp), when applied at 45 degrees angle to the footing. The maximum pile compressive load is 335 kips (max allowable 400 k)and maximum uplift force is -163 kips (max allowable -200 k). For pile layout see Fig. 6.

Table (8) below summarizes the resultant design

Table 8- COLUMN DESIGN COMPARISON

DESCRIPTION	CALTRANS METHOD	JAPAN METHOD
COLUMN SIZE	8'-0" Φ	2.8X6.0 m (Rectangular)
COL GROSS AREA	50.27 sq. ft (4.67 sq. m)	16.8 sq. m (180.74 sq. ft)
COLUMN REINFORCEMENT	#14 total 44 A_S= 99 in² (1.368 %) #6 Spiral @ 4 1/4 " (0.45 %)	
FOOTING DEPTH	4'-3" (1300 mm)	2200mm minimum
FOOTING SIZE	21'X21' (6400mmX6400mm)	9000mmX9000mm
FOOTING REINFORCEMENT	Top #6 total 52 (both ways) Bottom #10 total 65 Transverse #10 total 48 Longitudinal	
PILES	40 -15" Diam. Piles/Length (60') 100 Ton Capacity	28 Piles Φ 600X18.3 m

The abutment footing required a total of 24, 15 inch diameter, piles with 70 ton capacity (Class 70) using the Caltrans method (Fig. 8). By comparison, it required 8, 600 mm diameter, piles using the Japan method. Under the California method, abutments are designed such that no earthquake loads can be transferred into their foundation. Therefore, abutment footings and piles are not designed to withstand seismic forces .

6. CONCLUSION

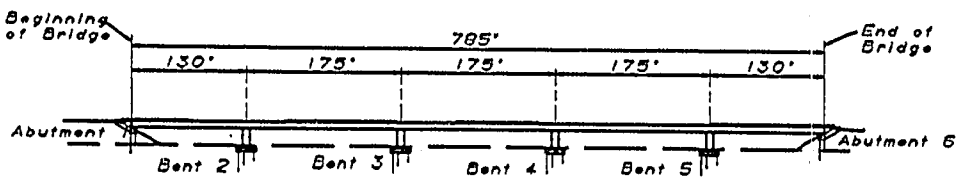
Design data for an example bridge were presented along with factors affecting the final design. One of the most obvious results of the comparison is the size of substructure components (columns), size of foundations (footings), and the natural period of the structure. In this example, the Japanese bridge uses a rectangular pier three times larger than the Caltrans round column. The Japanese footing area and depth are approximately 75 % larger than the Caltrans footing. Length of piles used with both approaches is very similar. Finally, primarily due to the larger substructure, the Japanese bridge has about half the natural period of its Caltrans equivalent, and as such, is twice as stiff.

7. ACKNOWLEDGMENT

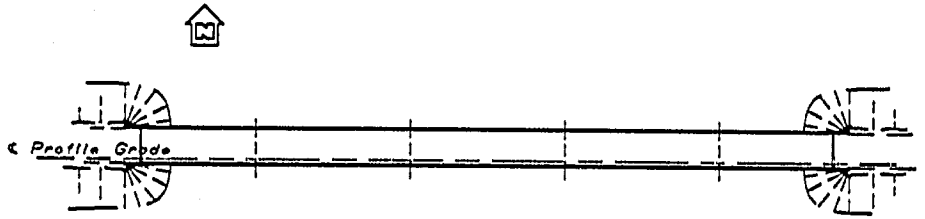
The authors wish to acknowledge the Japan Science and Technology Agency (STA), the U.S. National Science Foundation (NSF), the Public Works Research Institute (PWRI) in Tsukuba, Japan, and the California Department of Transportation for their support and cooperation with the authors and who made their collaboration possible.

8. REFERENCES

1. Kawashima, K. and Hasegawa, K., "Evaluation of Lateral Inertia Force of Bridges for Seismic Design", Seventh US-Japan Bridge Workshop, Tsukuba Science City, Japan. May 8 and 9, 1991.
2. Iwasaki, T., Kawashima, K. and Hasegawa, K., "New Seismic Design Specifications for Road Bridges in Japan.", 22nd Joint Meeting, US-Japan Panel on Wind and Seismic Effects, U.J.N.R, Gaithersburg, Maryland, May 1990.
3. "Standard Specifications for Highway Bridges", Thirteenth Edition, 1983, by the American Association of State Highway and Transportation Officials, Inc. (AASHTO) with Revisions by Caltrans through June 1990.
4. "Abutment Investigation", Bridge Design Aids by Caltrans, January 1988.
5. "Dynamic Model Assumptions and Adjustments", Bridge Design Aids by Caltrans, October 1989.
6. Sultan, M. "Countermeasures at Caltrans following the Loma Prieta Earthquake", Proceedings of the Nineteenth Japan Road Conference, Japan Road Association, Tokyo, Japan, October 1991.



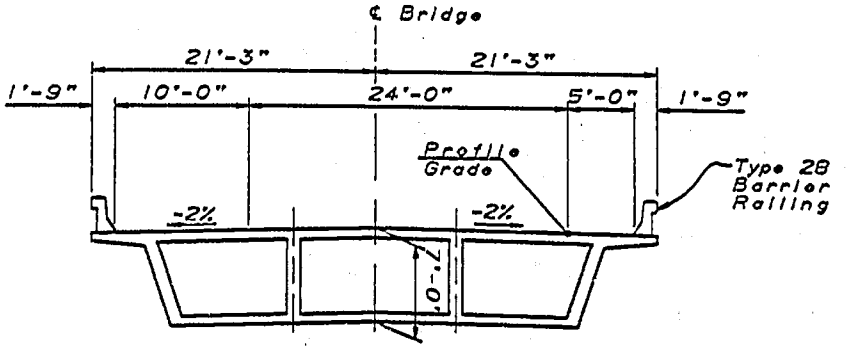
ELEVATION

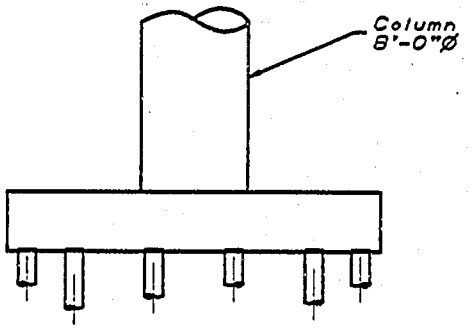


PLAN

GENERAL PLAN - CALTRANS METHOD

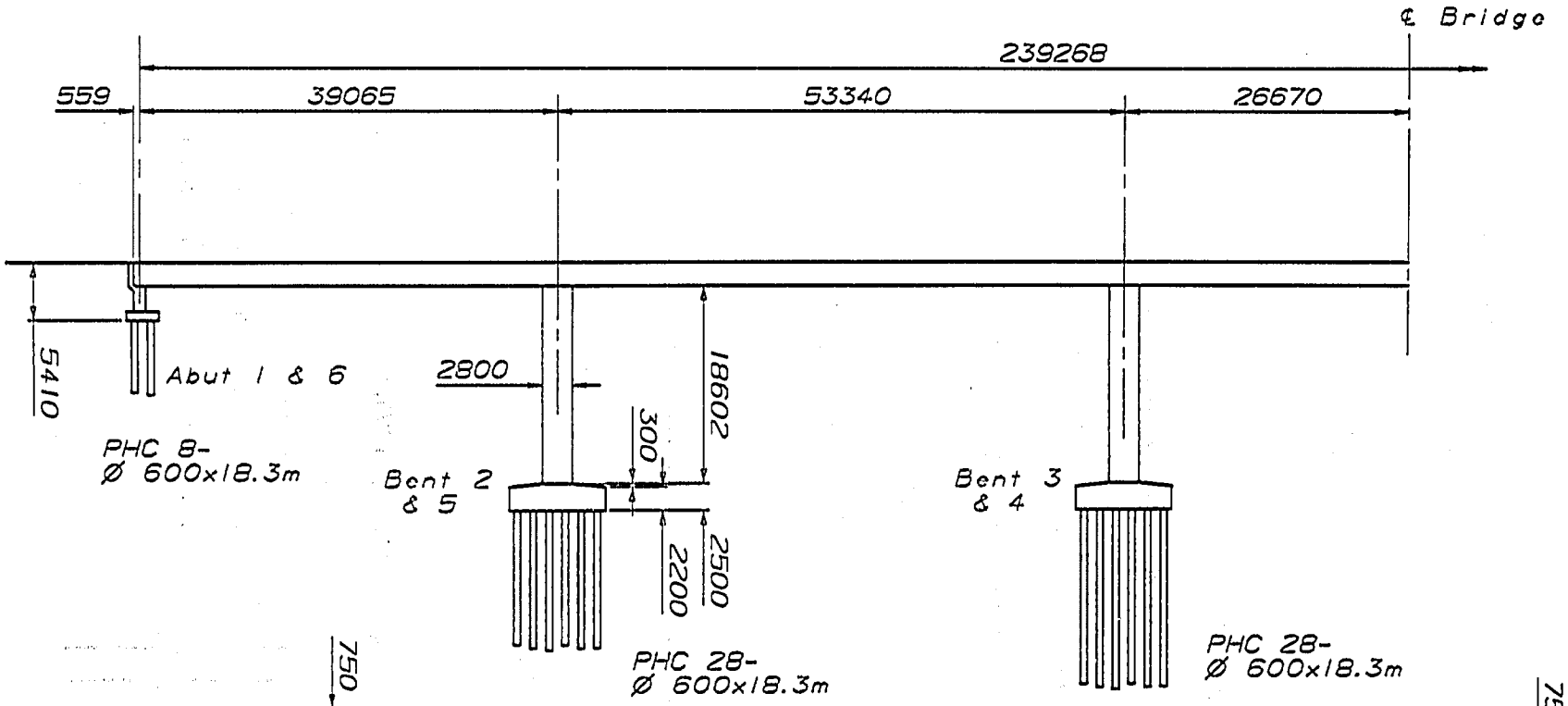
Fig 1 (a)



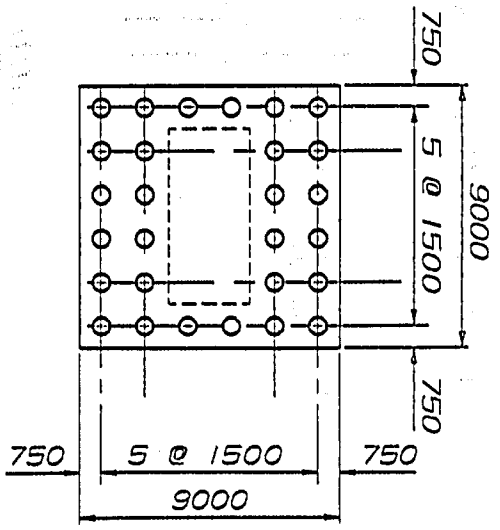


TYPICAL SECTION - CALTRANS METHOD

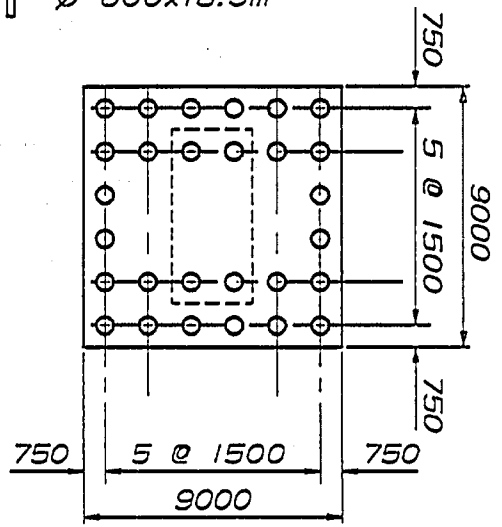
Fig 2



ELEVATION
NO SCALE

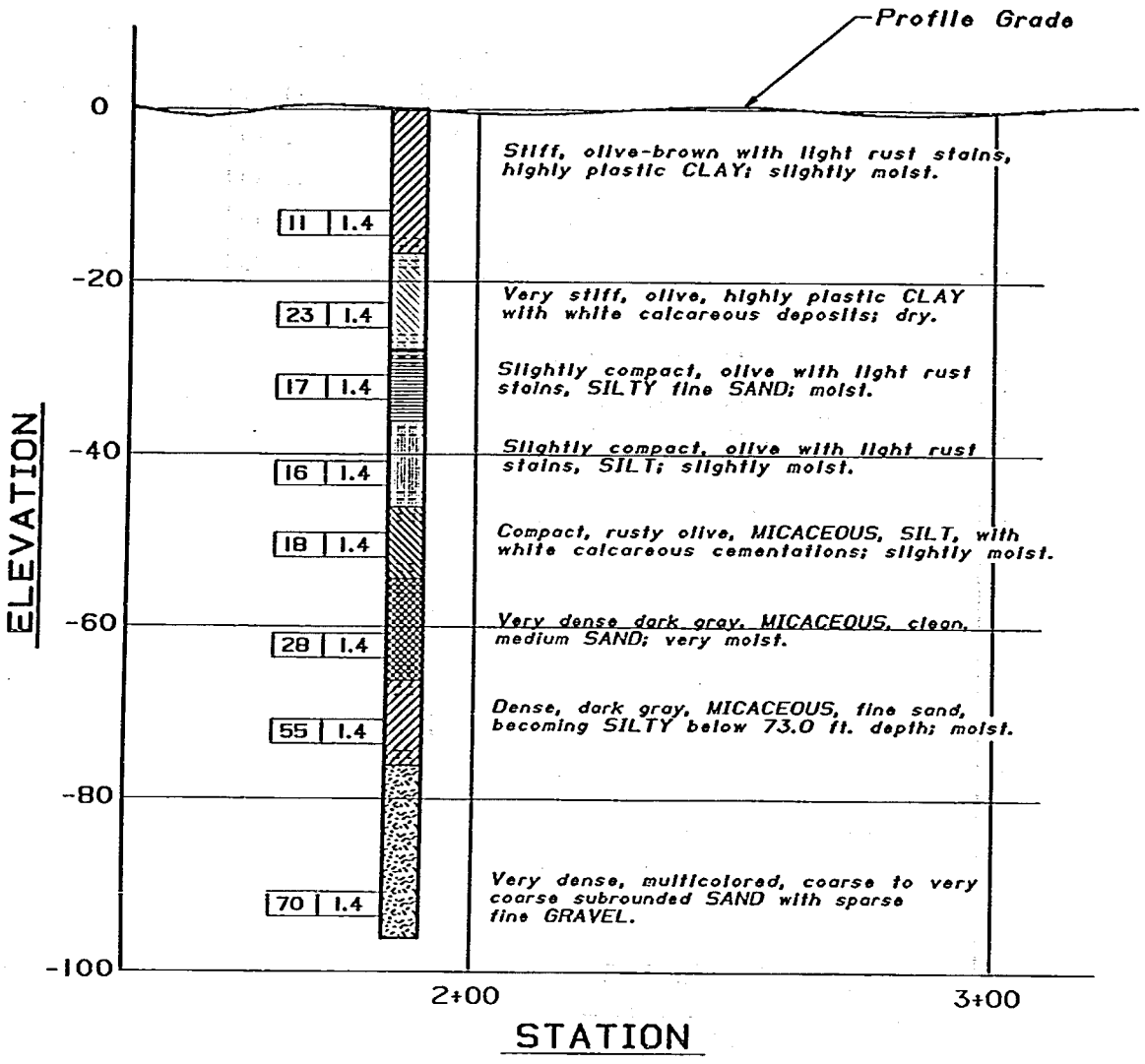


(BENT 2 & 5)
PILE LAYOUT
NO SCALE

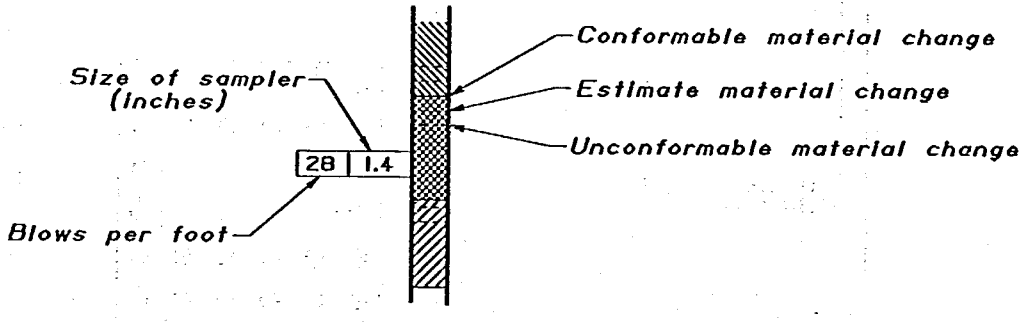


(BENT 2 & 5)
PILE LAYOUT
NO SCALE

GENERAL PLAN - JAPAN METHOD
Fig 1 (b)

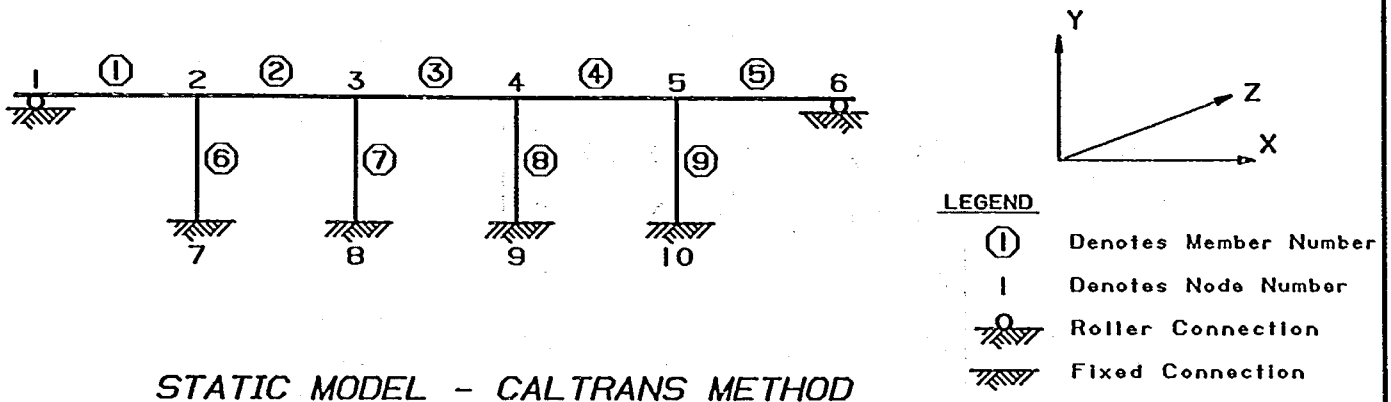


LEGEND OF BORING OPERATIONS



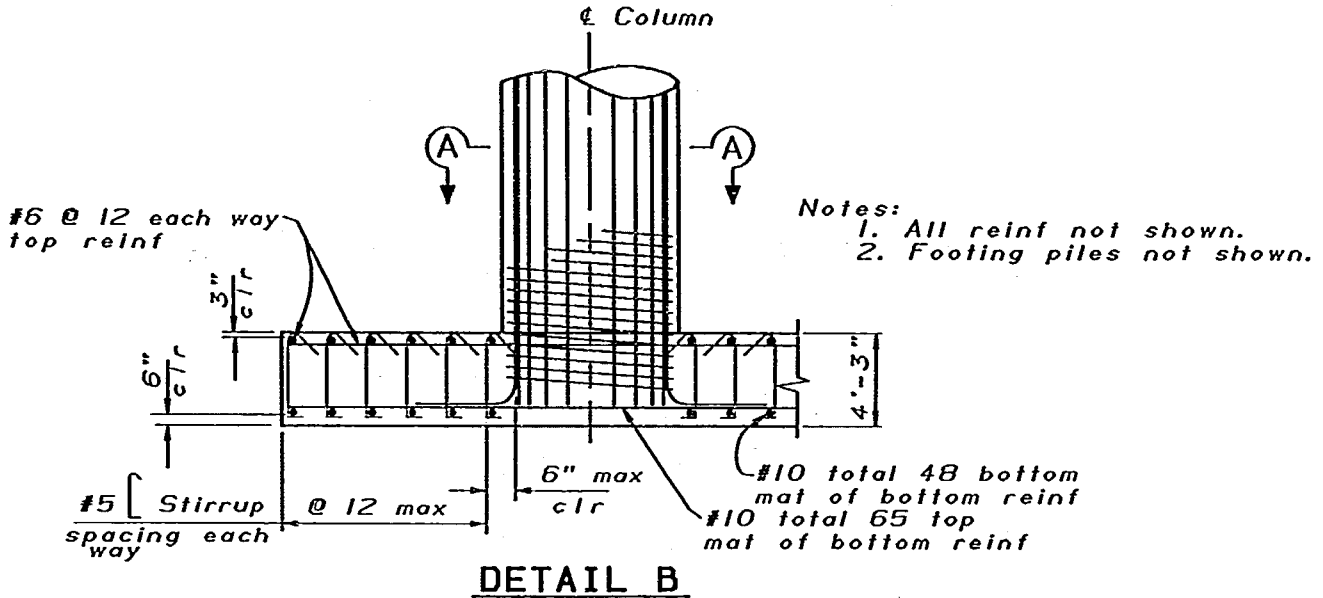
SOIL PROFILE

Fig 3

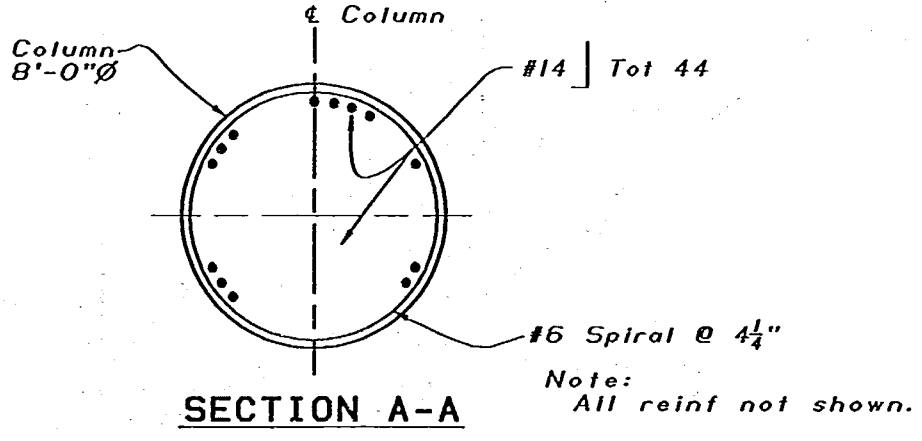


STATIC MODEL - CALTRANS METHOD

Fig 4



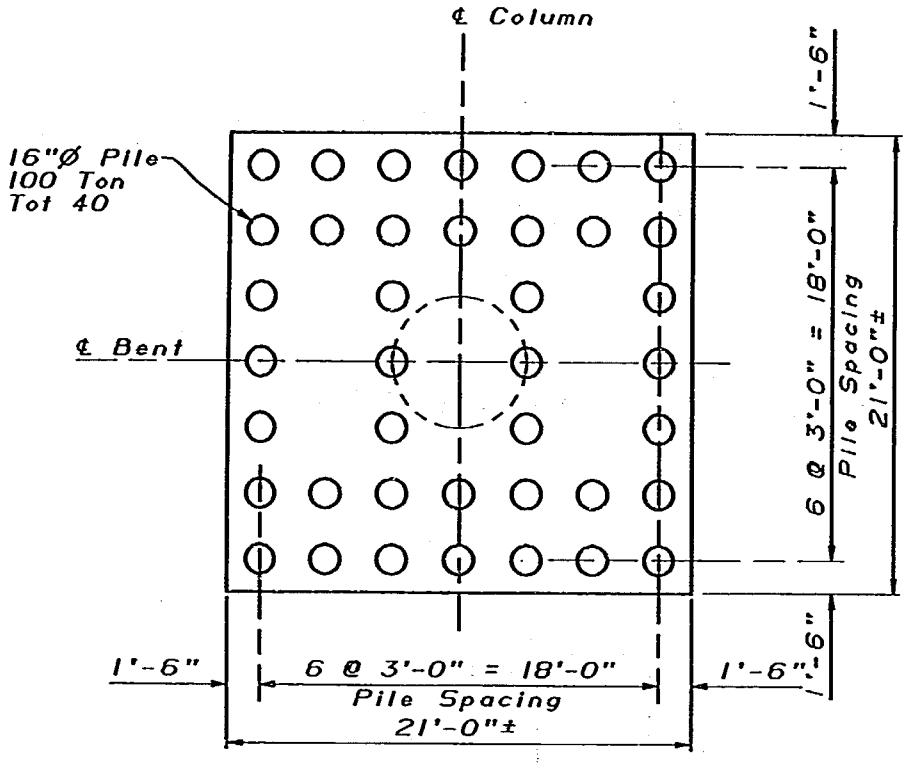
DETAIL B



SECTION A-A

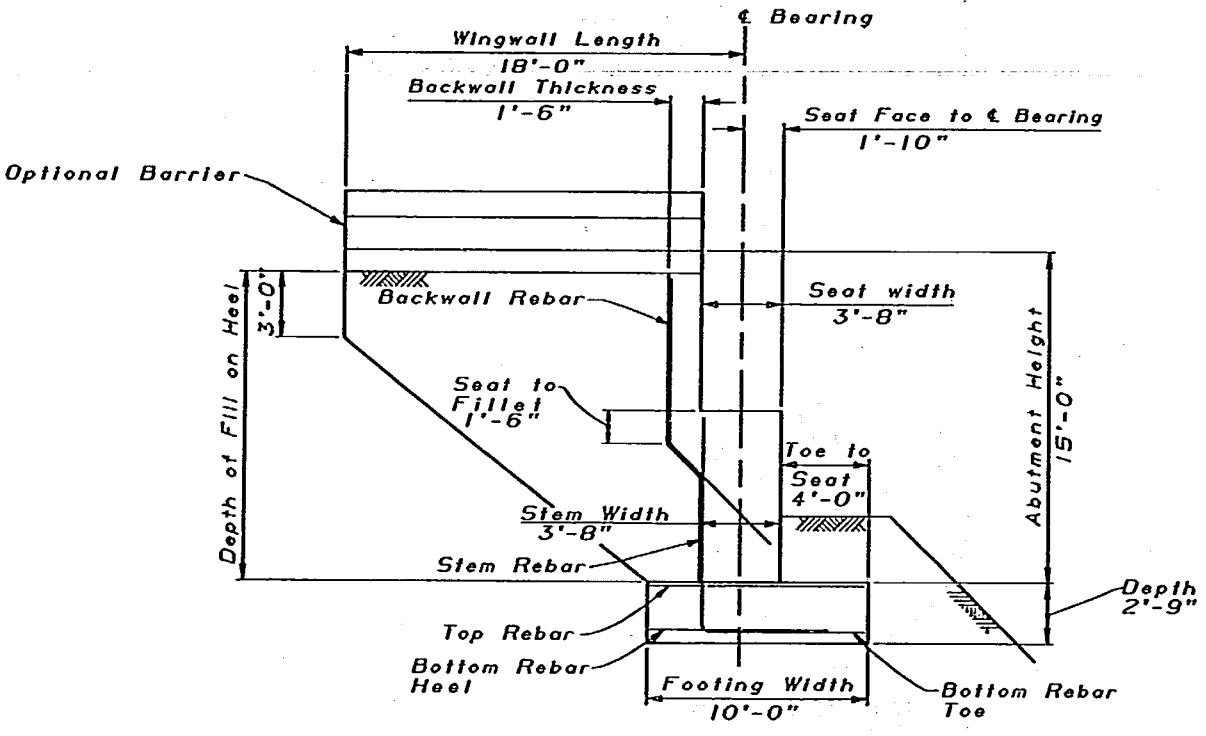
COLUMN & FOOTING DETAILS - CALTRANS METHOD

Fig 5



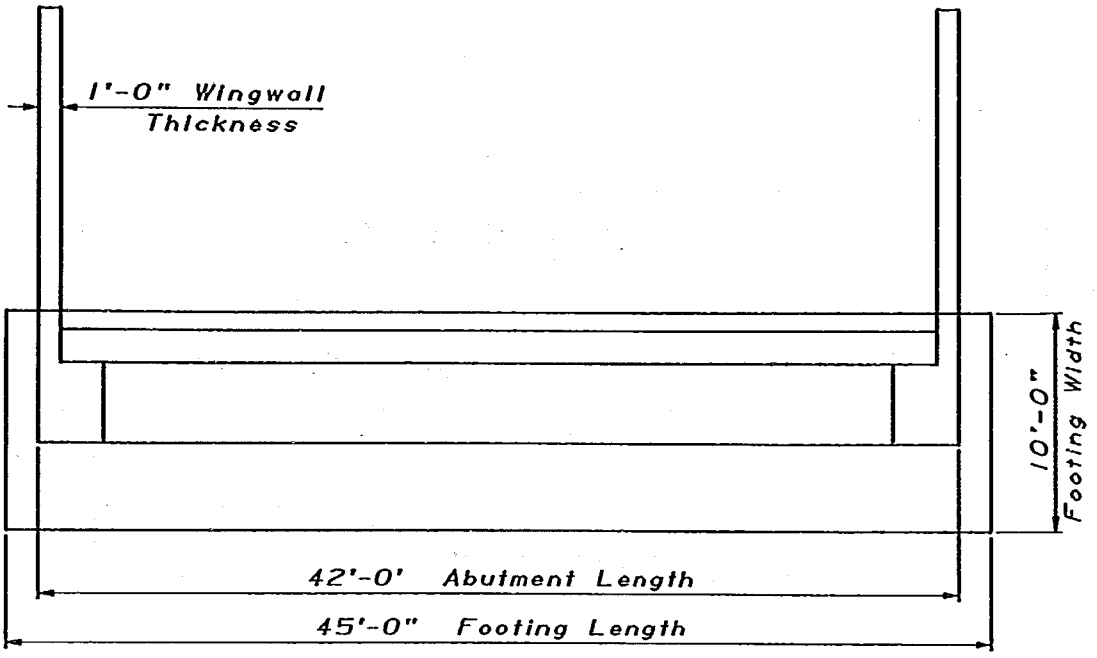
FOOTING PLAN & PILE LAYOUT - CALTRANS METHOD

Fig 6



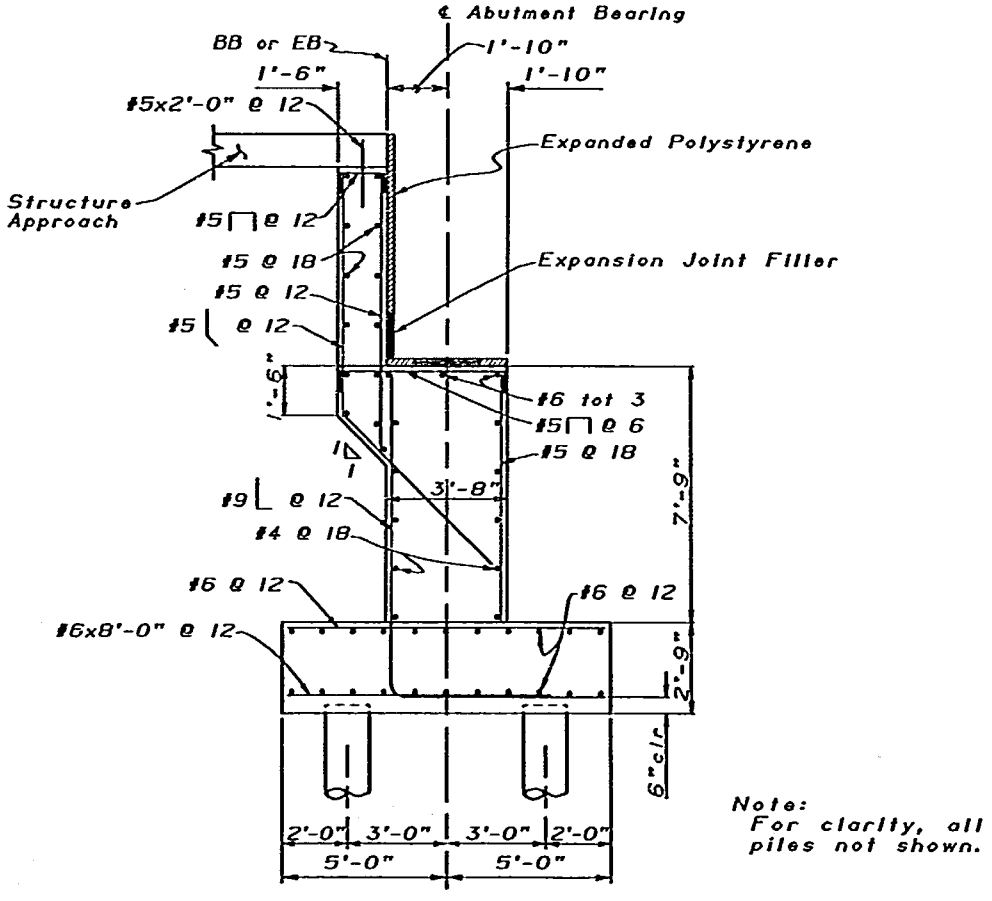
ABUTMENT ELEVATION - CALTRANS METHOD

Fig 7 (a)



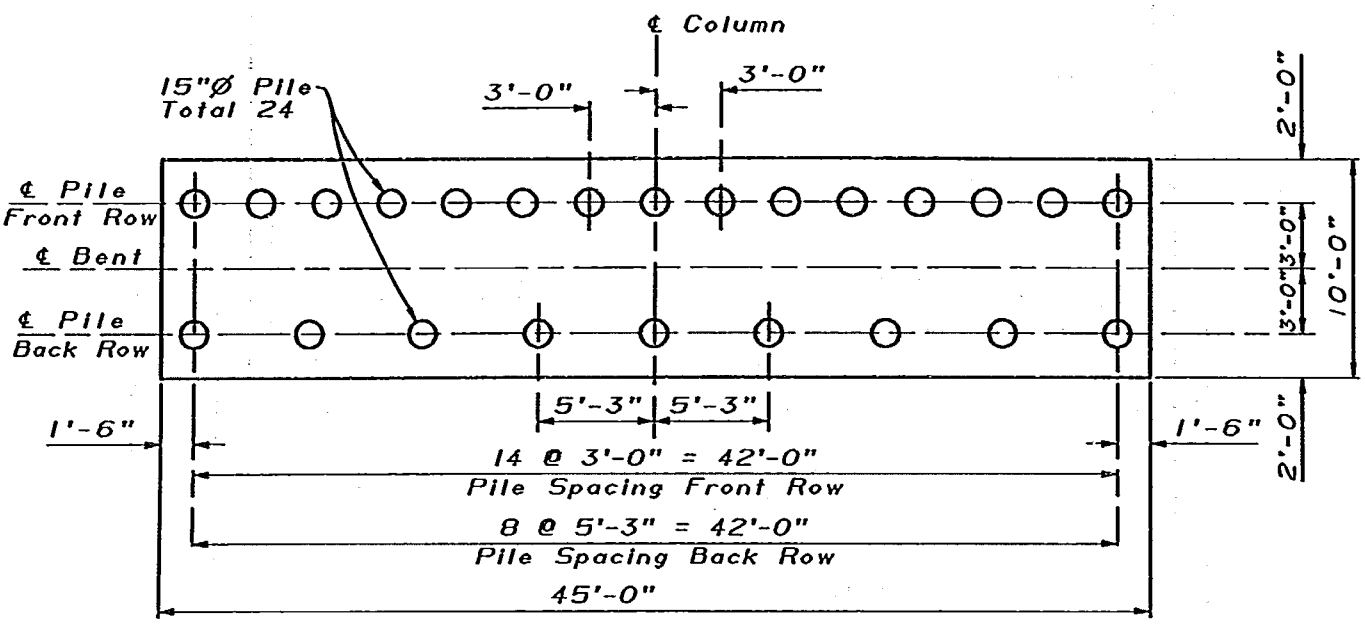
ABUTMENT PLAN - CALTRANS METHOD

Fig 7 (b)



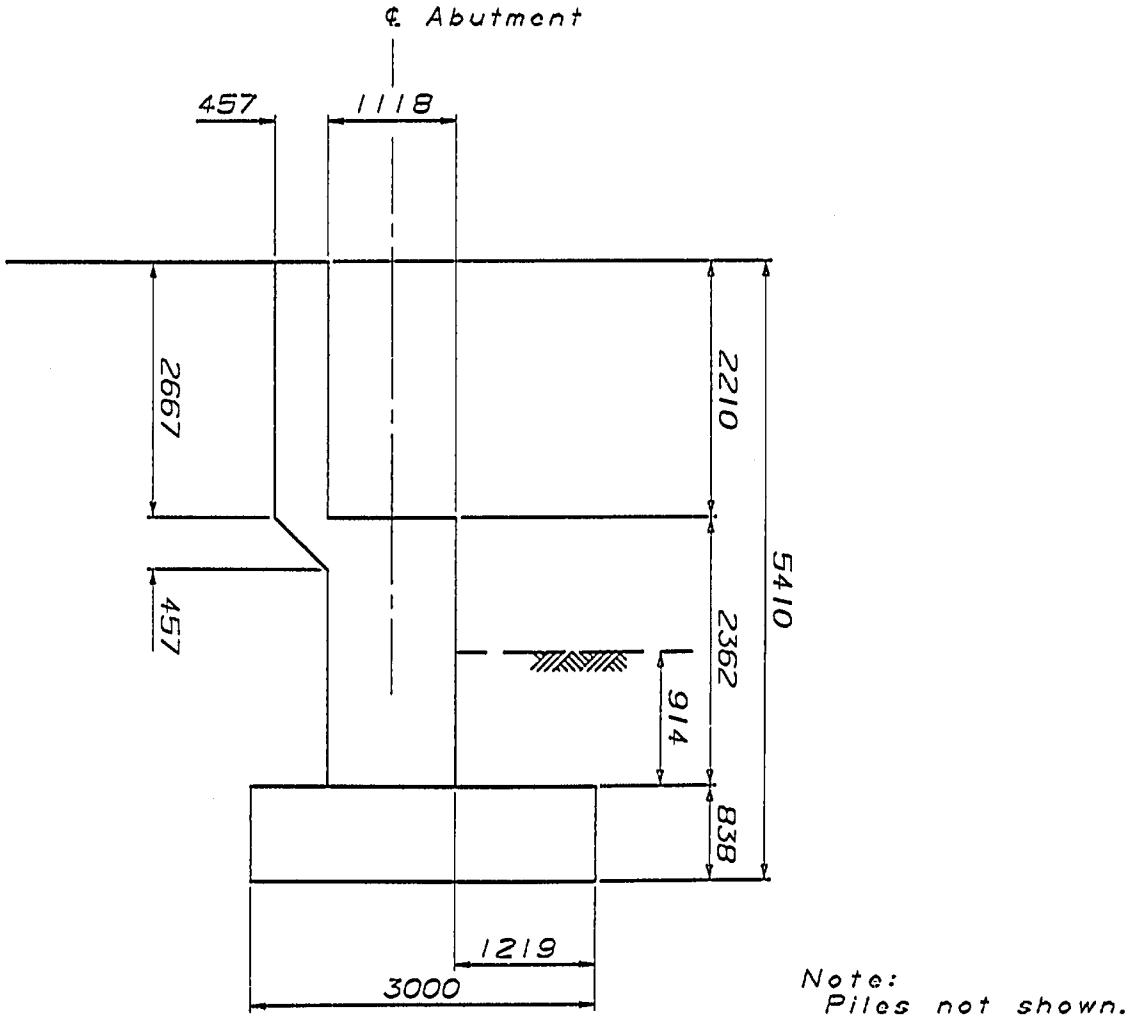
ABUTMENT SECTION - CALTRANS METHOD

Fig 7 (c)



ABUTMENT PILE LAYOUT - CALTRANS METHOD

Fig 8



ABUTMENT DETAIL - JAPAN METHOD

Fig 9

Guidelines for Disaster Information Systems for Important Infra-Structures

Kazuhiko KAWASHIMA
Ken-ichi TOKIDA
Hideki SUGITA
Tomoru NAKAJIMA
and
Hideo MATSUMOTO

25th Joint Meeting of The U.S.-Japan
Cooperative Program In
Natural Resources Panel on
Wind and Seismic Effects
Tsukuba, Japan
May, 1993

GUIDELINES FOR DISASTER INFORMATION SYSTEMS FOR IMPORTANT INFRA-STRUCTURES

By Kazuhiko KAWASHIMA*, Kenichi TOKIDA**, Hideki SUGITA***, Tomoru NAKAJIMA***
and Hideo MATSUMOTO****

ABSTRACT

This paper outlines the "Guidelines for Disaster Information Systems for Infra-structures". This is a part of the "Guidelines for Disaster Information Systems" which was compiled in March 1992 as a final accomplishments of a comprehensive five year research project on Development of Disaster Information Systems. Description is given to proposed seismic damage information systems for the Ministry of Construction. Emphasis is placed on the Damage inspection with use of video cameras from helicopters and visual information systems for seismic zonation of ground hazard.

KEYWORDS: Disaster, Information, Earthquake, Damage Inspection, Ground Hazard

1. INTRODUCTION

When a destructive earthquake occurs, it is of significant importance to immediately collect accurate information on the extent of damage in the area affected by the earthquake. Road transportation is likely to be interrupted in urban area such as Tokyo as a direct result of damage of not only transportation facilities but buildings and lifeline facilities along roads. Confusion caused by people in evacuation and automobiles left on roads are anticipated, and they would also cause considerable disruption of transportation. It is required therefore to develop a new information collecting and processing systems which enable the extent of damage to be recognized immediately after an earthquake for formulating the repair and restoration strategy promptly.

A comprehensive 5 year research program entitled "Development of Information Collecting and Processing Systems for Disaster Mitigation" was initiated in 1987 by the Ministry of Construction. Public Works Research Institute, Building Research Institute and Geographical Survey Research Institute are involved in the research. The objectives of this research project were to develop new information collecting and processing systems, using advanced new technologies, for various disasters such as earthquakes, floods and debris flows. As shown in Fig.1, key items of the research development were :

a) bird's eye information collecting systems from helicopters,
b) on-line information processing systems, and
c) real-time digital mapping systems.

For this purpose, measuring and assessing technology of damage degree of structures using moving picture information detected from helicopters and new media oriented high-grade disaster prediction methods as well as planning systems for repair and restoration in damaged areas was developed. To avoid distortion of information during transferring from regional offices to headquarters, it was aimed to adopt visual motion picture systems.

This paper presents the outline of "Guidelines for Disaster Information Systems for Infra-structures", which is a part of the "Guidelines for Disaster Information Systems".

2. SCOPES AND CONTENTS OF THE GUIDELINES

The Guidelines is of five parts as :

Part I General Remarks and Proposals
Part II DEvelopment of Principal Technology for Disaster Information Systems
Part III Damage Information Systems for Important Infra-structures
Part IV Damage Information Systems for Urban Disaster

In Part I, summary of the 5 year project is presented with the background and needs of the project. Details of the program is presented in Parts II, III and IV. In Part II, various new and advanced technology for disaster information systems are presented. They include utilization of GPS positioning system, thermal image sensors, aero photo and video image camera. In Part IV, governments is presented. Data base required for disaster information systems, real time simulation of fire spreading and evacuation systems are included. GSI, PWRI and BRI are in charge of making Part II, III and IV, respectively.

In the Part III, which will be briefly introduced in this paper, the following issues are described :

---

* Head, Earthquake Engineering Division, Public Works Research Institute
** Director, Kanazawa Construction Office
*** Research Engineer, Earthquake Engineering Division, Public Works Research Institute
**** Hiigawa and Kandogawa Construction Office, Ministry of Construction

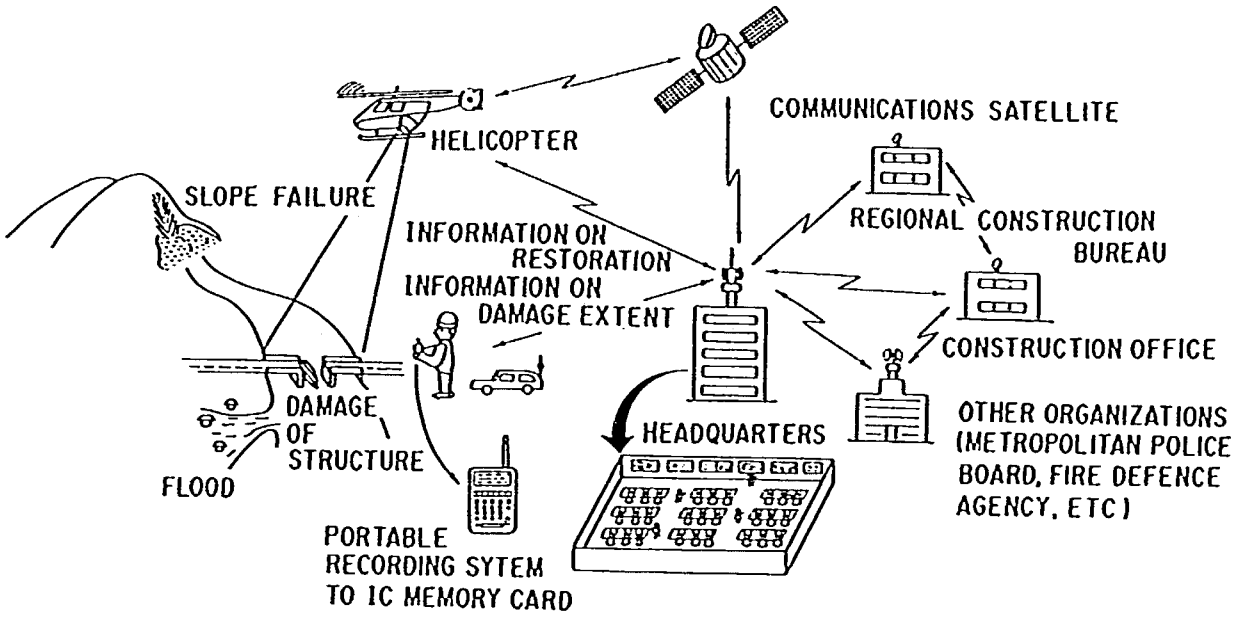


Fig. 1 Disaster Information Systems for Important Infra-structures

1 Common Part
- 1.1 General
- 1.2 Information Required during Disasters
- 1.3 Information Collecting and Processing before an earthquake
- 1.4 Damage Information System with use of Electric Still Cameras and Electric Handy Recorders
- 1.5 Outline of Damage Information Systems Common System Required for Various Disasters
- 1.6 Application to Normal Work
- 1.7 Organization Required for Application of Damage Information Systems

2 Damage Information Systems for Earthquakes
- 2.1 Damage Information Collecting Systems
- 2.2 Damage Information Transferring Systems
- 2.3 Damage Information Processing Systems

3 Damage Information Systems for Ground Failure during Earthquakes
- 3.1 Estimation of Ground Movement
- 3.2 Damage Inspection of Embedded Underground Structures
- 3.3 Damage Inspection of Road Facilities
- 3.4 Information Processing System for Ground Hazard

4 Damage Information Systems for Flooding
- 4.1 Damage Information Collecting Systems
- 4.2 Damage Information Processing Systems
- 4.3 Damage Information Transferring Systems

5 Damage Information System for Land Slide
- 5.1 General
- 5.2 Damage Information Collecting Systems
- 5.3 Damage Information Processing Systems Required for Restoration
- 5.4 Damage Information Processing Systems Required for Management of Construction Materials, Driftwood and Sand

3. PROBLEMS OF CURRENT DAMAGE INFORMATION COLLECTING SYSTEMS AND BASIC REQUIREMENTS FOR DEVELOPING NEW SYSTEMS

Although there were not destructive earthquakes which seriously hitted urban area in the last 40 years in Japan, it has been repeatedly pointed out from the experience of seismic damage in local areas that information collection and dissemination are the most important but difficult issue for central and regional governments in charge of control of public facilities[2)3)]. This was also pointed out at the Loma Prieta, U.S.A., Earthquake in October 1989[4)5)]. From the past experiences, various obstacles for collecting damage information are anticipated[2)3)]. The most important one is unexpectedly long time required for collecting damage information due to interruption of roads and damage of information transferring media such as telephone. Even if telephone could survive an earthquake, disruption of communication repeatedly happened due to concentration of call to a specific region.

Inadequate accuracy of the collected information is the second problem. Unconfirmed and sometimes uncorrect information were sent. Only a part of total information arrived. It is difficult to know the accuracy and correctness. Sometimes the same information arrived through different routes, and they were misunderstood as different information. Confirmation of source of information is very important. When a series of

events occurred, information on subsequent event sometimes arrived earlier than the information of the preceding event. There are examples that this caused significant misunderstanding on what were going on the events and the repair.

Because most of information is transferred by a voice and letters, correct evaluation on the information is difficult. Distortion of information always occurs. Therefore it is required to send information in a form of visible information. Still picture and moving picture information are quite effective.

Basic requirements for solving the problems of the current damage information collecting systems are:

(1)Prompt Information Collection

Collection of damage information in wide areas has to be made at not only day time but night time. Because accuracy of the damage information required changes in accordance with time following an earthquake, it is important to be able to collect damage information with reasonable accuracy depending on the time after an earthquake. Visible information through video cameras is quite important.

(2)Delivery of Updated and Same Information for All Bodies Involved in Repair and Restoration

Although quality of the information required depends on the task of individuals involved in repair and restoration, it is essentially important that the same and updated damage information is able to be delivered for all individuals from site engineers to decision makers. The real-time damage information has to be displayed in the form of not only letters but moving pictures. Because it is important for site engineers involved in inspection and emergency treatment to know real-time progress of damage and repair even in other area for which they are not in charge of, the systems should have capability to display the damage information of not only inside but outside of the controlled area.

(3)Data Processing Systems for Repair and Restoration

The data processing systems has to be capable to control all the damage information in a system, and can be used from the first stage (immediately after an earthquake) to third stage (stage of permanent repair and restoration) [2][3]. It should also have a capability to execute various simulation for studying restoration strategy.

4. PROPOSED SEISMIC DAMAGE INFORMATION SYSTEMS

For enabling the requirements presented in the preceding chapter, Seismic Damage Information Systems was proposed for collecting and processing seismic damage information for repair and restoration of roads and river facilities. The Seismic Damage Information Systems is to be operated at the Main Headquarters for Disaster Countermeasures (Headquarters Office at the Ministry of Construction), the Headquarters for Disaster Countermeasures (Headquarters Office at Regional Construction Bureaus) and the Branch for Disaster Countermeasures (Regional Construction Offices).

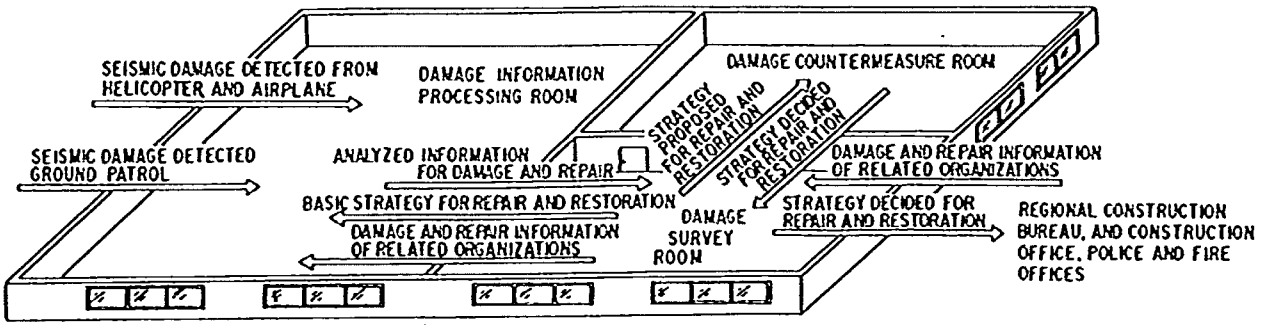
Fig.2 shows layout and role of three sub-sections of the Seismic Damage Information Systems. At Damage Information Processing Room, all damage information are collected from various sources such as ground patrol teams, helicopter patrol teams, other organizations and public. From such information from various sources, important information required for repair and restoration of roads and river facilities are identified. Preliminary statistical analysis of the damage are made. At Damage Survey Room, repair and restoration plan based on the damage information compiled at the Damage Information Processing Room are formulated. Communication and adjustment for restoration with related organizations such as police, fire departments and local governments have to be made at this stage. At Damage Countermeasure Room, basic policy and strategy for repair and restoration based on the information compiled at the Damage Survey Room is decide.

Fig.3 shows an image of the Damage Survey Room and the Damage Information Processing Room which should be placed at the Headquarters Office at Regional Construction Bureaus.

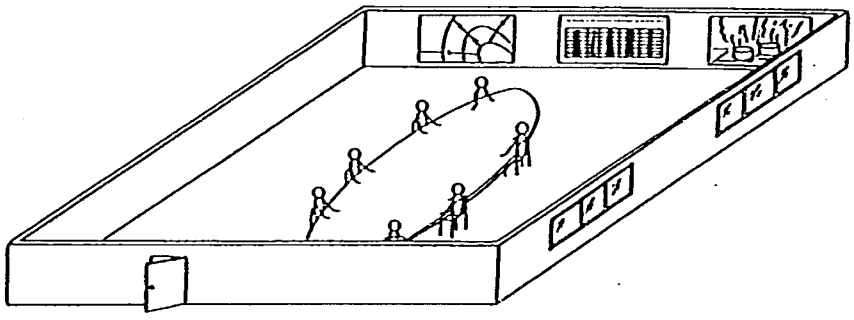
The Seismic Damage Information Systems is of four sub-systems for collecting, transferring, processing and maintenance of the damage information. The outline of the sub-systems are as follows.

(1) Seismic Damage Information Collecting Systems

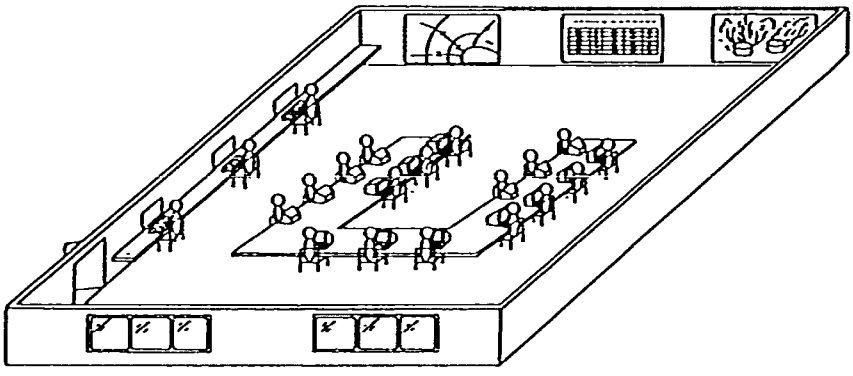
Information on seismic damage detected by helicopter patrol teams and ground patrol teams is collected and processed in this systems. The damage information is of moving picture, still picture and letters. They have to be detected by video cameras, electric still cameras and electric hand notes. The electric hand notes are specially designed man-machine handy type personal computers for exclusive use for recording seismic damage. When the electric notes are operated by field engineers, the notes automatically display and ask important items for identifying the damage situation such as



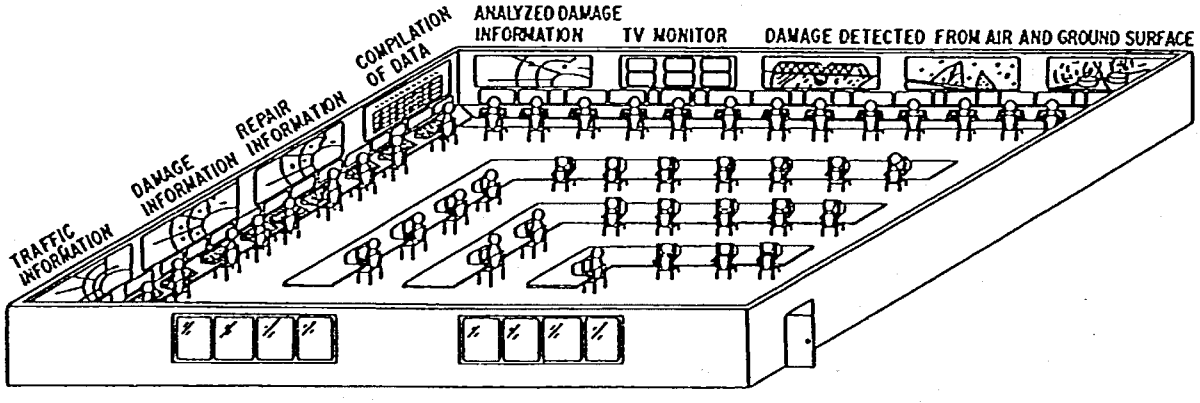
(a) FLOW OF INFORMATION



(b) DAMAGE COUNTERMEASURE ROOM

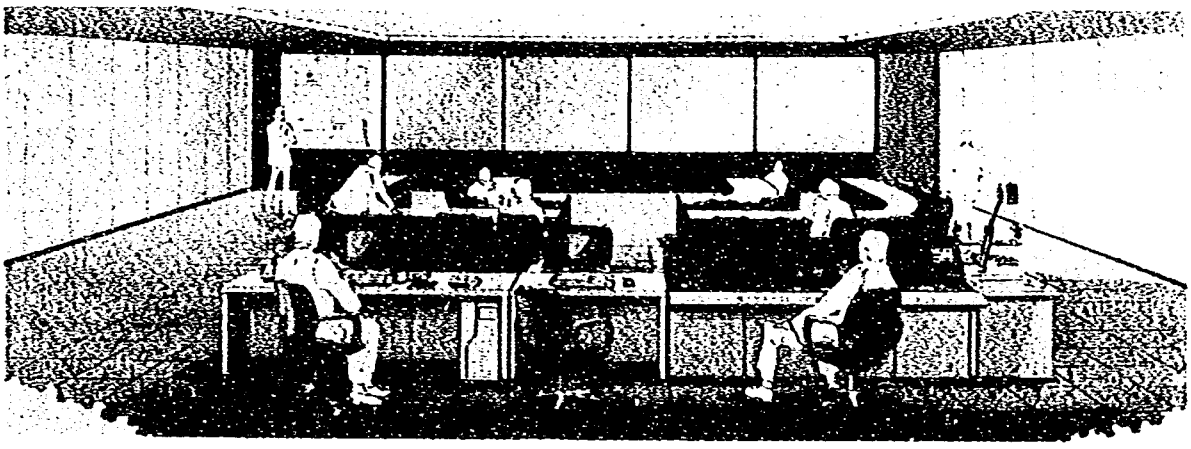


(c) DAMAGE SURVEY ROOM

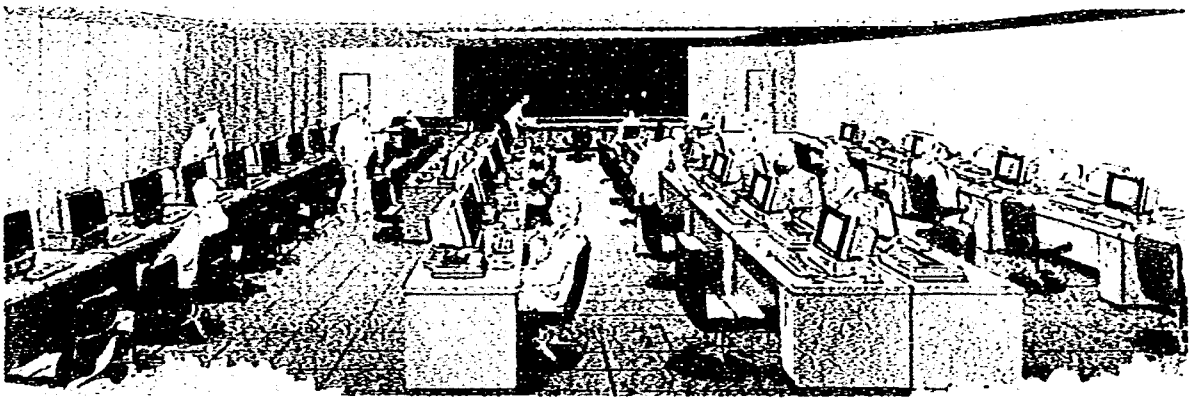


(d) DAMAGE INFORMATION PROCESSING ROOM

Fig. 2 Layout and Role of Headquarters



(a) Damage Survey Room (Regional Construction Bureau)



(b) Damage Information Processing Room (Regional Construction Bureau)

Fig. 3 Image of Damage Information Processing Room and Damage Survey Room

location, size, type and degree of damage. The data are stored on floppy disk, and they can be sent to a host computer at the Headquarters by cables or radio communication systems.

(2) Data Transferring Systems

Fig.4 shows an image of the Data Transferring Systems for transferring the damage information between Headquarters, Regional Construction Bureaus, Regional Construction Offices, patrol helicopters and ground patrol teams. The information to be covered by the systems includes;

a) moving picture motion detected by video cameras on helicopters
b) moving picture motion by video cameras of ground patrol teams
c) still picture motion by still cameras of ground patrol teams
d) character and mapping data used in the Seismic Damage Information Processing Systems
e) telemetered data on earthquake and meteorology
g) Information through telephone and faximile

Main facilities required for the Data Transferring Systems are presented in Fig.5. Main facilities included in the systems are of satellite communication systems and ground communication systems. The satellite communication systems includes satellite, fixed receivers, portable receivers and moving picture transmitting systems. The fixed receiver and portable receivers were already installed at two and five of eight Regional Construction Bureaus, respectively. The ground communication systems are of radio network for exclusive use of the Ministry of Construction and picture motion communication systems. The radio network of the Ministry of Construction covers about 800 locations including Regional Construction Offices and local governments throughout the country.

(3) Seismic Damage Information Processing Systems

Fig.6 shows ten sub-systems for operating the Seismic Damage Information Processing Systems. Whole seismic damage data, repair and restoration data, mapping information, and

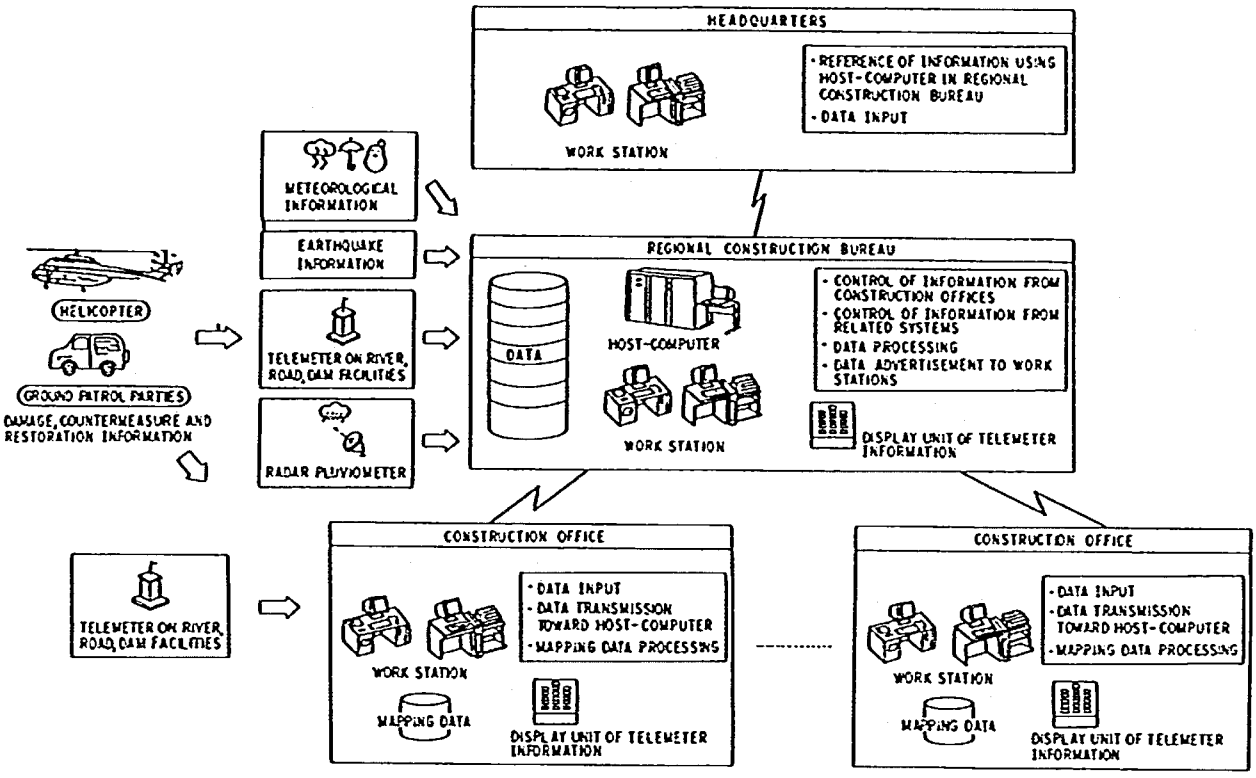


Fig. 4 Image of Data Transferring Systems

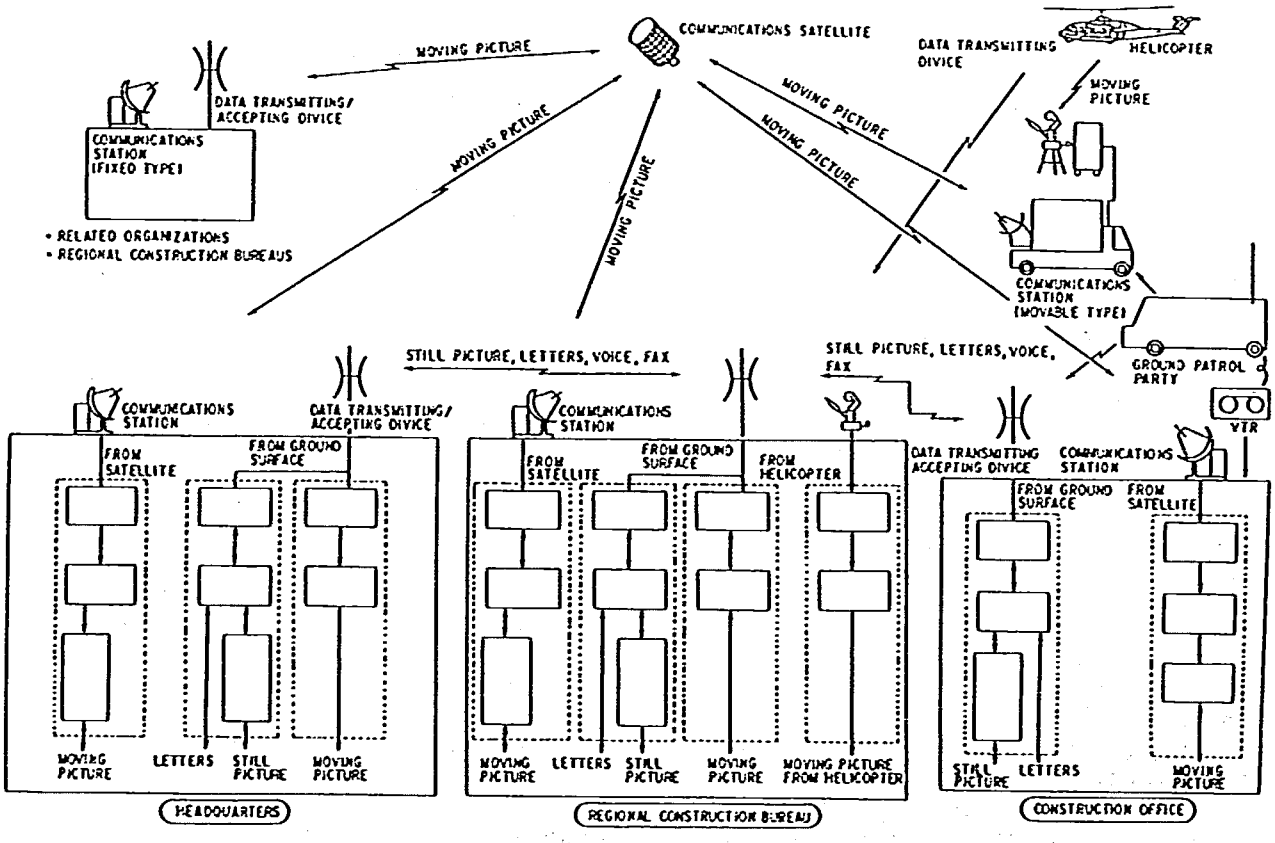


Fig. 5 Main Facilities for Data Transferring Systems

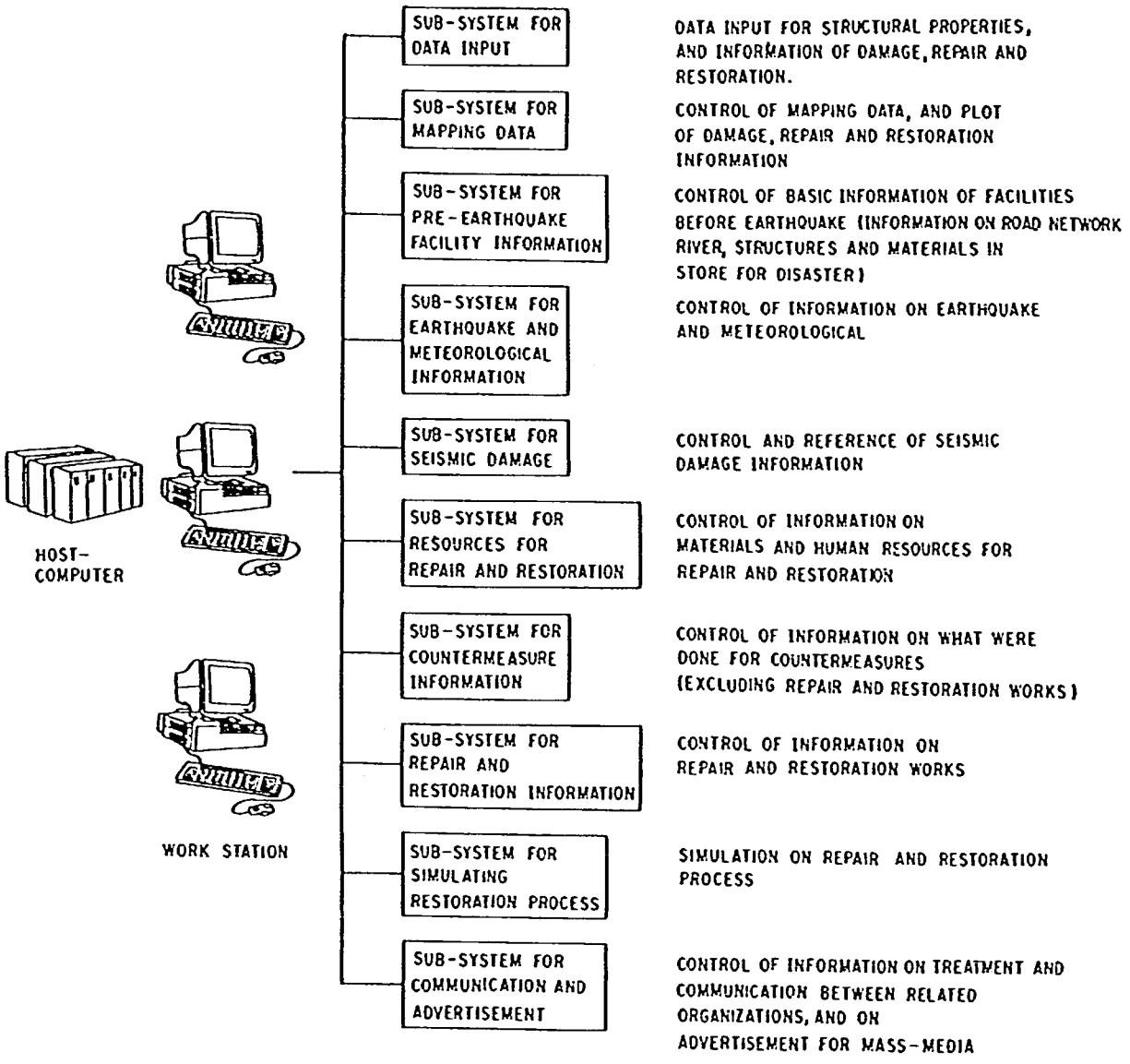


Fig. 6 Sub-systems of Seismic Damage Information Processing Systems

facilities information prior to an earthquake are compiled and controlled in this systems. Simulation of restoration strategy can be made for clarifying the most appropriate way of restoration. Control of information on adjustment with other organizations are made. Notice and announcement on damage and repair to mass-media is also controlled by this systems. It is of host computer for data processing and work-stations for data input and output. Analyzed data should be displayed on monitor in a well organized form for deciding repair and restoration strategy.

(4) Audio Visible Systems

Fig.7 shows an image of the Audio Visible systems. It includes screens with 200 inches and 70 inches, monitor of telemeters, projectors and electric black boards. The Audio Visible Systems should have the capability to monitor the damaged area through large screen, to understand the damage feature by comparing the still and moving pictures taken prior to the earthquake, and to conduct TV conference.

5. DAMAGE INSPECTION FROM HELICOPTERS

Damage inspection from helicopter seems attractive to collect damage information promptly because it is not interrupted by traffic congestion and road suspension. To investigate the effectiveness of the damage survey from helicopter, model damages were intentionally placed on various road and river facilities. A helicopter owned by the Ministry of Construction was used for this test. It is for exclusive use for disaster prevention as shown

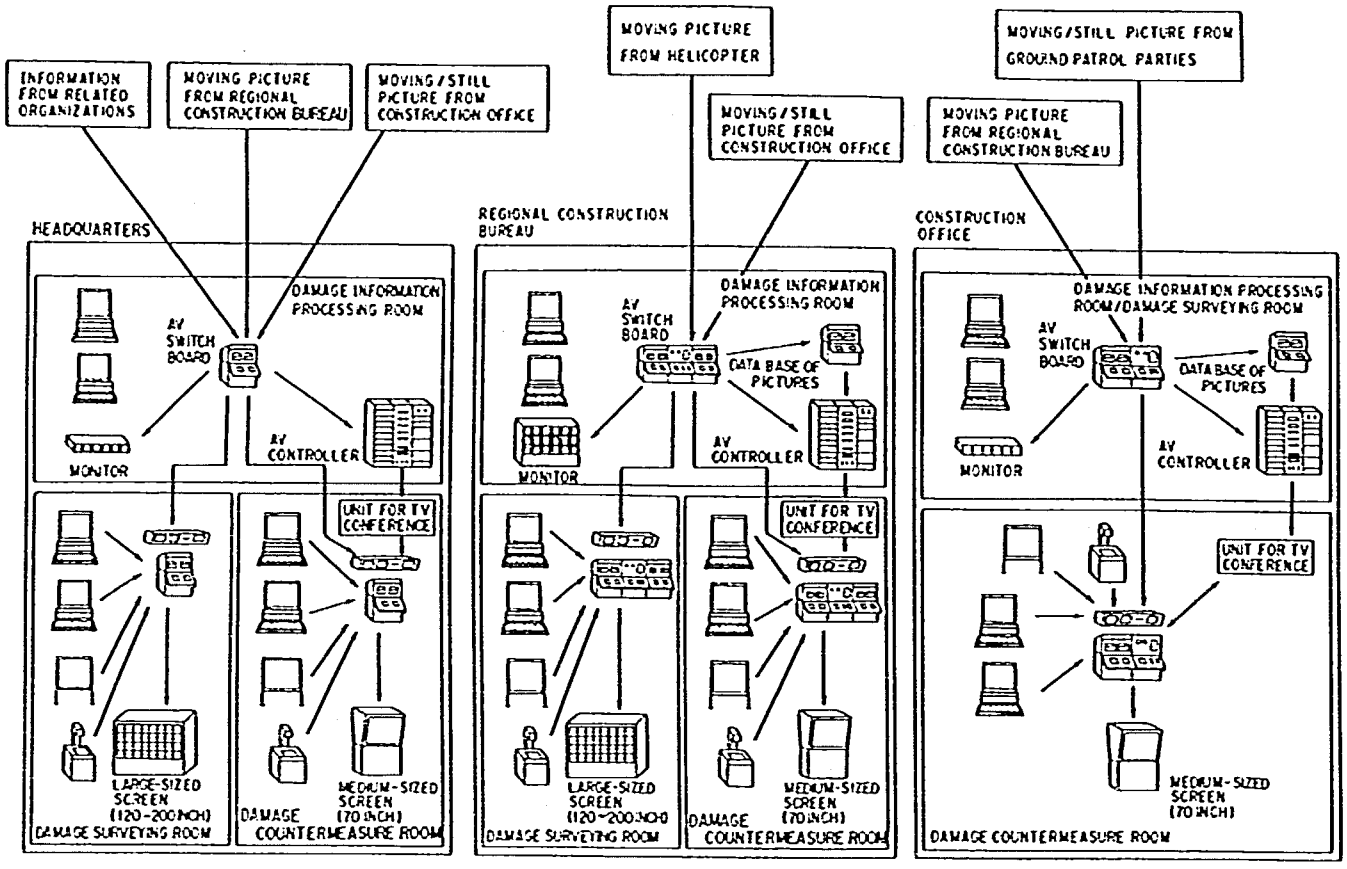


Fig. 7 Image of Audio Visible Systems

in Photo 1.



Photo 1 Helicopter for Disaster Prevention Owned by Ministry of Construction

A video camera which is set in a specially designed camera case for isolating the camera from vibration of the helicopter was used to detect artificial damage. The focal distance of the video camera is from 12.5 mm to 550 mm. By using the focal distance of 550 mm, a flame of 4.8 m by 3.6 m can be recorded when the height of the helicopter is 300 m which is regulated minimum height at city area. Real time transferring of the picture from the helicopter to the ground receiver can be made. A thermal image sensor is also provided on the helicopter. It can detect the difference of temperature with the resolution of 0.25 degree in Centigrade. Because zoom as large as 4 times is provided in the thermal image sensor, a flame with 37 m by 21 m can be recorded.

Various seismic damage was intentionally developed on bridges, pavement, road embankment and river structures. Photo 2 shows cracks which were made by placing white vinyl tape with width of 5 cm for aiming to represent a damage developed at mid-height of reinforced concrete pier and a damage of prestressed concrete deck. The former damage is likely to be developed when reinforcing bars are terminated at mid-height with inadequate anchoring length[3] and the latter damage tends to be developed on the concrete near the bearing supports[7] when the deck is pulled laterally. Photo 3 shows how such damages are detected from helicopter flying 321 m above the ground surface with velocity of 60 km/h[3]. The focal distance was 550 mm. It is apparent that the cracks at pier and deck can be clearly detected. The test was made by varying the velocity and height of flight.

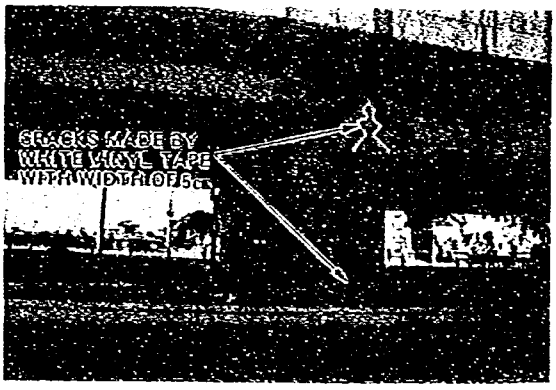


Photo 2 Cracks Placed on Mid-height of Pier and Girder



Photo 3 Damage Detected by Video Camera Placed on Helicopter (Height is 321m, Focal Distance is 550mm)

Photo 4 shows picture representing a new bridge construction along an existing bridge in use for traffic. This was detected by the thermal image sensor at night. Flight height was 338m from the ground surface. Automobiles driving on he existing bridge and four girders under construction can be apparently seen[3]. The thermal image sensor is effective to detect large damage of steel and concrete structures.

Photos 5 and 6 show the seismic damage of road along natural slope , which was caused by the Izu Ohshima-kinkai Earthquake[2] with the Richter magnitude of 7.0 in January 1978. Extensive slope failure was developed along the road with total distance of about 125 m and height of 30 to 50 m , and this embedded a public bus with three being killed. Photo 6 shows the repairing job by a crane. Because this is a part of video taken by a TV company for broadcasting, the flight information such as height and velocity is unknown. By carefully examining the video record, length, depth and soil volume were surveyed by three geologists with different professional careers[3]. The geologist with 17, 10 and 5 years professional career is designated herein as A, B and C geologist, respectively.

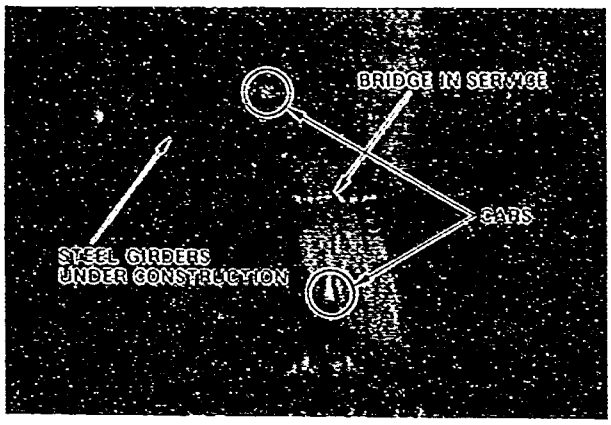


Photo 4 Bridges Detected by Thermal Image Sensor at Night (Height is 338m)

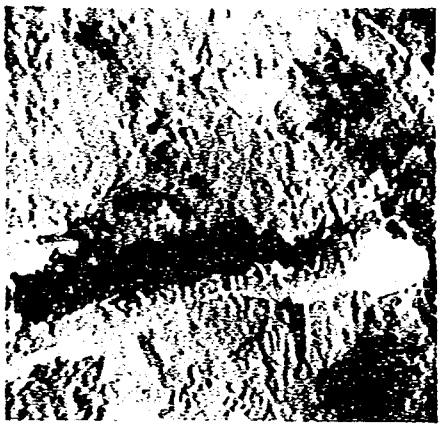


Photo 5 Slop Failure at Nashimoto District of Izu Peninsula Detected by Video Camera from Helicopter

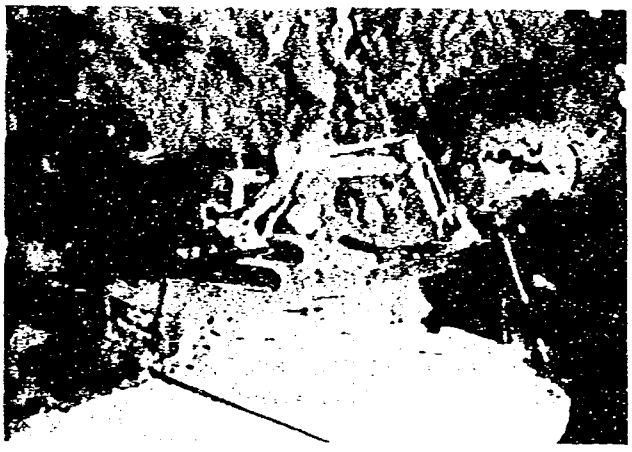


Photo 6 Repair Work Detected by Video Camera from Helicopter

Table 1 compares the accuracy of the estimation by three geologists based on the video film. It is interesting to note that the geologist A gives the most appropriate estimation, and that the geologists with shorter professional career tends to give 30 to 50 % smaller estimation. Because estimation was made through video picture which is, of course, much smaller in size

than the actual damage, the surveyors tend to give smaller estimation in size.

Table 1 Accuracy of Estimation by Three Geologists with Different Professional Career

DAMAGE	GEOLOGISTS			MEASURED
	A	B	C	AT SITE
AVERAGE WIDTH	70(CRANE(10m)x7)	60~80	10~30	100m
AVERAGE DEPTH	10(AVERAGE WIDTHx 1/7~1/10)	5~10	•	5m
FAILURE AREA	•	320~430	•	-
SOIL VOLUME	20,000(30mx70mx10m)	20,000	•	26,500
LENGTH OF ROAD INTERRUPTED BY SLOPE FAILURE	100(AVERAGE WIDTH •α)	80	•	125

1. • MEANS THAT IT WAS UNABLE TO ESTIMATE FROM VIDEO TAPE
2. ( ) REPRESENTS HOW GEOLOGISTS EVALUATED LENGTH, DEPTH AND DISTANCE

Fig. 8 shows the geological feature detected by the geologist A based on the video film. Various information which is useful to judge the cause of failure and probability to cause further progress of the failure can be obtained if the video picture is carefully evaluated by a person with enough professional knowledge.

It was found from the study that estimation of the volume and length of failure is easier when artificial goods and facilities such as car, gird rails, house are found in the moving picture because they can be used as a reference to measure the distance[10] On the other band, it was found difficult to estimate the distance and length when the failure is enormously large as compared with the size of such artificial goods and facilities.

The study presented here is now being extended for studying the maximum flight velocity to detect a certain size of damage[11], effect of temperature and wind velocity for detecting damage by thermal image sensor[12], and the most appropriate way of flight[13].

6. DEVELOPMENT OF GRAPHIC SYSTEMS FOR EARTHQUAKE DAMAGE INFORMATION

Graphic display with use of a computer system is effective for realizing various information and data. However development of a graphic system for disaster information system includes various problems such as in core memory and computer time required. Therefore a pilot-system for earthquakes disaster information system was developed to study the feasibility and display method.

The pilot system can display information on seismic ground motion and hazard which are required immediately after an earthquake as the

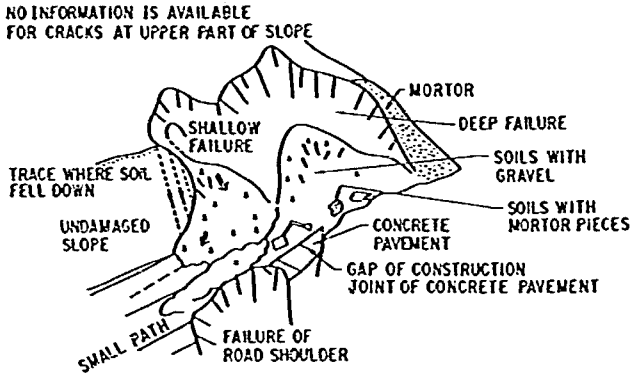


Fig. 8 Geological Feature Detected by Geologist A based on Video Film

basic disaster information for damage evaluation and restoration. The system can display an epicenter, magnitude of earthquake, ground motion records and ground failures.

As a case study, a pilot model was formulated for southern Kanto district around Tokyo-Bay. The system can display a monitor with three different scales. Map A indicates wide area of 158km × 130km with 14 × 14=196 cells. Map B indicates middle areas of 11.3km× 9.25km with 20 × 20 = 400 cells. A whole Map B corresponds to one cell of the Map A. Map C represents small area of 566m × 466m scale, and a whole Map C corresponds to one cell of the Map B.

The hardware of the pilot system is of a memory, a display, a keyboard with a mouse, a printer and a mainframe computer as shown in Photo. 7. Photos 8 and 9 show the graphics on peak acceleration and liquefaction potential.

7. CONCLUDING REMARKS

When the Kanto Earthquake which resulted in about 120 thousands of death occurred in September 1923, there were only about 4,500 vehicles in Tokyo City. People evacuated by either walking or bicycle. This clearly indicates the great difference of anticipated damage situation, between in 1923 and current time, in urban area hitted by a destructive earthquake. It is important to note that there have not be destructive earthquakes which hitted badly urban areas in the last 40 years, and during this time the size, structures of living, lifelines and techniques completely changed. It is therefore anticipated to face a new situation when a large event happens near urban area. It is quite important to develop and introduce a new systems for collecting and processing seismic damage information.

Because the proposed systems would become a large systems consisting of a number of hardwares and softwares, further study needs to

be made for an integrated architecture so that they can be used even after a destructive earthquake. Special training for operating the systems is inevitably important. Because sudden operation immediately after an earthquake can not be made, it has to be used as a part of the comprehensive systems for dally use. Appropriate form of the emergency operation systems in normal time has to be well examined.

Although the thermal image sensors are effective to detect large damage at night, they can be used for surveying more detailed damage if the camera with longer focus distance was developed. The use of new technology such as the high vision camera is promising.

ACKNOWLEDGEMENTS

In executing the project, the Technical Research Center for National Land Development established the Committee for the Development of Disaster information Systems, which is chaired by Dr. H. Umemura, Professor Emeritus of the University of Tokyo, with the commitment of the Ministry of Construction. The reports presented in this paper are being executed with the supervision by the Subcommittee for the Development of Supporting Systems for Disaster Restoration Plan (Chairman : Professor Emeritus K. Kubo).). The authors express their sincere thanks to all committees members for their invaluable suggestions and guidance. Special thanks go to Professor E. Kuribayashi, T. Katayama and Prof. H. Kameda for their invaluable suggestions.

REFERENCES

1) Ministry of Construction : Guidelines for Disaster information Systems, March 1992
2) Public Works Research Institute: Guidelines for Disaster Information Systems for Important Infra-structures, Technical Note of Public Works Research Institute, Vol.58, March 1992
3) Public Works Research Institute : Manuals for Repair Methods for Civil Engineering Structures Damaged by Earthquakes, Technical Note of the Public Works Research Institute, Vol. 45, December 1986 (in Japanese). Translated version is available from the National Center for Earthquake Engineering Research, University of New York, Buffalo, U.S.A.
4) Japan Road Association Guide Specifications for Earthquake Hazard Mitigation for Transportation Facilities - Repair and Restoration -, February 1987
5) Public Works Research Institute: Report on the Disaster Caused by the Izu-ohshima-kinkai Earthquake, Report or the Public Works Research Institute, Vol.158, March 1982
6) Kawashima, K., Sugita, H. and Kanoh, T. : Survey of Seismic Damage by Video Tapes Taken from Helicopter, Civil Engineering Journal, Vol. 33-1, January 1991
7) Kawashima. K., Sugita, H. and Kanoh, T. : Maximum Flight Velocity of Helicopter for Surveying Seismic Damage With Use of Audio Visual Picture, Civil Engineering Journal, Vol.33-9, 1991
8) Kawashima, K., Sugita,H., Kanoh, T. and Iida, H. : Application of Thermal Image Sensor for Survey of Seismic D,,Image, Civil Engineering Journal, Vol. 33-1,
January 1991
9) Kawashima, K., Sugita, H. and Kanoh, T. : Flight Method of Helicopter for Surveying Damage Information Immediately After An Earthquake, Civil Engineering Journal, Vol.33-9. 1991

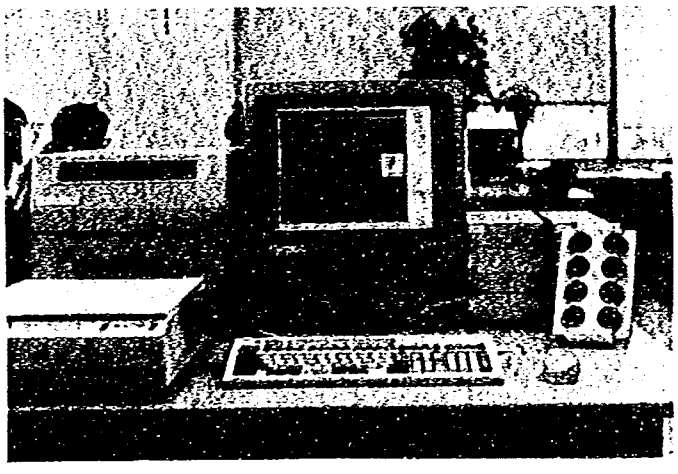


Photo 7 Visual Information Pilot System

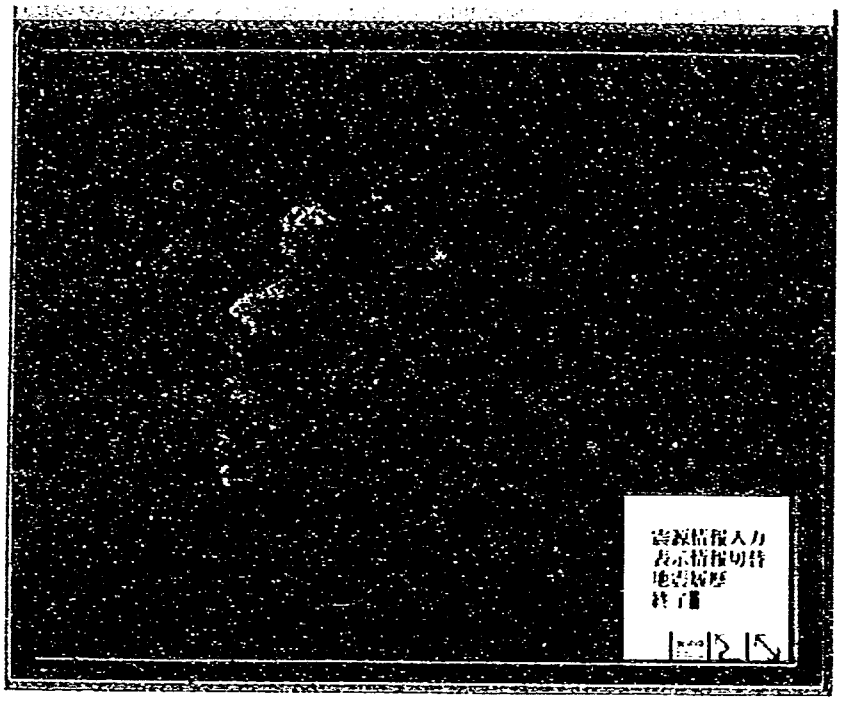


Photo 8 Maximum Acceleration of Ground Surface and Seismic Intensity

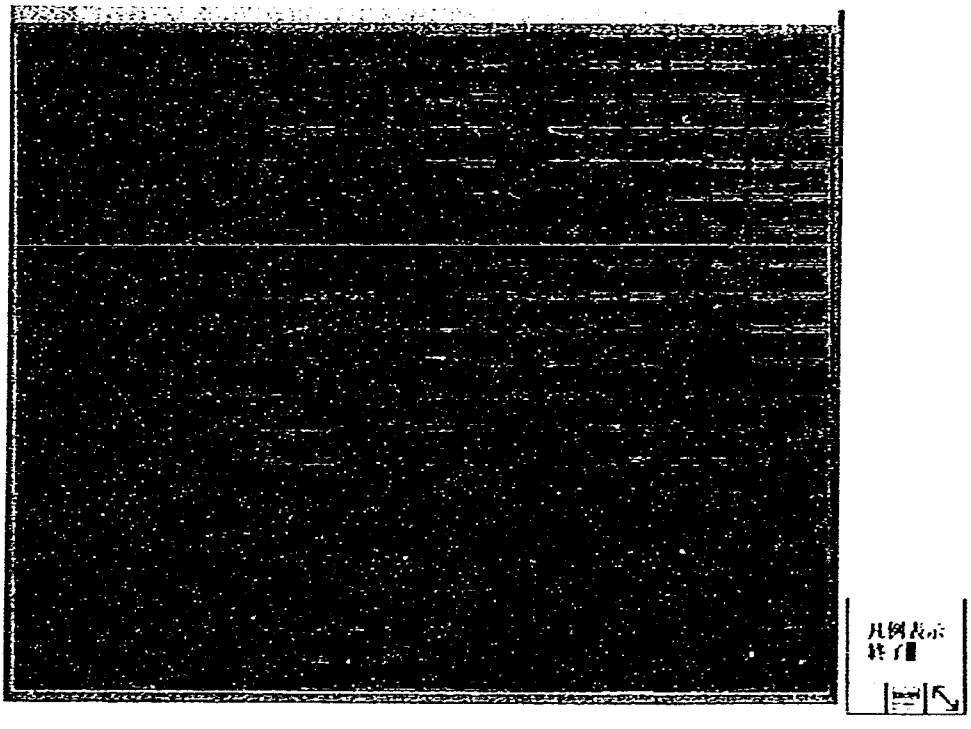


Photo 9 Liquefaction Potential Estimated for Each Cell

Seismic Response Control of Highway Bridges by Variable Damper

Kazuhiko KAWASHIMA
Shigeki UNJOH
and
Hidetoshi MUKAI

25th Joint Meeting of The U.S.–Japan
Cooperative Program In
Natural Resources Panel on
Wind and Seismic Effects
Tsukuba, Japan
May, 1993

SEISMIC RESPONSE CONTROL OF HIGHWAY BRIDGES BY VARIABLE DAMPER

by

Kazuhiko Kawashima[1], Shigeki Unjoh[2] and Hidetoshi Mukai[3]

ABSTRACT

This paper presents experimental studies on the effectiveness of a variable damper developed at the Public Works Research Institute. A prototype model of the variable damper is developed and the dynamic characteristics and the controllability through the dynamic loading tests are presented. The shaking table tests of a model bridge to verify the effectiveness of the variable damper for reducing seismic response of highway bridges are also presented. Furthermore, the variable stiffness concept in which the natural period of highway bridges is shifted to avoid resonance using the variable damper is formulated, and the effectiveness is analytically studied.

KEY WORDS : Seismic Response Control, Highway Bridges, Variable Damper, Prototype Model, Shaking Table Test, Variable Stiffness

1. INTRODUCTION

The variable damper is a viscous damper in which the viscous damping force is variable depending on the response of highway bridges so that the variable damper have the advantages of an usual viscous damper stopper, a passive energy dissipator and a stopper with a shock absorber function. Because integration of functions of a damper-stopper and a energy dissipator is effective for increasing seismic safety of highway bridges, the applicability and practicability of the variable damper has been studied at the Public Works Research Institute.[1)-4)]

This paper presents experimental studies on the effectiveness of the variable damper developed. A prototype model of the variable damper is fabricated and the dynamic performance and the controllability is verified through dynamic loading tests. Shaking table tests of a model bridge to verify the effectiveness of the variable damper for reducing seismic response of highway bridges are also presented. Furthermore, an application of the variable damper to the variable stiffness control is presented. In the variable stiffness control, the natural period of highway bridges is shifted for avoiding resonance.

2. DEVELOPMENT OF A PROTOTYPE MODEL OF THE VARIABLE DAMPER

2.1 Outline of A Prototype Model of the Variable Damper

Fig.1 and Photo 1 show a design plan and a view of a prototype model of the variable damper developed. The model is designed so that the maximum damping force is 20tf, maximum stroke is within ± 13cm. The control of the damping ratio is arbitrarily made by a personal computer depending on relative displacement and/or velocity developed between deck and substructures.

The piston-cylinder has total length of 118.4cm, and the pressure area of the piston is 137.4cm^2. A steel pipe by-pass with servo valves is installed between the cylinder-cells divided by the piston.

The servo valve is a D.C. proportional relief valve and the oil pressure through the valve is adjusted. The servo valve relieves the pore oil pressure over a certain value. This pressure is defined hereafter as the control pressure. Since the damping force of the piston is caused due to the difference of the pressure between the two cells in the cylinder, it increases up to the control pressure, and then becomes constant over the control pressure. Therefore, the damping force is dependent on neither displacement nor velocity of the piston.

The input voltage from a servo amplifier to the servo valve is designed to be in the range of 0 to 5V. The control pressure is 0 at the input voltage of 0V and increases with increase of the input voltage. The viscous material used for the variable damper is an usual oil for a dynamic loading actuator. The variable damper also has a fail-safe function for emergency conditions such

1) Head of Earthquake Engineering Division, Earthquake Disaster Prevention Department, Public Works Research Institute, Ministry of Construction
2) Senior Research Engineer, ditto
3) Assistant Research Engineer, ditto

as power failure. The control pressure can be preset at arbitrary pressure in such case.

2.2 Dynamic Loading Tests of the Prototype Model of the Variable Damper

In the controlling algorithm, it is the most important critical point to assure the relation between the input voltage and damping force of the variable damper. For verifying the algorithm, a dynamic loading test are made.

Fig.2 shows the set-up of the dynamic loading test. Loading was applied to the piston by a dynamic actuator under the displacement control. The control pressure of the servo valve was kept constant. The input voltage to the servo valve, reaction force and stroke of the piston were measured. Ten cyclic loading was made for each loading displacement.

Two tests as shown in Table 1 was made. In Case 1, the friction force of the damper piston was measured. Because loading rate is not important for measuring the friction force, loading frequency was 0.05Hz with loading displacement of $\pm$ 10cm. The input voltage of the variable damper was assumed to be 0V so that the control pressure be 0. In Case 2, the relation between the input voltage to the servo valve and damping force of the variable damper was tested. Combination of loading frequency, loading displacement and input voltage were varied. All loading were made with the peak loading rate less than 7cm/s because of the capability of the loading apparatus.

2.3 Performance of the Prototype Model of the Variable Damper

(1) Friction Force of the Damper Piston

Fig.3 shows hysteresis loops of the load-displacement relation in Case 1. The hysteresis loops show almost rectangular shape, i.e., typical friction type load-displacement relation. The hysteresis is stable for a number of loading cycles. The average friction force is about 1tf.

(2) Hysteresis Loops of the Load-Displacement Relation

Fig.4 shows hysteresis loops of the load-displacement relation with loading frequency of 0.1Hz in Case 2. Variation of the hysteresis loops with the input voltage are also shown. Although overall shape of hysteresis loops are rectangular, some distortion is seen at the instance when the direction of movement of the piston changes at peak displacement. This is because of time-lag for increasing the oil pressure from 0 to the control pressure. But this effect becomes less as the loading stroke increases. This may be resolved by adopting servo valve with large capacity. Turbulence is also found at the instance when the damping force reaches the preset peak force. This may be because of the pressure wave motion by sudden increase of the pressure.

(3) The Relation between the Input Voltage and Damping Force

Fig.5 shows the relation between the damping force and the input voltage. The damping force varies as a power function of the input voltage in the range of 0V and 1.8V. When the input voltage is greater than 1.8V the relation becomes almost linear. An empirical equation was obtained by a least square method as

$$F = \begin{cases} 0.42V^{2.7} + 1.0 & (0 \leq V \leq 1.8) \\ 8.14V - 9.95 & (V > 1.8) \end{cases} \qquad (1)$$

where, F and V represent the damping force (tf) and the input voltage (Volt), respectively. In Eq.(1), the constants are determined as averaged values of those obtained in each loading case.

2.4 Controllability of the Prototype Model of the Variable Damper

The controllability of the variable damper using Eq.(1) was tested. The control of the variable damper is made by controlling a signal from a personal computer depending on the measured displacement. Since digital control is made by the computer, sampling time to detect displacement is preset.

Fig.6 shows hysteresis loops of the load-displacement relation thus obtained. The commanded damping force and the measured one are compared in Fig.6. The damping force is perfectly found to be controlled. Some corrugation in the sampling time of 0.1 sec. Therefore, in order to control accurately, it is required to determine the appropriate sampling time in consideration with the loading velocity.

3. SHAKING TABLE TESTS OF A MODEL BRIDGE CONTROLLED BY THE VARIABLE DAMPER

3.1 Model Bridge

In order to verify the effectiveness of the variable damper, shaking table tests of a model bridge were made. The tests were made using the shaking table at the Public Works Research Institute.

Photo 2 and Fig.7 show the set up of shaking table test and the model bridge. The model bridge is an elastically supported single span girder. It has a pier height of 1.6m, deck length of 7.6m and deck weight of 39.8tf. The deck is supported by 4 rubber bearings as shown in Fig.8. The stiffness of the rubber bearings are designed so that the fundamental natural period of the model bridge be 1sec. Therefore, the stiffness of rubber bearing is designed as 160tf/m at 50% shear strain. Total thickness and shear modulus of the rubber is 10cm and 6kgf/cm^2, respectively.

The variable damper is installed between the deck and the top of left pier as shown in Photo 3.

Fig.9 shows the control algorithm of the variable damper.[3)4)] The displacement dependent damping was assumed and the variable damper is controlled by the displacement of deck relative to the pier top.

3.2 Dynamic Response Characteristics of A Model Bridge

Because the rubber bearings have some nonlinearity, the stiffness and energy dissipation depend on the shear strain (shear displacement). For clarifying these characteristics, the model bridge was firstly excited by a series of harmonic motions without controlling by means of the variable damper.

Fig.10 shows the frequency response function of deck displacement. Peak deck displacement increases from 2.8cm to 9.8cm by increasing the peak acceleration of harmonic table motion from 20cm/s^2 to 40cm/s^2. The predominant frequency of the deck also shifts from 1.15Hz to 1.0Hz by doubling the table motion.

From the harmonic excitation tests, the load-displacement hysteresis of the bearing as shown in Fig.11 was evaluated. The equivalent stiffness and equivalent damping ratio was computed as :

$$h_e = \frac{1}{2\pi}\frac{\Delta W}{W} \qquad (2)$$

$$K_e = \frac{F(u_{max}) - F(u_{min})}{u_{max} - u_{min}} \qquad (3)$$

where,

h_e : equivalent damping ratio
K_e : equivalent stiffness
W : strain energy
ΔW : energy dissipation
u_{max} : maximum displacement developed in bearings
u_{min} : minimum displacement developed in bearings
$F(u_{max})$: force developed at displacement u_{max}
$F(u_{min})$: force developed at displacement u_{min}

Fig.12 shows the equivalent stiffness and the equivalent damping ratio of the rubber bearings by Eqs.(2) and (3). The equivalent stiffness decreases with increase of displacement. The displacement dependence of the equivalent damping ratio is less significant.

3.3 Earthquake Response Characteristics of the Model Bridge Controlled by the Variable Damper

In order to verify the effectiveness of the variable damper, the model bridge was excited by an earthquake motion. An acceleration ground motion, which recorded on the ground around Hachirogata during the Nihon-kai-chubu Earthquake of 1983, was used as an input acceleration by reducing the time axis one half so that the predominant frequency of the record matches with the fundamental natural frequency of the bridge model. Peak acceleration was modified to be 200cm/s^2 and 500cm/s^2.

Three cases in total were made. In Case A, the model bridge was not controlled by the variable damper and the peak acceleration was assumed as 200cm/s^2. In Case B, the model bridge was controlled by the variable damper and the peak acceleration was assumed as 200cm/s^2. In Case C, the model bridge was controlled and the peak acceleration was increased to 500cm/s^2.

Figs.13 to 15 show the measured responses of above three cases, respectively. The displacement and acceleration of the model bridge and the damping force of the variable damper are shown. The simulation results described later is also shown.

Fig.13 shows the input acceleration and the deck responses of the Case A (no control). The deck responses with the period of about 1sec which is the fundamental natural period of the model bridge. The peak displacement and peak acceleration of deck are 376cm/s^2 and 9.2cm, respectively. The deck acceleration is amplified to 2.2 times the input acceleration. Fig.14 shows those in Case B (with control). The deck responses contain the faster frequency

components and the peak displacement and peak acceleration of deck decrease to 203cm/s^2 and 1.3cm, respectively. The amplification of the deck acceleration is 1.1 times the input acceleration. Fig.15 shows those in Case C (with control). The peak displacement and the peak acceleration of deck are 412cm/s^2 and 3.5cm, respectively.

Table 2 summarizes the peak responses of the model bridge and the variable damper. Comparing Cases A and B, the peak acceleration and peak displacement of deck controlled by the variable damper decrease to 54% and 14% of those with no control, respectively. The peak damping force of the variable damper in Case B is 7.2tf.

3.4 Simulation of the Shaking Table Tests

In order to simulate the tests results, a computer program "VDAM" which can analyse earthquake response of a multi-degree-of-freedom system with the variable damper developed at PWRI was used.[3] The simulation results are shown in Fig.13 to 15 described in the above. Equivalent stiffness and equivalent damping ratio of the rubber bearing obtained through the harmonic excitation in the above were used for the simulation.

In case A (no control), fair agreement between measured and computed responses are found in displacement and acceleration responses.

In case B and C (with control), computed deck displacements are larger than the measured ones. On the other hand, the measured damping force is greater than computed one. The difference between measured and computed peak displacements is about twice. This is because of the over-shooting of the damping force of the variable damper. Therefore, the servo valve which has quick response capability should be adopted so as to decrease the over-shooting of damping force. However, the computed and measured responses in Cases B and C show the fair agreement.

4. SEISMIC RESPONSE CONTROL OF HIGHWAY BRIDGES BY VARIABLE STIFFNESS

4.1 Algorithm of the Variable Stiffness

Most of bridges with usual size have the natural period ranging from 0.3 to 1.5 second, and this natural period range corresponds to the predominant period of earthquake-induced ground motions. Thus the resonance of the bridges response with the ground motion tends to be developed during an earthquake. The bridge response could be reduced provided the resonance of bridge response with the ground motion could be avoided.

Although it is hard to predict the predominant period of ground motion prior to an earthquake, it can be evaluated time by time during an earthquake. The moving window analysis may be used for evaluating the instantaneous predominant period of ground motion T^*. The resonance of bridge response with the ground motion may be avoided if the instantaneous natural period of bridges T be shifted from the instantaneous predominant period of ground motion T^* during an earthquake.

There are various methods to shift the instantaneous natural period of bridges during an earthquake. Flexibility of bearings may be changed, and active tendons/bracings may be adopted.

If one provides the variable dampers for a bridge which is elastically supported by rubber bearings, the natural period of the bridge can be varied by changing the damping coefficient of the variable dampers. If one makes the damping ratio of the variable damper very large, the variable damper would acts as the damper stopper. On the other hand, if one makes the damping ratio small, the natural period of the bridge takes the value computed from the stiffness of the rubber bearings and piers. The variable dampers have various advantage for controlling the instantaneous natural period of bridges because it is more stable for long term use than the active tendons/bracing systems.

Fig.16 shows the algorithm of the variable stiffness control. The instantaneous predominant period of ground motion T^* at time t_i is computed by the moving window Fourier Spectrum. The damping coefficient of variable dampers is varied so that the instantaneous natural period of the bridge T be shifted to prevent the resonance with the ground motion.

Although several algorithm can be considered, the period shift is assumed here as

$$T = \alpha T^* \qquad (4)$$

where,

T : instantaneous natural period of a bridge at time t_i

T^*: instantaneous predominant period of an earthquake ground motion at time t_i

α : control coefficient

The coefficient α has to be determined depending on the undamped natural period of the

bridge T and the instantaneous predominant period T^s of an ground motion. It is proposed that α is set as

$$\begin{aligned} \alpha &< 1/2 \quad (T < T^s) \\ \alpha &> 2 \quad (T \geq T^s) \end{aligned} \tag{5}$$

4.2 Earthquake Response Analysis Method of Multi-Degree of Freedom System with Variable Stiffness Control

The equations of motion for a linear multi-degree-of-freedom system with the variable stiffnesses control may be written as

$$\underline{M}\,\ddot{\underline{x}} + (\underline{C} + \underline{C}_v)\,\dot{\underline{x}} + \underline{K}\,\underline{x} = -\underline{M}\,\ddot{x}_0 \tag{6}$$

in which $\underline{M}$, $\underline{C}$ and $\underline{K}$ represent mass, damping and stiffness matrices of the system, respectively. $\underline{x}$ and x_0 denote displacement vector of the system and an earthquake ground motion, respectively. $\underline{C}_v$ denotes a damping matrix of the variable dampers and is assumed as

$$\underline{C}_v = \sum_{k=1}^{n_v} \underline{c}_{ij}^{\,v} \tag{7}$$

where

$$\underline{c}_{ij}^{\,v} = \begin{bmatrix} V & -V \\ -V & V \end{bmatrix} \tag{8}$$

in which $\underline{c}_{ij}^{\,v}$ and n_v represent damping matrix of the variable dampers, which is installed between the i-th node and the j-th node, and a number of the variable dampers installed, respectively. V is the damping coefficient of an each variable dampers and is given according to the control algorithm as shown in Fig.16.

Although there are various methods to prescribe the damping matrix $\underline{C}$ of the structure, it is assumed here to be written as Eq.(9) assuming that the damping matrix $\underline{C}$ can be diagonalized by the modal matrix.

$$\underline{C} = (\underline{\Phi})^{-1}\,\mathrm{diag}[2h_k\omega_k]\,(\underline{\Phi}^T)^{-1} \tag{9}$$

in which, $\underline{\Phi}$ denotes a modal matrix of the system and $\mathrm{diag}[2h_k\omega_k]$ denotes a diagonal matrix with elements of $2h_k\omega_k$ (k=1,2,3,$\cdots\cdots$; mode number).

Since $\underline{C}_v$ is time-varying, Eq.(6) has to be solved by a direct integration method. According to the above analytical method, a computer program "VSTIFF," which can analyze earthquake response of a multi-degree-of-freedom system with the variable stiffnesses, was developed.

4.3 Highway Bridge Analyzed and Analytical Conditions

In order to analytically investigate the effectiveness of the variable stiffness, a three-span continuous girder bridge, as shown in Fig.17, with a span length of 90m is analyzed. The response in longitudinal direction is considered. The superstructure of the model is supported by elastic isolators in longitudinal direction and the 4 same variable stiffnesses are assumed to be installed between the superstructure and each pier top.

The weight of the superstructure and spring stiffness of the isolator are assumed as 481.2tf and 637tf/m, respectively. The flexural stiffness of piers is assumed so that the fundamental natural period of the model be 0.5sec when the 4 bearing supports are hinged. The stiffness of isolators result in the fundamental natural period of 1 sec for the model with elastic isolators. When the variable damper is not provided, the modal damping ratio of the bridge is assumed to be 2% of critical.

An acceleration ground motion as shown in Fig.18(a) is used as an input acceleration. The acceleration, recorded on the ground around the Tsugaru Bridge during the Nihon-kai-Chubu Earthquake of 1983, was modified so that the response spectrum matches with the target spectrum. The acceleration spectrum, which is specified in "Part V Seismic Design" of the "Design Specifications for Highway Bridges", for the check of bearing capacity of reinforced concrete piers on soft soil site (ground condition III), is assumed as the target spectra.

Fig.18(b) shows the intantaneous predominant frequency ($1/T^s$) of the input acceleration. Because the predominant period of ground motion is about 1 sec., α in Eq.(4) was assumed as 1/2.

4.4 Effectiveness of Variable Stiffness Control

Figs.19 shows how the natural period of the bridge change depending on the damping coefficient of the variable dampers. At the damping coefficient C of about 430 tf·sec/m, the fundamental natural period of bridge take very large value, because this corresponds to the critical damping of the structure. Although the period shift may be made in the damping coefficient range of 0 to over 800 tf·sec/m, it is assumed here that the period shift be made in the range of damping coefficient C over 430 KN·sec/m.

Fig.20 compares the deck acceleration and

displacement of the bridge with and without control. The peak displacement and peak acceleration of deck decreases to 17% and 50% of those without control. The bending moment of pier bottom decreases to 52% of the one without control. The peak damping force required for the four variable dampers is 77.6 tf × 4 = 310 tf and peak stroke is 3.1cm.

5. CONCLUDING REMARKS

The effectiveness of the variable dampers was experimentally studied. A prototype model of the variable damper was developed and the performance was studied through the dynamic loading tests and shaking table tests. The variable stiffness control in which the natural period of bridges is shifted to avoid resonance with the ground motion was proposed, and its effectiveness was analytically studied. According to the investigations presented herein the following conclusions may be deduced:

1) Based on the dynamic loading tests of the prototype model developed, the damping force of the variable damper can be controlled as commanded.

2) Based on the shaking table tests of the model bridge, the peak acceleration and peak displacement of deck controlled by the variable damper decreases to 54% and 14% of those with no control, respectively. The peak damping force of the variable damper is 7.2tf.

3) The measured responses in 2) can be predicetd by the analytical model presented herein.

4) By the variable stiffness control, the peak displacement and peak acceleration of the deck decreases to 17% and 50% of those without control, respectively. The bending moment of pier bottom decreases to 52% of that without control. The peak damping force required for the four variable dampers is 77.6tf × 4 = 310tf and peak stroke is 3.1cm.

REFERENCES

1) Taguchi, J., Iwasaki, T., Adachi, Y., Sasaki, Y. and Kawashima, K. : U.S.-Japan Cooperative Research Program on Hybrid Control of Seismic Response of Bridge Structures, 22nd Joint Meeting, U.S.-Japan Panel on Wind and Seismic Effects, UJNR, Gaithersburg, Maryland, USA, May, 1990

2) Kawashima, K., Unjoh, S., Nagashima, H. and Shimizu, H. : Current Research Efforts in Japan for Passive and Active Control of Highway Bridges Against Earthquakes, 23rd Joint Meeting, U.S.-Japan Panel on Wind and Seismic Effects, UJNR, Tsukuba, May, 1991

3) Kawashima, K., Unjoh, S. and Shimizu, H. : Seismic Response Control of Highway Bridges by Variable Damper, 24th Joint Meeting, U.S.-Japan Panel on Wind and Seismic Effects, UJNR, gaithersburg, May, 1992

4) Kawashima, K., Unjoh, S., Iida, H. and Mukai, H. : Effectiveness of the Variable Damper for Reducing Seismic Response of Highway Bridges, Proc. of the 2nd U.S.-Japan Workshop on Earthquake Protective Systems for Bridges, Tsukuba, Dec. 7-8, 1992

5) Liu, S., C., Lagorio, H., J. and Chong, K., P. : Status of U.S. Research on Structural Control Systems, 23rd Joint Meeting, U.S.-Japan Panel on Wind and Seismic Effects, UJNR, Tsukuba, May, 1991

6) Kawashima, K., Unjoh, S. and Shimizu, H. : Earthquake Response Control of Highway Bridges by Variable Damper, Proceedings of Colloquium on Control of Structures, Japan Society of Civil Engineers, Part. B, pp.221-224, July, 1991 (in Japanese)

7) Feng, Q. and Shinozuka, M. : Use of A Variable Damper for Hybrid Control of Bridge Response Under Earthquake, U.S. National Workshop on Structural Control Research, University of Southern California, CA., U.S.A., October, 1990

8) Shinozuka, M., Feng, Q. and Kawamura, S. : New Perspectives for Sliding Base Isolation Systems, Proceedings of International Workshop on Recent Developments in Base-Isolation Techniques for Buildings, Tokyo, Japan, 27-30 April, 1992

9) Kawashima, K., Unjoh, S. and Shimizu, H. : Earthquake Response Control of Highway Bridges by Variable Damper, Transactions of the Japan National Symposium on Active Structural Response Control, Japan Science Council, pp.311-317, March, 1992 (in Japanese)

10) Kawashima, K., Unjoh, S. and Shimizu, H. : Experimental Study on Dynamic Characteristics of Variable Damper, Transactions of the Japan National Symposium on Active Structural Response Control, Japan Science Council, pp.311-317, March, 1992 (in Japanese)

Table 1 Test Cases

Case	Objective	Loading Frequency (Hz)	Loading Displace-ment (cm)	Input Voltage (Volt)
1	Measurement of Friction Force of Damper-Piston	0.05	±100	0
2	Relation between Damping Force and Input Voltage	0.1~1.0	±2~±100	0~5

Table 2 Peak Responses of A Model Bridge and Variable Damper

Test Cases	Peak Accel. of Shaking Table (cm/s^2)	Measured			Computed		
		Deck	Variable Damper		Deck	Variable Damper	
		Accel. (cm/s^2)	Force (tf)	Stroke (cm)	Accel. (cm/s^2)	Force (tf)	Stroke (cm)
A No Control	172	376	---	---	361	---	---
B With Control	185	203	7.2	1.3	148	5.2	2.5
C With Control	413	412	13.8	3.5	442	13.5	6.2

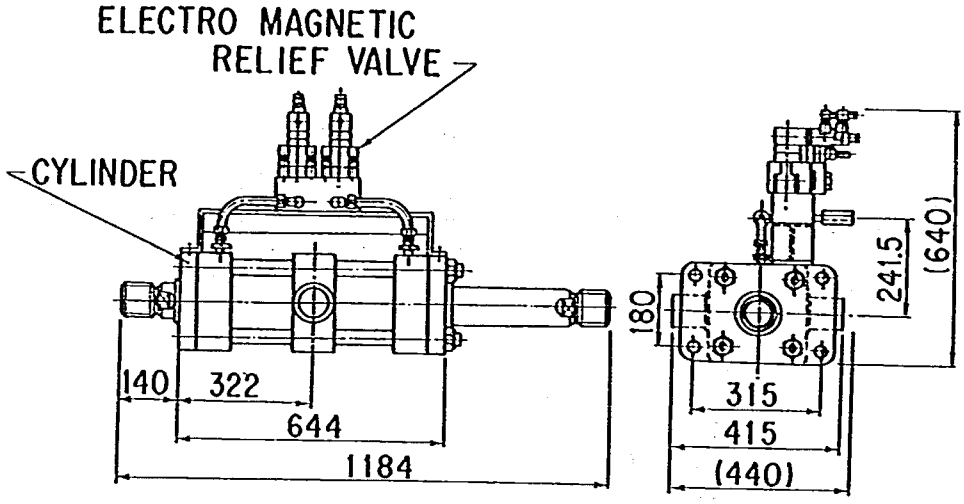


Fig.1 Prototype Model of Variable Damper Developed

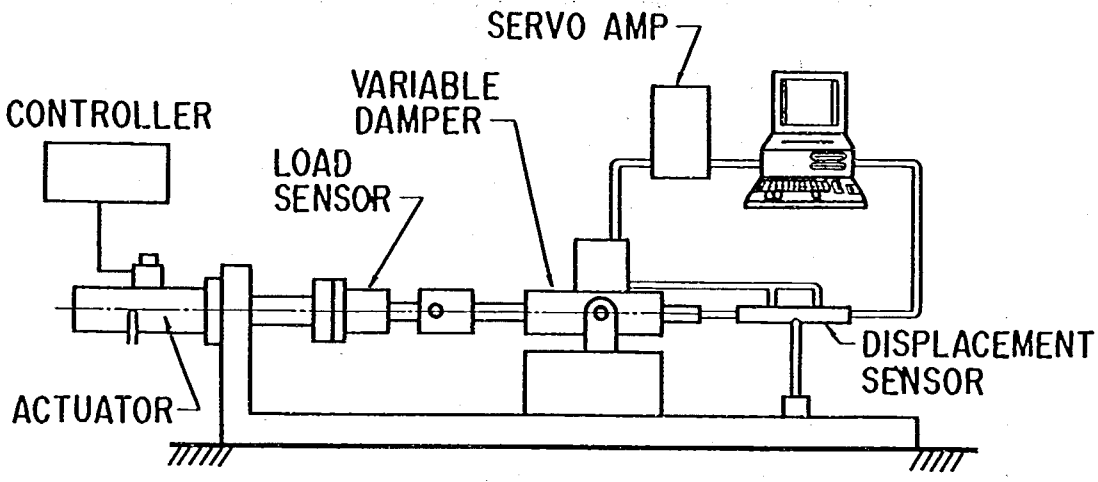


Fig.2 Set up of Dynamic Loading Tests of Variable Damper Developed

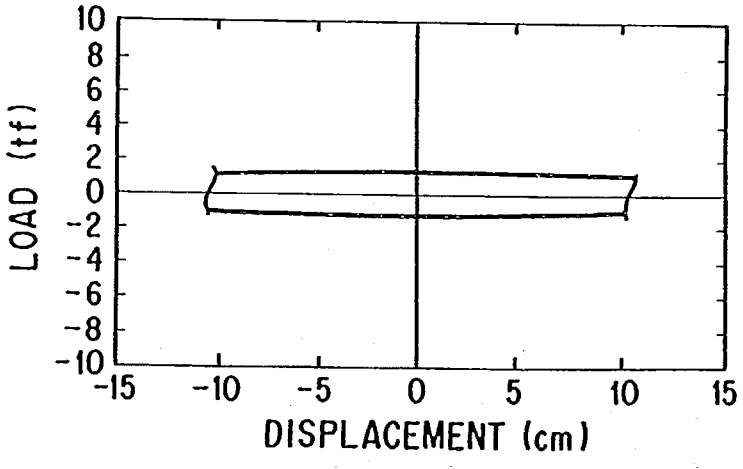
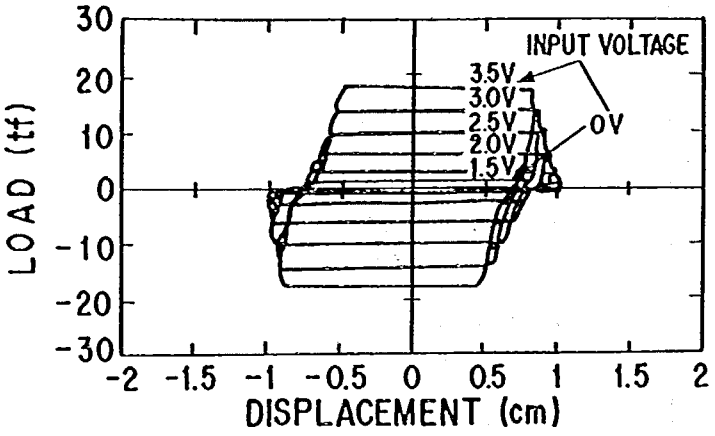
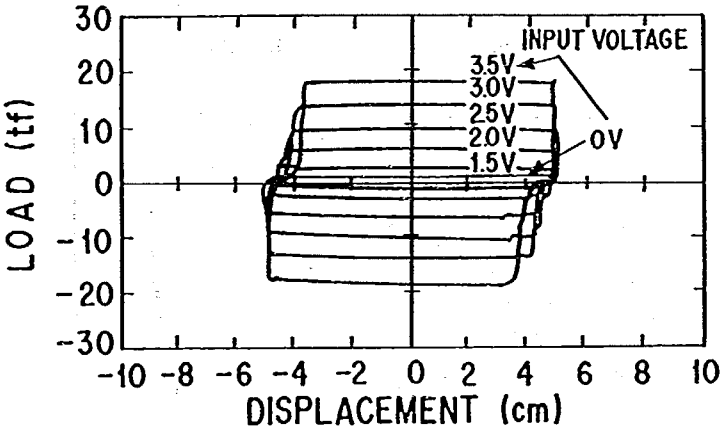


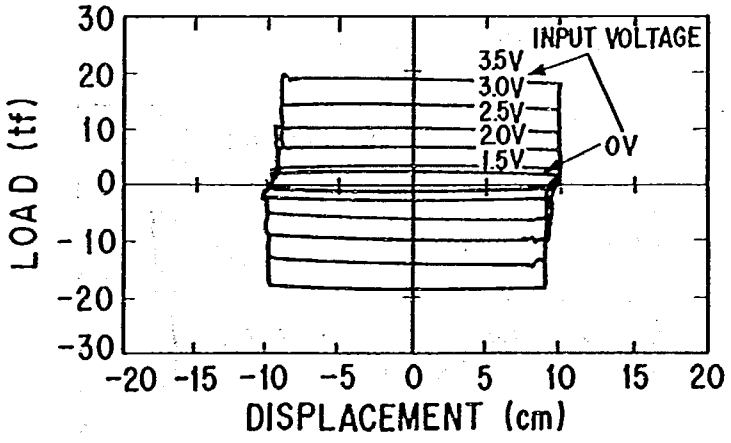
Fig.3 Hysteresis Loops of Load-Displacement Relation
(Displacement = 10cm, Frequency = 0.05Hz)



(1) Displacement 1cm



(2) Displacement 5cm



(3) Displacement 10cm

Fig.4 Hysteresis Loops of Load-Displacement Relation (Frequency = 0.1Hz)

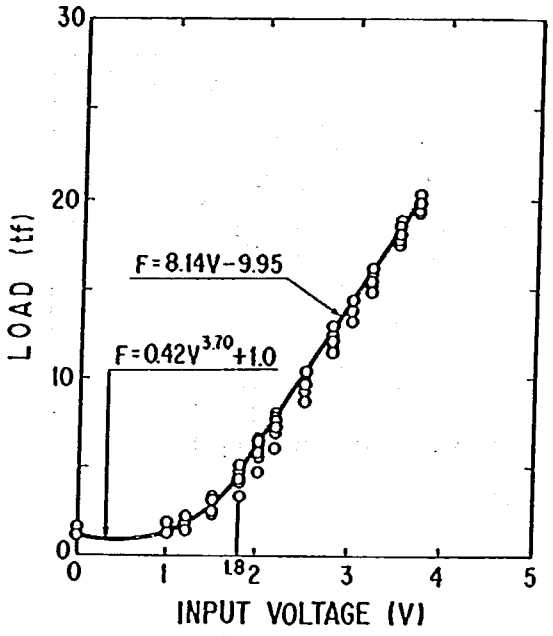
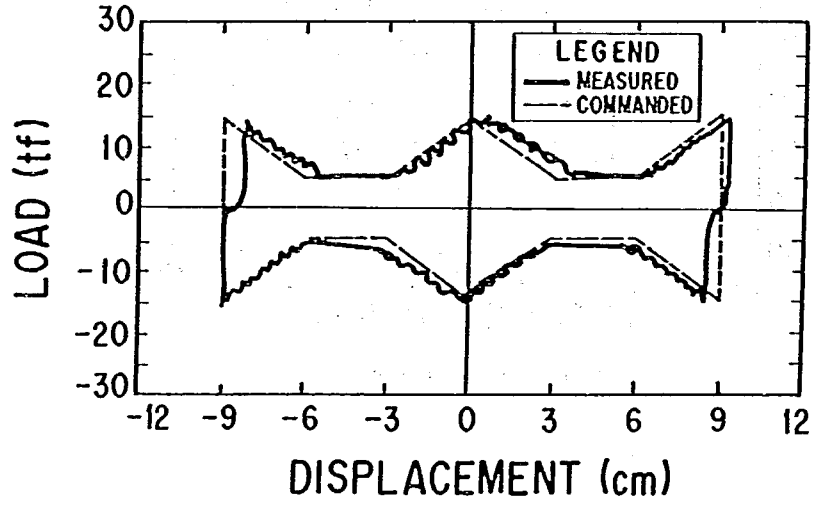
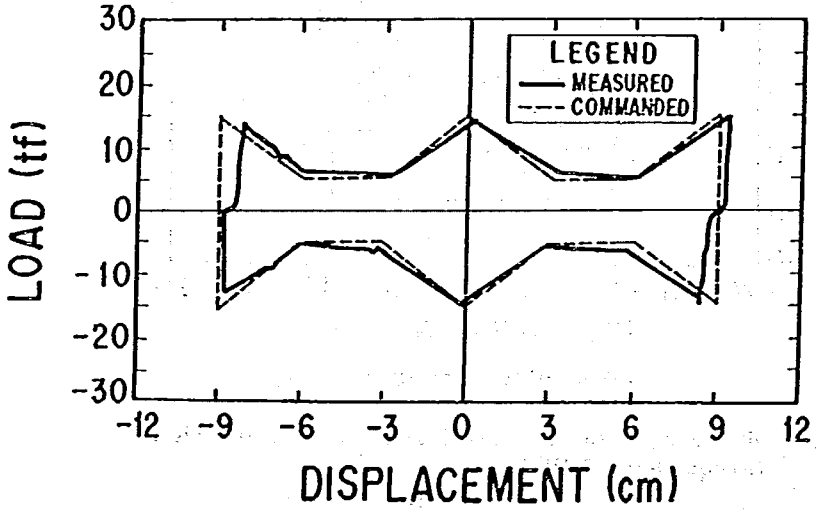


Fig.5 Damping Force vs. Input Voltage Relation



(1) Sampling Time 0.1sec



(2) Sampling Time 0.01sec

Fig.6 Controllability of the Variable Damper Developed

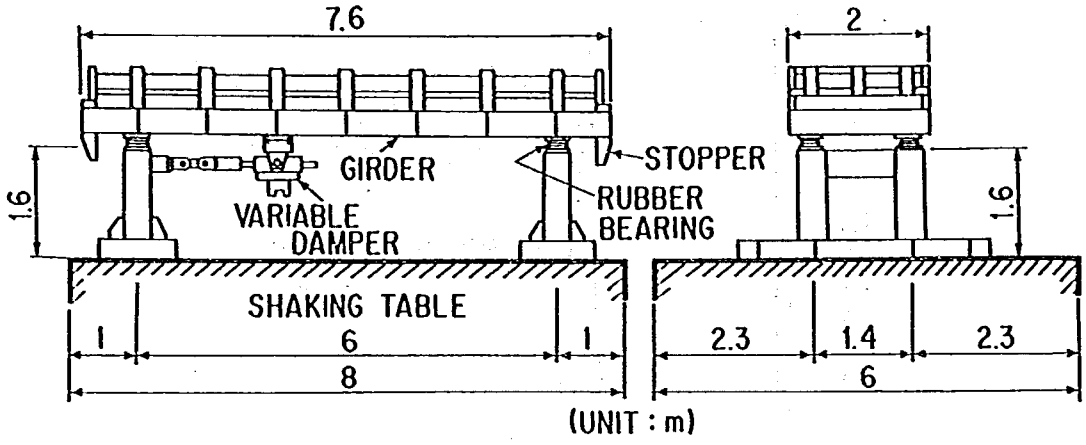


Fig.7 Model Bridge Studied

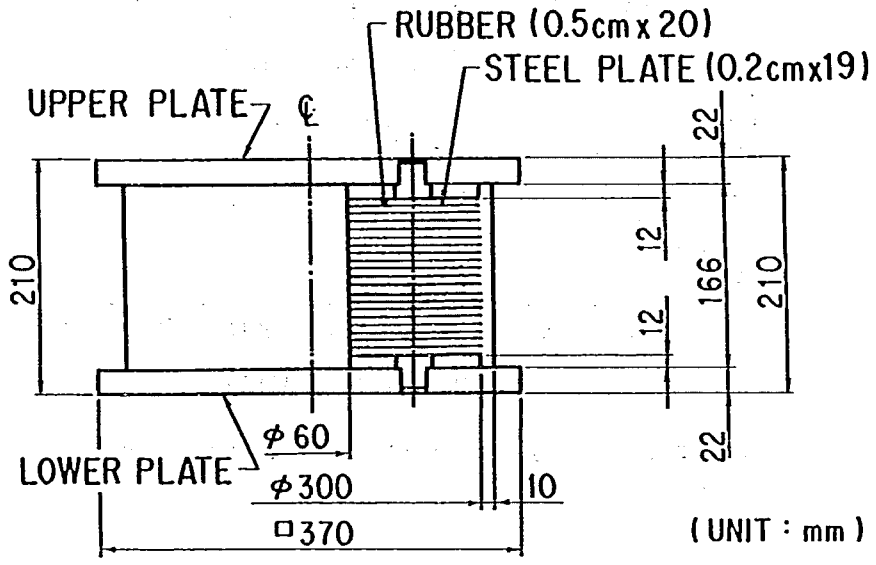


Fig.8 Rubber Bearing used for A Model Bridge

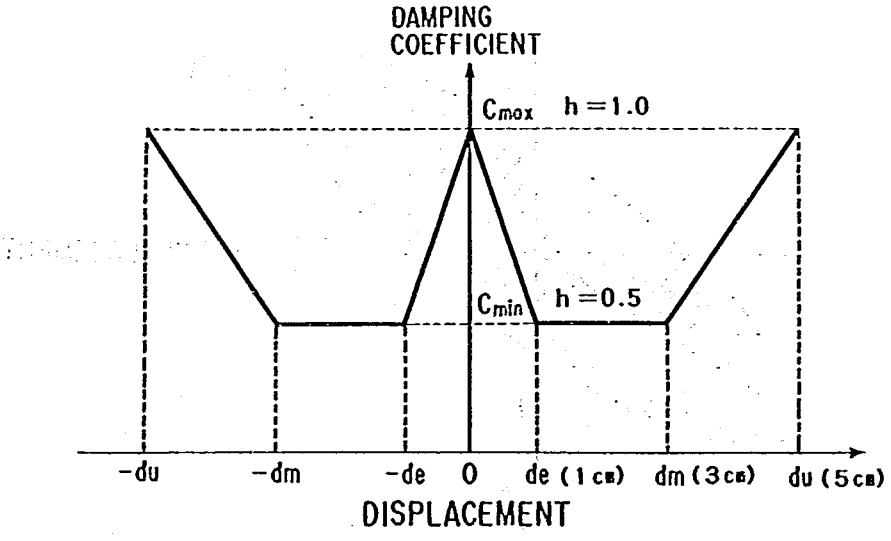


Fig.9 Control Algorithm of Variable Damper (Displacement Dependent Damping)

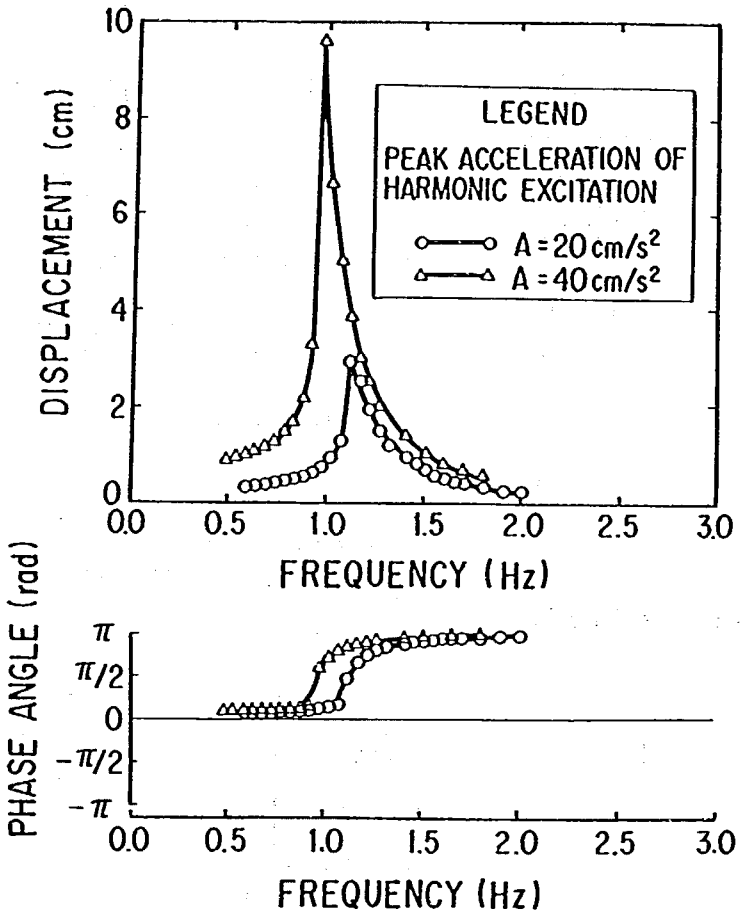


Fig.10 Frequency Response Function of A Model Bridge

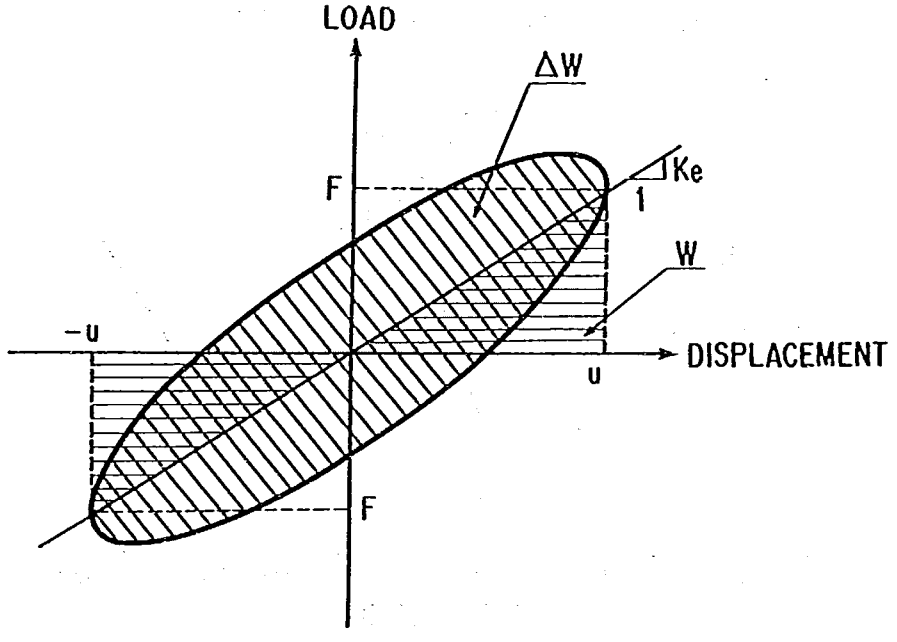
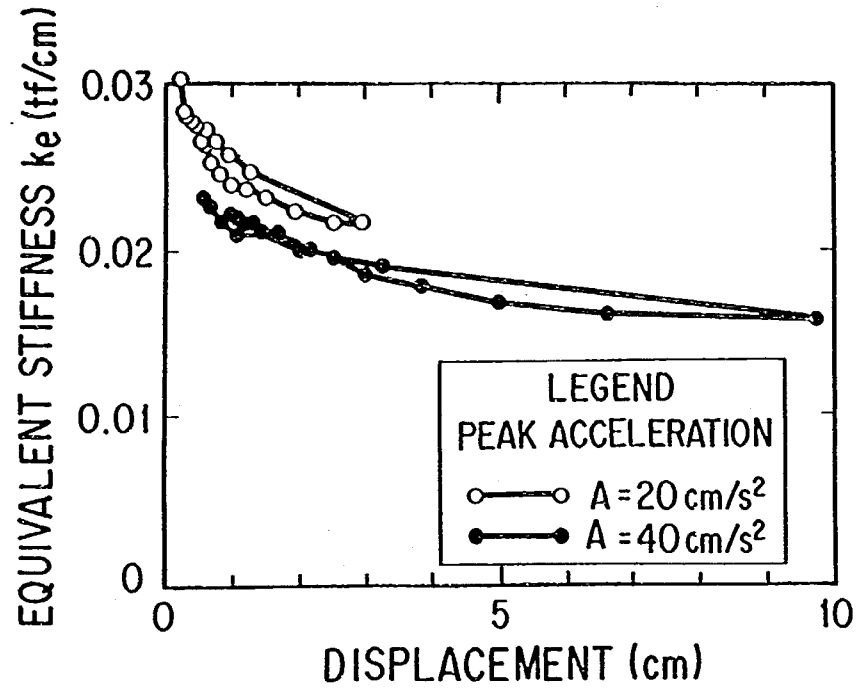
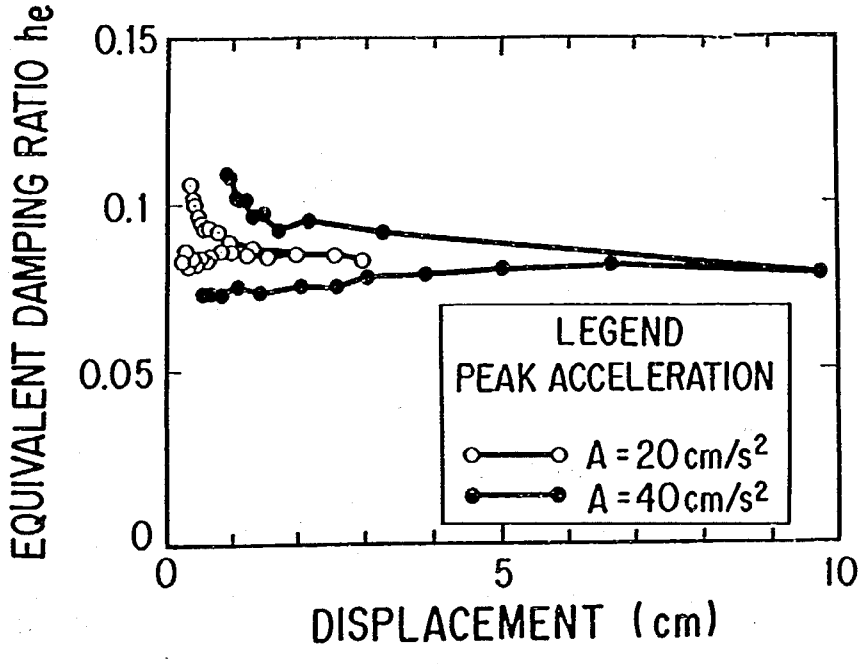


Fig.11 Hysteresis Loop of Load-Displacement Relation of Rubber Bearing



(1) Equivalent Stiffness



(2) Equivalent Damping Ratio

Fig.12 Equivalent Stiffness and Equivalent Damping of Rubber Bearing obtained through Harmonic Excitation Test

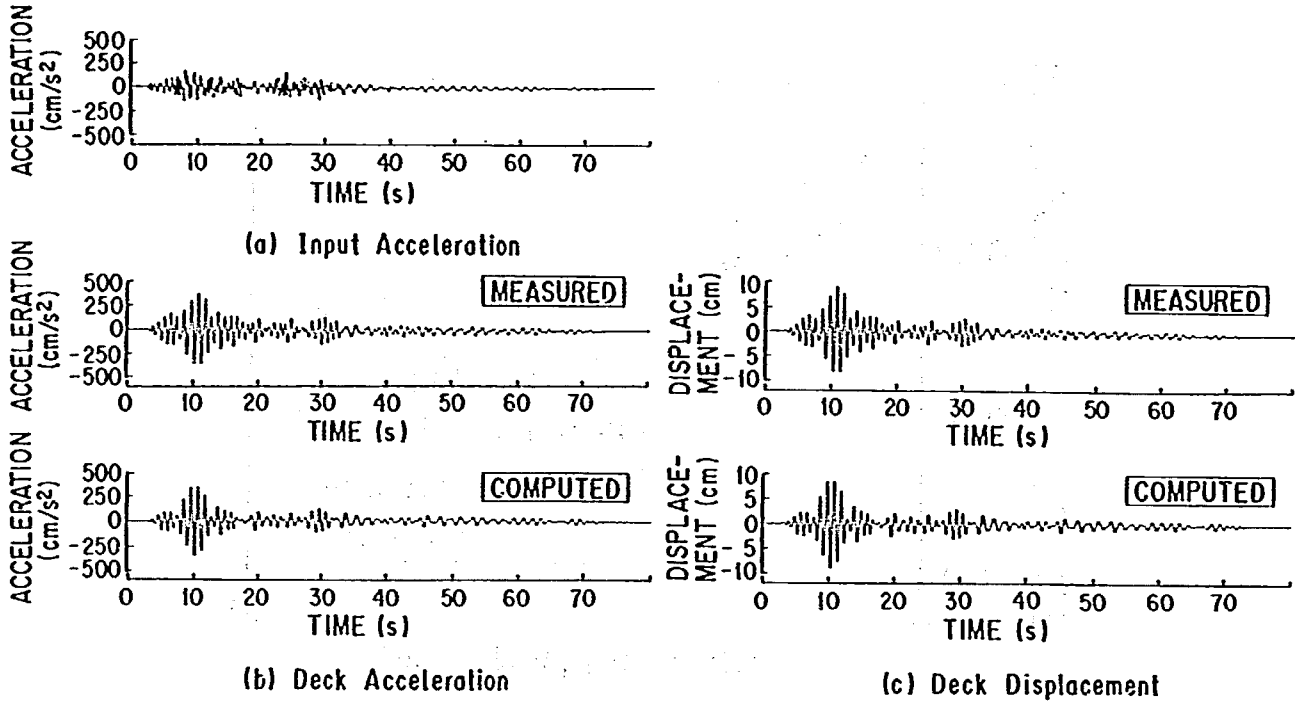


Fig.13 Responses of the Model Bridge without Control

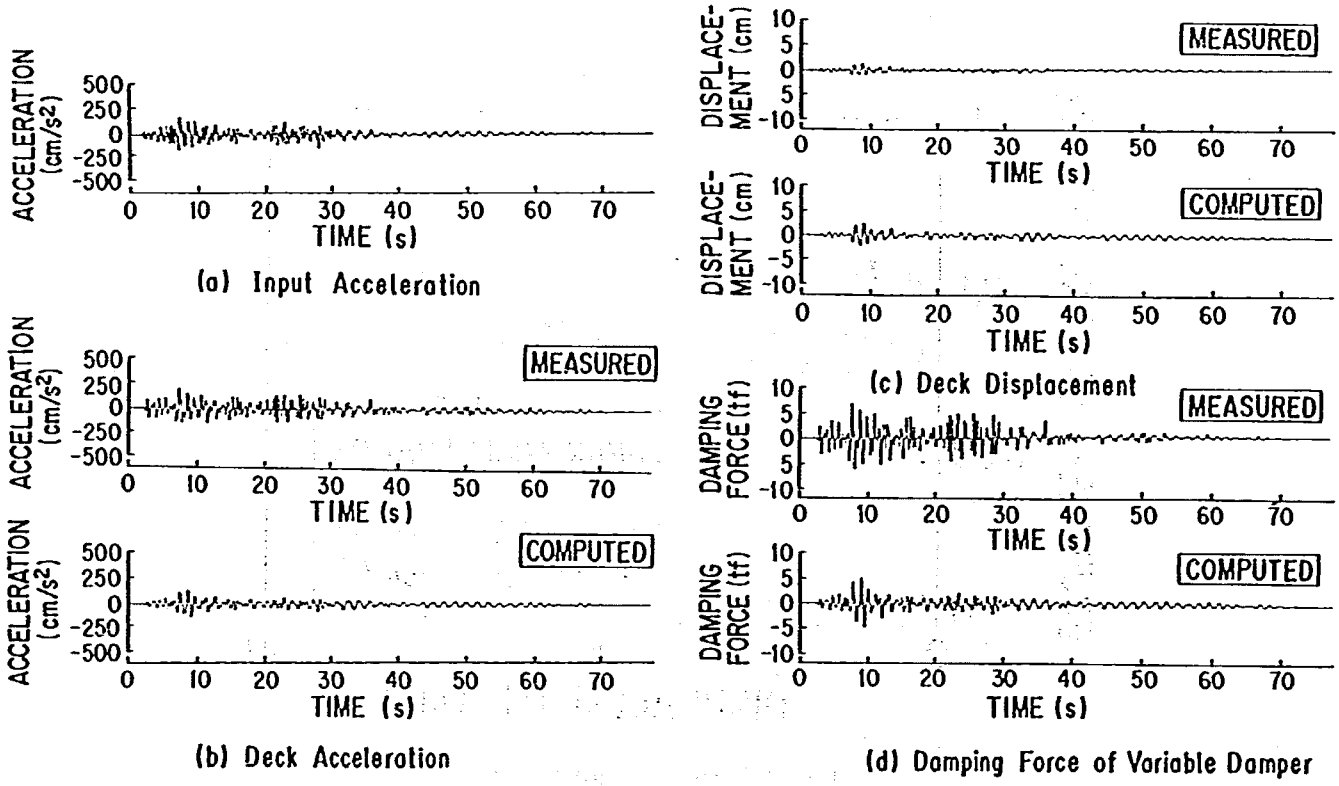


Fig.14 Responses of the Model Bridge with Control against a Table Motion with Peak Acceleration of 200cm/s²

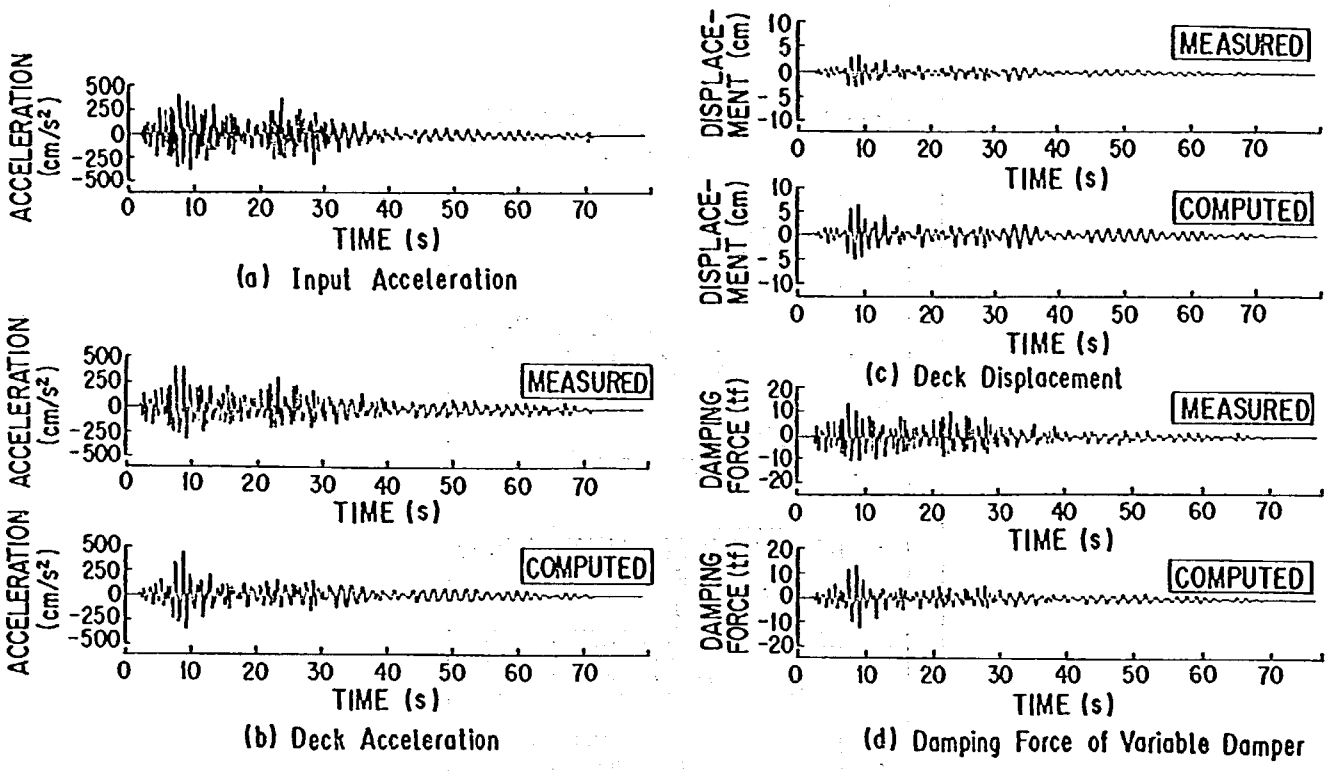


Fig.15 Responses of the Model Bridge with Control against a Table Motion with Peak Acceleration of 500cm/s²

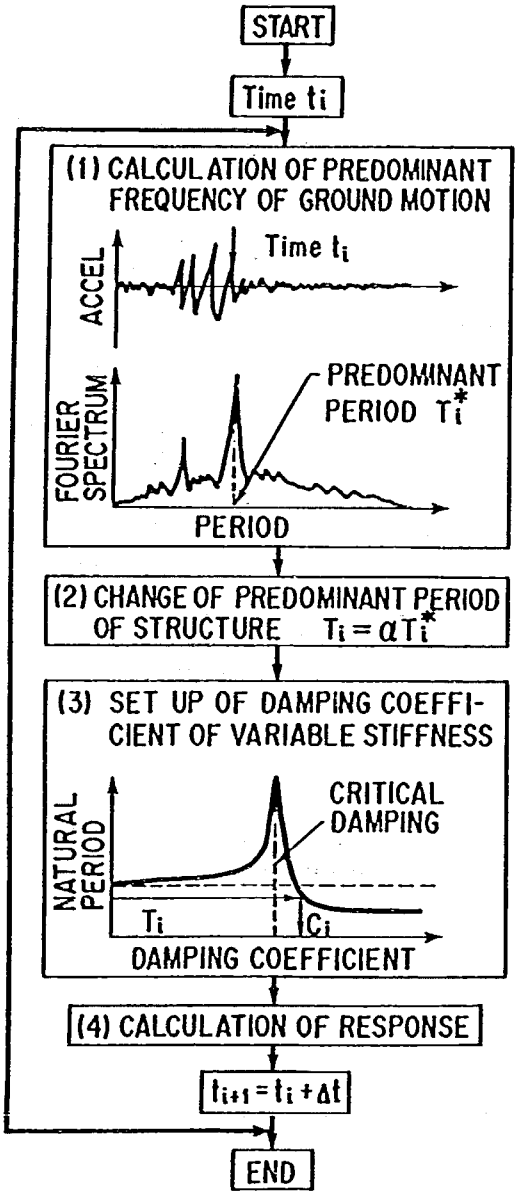


Fig.16 Control Algorithm of Variable Stiffness

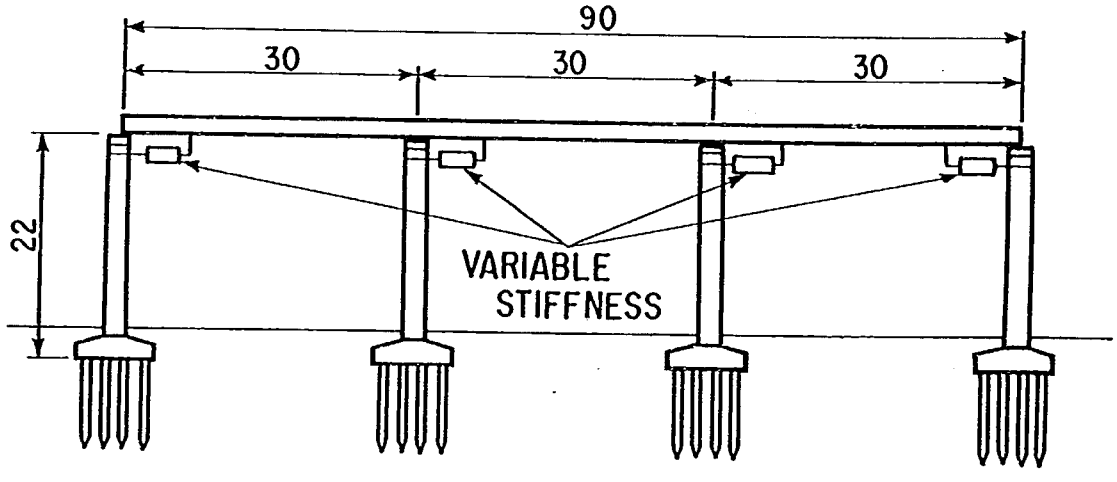


Fig.17 Model Bridge Analysed

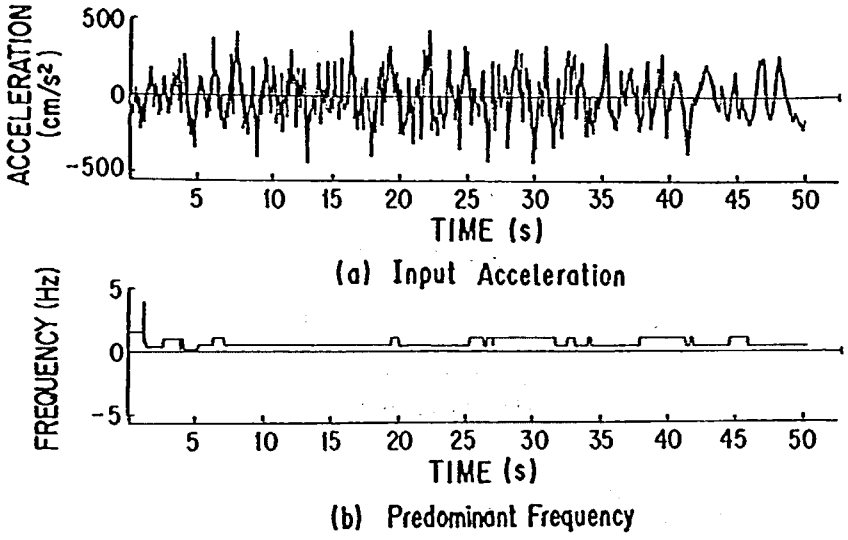


Fig.18 Input Acceleration and the Predominant Frequency

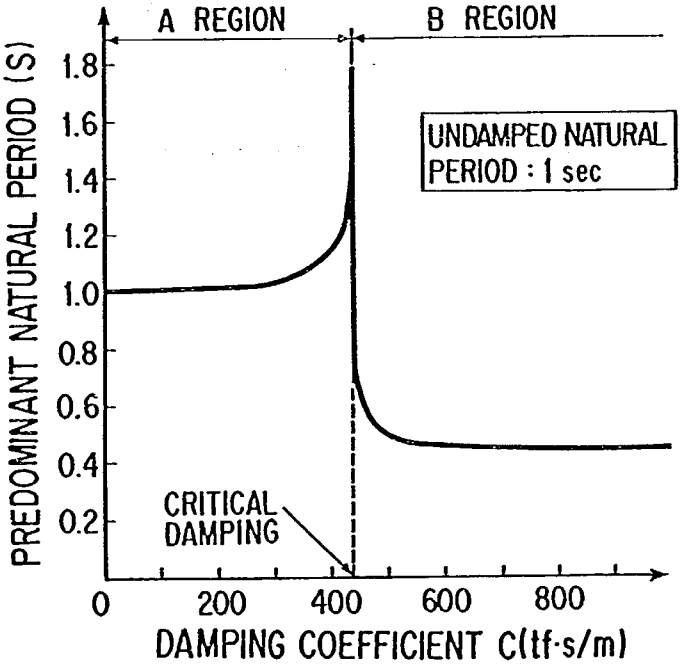


Fig.19 Relation between Damping Coefficient of Variable Stiffnesses and Predominant Natural Period of the Bridge

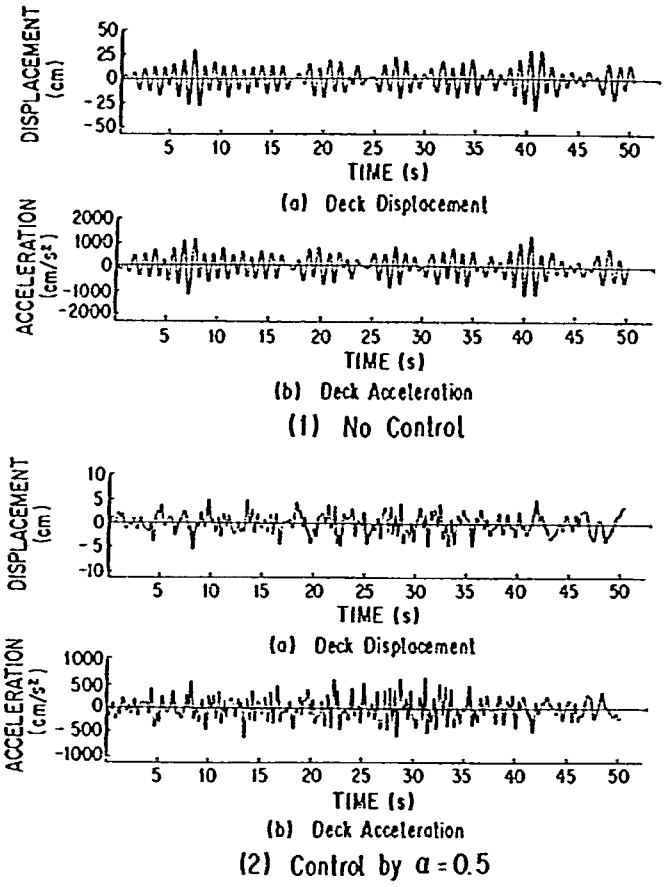


Fig.20 Comparison of Deck Responses

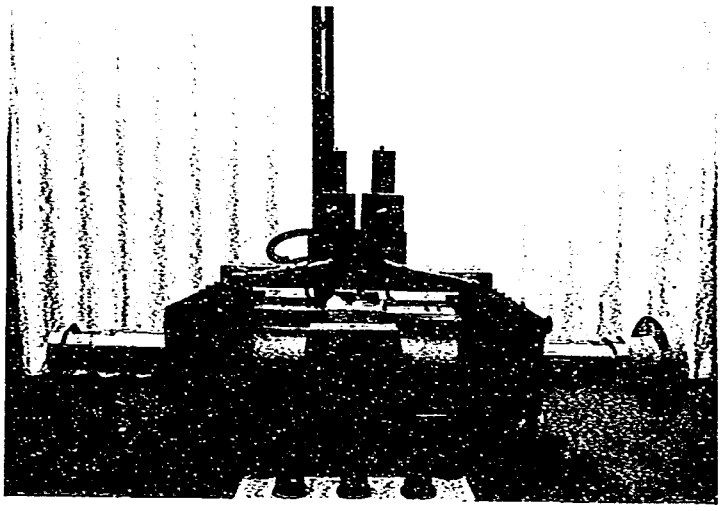


Photo 1 Prototype Model of Variable Damper Developed



Photo 2 Set up of Shaking Table Test

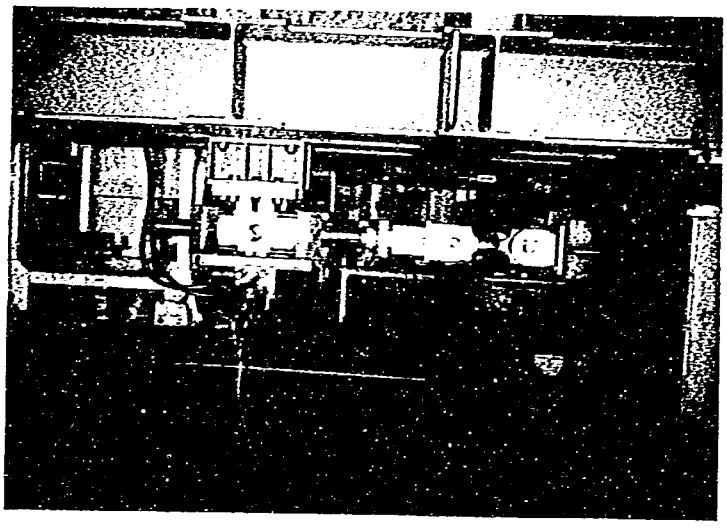


Photo 3 Set up of Variable Damper

Infrastructures Damage by Cairo, Egypt, Earthquake of October 1992 and Flores Island, Indonesia, Earthquake of December 1992,.

Tomomitsu FUJII
and
Kazuhiko KAWASHIMA

25th Joint Meeting of The U.S.–Japan
Cooperative Program In
Natural Resources Panel on
Wind and Seismic Effects
Tsukuba, Japan
May, 1993

INFRASTRUCTURES DAMAGE BY CAIRO, EGYPT, EARTHQUAKE OF OCTOBER 1992 AND FLORES ISLAND, INDONESIA, EARTHQUAKE OF DECEMBER 1992

by Tomomitsu FUJII[1] and Kazuhiko KAWASHIMA[2]

ABSTRACTS

Presented in this paper is the damage of infrastructures caused by the Cairo, Egypt Earthquake of October 12, 1992 and the Flores Island, Indonesia Earthquake of December 12, 1992. Ground motion estimation, damage feature, liquefaction, tsunami and earthquake preparedness are described. Importance of training and education as well as damage information dissemination are also presented.

KEY WORDS : Cairo Earthquake, Flores Island Earthquake, Ground Motion, Damage Feature, Liquefaction, Tsunami, Earthquake Preparedness

1 INTRODUCTION

Although earthquake preparedness is extremely important for preventing damages due to an earthquake, it is generally quite difficult in the areas where frequency of occurrence of earthquakes is low. In such areas, the accumulation of scientific knowledge on an earthquake and earthquake damage has not been made, and this sometimes amplifies the damage.

In late 1992, the Cairo, Egypt, Earthquake and Flores Island, Indonesia, Earthquake occurred. For cooperating disaster mitigation and restoration, the Japan International Cooperation Agency dispatched the Japan Disaster Relief Team to Egypt and Indonesia. The mission dispatched to Egypt was consisted of 9 members and was headed by Professor Tsuneo Ohkada, Institute of Industrial Science of University of Tokyo. The mission dispatched to Indonesia included 8 members and was headed by Professor Katsuyuki Abe, Earthquake Research Institute of University of Tokyo. Because two authors of this paper joined into the two missions, summary of the damage[1][2] and lessons learned from the two earthquakes are presented.

2 CAIRO, Egypt, EARTHQUAKE

2.1 Outline of the Cairo Earthquake

An earthquake with moment magnitude of 5.8 occurred at 15:09 (local time) on October 12, 1992 at about 30 km south-west of Cairo city as shown in Fig. 1. Because Egypt has long history, the data on historical earthquakes can be traced as old as B.C. 2,800[3]. Fig. 2 shows the epicenters of the earthquakes which occurred around Cairo. The epicenters of historical earthquakes which were determined from old documents are included in Fig. 2. The latest earthquake which hit the Cairo area occurred on August 7, 1847 at Faiyum[4]. About 185 persons were killed by this earthquake. There have been no disastrous earthquakes around Cairo for about 150 years till the Cairo Earthquake of October 12, 1992.

Fig. 3 shows the accumulated number of earthquake vs. earthquake magnitude within 300 km around the north Cairo from 1952 to 1985[5]. It is seen from Fig. 3 that the averaged annual number of an earthquake with magnitude of 6 or larger is 0.05. The maximum credible earthquake is said about 6.8. On the other hand, Fig. 4 shows the same relation within 300 km around the Tokyo Bay, Japan from January 1885 to December 1979[6]. The averaged annual number of an earthquake with magnitude of 6 or larger is about 3. This means that the frequency of occurrence of an earthquake in Egypt is about 1/69 of that in Tokyo, Japan. As can be anticipated from this evidence, it has been believed by public that no earthquake occurs in Egypt.

The main damage by the Cairo Earthquake is summarized as shown in Table 1. The casualties and injured were mostly developed in Cairo, Giza and Faiyum. Almost 200 students were killed in panicked stampede rather than by the collapse of school buildings. 73 peoples were killed at Heliopolis by a collapse of an apartment building in which number of story was illegally increased from 8 to 14. Photos 1 and 2 show the damaged building soon after the collapse and the foundation after debris was removed. Because no evidence showing failure of the foundation and surrounding soils were seen, it is considered that the damage was developed due to inadequate strength of the building.

Fire by the earthquake did not fortunately occurred.

Damage mostly occurred at old un-reinforced masonry and adobe housings as shown in Photos 3 and 4. Damage to new buildings was generally small. Damage to infrastructures was also limited.

1) Director of Earthquake Disaster Countermeasures Division, Disaster Prevention Bureau, National Land Agency
2) Head of Earthquake Engineering Division, Earthquake Disaster Prevention Department, Public Works Research Institute, Ministry of Construction

2.2 Ground Motion and Soil Condition

Because no strong motion accelerographs were installed in the vicinity of Cairo and the epicentral area, strong motion records were not obtained. Because evaluation of the intensity of ground shaking at the damaged area is difficult based on the instrumental records, it was made based on the empirical attenuation equation.

Based on the analysis of 394 components of free field strong motion records, the peak ground acceleration may be estimated as[7] :

$$a_{max} = 233 \times 10^{0.3131M} \times (R + 30)^{-1.218} \quad (1)$$

where

a_{max} : peak ground acceleration (cm/sec2)
M : earthquake magnitude
R : epicentral distance (km)

Assuming the surface magnitude of 5.3, the attenuation of peak ground acceleration is predicted by Eq.(1) as shown in Fig. 5. Because the epicentral distance is ranging from 30 km to 40 km at Giza and Cairo area, respectively, the peak ground acceleration a_{max} predicted by Eq. (1) is about 70 cm/sec^2 at Giza and 60 cm/sec^2 at Cairo. These values provide the preliminary insight for the ground acceleration developed at the damaged areas. It should be however noted that Eq.(1) gives the mean value of the measured acceleration, and has a large scatter around the mean value. When one considers one standard deviation from the mean value, the value predicted by Eq. (1) has to be multiplied by 1.7 and 1/1.7.

Fig. 6 shows a soil condition at Cairo city across the Nile River. Cairo city is located on the river terrace and soft alluvial deposits along the river.

2.3 Seismic Codes

Because of low frequency of occurrence of an earthquake, no seismic design seems to be presently made in Egypt for infrastructures. However design and construction of infrastructures are apparently better than those for ordinary buildings which suffered destructive damages due the the earthquake.

An example of the better design and construction is seen for road bridges. Comprehensive descriptions on loads, materials and allowable stress are specified in the Egyptian Code of Practice for Steel Constructions and Bridges (Ministerial Decree, No. 451-1989) and the Egyptian Code of Practice for Soil Mechanics and Foundation (Part 1 - Part 10, Ministerial Decree, No. 451-1989). Descriptions on seismic effects are few, and only some descriptions on soil liquefaction are provided in the Egyptian Code of Practice for Foundations Subjected to Vibrations and Dynamic Loads (Ministerial Decree, No. 449-1991). The treatment of the liquefied soil in design is not precisely stipulated.

However according to the General Authority of Roads and Bridges, various considerations which are effective for increasing seismic safety of bridges have been implemented as :

1) In-situ loading test is generally made for at least two piles per site for studying the load bearing capacity in vertical direction. Piles are subjected to vertical loading up to 2 times and 3 times of the design loading for the bearing piles and the friction piles, respectively, so as to confirm the yielding load. For example, a pile as shown in Photo 5 was subjected to 480 tf, which is twice as large as the design loading, at Faraskour Bridge.

2) Soils up to 8 m below the river bottom is generally disregarded in design of pile foundations as a design measure against scouring effect. Although the effect of soil liquefaction is not considered in design, such consideration is effective for increasing lateral stiffness of piles.

2.4 Damage of Roads and Bridges

Damage survey was made for Zamalek Overcrossing (Photo 6), Beni Suef Bridge, Faraskour Bridge (Photo 7) and Dessuk Bridge. No seismic damage was observed at those bridges. As was described in 2.3, design and construction seem conservative although seismic effects are not considered.

2.5 Damage of Lifelines

A visit to Rod El Farag Water Plant, Greater Cairo Water Supply Authority was made. No serious damage so as to affect the water supply was not developed by the earthquake. Only minor damage was developed at :

a) Cracks at masonry wall of a finished water pump station.
b) Increase of water leakage at a duct in the filters.
c) Offset and dislocation of a concrete wall of the clarifier (Photo 8).

2.6 Soil Liquefaction

Soil liquefaction was observed at Barmasht - El Alyat area. Several sand blow holes with a diameter as large as 4 m and a depth of 2 m were developed as shown in Photo 9. The sand spread over a paddy field. Fig. 7 shows the grain size accumulation curve of the sand. The average grain size D_{50} is 0.17 mm - 0.25 mm.

Although soil boring data at the site is not available, it is considered from the site inspection that the soil consists of saturated loose fine sand overlaid by cohesive clay with thickness of 1 - 2 m. Because the cohesive soil prevented the blow-up of water associated with the increase of pore-water pressure of sandy layer, the diameter of sand blow became quite large.

According to the eyewitnesses, the water and sand blew up as high as 3 m, and it continued about 45 minutes.

Based on the past experiences, it is known that the soil liquefaction tends to be developed in the area with a radius R from the epicenter as[2]

$$\log R = 0.77 M - 3.6 \qquad (2)$$

where

R : radius (epicentral distance, km)
M : earthquake magnitude

Fig. 8 shows the relation predicted by Eq. (2) as well as the observed data at Barmasht - El Aiyat (M = 5.3, R = 19 km). It is clearly seen that during the Cairo Earthquake the liquefaction occurred far from the threshold predicted by Eq. (2). This may be attributed to the fact that the sand at Barmasht area is extremely loose.

2.7 Restoration and Education on Earthquake

The Civil Defense Department, Ministry of Interior is responsible for rescuing victims under collapsed buildings by various disasters such as an earthquake and fire. The equipments in the department seem to be well maintained and the moral of the rescue team is excellent. Training for rescuing victims have been occasionally made.

Education on disaster to the public is also made in a room of the Public Relations Section of the Department, using video equipment. This kind of rooms are located in some other places. Even before the Cairo Earthquake, education and drill were made to the public in consideration of their importance.

However, panic of citizens in fear of the earthquake unfortunately occurred widely in Cairo and its vicinity. Especially, at scholar students panicked and many of them were injured or pressed to death when they tried to evacuate from the school buildings. For preventing such panic, public education and information dissemination in proper way are essential. Taking into account the evidence of the earthquake that affected variety of citizens in wide area, earthquake preparedness is very important not only at the central government but at local governments, schools and other agencies.

Because strength of buildings is not the same, it can not be compared in general sense, but it is educated in Japan through daily training not to evacuate confusedly from school buildings to outside but to keep staying underneath stable desks when an earthquake occurs. Because it is very important to respond without confusion against an earthquake, educations and training are repeatedly made through various opportunities and methods including dissemination of information by pamphlets which can be easily understood by the public. And also because the Great Kanto Earthquake which caused more than 140, 000 victims occurred on September 1, 1923, this day is designated as a special day for Disaster Prevention. Various trainings are made nation-widely on the Disaster Prevention Day so that citizens can have experience and training against disasters.

A number of persons who lost their housings stayed in tents provided by the Government as shown in Photo 10. At the area where aid could not be provided, people lived in a private tent as shown in Photo 11. Many people lived in tents not only because they lost their housing but because they had strong feared of the occurrence of aftershocks.

Egyptian people had been in fear of aftershocks for long time since October 12. Every time when a small aftershock occurred many people evacuated from housings, and some of them stayed outside in fear of possible collapse of the housings.

Furthermore the Japan Disaster Relief Team members had many inquiries from individuals and mass-media on the potential occurrence of a next large earthquake. Some peoples were in fear of occurrence of volcanic eruption.

The NRIAG (National Research Institute of Astronomy and Geophysics) immediately determined, on the basis of available seismic data in Helwan Station, the preliminary epicenter of the mainshock and sent this information to the Ministry of Scientific Research. And the NRIAG reports the number of aftershock twice a day at 9:30 and 15:30 to the Ministry. The earthquake information on the mainshock was officially announced on October 14.

There is no section responsible for releasing earthquake information to press and citizens in NRIAG nor in the Egyptian Government Offices. Thus, seismologists and researchers in NRIAG are faced to respond to various inquiries from press and citizens.

When a large earthquake occurs, it is extremely important to provide fast and accurate information about the earthquake not only to

administrative organizations but to public for mitigating earthquake disaster. In Japan, the Japan Meteorological Agency is responsible for this task, and reliability of the Agency is well recognized.

Timely and proper dissemination of the information on evaluation of future seismic activities based on scientific basis is very important together with public education. However, improvident information dissemination, to the public without enough scientific knowledge on the earthquake activity, based only on pure seismological point of view may cause panic. On the other hand, lack of information causes unnecessary fear among the public. It is therefore important to disseminate the earthquake information so that the public easily understands it and so that it is consistent with various aid activities. It is essentially important to disseminate scientific information on an earthquake, volcanic eruption and disasters before disasters occur.

3 FLORES ISLAND, INDONESIA, EARTHQUAKE

3.1 Outline of the Flores Island Earthquake

An earthquake with surface magnitude of 7.5 occurred at 13:29 (local time) on December 12, 1992 at north coast of the Flores Island, Indonesia as shown in Figs. 9 and 10. The epicenter is 8.48 ° S and 121.93° E.

The Flores Island has the length of about 360 km and width of 12 - 70 km. There are 19 volcanoes in the island. The Flores Island, which is a part of Nusatenggara Timur Province, is of Manggarai, Ngade, Ende, Sikka Flores Timur Regency.

Table 2 shows the human and building damage. Major damage was developed at Sikka, Ende, Ngada and Flores Timur Regency. Number of death was 2,080, and about 70 % of the total death concentrated at Sikka Regency. Damage was especially destructive at Maumere city which is on the alluvial fan deposit formed by the River Kalimati.

Tsunami damage was destructive, and occurred extensively over at least 100 km along the cost of Flores Sea. About 50 % of the death was caused by tsunami. Major tsunami damage was developed at Babi Island and Wuring area near Maumere.

Building damage concentrated on unreinforced masonry buildings as shown in Photo 12.

3.2 Ground Motion

Although it is said that 57 strong motion accelerographs are installed in Indonesia, no information regarding the location of the accelerographs and the strong motion records by the earthquake was obtained.

Assuming that the earthquake magnitude M of 7.5, the peak ground acceleration predicted by Eq. (1) attenuates as shown in Fig. 11. Because the sites are so close with the fault, it was assumed that the epicentral distance in Eq. (1) be measured from the center of the fault zone instead of the epicenter. The distance at Maumere and Ende is then approximately 25 km and 80 km, respectively. The peak ground acceleration from Eq. (1) is therefore evaluated as 0.4 g at Maumere and 0.2 g at Ende.

3.3 Damage by Tsunami

Extensive damage was developed due to tsunami along the coast of Flores Sea. In particular, damage at Babi Island and Wuling was destructive. At Babi Island, a village with population of about 950 was completely damaged as shown in Photos 13, 14 and 15. About 750 were killed by the tsunami at this island. The tsunami height is estimated as high as 3.7 m.

Photos 16, and 17 show the destructive damage at Wuling. The maximum tsunami height is estimated as 2.45 m.

3.4 Damage of Roads and Bridges

Extensive damage was developed in roads and bridges in Flores Island. Fig. 12 shows the major National Roads and Provincial Roads in the damaged area. Major damage was concentrated on the National Road connecting Ende and Maumere, National Road connecting Maumere and Larantuka, and the Provincial Road connecting Maumere and Magapanda.

The most serious damage was developed at National Road between Ende to Maumere which crosses in mountainous area. Because Ende and Maumere are the two major cities in the island, suspension of traffic between the two cities cause various problems for transportation in the island. As shown in Fig. 13 the road was suspended at 18 sites between Ende and Maumere.

Major damage at this route was developed by slope failure as shown in Photo 18. Fig. 14 classifies the type of failures. At the site where one side was cut and the other side was embanked (cut and filled embankment), the filled embankment often settled and this caused extensive cracks on the pavement. Failure also occurred at cut slopes and natural slopes. Destructive failure in which not only the cut slope but the natural slope failed as shown in Photo 19 were also observed at several sites.

Stone falling as shown in Photo 20 was observed

at several sites.

Extensive damage of pavement and bridges were developed by soil instability along the Flores Sea. Single span or two span simply supported girder bridges, which were probably constructed before the Second World War, often suffered settlement and tilting of abutments and back soils as shown in Photo 21: The settlement was as large as 1m. Such settlement and tilting of abutments were mostly caused by sliding of surrounding soils as shown in Fig. 15.

There are several new steel truss girders supported by reinforced concrete single columns or frame piers as shown in Photo 22. Damage was generally less in the truss bridges. The rubber cushion as shown in Photo 23 placed at the end of the deck behaved quite well for reducing the impact between the deck and the abutment wall.

3.5 Damage of Irrigation Facilities

A water barrier on a river near Nebe suffered damage on the parapet wall of water gate as shown in Photos 24 and 25. The parapet wall tilted with the back side being apart from the soil. Large settlement was developed at the back soils along the wall. Leakage of water from the parapet wall was seen. Photo 26 shows damage of the water gate.

3.6 Damage of Ports

The Maumere Port as shown in Photo 27 suffered extensive damage due to tsunami and soil liquefaction in addition to the ground shaking. The quay wall and retaining wall for the apron overturned toward sea side and was badly damaged as shown in Photo 28.

Photo 29 shows a boat and a truck attacked by the tsunami.

3.7 Damage of Airport

The Control Tower of the Maumere Airport and the Ende Airport was badly damaged. The Control Tower at the Maumere Airport is four story masonry building, and was subjected to extensive shear failure at the wall with the glass being broken. The control Tower at Ende Airport is three story masonry building, and was suffered significant shear failure at the wall as shown in Photo 30. The damage was so extensive that they could not be used. The apron and run-way suffer no damage at both Airports.

3.8 Damage of Lifelines

Water supply was interrupted at wide area in Flores Island. In Maumere a number of main wells were badly damaged due to the earthquake. This caused suspension of water supply for three days after the earthquake. Although the damage was repaired, amount of the supply was still about 50 % of the normal supply even two weeks after the earthquake. The water was delivered by water-tank vehicles as shown in Photo 31.

At Ende, the electricity is generated by 7 diesel engine generators as shown in Photo 32. They did not suffer damage. Masonry wall of the building storing the generators fell down at two locations. Because cables distributing electricity were ruptured at several sites, the electricity was suspended for two days after the earthquake. This caused problems for water supply.

3.9 Soil Liquefaction

Soil liquefaction was developed extensively along the coast of Flores Sea.

Fig. 16 shows a soil profile at Maumere. The ground condition is of sandy soils with the thickness of about 30 m - 50 m overlaid by top soil with about 5 m thickness. Because water table is shallow, the sand at Maumere is quite vulnerable to liquefaction.

Fig. 17 shows the grain size accumulation curve for the three specimens obtained at three sites along the Flores Sea. The averaged grain size D_{50} is 0.15 - 0.44 mm.

From Fig. 8 which shows the empirical relation by Eq. (2), it is anticipated that liquefaction occurred as far as 150 km from the epicenter.

Special interest was large soil settlement and lateral soil movement developed widely along the coast of Maumere city as shown in Photo 33. At this site large settlement probably as large as 1 $\sim$ 2 m was developed along the coast. Photo 34 shows the settlement of storage yard. Several cracks on soils and road pavement were seen as shown in Photo 35 parallel to the coast. It is considered that the lateral spreading due to liquefaction caused such large settlement and lateral movement of top soils.

3.10 Restoration and Rehabilitation

Emergency activities were made based on the Declare of the President of Republic of Indonesia under the cooperation of central government, province, regency, sub-regency and Armed Forces as shown in Fig. 18. Because the regency office suffered damage, the Chief of the regency took command of the Headquarters for Disaster Countermeasures at the Governor's official residence.

The first-aid stations were placed in Maumere to

provide the first-aid treatment. Fortunately hospitals were functional after the earthquake, and medical care could be made as shown in Table 3. There were sufficient supply for medical and pharmaceutical products in Maumere. But at Ende, the relief supplies were not enough because road transportation between Maumere and Ende was interrupted.

There were no serious trouble for daily living at Maumere because business service was resumed soon after the earthquake and relief supplies were provided. At Ende, however, the relief supplies were not enough because of road damage between Maumere and Ende. Although helicopters were used for distributing supplies, the amount of distribution was limited.

Many peoples stayed in tents after the earthquake. Lack of tents made many peoples be accommodated in open space like the military camp. Approximately 100 tents were pitched as shown in Photo 36 in a park near the official residence at Maumere. Because almost 10 families were accommodated in a large tent, there seems to be approximately 3,000 - 4,000 peoples in the tents.

It was planned to complete the emergency actions and the rehabilitation works by the early January 1993 and the end of March 1993, respectively. The rehabilitation of public facilities such as roads had the highest priority. It was planned to complete the repair of the National Road connecting Maumere and Ende by the early January, 1993. Many heavy construction machines such as bulldozer were transported from main island. The rehabilitation of public facilities and schools need the high priority. The target date for resuming schools was the early January 1993.

Because there are no major cities and sufficient road network in Flores Island, materials required for restoration and daily living needed to be supplied by sea and air transportation from Jawa Island. This resulted in two weeks for initiating the full restoration. It is learned from the evidence that active support of the central and regional governments is inevitable for prompt restoration. For such purpose, it is of great importance to evaluate damage degree immediately after an earthquake based on close collaboration among related ministries, and to restore the damage under clear strategy.

4 CONCLUDING REMARKS

Damage feature of infrastructures in the Cairo, Egypt, Earthquake of October 1992 and the Flores Island, Indonesia, Earthquake of December 1992, were briefly described. Based on the survey on the damage and earthquake preparedness in Egypt and Indonesia, the following conclusions may be pointed out :

1) Design and construction of infrastructures are far better in both countries than those for private buildings. Seismic damage of important infrastructures was limited.

2) Because infrastructures which have been so far constructed are small in size, seismic damage developed was limited in the two earthquakes even if seismic effects were not considered. But seismic effects are required to be considered in design for constructing modern infrastructures with large size.

3) Damage of roads caused serious problems in wide areas in Flores Island. Because damage of infrastructures considerably affects function of the region, significant attention needs to be paid for preventing damage of infrastructures.

4) Tsunami caused destructive damage along coastal areas. Education on tsunami behavior and training for evacuation are extremely important as well as appropriate tsunami warning systems and countermeasures for mitigating propagation of tsunami.

5) Improvident information dissemination to the public on future earthquake activities may cause panic when the public does not have enough scientific knowledge on an earthquake. It is important to disseminate the information so that it can be easily understood and that it is consistent with the aid-activities.

6) There are no special advises for two countries for mitigating seismic damage. Because earthquakes repeat in the future, it is the only way to provide appropriate preparedness. It includes seismic design, seismic evaluation, seismic strengthening, disaster information systems, and education and dissemination on damage of disaster. A standard procedure for evaluating vulnerability of exiting structures needs to be established with the highest priority.

7) If one classifies the earthquake environment in terms of the frequency of occurrence and the earthquake magnitude, a matrix such as the one presented in Table 4 may be obtained. It is generally difficult to take an appropriate measure against earthquakes at the areas where frequency of occurrence of earthquakes is low as shown in Table 5. Special attention needs to be paid in such areas for preventing seismic damage.

Because safety of structures is a matter to be evaluated from economic and benefit point of view, relative importance between economy and safety of structures needs to be carefully

considered. For example, in designing nuclear power stations, the highest priority is placed on safety of the facilities. They are designed against the maximum credible earthquakes at the site. On the other hand, ordinary infrastructures and buildings are designed so that essential function be maintained for JMA (Japan Meteorological Intensity) Intensity V, and fatal damage be prevented even for JMA Intensity VI. It is often evaluated that JMA Intensity V and VI is referred to the peak ground acceleration of 0.08 - 0.25 g and 0.25 - 0.4 g, respectively, although it is very rough because such intensity depends both on strength of ground motion and strength of structures. This is concept that structures need to keep their function against the earthquakes with high probability to occur within the structures lifetime, and to prevent collapse even against the larger earthquakes.

8) Avoiding unreinforced brick and adobe structures is the most essential measure for preventing seismic damage of structures developed in the two earthquakes. This is true for reducing structural damage by an earthquake all over the world. In Japan, construction of unreinforced brick structures which was imported from European countries after the Meiji Restoration in 1867 was prevented after the destructive damage developed in Nohbi Earthquake in 1892 and the Kanto Earthquake in 1923. If brick structures continue to be constructed, destructive damage may be developed still now. Because it is generally difficult in low seismic areas to consider seismic effect in design, technical development which enables to adopt more ductile materials is required. Because Japanese did not have an impression that wooden housings are poor construction, it was not so difficult to avoid the brick constructions. Because wooden constructions are vulnerable to fires, various countermeasures for preventing spread of fires such as an increase of road apace and adoption of fire-proof sidings and walls are being made. It is also repeatedly educated to extinguish fires at kitchen and stoves for preventing fire ignition.

ACKNOWLEDGEMENTS

The authors would like to express their sincere appreciation to the invaluable supports provided by various governmental organizations of Arab Republic of Egypt and Republic of Indonesia. Without supports provided by the Japanese Embassy and JICA Office in Egypt and Indonesia, survey could not be made so smoothly. Voluntary effort by the Japanese who were in Egypt and Indonesia is also greatly appreciated. Special appreciation also goes to the kind cooperation and assistance of the members of Japan Disaster Relief Team of the Japan International Cooperation Agency.

References

1) Japanese Expert Team as Dispatched by the Japanese Government through Japan International Cooperation Agency : Preliminary Report on Cairo, Egypt Earthquake of October 12, 1992, October 1992
2) Japanese Expert Team as Dispatched by the Japanese Government through Japan International Cooperation Agency : Preliminary Report on Flores Island, Indonesia Earthquake of December 12, 1992, December 1992
3) Kebeasy, R. M. : Seismicity of Egypt, Proc. Workshop on the Broad-band Seismic Network for the Mediterranean, CCSEM, September 1990
4) Ibrahim, E. M. : Seismic Activity in the Different Techtonic Provinces of Egypt, 4th Egyptian Training Course on Earthquake Engineering, Egyptian Society for Earthquake Engineering, November 1990
5) Albert, R. N. H. : Seismicity and Earthquake Hazard at the Proposed Site for a Nuclear Power Plant in the Anshars Area, Nile Delta, Acta Geophysica Polonia, Vol. 35, No. 4, 1987
6) Kawashima, K. : Seismic Damage of the Cairo, Egypt Earthquake of October 1992, Civil Engineering Journal, Vol. 35-3, March 1993
7) Kawashima, K. and Aizawa, K. : Attenuation of Peak Ground Acceleration, Velocity and Displacement Based on Regression Analysis of Japanese Strong Motion Records, Earthquake Engineering and Structural Dynamics, Vol. 14, pp.199-215, 1986
8) Kuribayashi, E. and Tatsuoka, F. : History of Earthquake Induced Soil Liquefaction in Japan, Bulletin of Public Works Research Institute, Vol. 31, 1977
9) Kawashima, K. and Uda, T. : Seismic Damage of Flores Island, Indonesia Earthquake of December 12, 1992, Civil Engineering Journal
10) Fujii, T. and Kawashima, K. : Seismic Damage of Cairo, Egypt Earthquake of October 1992 and the Flores Island, Indonesia Earthquake of December 1992, Journal of the Japan Society of Civil Engineers

Table 1 Major Damage by the Cairo Earthquake

(1) Human Damage	Casualty	561
	Injured	12,192
	Needs treatment in Hospital	2,270
	No needs treatment in Hospital	9,922
(2) Damage to Educational Facilities	Major Repair	2,301
	Minor Repair	3,569
	No use	1,087
(3) Damage to Mosque	Major Repair	211
	Minor Repair	544
(4) Damage to Monuments	Major Repair	14
	Minor Repair	104
(5) Damage to Homes and Houses	Major Repair	4,395
	Minor Repair	22,235
	No use	7,796

Table 2 Main Damage of the Flores Island Earthquake

Regency	Population ('85) (Prs)	Area (km^2)	Human Damage				Building Damage				
			Dead (Prs)	Injured		Missing (Prs)	Office (house)	Church Mosk (house)	People House (house)	School (house)	Others (house)
				Heavy (Prs)	Light (Prs)						
Sikka	236,691	1,731.9	1,457	252	1,256	8	56	47	10,200	324	4
Ende	212,349	2,046.6	229	106	227	—	344	193	13,804	281	154
Ngada	188,353	3,037.9	18	2	4	—	67	45	1,194	100	68
Flores Timur	267,295	3,079.2	376	15	241	61	26	22	2,920	80	50
Total	904,688	9,895.6	2,080	375	1,728	69	493	307	28,118	785	276

Note : 1) Human damage (Dead) in Flores Timur includes about 200 victims by Tsunami.
2) Building damage (Housing) includes partially damaged houses.
Souse : Army's Headquarters for Emergency Activities in WAIOTI Airport in Maumere on December 26, 1992.

Table 3 Number of Injured Who Had Medical Care at a hospital in Maumere

Date	Persons Who Visit Hospital	Persons in Hospital	Persons Who Took Medical Care	Dead	Persons Discharged From Hospital
12 Dec.'92	128	82	10	36	—
13	68	46	20	2	15
14	39	23	16	—	30
15	287	27	260	—	21
16	222	25	197	—	28
17	205	6	199	—	3
18	229	5	224	—	3
19	322	3	319	—	4
20	154	5	149	—	—
21	225	6	219	—	—
Total	1,879	228	1,613	38	104

Source : Army's Headquarters for Emergency Activities in WAIOTI Airport in Maumere.

Table 4 Classification of Earthquake Environment in terms of Frequency of Occurrence and Magnitude of Earthquakes

		MAGNITUDE OF EARTHQUAKE		
		Small ($M \leqq 7$)	Medium ($7 < M < 8$)	Large ($M \geqq 8$)
FREQUENCY	Low	Egypt Spain	Canada, Philippines, Indonesia	U.S.A. (Central and South)
	Medium	Armenia	Turkey	U.S.A. (West), New Zealand, China, India Mexico
	High			Japan, Chile Peru

Table 5 Difficulty of Preparedness against Earthquakes Depending on Frequency of Occurrence and Magnitude of Earthquakes

		MAGNITUDE OF EARTHQUAKE		
		Small ($M \leqq 7$)	Medium ($7 < M < 8$)	Large ($M \geqq 8$)
FREQUENCY	Low			
	Medium			
	High			

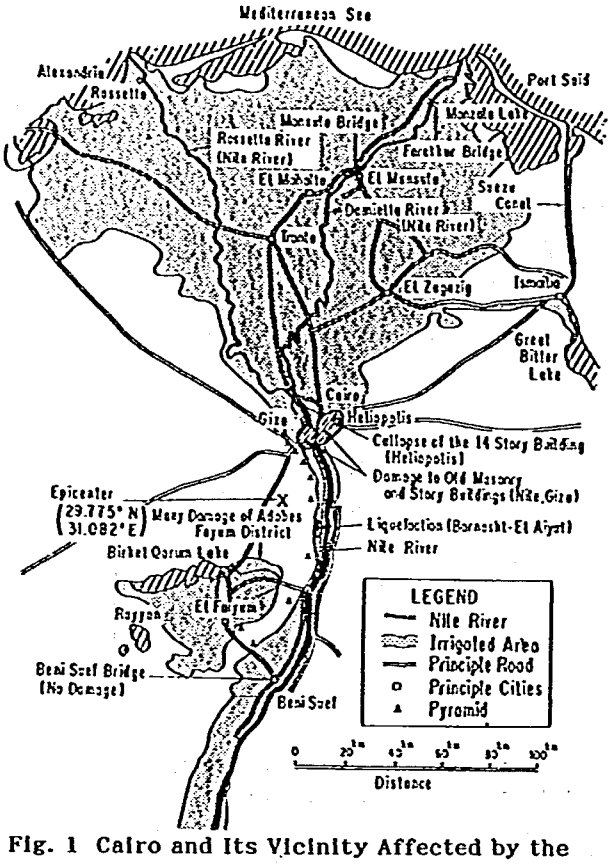


Fig. 1 Cairo and Its Vicinity Affected by the Cairo Earthquake

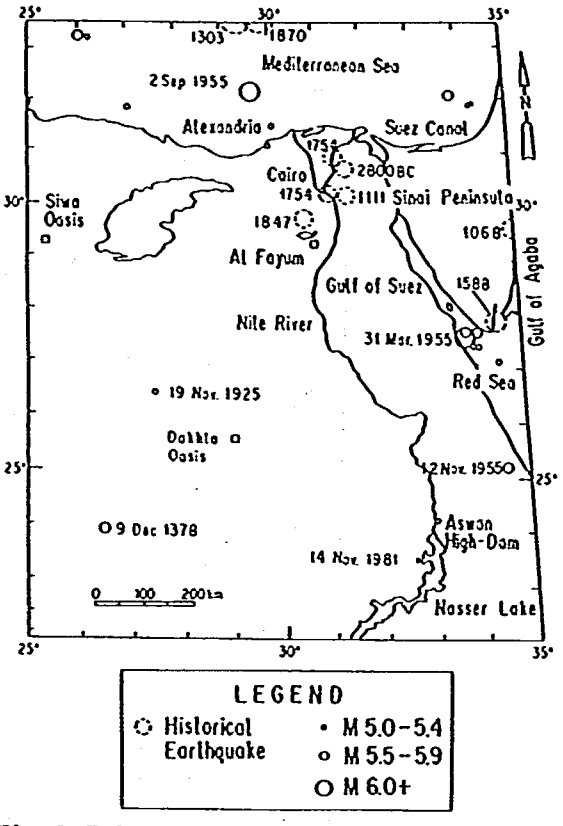


Fig. 2 Epicenter of the Past Earthquakes around Cairo

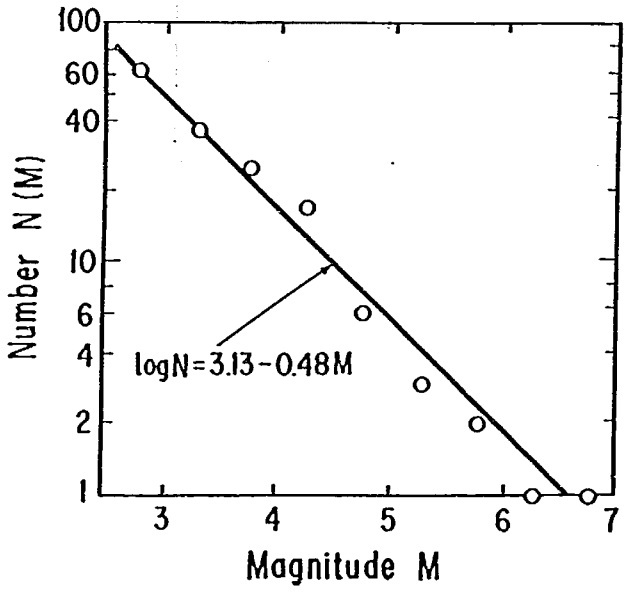


Fig. 3 Accumulated Number of Earthquakes within 300 km around north Cairo between 1952 and 1985[6]

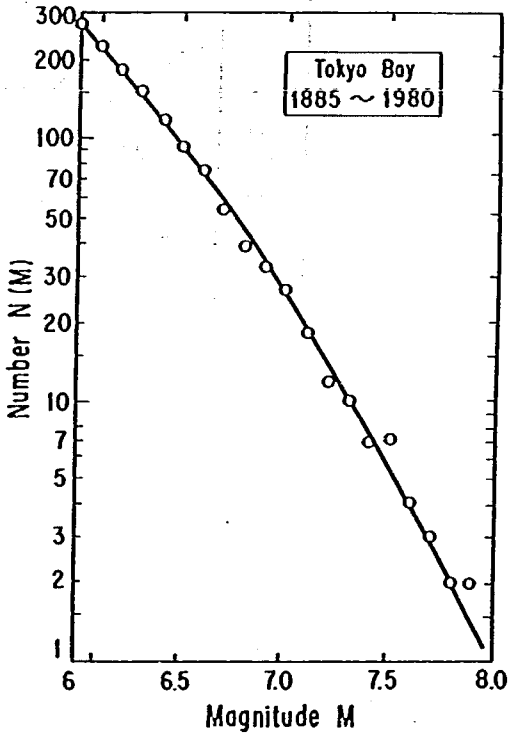


Fig. 4 Accumulated number of Earthquakes within 300 km around Tokyo Bay between 1885 and 1979

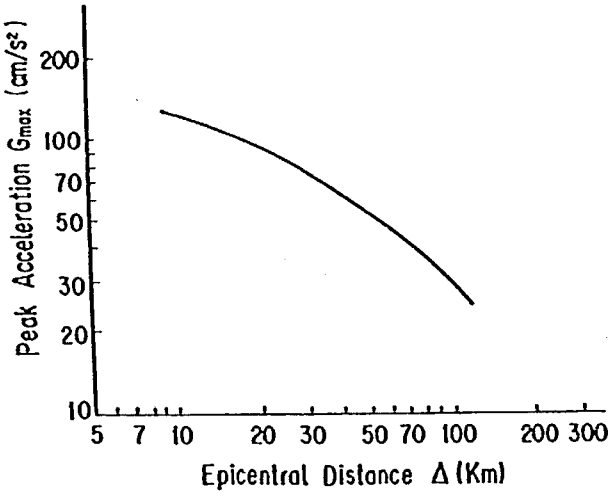


Fig. 5 Attenuation of Peak Ground Acceleration Predicted by Eq. (1)

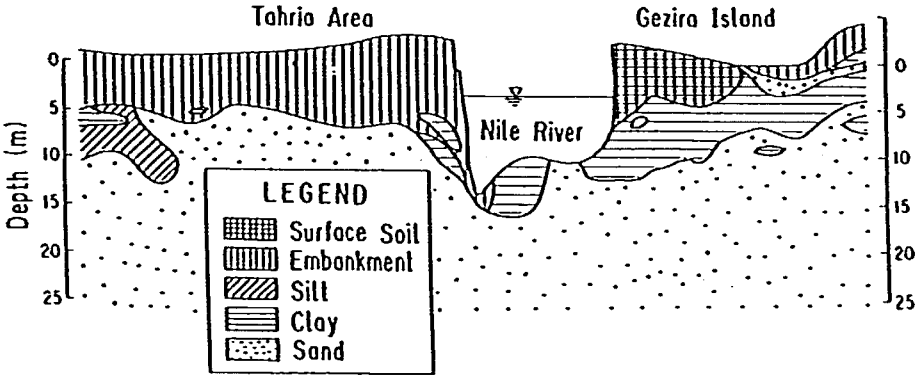


Fig. 6 Soil Condition at Cairo city

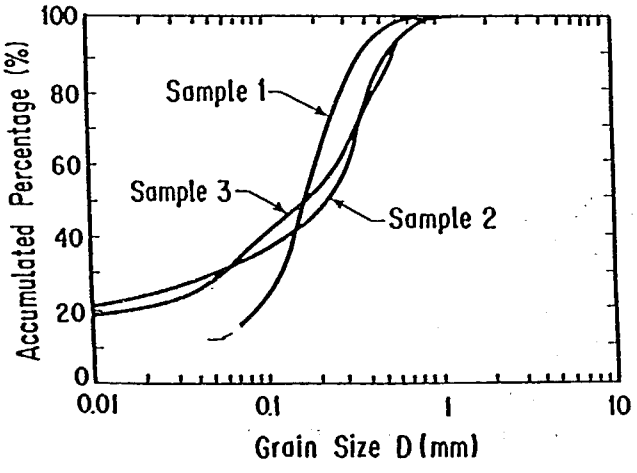


Fig. 7 Grain Size Accumulation Curve of the Liquefied Sand at Barmasht - El Alyat Area

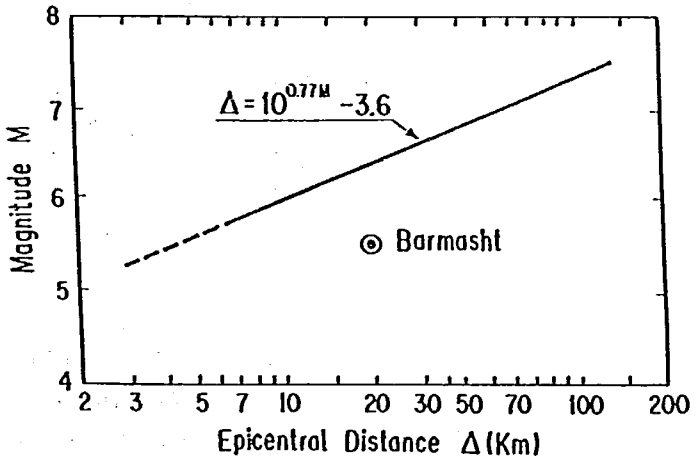


Fig. 8 Threshold for Causing Liquefaction

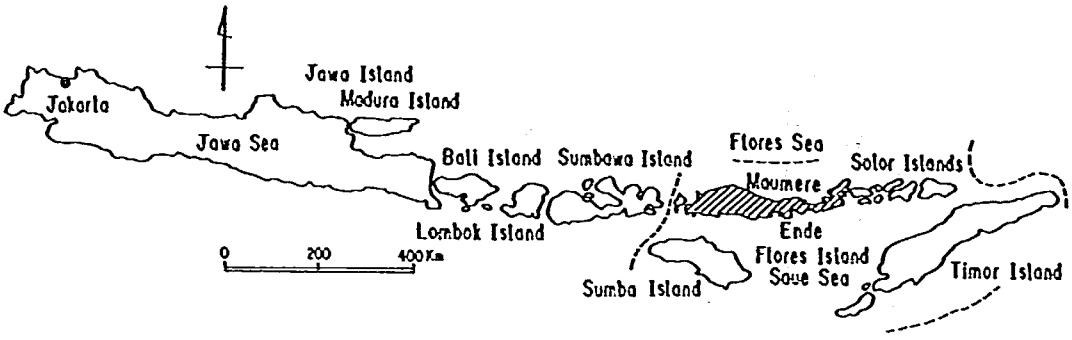


Fig. 9 Flores Island

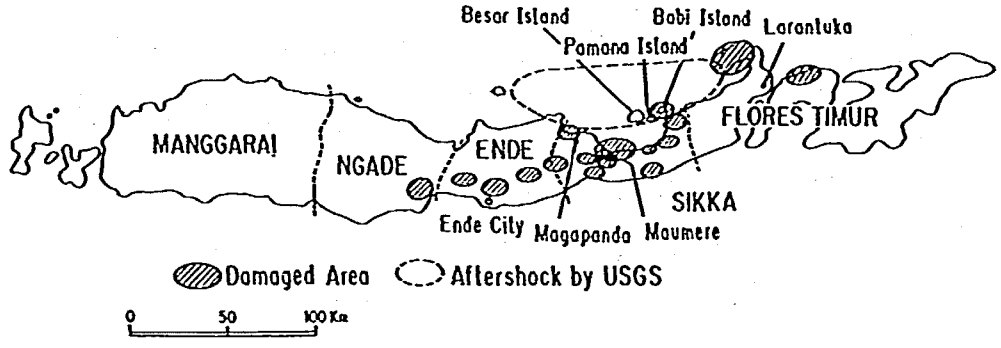


Fig. 10 Damaged Region and Aftershock Area

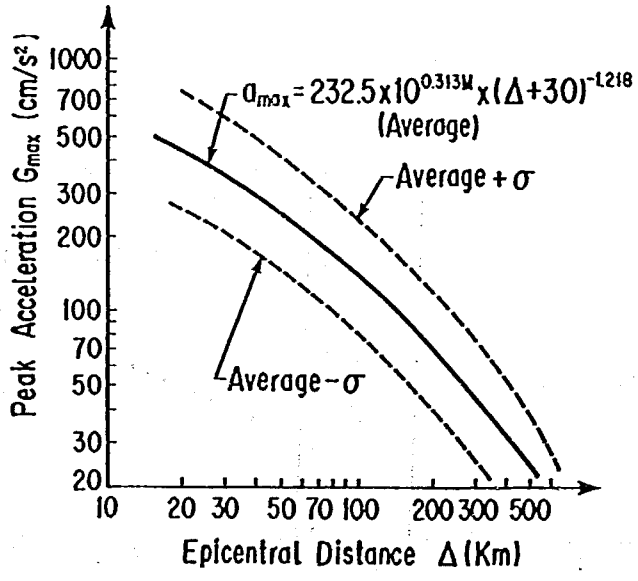


Fig. 11 Attenuation of Peak Ground Acceleration Predicted by Eq. (1)

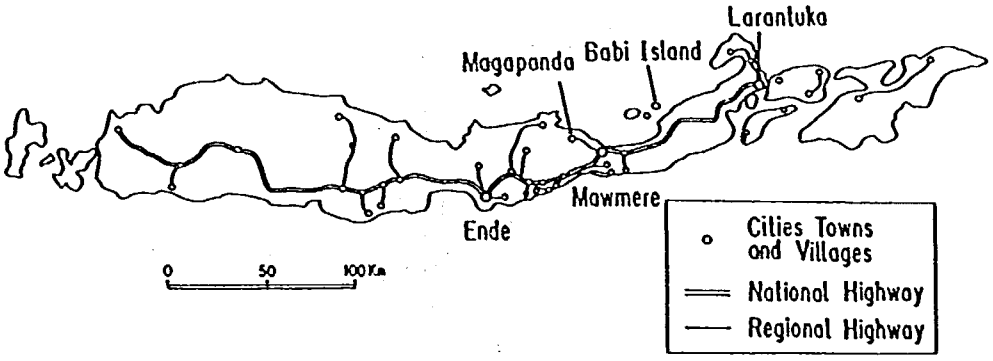


Fig. 12 Major National Roads and Provincial Roads in Flores Island

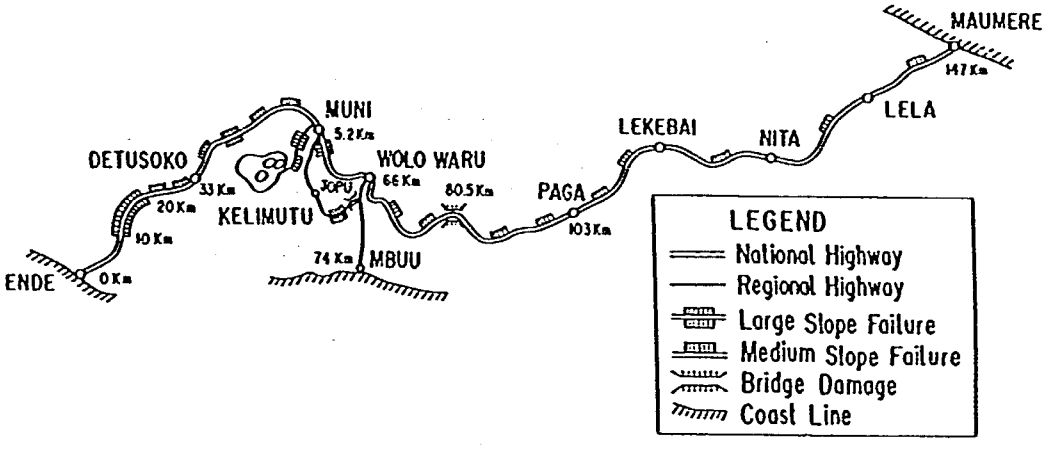


Fig. 13 Major Damage on National Road from Ende to Maumere

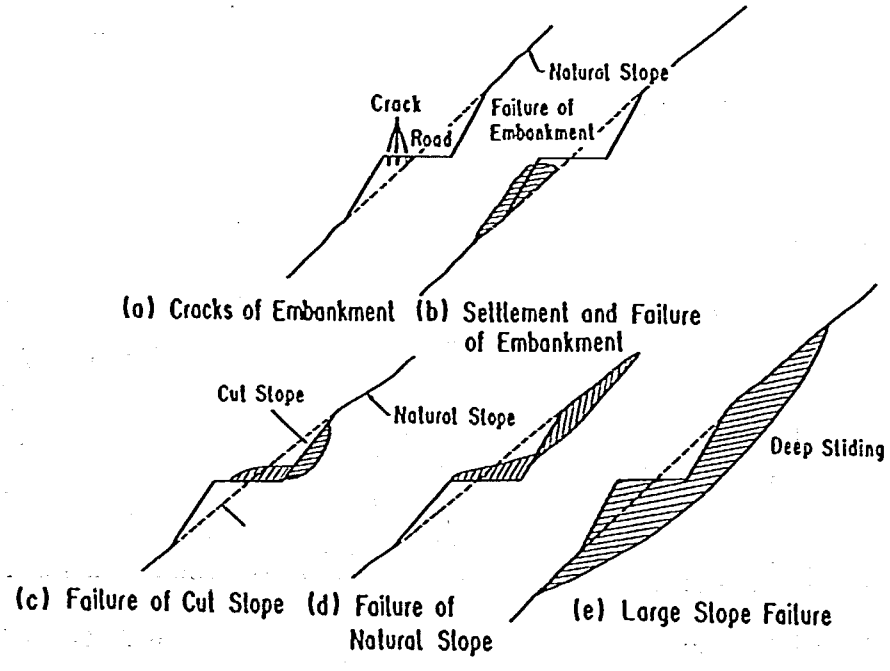


Fig. 14 Types of Slope Failure

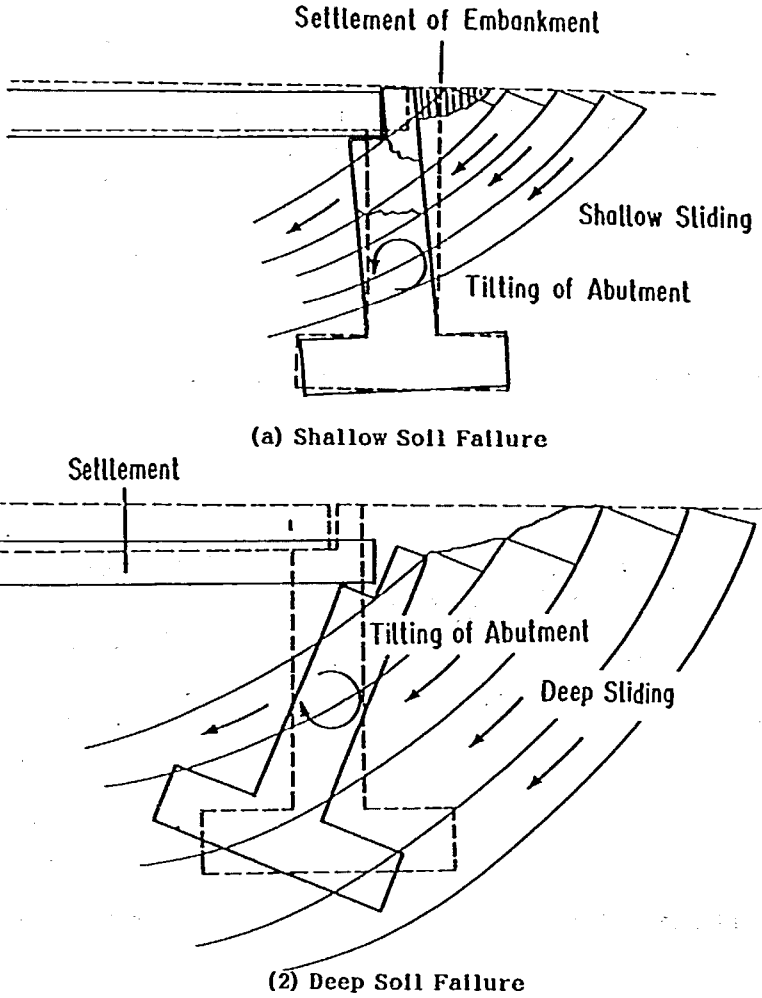


Fig. 15 Damage of Bridge Abutments due to Soil Instability

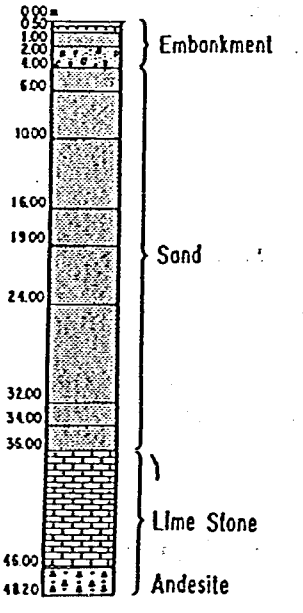


Fig. 16 Soil Profile at Maumere City

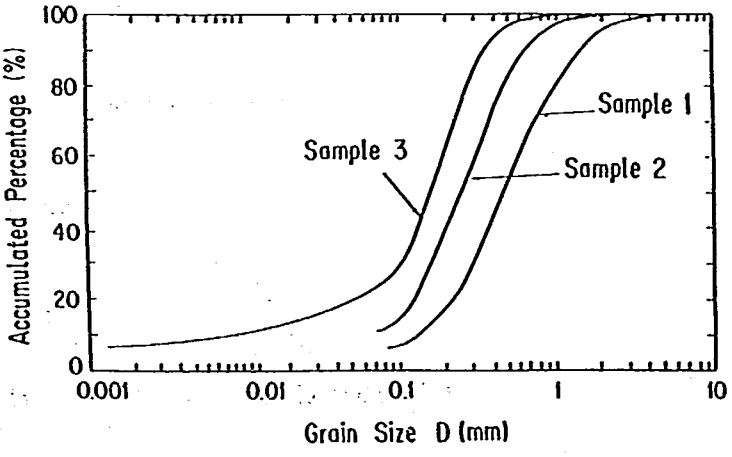


Fig. 17 Grain Size Accumulation Curve of Sand

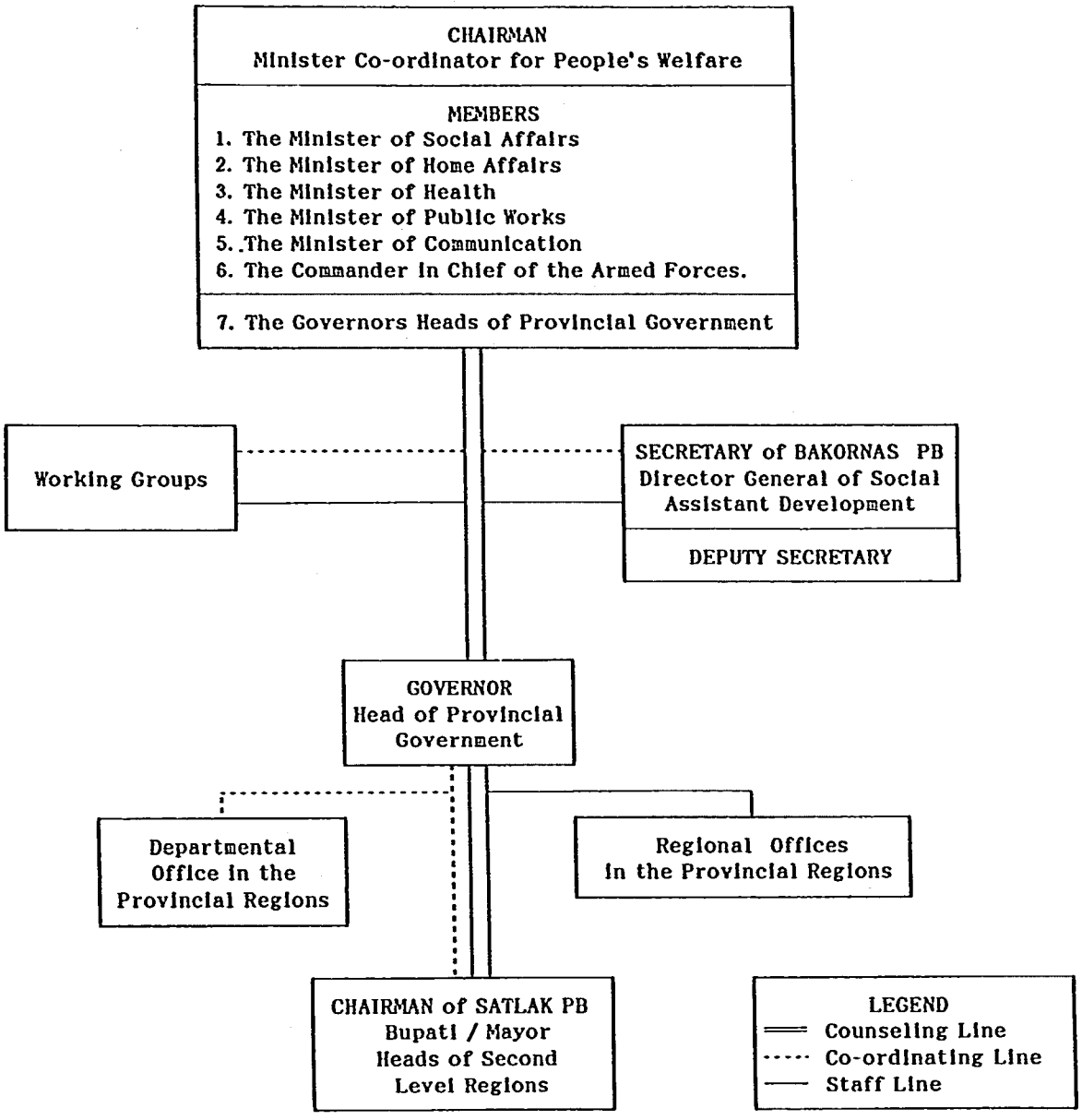


Fig. 18 Structure of Bakornas

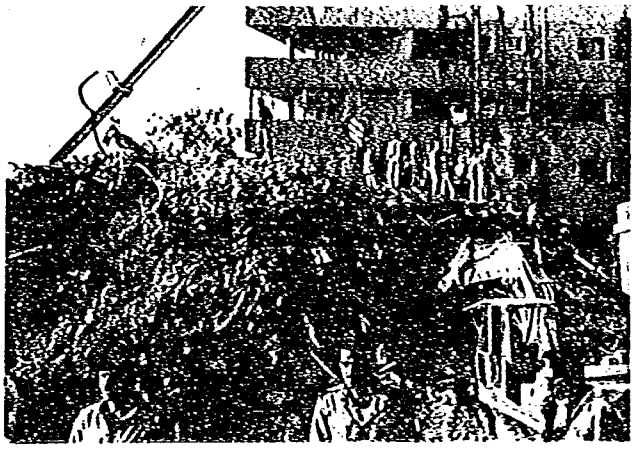


Photo 1 Collapse of 14-story Building at Heliopolis

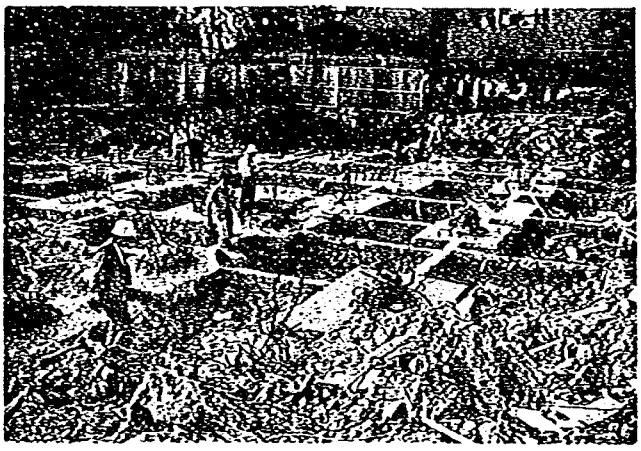


Photo 2 Foundation of 14-story Building



Photo 3 Damage of Adobe Housing at Faiyum

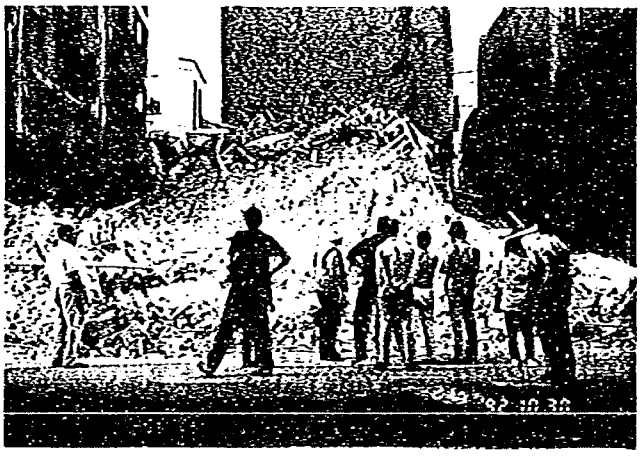


Photo 4 Damage of Unreinforced Masonry Buildings at Downtown Cairo

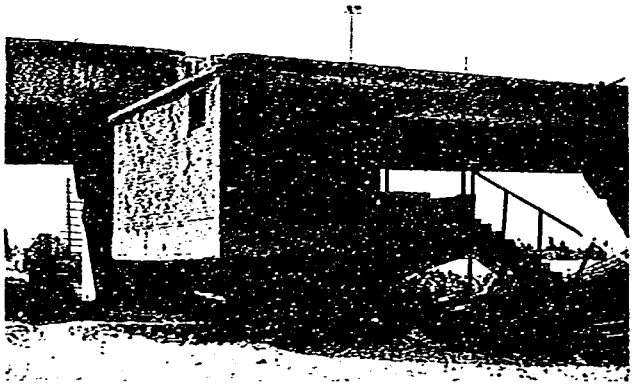


Photo 5 Test Pile Subjected to 480tf Loading (now used for Controlling House for the Site)

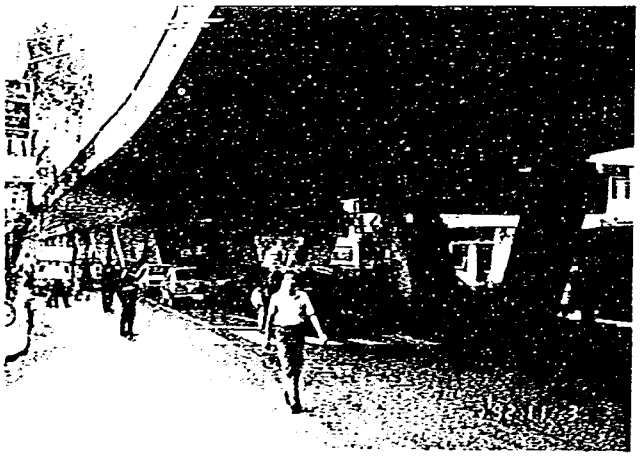


Photo 6 Zamalek Overcrossing (No Damage)

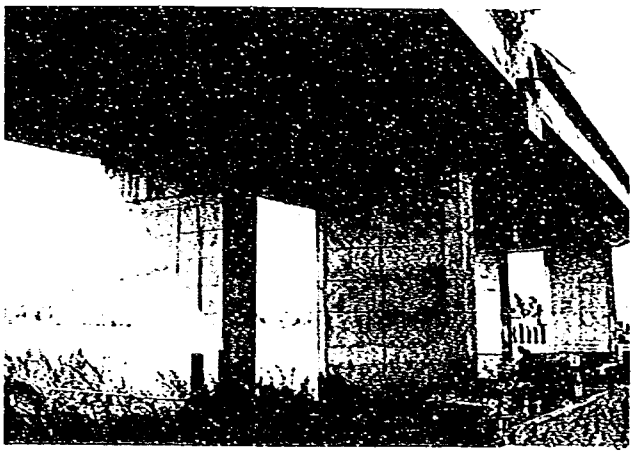


Photo 7 Fsaraskour Bridge (No Damage)

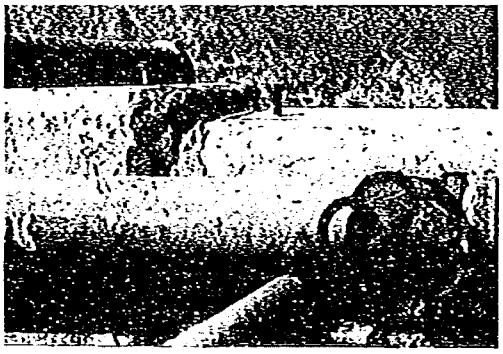


Photo 8 Offset of Concrete Wall of Clarifier



Photo 9 Sand Blow Hole due to Liquefaction at Barnasht - El Alyat



Photo 10 Emergency Tents

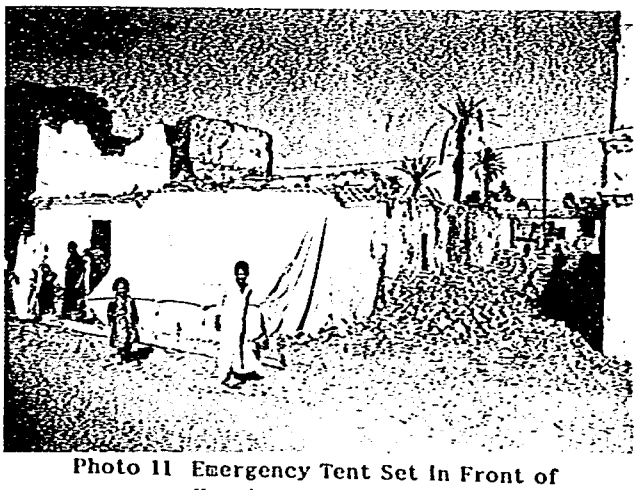


Photo 11 Emergency Tent Set in Front of Housing



Photo 12 Damage of Masonry Building



Photo 13 Damage of Babi Island due to Tsunami



Photo 14 Damage of Babi Island due to Tsunami



Photo 15 Damage of Babi Island due to Tsunami



Photo 16 Tsunami Damage at Wuling



Photo 17 Tsunami Damage at Wuling



Photo 18 Large Slope Failure



Photo 19 Destructive Slope Failure Including Cut Slope and Natural Slope



Photo 20 Stone Falling



Photo 21 Settlement of Bridge Abutment and Back-Fill

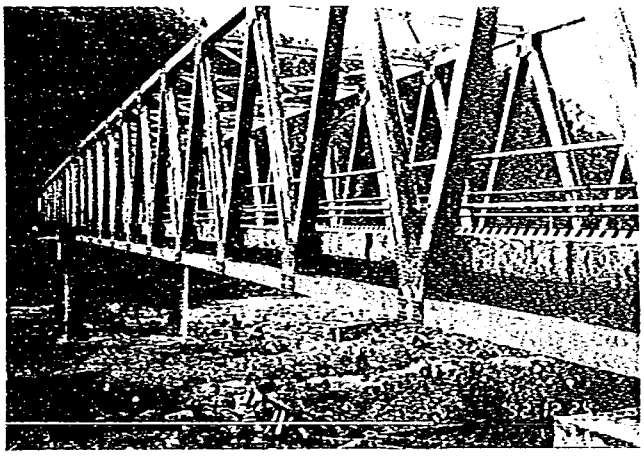


Photo 22 Truss Bridge

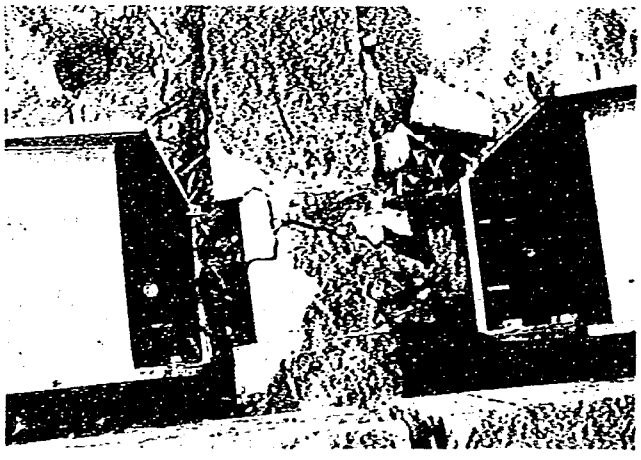


Photo 23 Longitudinal Stopper with Rubber Cushion

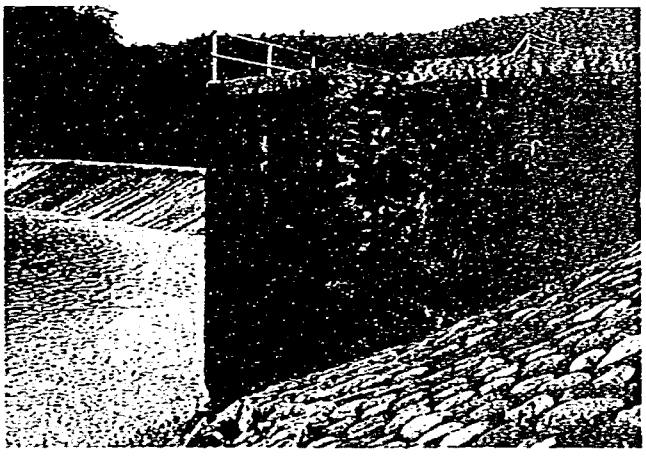


Photo 24 Damage of Concrete Block Cover along Water Barrier

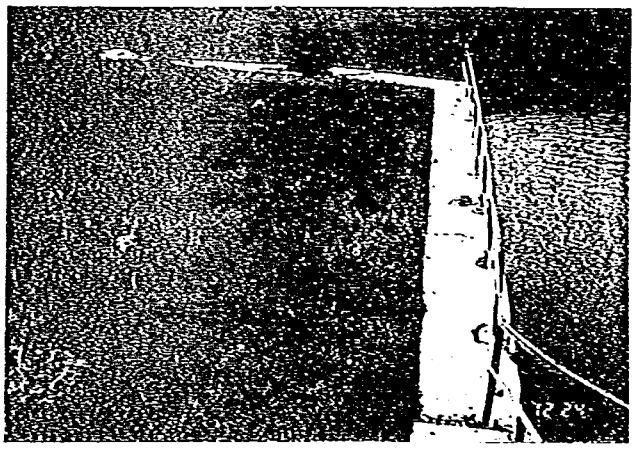


Photo 25 Tilting of Parapet Wall and Settlement of Back-fill



Photo 26 Cracks of Water Gate

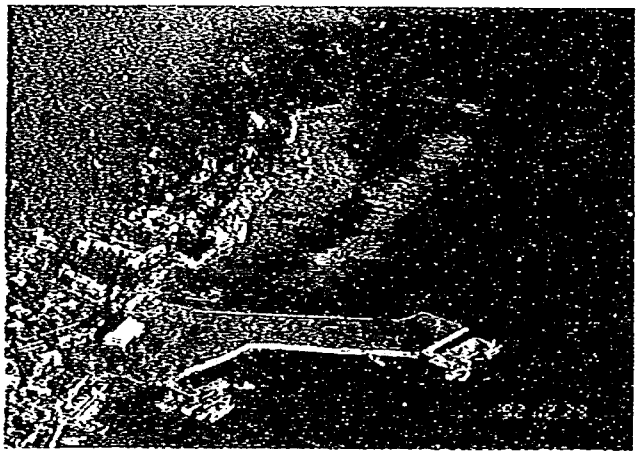


Photo 27 Maumere Port

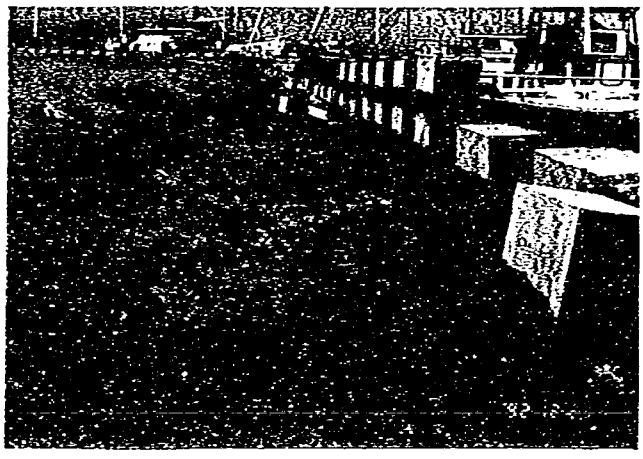


Photo 28 Tilting of Retaining Wall and Settlement of Back-Fill



Photo 29 Settlement of Apron and Failure of Wall (A Ship and A Boat which were surged by the Tsunami could be seen)

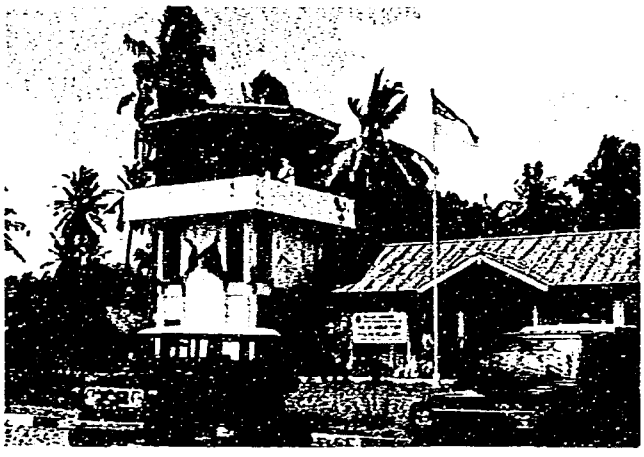


Photo 30 Damage of Control Tower at Ende Airport

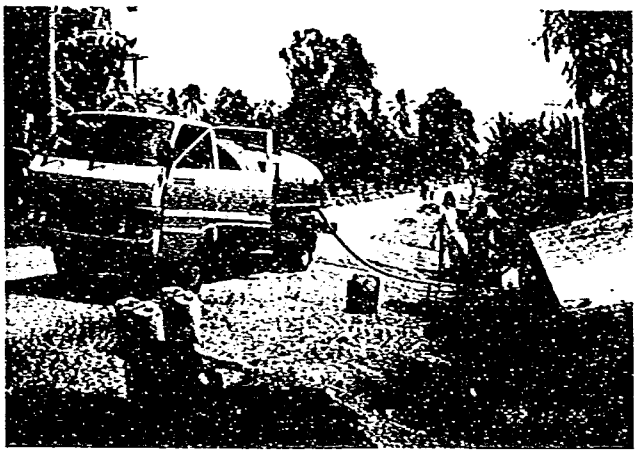


Photo 31 Emergency Water Supply by Water-Tank Vehicle near Ende

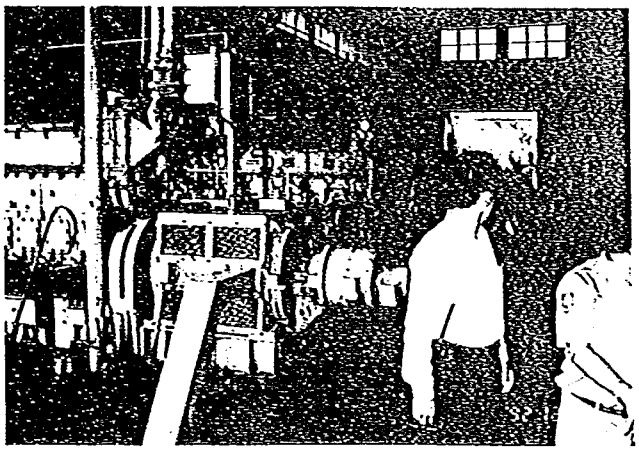


Photo 32 Diesel Generator for Electricity at Ende



Photo 33 Settlement and Lateral Soil Movement Developed around Maumere City



Photo 34 Settlement of Coast Line and Settlement of Storage Yard along the Coast



Photo 35 Cracks on Ground Surface along the Coast (Maumere city)

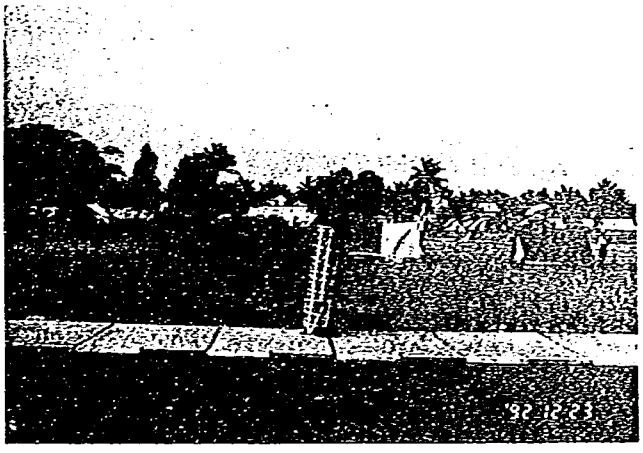


Photo 36 Emergency Tent Camp

Variable Dampers and Variable Stiffness for Seismic Control of Bridges

Kazuhiko KAWASHIMA
and
Shigeki UNJOH

International Workshop on
Structural Control
Hawaii, U.S.A.
August, 1993

VARIABLE DAMPERS AND VARIABLE STIFFNESS FOR SEISMIC CONTROL OF BRIDGES

by

Kazuhiko Kawashima [1] and Shigeki Unjoh [2]

1 Head, Earthquake Engineering Division, Public Works Research Institute, Ministry of Construction, Tsukuba Science City, Ibaraki-ken, Japan 305.
2 Senior Research Engineer, Earthquake Engineering Division, Public Works Research Institute, Ministry of Construction, Tsukuba Science City, Ibaraki-ken, Japan 305.

SUMMARY

This paper proposes the variable dampers which vary the damping coefficient depending on structural response, and the variable stiffness control in which the natural period of structures is varied depending on the structural response. Effectiveness of the variable dampers is presented through a numerical analysis and a series of shake table tests. The effectiveness of the variable stiffness control is also presented through a numerical analysis.

INTRODUCTION

Variable damper, in which damping coefficient can be variable dependent on structural response, for structural response control against an earthquake was proposed by the authors in 1989 (Kawashima and Unjoh 1989), and various studies have been made at the Public Works Research Institute. The variable damper has been effectively adopted in a field of mechanical engineering, in particular in a suspension system for an aircraft and an automobile. An active suspension for improving driving comfortableness and stability of automobiles is one of such examples (Sugawara 1986; Millikan 1987). However, it is a new idea to apply the variable damper for structural response control against an earthquake.

Variable stiffness is another interesting field of extension of the variable damper. If one shifts the natural period of structures, the structural response may be significantly reduced by avoiding the resonance with the ground motion.

This paper presents the current studies for the variable dampers and variable stiffness for response control of bridges against an earthquake.

VARIABLE DAMPERS

A unique technic in application of dampers to bridges is distribution of lateral force to as many piers as possible. Although damper is effective for reducing deck response, it is also effective for transmitting lateral force from deck to piers when it is used at over–damper range. Thus the damper stoppers have been successfully implemented in many bridges.

Because few energy dissipation is made in the damper stopper, it is effective to decrease the damping ratio so that energy dissipation can be made when the bridge is subjected to a ground motion caused by a large earthquake. Because the damper stopper is effective for preventing a small deck vibration associated with breaking loads and wind effects, the function as the damper stopper is effective at small deck displacement. On the other hand when the deck response becomes excessive during an earthquake, the stopper is required to present further build up of the deck response.

Thus, the variable dampers with the following requirements may be superior to the existing dampers and damper stoppers:

1) Damping coefficient is very large during a small deck vibration for preventing the deck vibration due to breaking loads of vehicles and wind effects. It is movable against the low rate motions such as the elongation of deck by temperature change.

2) Against the seismic response with the deck response over a certain value, the damping coefficient needs to be set so as to make energy dissipation maximum.

3) Against excessive deck response during an earthquake, high damping coefficient is required to function as a stopper. Smooth and gradual increase of the damping force may be effective for preventing shocks.

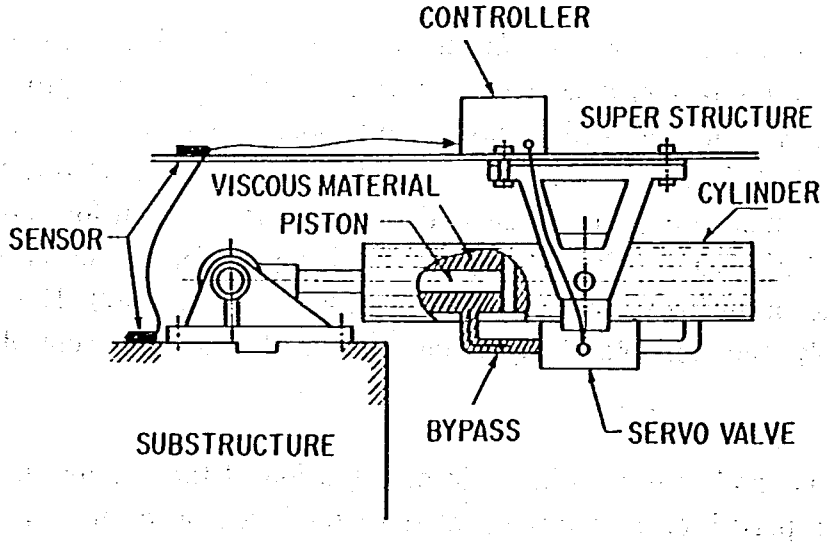


Fig. 1 Variable Damper

Although various types of the variable damper can be made, the simplest structure may be an piston–cylinder viscous damper as shown in Fig. 1. A by–pass is installed between the cylinder–cells divided by the piston. Damping coefficient of the damper can be controlled by varying an amount of viscous flow of the by–pass. Various technologies for controlling such flow are available. External energy required for such control is generally much smaller than that required for the active control.

EFFECTIVENESS OF VARIABLE DAMPERS

Fig. 2 shows the deck displacement dependent damping ratio of the variable damper proposed for bridges (Kawashima, Unjoh and Shimizu 1991, Kawashima, Unjoh, Nagashima and Shimizu 1991, Kawashima, Unjoh and Shimizu 1992). Various control algorithm may be used such as to vary h_1, h_2 and h_3 in time depending on bridge response for optimizing the deck response. The damping ratio can be varied depending on both the deck velocity and the deck displacement (Kawashima, Unjoh and Shimizu 1991). Partial control in which the control is made only partially in time can be made (Kawashima, Unjoh and Shimizu 1991). It should be noted that any relation between the damping ratio vs. the relative displacement and/or relative velocity can be incorporated in the analysis. The damping ratios h_1, h_2 and h_3 are assumed here to be constant during an earthquake.

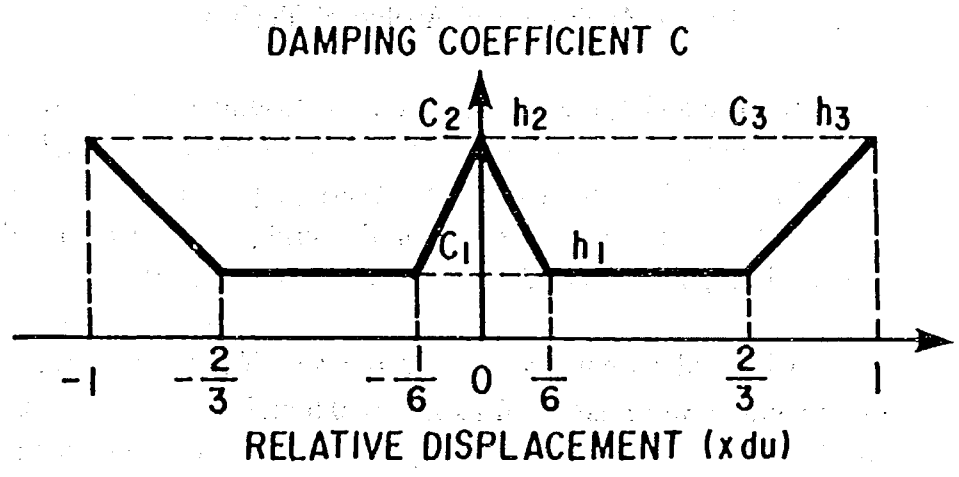


Fig. 2 Analytical Idealization of Damping Force vs. Relative Displacement Relation

For studying the effectiveness of the variable damper, a simple span girder bridge, as shown in Fig.3, with a span length of 30m was analyzed. The response in longitudinal direction was considered. Although the variable damper has better implementation for

multi-span continuous bridges, a simple span bridge was considered for analysis for simplicity. The deck was assumed to be supported by elastic bearings, and two variable dampers were installed between the deck and the piers.

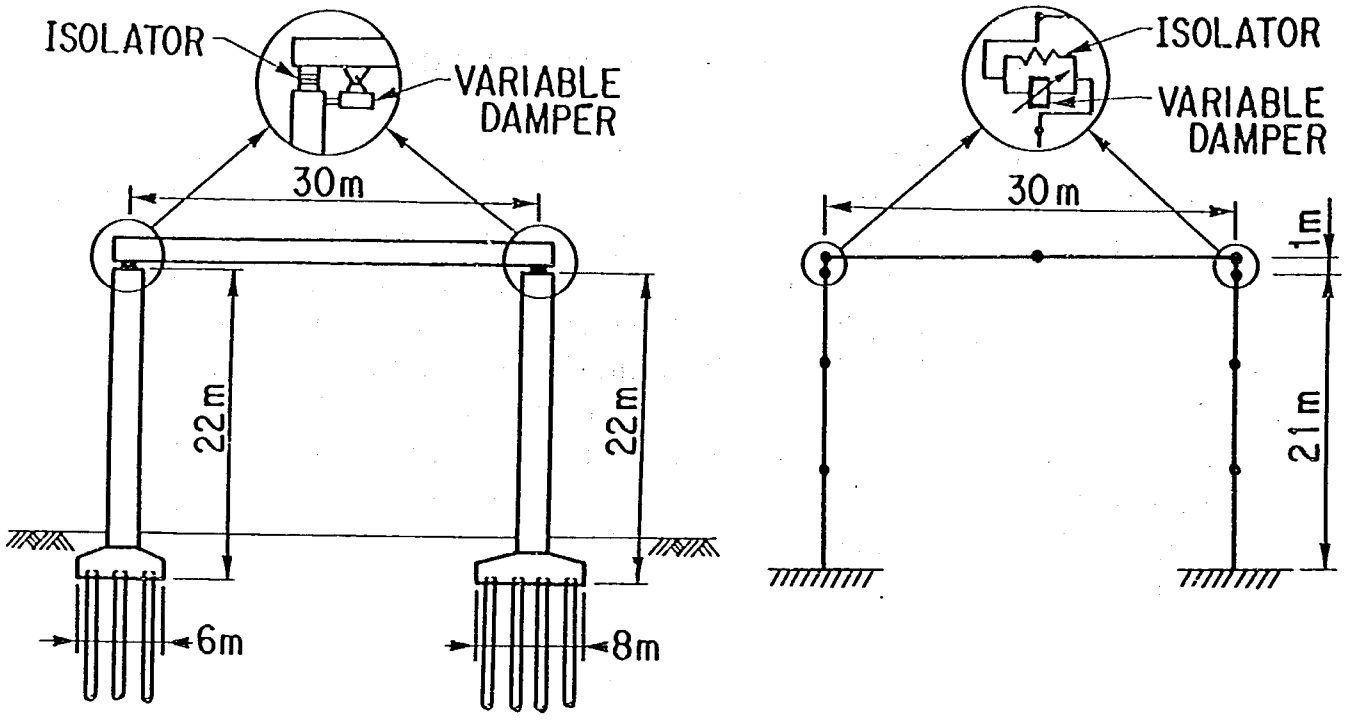


Fig. 3 Bridge Analyzed and Analytical Idealization

The weight of superstructure and stiffness of a pier were assumed as 2368 KN and 17350 KN/m so that the fundamental natural period of the bridge is 0.5 second if the both bearings are hinged. The lateral stiffness of rubber bearings per pier is assumed as 6276 KN/m so that the fundamental natural period of the bridge supported by the rubber bearings be 1.0 second. Damping ratio of the bridge was assumed as 0.02.

The bridge response with and without control by the variable dampers was computed. The damping ratios in Fig. 2 were assumed as $h_1 = 0.5$ and $h_2 = h_3 = 3$. As shown in Table 1, the peak deck displacement and the peak deck acceleration decrease to 26% and 44% of those without control, respectively.

The damping force and stroke required for the variable dampers are 632 KN × 2 = 1264 KN and 5.78 cm, respectively. Because the weight of deck is 2368 KN, the damping force is 53 % of the deck weight. The variable dampers with this specification can be designed and fabricated within the current scope of dampers technology.

Table 1 Peak Responses

Analytical Cases	Deck			Pier		Variable Damper		
	Displacement (cm)	Velocity (cm/s)	Acceleration (cm/s^2)	Shear Force (KN)	Bending Moment (KN·m)	Damping Force (KN)	Relative Displacement (cm)	Relative Velocity (cm/s)
NO CONTROL	33.00	189.0	1.300	1.637	32.333	———	———	———
WITH CONTROL	8.46	48.4	567	786	15.102	614	5.78	60.7

VERIFICATION OF VARIABLE DAMPER THROUGH SHAKE TABLE TEST

For verifying the feasibility of the variable dampers, a prototype variable damper was developed as shown in Photo 1 (Kawashima, Unjoh and Mukai 1993). It is a piston–cylinder type viscous damper with a by–pass installed between two cylinder–cells divided by the piston. The model was designed so that the maximum damping force is 200 KN and the stroke is ± 13 cm. Damping force can be controlled by a personal computer depending on a relative displacement and/or a velocity between a deck and a pier. The electricity required for control is only 50 W. This is extremely small as compared with the energy required for the active control.

A series of dynamic loading tests was made for the model. Fig. 4 shows a hysteresis loop of the damping force vs. stroke. Both command signal and actual data are presented. The hysteresis loop obtained by the loading test is very close with the command.

For verifying the effectiveness of the variable damper, a series of shake table tests was made. A simple span bridge model was fabricated on a shake table as shown in Fig. 5. The deck is 7.6 m long and 390 KN in weight. The piers are 1.6 m long. The deck is supported by four rubber bearings, and the prototype variable damper was installed between the deck and the pier as shown in Photo 2.

The model bridge was excited by a ground acceleration. The peak table acceleration was set as about 180 cm/sec^2 and 413 cm/sec^2. The excitation by the table motion with peak acceleration of 413 cm/sec^2 was not made for the model without control, because the deck response became excessive.
Figs. 6 and 7 compares the deck displacement of the model bridge, with and without control by the variable damper, subjected to the table acceleration with peak acceleration of about 180 cm/sec^2. Predicted response by the analysis which will be described later is also presented. The deck responses are 376 cm/sec^2 and 9.2 cm for no control, and they are decreased to 203 cm/sec^2 and 1.3 cm by the variable damper. The maximum damping force required for this control is 71 KN, which corresponds to 18% of the deck weight.

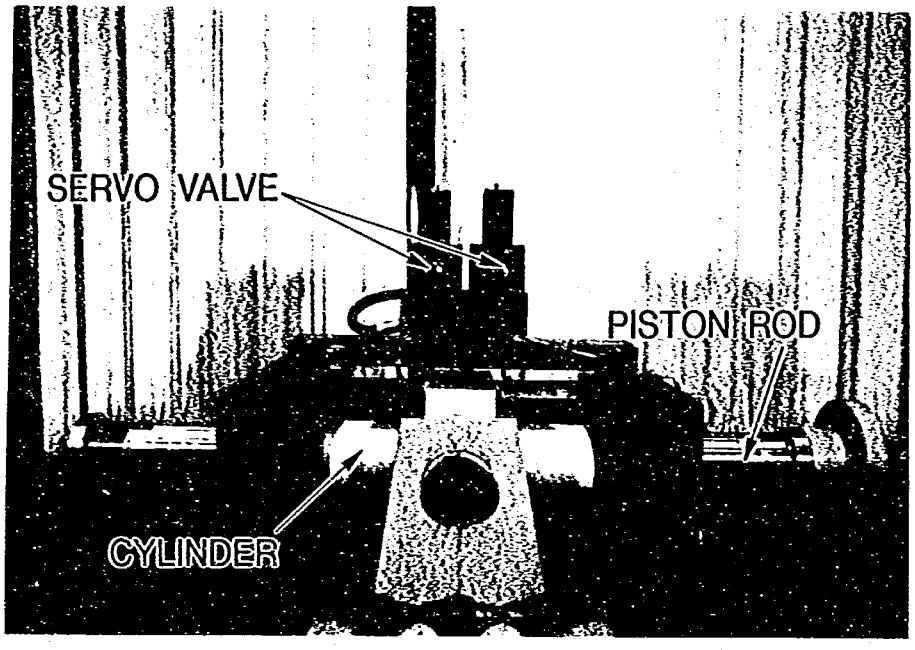


Photo 1 Prototype Model of Variable Damper

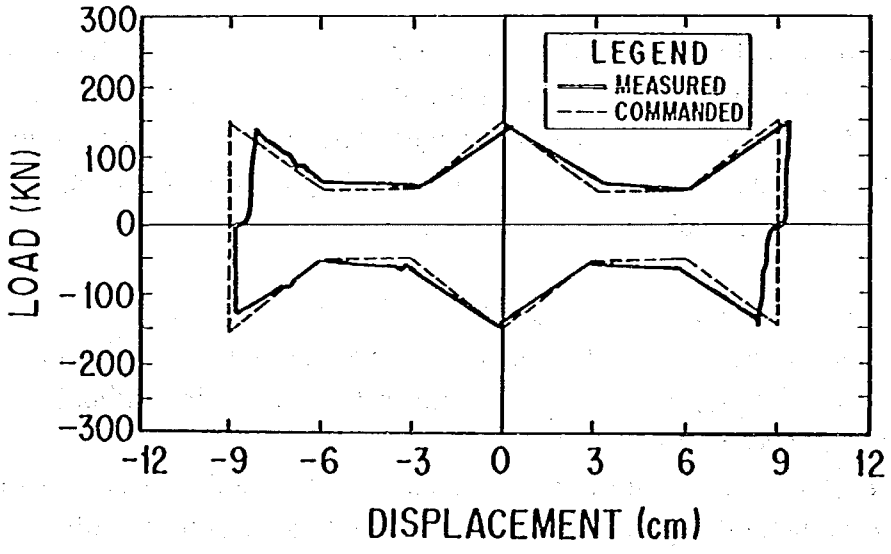


Fig. 4 Damping Force vs. Relative Displacement Relation from Dynamic Loading Test of Variable Damper

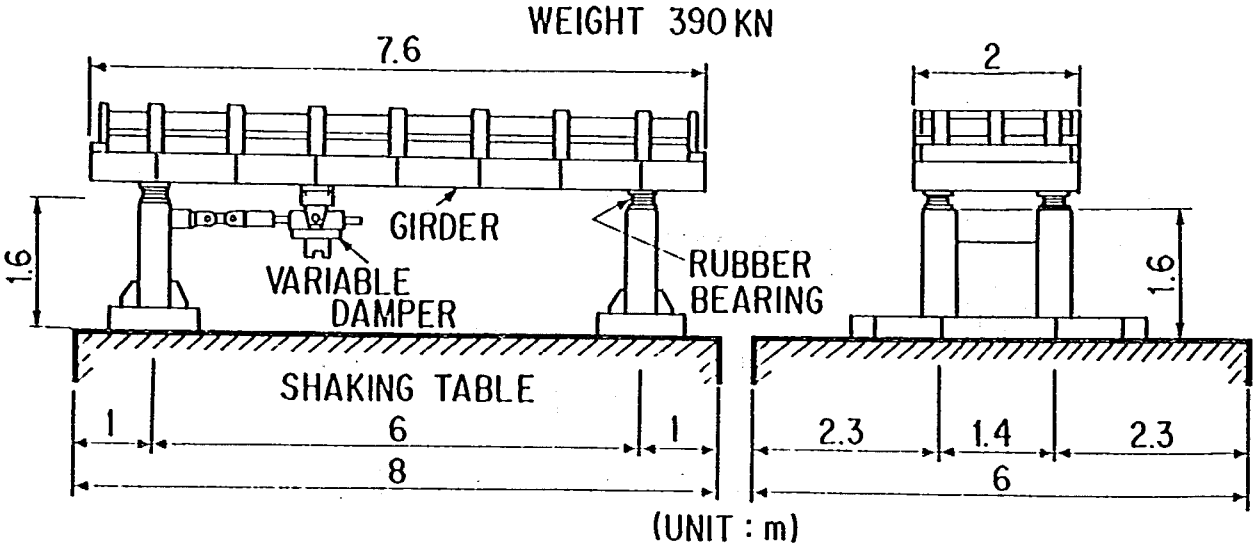


Fig. 5 Shake Table Test of a Model Bridge with a Variable Damper

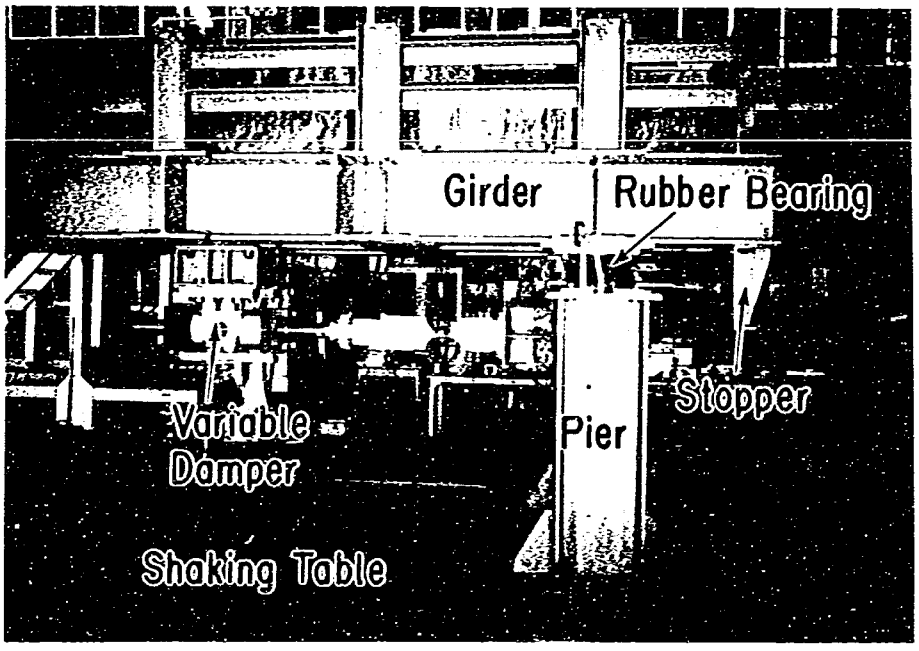


Photo 2 Model Bridge and Prototype Variable Damper Model

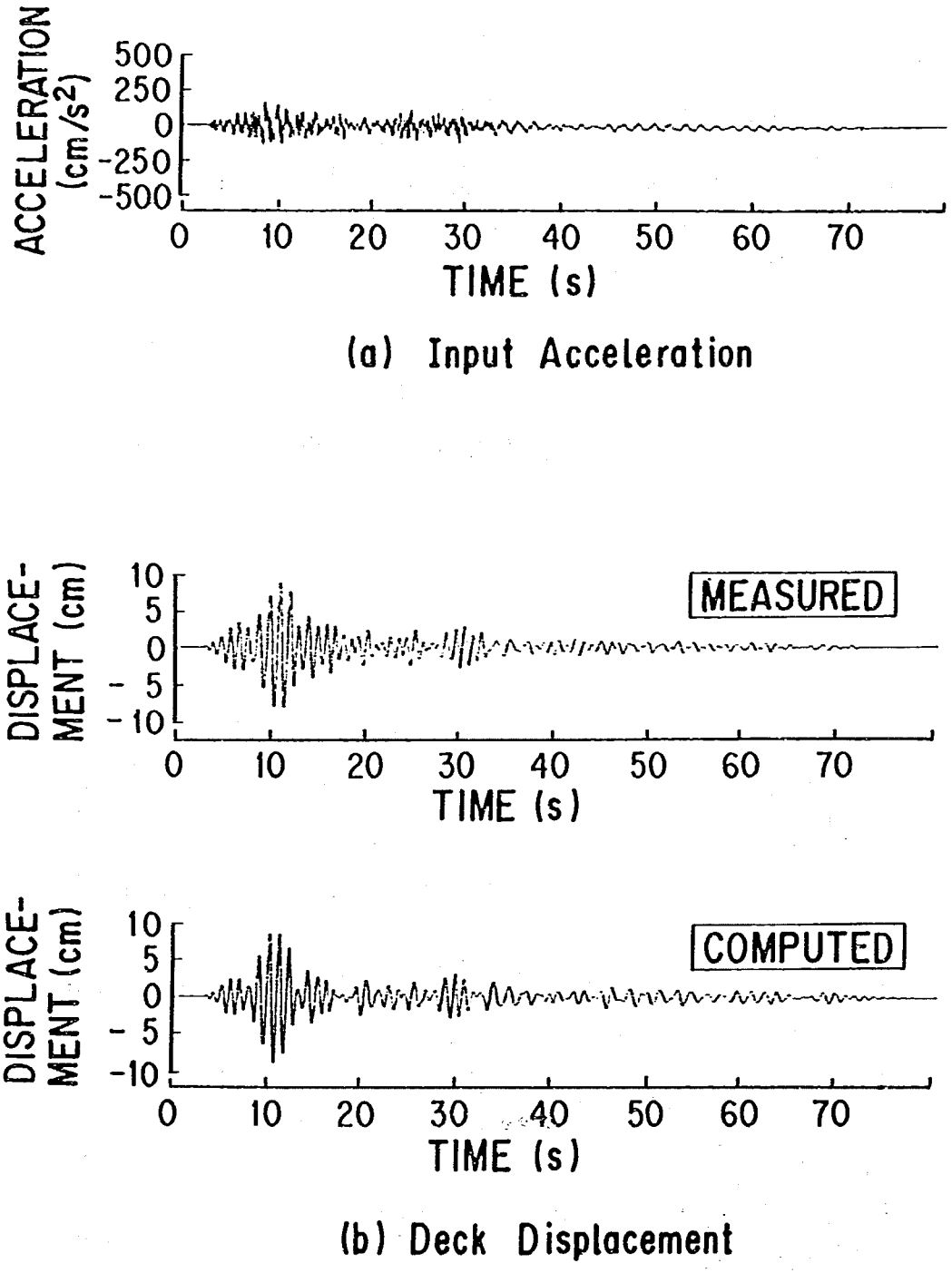


Fig. 6 Measured and Predicted Response of a Model Bridge without Control, subjected to a Table Motion with Peak Acceleration of 172 cm/sec ^{2}

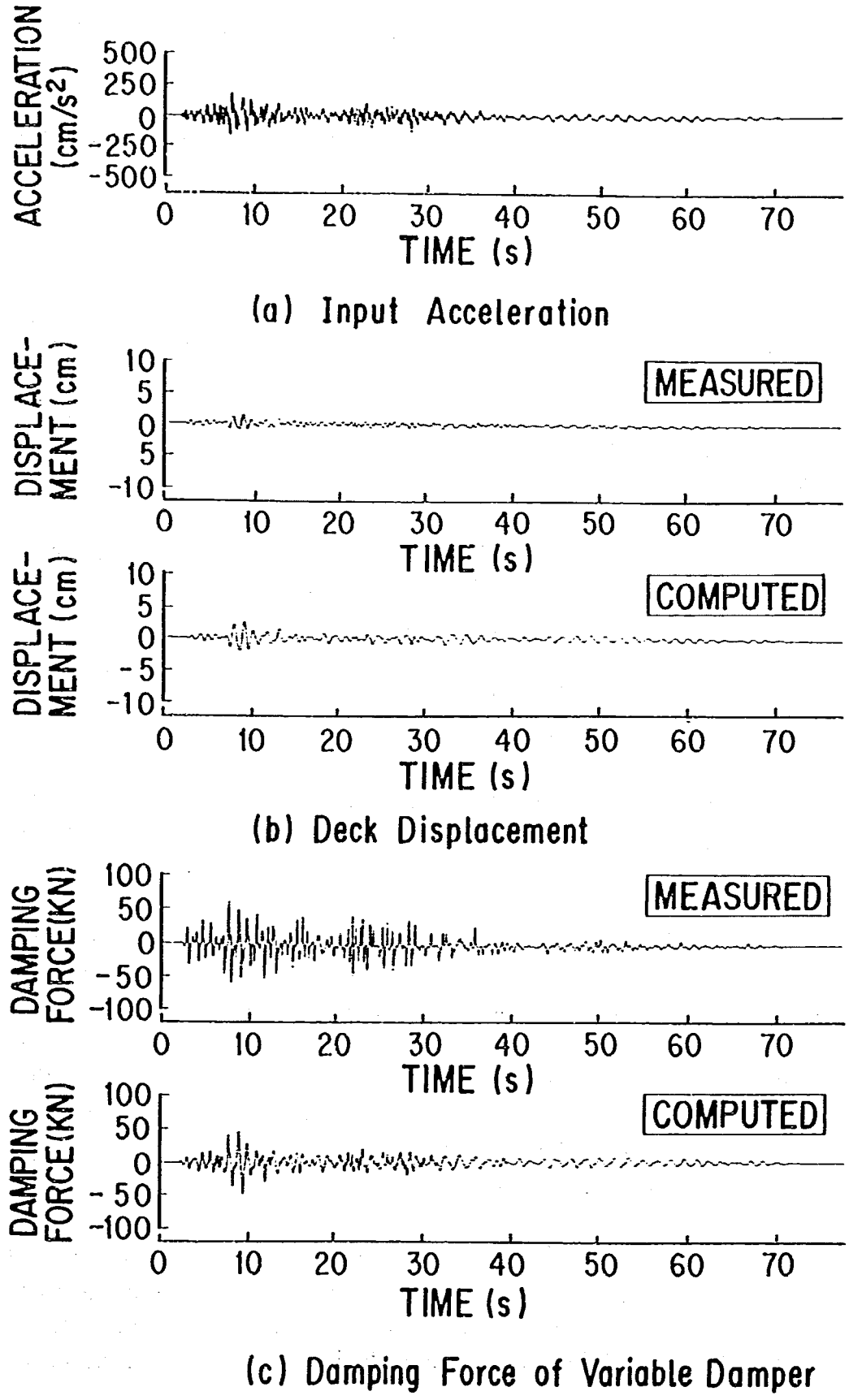


Fig. 7 Measured and Predicted Response of a Model Bridge with Control, subjected to a Table Motion with Peak Acceleration of 185 cm/sec ^{2}

A simulation of the experiments by the analytical method presented in the previous chapter was made. The deck, piers and rubber bearings were idealized by a discrete linear frame. Figs. 6 and 7 compare the deck displacement and the damping force developed in the variable damper between the experiments and analyses. The predicted responses are quite close with the measured responses.

VARIABLE STIFFNESS CONTROL

Most of bridges with usual size have the natural period ranging from 0.3 to 1.5 second, and this natural period range corresponds to the predominant period of earthquake–induced ground motions. Thus the resonance of the bridges response with the ground motion tends to be developed during an earthquake. The bridge response could be reduced provided the resonance of bridge response with the ground motion could be avoided.

Although it is hard to predict the predominant period of ground motion prior to an earthquake, it can be evaluated time by time during an earthquake. The moving window analysis may be used for evaluating the instantaneous predominant period of ground motion T^*. The resonance of bridge response with the ground motion may be avoided if the instantaneous natural period of bridges T be shifted from the instantaneous predominant period of ground motion T^* during an earthquake.

There are various methods to shift the instantaneous natural period of bridges during an earthquake. Flexibility of bearings may be changed, and active tendons/bracings may be adopted.

If one provides the variable dampers for a bridge which is elastically supported by rubber bearings, the natural period of the bridge can be varied by changing the damping coefficient of the variable dampers. If one makes the damping ratio of the variable damper very large, the variable damper would acts as the damper stopper. On the other hand, if one makes the damping ratio small, the natural period of the bridge takes the value computed from the stiffness of the rubber bearings and piers. The variable dampers have various advantage for controlling the instantaneous natural period of bridges because it is more stable for long term use than the active tendons/bracing systems.

Fig. 8 shows the algorithm of the variable stiffness control. The instantaneous predominant period of ground motion T^* at time t_i is computed by the moving window Fourier Spectrum. The damping coefficient of variable dampers is varied so that the instantaneous natural period of the bridge T be shifted to prevent the resonance with the ground motion.

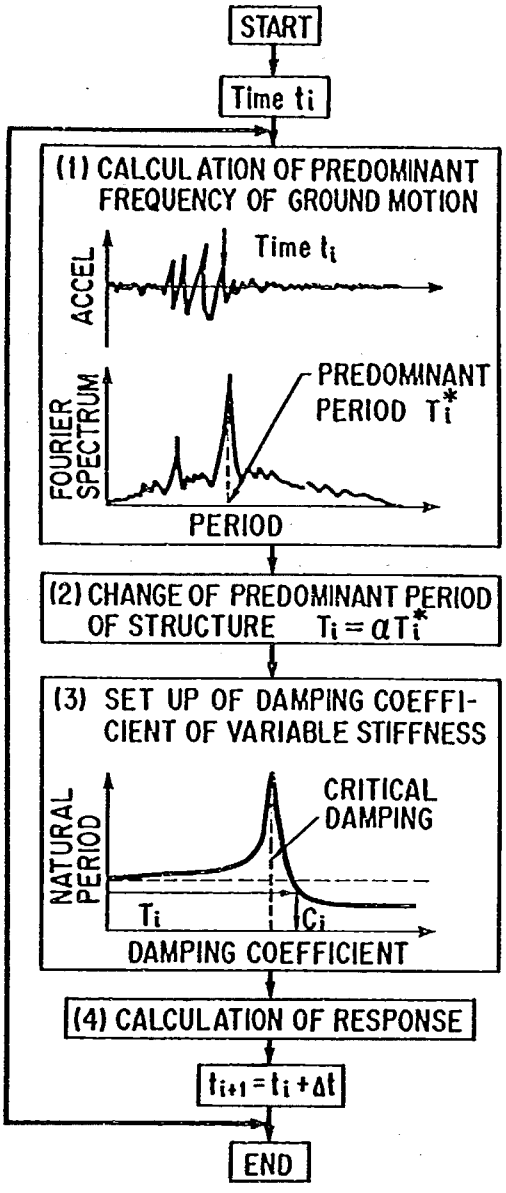


Fig. 8 Control Algorithm of Variable Stiffness

Although several algorithm can be considered, the period shift is assumed here as

$$T = \alpha T^* \qquad (1)$$

where,

T : instantaneous natural period of a bridge at time t_i

T^* : instantaneous predominant period of an earthquake ground motion at time t_i

α : control coefficient

The coefficient α has to be determined depending on the undamped natural period of the bridge T_0 and the instantaneous predominant period T^* of an ground motion.

EFFECTIVENESS OF VARIABLE STIFFNESS CONTROL

To study the effectiveness of the variable stiffness control, a three-span continuous girder bridge, as shown in Fig. 9, with a span length of 90m is analyzed. The response in longitudinal direction is considered. The superstructure of the model is supported by elastic bearings, and four variable dampers with the same characteristics are installed between the deck and the piers. The weight of the superstructure and spring stiffness of the rubber bearings are assumed as 4719 KN and 6247 KN/m, respectively. The stiffness of piers is assumed so that the fundamental natural period of the bridge is 0.5sec when the deck is supported by hinges. The stiffness of rubber bearings is set so that the fundamental natural period of bridge is 1 sec when the deck is supported by the elastic bearings. The damping ratio of the bridge without control is assumed as 0.02.

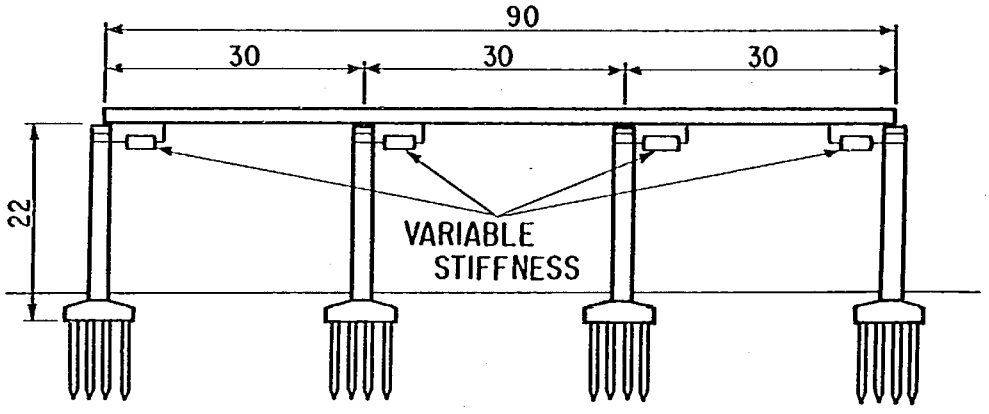


Fig. 9 Model Bridge Analysed

An acceleration ground motion as shown in Fig.10 is used as an input acceleration. The instantaneous predominant frequency ($1/T^*$) of the input acceleration is also shown in Fig. 10. Because the predominant period of ground motion is about 1 sec., α in Eq. (1) was assumed as 1/2.

Figs. 11 shows how the natural period of the bridge change depending on the damping coefficient of the variable dampers. At the damping coefficient C of about 4200 KN·sec/m, the fundamental natural period of bridge take very large value, because this corresponds to the critical damping of the structure. Although the period shift may be made in the damping coefficient range of 0 to over 8000 KN·sec/m, it is assumed here that the period shift be made in the range of damping coefficient C over 4200 KN·sec/m.

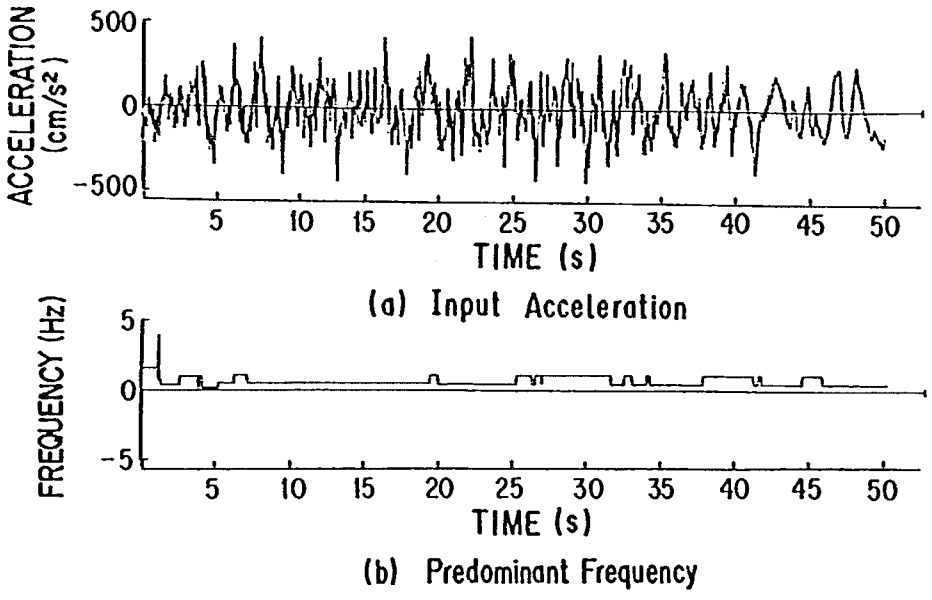


Fig. 10 Input Acceleration and the Predominant Period

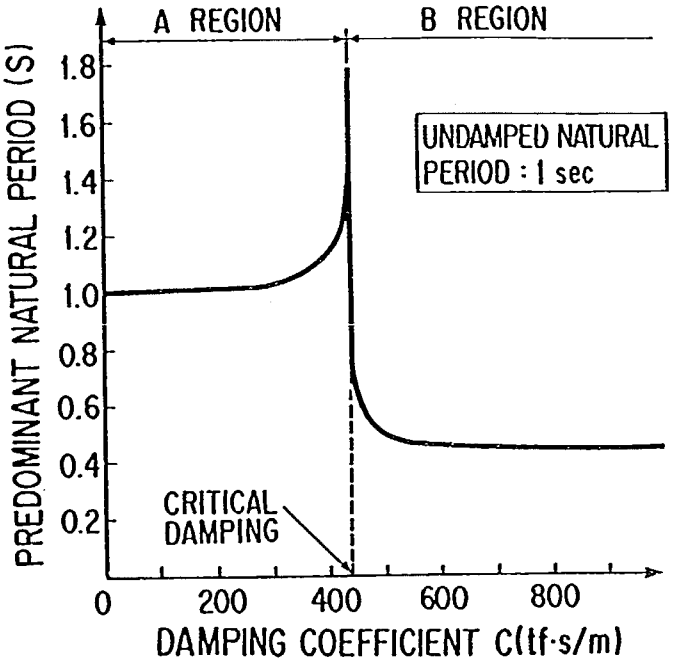


Fig. 11 Dependence of Natural Period of the Bridge on Damping Ratio of Variabl Dampers

Fig. 12 compares the deck acceleration and displacement of the bridge with and without control. The peak displacement and peak acceleration of deck decreases to 17% and 50% of those without control. The bending moment of pier bottom decreases to 52% of the one without control. The peak damping force required for the four variable dampers is 761 KN × 4 = 3040 KN and peak stroke is 3.1cm.

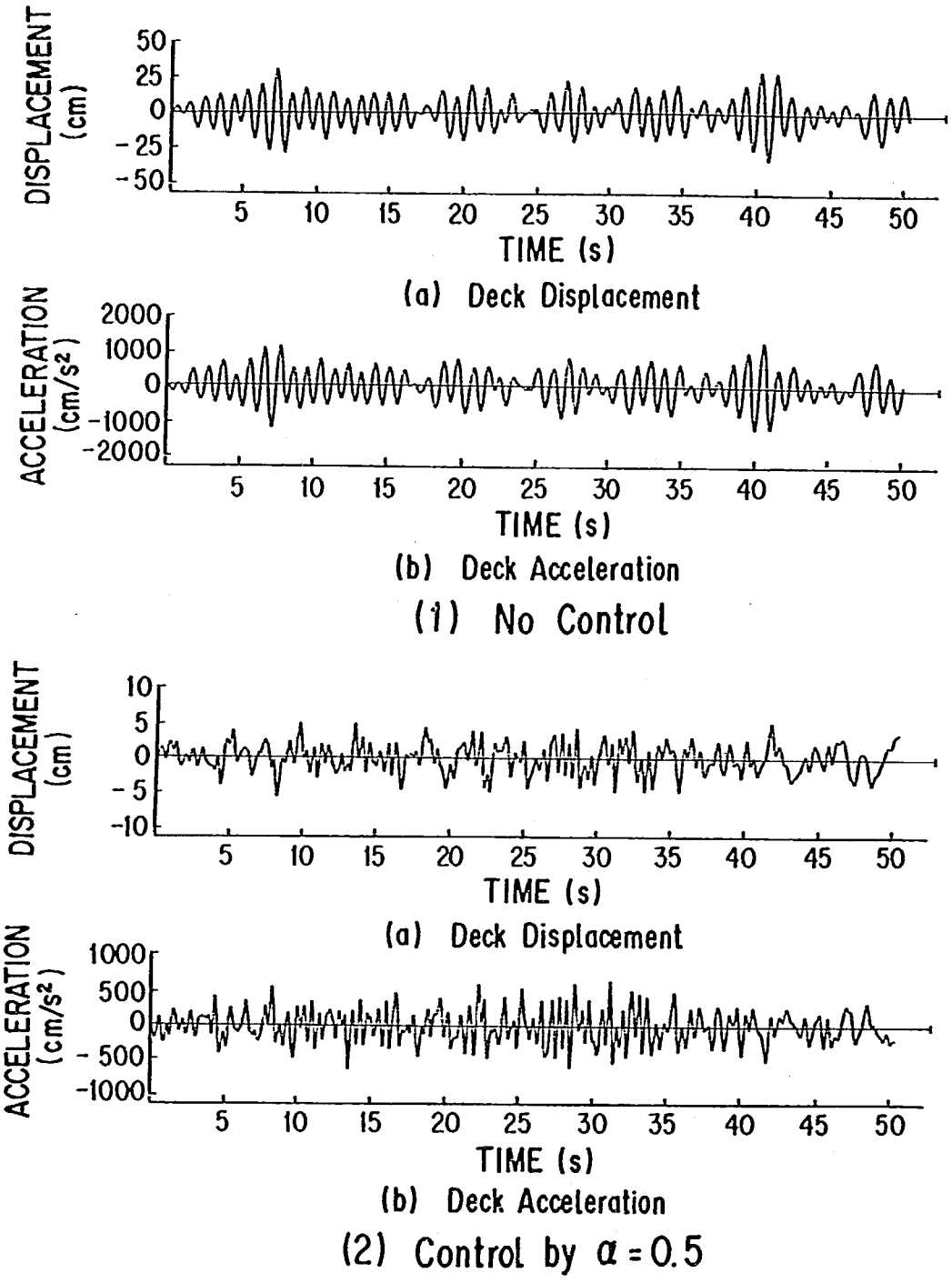


Fig. 12 Effectiveness of Variable Stiffness Control

CONCLUDING REMARKS

The variable dampers and variable stiffness control which are being developed at the Public Works Research Institute was described. Because the variable damper is a simple extension of the damper stopper technology which has been used in Japan for long time,

it is expected that the variable dampers be implemented in near future. Various research on the variable stiffness including development of the prototype model and shake table tests are currently being made.

The research presented herein is being made as a part of the U.S.–Japan Cooperative Research on Hybrid Control of Bridges under auspices of the Panel on Wind and Seismic Effects, UJNR. The authors extend their sincere appreciation to the strong support of Dr. S. C. Liu, NSF, Dr. H. S. Lew, NIST, Mr. J. D. Cooper, FHWA, Professor M. Shinozuka, Princeton University and Professor J. N. Yan, University of California at Irvine.

REFERENCES

1) Kawashima, K. and Unjoh, S. (1989). "Development of Hybrid Control Technology." Civil Engineering Journal, Tokyo, Japan, pp. 2–5, Vol. 32–6 (in Japanese).
2) Taguchi, J., Iwasaki, T., Adachi, Y., Sasaki, Y. and Kawashima, K. (1990). " U.S.–Japan cooperative research program on hybrid control of seismic response of bridge structures." 22nd Joint Meeting, U.S.–Japan Panel on Wind and Seismic Effects, UJNR, Gaithersburg, Maryland, USA, May, 1990, NIST Special Publication.
3) Kawashima, K., Unjoh, S., Nagashima, H. and Shimizu, H. (1991). "Current research efforts in Japan for passive and active control of highway bridges against earthquakes." Proc. 23rd Joint Meeting, U.S.–Japan Panel on Wind and Seismic Effects, UJNR, Tsukuba, Japan, 187–209.
4) Kawashima, K., Unjoh, S. and Shimizu, H. (1991). "Earthquake response control of highway bridges by variable damper." Proc. of Colloquium on Control of Structures, Japan Society of Civil Engineers, Part. B, pp.221–224, July, 1991 (in Japanese)
5) Kawashima, K., Unjoh, S. and Shimizu, H.(1992). "Seismic response control of highway bridges by variable damper." 24th Joint Meeting, U.S.–Japan Panel on Wind and Seismic Effects, UJNR, Gaithersburg, May, 1992, NIST Special Publication 843
6) Kawashima, K., Unjoh, S., Iida, H. and Mukai, H. (1992). "Effectiveness of the variable damper for reducing seismic response of highway bridges, Proc. of 2nd U.S.–Japan Workshop on Earthquake Protective Systems for Bridges, Tsukuba, Dec. 7–8, 1992, Technical Note of the Public Works Research Institute, No. 3196.
7) Kawashima, K., Unjoh, S. and Mukai, H. (1993). "Seismic response control of highway bridges by variable dampers." 25th Joint Meeting, Panel on Wind and Seismic Effects, UJNR, Tsukuba, Japan, Technical Note of Public Works Research Institute.
8) Milliken, Jr., W., F. (1987). "Lotus active suspension system." Proc. 11th International Conference on Experimental Safety Vehicles, Washington D.C., U.S.A., 467–475.
9) Sugawara, F. (1986). "Electronically controlled shock absorber system used as a road sensor which utilizes super sonic waves." Proc. Society of Automotive Engineers, Milwaukee, Wisconsin, U.S.A., 6.15–6.25.

Seismic Isolation of Bridges In Japan

Kazuhiko KAWASHIMA
Shigeki UNJOH
and
Hidetoshi MUKAI

First Egyptian Conference on
Earthquake Engineering
August, 1993

SEISMIC ISOLATION OF BRIDGES IN JAPAN

by

Kazuhiko Kawashima [1], Shigeki Unjoh [2] and Hideki Sugita [3]

ABSTRACT

This paper presents the current practice for seismic isolation of bridges in Japan. Description is given to the Manual for Menshin Design of Highway Bridges, which describes the basic requirements and design method. Emphasis is placed to describe the unique application of the seismic isolation. Implementation of the Menshin Design is also presented.

INTRODUCTION

Seismic isolation is increasingly adopted for bridges because it is advantageous for constructing multi-span continuous bridges. Various investigations have been made for the seismic isolation of bridges such as the response characteristics of base isolated bridges, development of isolators and energy dissipators, and testing methods for verifying the characteristics of devices. Compiling those studies, a design manual was formulated in 1992 for enhancing the construction of seismic isolated bridges.

This paper presents the current practice for designing the seismic isolated bridges. The outline of the manual and implementation are described.

MENSHIN DESIGN

One of the important decision in design of seismic isolated bridges is how much elongation of the natural period need to be made. In Japan, soils are mostly very weak at bridge sites. Significant earthquakes with magnitude over 8, which would produce long period ground motions, occur at shorter recurrence interval than other countries. Taking account of such evidence, the design seismic force is taken higher and the natural period at which the design acceleration decreases with increasing the natural period is taken longer, as shown in Fig. 1, in Japan than in other countries such as U.S.A., New Zealand

1) Head, Earthquake Engineering Division, Earthquake Disaster Prevention Department, Public Works research Institute, Ministry of Construction, Tsukuba-shi, 305
2) Senior Research Engineer, ditto
3) Research Engineer, ditto

and Italy. The advantage for reducing deck response can therefore be realized only by elongating the natural period longer than 1.4 ~ 2.0 second.

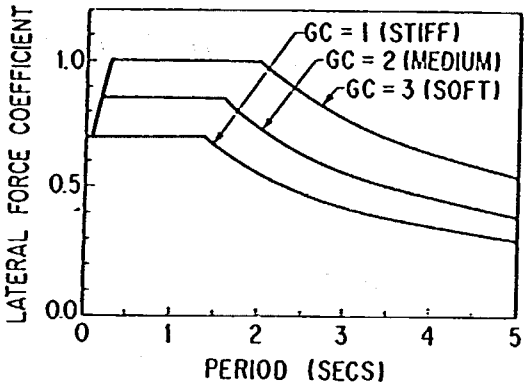


Fig. 1 Lateral Force Coefficient ($c_z = c_I = 1.0$)

However elongation of the natural period would bring the increase of the deck response displacement resulting to adopt the joints with long legs. This is, however, a crucial requirement difficult to adopt, in particular, for overcrossing in city area because it causes noise and vibration pollution, which is the most serious concern in city area. Furthermore it would cause the disadvantage for maintenance because of frequent replacement of the expansion joints damaged by traffic load.

Based on these reasons, it is not appropriate to forcibly elongate the natural period for reducing the deck response acceleration. It is appropriate to adopt the base isolation not for elongating the natural period but for increasing the energy dissipating capability. Distribution of the inertia force to as many substructures as possible, which is the long practice in Japan, is significantly advantageous (Kawashima, Hasegawa and Nagashima 1991).

Therefore basic principle for introducing the base isolation to highway bridges is as follows :

1) Distribute the inertia force to as many substructures as possible, and reduce the deck response by increasing the energy dissipating capability.

2) Do not forcible elongate the natural period, but select it so that the resonance of bridge response with the natural period of ground be avoided.

Such design criteria is not "isolation" of "base". It is therefore called here as "Menshin Design". The "Menshin" means "reduction of seismic response" in Japanese.

MENSHIN DESIGN OF HIGHWAY BRIDGES

Menshin Manual

The Manual for Menshin Design of Highway Bridges was developed by the Public Works Research Institute as the final accomplishment of the 3 years Joint Research Program with 28 private companies (PWRI 1992, Kawashima, Hasegawa and Nagashima 1992). Although this is not the mandate specifications, it is recommended to adopt the basic requirements of the Manual in addition to the Seismic Design Specifications of

Highway Bridges (JRA 1990).

The Manual consists of 9 chapters and 10 appendices. The table of contents is presented in the appendix of this paper. In the Menshin design, bridges are designed following the standard static design method. Precise evaluation of the seismic safety is made by the dynamic response analysis. In Menshin design, isolators and dampers are idealized by a set of equivalent linear springs with the equivalent stiffness and the equivalent damping ratio.

Design Force

Menshin devices are designed by the seismic coefficient method and the bearing capacity method. In the seismic coefficient method, the allowable stress approach is adopted, while in the bearing capacity method, the bearing capacity approach is adopted. Bridges are designed by the seismic coefficient method, and then the ductility of reinforced concrete piers is checked by the bearing capacity method.

In the seismic coefficient method, the design lateral force coefficient k_h is given as

$$k_h = c_z \cdot c_G \cdot c_I \cdot c_T \cdot c_E \cdot k_{h0} \geqq 0.1 \qquad (1)$$

where

$$c_T \cdot c_E \geqq 0.8$$

in which c_z : modification factor for zone, c_G : modification factor for ground condition, c_I : modification factor for importance, c_T : modification factor for structural response, c_E : modification factor for energy dissipation capability, and k_{h0} : standard design horizontal seismic coefficient $(=0.2)$.

The modification factors c_z , c_G , c_I and c_T are specified in the Design Specifications of Highway Bridges (JRA 1990, Kawashima and Unjoh 1993). The modification factor c_E takes a value shown in Table 1 depending on the first modal damping ratio of the bridge. The design lateral force is reduced as large as 20 % .

Table 1 Modification Factor for Energy Dissipation Capability c_E (Seismic Coefficient Method)

Damping Ratio h	Modification Factor c_E
$h<0.1$	1.0
$h \geqq 0.1$	0.9

In the bearing capacity method, the lateral force coefficient k_{hc} and the equivalent lateral force coefficient k_{he} are given as

$$k_{he} = \frac{k_{hc}}{\sqrt{2\mu - 1}} \geqq 0.3 \qquad (2)$$

$$k_{hc} = c_z \cdot c_I \cdot c_R \cdot c_E \cdot k_{hc0} \qquad (3)$$

in which c_z : modification factor for zone, c_I : modification factor for importance, c_R : modification factor for structural response, c_E : modification factor for energy dissipation capability, k_{hc0} : standard lateral force coefficient for bearing capacity method $(=1.0)$, and μ : allowable ductility factor of reinforced concrete piers.

The modification factors c_z , c_I , and c_R are specified in the Seismic Design

Specifications of Highway Bridges (JRA 1990). The modification factor c_E depends on the modal damping ratio of the bridge, and takes a value of Table 2. The design force is reduced as large as 30 %.

Table 2 Modification Factor for Energy Dissipation Capability c_E (Bearing Capacity Method)

Damping Ratio h	Modification Factor c_E
$h<0.1$	1.0
$0.1\leqq h<0.12$	0.9
$0.12\leqq h<0.15$	0.8
$0.15\leqq h$	0.7

Design of Isolators and Energy Dissipators

In the design of isolators and energy dissipators, the "displacement assumed in design for the devices u_B " (design displacement of menshin device), the equivalent stiffness K_B and the equivalent damping ratio h_B of the menshin device are the key factors.

The design displacement of menshin device u_B is evaluated as

$$u_B=\frac{k_h\cdot W_u}{K_B} \quad \text{(S.C.Method)} \tag{4}$$

$$u_B=\frac{k_{hc}\cdot W_u}{K_B} \quad \text{(B.C.Method)} \tag{5}$$

in which k_h : lateral force coefficient by Eq.(1), k_{hc} : lateral force coefficient by Eq.(3), K_B : equivalent stiffness (tf/m) of menshin device, and W_u : weight of the superstructure (tf) supported by the menshin device.

Various requirements for the devices against static load and dynamic load are described in the Manual. It is unique that precise loading test procedures for both dynamic and static loads are described in the Manual. Some of the important requirements for dynamic load is as:

(1) Menshin devices have to be designed and fabricated so that their equivalent stiffness K_B and equivalent damping ratio h_B be within ± 20 % of the design values.

(2) Menshin devices have to be stable against 50 cycles of harmonic loading with displacement of u_B given by Eq.(5).

(3) Deck should return to the rest position even after it was subjected to a large earthquake. The residual displacement u_{BR} developed in menshin devices after one smoothly releases from the deformed displacement of u_B given by Eq.(5) needs to satisfy.

$$u_{BR}\leqq 0.1\cdot u_B \tag{6}$$

(4) The equivalent stiffness and the equivalent damping ratio of menshin devices need to be stable against the change of load condition at normal time, change of natural environment such as the temperature change and earthquake-induced cyclic loading. Stability has to be examined for 1) cyclic loading associated with the elongation and shrinkage of deck due to temperature change and traffic load, 2) effect of loading

hysteresis, 3) variation of vertical loading, 4) effect of loading rate, 5) effect of pre-deformation due to creep and shrinkage, 6) direction of excitation, and 7) change of the equivalent stiffness and the equivalent damping ratio depending on the temperature change.

On the other hand, major requirements for static load include :

(1) Materials and mechanism of the menshin devices need to give credit to long term use. They need to be stable against the daily and annual cyclic elongation and shrinkage of deck due to the temperature change.

(2) The menshin devices need to be stable against local shear strain. Check of the local shear strain needs to be made in accordance with the Design Guidelines of Bearings JRA 1991).

(3) In the rubber-type menshin devices, the creep of rubber which would be developed for the life time of bridges in vertical direction due to the dead weight of superstructure needs not to exceed 5 % of the total thickness of rubber.

(4) The equivalent stiffness of menshin device at −10 ℃ need not to exceed 1.5 time the equivalent stiffness at 40 ℃.

Modal Damping Ratio of Bridges

The modal damping ratio of bridges, which is required for c_E in Eqs.(1) and (3), is evaluated as

$$h=\frac{\sum_{j=1}^{n}\phi_{ij}^{T}\cdot h_j\cdot k_j\cdot\phi_{ij}}{\phi_i^{T}\cdot K\cdot\phi_i} \qquad (7)$$

in which ϕ_{ij} : mode vector of j-th structural component for i-th mode, h_j : damping ratio of j-th structural component, k_j : stiffness matrix of j-th structural component, ϕ_{iT} : mode vector of bridge for i-th mode, K : stiffness matrix of bridge.

Table 3 shows the damping ratio h_j recommended for structural components in Eq.(7).

Table 3 Damping Ratio h_j Recommended for Structural Components

Structural Components	Steel	Concrete
Superstructures	0.02 ~ 0.03	0.03 ~ 0.05
Menshin Device	Damping Ratio by Eq.(11)	
Pier/Columns	0.03 ~ 0.05	0.05 ~ 0.1
Footing	0.1 ~ 0.3	

Eq.(7) may be approximated as

$$\left.\begin{aligned} h&=\frac{\sum K_{Bi}\cdot u_{Bi}^{2}\cdot c_{hi}}{\sum K_{Bi}\cdot u_{Bi}^{2}\cdot c_i}\\ c_{hi}&=h_{Bi}+\frac{h_{Pi}}{K_{Pi}}+\frac{h_{Pui}}{K_{Pui}}+\frac{h_{P\theta i}\cdot H^{2}}{K_{P\theta i}}\\ c_i&=1+\frac{K_{Bi}}{K_{Pi}}+\frac{K_{Bi}}{K_{Pui}}+\frac{K_{Bi}\cdot H^{2}}{K_{P\theta i}}\end{aligned}\right\} \qquad (8)$$

Table 4 Directory of Menshin Bridges in Japan

Bridge	Location	Deck Length	Administrator	Year Constructed	Super-Structure Type	Bearing Type
Onnetoh Bridge	Hokkaido	102.2m	Hokkaido Development Bureau	1992	4-Span Continuous Steel Plate Girder	LRB
Nagakigawa Bridge	Akita	97m	Noshiron Construction Office, MOC	Under Construction (1993)	3-Span Continuous Steel Plate Girder	LRB
Maruki-bashi Bridge	Iwate	92.5m	Iwate-ken	1992	3-Span Continuous Prestressed Concrete Box Girder	LRB
Yama-age Bridge	Tochigi	250m	Tochigi-ken	1993	6-Span Continuous Prestressed Concrete Box Girder	HDR
Miyagawa Bridge	Sizuoka	110m	Sizuoka-ken	1991	3-Span Continuous Steel Box Girder	LRB
Hirao Bridge	Yamaguchi	350m	Yamaguchi-ken	Under Construction (1993)	5-Span Continuous Prestressed Concrete Box Girder	LRB
Uehara Bridge	Nagoya	65m	Nagoya City	1991	2-Span Continuous Steel Box Girder	LRB
Route #12 Interchange Bridge	Tokyo	136.6m	Metropolitan Expressway Public Corp.	1991	6-Span Continuous Concrete Slab	LRB
Bay Shore Route	Tokyo	417.6m	Metropolitan Expressway Public Corp.	Under Construction (1993)	9-Span Continuous Prestressed Concrete Box Girder	LRB
Komatsukawa Route	Tokyo	240m	Metropolitan Expressway Public Corp.	1991	Interconnection of Simply-Supported Girder	LRB
Route #6	Tokyo	200m	Metropolitan Expressway Public Corp.	1992	Interconnection of Simply-Supported Girder	LRB
Matsunohama Bridge	Osaka	211.5m	Hanshin Expressway Public Corp.	1992	4-Span Continuous Steel Box Girder	LRB
Izumisano Bridge	Osaka	318m	Hanshin Expressway Public Corp.	Under Construction	6-Span Continuous Steel Box Girder	LRB
Moriguchi Route	Osaka	90m	Hanshin Expressway Public Corp.	1991	Interconnection of Simply-Supported Girder	LRB
Trans Tokyo Bay	Tokyo	880m	Trans Tokyo Bay Highway Corp.	Under Construction (1994)	11-Span Continuous Steel Box Girder	LRB
Karasaki Bridge	Fukushima	76.95m	Soma Kyodo Power Company Ltd.	1991	2-Span Continuous Prestressed Concrete Box Girder	HDR

in which h : modal damping ratio of bridge for 1st mode, h_{Bi} : damping ratio of i−th damper, h_{Pi} : damping ratio of i−th pier/abutment, h_{Fvi} : damping ratio of i−th foundation associated with translational movement, $h_{F\theta i}$: damping ratio of i−th foundation associated with rotation, K_{Pi} : equivalent stiffness of i−th pier/abutment, h_{Fvi} : translational stiffness of i−th foundation, $K_{F\theta i}$: rotational stiffness of i−th foundation, u_{Bi} : design displacement of i−th menshin device, and H : height from the bottom of pier to the gravity center of deck.

IMPLEMENTATION OF MENSHIN DESIGN

Table 4 shows the directory of implementation of the Menshin design. The first Menshin bridge in Japan is Miyagawa Bridge, and it was completed in 1991. Photos 1 and 2 show the general view and the lead rubber bearings. A series of forced excitation tests by an eccentric mass−shaker and quick−release test were conducted for verifying the design (Masumoto and Hara 1991). Strong motion observation has been made since the completion, and an analysis of the data was made (Kawashima, Nagashima, Masumoto and Hara 1992). Similar tests were made for several bridges as shown in Photos 3 and 4. Further accumulation of strong motion records are being made to confirm the bridge response during large earthquakes.

CONCLUDING REMARKS

Current practice of the seismic isolation of highway bridges in Japan was briefly introduced. It is unique in the Menshin Design that the emphasis is placed for increasing energy dissipating capability and distribution of lateral force of the deck to as many piers as possible. Forcible elongation of the natural period of bridges is avoided due to the

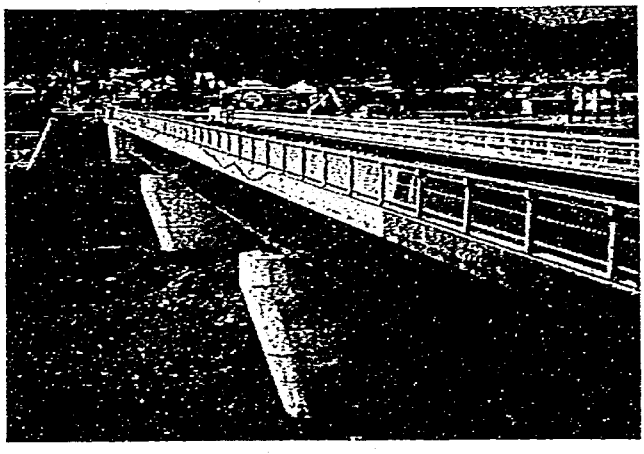


Photo 1 Miyagawa Bridge (Shizuoka−ken)

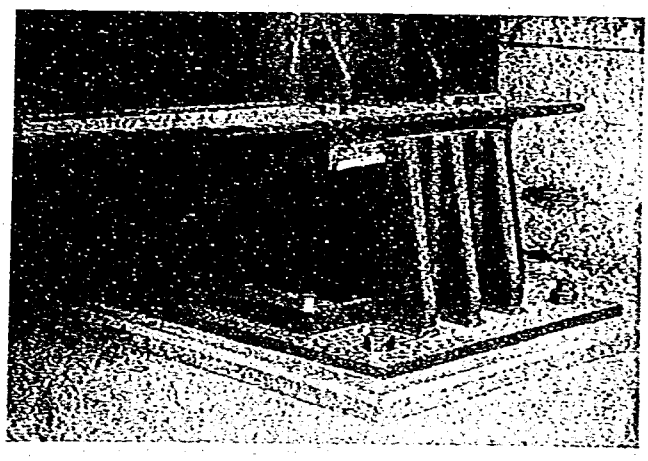


Photo 2 LRB used for Miyagawa Bridge

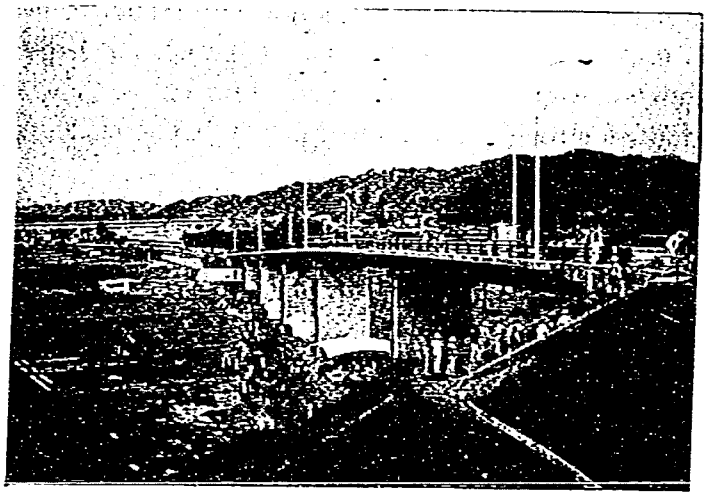


Photo 3 Yama-age Bridge (Tochigi-ken)

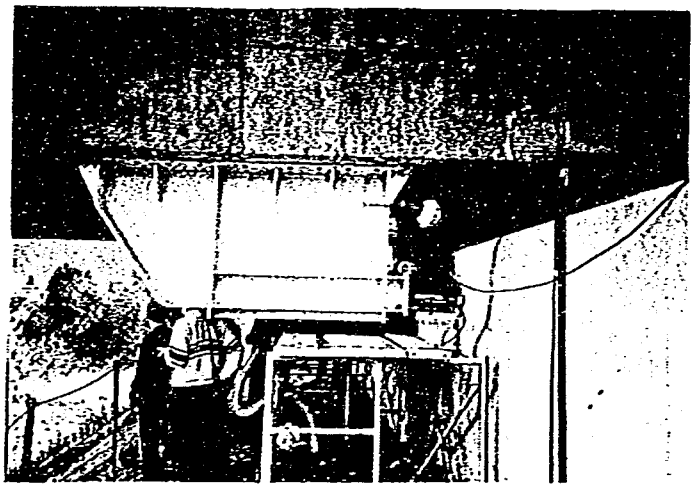


Photo 4 HDR used for Yama-age Bridge and Static Jack for Quick-Release Test

environmental and maintenance problems. More technical development which enables to construct super multi-span continuous bridges with the deck length over 1km without expansion joints is being made at the Public Works Research Institute.

REFERENCES

1) Public Works Research Institute (1992). "Manual for menshin design of highway bridges." Technical Note of Public Works Research Institute, Vol. 60 (in Japanese)
2) Japan Road Association (1990). "Part V seismic design" of the"Specifications of design of highway bridges" (in Japanese)
3) Japan Road Association (1991). "Guide-specifications of design of bearings." (in Japanese)
4) Kawashima, K., Hasegawa, K. and Nagashima, H. (1991). "A perspective of Menshin Design for highway bridges in Japan." Proc. 1st U.S.-Japan Workshop on Earthquake Protective Systems of Bridges, National Center for Earthquake Engineering Research, Buffalo, N.Y., U.S.A., September 1991
5) Kawashima, K., Hasegwa K. and Nagashima, H. (1992). " Manual of menshin design of highway bridges." Proc. 24th Joint Meeting, Panel on Wind and Seismic Effects, UJNR, Gaithersburg, MD, U.S.A., NIST Special Publication 843.
6) Masumoto, Y. and Hara, K. (1991). " Design and construction of Miyagawa Bridge." Proc. 1st U.S.-Japan Workshop on Earthquake Protective Systems of Bridges, State University of New York at Buffalo.
7) Kawashima, K., Nagashima, H., Masumoto, H. and Hara, K. (1992). "Response analysis of Miyagawa bridge based on a measured acceleration record." Proc. 2nd U.S.-Japan Workshop on Earthquake Protective Systems of Bridges, Tsukuba, Japan, Technical Note of PWRI, No. 3195.
8) Kawashima, K. and Unjoh, S. (1993). "Seismic design of highway bridges in Japan." 1st Egyptian Conference on Earthquake Engineering, Hurgada, Egypt.

APPENDIX

TABLE OF CONTENTS OF MANUAL FOR MENSHIN DESIGN OF HIGHWAY BRIDGES

1. General
   - 1.1 Scope of Application
   - 1.2 Definition of Terms
2. Basic Principle of Menshin Design
3. Menshin Design
   - 3.1 General
   - 3.2 Lateral Force Coefficient for Seismic Coefficient Method
   - 3.3 Lateral Force Coefficient and Equivalent Lateral Force Coefficient for Bearing Capacity Method
   - 3.4 Characteristics value for Menshin Devices

3.5 Computation of Natural Period of Bridge
3.6 Computation of Modal Damping Ratio of Bridges
4. Design of Menshin Devices
4.1 Basic Principle for Design of Menshin Devices
4.2 Design of Laminated Rubber Bearings
4.3 Design of Lead Rubber Bearings
4.4 . Design of High Damping Rubber Bearings
4.5 Design of Steel Dampers
4.6 Design of Friction Dampers
4.7 Design of Viscous Dampers
4.8 Design of Roller Dampers
5. Dynamic Response Analysis
5.1 General
5.2 Dynamic Response Analysis Method
5.3 Analytical Models
5.4 Design Seismic Forces
5.5 Check of Safety
6. Design Details
6.1 General
6.2 Gap between Structures
6.3 Falling-off Prevention Devices
6.4 Knock-off Devices
6.5 Details of Expansion Joints
7. Approving Tests of Menshin Devices
7.1 General
7.2 Approving Tests for Confirming Requirements for Dynamic Loads
7.3 Approving Tests for Confirming Requirements for Static Loads
8. Seismic Retrofit of Existing Bridges with Use of Menshin Design
9. Application of Menshin Design for Making Existing Simply Supported Girder Bridges Continuous
Appendices
1. Procedure of Menshin Design
2. Menshin Devices for Highway Bridges
3. References for Dynamic Response Analysis
4. Expansion Joints and Falling-off Prevention Devices for Highway Bridges
5. Design Example of Prestressed Concrete Bridges
6. Design Examples of Steel Girder Bridges
7. Design Examples of Super-multi-span Continuous Bridges
8. Design Examples for Seismic Retrofit
9. Design Examples for Making Existing Simply Supported Girders Continuous
10. Standard Acceleration Ground Motions Recommended for Dynamic Response Analysis

Seismic Design Method of Underground Structures

Kazuhiko KAWASHIMA
Hideki SUGITA
and
Tomoru NAKAJIMA

First Egyptian Conference on
Earthquake Engineering
August, 1993

SEISMIC DESIGN METHOD OF UNDERGROUND STRUCTURES

by

Kazuhiko Kawashima [1], Hideki Sugita [2] and Tomoru Nakajima [2]

ABSTRACT

This paper outlines the seismic design methods of underground structures by means of the Seismic Deformation Method. Because the underground structures behave quite differently from the structures on ground, a unique design method which is distinguished from the Lateral Force Coefficient Method is adopted. This paper presents the Seismic Deformation Method for design of cross section and for axial deformation.

INTRODUCTION

Seismic design of underground structures is made by the Seismic Deformation Method, in which the displacement and deformation developed in the subsurface ground during an earthquake are taken as the major seismic effects. The seismic response of underground structures is distinguished by the small mass effect and the large damping ratio from regular structures on ground, i.e.,

a) mass effect is small because unit weight of underground structures is in most cases smaller that that of subsurface ground, and

b) damping is very large because the radiational damping due to energy dissipation from underground structures to subsoils is very large.

Therefore, it is assumed in the Seismic Deformation Method that during an earthquake underground structures deform following the deformation of subsurface ground. Modelling of underground structures has to be made so that structural response of the underground structures be correctly represented. Because the increase of stress and deformation of underground structures due to seismic effects are evaluated by the Seismic Deformation Method, the stress and deformation actually developed during an earthquake have to be computed by adding them with those developed due to the static loads such as the dead weight.

Evaluation of seismic safety of underground structures can be made by either the

---

1) Head, Earthquake Engineering Division, Earthquake Disaster Prevention Department, Public Works Research Institute, Ministry of Construction, Tsukuba-shi, 305

2) Research Engineer, ditto

allowable stress design method or the bearing capacity design method. In the allowable stress design method the stress and the displacement developed in structural components are required to be less than the allowable stress and allowable displacement. In the bearing capacity design method the sectional forces developed in structural components are required smaller that those of dynamic bearing capacity of structural systems considering ductility. Displacement of structures are also required to be smaller than the critical displacement.

After the design by means of the Seismic Deformation Analysis, dynamic response analysis is recommended for the underground structures with complex structural response.

SEISMIC DESIGN FOR CROSS SECTION

In seismic design of underground structures in cross section, the dead weight, the earth pressure, the water pressure, the uplift force, the ground settlement and the seismic effects are to be considered. The loads have to be combined so that the most critical stress or displacement be developed. As the seismic effects, the following loads need to be considered:

Inertia Force

The lateral force coefficient is evaluated as

$$k_h = c_z \cdot c_G \cdot c_U \cdot k_{h0} \qquad (1)$$

in which k_h : lateral force coefficient, k_{h0} : standard lateral force coefficient (= 0.2), c_z : modification factor for zone (1.0, 0.85, 0.7 depending on the region), c_G : modification factor for ground condition (refer to Table 1), c_U : modification factor for depth, and is evaluated as

$$c_U = 1.0 - 0.015z \qquad (2)$$

in which z : depth from ground surface (m).

Table 1 Modification Factor for Ground Condition

Ground Group	I	II	III
c_G	0.8	1.0	1.2

Design Ground Displacement

The design ground displacement is evaluated depending on the depth and the distance as (refer to Fig. 1) :

$$u(z, x) = \frac{1}{\pi^2} S_V \cdot T_S \cdot \cos\left(\frac{\pi z}{2H}\right) \cdot \sin\left(\frac{\pi x}{2L}\right) \qquad (3)$$

in which $u(z, x)$: design ground displacement (m) at depth z (m) and at distance x (m), S_V : design velocity response spectrum at design base rock (cm/sec), H :

thickness of subsurface ground (m), T_S : natural period of subsurface ground (sec), and L : design wave length of ground motion (m). S_V is evaluated as

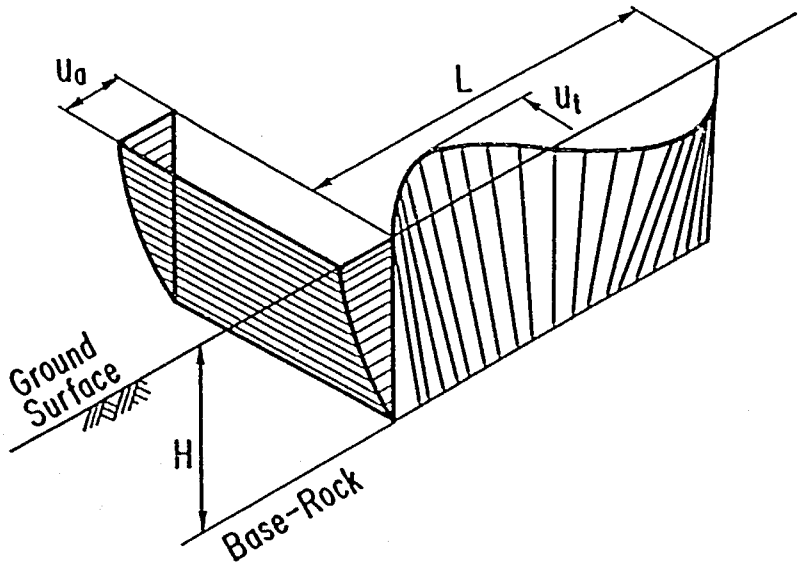


Fig. 1 Deformation of Subsurface Ground Assumed in Seismic Deformation Method

$$S_V = c_z \cdot S_{V0} \tag{4}$$

in which c_z : modification factor for zone and S_{V0} : standard velocity response spectrum (cm/sec) at design base rock, and is given by Fig. 2(a) for the allowable stress design method and by Fig. 2(b) for the bearing capacity design method. The design wave length of ground motion is evaluated as

$$L = \frac{2L_1 \cdot L_2}{L_1 + L_2} \tag{5}$$

in which L_1 and L_2 : design wave length (m) at subsurface ground and base rock, respectively, and are evaluated as

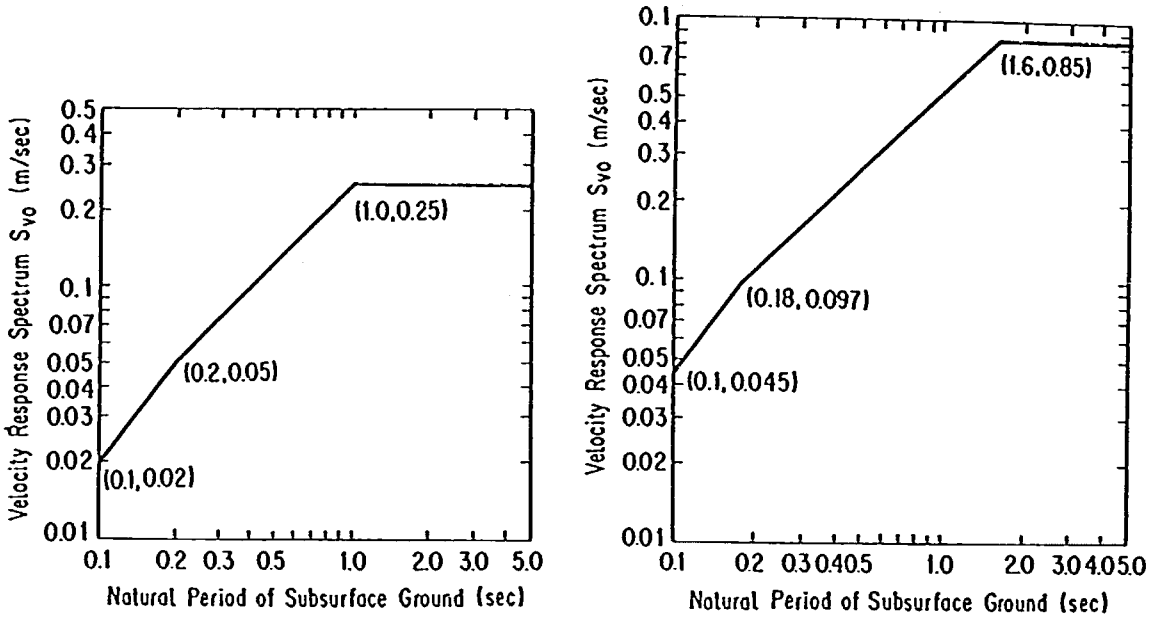
$$L_1 = T_S \cdot V_{SD}\ ,\ L_2 = T_S \cdot V_{SDB} \tag{6}$$

in which V_{SD} : averaged shear wave velocity of subsurface ground (m/sec), and V_{SDB} : shear wave velocity at design base rock (m/sec).

Design Shear Stress around Surface

At the surface of underground structures contacting with soils, the design shear stress around surface needs to be applied to the underground structures as shown in Fig. 3. The design shear stress around surface is given by Eq.(7). If the design shear stress around surface by Eq.(7) is larger than the strength of soils, the strength of soils needs to be taken as the shear stress around surface.

$$\tau = \frac{G_D}{\pi H} S_V \cdot T_S \cdot \sin\left(\frac{\pi z}{2H}\right) \tag{7}$$



(a) Allowable Stress Design (b) Bearing Capacity Design

Fig. 2 Standard Velocity Response Spectrum

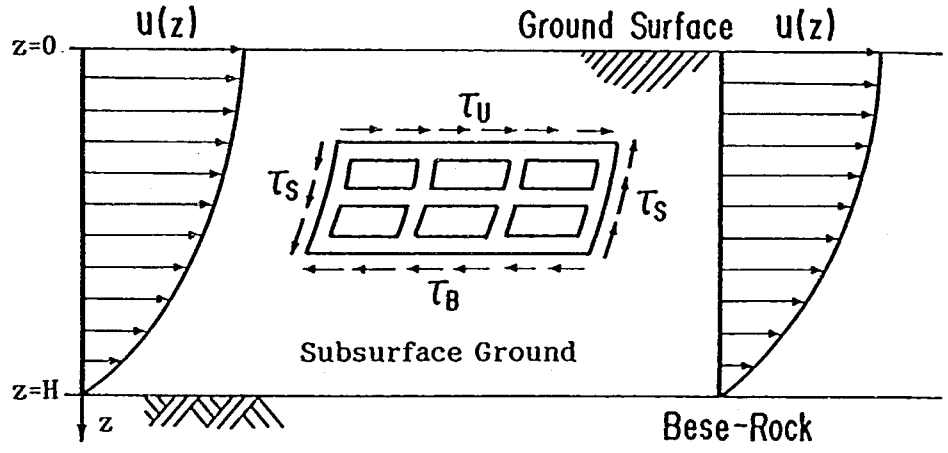


Fig. 3 Design Shear Stress around Surface of Underground Structures

in which P_V^c : Design shear stress around surface (tf/m ^{2}), S_V : design velocity response spectrum at the design base rock (cm/sec), G_D :shear modulus of subsurface ground (tf/m ^{2}), T_S : natural period of subsurface ground (sec), and H : thickness of subsurface ground (m).

Dynamic Earth Pressure

Dynamic earth pressure by Eq.(8) is applied to the side wall of underground structures as shown in Fig. 4.

$$p(z) = k_H \cdot \{u(z) - u(z_B)\} \qquad (8)$$

in which $p(z)$: dynamic earth pressure per unit area (tf/m ^{2}) at depth z (m), k_H : spring stiffness of soils per unit area (tf/m ^{2}), $u(z)$: design ground displacement (m), and z_B : depth of base of underground structure (m).

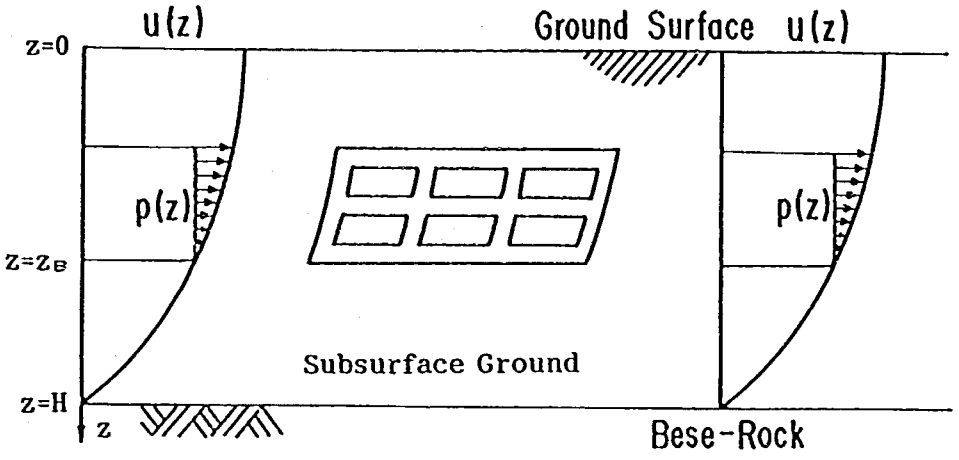


Fig. 4 Dynamic Earth Pressure

SEISMIC DESIGN METHOD FOR AXIAL DIRECTION

Seismic design method for axial direction of tubular underground structures is shown for shield tunnels. Shield tunnels are constructed by assembling a number of segments, ring bolts and segment bolts as shown in Fig. 5. Although there are various idealizations for shield tunnels, the idealization of the shield tunnels as a beam with equivalent stiffness may be the most appropriate for seismic design. Assuming a shield tunnel as a beam, elastically supported by subsurface ground, with equivalent stiffness as shown in Fig. 6, the seismic forces developed in the shield tunnel are evaluated by assuming the ground deformation as shown in Fig. 7 as :

$$\left.\begin{aligned}
&P_h^C=\alpha_1^C\frac{\pi u_h}{L}(EA)_{eq}^C\ ,\ P_h^T=\alpha_1^T\frac{\pi u_h}{L}(EA)_{eq}^T\\
&P_V^C=\alpha_1^C\frac{\pi(u_h+u_V)}{L}(EA)_{eq}^C\ ,\ P_V^T=\alpha_1^T\frac{\pi(u_h+u_V)}{L}(EA)_{eq}^T\\
&M_h=\alpha_3\frac{4\pi u_h}{L^2}(EI)_{eq}\ ,\ M_V=\alpha_3\frac{4\pi u_V}{L^2}(EI)_{eq}\\
&Q_h=\alpha_3\frac{8\pi u_h}{L^3}(EI)_{eq}\ ,\ Q_V=\alpha_3\frac{8\pi u_V}{L^3}(EI)_{eq}
\end{aligned}\right\}\quad(9)$$

where,

P_h^C ,P_h^T : compression and tension force (tf), respectively, developed due to the design ground displacement in lateral direction

P_V^C ,P_V^T : compression and tension force (tf), respectively, developed due to the design ground displacement in vertical direction

M_h ,M_V : bending moment in horizontal plane and vertical plane (tf·m), respectively

Q_h ,Q_V : shearing force in horizontal plane and vertical plane (tf),

respectively

$(EA)^{c}_{eq}$,$(EA)^{T}_{eq}$: equivalent compression rigidity (tf) and equivalent tension rigidity (tf) of shield tunnel

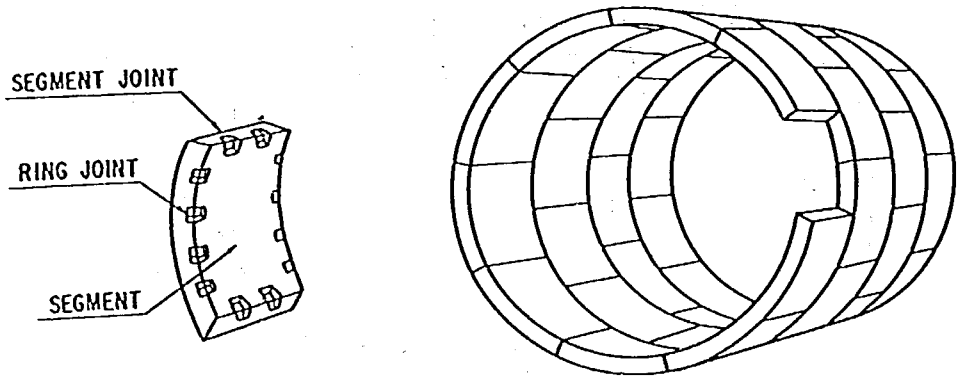


Fig. 5 Segments and Joints of Shield Tunnels

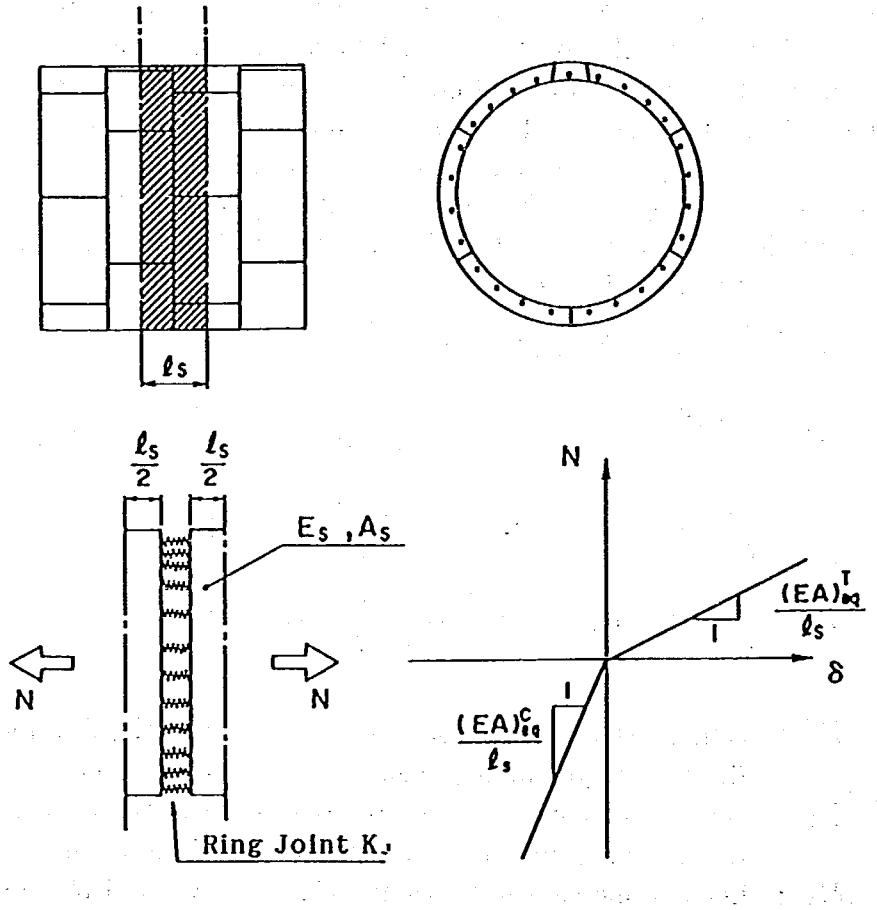


Fig. 6 Axial Stiffness of Segments–Ring Joints

$(EA)_{eq}$: equivalent flexural rigidity (tf)

u_h : design lateral ground displacement (m) at depth of gravity center of shield tunnel

u_v : design vertical ground displacement (m) at depth of gravity center of shield tunnel, and is given as 1/2 of u_h

L : design wave length (m)

$\alpha_1^C, \alpha_1^T, \alpha_2, \alpha_3$: coefficients to represent the degree of transmission of response displacement from the subsurface ground to shield tunnel, and is given by Eq.(10).

$$\left.\begin{aligned} \alpha_1^C &= \frac{1}{1+(2\pi/\lambda_1^C L_1)^2}, \quad \alpha = \frac{1}{1+(2\pi/\lambda_1^T L_1)^2} \\ \alpha_2 &= \frac{1}{1+(2\pi/\lambda_2 L)^4}, \quad \alpha_3 = \frac{1}{1+(2\pi/\lambda_2 L)^4} \end{aligned}\right\} \quad (10)$$

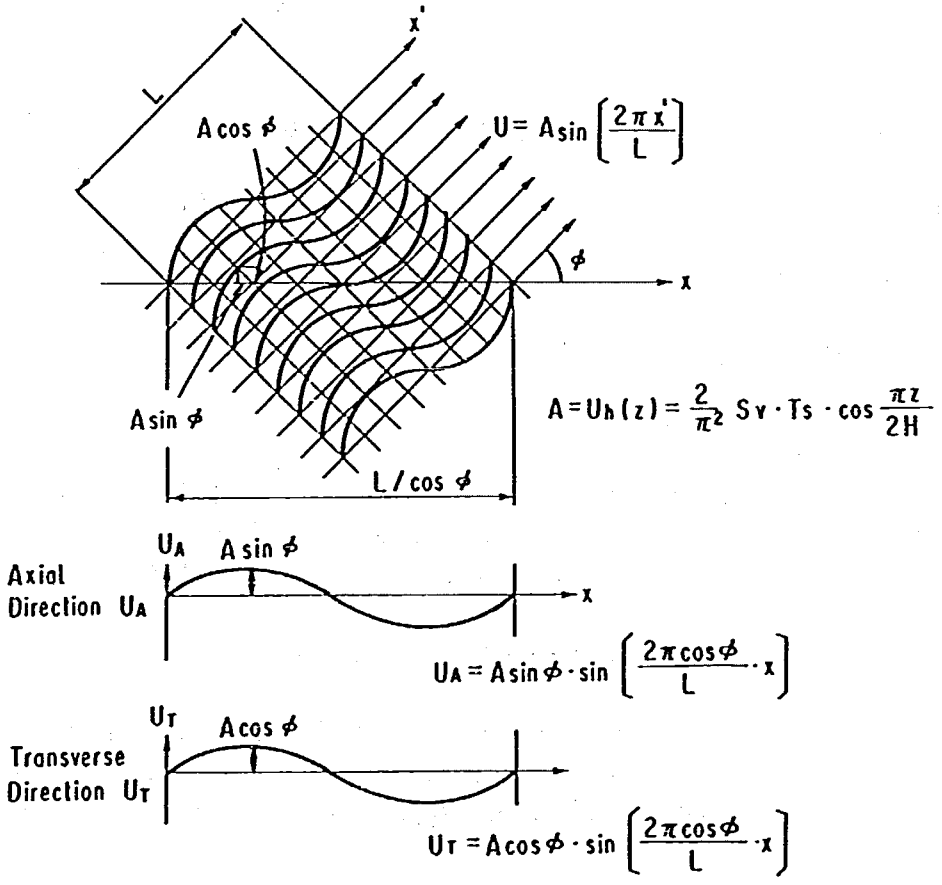


Fig. 7 Ground Displacement Assumed in Seismic Deformation Method

where,

$$\left.\begin{aligned} \lambda_1^C &= \sqrt{\frac{K_{g1}}{(EA)_{eq}^C}}\ ,\quad \lambda_1^T = \sqrt{\frac{K_{g1}}{(EA)_{eq}^T}} \\ \lambda_2 &= \sqrt[4]{\frac{K_{g2}}{(EA)_{eq}}}\ ,\quad \lambda_3 = \sqrt[4]{\frac{K_{g3}}{(EA)_{eq}}} \end{aligned}\right\} \qquad (11)$$

$$L_1 = \sqrt{2} \cdot L \qquad (12)$$

K_{g1} ,K_{g2} ,K_{g3} : soil spring in longitudinal, transverse and vertical direction, respectively (tf/m ^{2})

DYNAMIC RESPONSE ANALYSIS

In the dynamic response analysis, underground structures are idealized so that their response characteristics are well represented. Figs. 8 – 10 show some of the typical analytical idealizations.

Design ground motion at the design base rock is evaluated in terms of either response spectra or ground acceleration. The design acceleration response spectra at the design base rock is given as

$$S = c_z \cdot c_D \cdot S_0 \qquad (13)$$

in which S : design acceleration response spectrum (cm/sec) at the design base rock, S_0 : standard acceleration response spectrum at the design base rock and is given by Fig. 11(a) for the allowable stress design method and by Fig. 11(b) for the bearing capacity design method, c_z : modification factor for zone, and c_D : modification factor of damping ratio, and is given as

$$c_D(h_i) = \frac{1.5}{40h_i + 1} + 0.5 \qquad (14)$$

in which h_i : modal damping ratio of critical.

The input acceleration for the time response analysis is either selected from the strong motion records which have the close response spectral characteristics with S by Eq.(13) or obtained by adjusting the strong motion records in frequency domain so that the acceleration response spectrum be matched with S by Eq.(13).

CONCLUDING REMARKS

The outline of the seismic deformation method was described. The procedure is widely adopted to the design of underground tunnels, parking garage, common utility ducts, and water/gas tunnels. Details of the application however depend on the structures and the importance.

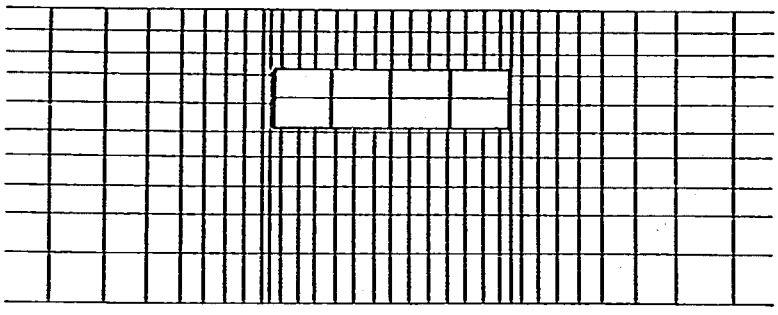


Fig. 8 Two Dimensional Finite Element Idealization

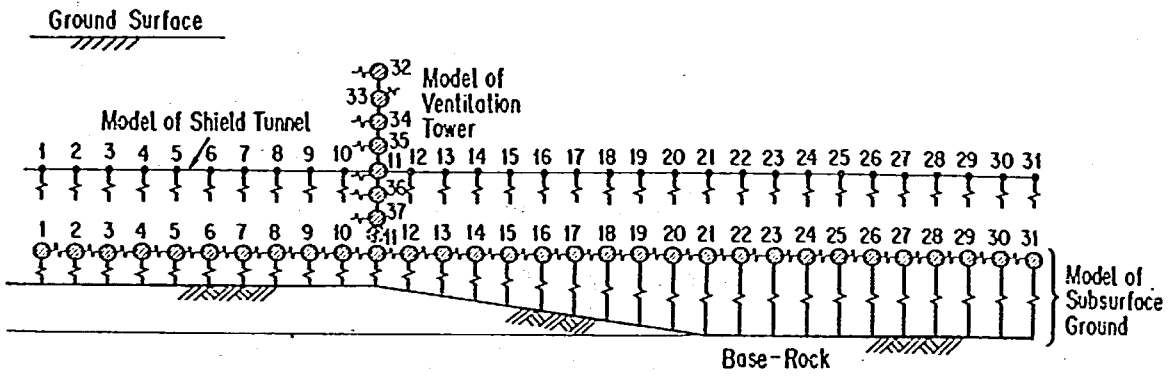


Fig. 9 Idealization by Springs–Masses Model of Tunnel, Ventilation Tower and Subsurface Ground

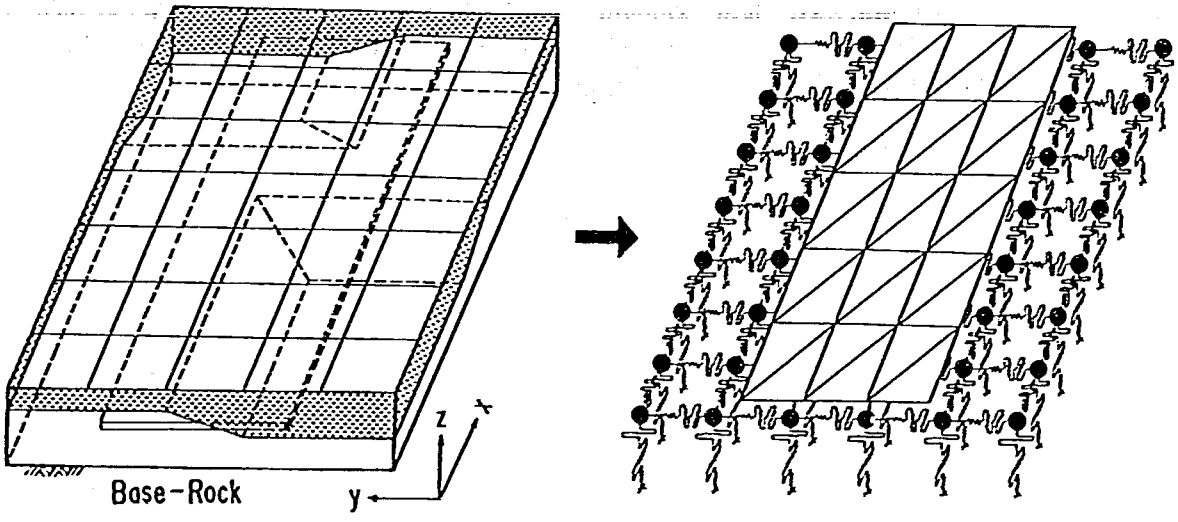
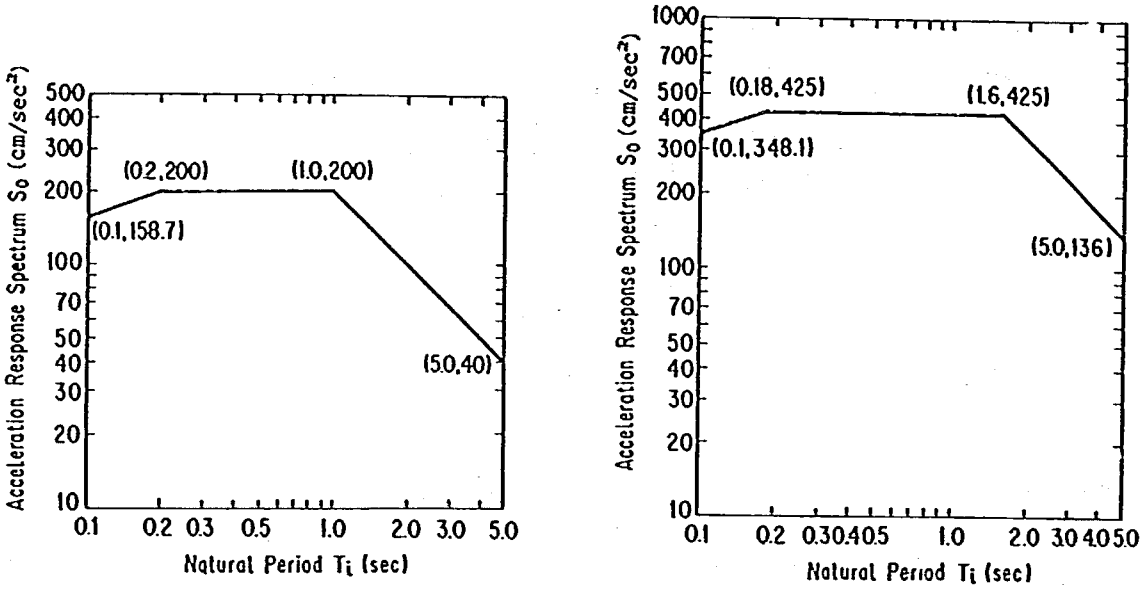


Fig. 10 Idealization by Plate Elements and Shell Elements



(a) Allowable Stress Design (b) Bearing Capacity Design

Fig. 11 Standard Acceleration Response Spectra

REFEPENCES

1) Public Works Research Institute (1992). "Guidelines for seismic design methods of underground structures." Technical Note, No. 3119
2) Asakura, H., Kawashima, K. and Sugita, H. (1992). "Guidelines for seismic design methods of large underground structures." 24th Joint Meeting, Panel on Wind and Seismic Effects, UJNR, Gaithersburg, MD, U.S.A., NIST SP 843.
3) Kawashima, K., Sugita, H. and Kanoh, T. (1990). "Deformation and failure characteristics of shield tunnel models subjected to alternative axial loading." Proc. Japan Society of Civil Engineering, Vol. 422, pp.225–233.

Seismic Design of Highway Bridges In JAPAN

Kazuhiko KAWASHIMA
and
Shigeki UNJOH

First Egyptian Conference on
Earthquake Engineering
August, 1993

SEISMIC DESIGN OF HIGHWAY BRIDGES IN JAPAN

by

Kazuhiko Kawashima [1] and Shigeki Unjoh [2]

ABSTRACT

This paper outlines the seismic design method of highway bridges in Japan. Description is given to the design force, evaluation of soil condition, liquefaction potential and its treatment, check of bearing capacity of reinforced concrete piers, dynamic response analysis and devices foe preventing superstructure from falling-down.

INTRODUCTION

Highway bridges are vital component of highway, and they have to be safe enough against earthquakes so that the function of highway be maintained. They have to be used without loosing any structural functions against small to moderate earthquakes which have high to moderate possibility of occurring at the site. Critical failures causing total collapse of a bridge have to be avoided even during significant earthquakes with the earthquake magnitude over 8.

The "Part V Seismic Design" of the "Design Specifications of Highway Bridges" is applied to the seismic design of highway bridges with span lengths not longer than 200 meters. The specifications adopts the static lateral force method (seismic coefficient method) based on the allowable stress design approach. The check of ductility for reinforced concrete piers (Check of Bearing Capacity of Reinforced Concrete Piers for Lateral Force) and dynamic response analysis are recommended in accordance with flow chart presented in Fig. 1. Emphasis is placed on the need to install devices for preventing falling-off of the superstructures from the substructures.

This paper outlines the seismic design method of highway bridges specified in the "Part V Seismic Design" of the "Seismic Design Specifications of Highway Bridges".

SEISMIC LATERAL FORCE

---

1) Head, Earthquake Engineering Division, Earthquake Disaster Prevention Department, Public Works Research Institute, Ministry of Construction, Tsukuba-shi, 305

2) Senior Research Engineer, ditto

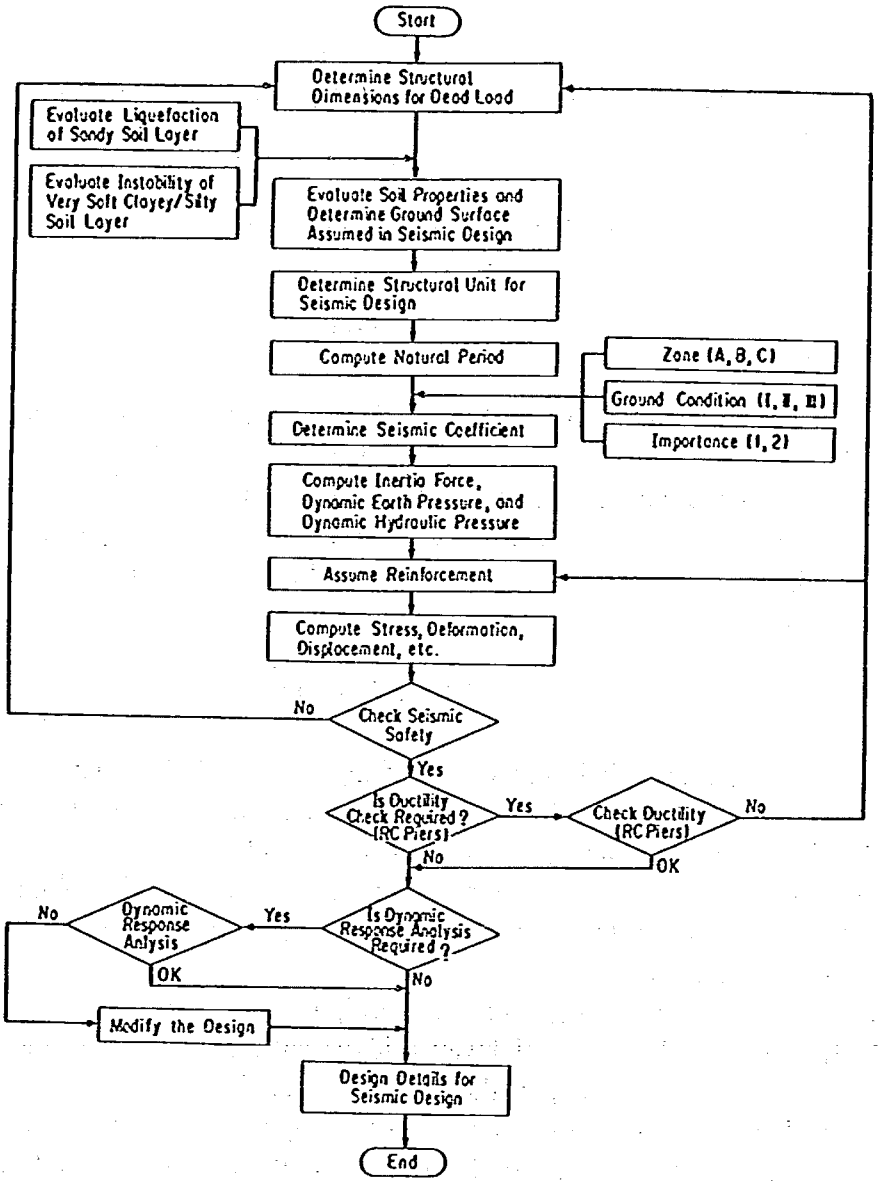


Fig. 1 Flow of Seismic Design of Highway Bridge

In the static lateral force method, the horizontal design seismic coefficient is determined by Eq.(1), but no less than 0.1.

$$k_h = c_z \cdot c_G \cdot c_I \cdot c_T \cdot k_{h0} \qquad (1)$$

in which k_h : design horizontal seismic coefficient, k_{h0} : standard design horizontal seismic coefficient (=0.2) , c_z : modification factor for zone, c_G : modification factor for ground condition (refer to Table 1), c_I : modification factor for importance (refer to Table 2), and c_T : modification factor for structural response (refer to Table 3). The coefficient c_z takes 1.0, 0.85 and 0.7 depending on the zone.

Table 1 Ground Condition Factor c_G

Ground Group	I	II	III
c_G	0.8	1.0	1.2

Table 2 Importance Factor c_I

Ground	c_I	Definition
1st class	1.0	Bridges on expressway (limited access highways), general national road. Important bridges on general prefectural road and municipal road.
2nd class	0.8	Other than the above

Table 3 Structural Response Factor c_R

Ground Group	Structural Response Coefficient c_R		
Group I	$T_{EQ} \leqq 1.4$ $c_R = 0.7$		$1.4 < T_{EQ}$ $c_R = 0.876 T_{EQ}^{-2/3}$
Group II	$T_{EQ} < 0.18$ $c_R = 1.51 T_{EQ}^{1/3} \geqq 0.7$	$0.18 \leqq T_{EQ} \leqq 1.6$ $c_R = 0.85$	$1.6 < T_{EQ}$ $c_R = 1.16 T_{EQ}^{-2/3}$
Group III	$T_{EQ} < 0.29$ $c_R = 1.51 T_{EQ}^{1/3} \geqq 0.7$	$0.29 \leqq T_{EQ} \leqq 2.0$ $c_R = 1.0$	$2.0 < T_{EQ}$ $c_R = 1.59 T_{EQ}^{-2/3}$

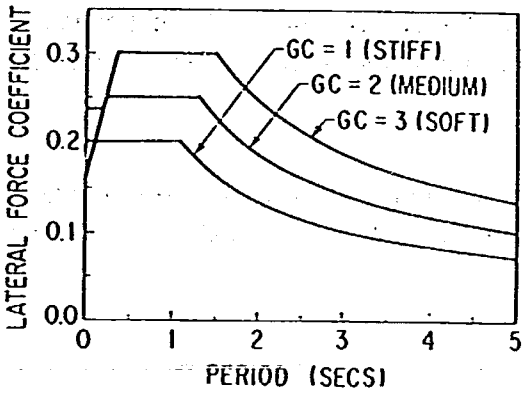


Fig. 2 Horizontal Seismic Coefficient k_h for Static Lateral Force Method ($c_Z = c_I = 1.0$)

Fig. 2 shows the horizontal seismic coefficient assuming $c_Z = c_I = 1.0$. The vertical design seismic coefficient is generally disregarded, except for the bearing supports, because the effect is less. The seismic lateral force is applied to those structural members, soils and water above the "ground surface assumed in seismic design". The ground surface assumed in seismic design depends on soil condition at the site, and is generally assumed at the base level of footing.

Against the lateral force by Eq.(1), the stress, strain and displacement at any part of the structures and soils contacting with the foundations need to be less than the allowable stress, strain and displacement which are specified in the Design Specifications. For seismic design, the allowable stress is increased 1.5 times for a load combination of primary load and the seismic effects.

Ground conditions are classified into three groups according to Table 4, in which characteristic value T_G is evaluated by Eq.(2).

Table 4 Classification of Ground Group

Ground Group	Definition	Approximate Estimation
Group I	$T_G<0.2$ sec	Tertialy or Older
Group II	$0.2\leqq T_G<0.6$ sec	Alluvium and Diluvium
Group III	$0.6\leqq T_G$ sec	Soft Alluvium

$$T_G=\sum_i \frac{4h_i}{V_{si}} \qquad (2)$$

in which H_i : thickness of i–th subsoil layer (m), V_{si} : shear wave velocity of i–th sublayer (m/sec), and i : sublayer's number counted from ground surface.

SOIL LIQUEFACTION

Saturated alluvial sandy layers which have the water table within 10m from the ground surface and have D_{50} –values on the grain size accumulation curve between 0.02 and 2.0mm are vulnerable to liquefaction up to a depth of 20m below the ground surface. For those soil layers which are vulnerable to liquefaction, liquefaction potential needs to be checked based on the liquefaction resistance factor F_L defined as

$$F_L=\frac{R}{L} \qquad (3)$$

in which F_L : liquefaction resistance factor, R : resistance of soil elements against dynamic load and L : dynamic load induced in soil elements during an earthquake. R and L are evaluated as

$$R=R_1+R_2+R_3$$

where,

$$R_1=0.0882\sqrt{\frac{N}{\sigma'_v+0.7}}$$

$$R_2=\begin{cases} 0.19 & (0.02\text{mm}\leqq D_{50}\leqq 0.05\text{mm}) \\ 0.225\log_{10}\left(\dfrac{0.35}{D_{50}}\right) & (0.05\text{mm}< D_{50}\leqq 0.6\text{mm}) \\ -0.05 & (0.6\text{mm}< D_{50}\leqq 2.0\text{mm}) \end{cases}$$

$$R_3=\begin{cases} 0.0 & (0\%\leqq FC\leqq 40\%) \\ 0.004FC-0.16 & (40\%< FC\leqq 100\%) \end{cases}$$

N : N–value of standard penetration test
D_{50} : averaged grain size on grain size accumulation curve
FC : fine sand (grain size less than 74 μ m) content

$$L=r_d\cdot k_s\cdot\frac{\sigma_v}{\sigma'_v}$$

where, $r_d=1.0-0.015x$
x : depth from the ground surface (m)
k_s : seismic coefficient for evaluating liquefaction, and is determined as

$$k_s = c_z \cdot c_G \cdot c_I \cdot k_{s0}$$

c_z, c_G and c_I : modification factors for zone, ground condition, and importance (refer to Eq.(1))

k_{s0} : standard design horizontal seismic coefficient for check of liquefaction (=0.15)

σ_v : total overburden pressure (kgf/cm^2), and

$$\sigma_v = \{\gamma_{t1} h_w + \gamma_{t2}(x - h_w)\}/10$$

σ'_v : effective overburden pressure (kgf/cm^2), and

$$\sigma'_v = \{\gamma_{t1} h_w + \gamma_{t2}(x - h_w)\}/10$$

Soil layers having the liquefaction resistance factors F_L smaller than 1.0 is judged to liquefy during an earthquake.

For those soil layers which were judged to liquefy in the above estimation and which are within 20 m from the ground surface, the spring stiffness and other soil constants need to be either neglected or reduced in seismic design as shown in Fig. 3, by multiplying the original spring stiffness and other soil constants by the reduction factor D_E which is determined in accordance with F_L and Table 5.

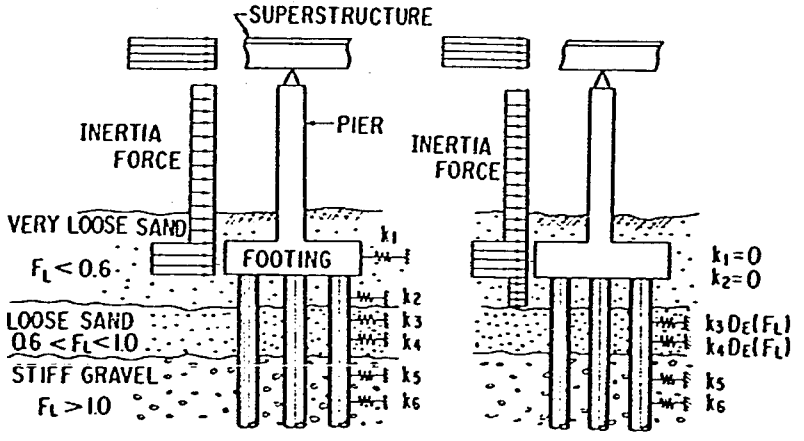


Fig. 3 Treatment of Soil Layers Vulnerable to Liquefaction

Table 5 Decreasing Rate D_E of Soil Constants Depending on F_L Value

F_L -value	Depth from Ground Surface	D_E
$F_L \leqq 0.6$	$0m \leqq x \leqq 10m$	0
	$10m \leqq x \leqq 20m$	1/3
$0.6 < F_L \leqq 0.8$	$0m \leqq x \leqq 10m$	1/3
	$10m \leqq x \leqq 20m$	2/3
$0.8 < F_L \leqq 1.0$	$0m \leqq x \leqq 10m$	2/3
	$10m \leqq x \leqq 20m$	1

CHECK OF BEARING CAPACITY OF REINFORCED CONCRETE PIERS

To prevent reinforced concrete piers from failing in a brittle manner, it is

recommended that the bearing capacity of the reinforced concrete piers be checked in accordance with the flowchart in Fig. 4.

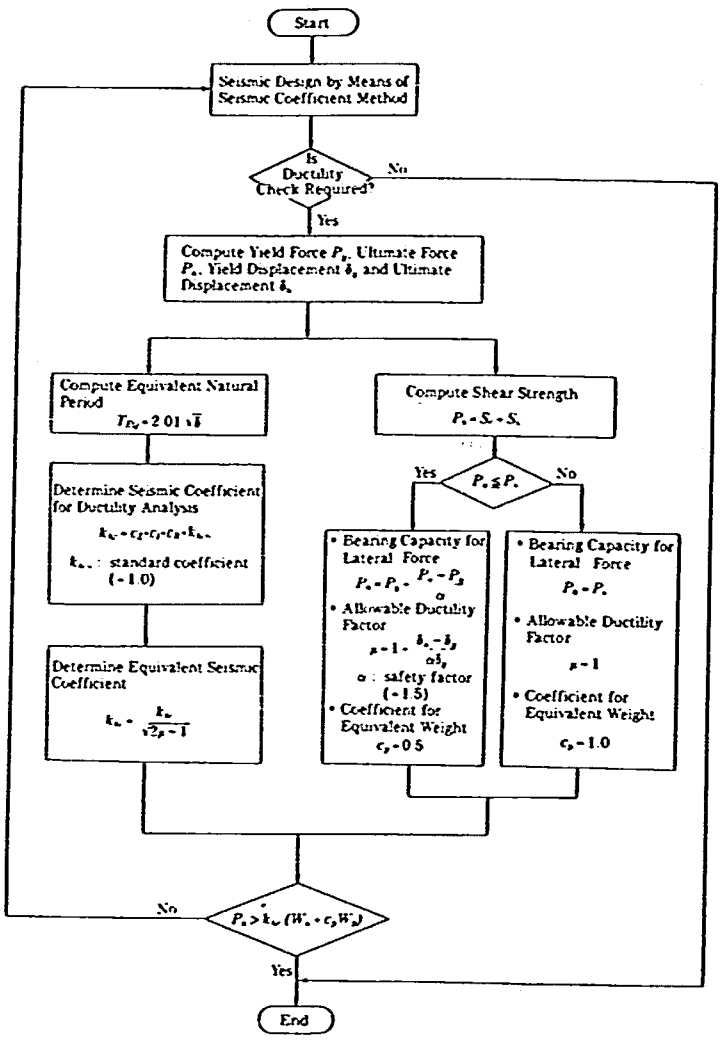


Fig. 4 Check of Bearing Capacity of Reinforced Concrete Pier For Lateral Force

In this check, the bearing capacity of reinforced concrete piers needs to satisfy

$$P_a > k_{he} W \tag{4}$$

in which P_a : bearing capacity of reinforced concrete piers (tf), k_{he} : equivalent horizontal seismic coefficient for check of bearing capacity, W : equivalent dead weight (tf), and is determined as

$$W = W_u + c_P W_P \tag{5}$$

$$c_P = \begin{cases} 0.5 & (P_u \leq P_s) \\ 1.0 & (P_u > P_s) \end{cases} \tag{6}$$

in which W_u : dead weight of a part of superstructure supported by the reinforced concrete piers (tf), W_P : dead weight of reinforced concrete piers (tf), P_u : bearing capacity of reinforced concrete piers for flexural failure (tf), and P_s : bearing capacity of

reinforced concrete piers for shear failure (tf).

Equivalent horizontal seismic coefficient for check of bearing capacity is determined according to the equal energy assumption as

$$k_{he}=\frac{k_{h0}}{\sqrt{2\mu-1}} \tag{7}$$

$$k_{hc}=c_z\cdot c_I\cdot c_R\cdot k_{hc0} \tag{8}$$

in which k_{he} : equivalent horizontal seismic coefficient for check of bearing capacity, k_{hc} : horizontal seismic coefficient for check of bearing capacity, μ : allowable ductility factor, c_z : modification factor for zone (refer to Eq.(1)), c_I : modification factor for importance (refer to Table 2), c_R : modification factor for structural response (refer to Table 6), and k_{hc0} : standard horizontal seismic coefficient for check of bearing capacity.

Table 6 Structural Response Factor c_T

Ground Group	Structural Response Coefficient c_T		
Group I	$T<0.1$ $c_T=2.69T^{1/3}\geqq 1.00$	$0.1\leqq T\leqq 1.1$ $c_T=1.25$	$1.1<T$ $c_T=1.33T^{-2/3}$
Group II	$T<0.2$ $c_T=2.15T^{1/3}\geqq 1.00$	$0.2\leqq T\leqq 1.3$ $c_T=1.25$	$1.3<T$ $c_T=1.49T^{-2/3}$
Group III	$T<0.34$ $c_T=1.80T^{1/3}\geqq 1.00$	$0.34\leqq T\leqq 1.5$ $c_T=1.25$	$1.5<T$ $c_T=1.64T^{-2/3}$

Fig. 5 shows the horizontal seismic coefficient k_{h0} for the check of bearing capacity when $c_z=c_I=1.0$.

The bearing capacity of reinforced concrete piers P_a and the allowable ductility factor μ is determined based on the failure mode as :

a) Flexural failure

$$P_a=P_y+\frac{P_u-P_y}{\alpha} \tag{9}$$

$$\mu=1+\frac{\delta_u-\delta_y}{\alpha\,\delta_y} \tag{10}$$

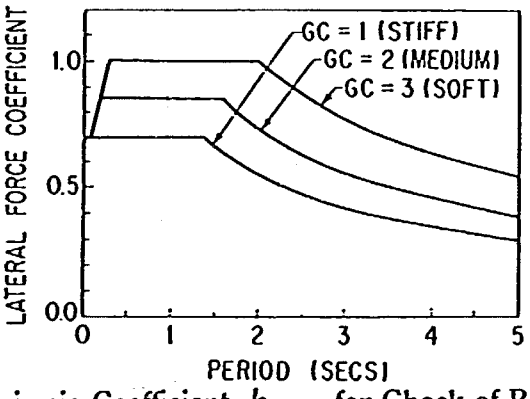


Fig. 5 Horizontal Seismic Coefficient k_{h0} for Check of Bearing Capacity of Reinforced Concrete Piers for Lateral Force ($c_z=c_I=1.0$)

in which P_u , δ_u : bearing capacity (tf) and ultimate displacement (m) for flexural failure, P_y , δ_y : yielding force (tf) and yielding displacement (m) for flexural failure, and α : safety factor (=1.5) .

b) Shear failure

$$P_a = P_s \tag{11}$$

$$\mu = 1 \tag{12}$$

in which P_s : bearing capacity (tf) for shear failure.

DYNAMIC RESPONSE ANALYSIS

For bridges with complicated dynamic response and for new types of bridges, dynamic response analysis is made to check seismic safety of the design made by means of the static lateral force method.

Dynamic response analysis is generally made by the modal response spectral analysis. Acceleration response spectrum for the analysis is given as

$$S = c_z \cdot c_I \cdot c_D \cdot S_0 \tag{13}$$

in which S : response spectrum for analysis (gal (=cm/sec^2)), S_0 : standard response spectrum (gal) (refer to Table 7), c_z : modification factor for zone (refer to Eq.(1)), c_I : modification factor for importance (refer to Table 2), and c_D : modification factor for damping ratio, and is given as

$$c_D = \frac{1.5}{40 h_i + 1} \tag{14}$$

Table 7 Standard Response Spectral Value S_0 for Modal Dynamic Response Analysis

Ground Group	S_0 (gal)		
Group I	$T_i < 0.1$ $S_0 = 431 T_i^{1/3} \geqq 160$	$0.1 \leqq T_i \leqq 1.1$ $S_0 = 200$	$1.1 < T_i$ $S_0 = 220 / T_i$
Group II	$T_i < 0.2$ $S_0 = 427 T_i^{1/3} \geqq 200$	$0.2 \leqq T_i \leqq 1.3$ $S_0 = 250$	$1.3 < T_i$ $S_0 = 325 / T_i$
Group III	$T_i < 0.34$ $S_0 = 430 T_i^{1/3} \geqq 240$	$0.34 \leqq T_i \leqq 1.5$ $S_0 = 300$	$1.5 < T_i$ $S_0 = 450 / T_i$

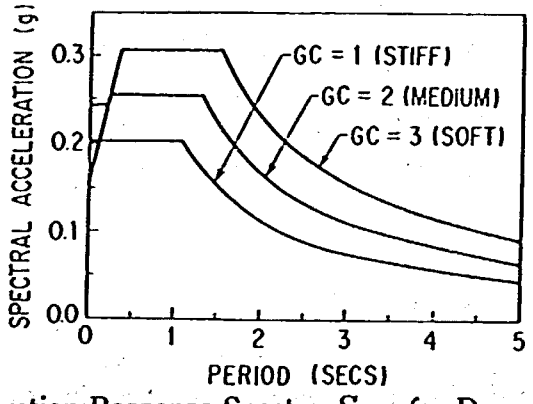


Fig. 6 Design Acceleration Response Spectra S_0 for Dynamic Response Analysis ($c_z = c_I = 1.0$ and $c_D = 1.0 (h_i = 0.05)$)

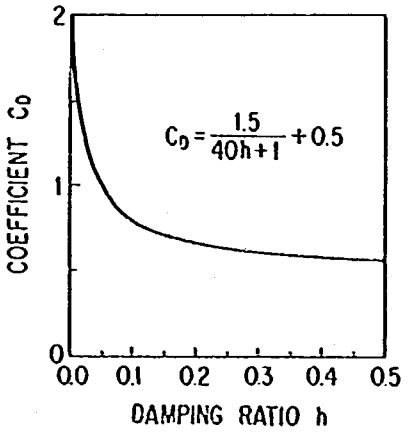


Fig. 7 Modification Factor c_D

in which h_i represents the modal damping ratio of the bridge for i−th mode.

Fig. 6 shows the design response spectra assuming $c_z = c_I = 1.0$ and $c_D = 1.0$ ($h_i = 5\%$). Fig. 7 shows the modification factor c_D.

When a time history analysis is required, several strong motion records which have the similar characteristics with S by Eq.(18) is used. Three ground acceleration records which were modified in frequency domain so that their response characteristics match with S_0 in Eq.(18) are provided in the Specifications as shown in Fig. 8.

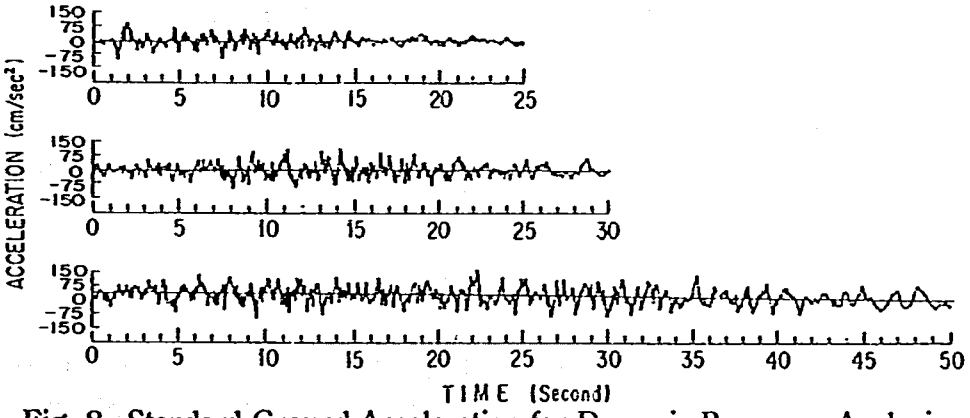


Fig. 8 Standard Ground Acceleration for Dynamic Response Analysis

DEVICES FOR PREVENTING SUPERSTRUCTURE FROM FALLING

Because the connection between the superstructure and substructure is susceptible to earthquake damage, special structural considerations are required to prevent the falling−down of superstructure due to the damage at this section. For such purpose, the following measures are applied as shown in Fig. 9 :

(1) At movable bearings, devices to prevent dislodgement of upper−bearings from the lower−bearings (stopper) are provided.

(2) At the both ends of superstructure, either of the following measures are used to prevent the superstructure from dislodging from the crest of the substructures :

a) The distance from the edge of superstructure to the edge of sub−structure (Seat

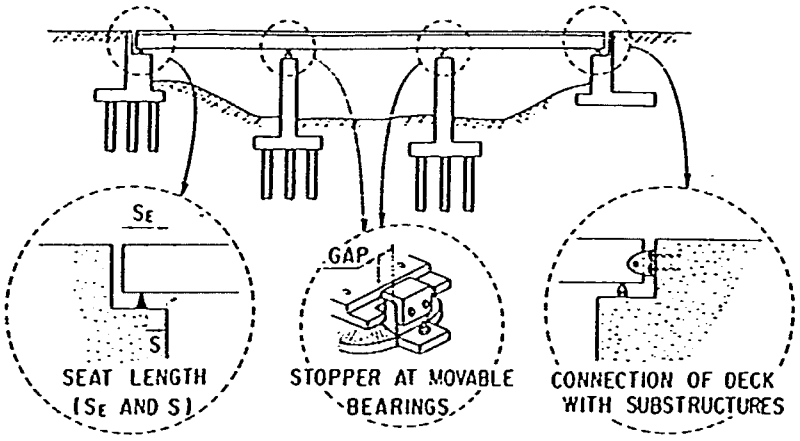


Fig. 9 Devices for Preventing Superstructure from Falling

Length) S_E needs to be longer than the value as

$$S_E = \begin{cases} 70+0.5\,l & (l \leq 100\text{m}) \\ 80+0.4\,l & (l > 100\text{m}) \end{cases} \qquad (15)$$

in which S_E and l represent the seat length in cm and the span length in m, respectively.

b) Installation of devices for preventing falling-off of superstructure from substructures

(3) In addition to the above (1) and (2), the distance from the edge of the bearing supports to the edge of substructure (Bearing Seat Length) S needs to be longer than the value as

$$S = \begin{cases} 20+0.5\,l \\ 30+0.4\,l \end{cases} \qquad (16)$$

in which S and l represent the bearing seat length in cm and the span length in m, respectively

CONCLUDING REMARKS

The current seismic design method issued in 1990 by the Ministry of Construction was briefly described. The design method has been modified and amended several times since 1926 by introducing lessons leaned from the earthquake experiences. Although the seismic damage developed in the past may be prevented by adopting this seismic design method, further attention needs to be paid for the new types of damages which are resulted from new construction practice.

REFERENCES

1) Japan Road Association : "Part V Seismic Design" of the "Design Specifications for Highway Bridges", 1990
2) Kawashima, K. : Seismic Design, Seismic Strengthening and Repair of Highway Bridges in Japan, U.S.-Japan Workshop on Seismic Retrofit of Bridges, Tsukuba Science City, Japan, December 1990

Seismic Strengthening of Highway Bridges

Kazuhiko KAWASHIMA
Shigeki UNJOH
and
Hidetoshi MUKAI

2nd U.S.–Japan Workshop on
Seismic Retrofit of Bridges
Berkeley, U.S.A.
January, 1994

SEISMIC STRENGTHENING OF HIGHWAY BRIDGES

Kazuhiko KAWASHIMA[1], Shigeki UNJOH[2] and Hidetoshi MUKAI[3]

1) Head, Earthquake Engineering Division, Public Works Research Institute, Ministry of Construction, Tsukuba Science City, Japan
2) Senior Research Engineer, ditto
3) Assistant Research Engineer, ditto

ABSTRACT

This paper presents current technical developments for seismic strengthening of existing highway bridges in Japan. Seismic strengthening for substructures is described based on the past practice. Emphasis is placed on the example of implementation.

INTRODUCTION

Japan is one of the most seismically disastrous countries in the world and has often suffered significant damage from large earthquakes. More than 3,000 highway bridges suffered damage in the past earthquakes since the Kanto Earthquake in 1923. The damage to highway bridges caused serious loss of function of road as an emergency evacuation route and a transportation route for emergency relief goods. Since repair of bridges damaged by an earthquake takes a long time, it significantly affects social and economical activities in the area. Therefore, it is important to provide appropriate seismic resistance for existing highway bridges.

This paper presents the seismic strengthening methods for substructures based on the case study of 121 examples of seismic strengthening.

HISTORY OF PROVISIONS OF SEISMIC DESIGN CODES FOR HIGHWAY BRIDGES

One year after the 1923 Kanto Earthquake, it was initiated to consider the seismic effect in design of highway bridges. The Civil Engineering Bureau of the Ministry of Interior notified "the method of seismic design of abutments and piers" in 1924. The seismic design method has been developed and improved through bitter experience in the number of past earthquakes and with progress of technical development in earthquake engineering. Table 1 shows the history of provisions in seismic design for highway bridges.

In particular, the seismic design method was integrated and upgraded by compiling the "Specifications for Seismic Design of Highway Bridges" in 1971, which exclusively provided issues related to seismic design. It was revised in 1980 and integrated as "Part V : Seismic Design" in "Design Specifications of Highway Bridges". It was further revised in 1990 and has been in practice for all highway bridges with span length shorter than 200m. In the latest Specifications, design seismic force, bearing capacity of reinforced concrete piers for lateral force, soil liquefaction, dynamic response analysis, and design detailings are prescribed.

HISTORY OF SEISMIC EVALUATION AND SEISMIC STRENGTHENING OF HIGHWAY BRIDGES

The Ministry of Construction made seismic evaluation of highway bridges 5 times throughout the country since 1971 as a part of the comprehensive earthquake disaster prevention measures for highway facilities. Seismic strengthening for vulnerable highway bridges has been successively made based on the seismic evaluations. Table 2 shows the history of past seismic evaluations[1)-8)].

The first seismic evaluation was made in 1971 to promote earthquake disaster prevention measures for highway facilities. The significant damage of highway bridges caused by the San Fernando Earthquake, U.S.A. in February 1971 triggered the seismic evaluation. Highway bridges with span length longer than or equal to 5m on all sections of national expressways and national highways, and sections of the others were evaluated. Attention was paid to detect deterioration such as cracks of reinforced concrete structures, tilting, sliding, settlement and scouring of foundations. Approximately 18,000 highway bridges in total were evaluated and approximately 3,200 bridges were found to require strengthening.

Following the first seismic evaluation, it has been subsequently made in 1976, 1979, 1986 and 1991 with gradually expanding highways and evaluation items. The seismic evaluation in 1986 was made with the increase of social needs to insure seismic safety of highway traffic after the damage caused by the Urakawa-oki Earthquake in 1982 and the Nihon-kai-chubu Earthquake in 1983. The highway bridges with span length longer than or equal to 15m on all sections of national expressways, national highways and principal local highways, and sections of the others, and overpasses were evaluated. The evaluation items included deterioration, devices for preventing falling-off of superstructure, strength of substructures and stability of foundations. Approximately 40,000 bridges in total were evaluated and approximately 11,800 bridges were found to require strengthening. Through a series of seismic strengthening works, approximately 25,000 bridges were strengthened by the end of 1991 fiscal year. Latest seismic evaluation was made in 1991. The results are being compiled.

In the seismic evaluation in 1986 and 1991, the evaluation was made based on a statistical

analysis of bridges damaged and undamaged in the past earthquakes[9]. Factors which affect seismic vulnerablity were detected as shown in Table 3. Table 4 shows the inspection sheet proposed to evaluate the seismic vulnerability. Because collapse of bridges tends to be developed due to the excessive relative movement between the superstructure and the substructures, and failure of substructures associated with inadequate strength, the evaluation is made in Table 4 based on both the relative movement and the strength of substructure.

Table 5 shows the feasibility of seismic strengthening against the 16 factors which would affect the seismic vulnerability of highway bridges as shown in Table 3. Among the 16 factors, ⑥ devices for preventing falling-off of superstructure, ⑦ type of substructures, ⑩ effect of soil liquefaction, ⑫ effect of scouring, ⑬ materials of substructures, ⑭ type of foundation, and ⑯ termination of main reinforcement at mid-height with inadequate anchoring length are the factors for which countermeasures are feasible. Countermeasures for other factors may not be feasible unless the whole bridge be replaced.

Fig. 1 shows how the countermeasures can be made for the above 7 factors. Installation of the devices for preventing falling-off of superstructure, strengthening of foundations, and strengthening of piers and abutments are the measures which are most often adopted for seismic strengthening.

Emphasis has been placed to install the falling-off prevention devices in the past seismic strengthening. Because the installation of the falling-off prevention devices is being completed, it now becomes important to promote the strengthening of substructures with inadequate strength and lateral stiffness.

SEISMIC STRENGTHENING FOR SUBSTRUCTURES

Practices of Strengthening

The Public Works Research Institute collected the data on the highway bridges in which substructures were strengthened based on the seismic evaluation in 1979 and 1986.[10)-12)] The first survey was made in 1987 to collect the data of seismic strengthening due to the seismic evaluation in 1979 and the second survey was made in 1991 to collect the data of seismic strengthening due to the seismic evaluation in 1986. Although the data base covers only a few bridges, it provides the most reliable information for seismic evaluation and strengthening.

The data base includes the year of construction, design specifications referred to, type of structures, results of the seismic evaluation, selection and comparison of seismic strengthening methods, design of strengthening, and construction method. In total the data for 121 bridges were collected.

Fig. 2(a) shows the year of construction of the bridges surveyed. About 70% of the strengthened bridges were constructed from 1950s to 1960s. The rate of bridges constructed before 1950 is only 22%. For such old bridges, replacement rather than the seismic strengthening has been made. Fig. 1(b) shows the design specifications referred to for the bridges surveyed. About 93% of the bridges strengthened were designed according to the pre−1971 specifications.

Reasons to Require Strengthening

Fig. 3 shows the number of bridges strengthened classified in terms of requirements for seismic strengthening. The requirements for strengthening, i.e., the reason for requiring the seismic strengthening, were classified from Table 3 into 10 as

- ·scouring around foundation
- ·abnormal displacement of foundation
- ·apparent deterioration of reinforced concrete structure
- ·weak reinforced concrete frame
- ·substructure placed on two independent caisson foundations
- ·bent piles with inadequate strength and lateral stiffness
- ·pier with inadequate strength
- ·soil liquefaction
- ·inadequate bearing capacity of piles
- ·inadequate bearing capacity of soil/foundation

The seismic strengthening was required mostly because of the inadequate bearing capacity of foundations associated with scouring, inadequate strength of reinforced concrete frame structure, and inadequate bearing capacity of piles. Forty bridges were strengthened because problem arose due to the scouring. Because the vulnerability of foundations due to scouring can be reliably evaluated, the strengthening has been made successively. Sixteen bridges were strengthened due to the weakness of reinforced concrete frame structure and inadequate bearing capacity of piles, respectively.

Strengthening Methods

Fig. 4 shows the methods adopted for seismic strengthening. They are presented for the 10 requirements presented above. Various methods were adopted depending on site conditions and other restrictions and requirements. Increase of number of piles, enlargement of footing, placing of new reinforced concrete section surrounding the existing structure, and construction of new lateral beams for increasing strength and lateral stiffness are the major methods.

IMPLEMENTATION OF SEISMIC STRENGTHENING

Seismic Strengthening of Weak Reinforced Concrete Frame Structures

Fig. 5 shows an implementation of seismic strengthening of a reinforced concrete frame. This bridge was constructed in 1959 and has a 5–span simply–supported steel plate girder with length of 176m. The substructures were of reinforced concrete frame structures with reinforced concrete piles.

Based on the 1979 seismic evaluation, an increase of the lateral strength of substructures in transverse direction was detected to be required. It was decided to place a new reinforced concrete wall to strengthen the substructures. Thickness of the wall was designed as 40cm, and it was assumed that the seismic lateral force is supported by the integrated structure consisting of the new and the existing reinforce concrete members. Therefore, the most crucial point of the design and construction was how reliably the integration between the new and the existing structures be made. To assure the reliable integration, the cover concrete of exciting substructures was chipped–out by about 1cm and anchor bars were installed with 30cm pitch at the columns. The anchor bars with diameter of 16mm (D16) were inserted in the drilled holes with diameter of 26mm and depth of 24cm. The spaces between the holes the and the anchor bars were filled with epoxy resin.

Seismic Strengthening of Bent Piles with Inadequate Lateral Stiffness

Fig. 6 and Photo 1 show a seismic strengthening for bent piles with inadequate lateral stiffness. This bridge was constructed in 1960 and has a 9–span simply–supported prestressed concrete slab with length of 54m. The substructures were of bent piles with 7 reinforced concrete piles with length of 12m and diameter of either 30cm or 50cm.

Based on the 1979 seismic evaluation, an increase of the lateral strength of the bent piles in longitudinal direction was detected to be required. It was decided to place a new reinforced concrete surrounding the piles at the river bottom level and to connect each bent pile by reinforced concrete slabs. The reinforced concrete slabs were placed to decrease the lateral displacement of bent piles at the river bottom level. This method was selected because the span length was short and the effectiveness of strengthening was apparent. Design was made assuming that the lateral force is supported by a new integrated structure.

Seismic Strengthening of Bent Piles in Liquefaiable Sandy Soils

Fig. 7, Photos 2 and 3 show a seismic strengthening of 11–span simply–supported pre–tensioned concrete slab bridge. It was constructed in 1959. Reinforced concrete bent plies were used for piers and abutments. The diameter and length of reinforced concrete piles were 60cm and 12m for piers and 50cm and 8m for abutments, respectively.

Based on the 1986 seismic evaluation, it was found that the bent piles were vulnerable to soil liquefaction. The Liquefaction Resistance Factor F_L at the sandy layer with thickness of 3.2m below the river bed was less than 1.0. The length of the part of piles which were supported by stable soil was only 1/3 of the total pile length of 12m. Based on the stability analysis of piles, the stress induced in concrete and reinforcing bars of piles significantly exceeded the allowable stresses. The displacement predicted at piles was 4.6cm at the design ground level and 12.8cm at the crest. Those were much larger than the allowable displacement.

Five strengthening measures were proposed. Those were ① to strengthen all 12 substructures, ② to strengthen one substructure per two spans, ③ to strengthen both abutments and connect all pier crests by continuous beams, ④ to replace liquefiable soil layer by stable soils, and ⑤ to increase soil strength by chemical grouting. Because the methods ④ and ⑤ were expensive in spite of unreliable effectiveness, they were decided to be not appropriate at this site. Among the three strengthening methods, ③ was adopted because cost performance was the most superior. Because strengthening of the substructures was required at only two end abutments, it was less expensive. It was decided that the seismic safety can be increased to the level required if the lateral displacement induced at pier crest was controlled by the continuous beams.

In the design, it was assumed that the lateral force in longitudinal direction is supported by both the new piles and the existing piles. Since the pier crests of bent piles are strengthened by the connecting beams, it was required to insure enough strength for the connecting beams and fix bearing set between the pier crests and the connecting beams. Therefore, they were designed adopting two times larger design lateral force. It should be noted that the connecting beams were also used as the girders for supporting a pedestrian deck installed to the bridge.

Seismic Strengthening of Weak Bent Piles

Fig. 8 and **Photo 4** show strengthening of 3–span continuous steel plate girder bridge with deck length of 75m. Steel pipe bent plies were used for piers. The diameters and length of the piles were 1m and 45.2m, respectively. The bridge was constructed in 1969.

Based on the 1986 seismic evaluation, it was found that the stress induced in the reinforced concrete lateral beam significantly exceeded the allowable stress when the seismic lateral force was applied in transverse direction. The stress induced in the steel–pipe piles is smaller than the allowable stress. Because it was not easy to strengthen the lateral beam, it was decided to place a new reinforced concrete wall surrounding the existing bent piles. Hollow section was adopted to mitigate the increase of the weight. The construction was made by drying–up the water using the steel sheet piles.

Seismic Strengthening of Foundations with Inadequate Soil Bearing Capacity

Fig. 9 shows seismic strengthening of foundations by increasing number of piles and enlarging footing. The bridge was constructed in 1960 and consisted of 14–span simply–supported prestressed concrete girder with length of 238m. The abutments were of a gravity type with wooden piles. Piers were of reinforced concrete frames with wooden piles.

Based on the 1979 seismic evaluation, the bearing capacity of soils around foundations was found to be insufficient. Two strengthening methods were proposed. The first was to increase number of piles and the second was to improve soils. Since it is reliable and the construction cost was cheaper in the first method, it was adopted as a principal countermeasure. However, since the construction space was very limited to place the new piles, the soil improvement as well as enlargement of the existing footing was adopted for some foundations.

In increasing number of new piles, the existing wooden piles were neglected and it was assumed that the lateral force is supported by only new piles. On the other hand, in the design of soil improvement and enlargement of footings, it was assumed that the lateral force is supported by shear force at the bottom of the new and the existing footings. Because the soil was improved so as to increase the N–value to 30, the bearing capacity of the soil could be increased. When the new footing was placed on the existing footing, the surface of existing footing was chipped–out by 2cm, and anchor bars with diameter of 22mm (D22) were installed with epoxy resin injection. The cement milk was injected to improve soil up to 3m deep below the bottom of the footing.

Seismic Strengthening of a Pile Foundation Vulnerable to Liquefaction

Fig. 10 shows seismic strengthening of pile foundations in liquefiable soil layers. This bridge was constructed in 1952 and consisted of a Langer girder and 15–span simply–supported plate girder with length of 575m. Abutments were of gravity type foundations and piers were of reinforced concrete walls. Foundations were of open caisson for the Langer girder and pile foundations for the others.

Based on the 1979 seismic evaluation, it was detected that the bearing capacity of soils at the pier foundations was inadequate, because the soil was vulnerable to liquefaction.

Three strengthening methods were proposed. They were ① to improve the ground by soil cement, ② to increase number of piles, and ③ to surround the existing foundations by steel sheet piles. Since ① was expensive, ② and ③ were investigated precisely, and ② was finally adopted. Effectiveness of strengthening was reliable and cost performance was

superior.

In the design, it was assumed that the existing piles would resist to the lateral seismic force up to the design level and that the lateral force beyond the design level be supported by the new piles. Since the piers were in the high water channel, a temporary road was constructed to the piers during the construction. The steel–pipe piles were placed using a vibro hammer. The new footing was constructed by drying–up water by steel sheet piles. Integration between the new and the existing footings was made by anchor bars with injection of resin mortar. **Photo 5** shows the construction of new piles. **Photos 6** and **7** show the connection of the new and the existing footings.

Seismic Strengthening of a Pile Foundation by Enlarging Footing and Increasing Number of Piles

Fig. 11 and **Photo 8** show Akisato Bridge on National Highway No.9 in Tottori City.[13] It was planned to be of two bridges in parallel with length of 264m. Because number of traffic was small at the construction stage, only one bridge was completed in 1975 with the substructures being completed so as to support the two bridges. Since number of traffic increased in recent years, it became required to construct one more bridge on the existing substructure. The existing bridge is of 7–span simply–supported steel plate girder and a simple prestressed concrete hollow slab. The substructures consist of reinforced concrete frame structures and wall type reinforced concrete piers. All substructures are supported by steel pipe piles with length of 40m. The ground is of very soft clay with thickness of about 30m.

Associate with the revision of the seismic map and the lateral force coefficient, it was required to increase the design lateral force coefficient from 0.2 to 0.3 to meet with the current design requirements. Some deterioration is also found at the substructures,

For the 50% increase of the lateral force, the superstructure was made continuous so as to distribute the lateral force to as many substructures as possible. The substructures required to increase number of piles, thickness and size of footing and strength of piers. Because the space on the footing was limited, the thickness of the footing was required to be increased not only on the footing but also at the bottom. An unique method with high fluid concrete was adopted.

Fig. 13 shows the construction procedure. After excavating the bottom of the existing footings, new piles were placed and the new footing was constructed. The high fluid concrete was placed from one side of the footing. It was placed from the other side. The new footing was completed by placing the concrete on the existing footing. It is very unique to place the new reinforced concrete under the existing footing and to adopt the high fluid concrete. The strengthening was completed in 1993. **Photo 9** shows the excavation at the

bottom of the existing footing. Although mini–back–hoes were used to excavate the soil under the footing, manpower was also required as shown in the **Photo 10. Photos 11** and **12** show the reinforcement at the top of new piles and the new footing. **Photo 13** shows the seismic strengthening of piers.

Fig. 14 shows the strengthening of the abutments. Instead of increasing the strength of the abutments, expanded polystyrene (EPS) was used behind the abutments to decrease the earth pressure on the abutments. Expanded polystyrene was placed with height of 1.75m and length of 13m.

CONCLUSIONS

This paper presented seismic strengthening of existing highway bridges with emphasis on case study of implementation. Emphasis has been placed by now to install the falling–off prevention devices. Because the installation of the falling–off prevention devices is being almost completed, it is now required to further promote the seismic strengthening of substructures. As described in this paper, the past strengthening of substructures has been made case by case basis.

Being different from the installation of the falling–off prevention devices, the seismic strengthening of substructures requires more cost. Because most of the substructures designed and constructed before 1971 do not meet with the current seismic requirements, it is urgently needed to study the level of seismic vulnerability requiring the strengthening. Upgrading of the reliability to predict the possible failure modes in the future earthquakes is also very important.

REFERENCES

1) Headquarters Office for Earthquake Disaster prevention Countermeasures, Ministry of Construction : Countermeasures against Large–scale Earthquakes, Monthly Journal of Construction, Vol.25, No.1, January, 1972 (in Japanese)
2) Fujii, T. : Road Disaster Prevention Measures, Journal of Road, September, 1978 (in Japanese)
3) Fujii, T. : Road Service and Road Disaster Prevention Measures, Journal of Road, June, 1980 (in Japanese)
4) Yamauchi, Y. : Present Status of Road Disaster Prevention Measures, Journal of Road, December, 1980 (in Japanese)
5) Yoshikoshi, H. : Present Status and Subjects of Road Disaster Prevention Measures, Journal of Road, September, 1982 (in Japanese)
6) Miyaji, A. : Road Disaster Prevention Measures, Journal of Road, September, 1990 (in Japanese)
7) Edited by Road Bureau, Ministry of Construction : Road Traffic and Economy Survey,

1992 Version, December, 1990 (in Japanese)
8) Kawashima, K. : Seismic Design and Earthquake Disaster Countermeasures for Highway Bridges, Journal of Road, September, 1990 (in Japanese)
9) Kawashima, K. and Unjoh, S. : An Inspection Method of Seismically Vulnerable Existing Highway Bridges, Structural Eng./Earthquake Eng., Vol.7, No.7, Proc. JSCE, April 1990
10) Kawashima, K., Unjoh, S. and Azuta, Y. : Case Survey of Seismic Strengthening Practices of Existing Highway Bridges Based on Seismic Inspection of 1979, Technical Memorandum of Public Works Research Institute, No.2674, October, 1989 (in Japanese)
11) Kawashima, K., Unjoh, S. and Iida, H. : Case Survey of Seismic Strengthening Practices of Existing Highway Bridges Based on Seismic Inspection of 1986, Technical Memorandum of PWRI, No. 69, 1990 (in Japanese)
12) Kawashima, K. and Unjoh, S. : Seismic Strengthening and Retrofitting of Highway Bridges in Japan, Proc. the 5th U.S.–Japan Workshop on Earthquake Disaster Prevention for Lifeline Systems, 1992, Technical Memorandum of PWRI, No.3198, 1992
13) Kaneyama, T., Suzuki, H. and Hashimoto, T. : Seismic Strengthening and Construction of Akisato Bridges, Proc. of the 20th Road Conference, 1993 (in Japanese)
14) Suzuki, H. and Kanoh, S. : Seismic Strengthening of an Existing Bridge Foundation – Akisato Bridge at Tottori New National Highway –, Seminar on Construction Technology, Shikoku Regional Office of Japan Construction Technology Association, October, 1993 (in Japanese)

Table 1 Development of Seismic Design Methods for Highway Bridges

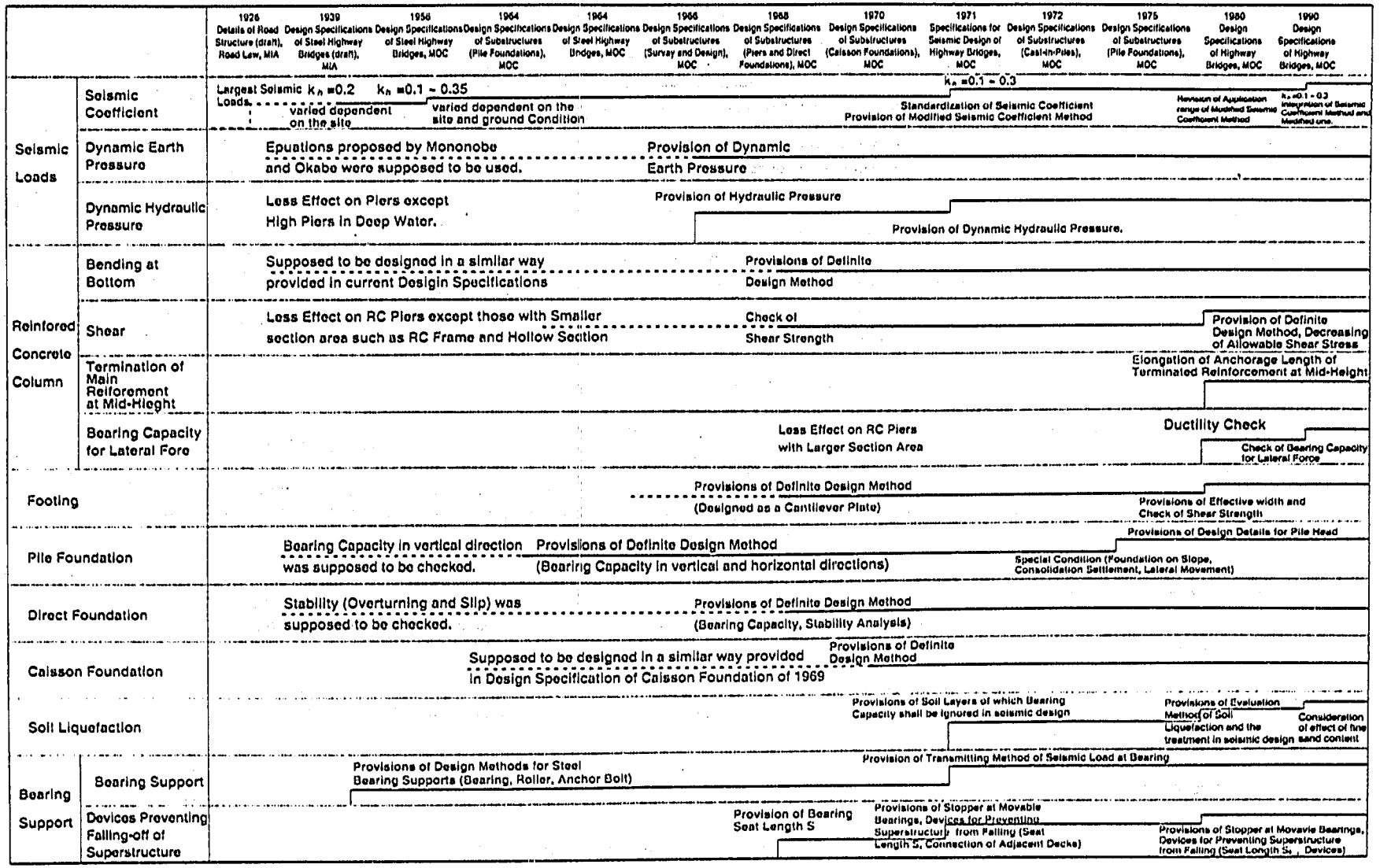


Table 2 Past Seismic Evaluations of Highway Bridges

Year	Highways Inspected	Inspection Items	Number of Bridges		
			Inspected	Require Strengthening	Strengthened
1971	All Sections of National Expressways and National Highways, and Sections of the Others (Bridge Length ≧ 5m)	① Deterioration ② Bearing Seat Length S for Bridges supported by Bent Piles	18,000	3,200	1,500
1976	All Sections of National Expressways and National Highways, and Sections of the Others (Bridge Length ≧ 15m or Overpass Bridges)	① Deterioration of Substructures, Bearing Supports and Girders/Slabs ② Bearing Seat Length S and Devices for Preventing Falling-off of Superstructure	25,000	7,000	2,500
1979	All Sections of National Expressways, National Highways and Principal Local Highways, and Sections of the Others (Bridge Length ≧ 15m or Overpass Bridges)	① Deterioration of Substructures and Bearing Supports ② Devices for Preventing Falling-off of Superstructure ③ Effect of Soil Liquefaction ④ Bearing Capacity of Soils and Piles ⑤ Strength of RC Piers ⑥ Vulnerable Foundations (Bent Pile and RC Frame on Two Independent Caisson Foundation)	35,000	16,000	13,000
1986	All Sections of National Expressways, National Highways and Principal Local Highways, and Sections of the Others (Bridge Length ≧ 15m or Overpass Bridges)	① Deterioration of Substructures, Bearing Supports and Concrete Girders ② Devices for Preventing Falling-off of Superstructure ③ Effect of Soil Liquefaction ④ Strength of RC Piers (Bottom of Piers and Termination Zone of Main Reinforcement) ⑤ Bearing Capacity of Piles ⑥ Vulnerable Foundations (Bent Piles and RC Frame on Two Independent Caisson Foundation)	40,000	11,800	8,000 (As of the End of 1991 Fiscal Year)
1991	All Sections of National Expressways, National Highways and Principal Local Highways, and Sections of the Others (Bridge Length ≧ 15m or Overpass Bridges)	① Deterioration of Substructures, Bearing Supports and Concrete Girders ② Devices for Preventing Falling-off of Superstructure ③ Effect of Soil Liquefaction ④ Strength of RC Piers (Piers and Termination Zone of Main Reinforcement) ⑤ Vulnerable Foundations (Bent Piles and RC Frame on Two Independent Caisson Foundation)	60,000	———	———

Note) Number of bridges inspected, number of bridges that required strengthening and number of bridges strengthened are approximate numbers.

Table 3 Factors which Affect Seismic Vulnerability of Highway Bridges

Items	Seismic Vulnerability
① Design Specifications	Those designed in accordance with 1926 or 1939 Specifications have higher vulnerability
② Type of Superstructure	• Gerber or simply supported girders with 2 or more spans have higher vulnerability • Arch, frame, continuous girders, cable-stayed bridges or suspension bridges have lower vulnerability
③ Shape of Superstructure	Skewed or curved bridges do not necessarily have higher vulnerability than straight bridges
④ Materials of Superstructure	Reinforced concrete bridges or prestressed concrete bridges have lower vulnerability than steel bridges although the difference is small
⑤ Slope in Bridge Axis	Bridges with slope in bridge axis have higher vulnerability
⑥ Device for Preventing Falling-off of Superstructure	Bridges with devices for preventing falling-off of superstructure have lower vulnerability
⑦ Type of Substructure	Bridges supported by single-line bent piles or by reinforced concrete frame placed on two separate caisson foundations have higher vulnerability
⑧ Height of Piers	Bridges supported by higher piers have higher vulnerability
⑨ Ground Condition	Bridges constructed on soft soil have higher vulnerability
⑩ Effect of Soil Liquefaction	Bridges constructed on sandy soil layers susceptible to liquefaction have higher vulnerability
⑪ Irregularity of Supporting Soil Condition	Bridges constructed on soils with irregularity of supporting conditions have higher vulnerability
⑫ Effect of Scouring	Bridges where the surface soils are scoured have higher vulnerability
⑬ Materials of Substructures	Bridges supported by plane-concrete substructures designed in accordance with 1926 or 1939 specifications have higher vulnerability
⑭ Type of Foundation	Bridges supported by timber, brick, masonry or other old unknown type substructures have higher vulnerability
⑮ Intensity of Ground Motion	Bridges subjected to higher intensity of ground acceleration have higher vulnerability. In particular, vulnerability becomes quite high when the bridges are subjected to peak ground acceleration larger than 400 gal (0.4g)

Table 4 Inspection Sheet to Evaluate Seismic Vulnerability of Highway Bridges

Point of Inspection		Factors of Inspection	Evaluation
Inspection for Vulnerability to Develop Excessive Deformation	Inspection Format (A) Inspection for Deformation of Superstructure	① Design Specifications	4.0: 1926 Specs. or 1939 Specs. 2.0: 1956 Specs. or 1964 Specs. 1.0: 1971 Specs. or 1980 Specs.
		② Superstructure Type	3.0: Gerber Girder or Simply-supported Girders with Two Spans or More 1.5: Simply-supported Girder or Continuous Girders Consisting of Two Spans or More 1.0: Arch, Flame, Continuous Girder (One Span), Cable-stayed Bridge, Suspension Bridge
		③ Shape of Superstructure	1.2: Skewed or Curved Bridge 1.0: Straight Bridge
		④ Materials of Superstructure	1.2: Rc or PC 1.0: Steel
		⑤ Gradient	1.2: 6% or Steeper 1.0: Less Than 6%
		⑥ Falling-off Prevention Device	2.0: None 1.0: One Device
		$P_A = ① \times ② \times ③ \times ④ \times ⑤ \times ⑥$	$P_A =$
	Inspection Format (B) Inspection for Deformation of Substructure	⑦ Type of Substructure	2.0: Single-line Bent Pile Foundation 1.0: Others
		⑧ Height of Pier H	2.0: $H \geq 10m$ 1.5: $5 \leq H < 10m$ 1.0: $H < 5m$
		⑨ Ground Condition	5.0: Extremely Soft in Group 4 2.5: Group 4 2.0: Group 3 1.2: Group 2 1.0: Group 1
		⑩ Effects of Liquefaction	2.0: Liquefiable 1.0: Non-liquefiable
		⑪ Supporting Ground Condition	1.2: Irregular 1.0: Almost Uniform
		⑫ Scouring	1.5: Recognized 1.0: None
		$P_B = ⑦ \times ⑧ \times ⑨ \times ⑩ \times ⑪ \times ⑫$	$P_B =$
Inspection for Vulnerability to Develop Failure Due to Inadequate Strength of Substructure	Inspection Format (C) Inspection for Strength of RC Pier at Termination of Reinforcement	⑬ Shear Span Ratio (h/D)	2.0: $1 < h/D < 4$ 1.0: $h/D \geq 4$ 0.5: $h/D \leq 1$
		⑭ Tension Cracks in Flexure at Terminated Point of Main Reinforcement	2.0: Cracks Will Occur 1.0: Cracks Will Possibly Occur 0.3: Cracks will Not Occur
		⑮ Safety Factor for Yield Strength at Terminated Section of Main Reinforcement ⑮-1 S_{sa}	3.0: $S_{sa} \leq 1.1$ 2.0: $1.1 < S_{sa} < 1.5$ 0.5: $S_{sa} \geq 1.5$
		⑮-2 S_{sma}	3.0: $S_{sma} \leq 1.1$ 2.0: $1.1 < S_{sma} \leq 1.3$ 1.0: $1.3 < S_{sma} < 1.5$ 0.5: $S_s \geq 1.5$
		⑯ Shear Stress σ (tf/m²)	3.0: $\sigma \geq 45$ 2.0: $30 \leq \sigma < 45$ 1.0: $15 \leq \sigma < 30$ 0.5: $\sigma < 15$
		$P_C = ⑬ \times ⑭ \times ⑮\text{-}1 \times ⑮\text{-}2 \times ⑯$	$P_C =$
	Inspection Format (D) Inspection for Strength of Substructure	⑰ Failure of Fixed Supports and Proximity	5.0: Extensive Failure 2.0: Small Failure 1.0: None
		⑱ Extraordinary Damage of Pier	5.0: Extensive Damage 2.0: Small Damage 1.0: None
		⑲ Materials of Substructure	2.0: Plane Concrete Older Than 1926 Excluding Gravity-type Abutment 1.0: Others
		⑳ Construction method of Foundation	2.0: Timer Pile, Masonry, Brick, Other Old Construction Methods 1.5: RC Piles, Pedestal Piles, Pier Supported by Two Independent Caissons 1.0: Foundation Designed by 1971 Specs. and Other Later Specs.
		㉑ Foundation Type	1.5: RC Flame Supported by Two Independent Caisson Foundations 1.0: Others
		㉒ Extraordinary Failure of Foundation	2.0: Recognized 1.0: None
		$P_D = ⑰ \times ⑱ \times ⑲ \times ⑳ \times ㉑ \times ㉒$	$P_D =$
Evaluation of Deformation and Strength			$X = P_A \times P_B =$ and $Y = P_C \times P_D =$

Table 5 Feasibility of Seismic Strengthening for 16 Factors Which Affect Seismic Vulnerability of Highway Bridges

Items	Feasibility of Seismic Strengthening	Principles of Countermeasures
① Design Specifications	×	———
② Type of Superstructure	×	———
③ Shape of Superstructure	×	———
④ Materials of Superstructure	×	———
⑤ Slope in Bridge Axis	×	———
⑥ Device for Preventing Falling-off of Superstructure	O	Installation of Devices
⑦ Type of Substructure	O	Strengthening of Substructures
⑧ Height of Piers	×	———
⑨ Ground Condition	×	———
⑩ Effect of Soil Liquefaction	O	Strengthening of Fundations or Strengthening of Surrounding Soils
⑪ Irregularity of Supporting Soil Condition	×	———
⑫ Effect of Scouring	O	Treatment for Prevention of Scouring, or Strengthening of Foundations
⑬ Materials of Substructures	O	Strengthening of Substructures
⑭ Type of Foundation	O	Strengthening of Foundations
⑮ Intensity of Ground Motion	×	———
⑯ Effect of Termination of Main Reinforcement at Mid-height	O	Strengthening of Substructures

Note O Items for which seismic strengthening is feasible
× Items for which seismic strengthening is not feasible

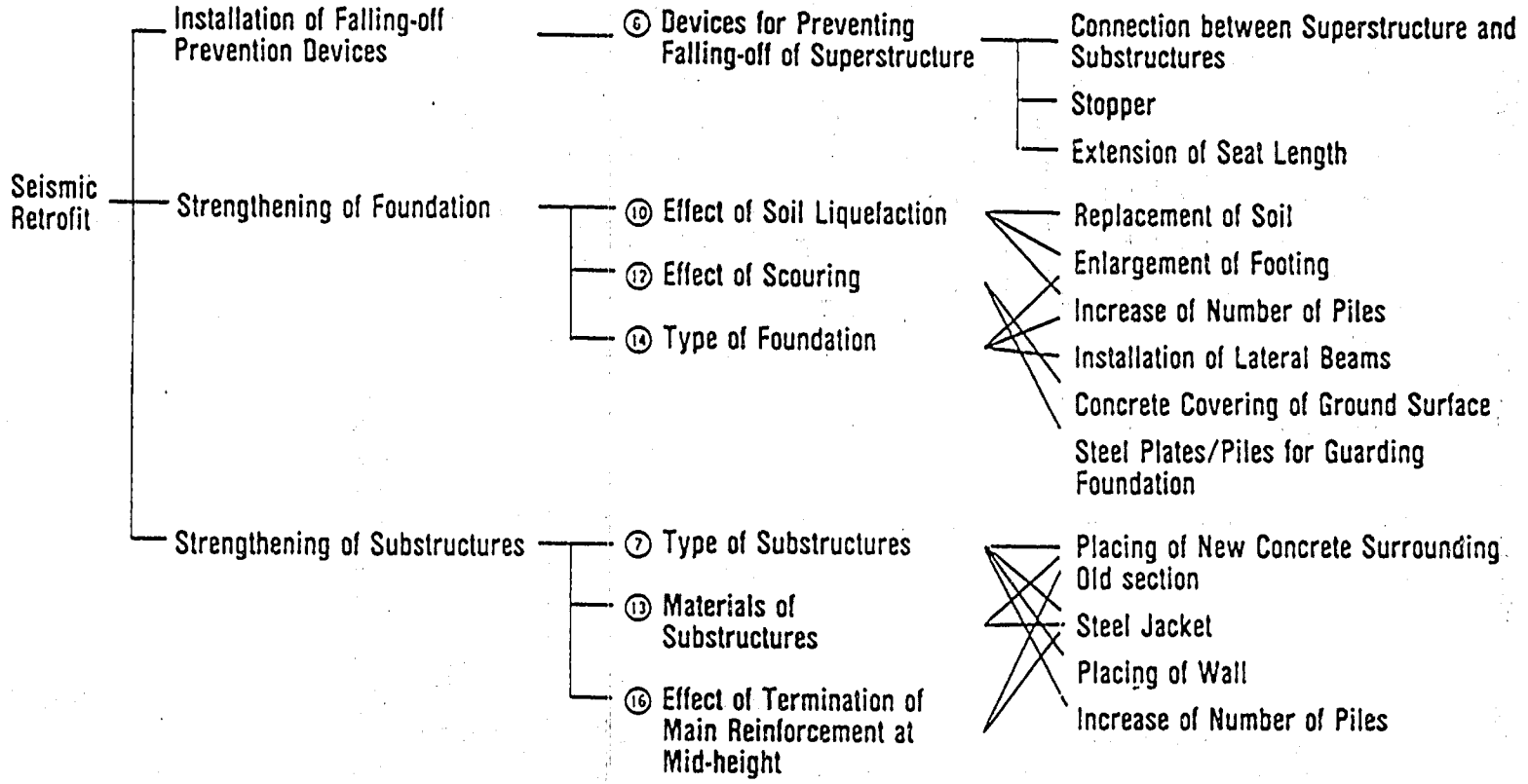
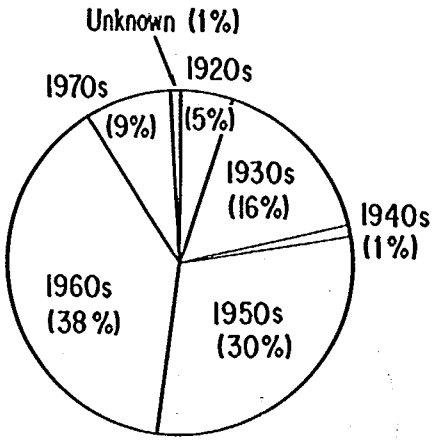
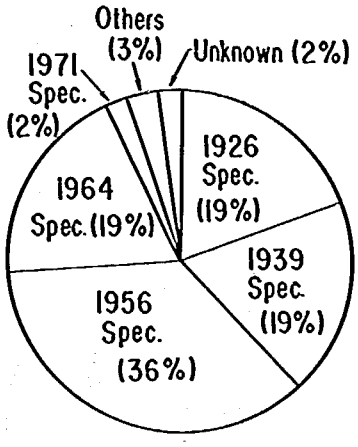


Fig. 1 Methods Adopted for Seismic Strengthening



(a) Year of Construction



(b) Design Specifications Referred to

Fig. 2 Bridges Surveyed

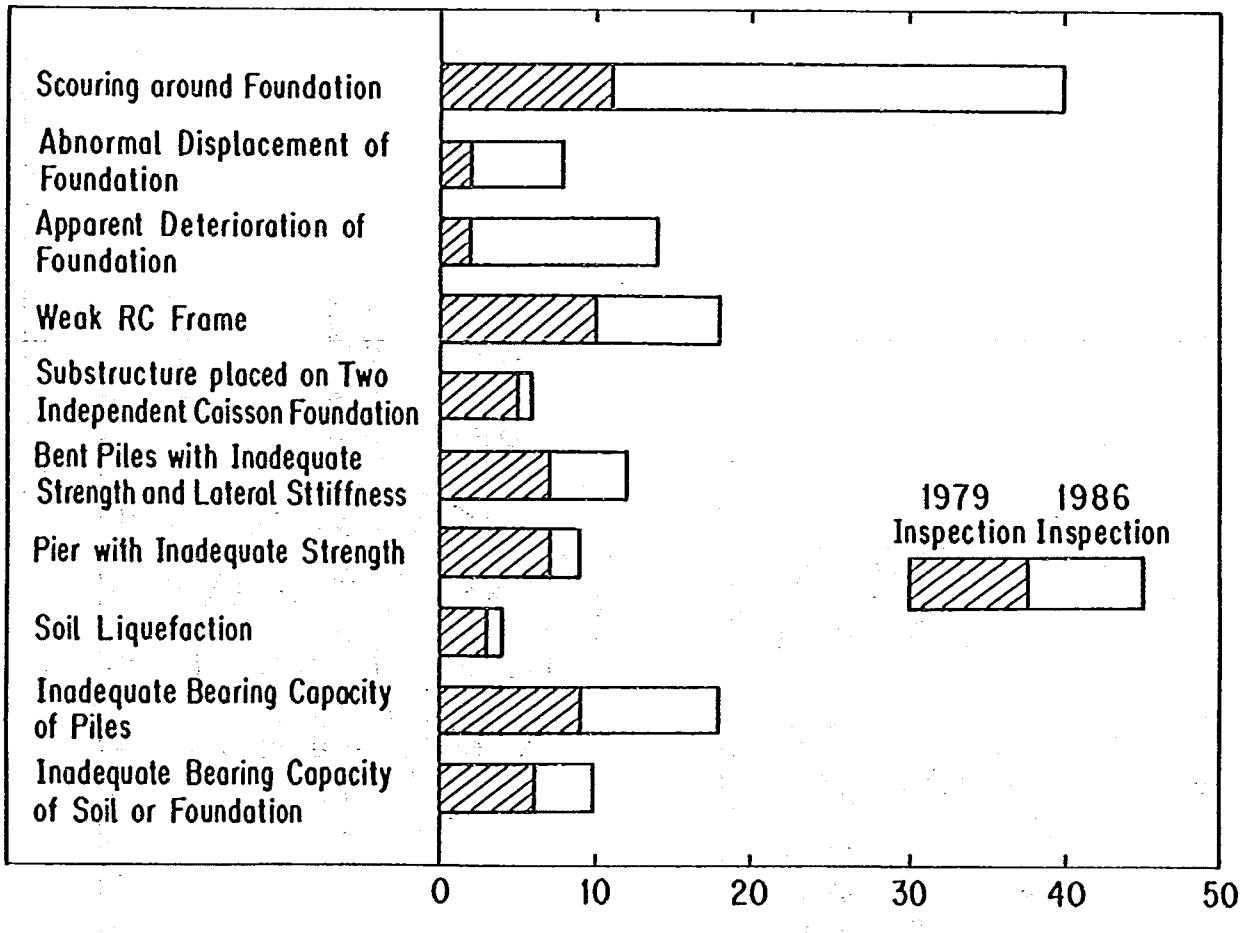
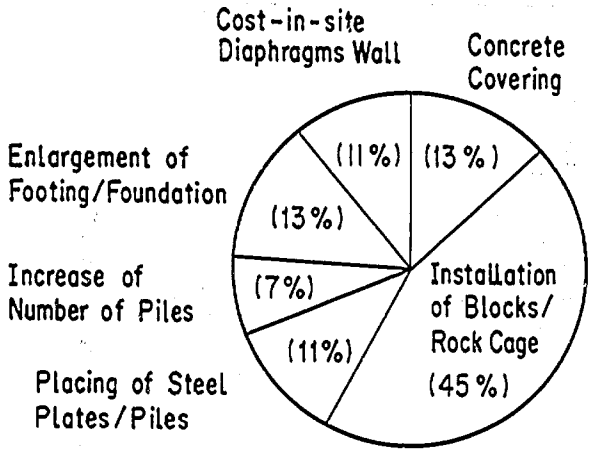
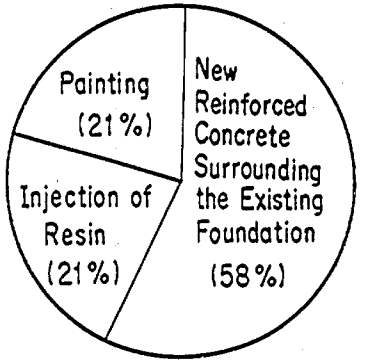


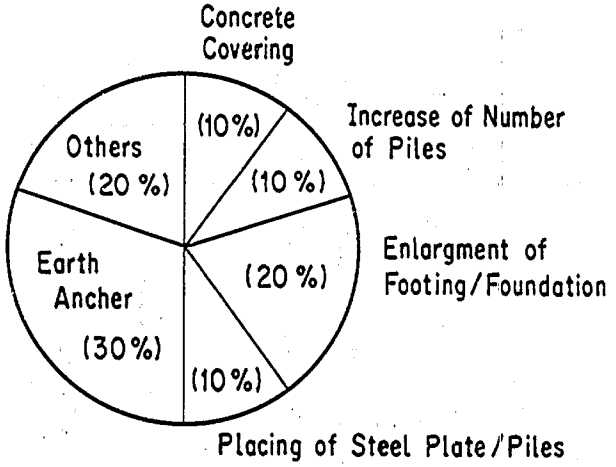
Fig. 3 Number of Bridges Strengthened Classified by Requirement for Seismic Strengthening



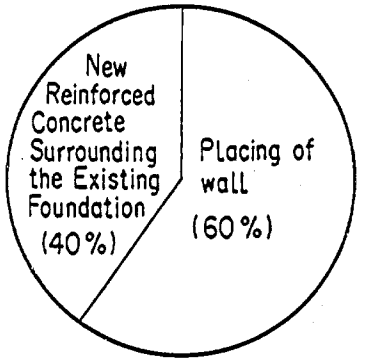
(a) Scouring around Foundation



(c) Apparent Deterioration of Reinforced Concrete Structure

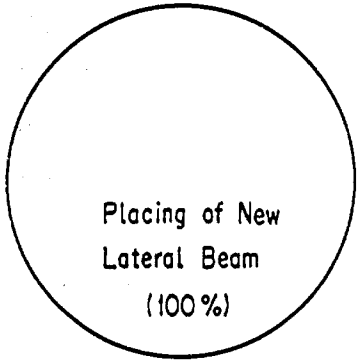


(b) Abnormal Displacement of Foundation

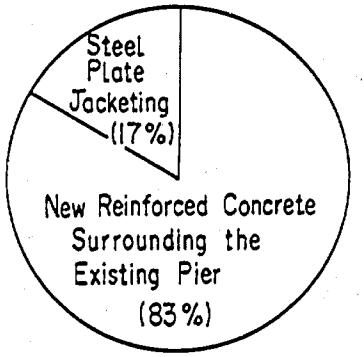


(d) Weak Reinforced Concrete Frame

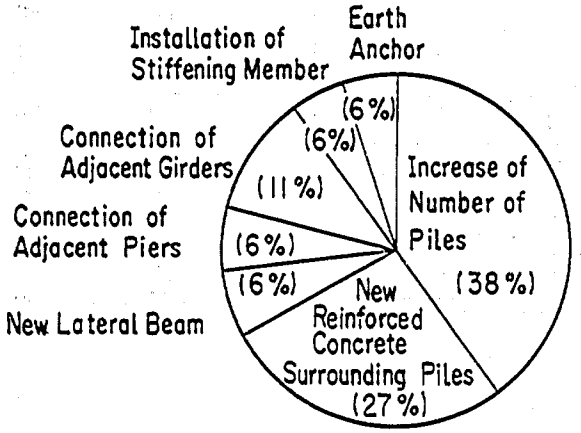
Fig. 4 Methods Adopted for Strengthening



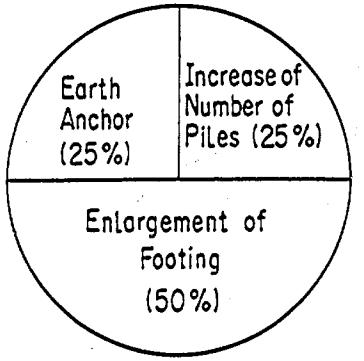
(e) Substructure Placed on Two Independent Caisson Foundations



(g) Pier with Inadequate Strength

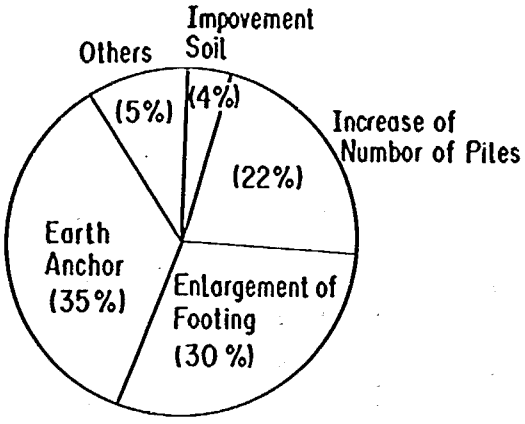


(f) Bent Piles with Inadequate Strength and Lateral Stiffness

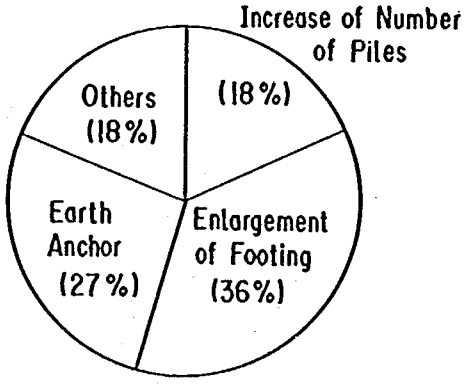


(h) Soil Liquefaction

Fig. 4 Methods Adopted for Strengthening



(i) Inadequate Bearing Capacity of Piles



(j) Inadequate Bearing Capacity of Soil/Foundation

Fig. 4 Methods Adopted for Strengthening

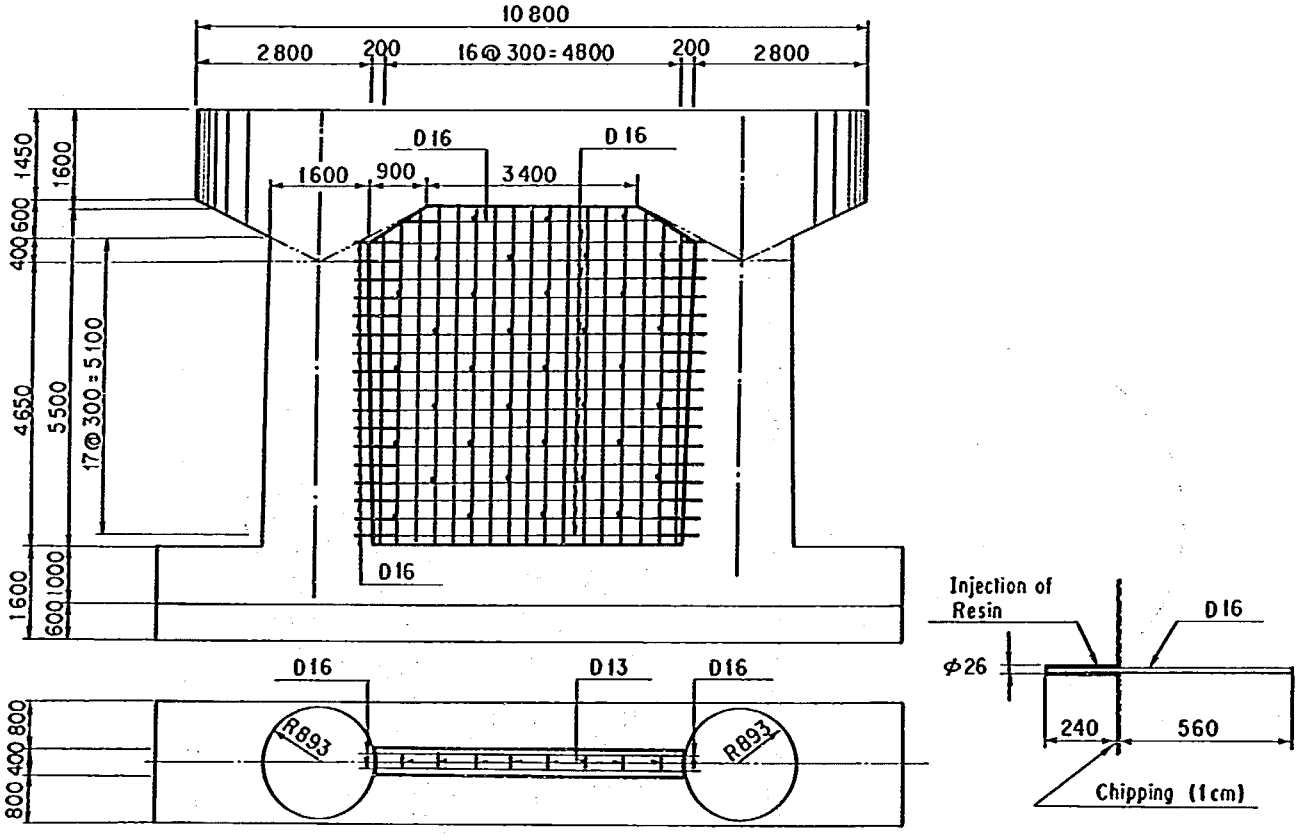


Fig. 5 Seismic Strengthening of A Reinforced Concrete Frame by Placing A New Reinforced Concrete Wall

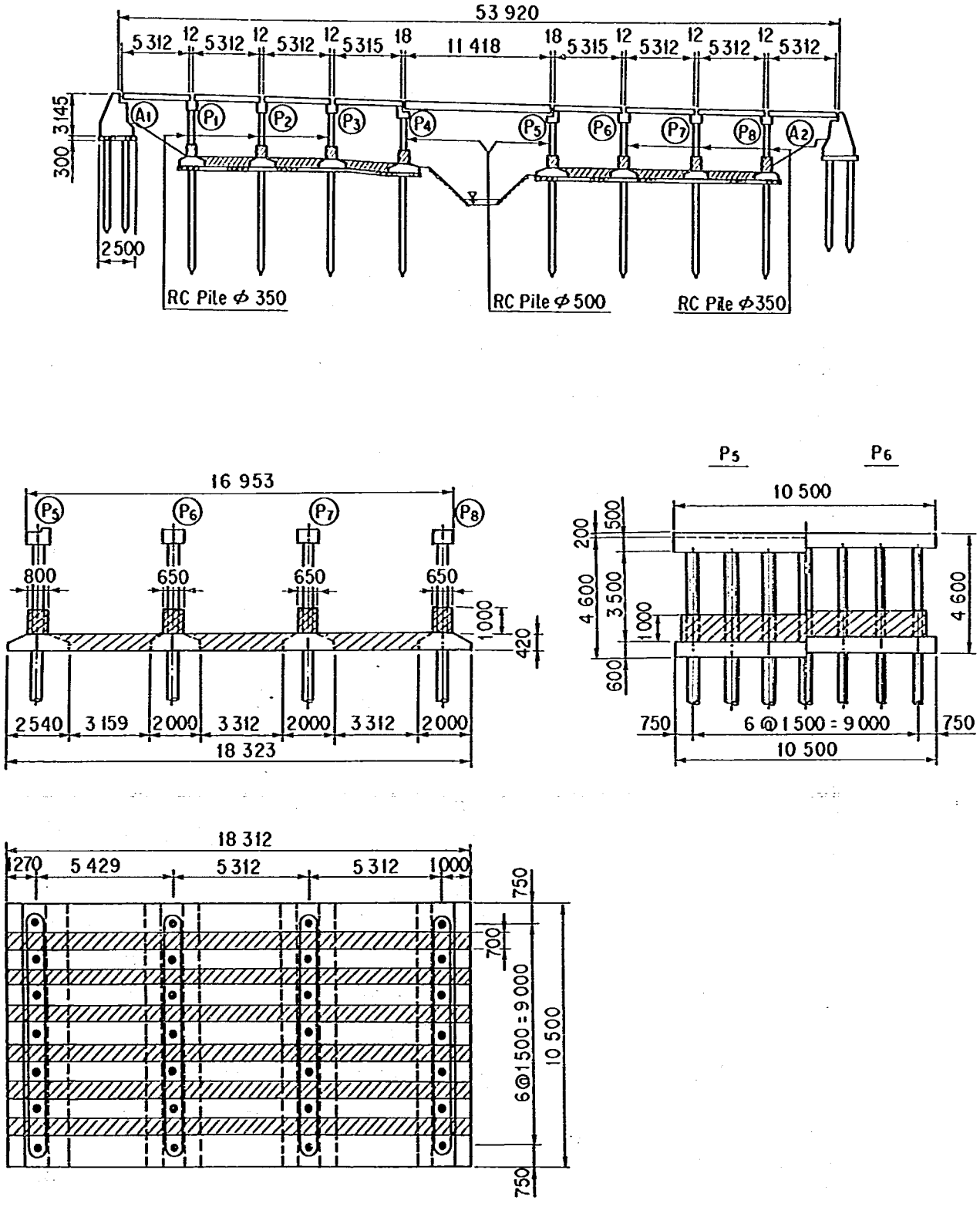


Fig. 6 Seismic Strengthening of Bent Piles by New Concrete Walls and New Connection Slabs

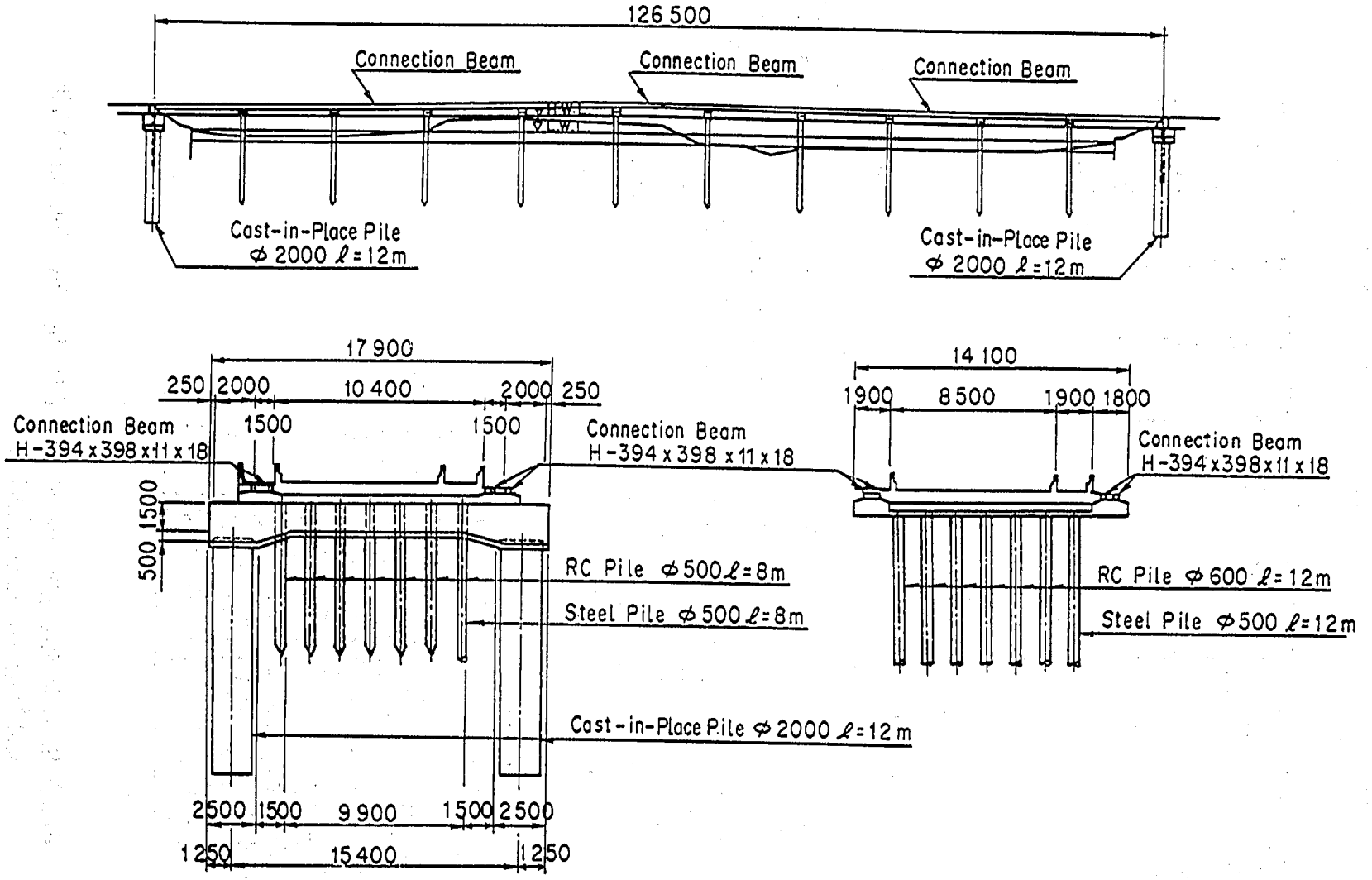


Fig. 7 Seismic Strengthening of Bent Piles in Liquefiable Sandy Soils by Connecting Beams

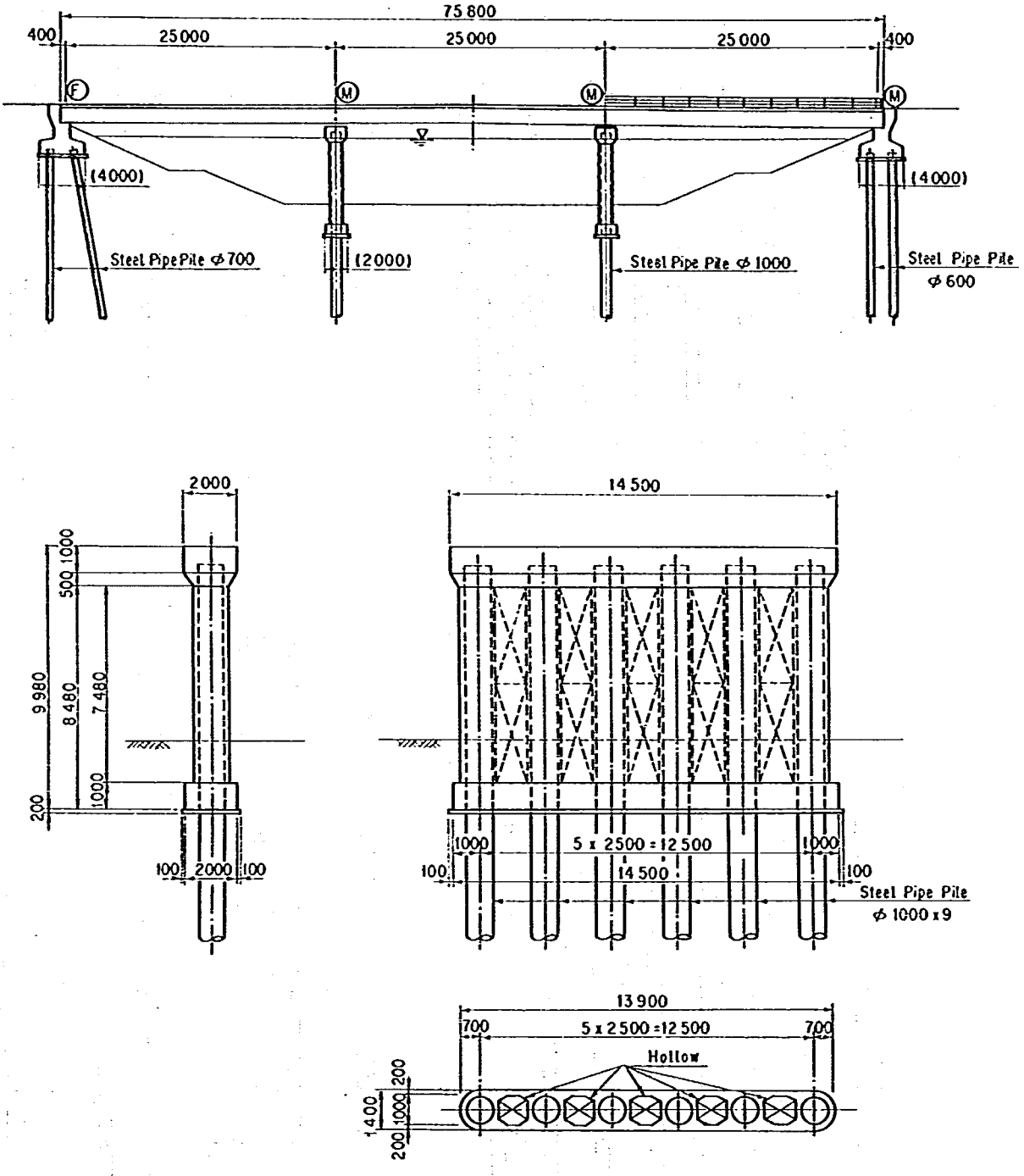


Fig. 8 Seismic Strengthening of Bent Piles by Placing A New Reinforced Concrete Wall

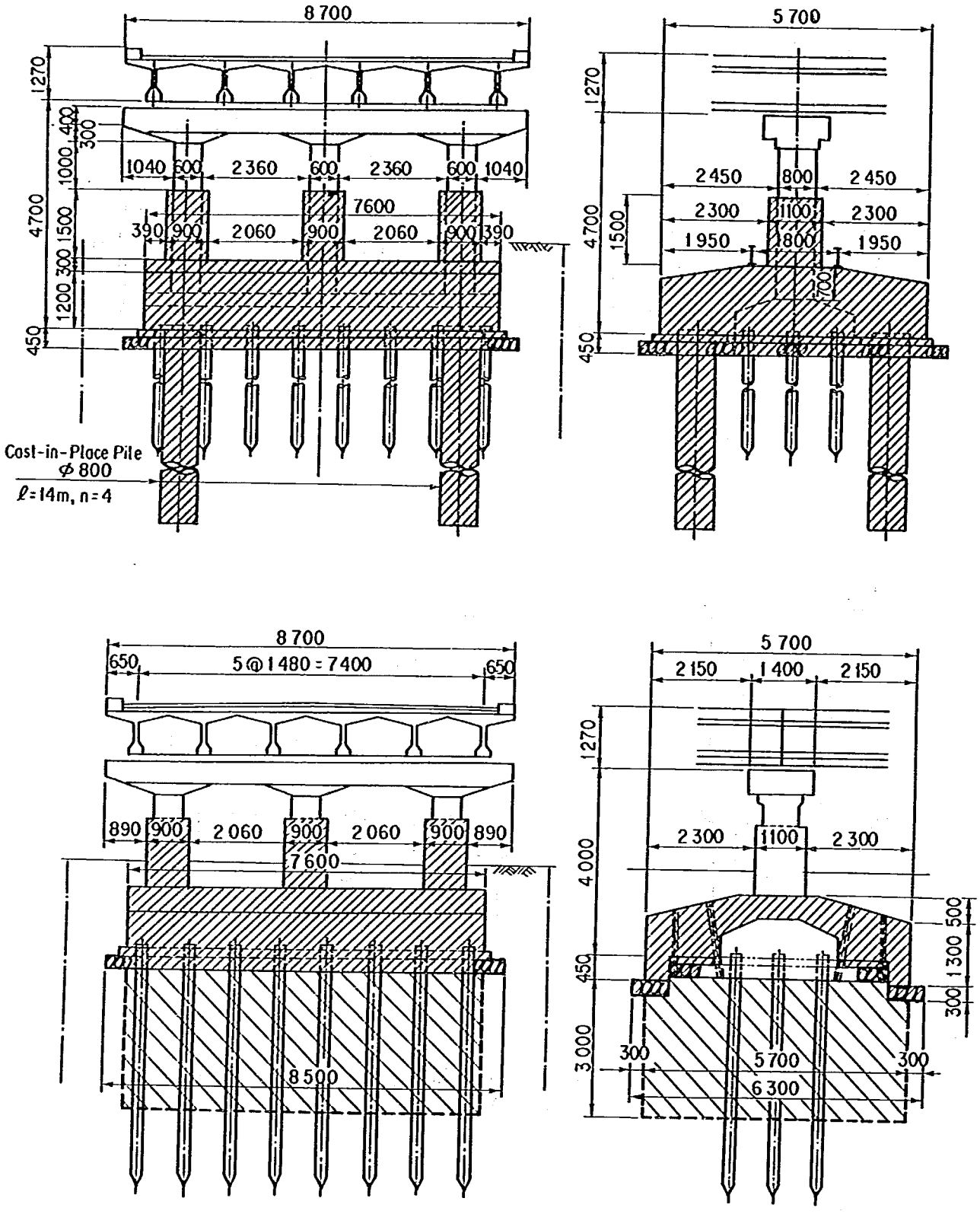


Fig. 9 Seismic Strengthening of Foundations by Increasing Number of Piles and by Enlarging Footing

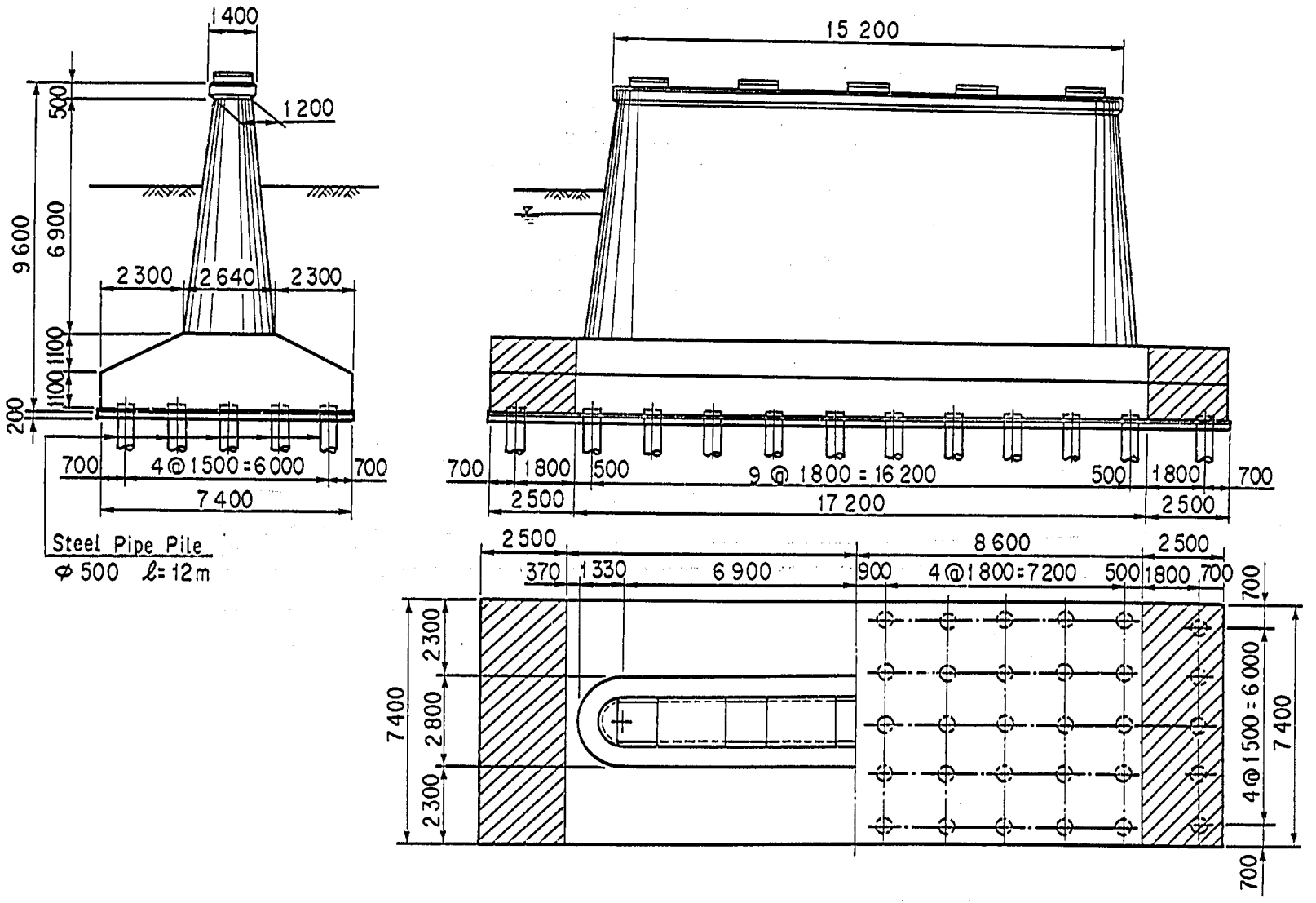


Fig. 10 Seismic Strengthening of A Pile Foundation in Liquefiable Soils by Increasing Number of Piles

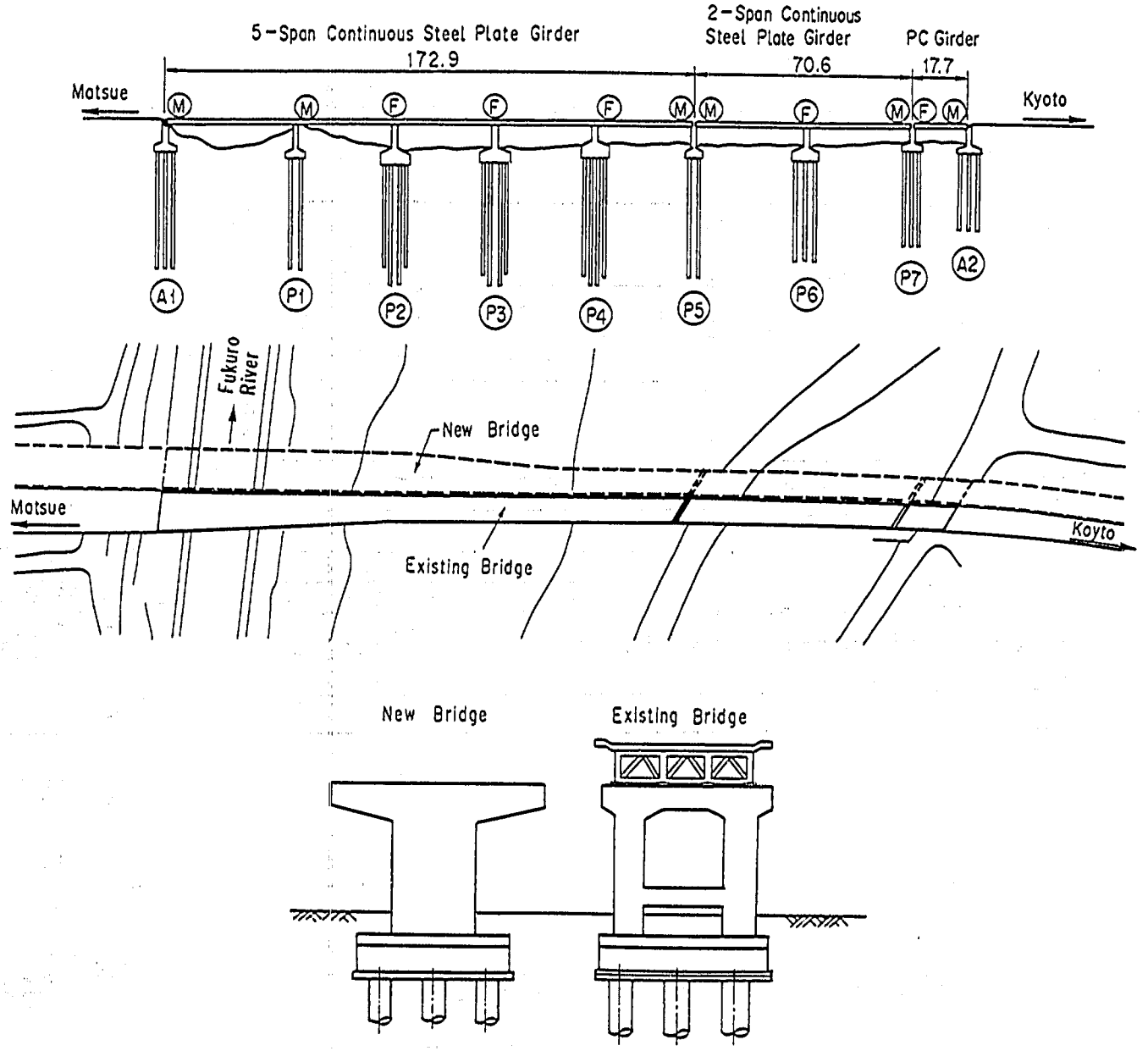


Fig. 11 General View of Akisato Bridge

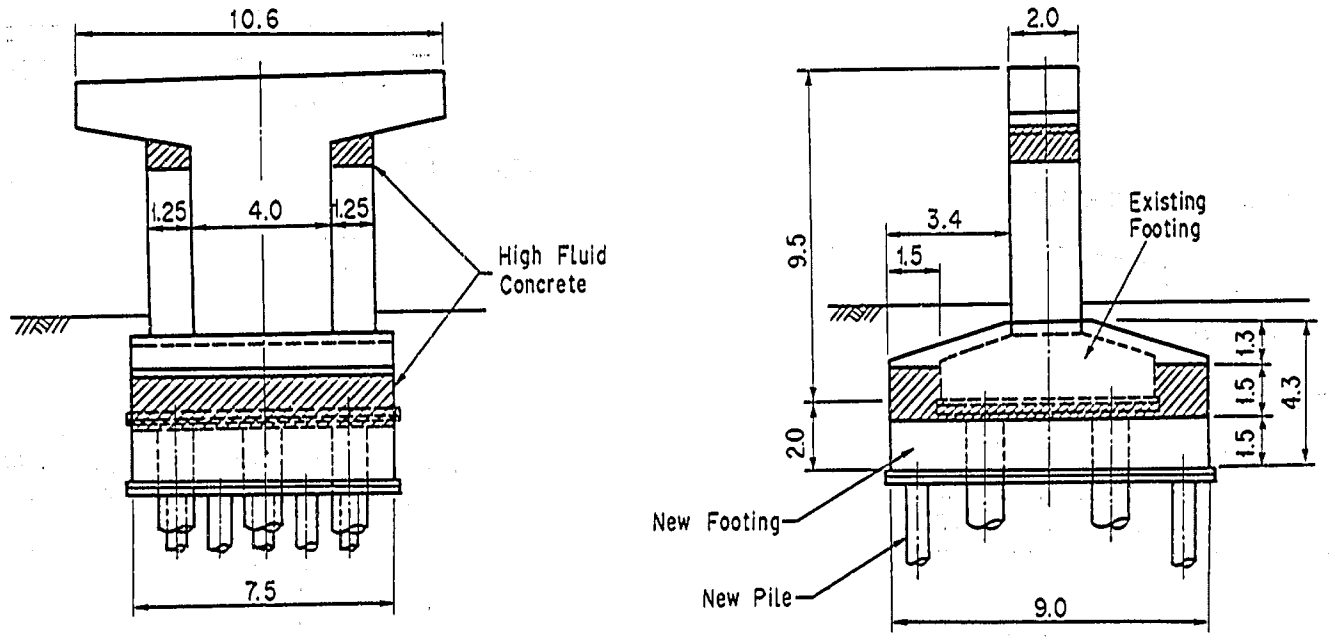


Fig. 12 Seismic Strengthening Method of Substructures (Akisato Bridge, Pier P4)

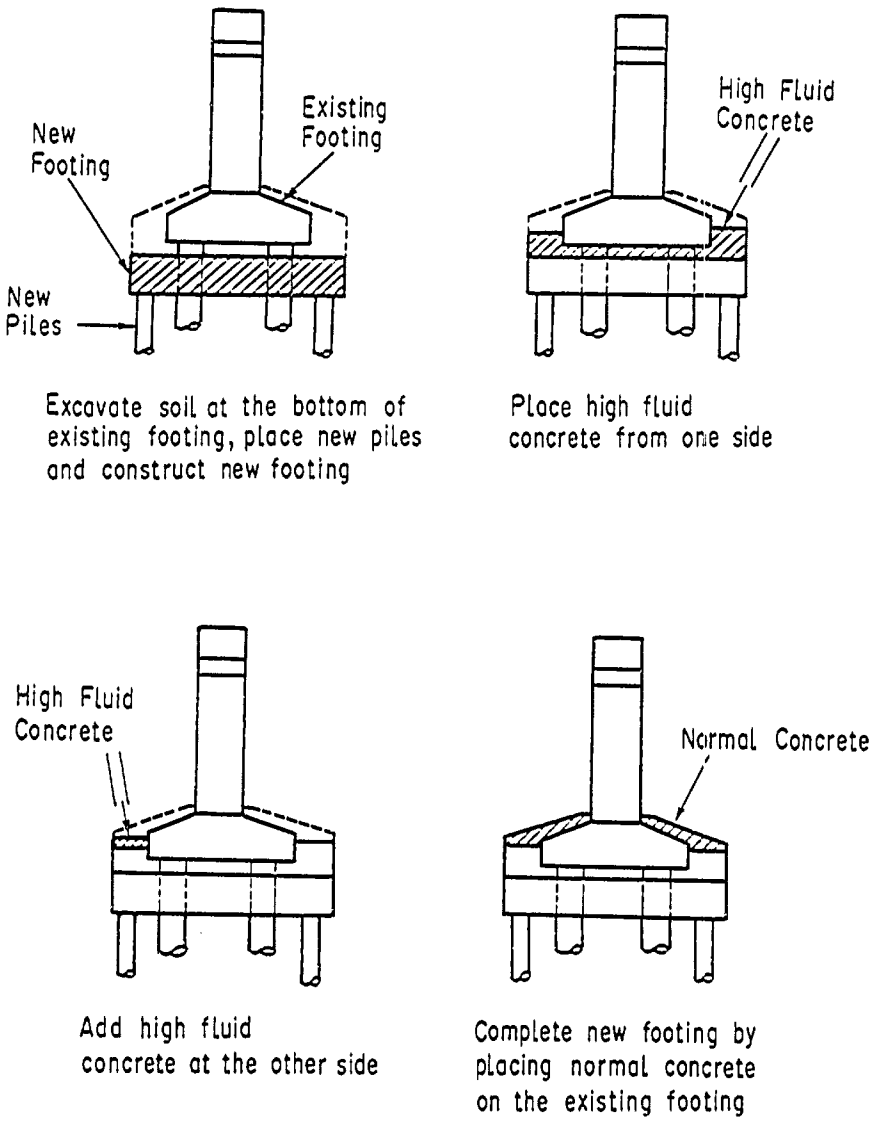


Fig. 13 Construction Procedure of Strengthening of Substructures

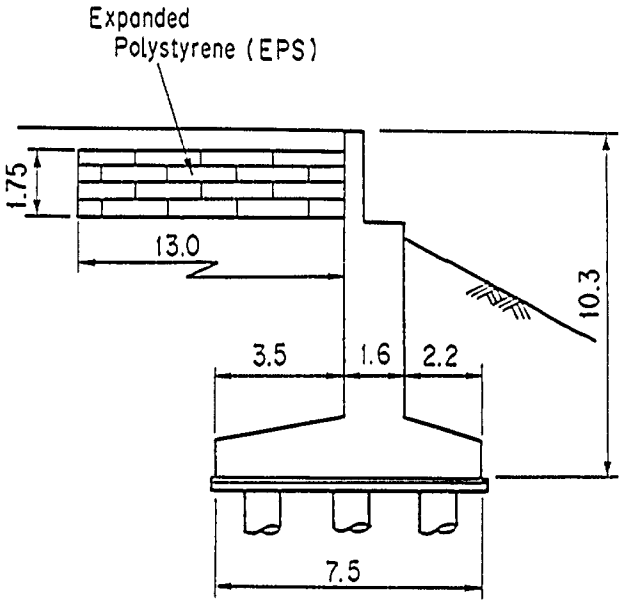


Fig. 14 Seismic Strengthening of Abutment

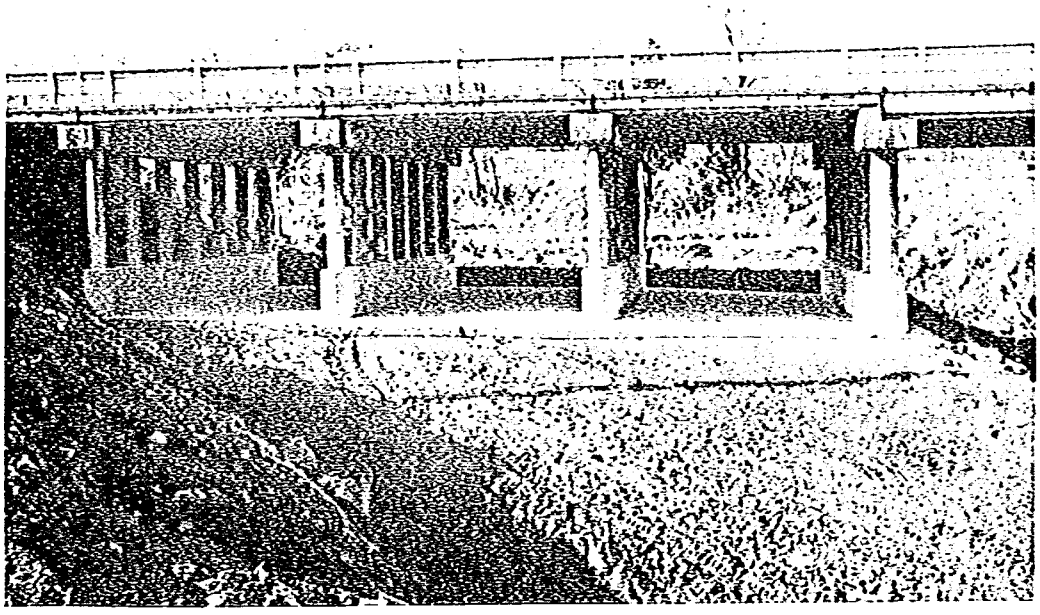


Photo 1 Seismic Strengthening of Bent Piles by New Concrete Walls and New Connection Slabs

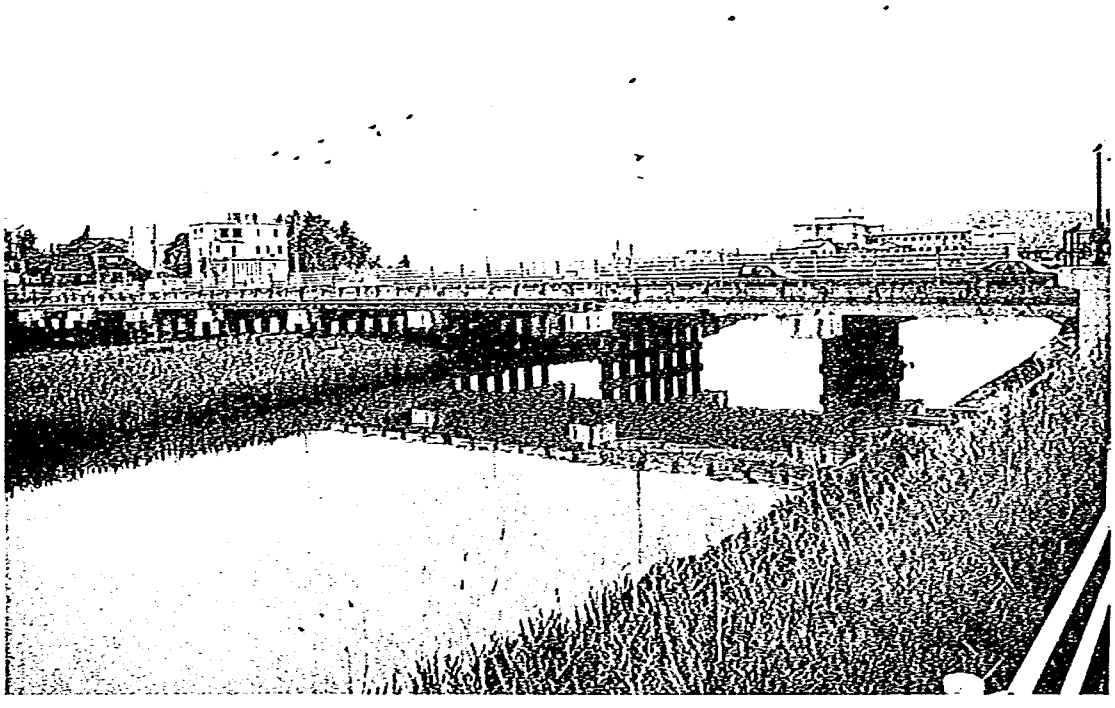


Photo 2 Seismic Strengthening by Connecting Beams

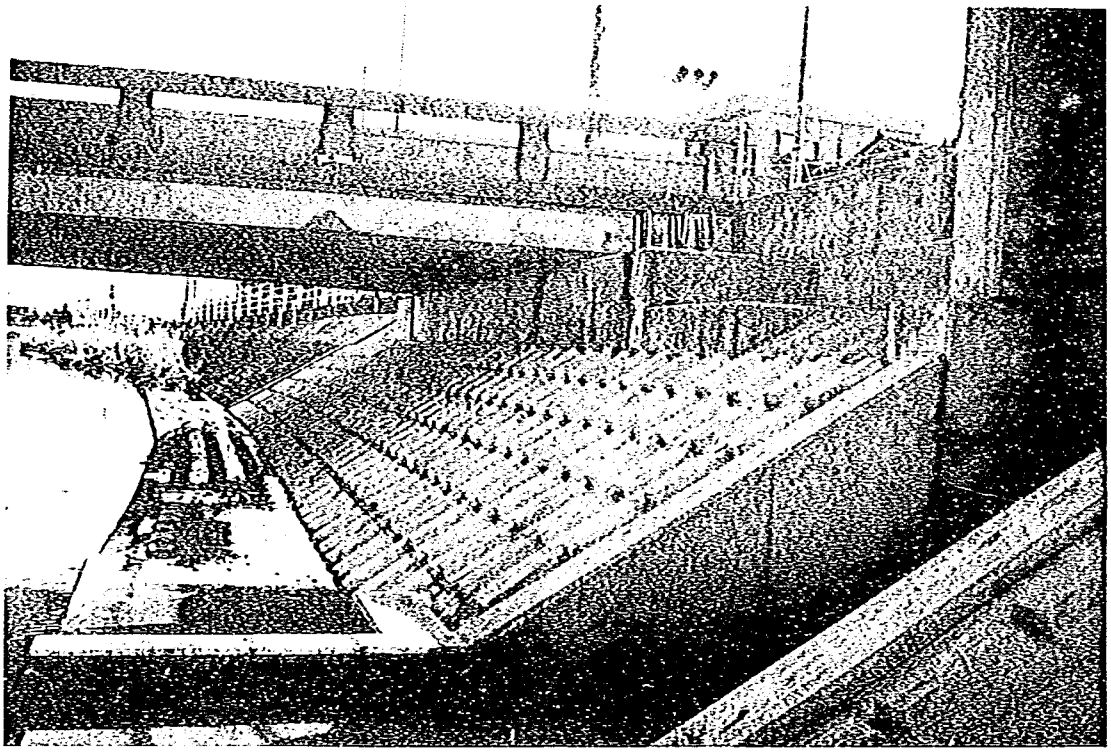
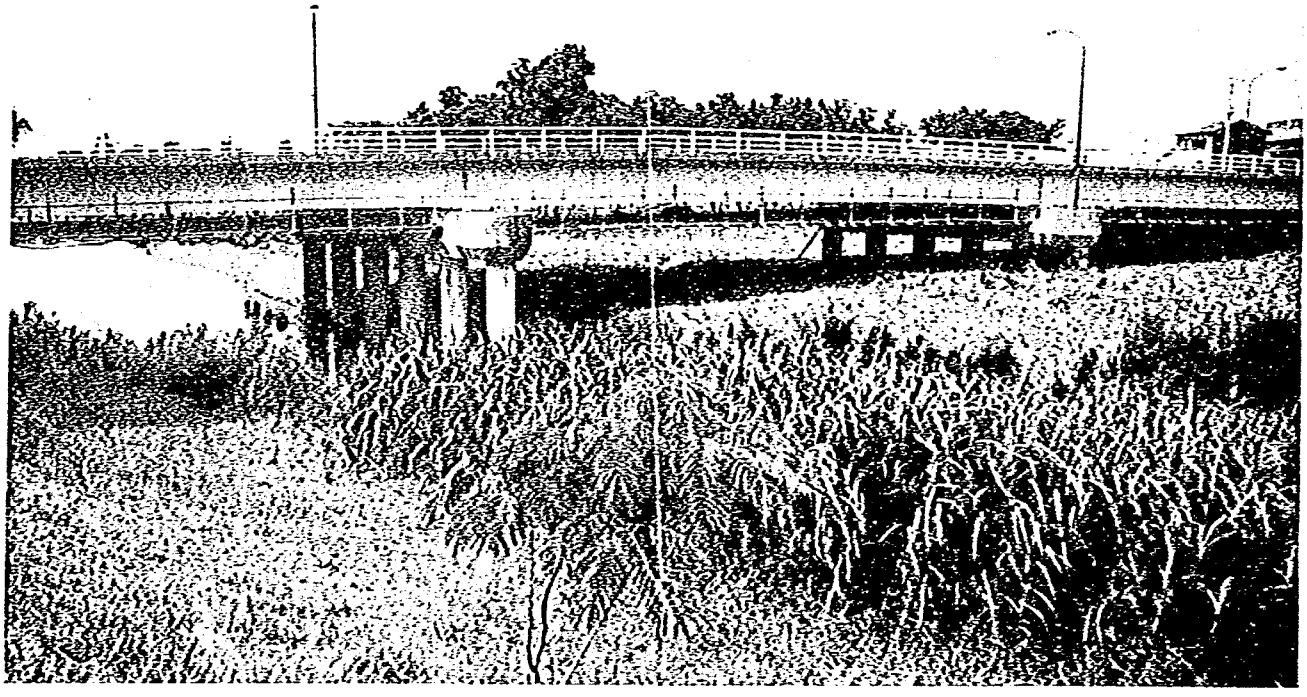
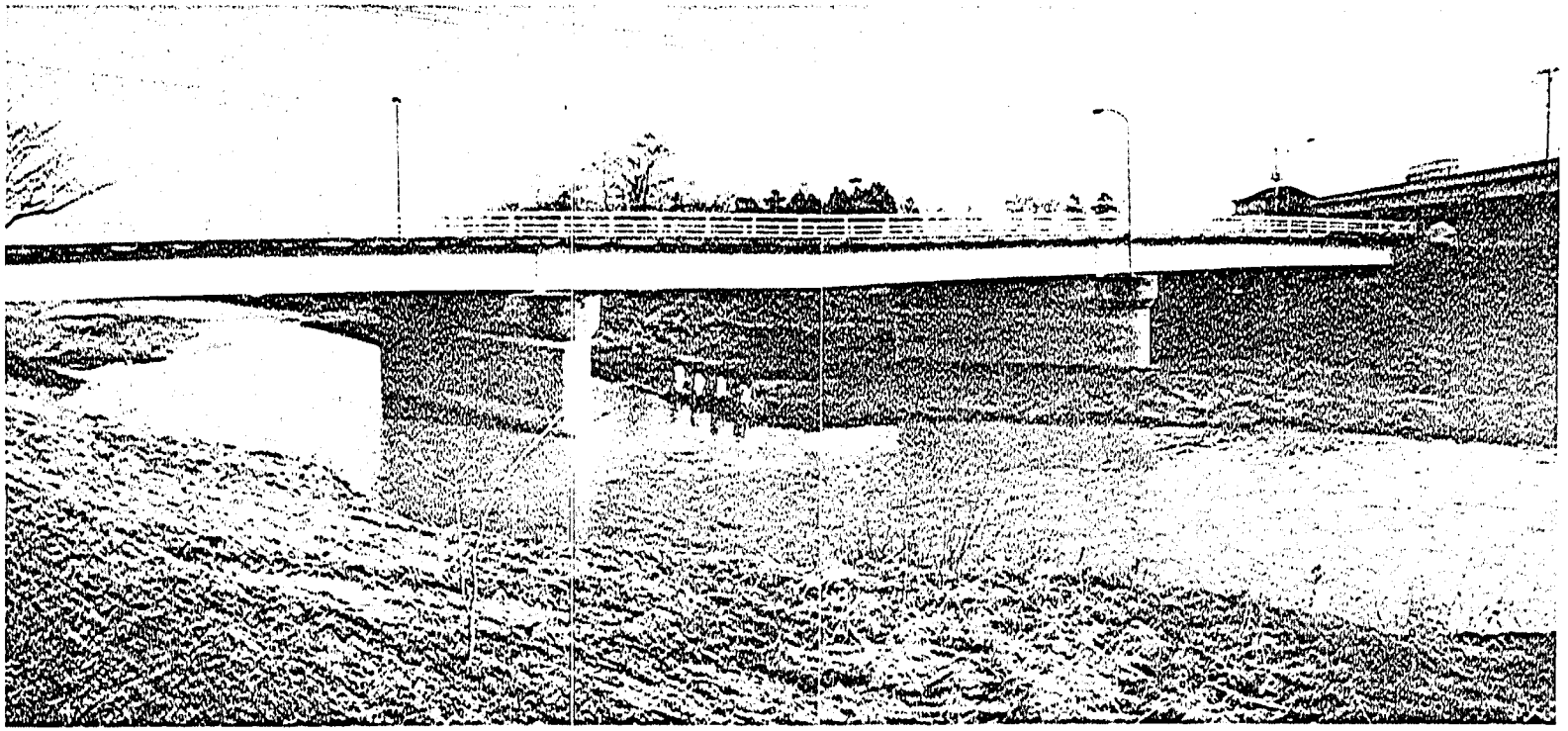


Photo 3 Seismic Strengthening of Abutment by Increasing Number of Piles



(a) Before the Seismic Strengthening

Photo 4 Seismic Strengthening by A New Reinforced Concrete Wall



(b) After the Seismic Strengthening

Photo 4 Seismic Strengthening by A New Reinforced Concrete Wall

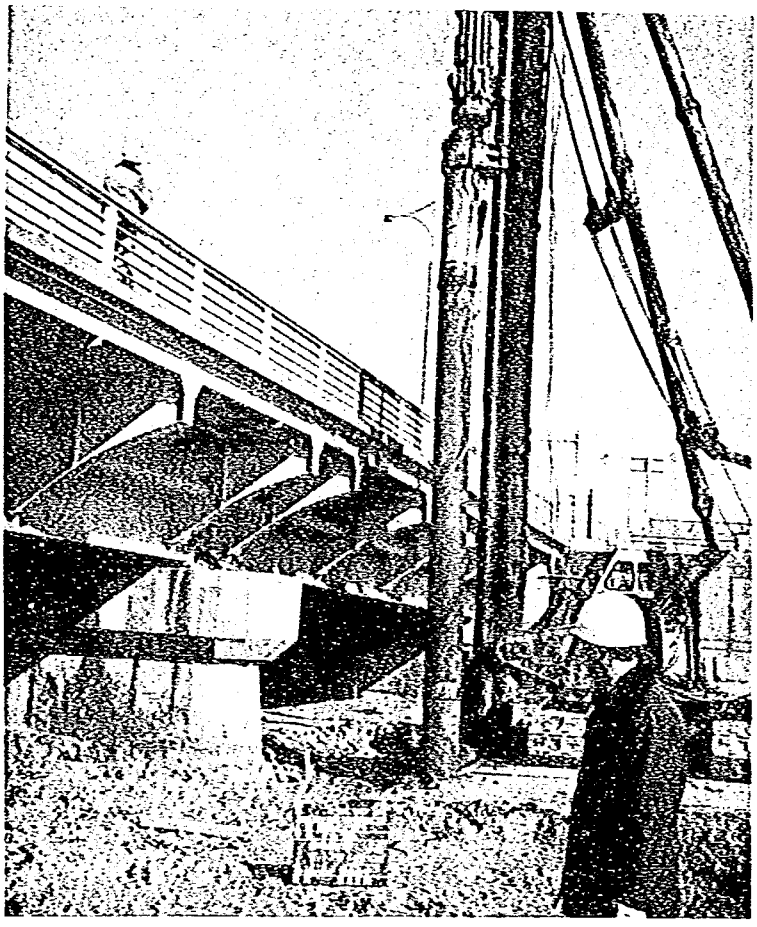


Photo 5 Construction of the New Piles

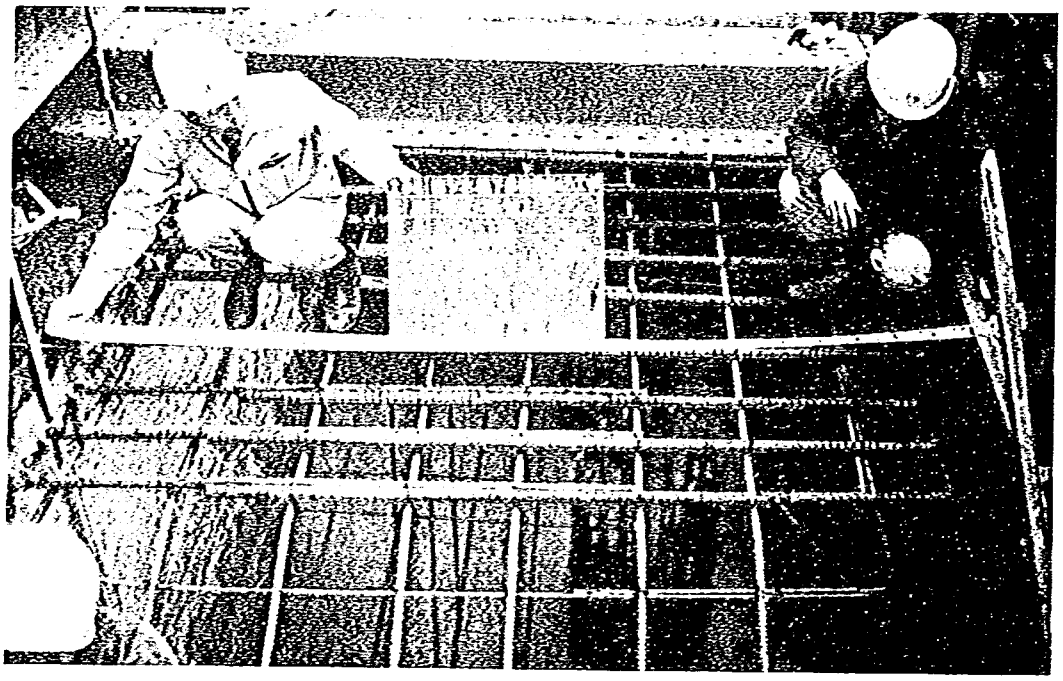


Photo 6 Reinforcement of at the New Footing

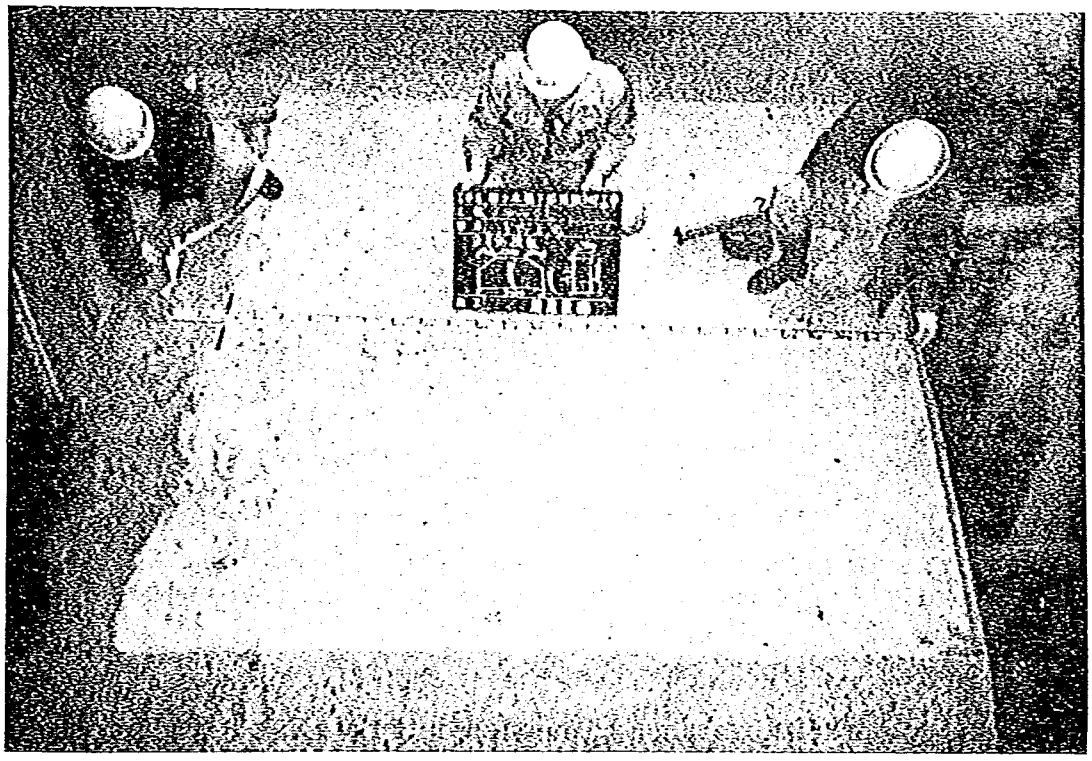


Photo 7 New Footing

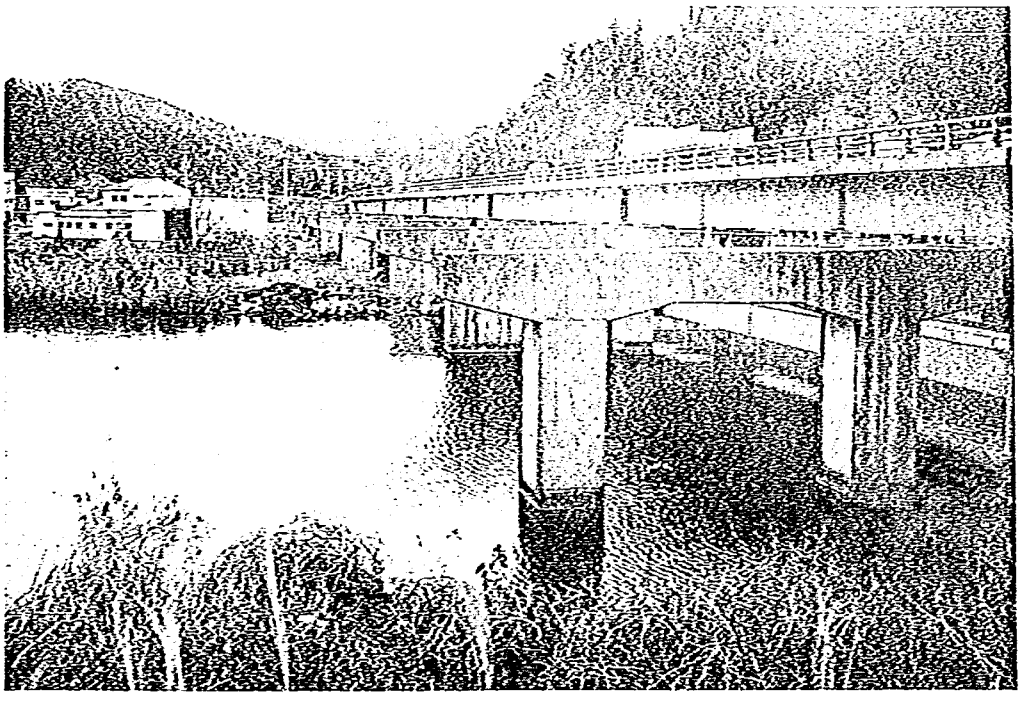


Photo 8 General View of Akisato Bridge and Existing Piers

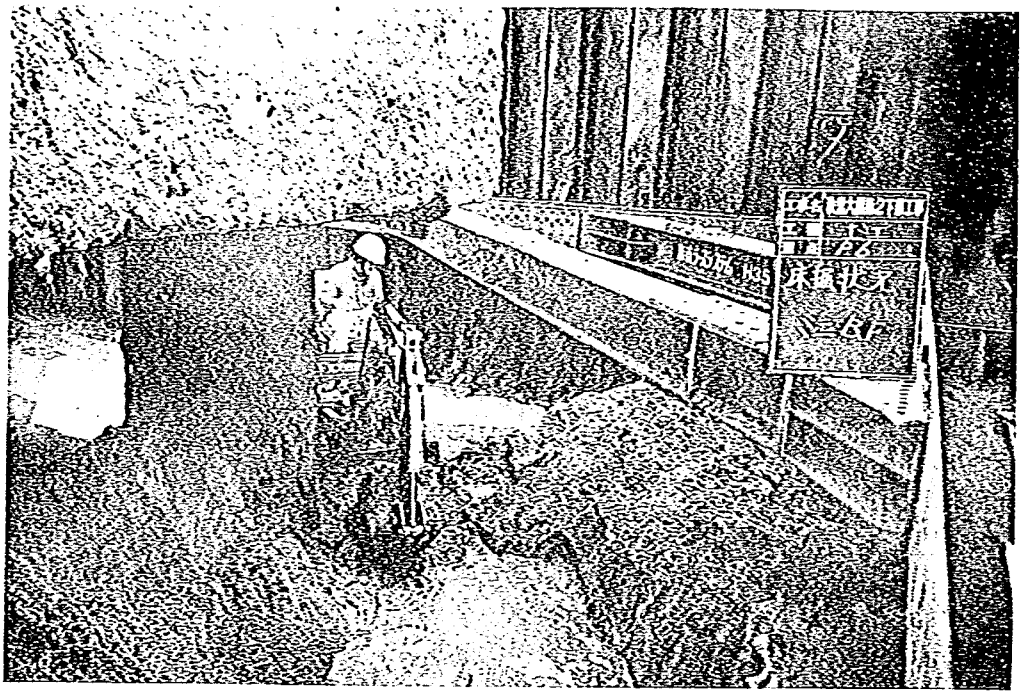


Photo 9 Excavation below the Bottom of Existing Footing

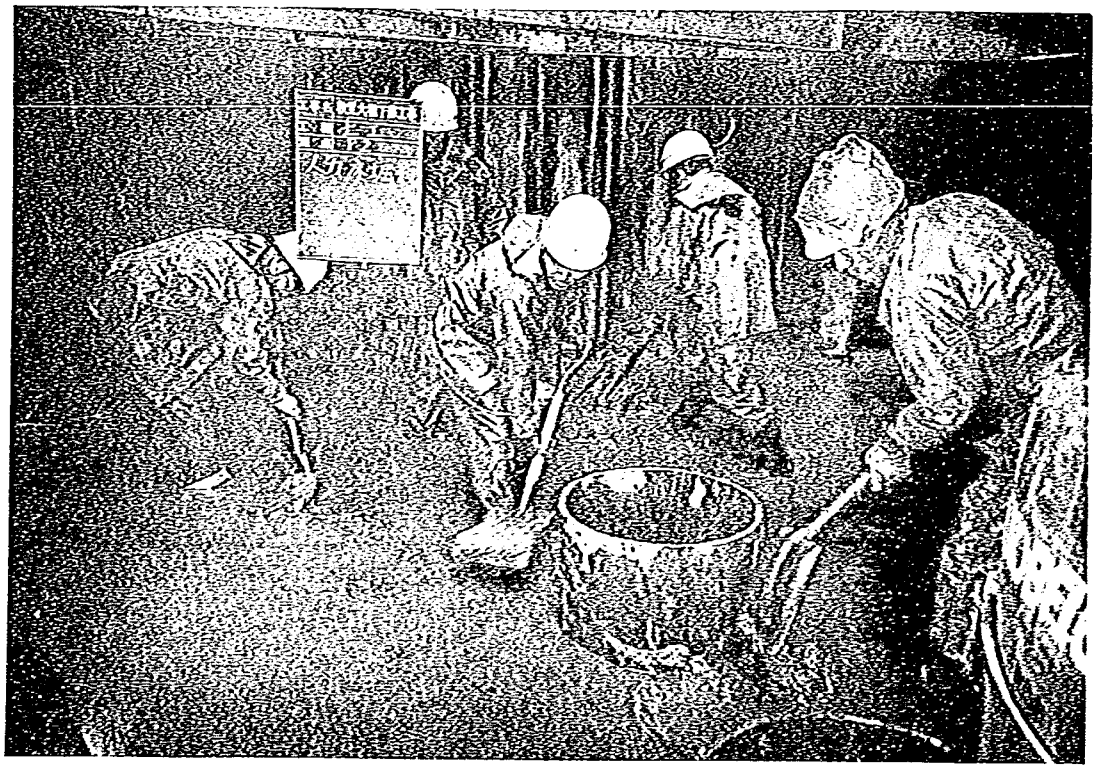


Photo 10 Excavation by Manpower and the Head of New Pile



Photo 11 Reinforcement around the New Pile

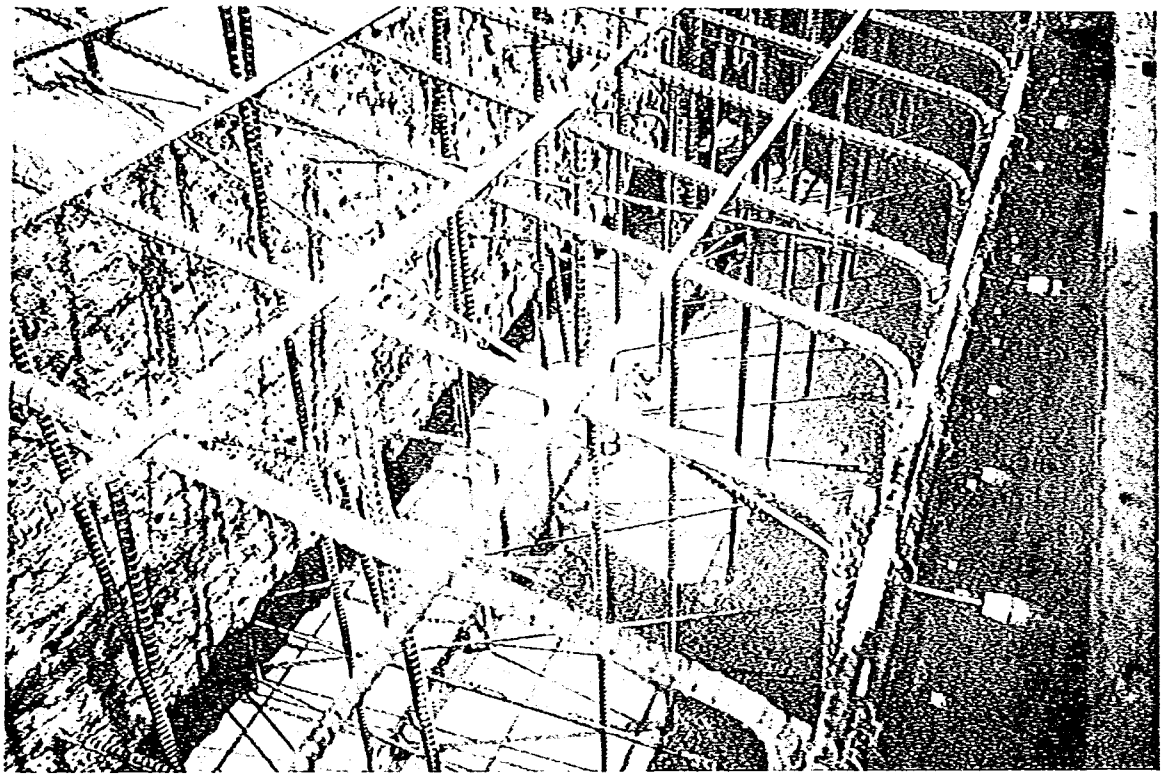


Photo 12 Reinforcement at the New Footing

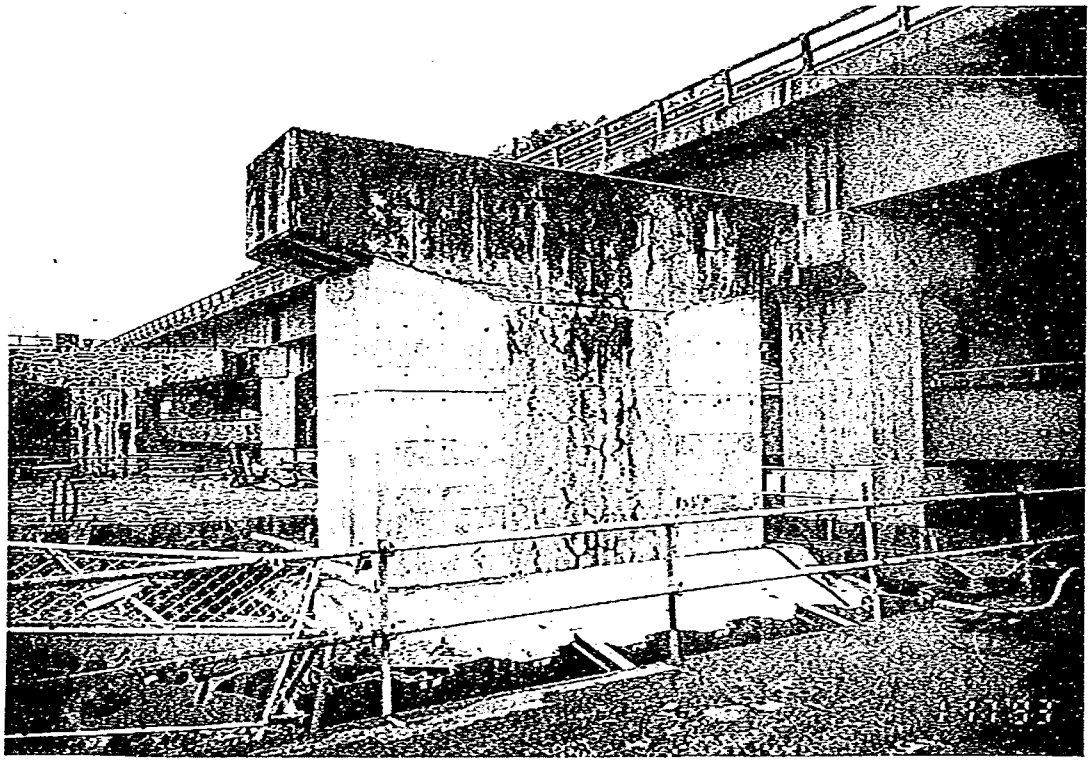


Photo 13 Seismic Strengthening of the Piers

Damage of Bridges by Kushiro-oki Earthquake, January 1993, and Hokkaido Nansei-oki Earthquake, July 1993

Kazuhiko KAWASHIMA
Shigeki UNJOH
Tomoru NAKAJIMA
and
Jun-ichi HOSHIKUMA

2nd U.S.-Japan Workshop on
Seismic Retrofit of Bridges
Berkeley, U.S.A.
January, 1994

DAMAGE OF BRIDGES BY KUSHIRO-OKI EARTHQUAKE, JANUARY 1993, AND HOKKAIDO NANSEI-OKI EARTHQUAKE, JULY 1993

Kazuhiko KAWASHIMA[1], Shigeki UNJOH[2], Tomoru NAKAJIMA[3] and Junichi HOSHIKUMA[3]

1) Head, Earthquake Engineering Division, Public Works Research Institute, Ministry of Construction, Tsukuba Science City, Japan
2) Senior Research Engineer, ditto
3) Research Engineer, ditto

ABSTRACT

This paper presents the damage to bridges caused by the recent earthquakes occurred in Japan. Sixty-two bridges were damaged by the Kushiro-oki Earthquake of January 15, 1993, and twenty-four bridges by the Hokkaido-nansei-oki Earthquake of July, 12, 1993 including slight damage which did not affect the trafficability of bridges.

INTRODUCTION

The Kushiro-oki Earthquake occurred on January 15, 1993, and Hokkaido-nansei-oki Earthquake occurred on July 12, 1993 both in Hokkaido island. They caused a lot of damages to highway, river and port facilities and buildings.

The Kushiro-oki-Earthquake with magnitude of 7.8 on the Richiter scale occurred approximately 15km from the Kushiro city. The Hokkaido-nansei-oki Earthquake with the magnitude of 7.8 occurred approximately 60km north-west from the Okushiri Island. Hokkaido-nansei-oki Earthquake caused heavy damage to Okushiri island by the Tsunami and the Fire. Although two earthquakes were a large-scale earthquake with the magnitude of 7.8, structural damages were not so heavy because the earthquakes hitted rural area with low population density and there are not large scale structures in the affected area.

Figs. 1 and 2 show the location of the damaged structures. On the highway bridges, large damage such as falling-off of superstructures was not found. However, based on the investigation of the damaged bridges important lessons on the seismic design of highway bridges and countermeasures to highway systems in the future were found. This paper presents damages to highway bridges caused by the Kushiro-oki Earthquake and Hokkaido-nansei-oki Earthquake.

DAMAGE TO REINFORCED CONCRETE BRIDGE PIERS WITH TERMINATION OF LONGITUDINAL REINFORCEMENT AT MID-HEIGHT

Common damage to bridges in the two earthquakes was damage to the reinforced concrete bridge piers where the longitudinal reinforcement was terminated at mid-height. This type damage was recognized by the heavy damage to the piers of Shizunai Bridge during the Urakawa-oki Earthquake of 1982. Shizunai bridge was damaged as almost falling-off of superstructure.

The damage to reinforced concrete piers were found for six bridges by the Kushiro-oki Earthquake and three bridges by the Hokkaido-nansei-oki Earthquake. All of eight bridges were constructed in 1960s to early 1970s and the bridges were designed according to the specifications before the revision of design details on the anchorage of reinforcement in 1980.

The followings show the interesting damage in which some spans were designed according to the older specifications and damaged by the Hokkaido-nansei-oki Earthquake, and the other designed according to the revised specifications was not damaged.

Photo 1 shows the Shin-Shiriuchi bridge on the municipal highway of Motomachi No.1. It is a 7 span simple post-tension T shaped girder bridge with length of 214m and width of 6m. Although the original bridge was constructed in 1970, the right side two spans with length of 66m were newly constructed in 1989 because of the river reconstruction. Existing piers have the height of 6.8mm for Piers P1 and P4, that of 7.04m for Piers P3 and P4. They all have the circular section with diameter of 1.8m. Newly constructed Pier P1 has the oval section of 3×1.8m, and P2 has that of $3\text{m} \times 1.5$m. The foundations are caisson type for all piers except that the new Pier P1 has a direct type foundation.

Sixty-four reinforcing bars with diameter 22mm (D22) were arranged for existing piers. In which, 32 reinforcing bars are terminated at the height of 2.47m from the bottom of piers and then 16 reinforcing bars are terminated at the height of 3.67m. On the other hand, for new Pier P2, 56 reinforcing bars are arranged at the bottom and 28 bars are terminated at the height of 3m from the bottom. No termination of the reinforcing bars for new pier P1 are made.

The damage was found at the termination section of all of the existing piers. **Photo 2** and 3 shows the damage situation. Cracks and spalling-off of cover concrete was found and the buckling and the deformation of reinforcing bars towards the outside of the piers were occurred.

Heaviest damage was found at Pier P3 and the pier was damaged with the height about 1m at the lower termination section. It was caused by the response in the transverse direction because the damage was found at the both side of the pier in the upper and lower stream sides of the river.

The judgement methods of the damage degree in terms of residual strength and

ductility characteristics of reinforced concrete piers are shown in the Manual of the Earthquake Disaster Prevention for Highways. The damage degree can be estimated according to Table 1. The damage to Pier P3 is estimated as "heavy damage" with requirement to close the traffic. The strength of the pier is estimated under the yielding strength.

It is interesting that the damage was found at the exciting piers but no damage was found newly constructed Pier P2 which also has the termination of main reinforcement. It is proved that this type damage was prevented by providing an enough anchorage length for the terminated reinforcing bars according to the 1980 specifications.

The strong motion records was obtained at the Shichihou Bridge (no damage) which is located about 10km form the Shin-Shiriuchi Bridge by the Hokkaido Development Bureau. Peak acceleration on the ground surface was about 200cm/sec^2. The wooden house is located at the just side of the bridge and the owner said that the house was excited heavily during the earthquake but the vibration was not so large and a cup was dropped from the case. It is an important damage to learn even if the excitation is not so heavy heavy damage will occurred if the anchorage length is not enough.

The same type damage was found at five bridges during the Kushiro-oki Earthquake, i.e., Matsnoe Bridge on national highway No.240 (Photo 4), Gojukkoku Bridge on national highway No.391 (Photo 5), Shin-tawa bridge on regional highway Nakashibetsu-Shibetya (Photo 6), Hatsune Bridge on regional highway Onbetsu-Teishajo (Photo 7), Akangawa Bridge on the regional highway of Akan-Shibetya (Photo 8), Yoda Bridge on the regional highway Horokayanto (Photo 9). And 2 bridges during the Hokkaido-nansei-oki Earthquake, i.e., Motoe Bridge on the municipal highway Motoebashi (Photo 10), and Motouriya Bridge on the municipal highway Uriya No.2 (Photo 11).

DAMAGES TO ABUTMENT AND BEARING SUPPORTS

Kamiisoshin Bridge is located on the National Highway No.228 at the Kamiiso in Hakodate city. Photo 12 shows the bridge with bridge length of 53.1m and the width of 8m. The bridge constructed in 1961 and was a three span simply supported steel plate girder bridge. The foundations are a caisson type.

Photo 13 shows the damage found at the A1 abutment (fixed bearing). The girder moved by about 5cm in the longitudinal direction and crashed into the parapet of the abutment. The web of the steel plate deformed and the crack was found at the parapet. The bearing supports were rotated with displacement of 5cm as shown in Photo 14. The bearing was damaged because the bearing was one anchor type bearing. This type bearing was easily rotated by the longitudinal lateral force. After and the bearing concrete was damaged, the anchorage was dislodged and then the bearing was floated up.

Although this type damage was commonly found in the past earthquakes, it is difficult

to repair this type damage. Generally, the parapet is reconstructed after the displacement of the girder was fixed. However, the repair work significantly affects the traffic. This type damage is easy to be developed during earthquakes, therefore, it is required to develop the structural details which is not affected by the earthquakes and also is easy to repair.

DAMAGE CAUSED BY SOIL LIQUEFACTION

During the both earthquakes, the effect of soil liquefaction was found in a wide area of Hokkaido especially in Kushiro area and south–west area of the Hokkaido. Many damages were found at the road embankment, submerged structures, port facilities and buildings. Although the bridge was not affected by the soil liquefaction, Oshamanbe bridge is an only bridge clearly damaged by the soil liquefaction.

Photo 15 shows the Osyamanbe bridge in the Oshamanbe on the National highway No.37. It is 5 span simply supported post tension T shaped girder bridge with bridge length of 150.1m and deck width of 7m. The foundations are a caisson type. The bridge was constructed in 1960 and the pedestrian bridge was added at the upper stream in 1976.

The bridge pier was inclined in the direction of upper stream of the river as shown in **Photo 16** resulting in the displacement of 42cm on the deck level. No inclination was found at the abutments. Since inclination angle is larger at the center of the bridge and smaller at the abutments, the bridge looks like a curved bridge as shown in **Photo 17.** The largest inclination of pier was found at the Pier P2, the height level at the bearing support in the upper stream side is higher by 38.6cm than that in the lower stream side. The inclination angle was about 0.035 radian.

Several boiling holes caused by the soil liquefaction were found around the bridge. **Fig. 3** shows the ground condition around piers. Gravel, fine sand, and gravel sand layers are around caisson foundation, it is estimated that the these layers in particular fine sand layer was liquefied. **Fig. 4** represent the liquefaction resistance factor, F_L , of the pier P2. In the computation of the liquefaction resistance factor, the seismic lateral force coefficient was assumed as 0.15 which is the design lateral force coefficient.

It should be noted here that the evaluation method for soil liquefaction was introduced in the design specification of highway bridges in 1971. And the evaluation method and treatment method which is almost the same method as a current design method for the design of highway bridges was revised in 1980. The bridge was constructed in 1960 and the effect of soil liquefaction was not considered in the design of the bridge.

DAMAGE TO FALLING–OFF PREVENTION DEVICES

Although damage to the stoppers which were installed at the bearings was found in the past earthquakes, there has been very few damage to the falling–off prevention devices because the large–scale earthquakes has not occurred recently. The bolts of the connection

devices between adjacent girders of Hatsune Bridge on the regional highway Onbetsu–teisyajo were failed during the Kushiro–oki Earthquake. On the other hand, the steel links connecting between girder and substructure were buckled at the Yanagisaki bridge on the national highway No.229 during the Hokkaido–nansei–oki Earthquake.

Hatsune Bridge as shown in **Photo 18** is 6 span simply supported steel plate girder bridge with bridge length of 172m. The bridge was constructed in 1969. **Photo 19** shows the connection devices between adjacent girders used for the Hatsune Bridge. The steel plate (SS400) with height of 68cm, width of 34.5cm and thickness of 9mm was connected by 7 bolts in one side, total 14 bolts for both sides. The bridge has 3 steel plate girders and one connection plate was installed for each steel plate girder. The one side of the connection plate was fixed to the plate girder and the other side had the oval holes so as to be movable in the longitudinal direction by ±20mm.

During the earthquake, the 3 to 10 bolts were cut by shear for 10 connection plates in the total 15 plates as shown in **Fig. 5. Photo 20** shows the connection plate at which 10 bolts in 14 were cut and all bolts of one side were cut resulting that the connection function was lost. All bolts at one side were cut at 7 connection plates of ten damaged plates.

Photo 21 shows the cutting surface of the bolts. **Photo 22** shows the 2000 times magnifications. According to the photos, the cutting surface shows the typical stretch failure type shape. The origin of the cut was estimated to occur from the thread of the screw at the B side as shown in **Fig. 5**, and the failure was occurred only in one direction. Therefore, the bolts were cut by the relative displacement between the adjacent girders during the earthquake. The damaged bolts with shear deformation were also found other than cut bolts and it was found that the reversed force was estimated to act the bolts.

The objective of the falling–off prevention devices is a fail–safe function to prevent destructive damage such as falling–off of superstructure when the main members are damaged during earthquake. Hatsune bridge was damaged at the reinforced concrete pier with termination of longitudinal reinforcement as shown in **Photo 7.**

Although the devices were functioned, the damage was found at Yanagisaki bridge on the national highway 229 as shown in **Photo 23.** The bridge is 5 span simply supported steel plate girder bridge. The connection devices using a steel link between girders and abutment were buckled as shown in **Photo 24.** Although the connection portion at the girder had the oval shape to release some amount of movement, the larger displacement was developed during the earthquake. The stoppers installed at the bearings at the other side abutment to prevent an excessive displacement were damaged as shown in **Photo 25.**

This type of falling–off prevention devices functions as a tension member when the girder moves in the center of the bridge, on the other hand, in the opposite direction it works as a compression member resulting in buckling of the devices.

Although this type of devices is recommended for the installation to the existing bridges in the current design specifications, the device should be designed so as to release the relative displacement between the girder and abutment. The appropriate design

displacement of the devices is necessary to be investigated.

CONCLUSIONS

This paper presents the typical damage of highway bridges caused by the recent earthquakes occurred in Japan. The following conclusions may be deduced :

1) The bending failure to shear failure of the reinforced concrete bridges were found at the section of the longitudinal reinforcement were terminated at mid-height. Six bridges during the Kushiro-oki Earthquake and three bridges during the Hokkaido-nansei-oki Earthquake were found. These bridges were designed according to the specifications of highway bridges before 1980 version and they all have RC piers with the circular section. The damage to Shinshiriuchi bridge showed that piers the bridge designed according to the specifications after 1980 were not damaged at the termination section of main reinforcement at mid-height. Since this type of damage tends to develop a brittle shear failure from the bending failure, the countermeasures to the vulnerable bridge piers is required to be promoted.
2) Although the damage to the parapet of abutment is not a destructive one, it is difficult to repair without closing of the exciting traffic. The structure of the abutments which is not damaged and is easy to repair should be investigated.
3) The damage to falling-off prevention devices were found at two bridges. Since the devices are to prevent a destructive damage such as falling-off of superstructure, the improvement of the devices should be investigated.

ACKNOWLEDGEMENT

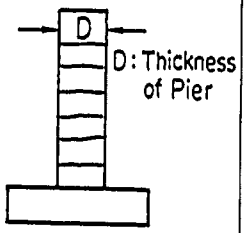
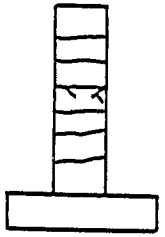
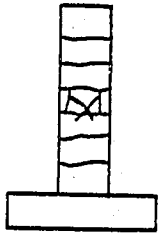
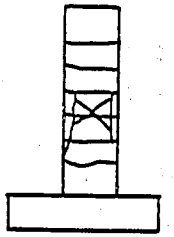
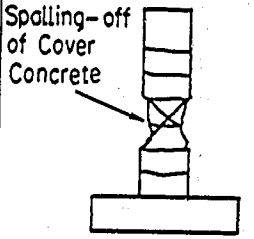
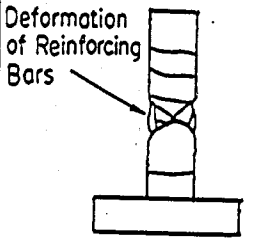
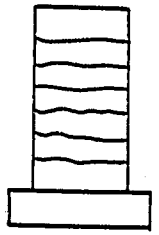
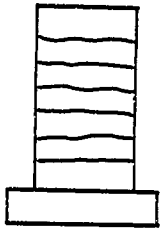
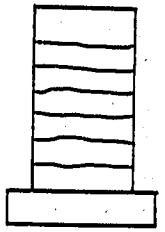
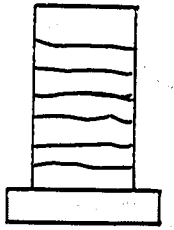
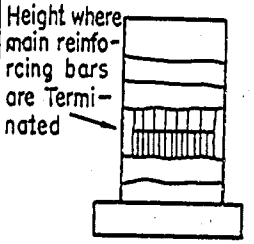
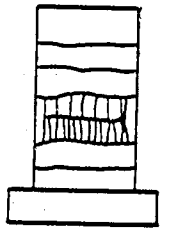
For conducting the damage investigation, invaluable supports were provided by the Kushiro, Obihiro and Hakodate Construction Departments of the Hokkaido Development Bureau, and Hokkaido Government. The damage investigation was made jointly with a U.S. Investigation Team (Liley Chung, NIST: Team Leader) as one of the activities of the Panel on Wind and Seismic Effects, UJNR. The authors sincerely thank various suggestions and discussions provided by various persons and organizations.

REFERENCES

1) Kushiro Development Department of Hokkaido Development Bureau : Prompt Report (Road Facilities) of the Kushiro-oki Earthquake of January 15, 1993, 1993 (in Japanese)
2) The First Investigation Team of the Public Works Research Institute : Prompt Report of the Kushiro-oki Earthquake of 1993, Civil Engineering Journal, Vol.35, No.4, 1993 (in Japanese)
3) Hakodate Development Department of Hokkaido Development Bureau : Prompt Report

(Road Facilities) of the Hokkaido-nansei-oki Earthquake of 1993, 1993 (in Japanese)
4) The First Investigation Team of the Public Works Research Institute : Prompt Report of the Hokkaido-nansei-oki Earthquake of 1993, Civil Engineering Journal, Vol.35, No.10, 1993 (in Japanese)
5) Kawashima, K., Unjoh, S. and Nakajima, T. : Prompt Report of the Hokkaido-nansei-oki Earthquake of July, 1993, Technical Memorandum of PWRI, No.3204, 1993 (in Japanese)
6) Narita, N., Murakami, P. and Asanuma, H. : Report of the Damage to Shizunai Bridge during the Urakawa-oki Earthquake of 1982, The 15th Joint Meeting of the Panel on Wind and Seismic Effects, UJNR, Tsukuba, 1983
7) Kawashima, K., Unjoh, S., Sugita, H. and Nakajima, T. : Damage to Bridges caused by the Kushiro-oki Earthquake, Bridges and Foundations, Vol.93, No.6, 1993 (in Japanese)
8) Kawashima, K., Unjoh, S. and Iida, H. : Damage to Reinforced Concrete Bridge Piers with Termination of Longitudinal Reinforcement at Mid-height and the Analysis, Civil Engineering Journal, Vol.34, No.5, 1992 (in Japanese)
9) Japan Road Association : Part IV, Substructures of Design Specifications of Highway bridges, 1980 (in Japanese)
10) Japan Road Association : Manual for Earthquake Disaster Prevention Measures of Road Facilities (Post Earthquake), 1988 (in Japanese)
11) Kawashima, K. and Nishikawa, K. : Damage to Bearings of Highway Bridges during the Miyagi-ken-oki Earthquake, Civil Engineering Journal, Vol.21, No.4, 1979 (in Japanese)
12) Japan Road Association : Seismic Design of Design Specifications of Highway bridges, 1971 (in Japanese)
13) Japan Road Association : Part V, Seismic Design of Design Specifications of Highway bridges, 1980 (in Japanese)

Table 1 Estimation Meshod of Damage Degree of Reinforced Concrete Piers at the Termination Section of Main Reinforcement

Observed Damage		① Horizontal Crack	② Diagonal Crack (Less Than the Width of D/2)	③ Diagonal Crack (More Than the Width of D/2)	④ Diagonal Crack (Vertical Crack)	⑤ Spalling-off of Cover Concrete	⑥ Deformation of Reinforcing Bars
Damage	Side View						
	Front View						
Damage Degree		C : Small	C : Small	C : Small	B : Medium	B : Medium	A : Large
Residual Strength		P_u ($1.05P_y \sim 1.1P_y$)	P_u ($1.05P_y \sim 1.1P_y$)	$1.0P_y$	$1.0P_y$	Less Than P_y	Less Than P_y
Residual Ductility $\frac{\delta_u-\delta}{\delta_u-\delta_y} \times 100$ (%)		100 %	70 %	40 %	10 %	0 %	0 %

P_y : Yielding Strength P_u : Ultimate Strength δ_y : Yielding Displacement δ_u : Ultimate Displacement, δ : Peak Displacement

Nate) D : Thickness Pier

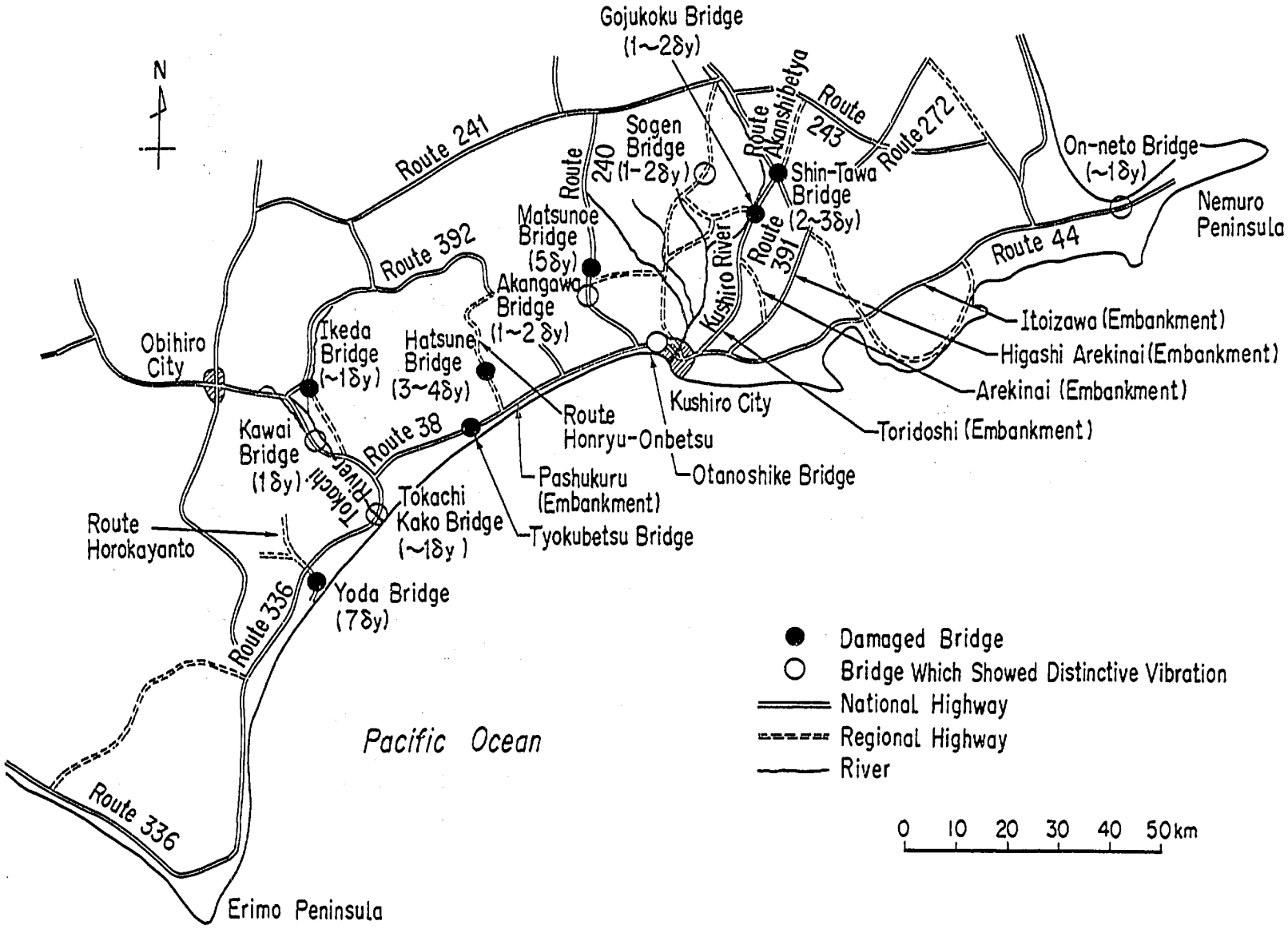


Fig. 1 Location of Damaged Bridges and Damage Degree of Piers caused by the Kushiro–oki Earthquake

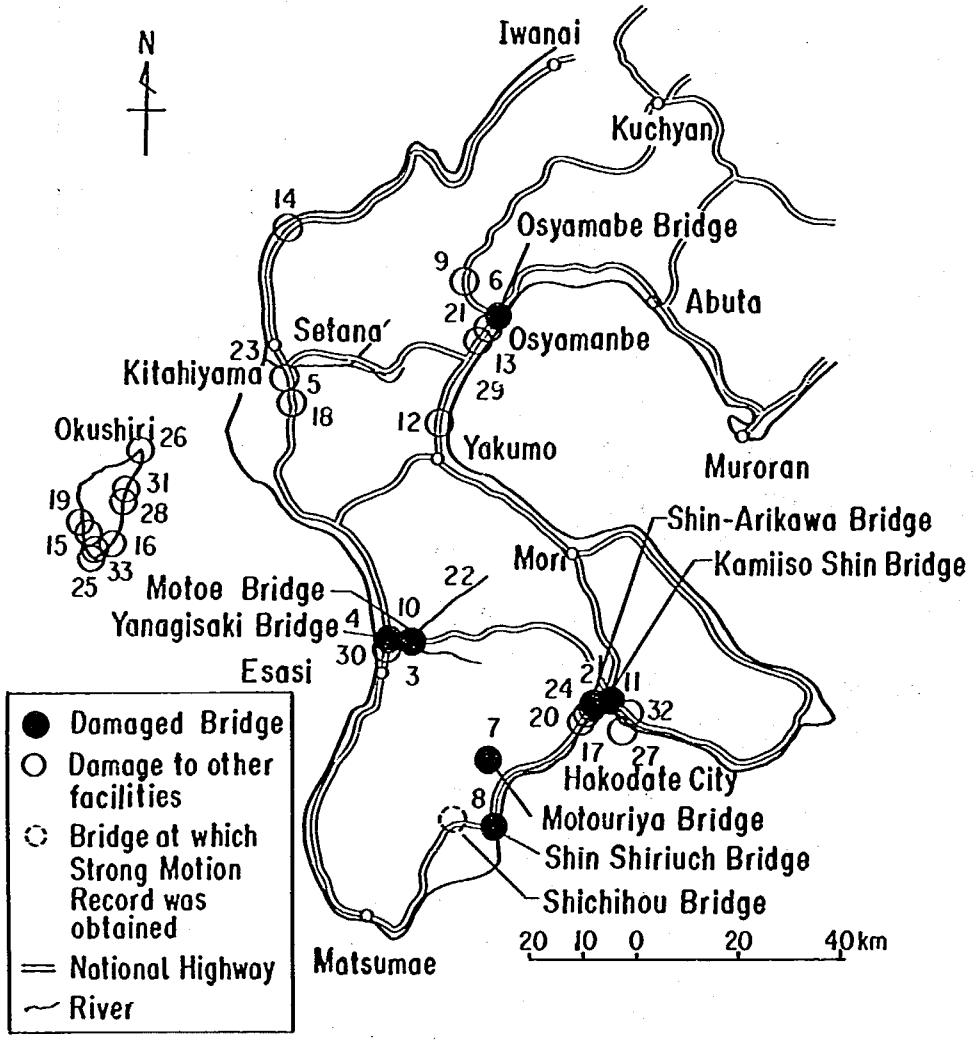


Fig. 2 Location of Damaged Bridges caused by the Hokkaido–nansei–oki Earthquake

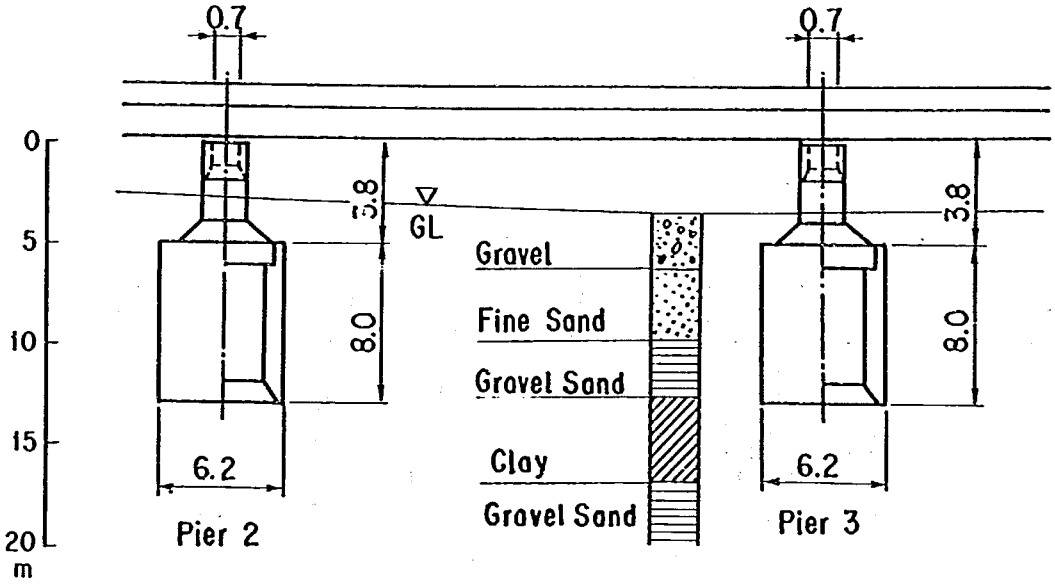


Fig. 3 Ground Condition of Osyamanbe Bridge (by Hokkaido Development Bureau)

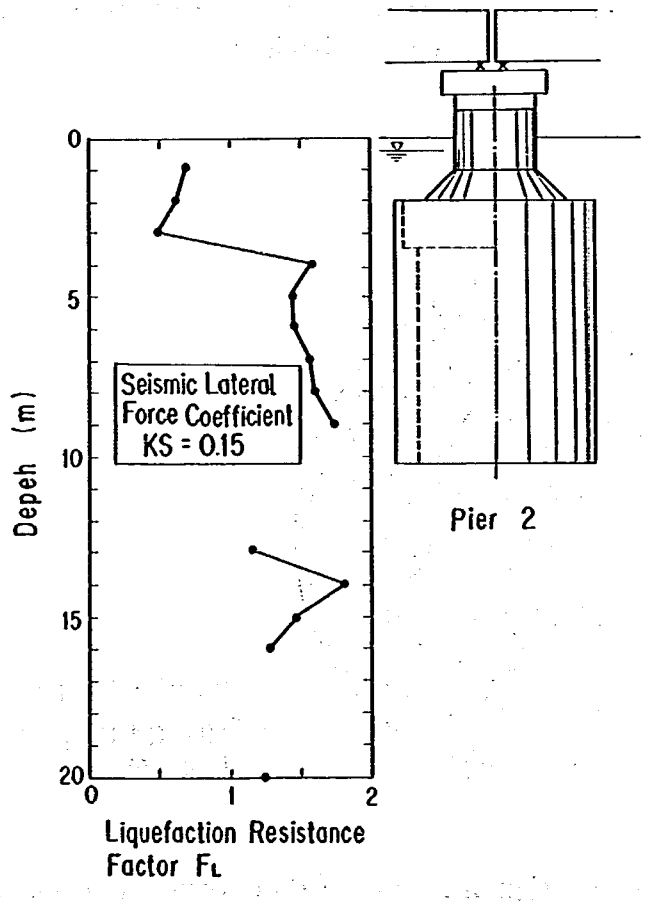


Fig. 4 Liquefaction Resistance Factor, F_L (Pire P2, Osyamanbe Bridge)

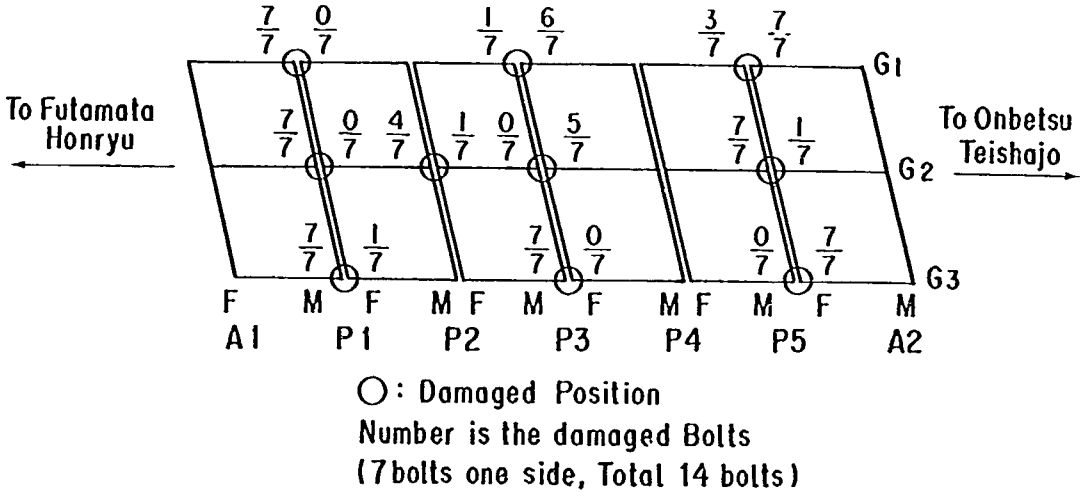


Fig. 5 Location of damage to the connection devices between adjacent girders (Hatsune Bridge)

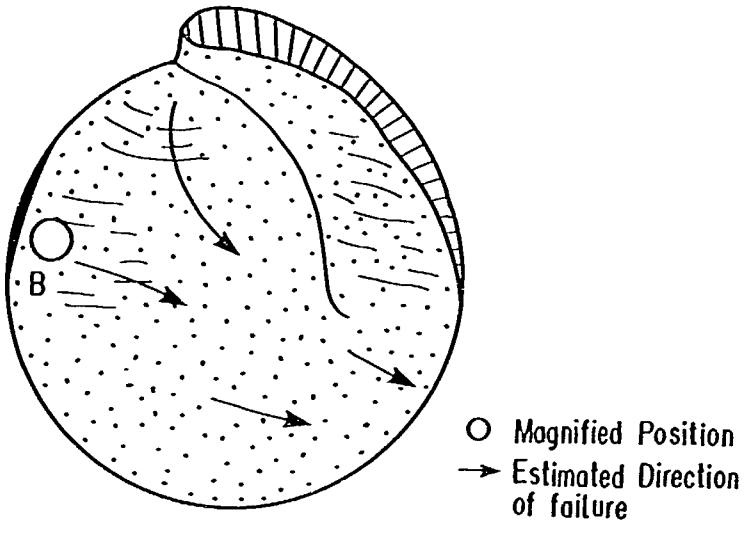


Fig. 6 Direction of Failure of Bolts (Hatsune Bridge)

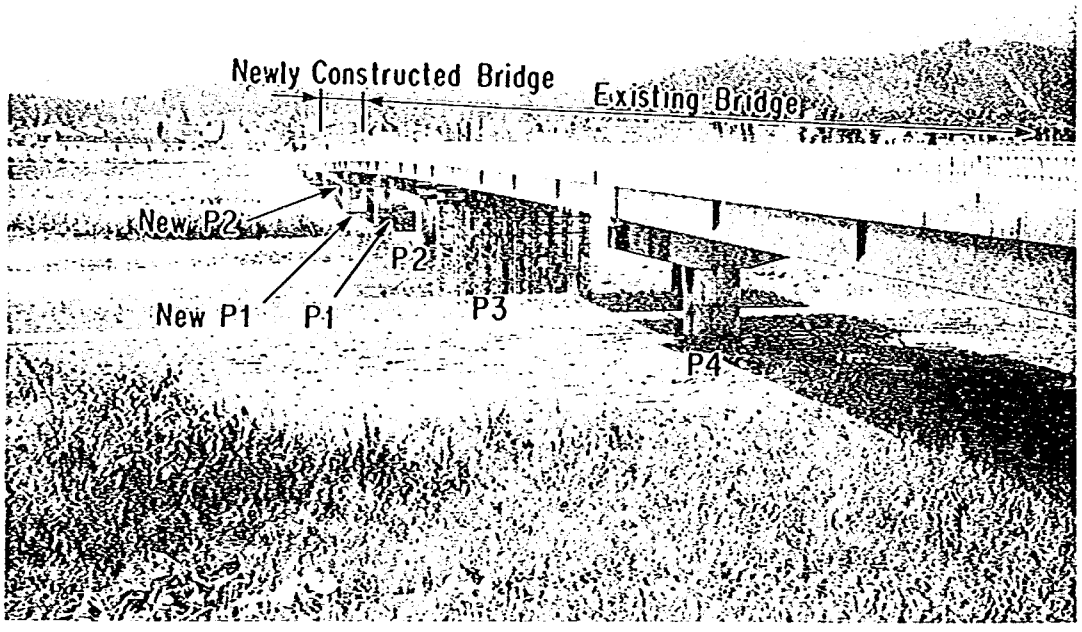


Photo 1 Shin–Shiriuchi Bridge

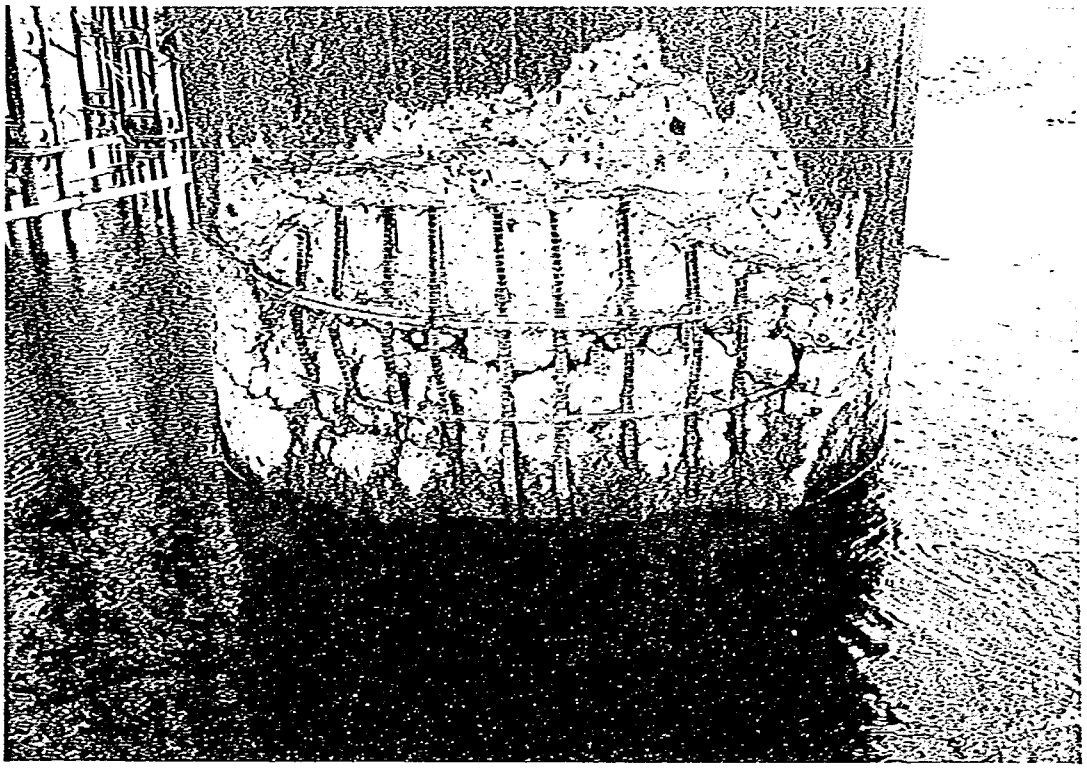


Photo 2 Damage of Pier P3 (from the lower stream side)

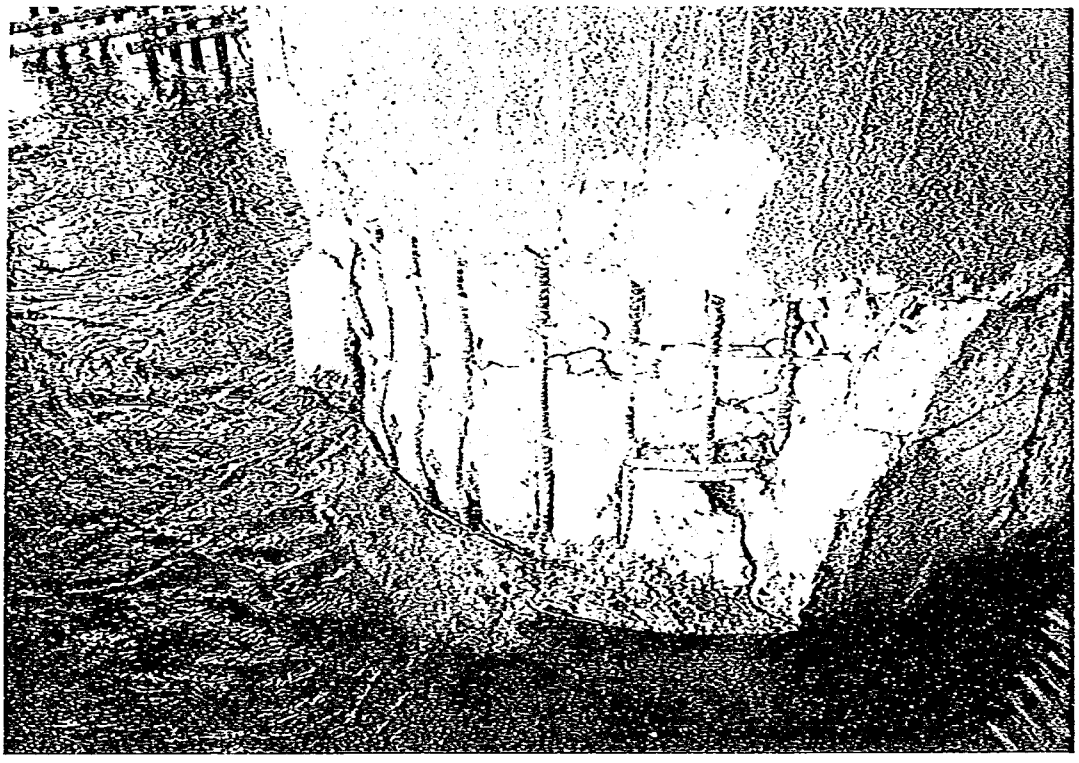


Photo 3 Damage of Pier P3 (from the upper stream side)

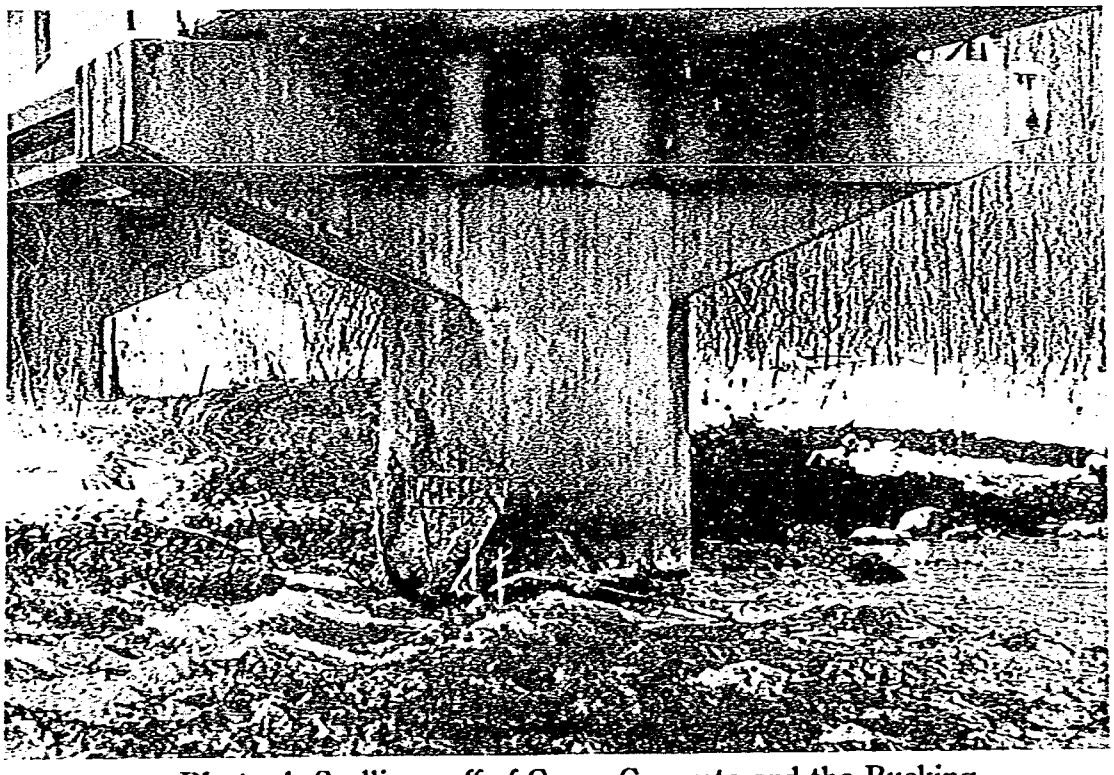


Photo 4 Spalling–off of Cover Concrete and the Bucking of Main Reinforcement of Matsunoe Bridge (Pier P4)

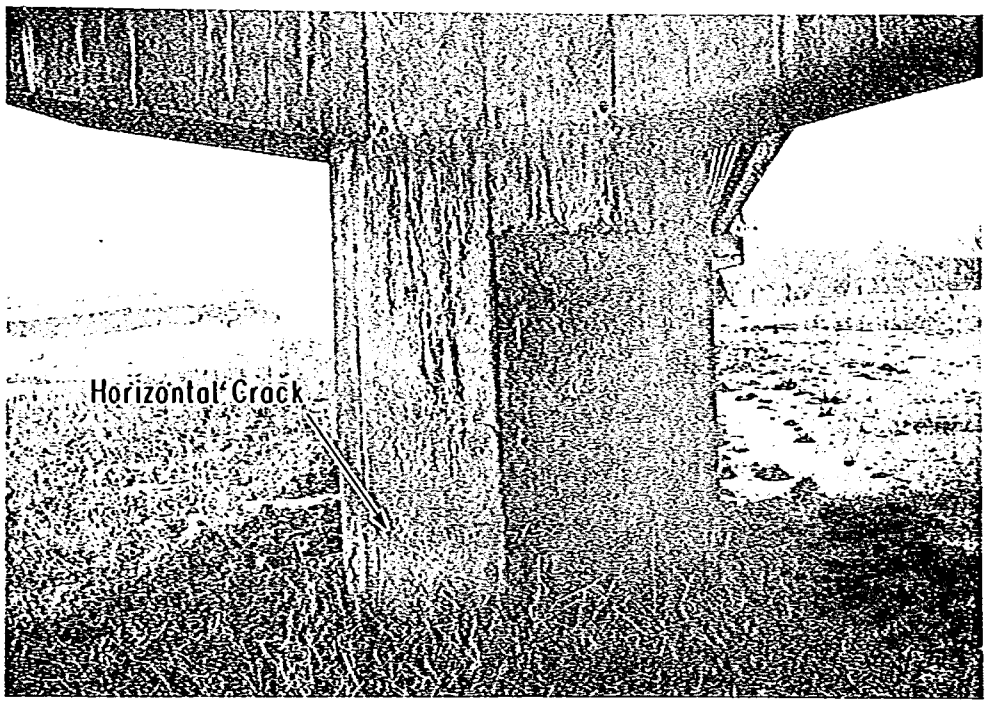


Photo 5 Cracks of Gojukkoku Bridge

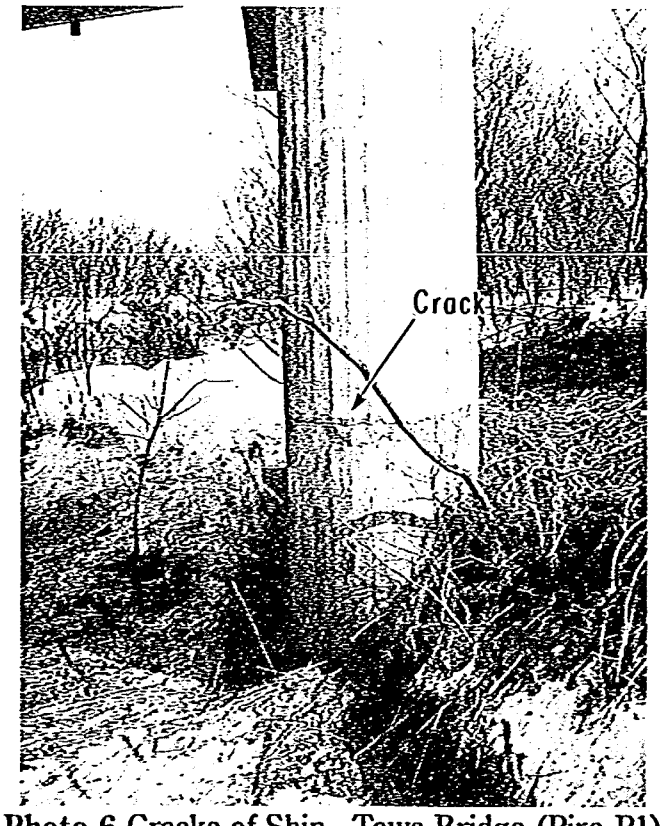


Photo 6 Cracks of Shin-Tawa Bridge (Pire P1)

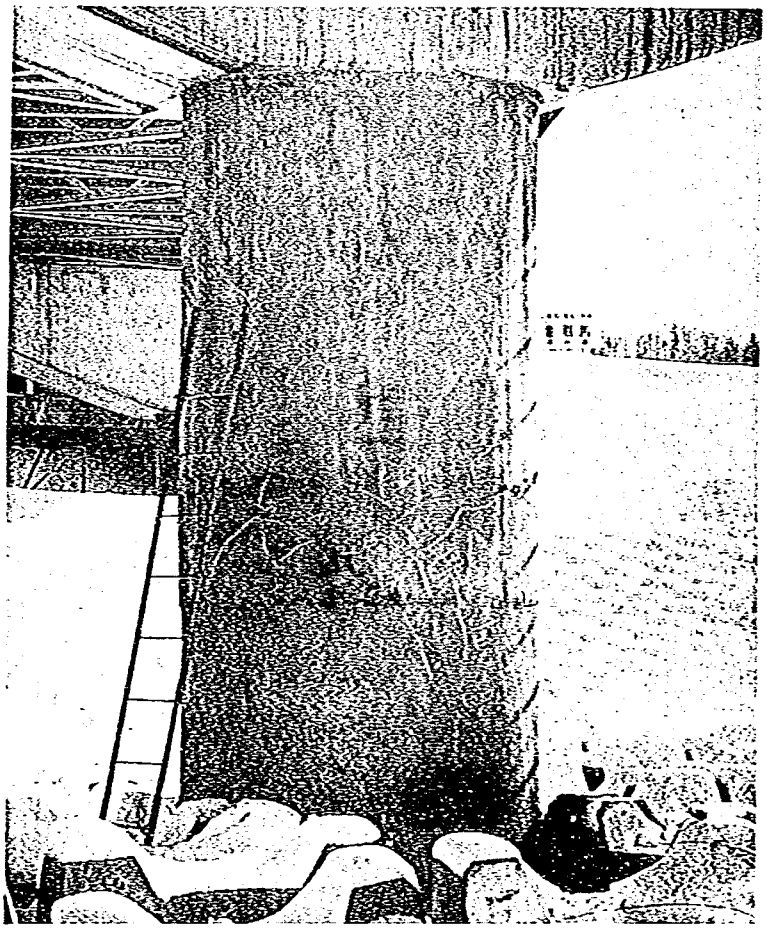


Photo 7 Diagonal Cracks of Hatsune Bridge (Pire P4)

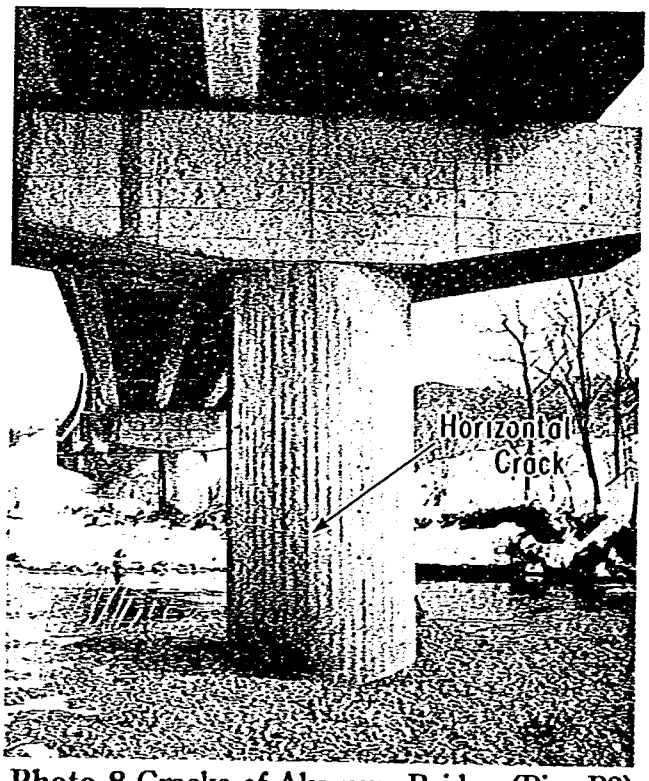


Photo 8 Cracks of Akagawa Bridge (Pire P2)

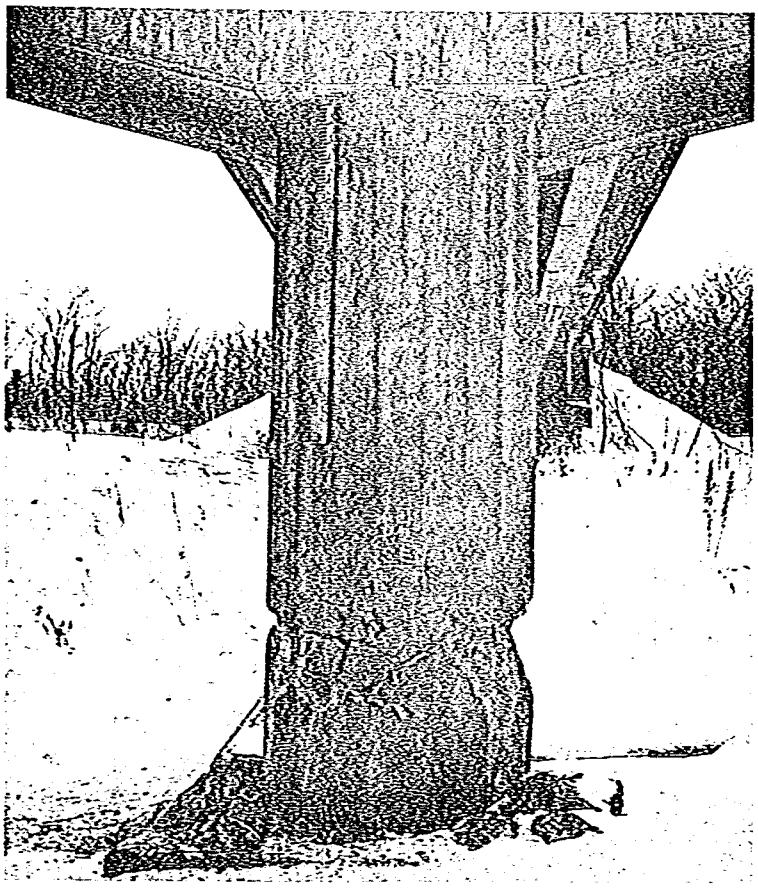


Photo 9 Damage to Pire P2 of Yoda Bridge

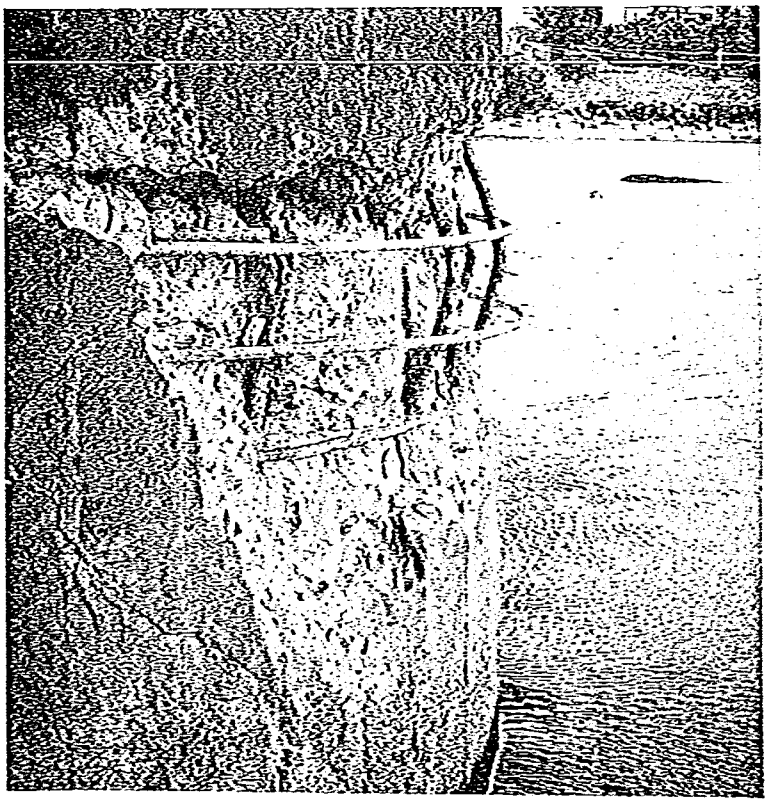


Photo 10 Damage to Pire P3 of Motoe Bridge

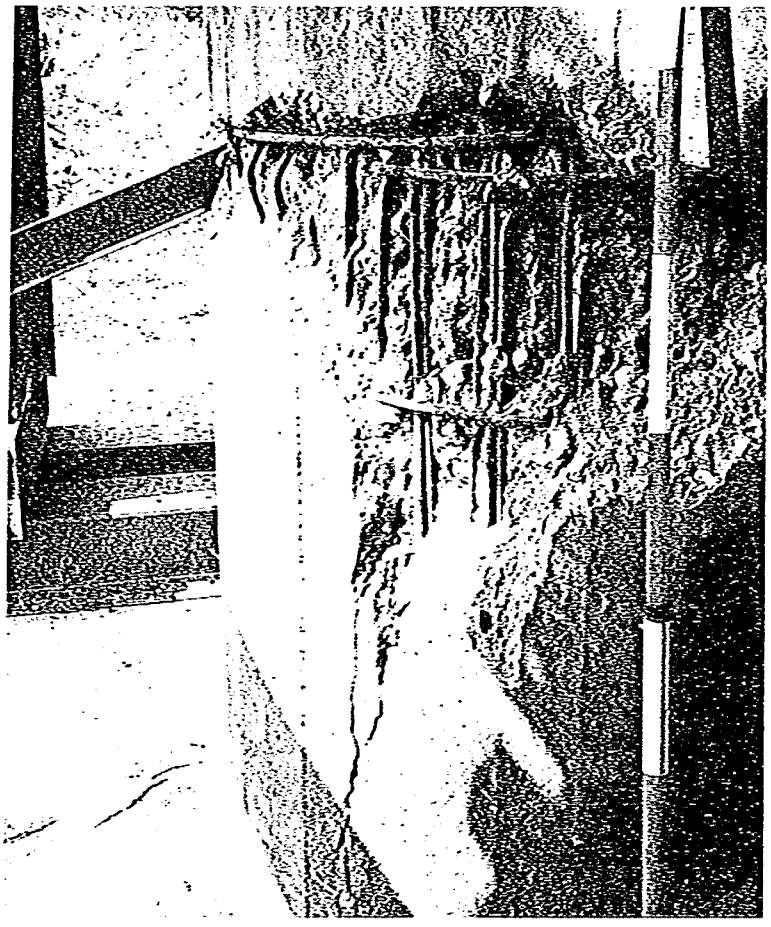


Photo 11 Damage to Pire of Motouriya Bridge

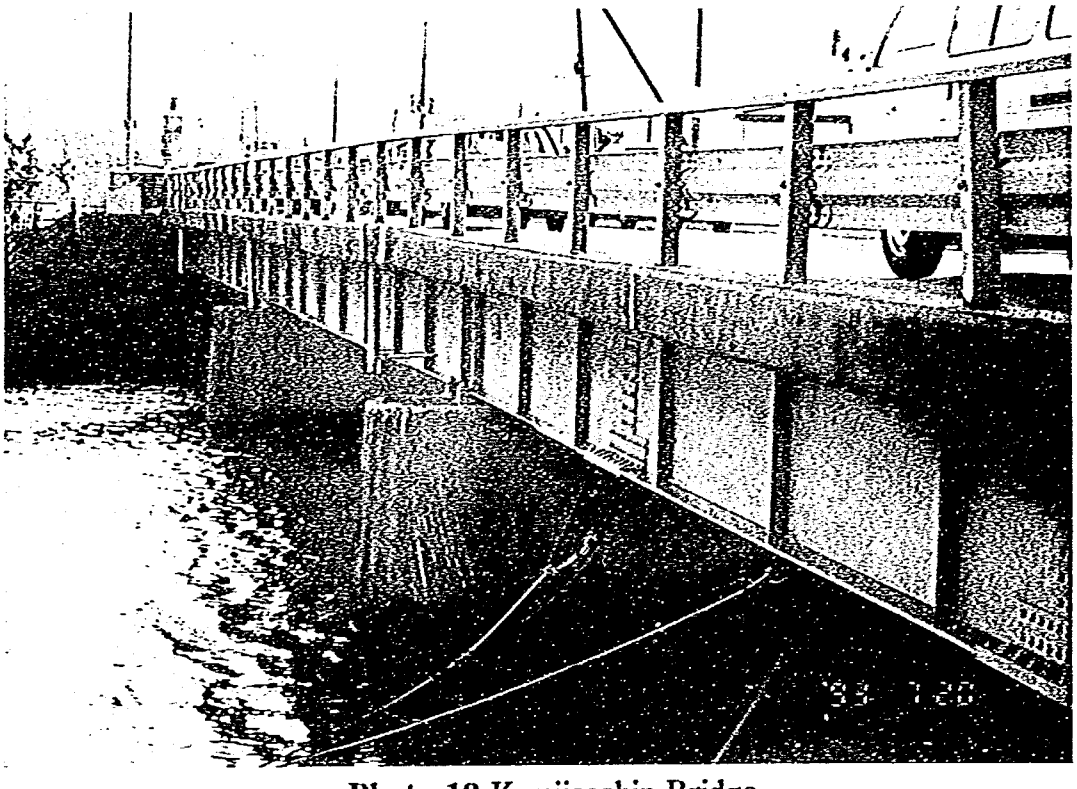


Photo 12 Kamiisoshin Bridge

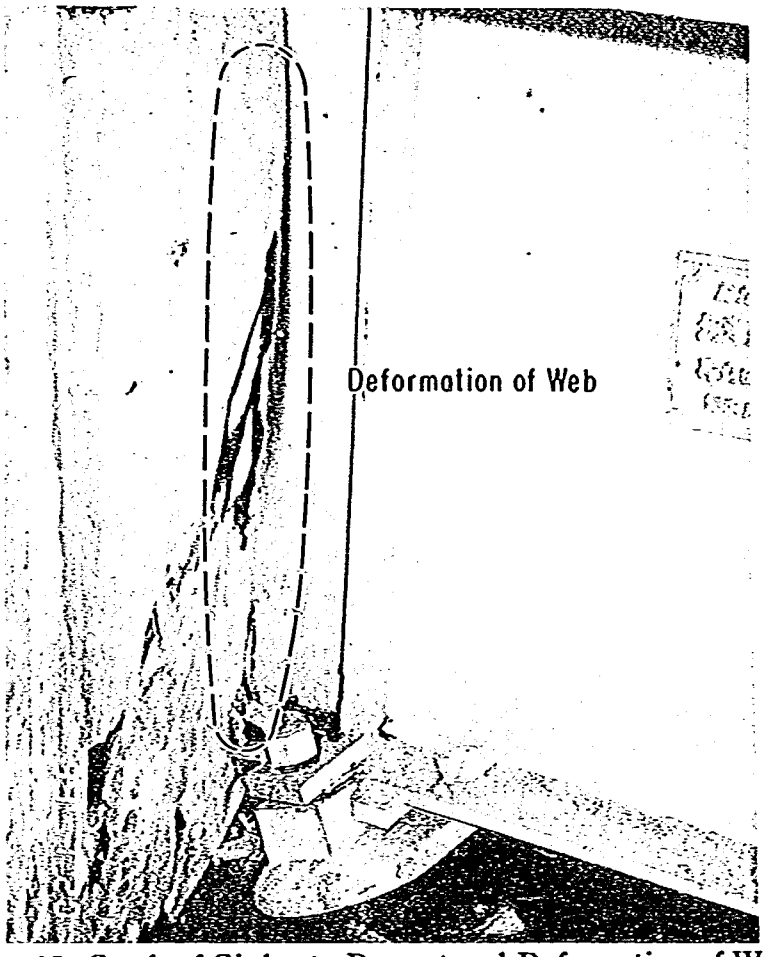


Photo 13 Crash of Girder to Parapet and Deformation of Web and Rotation of Bearings (Kamiisoshin Bridge)

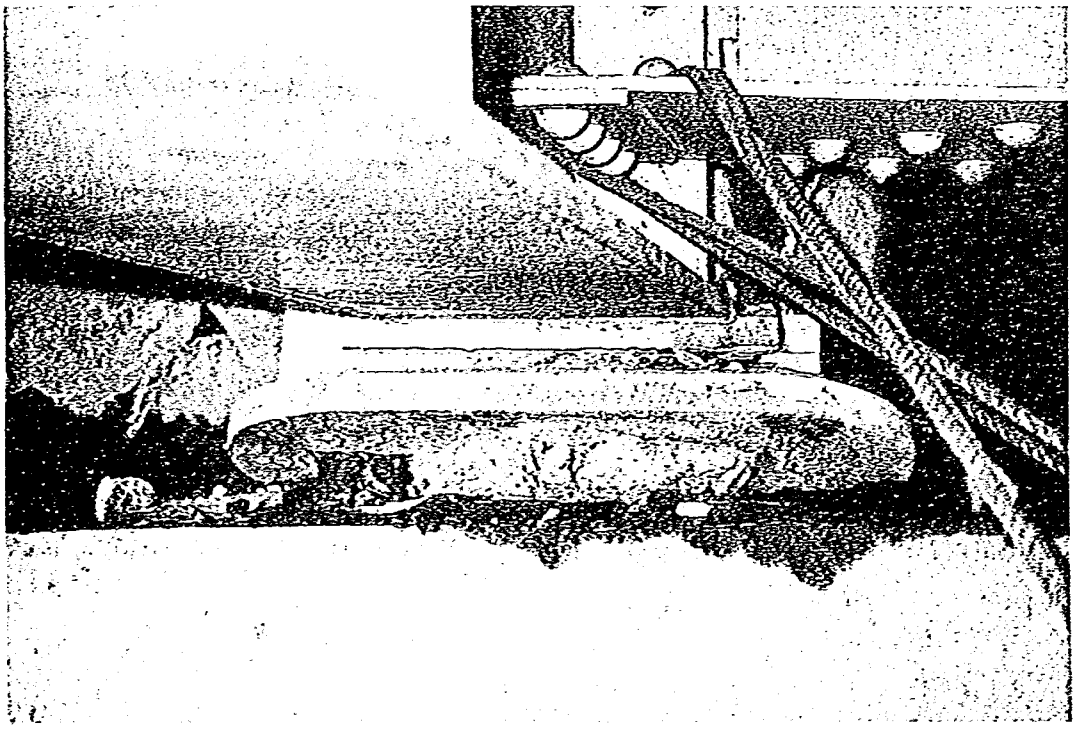


Photo 14 Rotation of Bearing (Kamiisoshin Bridge)

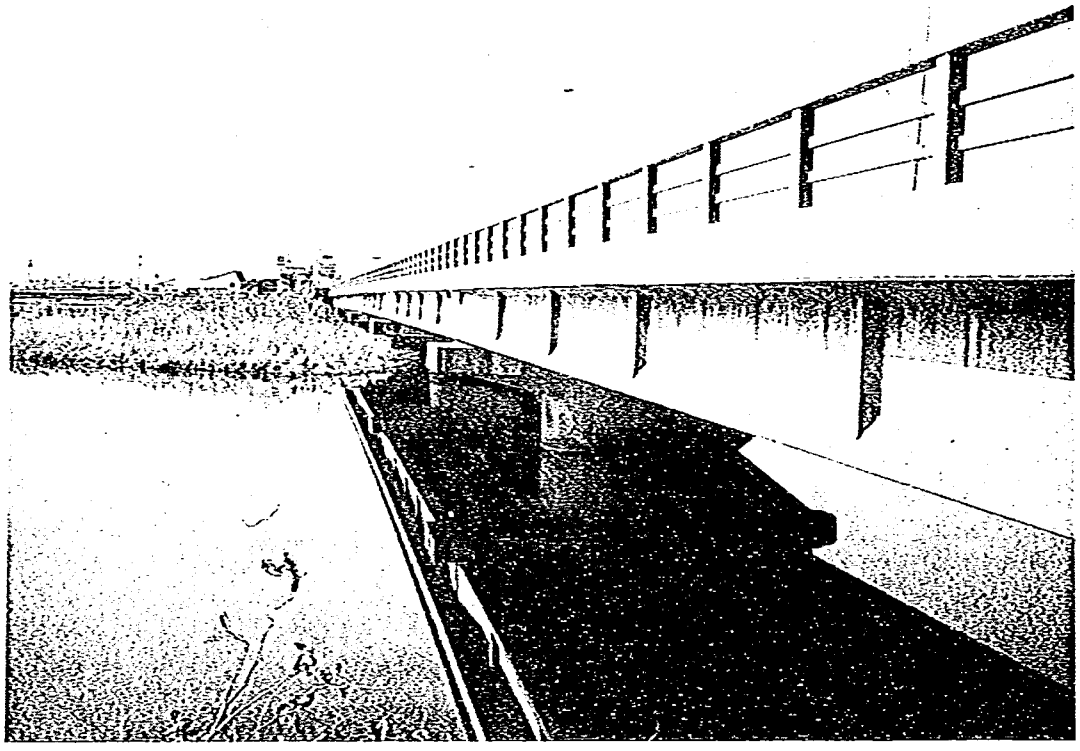


Photo 15 Osyamanbe Bridge



Photo 16 Inclination of Pire and soil Liquefaction (Osyamanbe Bridge, Pier P2)

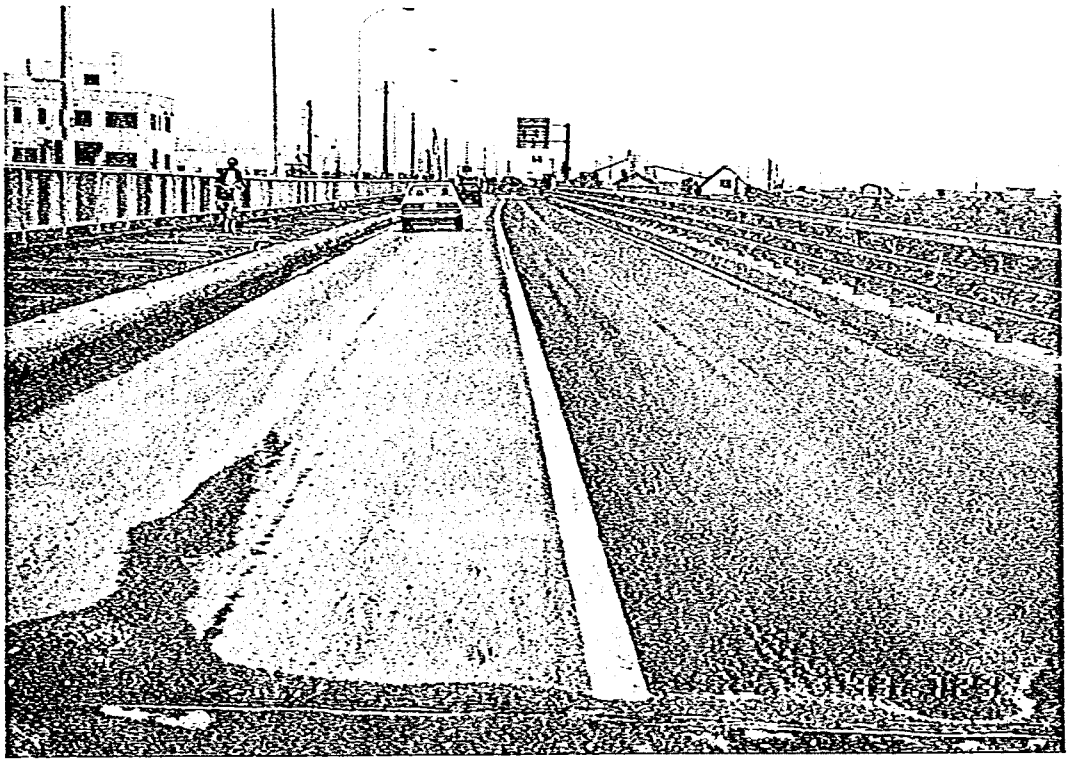


Photo 17 Residual Displacement found at the Deck caused by the Inclination of Piers (Osyamanbe Bridge)

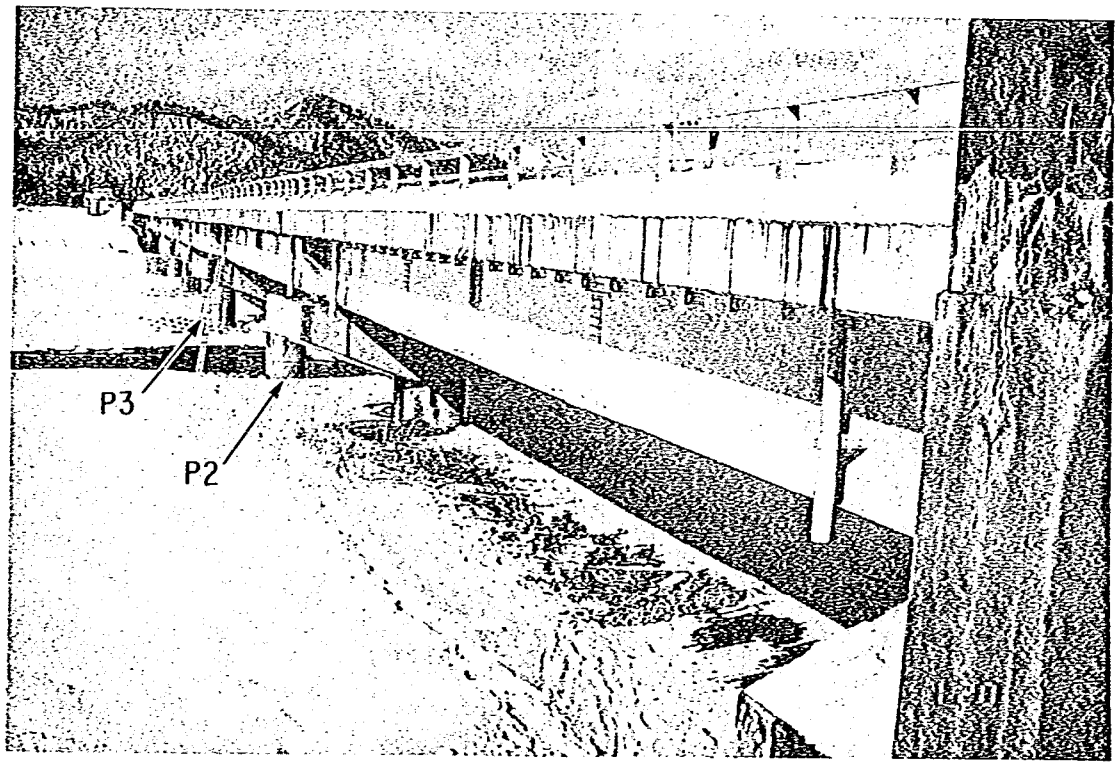


Photo 18 Hatsune Bridge

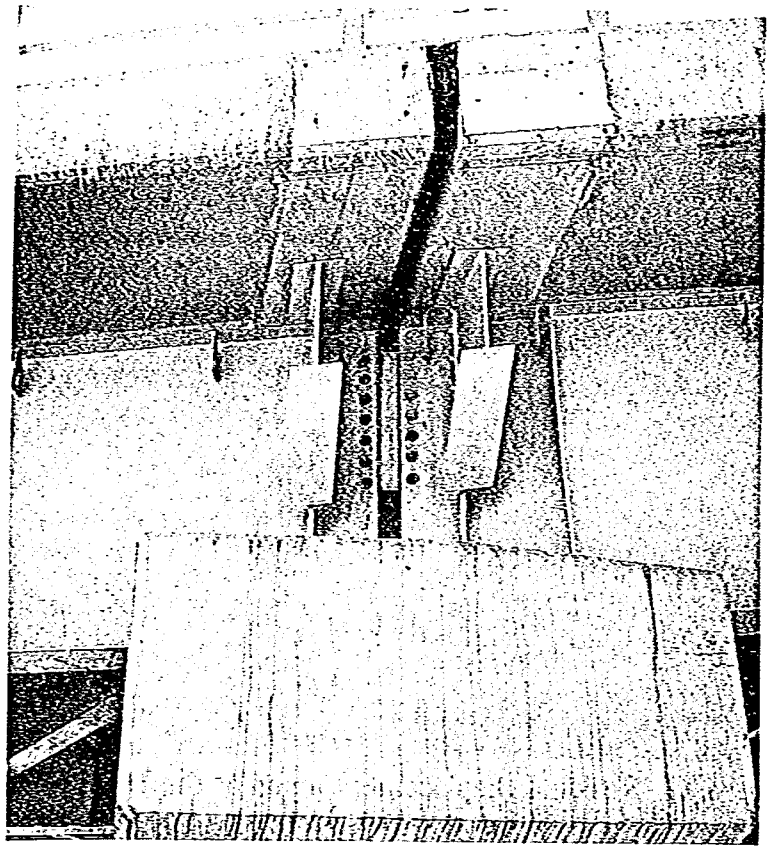


Photo 19 Damage of the Connection Devices (Hatsune Bridge)

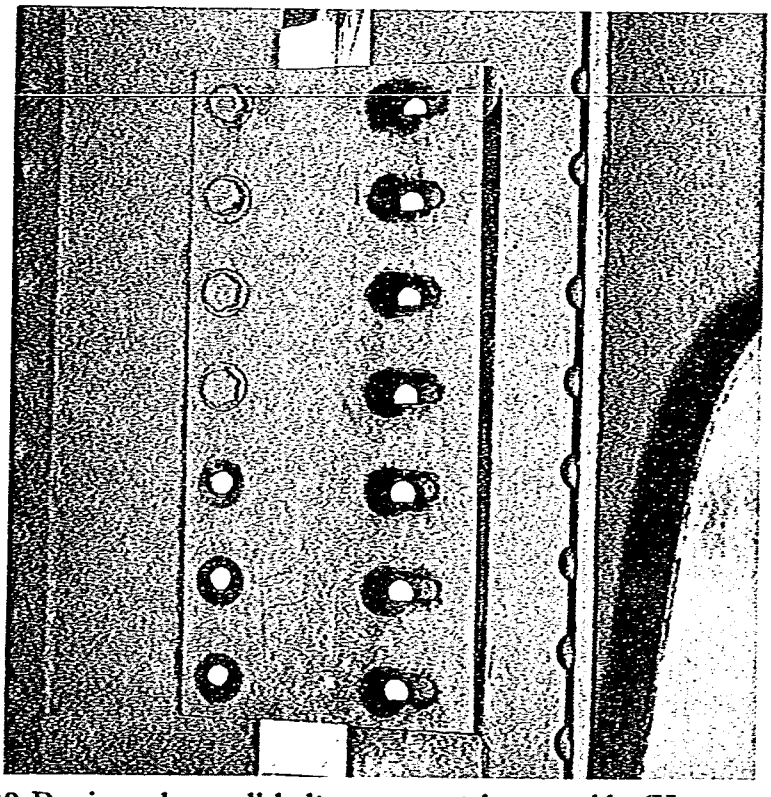


Photo 20 Device where all bolts were cut in one side (Hatsune Bridge)

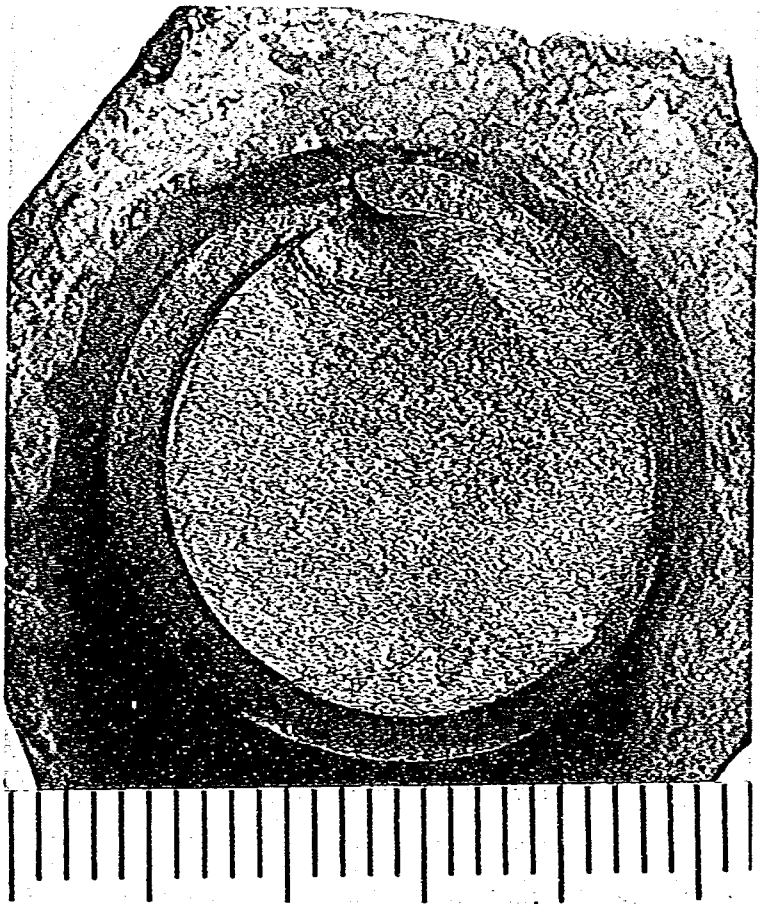


Photo 21 Cutting Surface of Bolts (Hatsune Bridge)

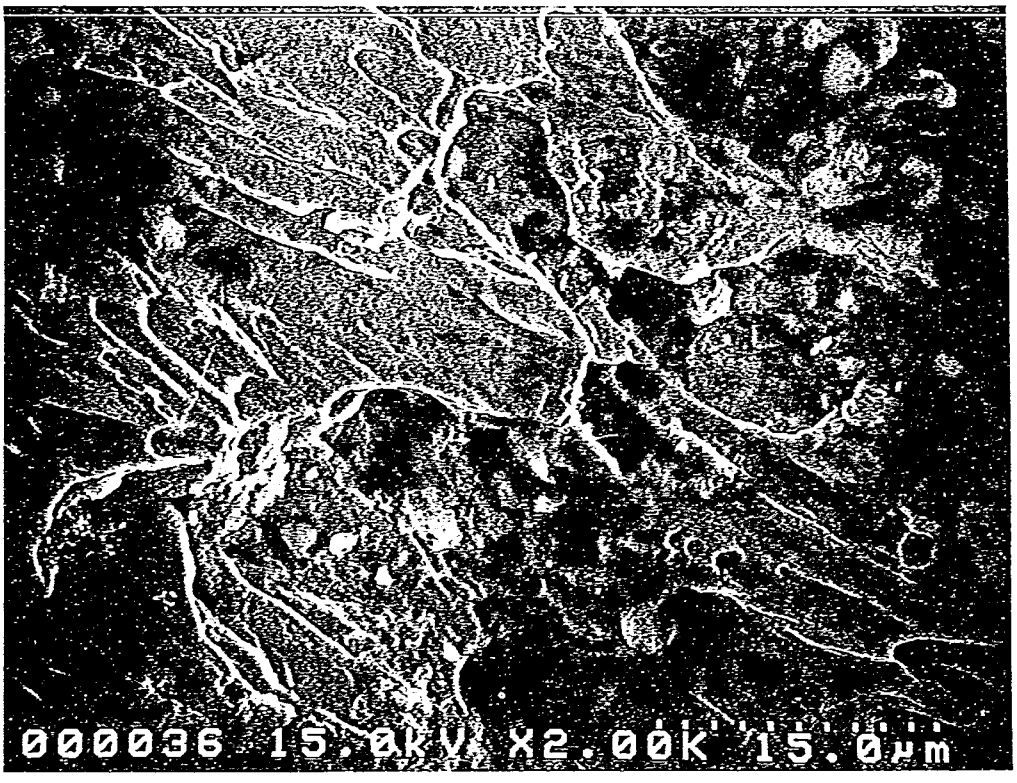


Photo 22 Magnification of Cutting Surface (Hatsune Bridge, Position B in Fig. 6)

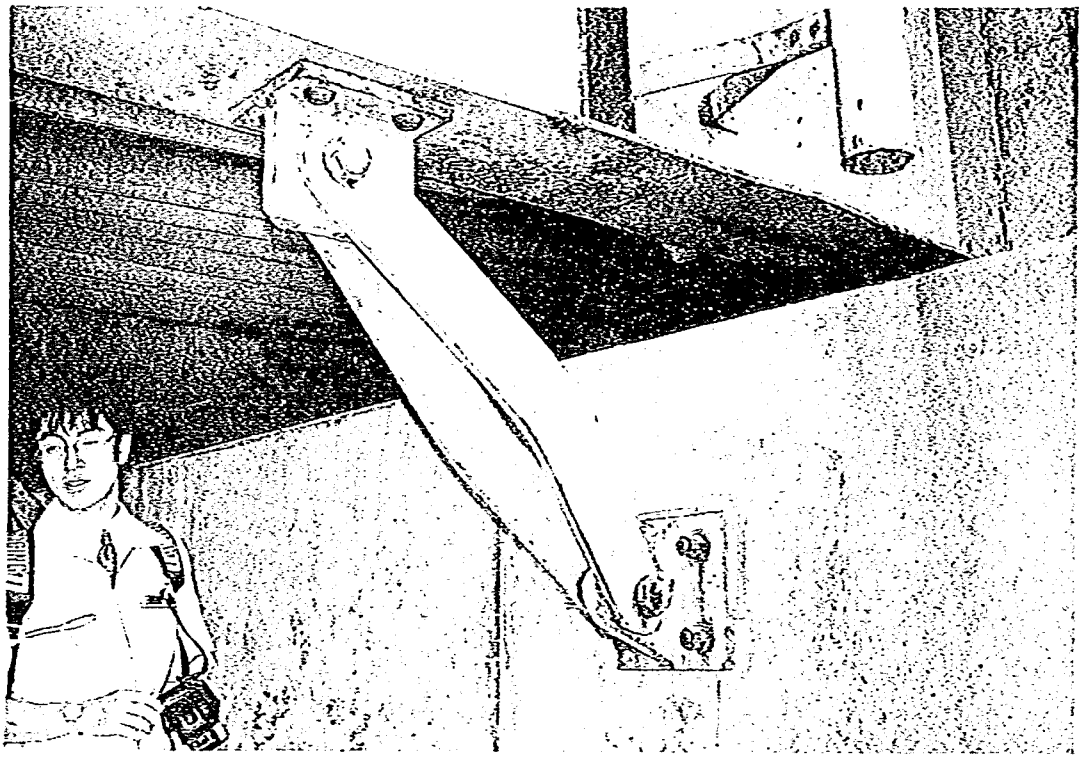


Photo 23 Yanagisaki Bridge

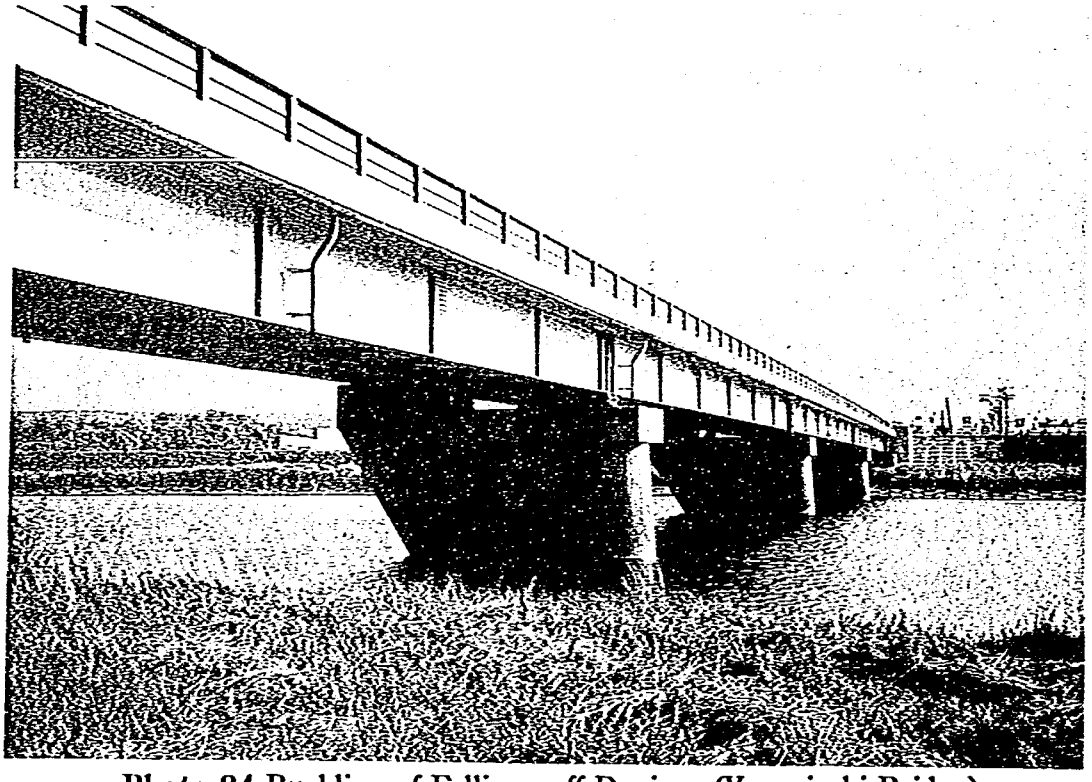


Photo 24 Buckling of Falling–off Devices (Yanagisaki Bridge)

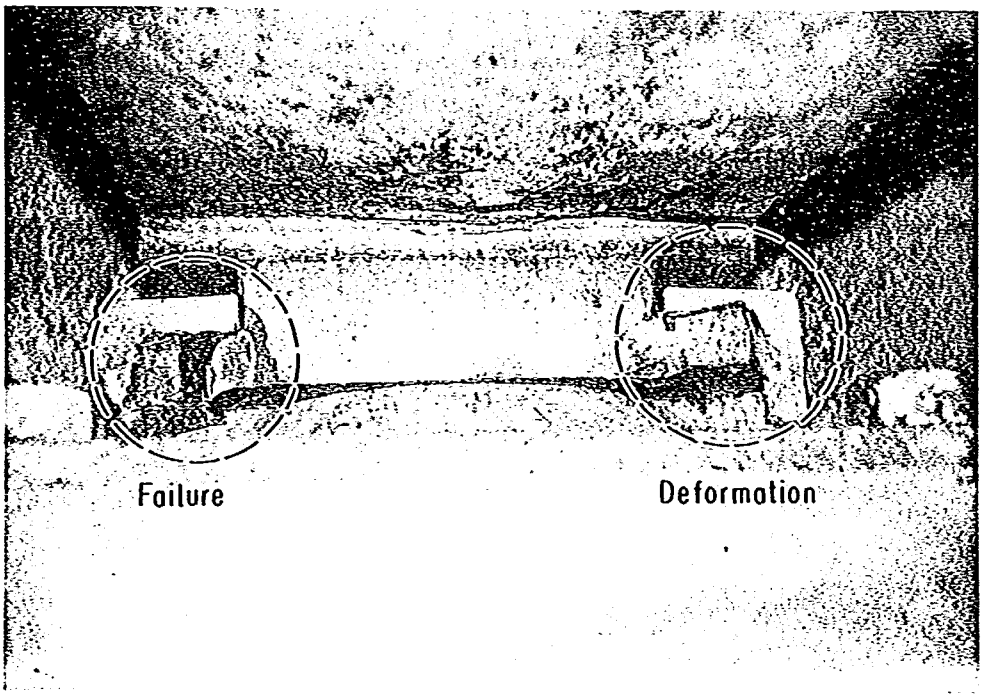


Photo 25 Damage of Stoppers (Bearing at Abutment, Yanagisaki Bridge)

Damage Analysis of Reinforced Concrete Bridge Piers by Kushiro-oki Earthquake, January, 1993 and Hokkaido Nansei-oki Earthquake, July, 1993

Kazuhiko KAWASHIMA
Jun-ichi HOSHIKUMA
and
Shigeki UNJOH

2nd U.S.-Japan Workshop on
Seismic Retrofit of Bridges
Berkeley, U.S.A.
January, 1994

DAMAGE ANALYSIS OF REINFORCED CONCRETE BRIDGE PIERS BY KUSHIRO-OKI EARTHQUAKE, JANUARY, 1993 AND HOKKAIDO NANSEI-OKI EARTHQUAKE, JULY, 1993

K. Kawashima[1], J. Hoshikuma[2] and S. Unjoh[3]

1) Head, Earthquake Engineering Division, Public Works Research Institute, Ministry of Construction, Tsukuba Science City, Japan
2) Research Engineer, ditto
3) Senior Research Engineer, ditto

ABSTRACT

This paper presents the effectiveness of a seismic evaluation method for reinforced concrete bridge piers with termination of longitudinal reinforcement at mid-height based on the damage due to the Kushiro-oki Earthquake and the Hokkaido Nansei-oki Earthquake. During these earthquakes, several reinforced concrete bridge piers with circular cross section suffered significant damage at mid-height. The piers were designed and constructed prior to 1980, when the Design Specifications of Highway Bridges was revised. The seismic vulnerability of damaged and undamaged piers was evaluated.

INTRODUCTION

During the Kushiro-oki Earthquake in January, 1993 and the Hokkaido Nansei-oki Earthquake in July, 1993, many bridges were damaged[1]. In particular, reinforced concrete piers suffered damage at mid-height, where the longitudinal reinforcement was terminated with inadequate anchorage length. The importance for this type of damage was firstly pointed out when Shizunai bridge was critically damaged during the Urakawa-oki Earthquake in 1982[2].The damage causes a brittle shear failure and may result in a collapse of substructures.

Before 1980, an anchorage length of terminated reinforcement was stipulated as[3]

$$l = \frac{\phi \sigma_{sa}}{6 \tau_{oa}} \tag{1}$$

where

l : anchorage length (cm)
σ_{sa} : allowable tensile stress of reinforcement (kgf/cm^2)
τ_{oa} : allowable adhesion stress of concrete (kgf/cm^2)

ϕ : diameter of reinforcement (cm)

In the revision of the Design Specifications of Highway Bridges in 1980[4], the anchorage length was increased as

$$l = \frac{\phi \sigma_{sa}}{4 \tau_{0a}} \tag{2}$$

and the allowable shear stress of concrete in anchorage zone was reduced to two thirds of the shear stress at the normal zone. Therefore, reinforced concrete piers designed and constructed in accordance with the Specifications after 1980 are redundant at the termination zone, however, the others require to be adequately evaluated and strengthened at need. To identify the seismic vulnerability at the termination point, a seismic evaluation method was proposed based on the study at PWRI and has been applied to the seismic evaluation in 1991 throughout the country.

This paper presents a result of seismic evaluation of piers which were damaged and undamaged during the Kushiro-oki Earthquake and the Hokkaido Nansei-oki Earthquake, and describes an application of the seismic evaluation method at the termination of longitudinal reinforcements.

SEISMIC EVALUATION METHOD FOR THE TERMINATION OF LONGITUDINAL REINFORCEMENT

The seismic evaluation method for the termination of longitudinal reinforcement was already reported[5) 6)], hence a summary of the evaluation method is described here briefly.

Fig. 1 shows a flow chart of the seismic evaluation for reinforced concrete piers with termination of longitudinal reinforcement. According to the evaluation method, the seismic vulnerability at the termination point is evaluated by two parameters, i.e., failure mode factor and safety factor. The safety factor is defined as a ratio of the yielding bending moment to the bending moment due to the lateral force for design as shown in Fig. 2 and is given as

$$F_y^T = \frac{M_y^T}{M^T} \tag{3}$$

$$F_y^B = \frac{M_y^B}{M^B} \tag{4}$$

where

F_y^T and F_y^B : safety factor at the termination point and base, respectively

M_y^T and M_y^B : yielding bending moment at the termination point and base, respectively

M^T and M^B : bending moment at the termination point and base, respectively, due to the lateral force for design

In this evaluation, the termination point is defined as the point with anchorage length below

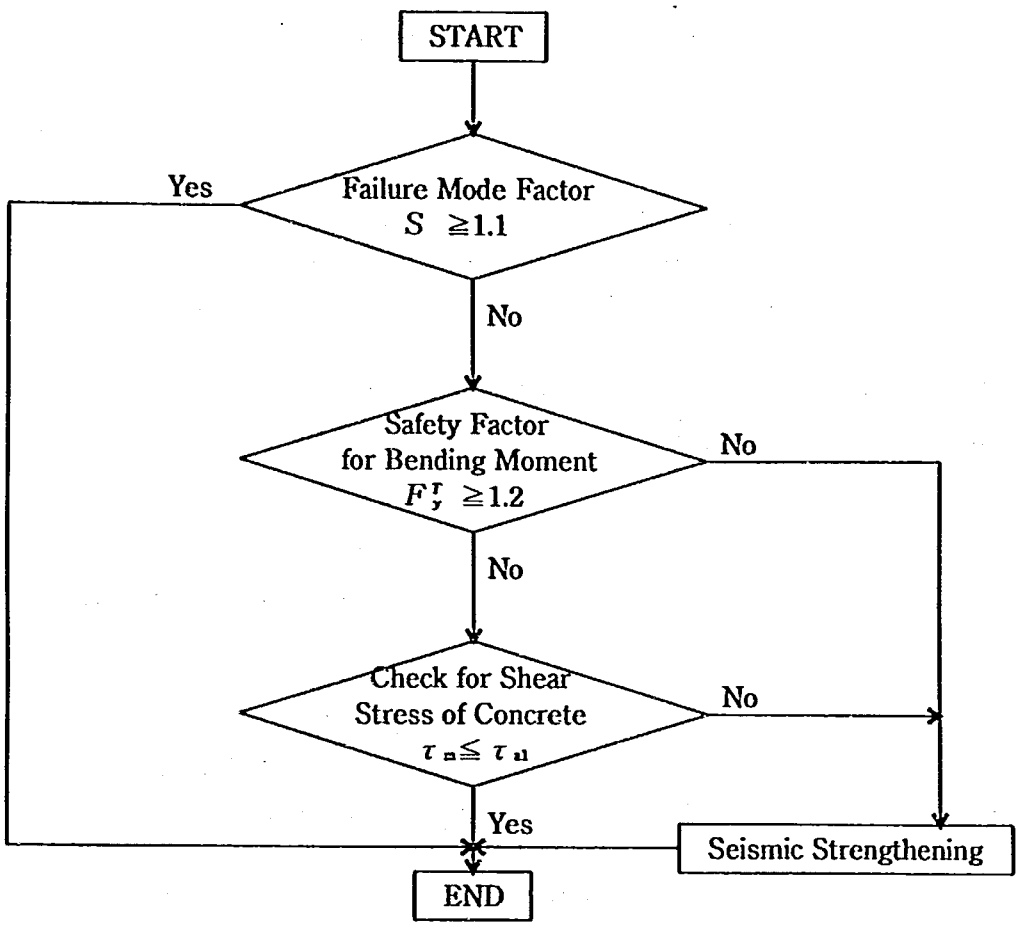


Fig. 1 Seismic Evaluation for Reinforced Concrete Bridge Piers with Termination

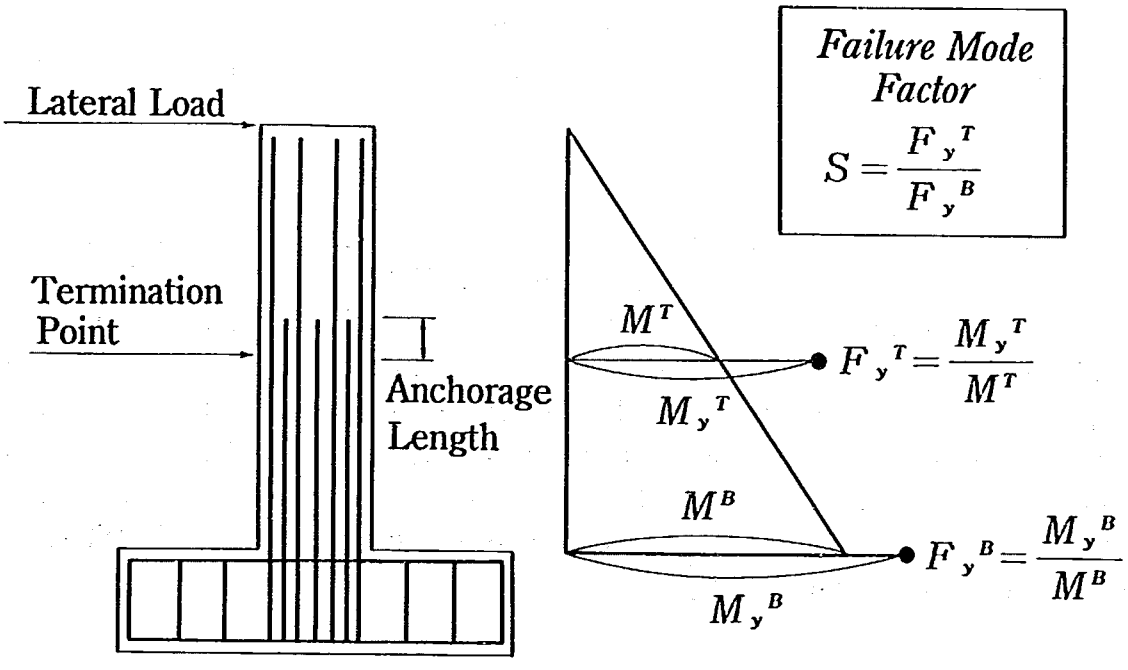


Fig. 2 Definition of Failure Mode Factor

the actual point of terminations.
To identify which zone the initial damage would be developed, the failure mode factor S is defined as

$$S=\frac{F_y{}^T}{F_y{}^B} \tag{5}$$

Based on a series of loading test results at PWRI, the seismic vulnerability at the termination point was evaluated by means of the failure mode factor S and the safety factor $F_y{}^T$ as shown in Table 1. The piers which are evaluated S as larger than 1.1 are not damaged at the termination point, while the others are predicted the damage degree by Table 1(b). Fig. 3 summarizes the damage degree at the termination point predicted by Table 1. The seismic strengthening is required for the piers evaluated S as less than 1.1 and $F_y{}^T$ as less than 1.2.

DAMAGE OF REINFORCED CONCRETE PIERS AT MID-HEIGHT DUE TO RECENT EARTHQUAKES

General

During the Kushiro-oki Earthquake and the Hokkaido Nansei-oki Earthquake, nine bridges suffered damage at mid-height. Fig. 4 and Table 2 show the locations and damage of the bridges. The remarkable points of damage are as follows.

a) All bridges damaged were designed and constructed prior to 1980. Therefore, the anchorage length of the terminated longitudinal reinforcement was inadequate.
b) Most of piers damaged have a circular cross section with smaller concrete area.
c) The damage was developed by the lateral force in transverse direction.

In this paper, the damage of Yoda bridge, Motoe bridge, Shin-shiriuchi bridge and Motouriya bridge, which are evaluated as the "Critical Damage" based on the Guide Specifications for Earthquake Hazard Mitigation for Transportation Facilities[7], is described below.

Damage of Yoda Bridge

The pier of Yoda bridge has a circular cross section with 1.4m diameter and 4.1m height. As shown in Fig. 5, forty eight D19 bars (deformed bars with diameter of 19mm) were used as the longitudinal reinforcement at the base. Twenty four bars were terminated at 0.78m above the base, and twelve bars were terminated at 1.58m above the base. The hoop reinforcement (D13) was placed every 20cm around the termination points. The P2 pier suffered the spalling-off of concrete and serious buckling of longitudinal reinforcement at the second termination point as shown in Photos 1 and 2. Among twelve bars above the second termination point, six bars were ruptured. Judging from such failure, almost no residual strength was left at the pier.

Table 1 Evaluation of Seismic Vulnerability

(a) Evaluation in terms of Failure Mode Factors S

Failure Mode Factor S	Failure Mode
$S \geqq 1.1$	Flexural Failure at Base
$S < 1.1$	Vulnerable to Failure at Termination Zone

(b) Evaluation in terms of Safety Factors F_y^T

Safety Factor F_y^T	Damage Degree at Termination Zone at the Loading Displacement of $5\delta_y$
$F_y^T < 1.2$	Rupture and serious buckling of longitudinal reinforcement are developed.
$F_y^T \geqq 1.2$	Diagonal racks, spalling-off of cover concrete, and slight buckling of longitudinal reinforcement are developed.

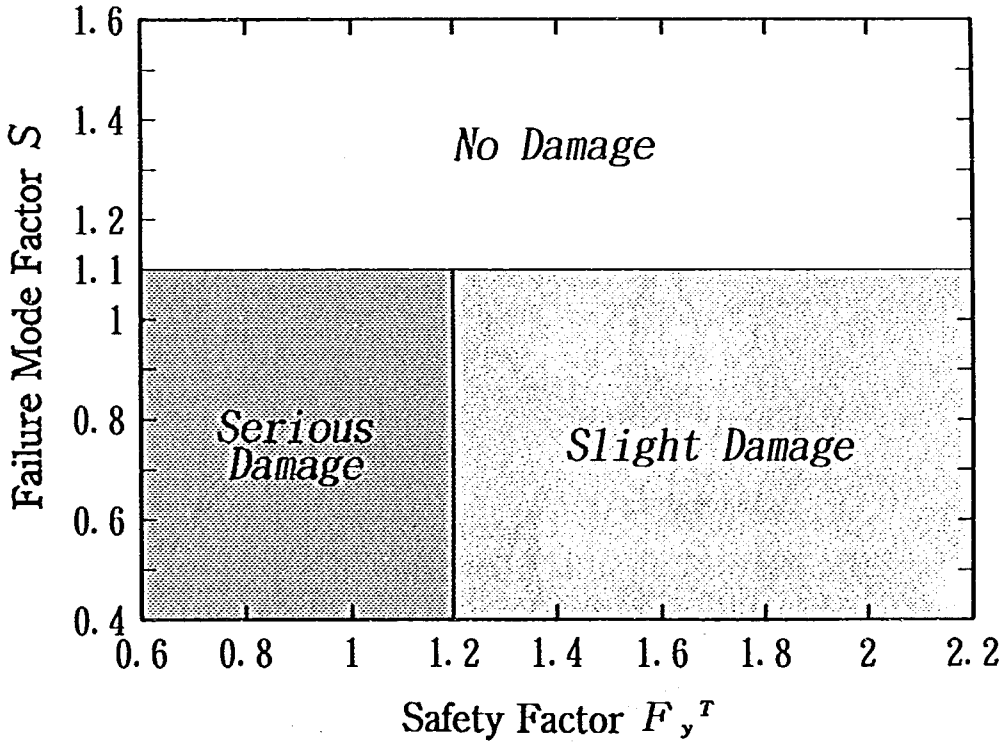
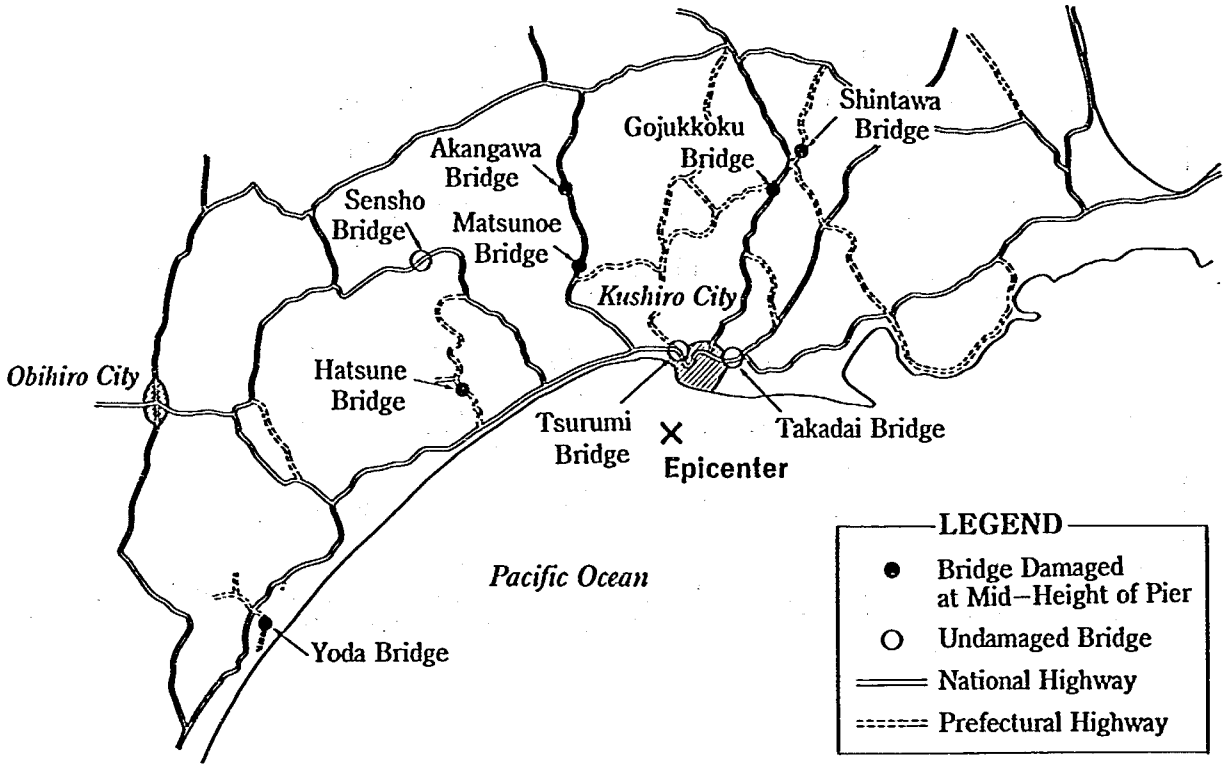
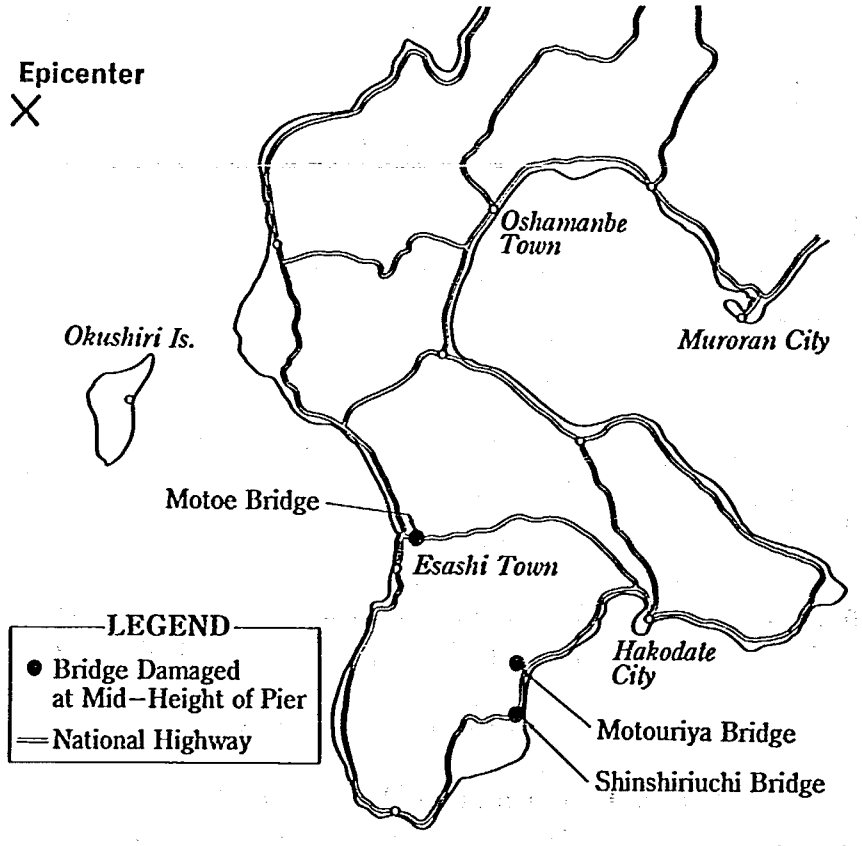


Fig. 3 Evaluation of Damage Degree



(a) Bridges Damaged Due to Kushiro-oki Earthquake



(b) Bridges Damaged Due to Hokkaido Nansei-oki Earthquake

Fig. 4 Location of Bridges

Table 2 Summary of Bridge Damaged

Earthquake	Bridge	Year of Design	Length(m)	Superstructure Type	Cross Section		Damage Degree
					Shape	Dimension(m)	
Kushiro-oki Earthquake	Yoda Br.	1969	70	3-Span Simple Supported Steel Girder Bridge	Circular	ϕ 1.4	Critical Damage
	Matsunoe Br.	1962	157	5-Span Simple Supported PC Girder Bridge	Circular	ϕ 2.5	Medium Damage
	Hatsune Br.	1967	172	6-Span Simple Supported Steel Girder Bridge	Circular	ϕ 1.8	Medium Damage
	Shintawa Br.	1974	60.3	3-Span Simple Supported Steel Girder Bridge	Oval	7.9 × 1.0	Slight Damage
	Gojukkoku Br.	1966	249	7-Span Simple Supported PC Girder Bridge	Circular	ϕ 2.2	Slight Damage
	Akangawa Br.	1973	126.5	4-Span Simple Supported PC Girder Bridge	Circular	ϕ 2.0	Slight Damage
Hokkaido Nansei-oki Earthquake	Motoe Br.	1968	165.7	7-Span Simple Supported Steel Girder Bridge	Circular	ϕ 1.8	Critical Damage
	Shinshiriuchi Br.	1970	214	7-Span Simple Supported PC Girder Bridge	Circular	ϕ 1.8	Critical Damage
	Motouriya Br.	1964	63	2-Span Simple Supported PC Girder Bridge	Circular	ϕ 1.5	Critical Damage

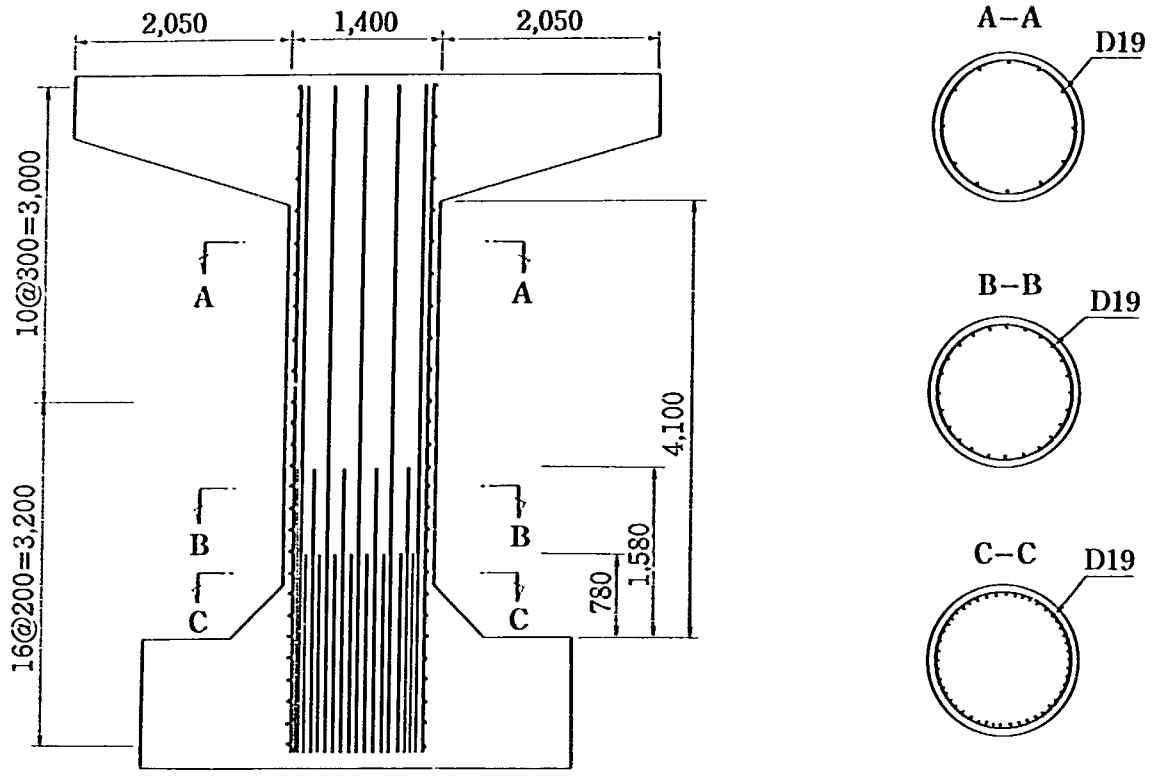


Fig. 5 Layout of Longitudinal Reinforcement in Yoda Bridge Pier

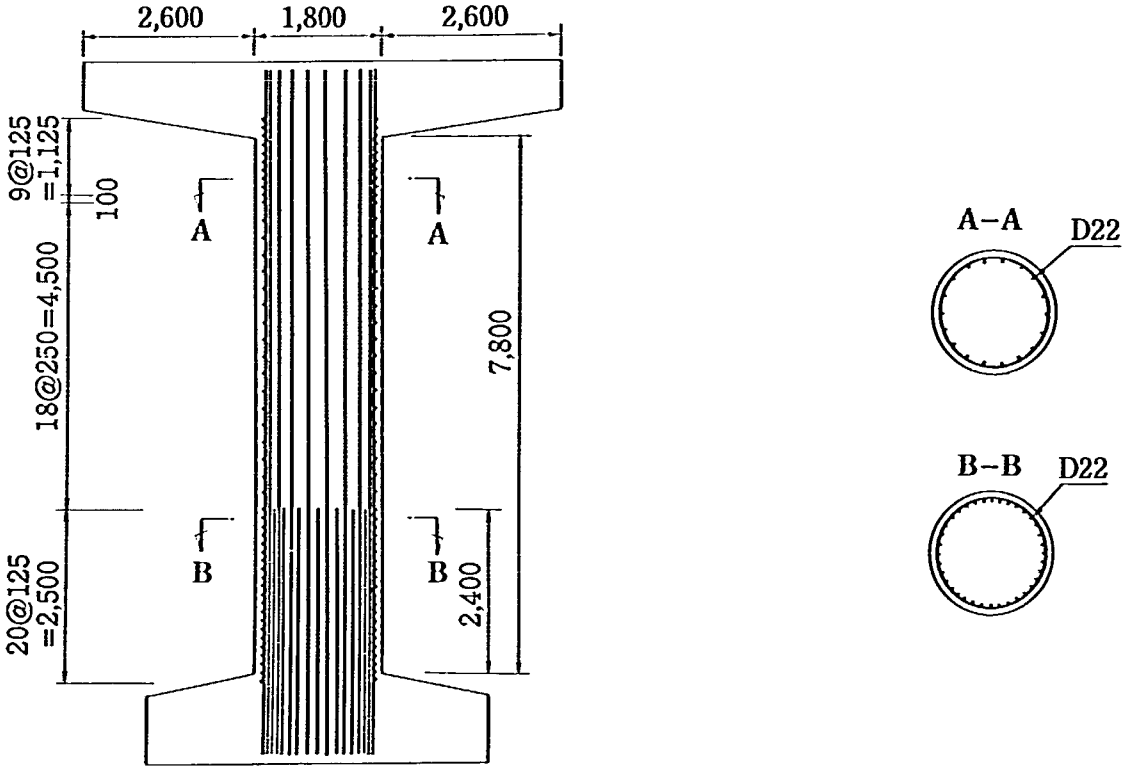


Fig. 6 Layout of Longitudinal Reinforcement in Motoe Bridge Pier



Photo 1 Damage of Yoda Bridge

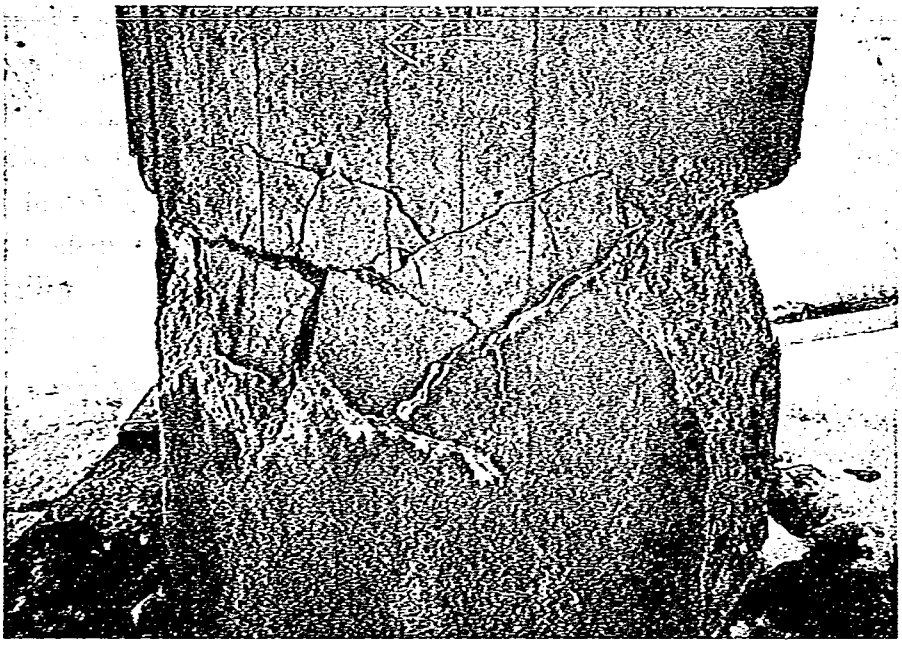


Photo 2 Failure at Termination Point

Damage of Motoe Bridge

The pier of Motoe bridge has a circular cross section with 1.8m diameter and 7.8m height. As shown in **Fig. 6**, thirty six D22 bars were placed as the longitudinal reinforcement at the base, and eighteen bars were terminated at 2.4m above the base. The hoop reinforcement (D13) was placed every 12.5cm between the base and the termination point. The P3 pier suffered the most serious damage as shown in **Photos 3** and **4**. The spalling–off of concrete and the buckling of longitudinal reinforcement were developed at the termination point. This was developed due to the lateral force in transeverse direction.

Damage of Shin–shiriuchi Bridge

Shin–shiriuchi bridge consists of seven simply supported girders as shown in **Fig. 7**. After the five spans at the left bank side were constructed in 1969, the other two spans were extended associated with the extension of Shiriuchi River in 1989. Among six piers, only new P1 pier did not have the termination of the longitudinal reinforcement. It was interesting that the old piers were damaged at the termination point, while the new piers were not damaged.

The old P3 pier has a circular cross section with 1.8m diameter and 7.04m height. As shown in **Fig. 8**, sixty four D22 bars were double–placed as the longitudinal reinforcement at the base. Thirty two inside bars were terminated at 2.47m above the base, and sixteen outside bars were terminated at 3.67m above the base. The hoop reinforcement (D13) was placed every 12.5cm at base and every 25cm around the termination points. Failure of concrete and buckling of longitudinal reinforcement were developed at the first termination point as shown in **Photo 5**. In the old P2 pier, the horizontal and diagonal cracks were developed at the second termination point as shown in **Photo 6**.

The new P2 pier has an oval cross section of 3m × 1.5m with 6.1m height. The cross sectional area of the new P2 pier is approximately 1.6 times larger than that of the old P3 pier. As shown in **Fig. 9**, fifty six D22 bars were placed as the longitudinal reinforcement at the base, and twenty eight bars were terminated at 3m above the base. The hoop reinforcement (D16) was placed every 10cm. The structure is quite different between the old pier and the new pier. It was proved that the damage at the termination point can be prevented by taking the anchorage length long enough in accordance with the current Specifications.

Damage of Motouriya Bridge

The pier of Motouriya bridge has a circular cross section with 1.5m diameter and 3.05m height. As shown in **Fig. 10**, thirty six ϕ16 round bars were placed as the longitudinal reinforcement below the termination point, and eighteen ϕ13 round bars were placed above it. These bars were spliced with lap length of 50cm. Two thirds of longitudinal reinforcement in terms of the gross area were terminated. The round hoop reinforcement

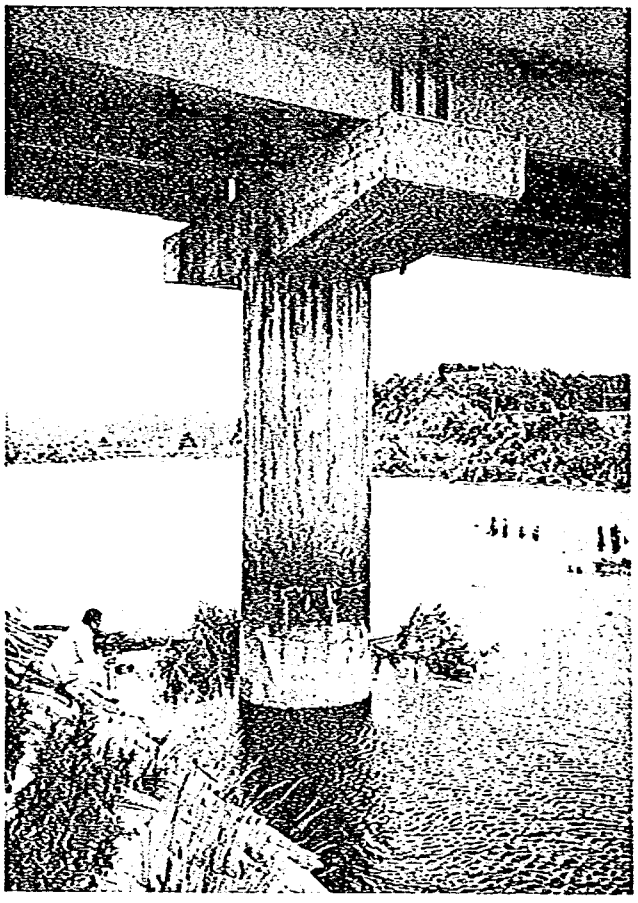


Photo 3 Damage of Motoe Bridge

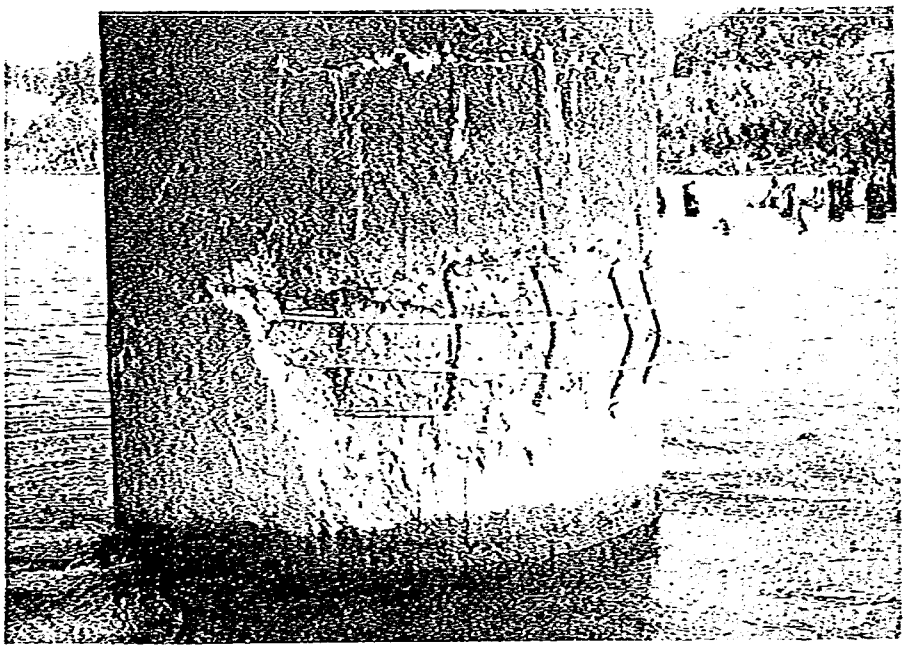


Photo 4 Failure at Termination Point

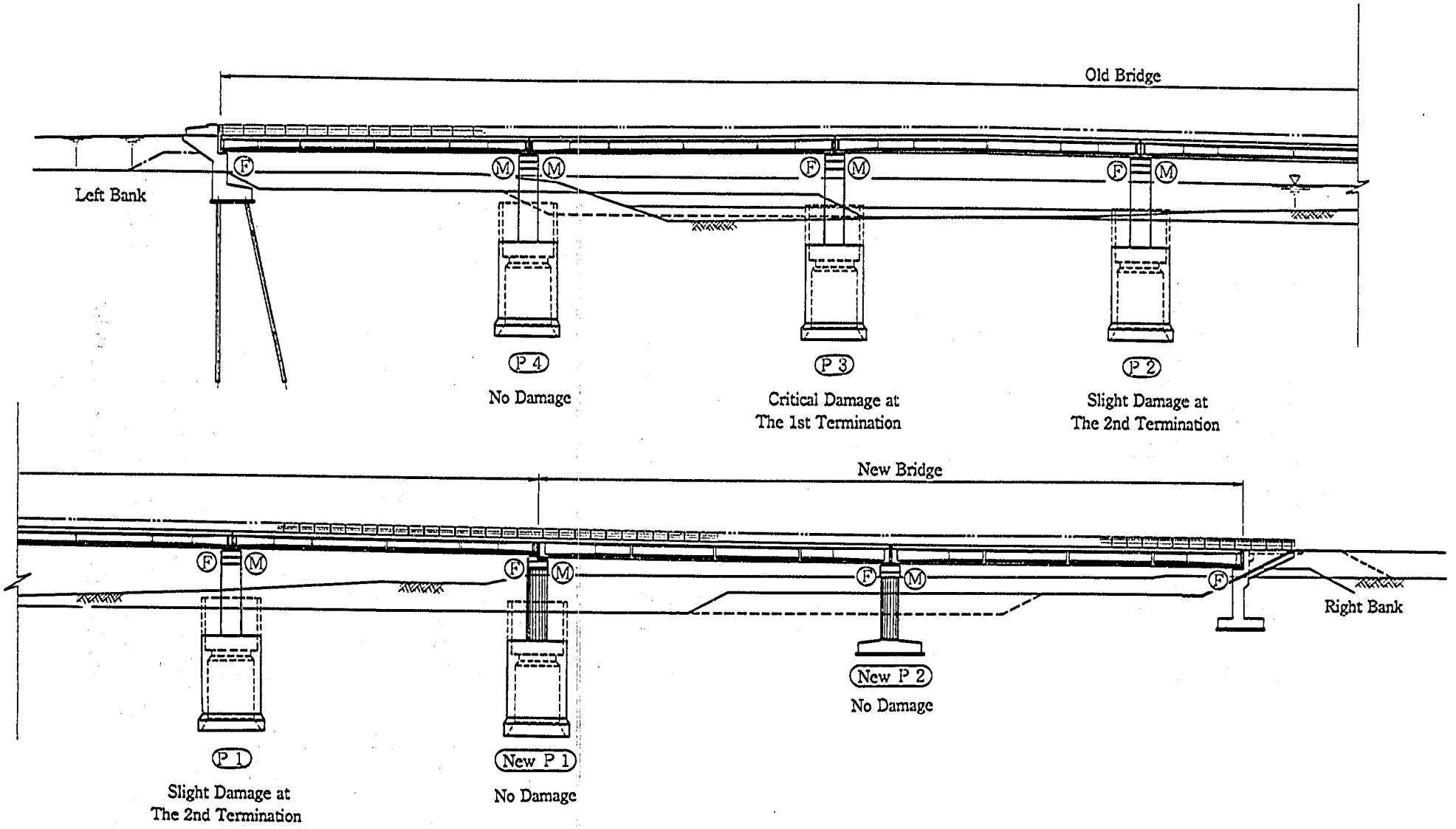


Fig. 7 General Schematic View of Shin−shiriuchi Bridge

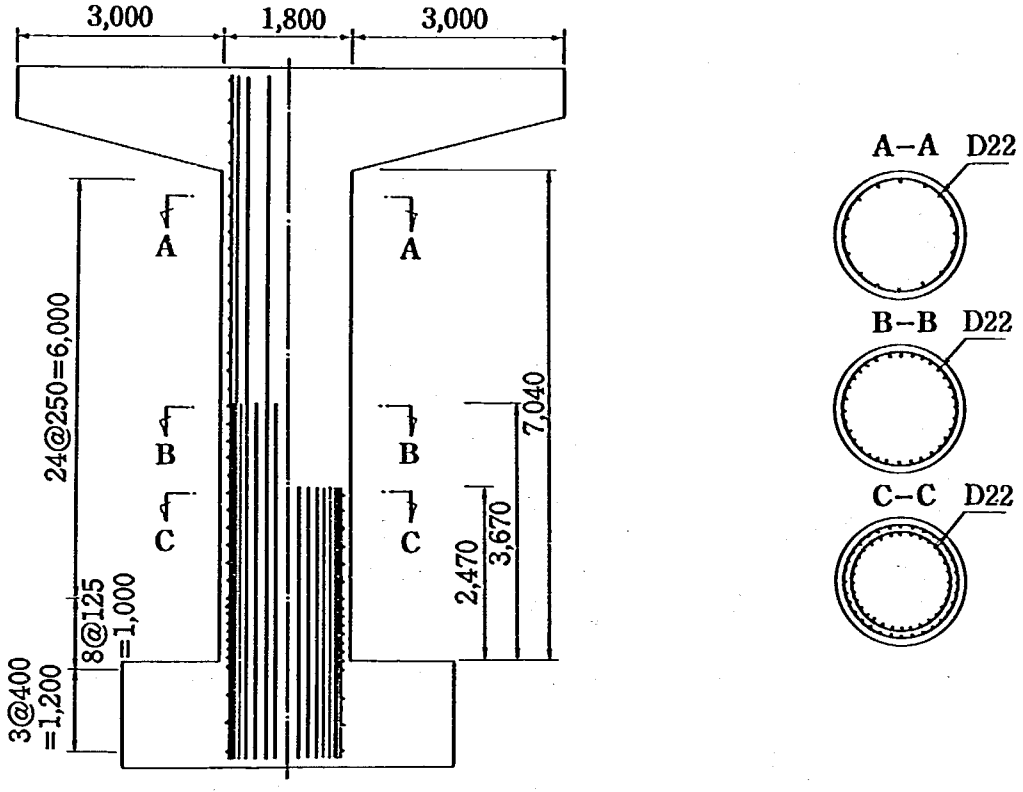


Fig. 8 Layout of Longitudinal Reinforcement in Shin–shiriuchi Bridge Pier (Old P3)

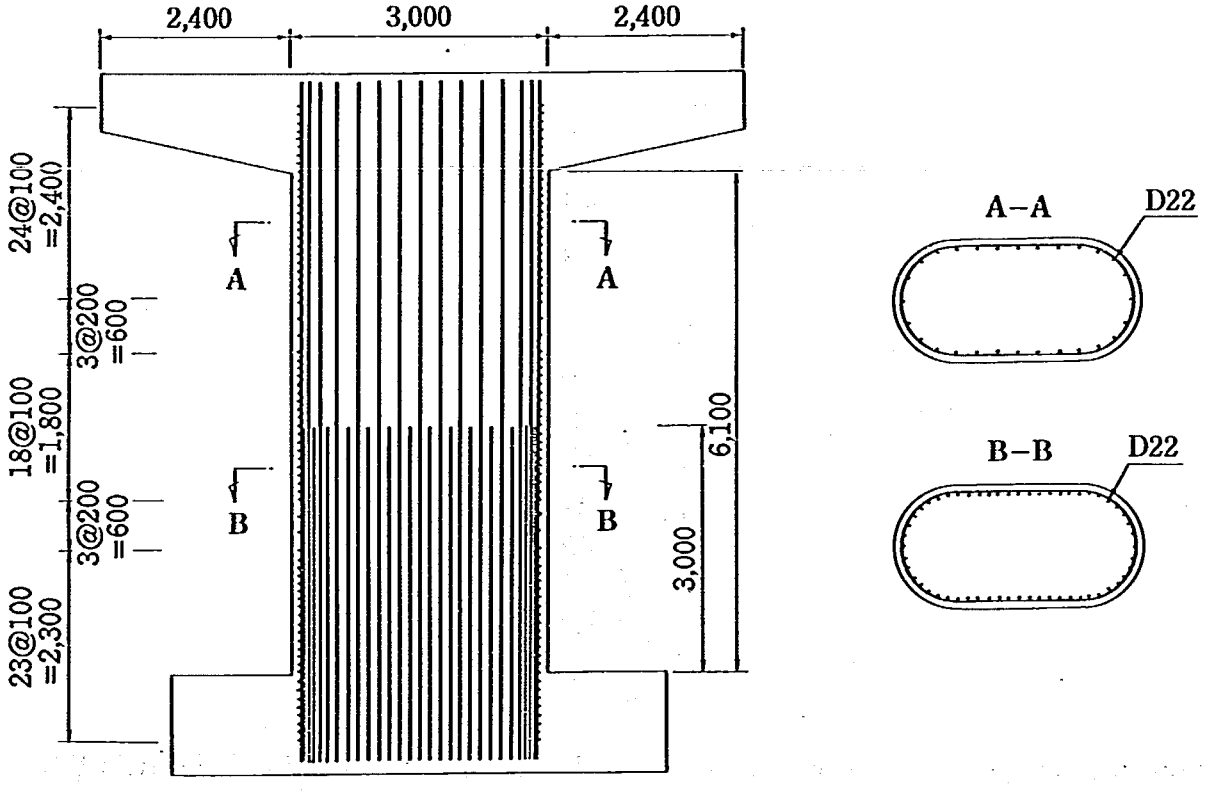


Fig. 9 Layout of Longitudinal Reinforcement in Shin–shiriuchi Bridge Pier (New P2)

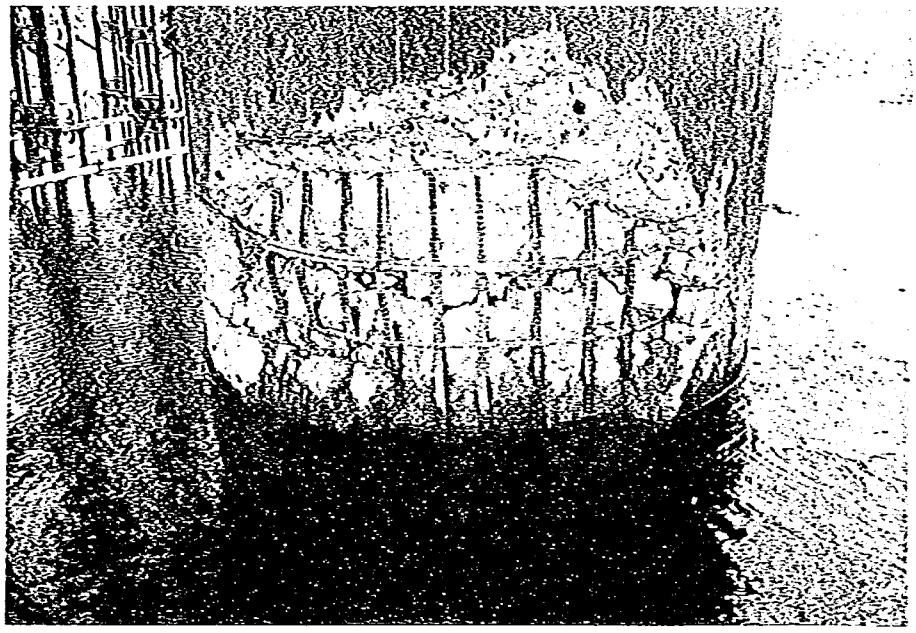


Photo 5 Damage of Shin−shiriuchi Bridge at The First Termination Point (Old P3)

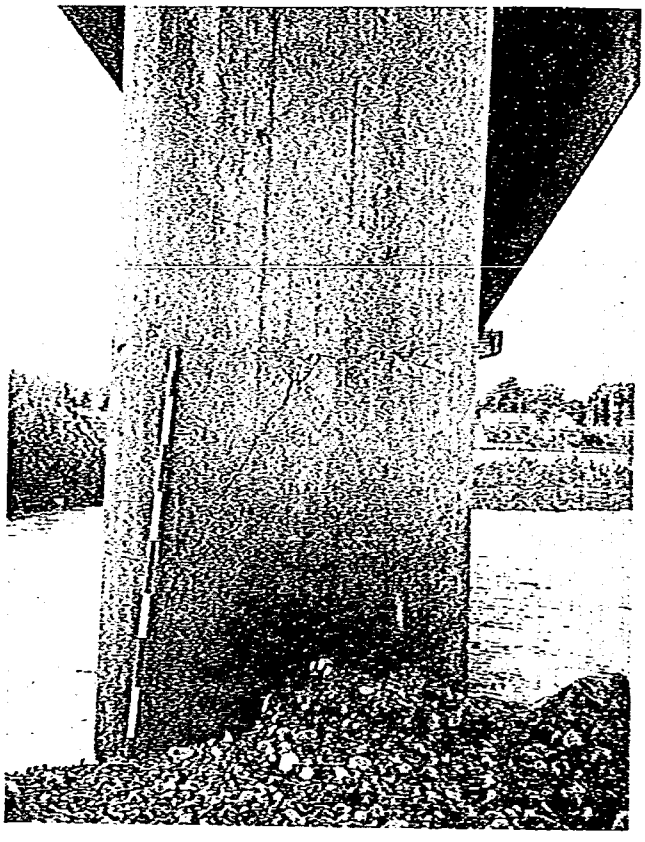


Photo 6 Damage of Shin−shiriuchi Bridge at The Second Termination Point (Old P2)

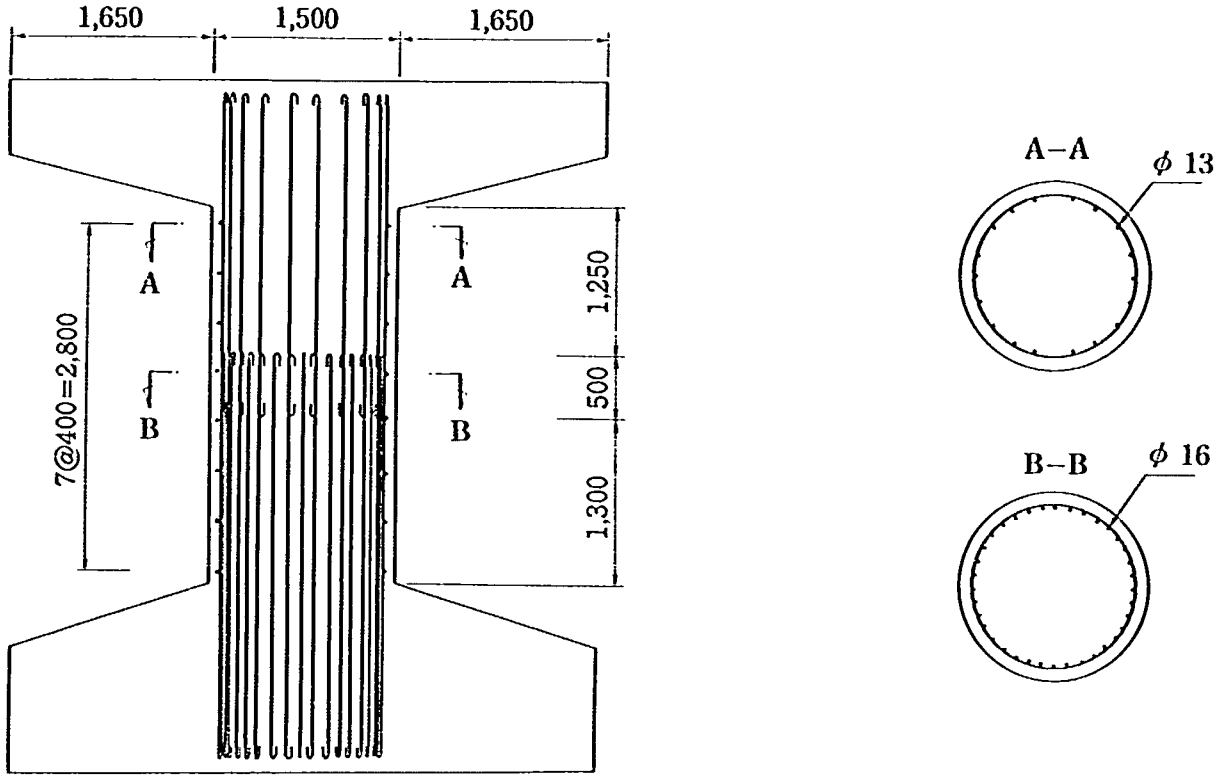


Fig. 10 Layout of Longitudinal Reinforcement in Motouriya Bridge Pier

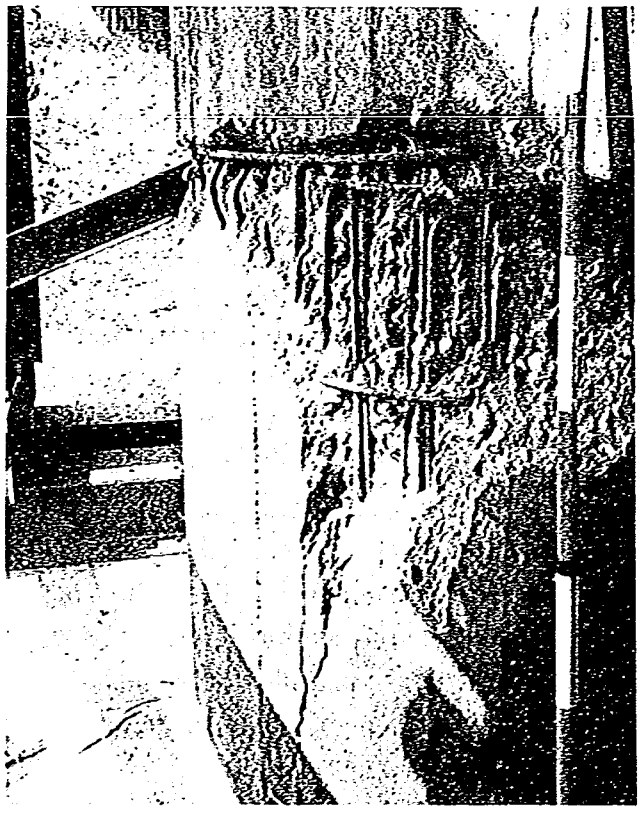


Photo 7 Damage of Motouriya Bridge at Splicing Zone

(ϕ 13) was placed every 40cm.

Spalling-off of concrete and buckling of longitudinal reinforcement were developed at the splicing zone as shown in **Photo 7.** The lap length of this pier is estimated as 53cm by Eq.(1) and as 80cm by Eq.(2). Because the actual lap length is only 50cm, it was inadequate.

ANALYSIS OF SEISMIC VULNERABILITY AT THE TERMINATION POINTS

Reinforced Concrete Piers Analyzed

Fourteen reinforced concrete piers were analyzed. They were selected from nine piers which suffered damage at the termination point due to the Kushiro-oki Earthquake and the Hokkaido Nansei-oki Earthquake, and five piers which were undamaged and located close to the fault zone. All piers undamaged were constructed after 1980. **Table 3** summarizes the bridges analyzed, and the analytical parameters required for the analysis, i.e. seismic coefficient, concrete strength and the material of reinforcement, are shown in **Table 4.** Because there were a few uncertain parameters, these were assumed from the past records.

Results of Analysis

Table 5 summarizes the failure mode factor S and the safety factor F_y^T at the termination points. **Fig. 11** shows the failure mode factor S vs. the damage degree. It is clearly observed that the serious damage is developed as the failure mode factor S becomes smaller. The failure mode factor S of the piers which were damaged is less than 1.1. This very much matches with **Table 1(a).** The failure at the termination point can be predicted quite well by the failure mode factor S .

Fig. 12 shows the safety factor F_y^T vs. the damage degree. It is also observed that the serious damage is developed as the safety factor becomes smaller. Matsunoe bridge is an only exception, in which the safety factor is evaluated as 2.01, while it suffered significant damage at the termination point. The reason for this is not clear. Lager lateral force than expected would be developed due to the response of adjacent decks. The safety factor F_y^T of the piers which were damaged is less than 1.1 except Matsunoe bridge. This also matches with **Table 1(b),** in which 1.2 was proposed as the critical F_y^T .

Fig. 13 compares the predicted damage (refer to **Fig. 3**) with the actual damage at the termination points (refer to **Table 2**). The piers predicted by **Fig. 3** as "Serious Damage" suffered at least horizontal cracks. Most of them suffered diagonal cracks, buckling of and rupture of longitudinal reinforcements. On the other bend, the piers predicted by **Fig. 3** as "No Damage" were not damaged during the two earthquakes. Therefore the damage degree predicted by **Fig. 3** provides reasonable estimation. As described previously, Matsuuoe bridge suffered slight buckling of longitudinal reinforcement, although it is predicted by **Fig. 3** to develop only slight damage.

Table 3 Bridge Piers Analyzed

Cross Sectional Shape	Circular		Oval	
	Damaged	Undamaged	Damaged	Undamaged
Kushiro-oki Earthquake	Yoda Br. Matsunoe Br. Hatsune Br. Gojukkoku Br. Akangawa Br.	Sensho Br.	Shintawa Br.	Takadai Br. Tsurumi Br.
Hokkaido Nansei-oki Earthquake	Motoe Br. Shin-shiriuchi Br. (Old Pier) Motouriya Br.	—	—	Shin-shiriuchi Br. (New Pier)

Table 4 Analytical Parameters

Bridge	Pier	Analytic Direction	Seismic Coefficient k_h	Concrete Strength (kgf/cm^2)	Material of Longitudinal Reinforcement
Yoda Br.	P1	Transversal	0.20*)	210	SD295
Matsunoe Br.	P3	Transversal	0.20	180	SD235
Hatsune Br.	P4	Transversal	0.20	210	SDC390
Shintawa Br.	P2	Longitudinal	0.20	210	SD295
Gojukkoku Br.	P1	Transversal	0.20	210	SDC390
Akangawa Br.	P1	Transversal	0.20*)	210	SD345
Sensho Br.	P4	Longitudinal	0.18	210	SD295
	P5	Transversal	0.18	210	SD295
Takadai Br.	P2	Longitudinal	0.24	210	SD295
Tsurumi Br.	P5	Longitudinal	0.24	210	SD295
Motoe Br.	P3	Transversal	0.20	210	SDC390
Shinshiriuchi Br.	P3	Transversal	0.15	210	SD295
	New P2	Longitudinal	0.14	210	SD295
Motouriya Br.	P1	Transversal	0.15*)	210	SR235*)

*) assumed from the past records

Table 5 Analytical Results

Bridge	Pier (Termination)		Yielding Bending Moment (tf·m)		Safety Factor		Failure Mode Factor S	Damage Degree Predicted at Termination Zone	Damage
			Base M_y^B	Termination M_y^T	Base F_y^B	Termination F_y^T			
Yoda Br.	P1	1st	218.3	148.9	1.24	0.87	0.70	Serious	No Damage
		2nd		111.9		0.74	0.60		Rupture and Serious Buckling of Longitudinal Reinforcement
Matsunoe Br.	P3		962.4	760.7	1.96	2.01	1.03	Slight	Slight Buckling of Longitudinal Reinforcement
Hatsune Br.	P4		657.4	433.8	1.51	1.15	0.76	Serious	Diagonal Crack
Shintawa Br.	P2		358.6	201.3	1.02	0.92	0.90	Serious	Horizontal Crack
Gojukkoku Br.	P1		915.8	634.4	1.26	1.12	0.89	Serious	Slight Horizontal Crack
Akangawa Br.	P1	1st	1161.1	772.9	1.30	1.00	0.77	Serious	No Damage
		2nd		551.5		0.87	0.67		Slight Horizontal Crack
Sensho Br.	P4		2193.8	1387.6	1.09	1.34	1.23	No Damage	No Damage
	P5		1174.6	790.3	1.08	1.31	1.21	No Damage	No Damage
Takadai Br.	P2		1179.8	599.9	1.33	1.83	1.38	No Damage	No Damage
Tsurumi Br.	P5		11113.8	6089.5	1.59	1.79	1.13	No Damage	No Damage
Motoe Br.	P3		425.1	294.9	1.00	0.82	0.82	Serious	Serious Buckling of Longitudinal Reinforcement
Shinshiriuchi Br.	P3	1st	562.2	408.7	1.19	1.02	0.86	Serious	Serious Buckling of Longitudinal Reinforcement
		2nd		325.6		0.96	0.81		No Damage
	New P2		530.2	407.5	1.02	1.17	1.15	No Damage	No Damage
Motouriya Br.	P1		184.7	141.0	1.08	1.01	0.94	Serious	Serious Buckling of Longitudinal Reinforcement

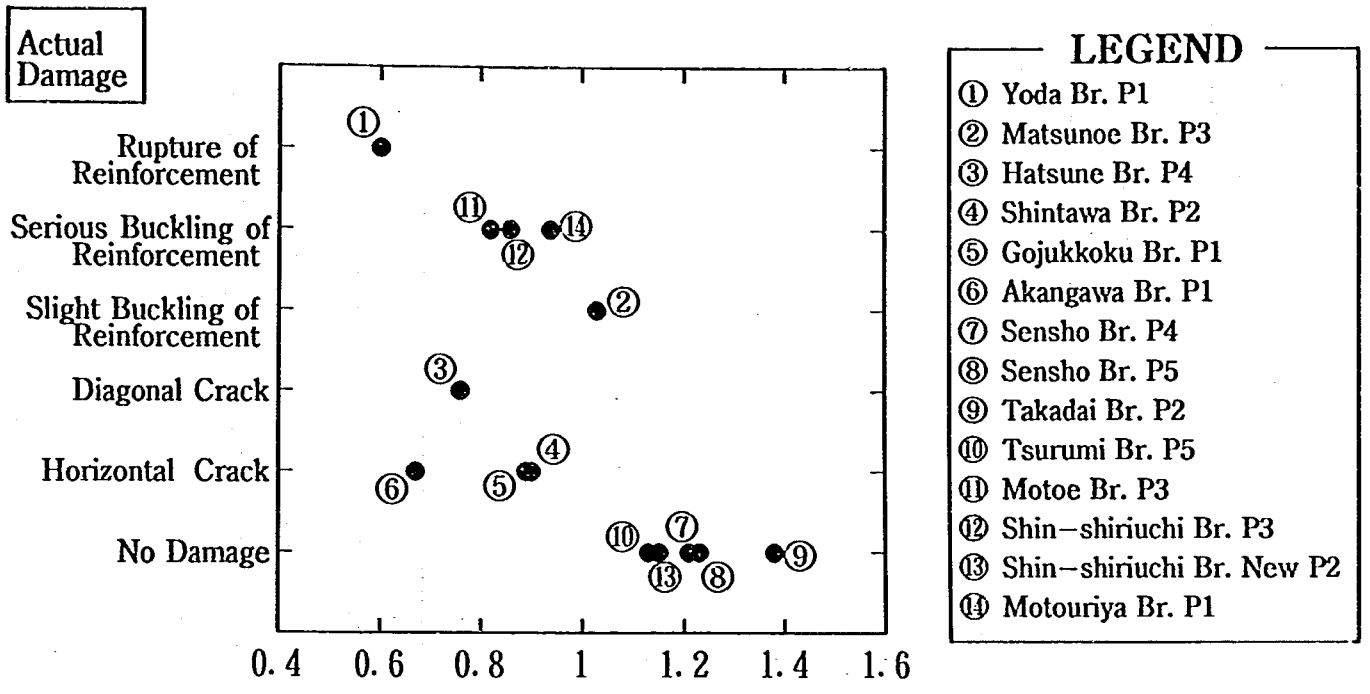


Fig. 11 Failure Mode Factor and Actual Damage

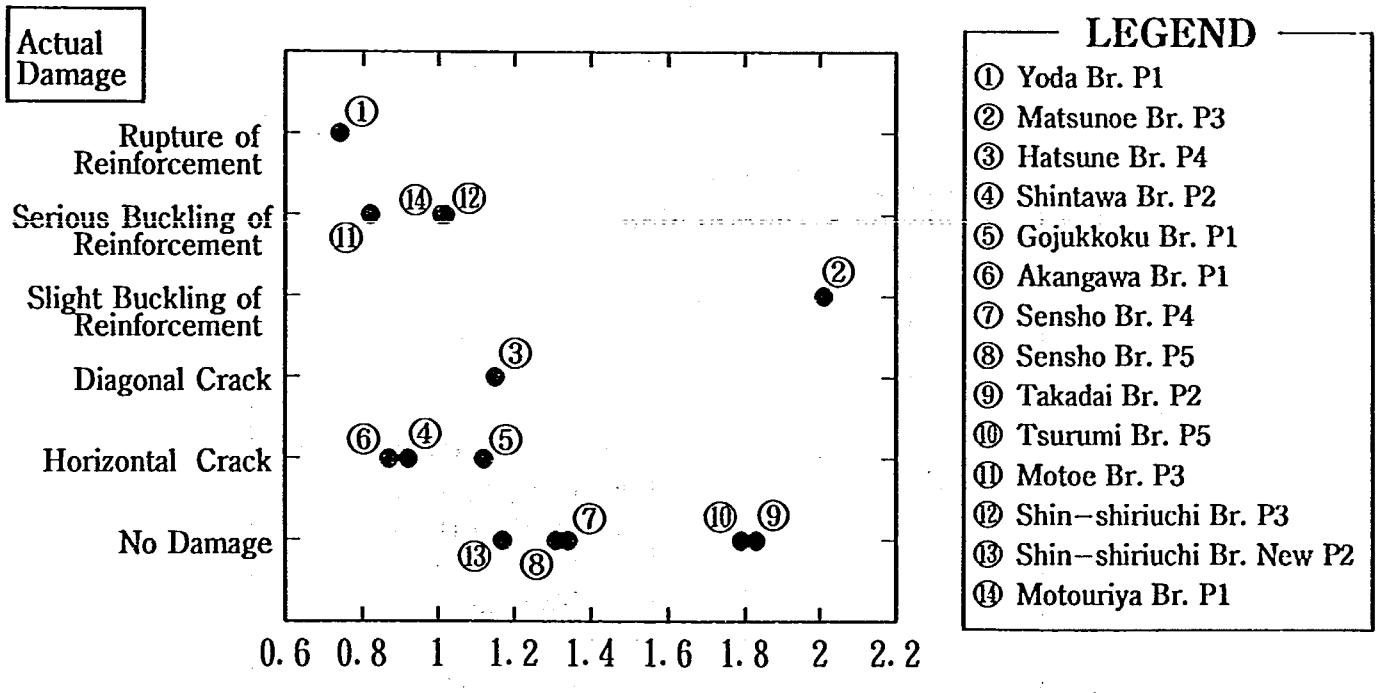


Fig. 12 Safety Factor and Actual Damage

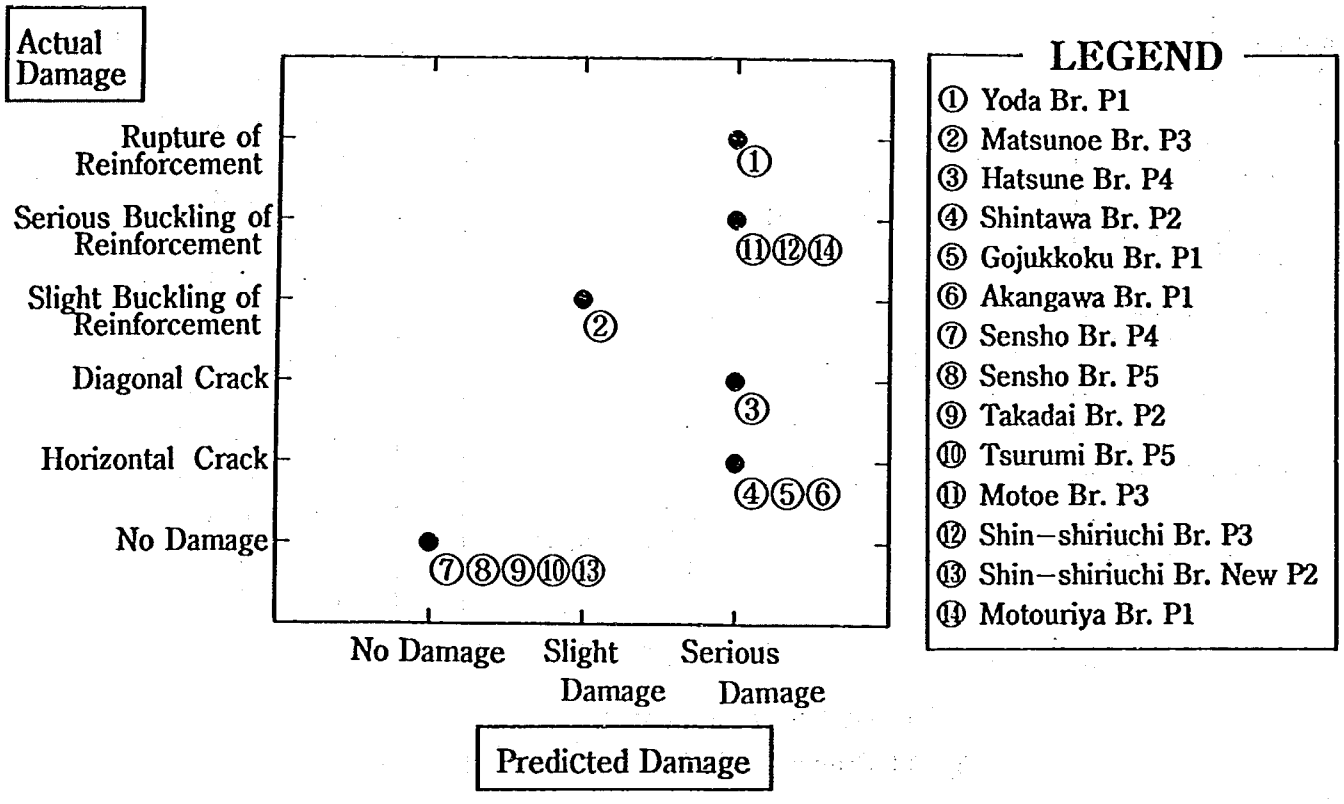


Fig. 13 Predicted Damage and Actual Damage

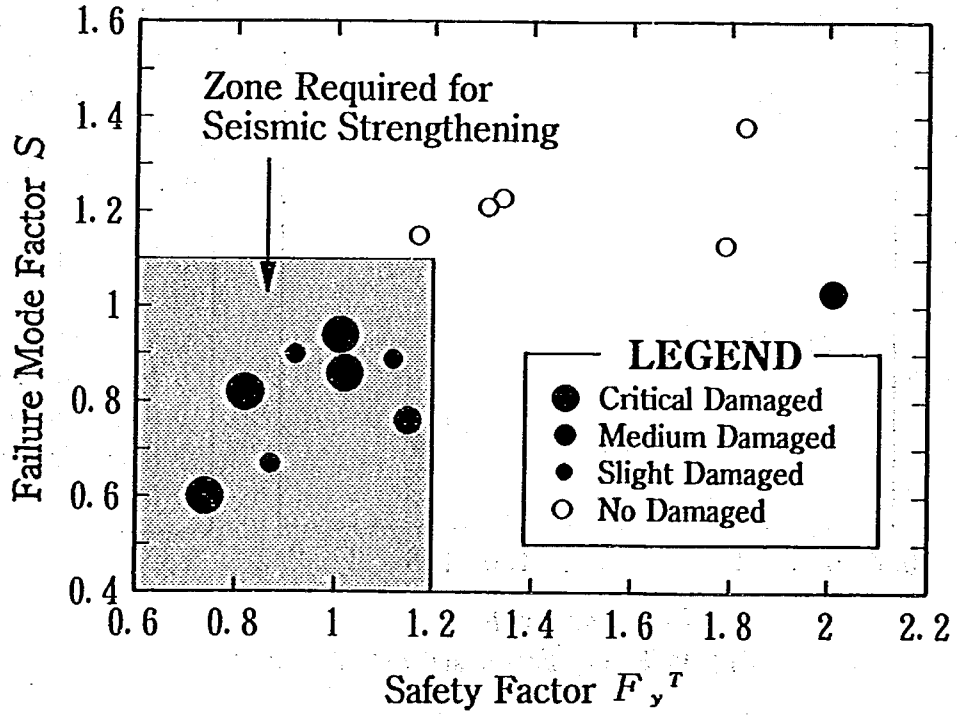


Fig. 14 Relation between Failure Mode Factor and Safety Factor

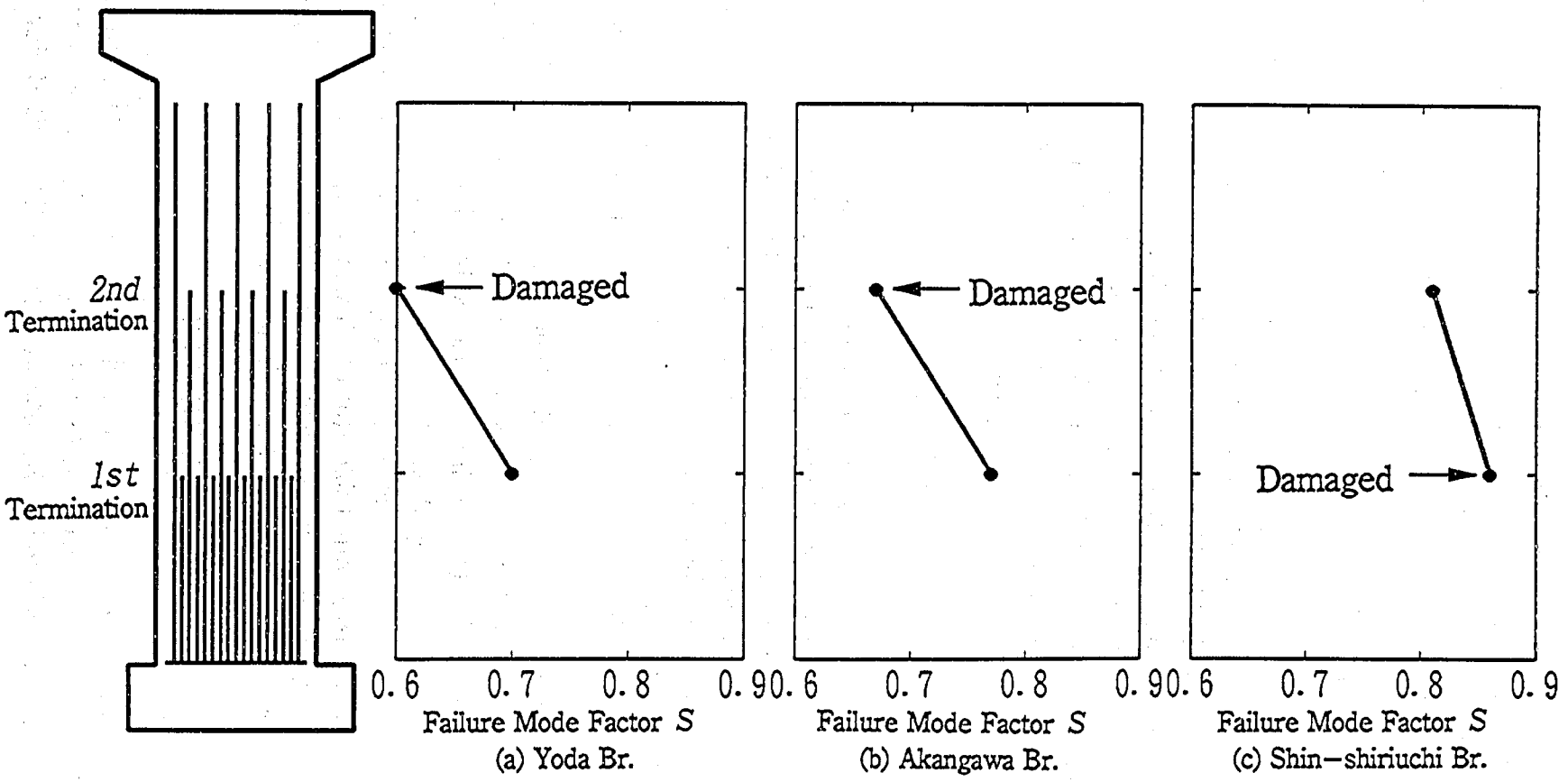


Fig. 15 Two Inadequate Terminations and Actual Damage

Fig. 14 summarizes the evaluation of damage degree in terms of S and F_y^T. Excluding only Matsunoe bridge, the damage degree developed during the two earthquakes agree quite well with the prediction by Fig. 3.

There were three bridges in which the longitudinal reinforcement were terminated at two different heights. It is interesting to clarify at which termination point the failure was developed between the two.

Fig. 15 compares the failure mode factors S at the two heights. At Yoda bridge and Akangawa bridge, the failure occurred at the 2nd (higher) termination point. Because the failure mode factor S is smaller at the 2nd termination point, the prediction by S is quite well. At Shin-shiriuchi bridge, on the other hand, the damage was developed at the first termination point, while S is smaller at the 2nd termination point. Because the difference of S between the 1st and the 2nd termination points is only 0.05 at Shin-shiriuchi bridge, this may be the reason for wrong prediction. But it should be noted that, at some other piers of Shin-shiriuchi bridge, cracks were developed not at the 1st termination point but at the 2nd termination point.

CONCLUDING REMARKS

This paper presented the damage of reinforced concrete bridge piers at the termination point of longitudinal reinforcements with inadequate anchorage length due to the Kushiro-oki Earthquake and the Hokkaido Nansei-oki Earthquake, and the application of the seismic evaluation method proposed by PWRI. The conclusions derived from the study presented herein are the following;

1) The reinforced concrete bridge piers which were designed and constructed in accordance with the Specification prior to 1980 suffered damage at the termination points. They had a circular cross section.

2) The damage degree becomes serious as the failure mode factor S by Eq.(5) becomes smaller. The failure mode factor S of the piers which were damaged is less than 1.1. This is quite close with Table 1(a) which was proposed based on the loadng tests.

3) The serious damage is developed as the safety factor F_y^T becomes smaller. The safety factor F_y^T of the piers which were damaged is less than 1.1 except Matsunoe bridge. This is also very closed with Table 1(b) which was proposed by the loading tests.

4) Based on this study, the seismic evaluation at the termination point by means of the failure mode factors and the safety factor F_y^T is appropriate.

REFERENCES

1) Kawashima, K., Unjoh, S., Nakajima, T. and Hoshikuma, J. : Damage of Bridges by Kushiro-oki Earthquake, January, 1993 and Hokkaido Nansei-oki Earthquake, July, 1993, 2nd U.S.-Japan Workshop on Seismic Retrofit of Bridges, Berkeley, USA, January

1994
2) Narita, N., Murakami, M. and Asanuma, H. : Report of the Investigation on Earthquake Damage to Shizunai Bridge, 15th Joint Meeting, U.S.–Japan Panel on Wind and Seismic Effects, UJNR, Tsukuba, Japan, May 1983
3) Japan Society of Civil Engineering : Standard Specifications for Concrete, December 1958
4) Japan Road Association : Part IV Design of Foudations, Design Specifications of Road Bridges, Feb. 1991
5) Kawashima, K., Unjoh, S. and Iida, H. : Seismic Inspection and Seismic Strengthening of Reinforced Concrete Bridge Piers with Termination of Main Reinforcement at Mid–Height, 1st U.S.–Japan Workshop on Seismic Retrofit of Bridges, Tsukuba, Japan, December 1990
6) Kawashima, K., Unjoh, S. and Iida, H. : Seismic Inspection and Seismic Strengthening of Highway Bridges in Japan, 4th U.S.–Japan Workshop on Earthquake Disaster Prevention for Lifeline Systems, Los Angeles, USA, August 1992
7) Japan Road Association : Guide Specifications for Earthquake Hazard Mitigation for Transportation Facilities – Post–Earthquake Countermeasures –, 1987

A Stress–Strain Model for Reinforced Concrete Bridge Piers Confined by Hoop Reinforcement

Jun–ichi HOSHIKUMA
Kazuhiko KAWASHIMA
and
Kazuhiro NAGAYA

2nd U.S.–Japan Workshop on
Seismic Retrofit of Bridges
Berkeley, U.S.A.
January, 1994

A STRESS–STRAIN MODEL FOR REINFORCED CONCRETE BRIDGE PIERS CONFINED BY HOOP REINFORCEMENT

J. Hoshikuma[1], K. Kawashima[2] and K. Nagaya[3]

1) Research Engineer, Earthquake Engineering Division, Public Works Research Institute, Ministry of Construction, Tsukuba Science City, Japan
2) Head, ditto
3) Assistant Research Engineer, ditto

ABSTRACT

In this paper, a stress–strain model of concrete which takes account of confinement effect is proposed based on a series of loading tests for reinforced concrete column specimens, with circular and square cross section, containing various hoop reinforcement. Predominant factors for controlling the stress–strain relation of the concrete columns were examined, and the stress–strain model consisting of an exponential function and a straight line was proposed. The predicted relation provides better agreement with test results than the previous models.

INTRODUCTION

A large seismic lateral force causes reinforced concrete bridge piers to be in inelastic range. However, the confinement associated with hoop reinforcement increases the ductility and the energy absorption of reinforced concrete bridge piers. It is, therefore, significant to incorporate the effect of hoop reinforcement into seismic design to evaluate the ductility of reinforced concrete bridge piers.

This paper proposes a stress–strain model of confined concrete which can be used in seismic design of reinforced concrete bridge piers. To examine the effect of confinement on ductility of concrete, a series of loading tests of confined concrete columns were conducted and modeling of the stress–strain curve is clarified.

BACKGROUND OF THE RESEARCH

Previous Researches

Prof. Park and other researchers have already made significant researches on the confinement effect on ductility of concrete. Table 1 compares typical previous

Table 1 Review of Stress–Strain Model for Confined Concrete

Proposer	Stress–Strain Model for Confined Concrete			Applicable Cross Sectional Shape
	Ascending Part	Descending Part	Residual Stress	
Park	$f_c = K f_{co}\left\{\frac{2\varepsilon_c}{0.002K} - \left(\frac{\varepsilon_c}{0.002K}\right)^2\right\}$	$f_c = K f_{co}\{1 - Z_m(\varepsilon_c - 0.002K)\}$	20% of maximum stress	Rectangle
Sheikh	$f_c = K f_{co}\left\{\frac{2\varepsilon_c}{\varepsilon_{s1}} - \left(\frac{\varepsilon_c}{\varepsilon_{s1}}\right)^2\right\}$	$f_c = f_{cc}\{1 - Z(\varepsilon_c - \varepsilon_{cc})\}$	30% of maximum stress	Rectangle
Mander	$f_c = \frac{f_{cc} x r}{r - 1 + x^r}$ where $x = \frac{\varepsilon_c}{\varepsilon_{cc}}$, $r = \frac{E_c}{E_c - E_{sec}}$			Circle Rectangle Wall
Muguruma	$f_c = E_t \varepsilon_c + \frac{f_{co} - E_t \varepsilon_m}{\varepsilon_m^2}\varepsilon_c^2$ and $f_c = \frac{f_{co} - f_{cc}}{(\varepsilon_{co} - \varepsilon_{cc})^2}(\varepsilon_c - \varepsilon_{cc})^2 + f_{cc}$	$f_c = \frac{f_{cu} - f_{cc}}{\varepsilon_{cu} - \varepsilon_{cc}}(\varepsilon_c - \varepsilon_{cc}) + f_{cc}$	———	Circle Rectangle
Fujii	$f_c = E_t \varepsilon_c + \frac{f_{co} - E_t \varepsilon_{co}}{\varepsilon_{co}^2}\varepsilon_c^2$ and $f_c = \frac{f_{co} - f_{cc}}{(\varepsilon_{co} - \varepsilon_{cc})^3}(\varepsilon_c - \varepsilon_{cc})^3 + f_{cc}$	$f_c = f_{cc} - E_{des}(\varepsilon_c - \varepsilon_{cc})$	20% of maximum stress	Circle Rectangle

stress–strain models proposed for confined concrete.

In 1971, Park proposed a stress–strain model consisting of a second order parabola and a straight line. In this model, confinement effect was incorporated into the gradient at the stress descending part and the parameters were determined based on the experimental tests by Soliman, Roy and Bertero[1]. In 1982, Park revised the original model by introducing an allowance for the enhancement in the concrete strength due to confinement effect, which was assumed to be proportional to volumetric ratio and yield strength of hoop reinforcement, and inversely proportional to strength of unconfined concrete[2].

Sheikh proposed a stress–strain model idealizing the confinement effect in terms of the peak stress and a confinement effectiveness coefficient[3][4]. The confinement effectiveness coefficient depends on the layout of hoop reinforcement. The gradient at the stress descending part is similarly evaluated with Park's.

Mander proposed a fractional expression which was applicable to both the stress ascending and descending parts[5]. To evaluate the peak stress, confinement effectiveness coefficients for circular, square and wall sections were proposed based on the similar method to Sheikh's. Furthermore, a constitutive model involving a specified ultimate strength surface for multiaxial compressive stresses was used in this model, which enabled to develop a theoretical model without depending on a statistical analysis of test results. This model was found to provide good prediction for the test results[6].

In Japan, Muguruma proposed two second order parabolas for the stress ascending part[7]. A confinement effectiveness coefficient which took account of ineffectively confined core was included to evaluate the confinement effect. An evaluation method for the peak stress and the ultimate strain in terms of the confinement effectiveness coefficient was proposed based on the test results[8].

Fujii proposed a model consisting of a second order curve and a third order curve for the stress ascending part[9]. A confinement effectiveness coefficient which referred to Park was proposed, and the peak stress and the gradient at the stress descending part were formulated by a linear function of the confinement effectiveness coefficient based on a regression analysis of the test results.

Objectives of This Research

It is pointed out that reinforced concrete bridge piers constructed in Japan have largely concrete section and lower hoop reinforcement ratio in comparison with ones constructed in U.S.A. and New Zealand. Table 2 shows a summary of the previous compressive loading tests for the confined concrete columns to study the effect of confinement. Table 3 shows a requirement of hoop reinforcement as provided in the Specifications[10]. Although reinforced concrete bridge piers generally have the volumetric ratio of hoop reinforcement of 0.3% to 0.5%, there are few researches in which test specimens with the volumetric ratio of hoop reinforcement of 0.3% to 0.5% were used. A few specimens containing the volumetric ratio of hoop reinforcement of less than 0.5%

Table 2 Test Specimens in Previous Researches

Researcher	Cross Sectional Shape	Size of Specimen (cm)	Volumetric Ratio of Hoop Reinforcement(%)	Remarks
Park[1]	Rectangle	10×15	0.35~1.87	by Soliman, eccentric loaded
		12.8×12.8	2.07~2.39	by Roy
		10×10	1.09~1.81	by Bertero, High strength Concrete
Sheikh[3]	Rectangle	30×30	0.76~2.40	
Mander[6]	Circle	ϕ50	0.60~2.50	Spiral Reinforcement
	Rectangle	45×45	1.86~1.97	
	Wall	15×70	1.62~7.87	
Muguruma[8]	Circle	ϕ15	0.76~2.79	Spiral Reinforcement Some Specimens Containing High Tensile Steel
	Rectangle	19.4×19.4	0.40~3.13	
Fujii[9]	Circle	ϕ15	0.62~4.02	
	Rectangle	15×15	0.62~2.50	

were tested by Park and Muguruma, however, these are special cases because some were subjected to eccentric loading and the others used high tensile steel for hoop reinforcement. Therefore, the previous models are not enough to study the effect of confinement in the range of low hoop reinforcement ratio.

Table 3 Requirement of Hoop Reinforcement

Ratio of Longitudinal Reinforcement p_t(%)	$0<p_t\leqq 0.5$	$0.5<p_t\leqq 1.0$	$1.0<p_t$
Volumetric Ratio of Hoop Reinforcement ρ_s(%)	0.3	0.4	0.5

In this research, a series of compressive loading tests on hoop reinforcement considering volumetric ratio, spacing and hook configuration of hoop reinforcement as parameters are conducted taking account of Japanese design practice. It is the main purpose of this research to propose a stress–strain model for reinforced concrete bridge piers.

LOADING TEST OF CONFINED CONCRETE COLUMNS

Specimens and Experimental Procedure

The details of the specimens are given in Table 4. Both small and large specimens which are designated herein as S Series and L Series were constructed to evaluate the confinement effect in terms of volumetric ratio, spacing and hook configuration of hoop reinforcement. The specimens with square cross section were tested in the S Series (S6 to S10). Specimens L6, L7 and L8 used hoop reinforcement with semicircular, rectangular and sharp–angled hook as shown in Fig. 1, respectively. The hook was fabricated in accordance with the Specifications[10].

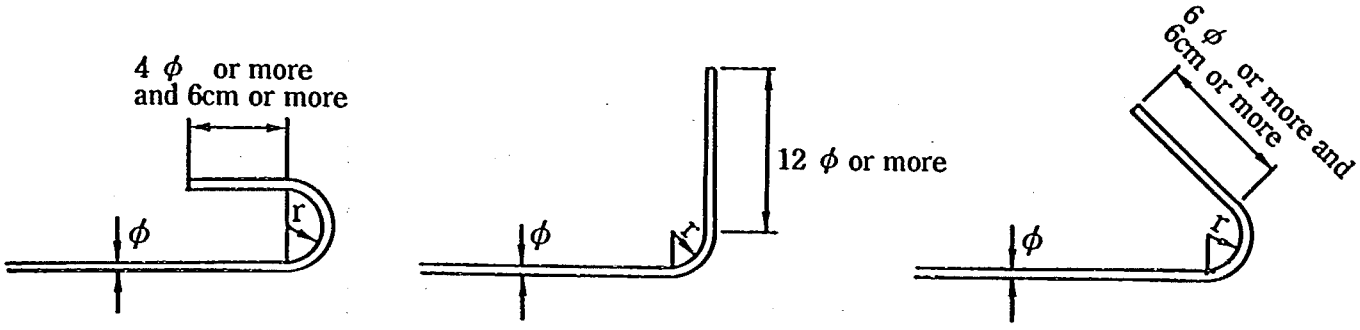
Photo 1 shows an experimental set–up with 30MN universal testing machine. All specimens were subjected to uniaxial compressive loading under displacement control, and loading rate was set as 1mm/min. The deformation of specimen between top and bottom was measured by linear potentiometers and the longitudinal strain was obtained by dividing the deformation by the height of specimen. To accurately record the stress–strain curve including the stress descending part, dynamic electric instrumentation was used.

Effect of Hoop Reinforcement Ratio

Fig. 2 shows stress–strain curves taking the hoop reinforcement ratio as parameter. In Fig. 2, a predicted relation which will be described later is also shown for comparison. Although the initial stiffness of each specimen is approximately equal, the peak stress and the strain corresponding to the peak stress increase as the hoop reinforcement ratio increases. Substantial deterioration of the compressive capacity after the peak stress is also

Table 4 Test Specimens

Series		Dimension of Specimens (mm)	Strength of Unconfined Concrete (MPa)	Hoop Reinforcement		Volumetric Ratio of Hoop Reinforcement (%)	Hoop Reinforcement Joint
				Material Diameter	Spacing (cm)		
S	S1	ϕ200 h=600	18.5	SR235 ϕ6	15	0.39	Weld
	S2				10	0.58	
	S3				5	1.17	
	S4				2.5	2.33	
	S5				1.25	4.66	
	S6	200 × 200 h=600	23.2	SR235 ϕ6	15	0.39	Weld
	S7				10	0.58	
	S8				5	1.17	
	S9				2.5	2.33	
	S10				1.25	4.66	
L	L1	ϕ500 h=1500	28.8	SD295 D10	15	0.39	Weld
	L2				10	0.58	
	L3				5	1.16	
	L4			SD295 D13	30	0.34	
	L5			SD295 D16	30	0.54	
	L6			SD295 D10	10	0.58	Rectangular Hook
	L7						Sharp-angled Hook
	L8						Semicircular Hook



(a)Semicircular Hook (b)Rectangular Hook (c)Sharp−angled Hook

Fig. 1 Hook Configuration of Hoop Reinforcement

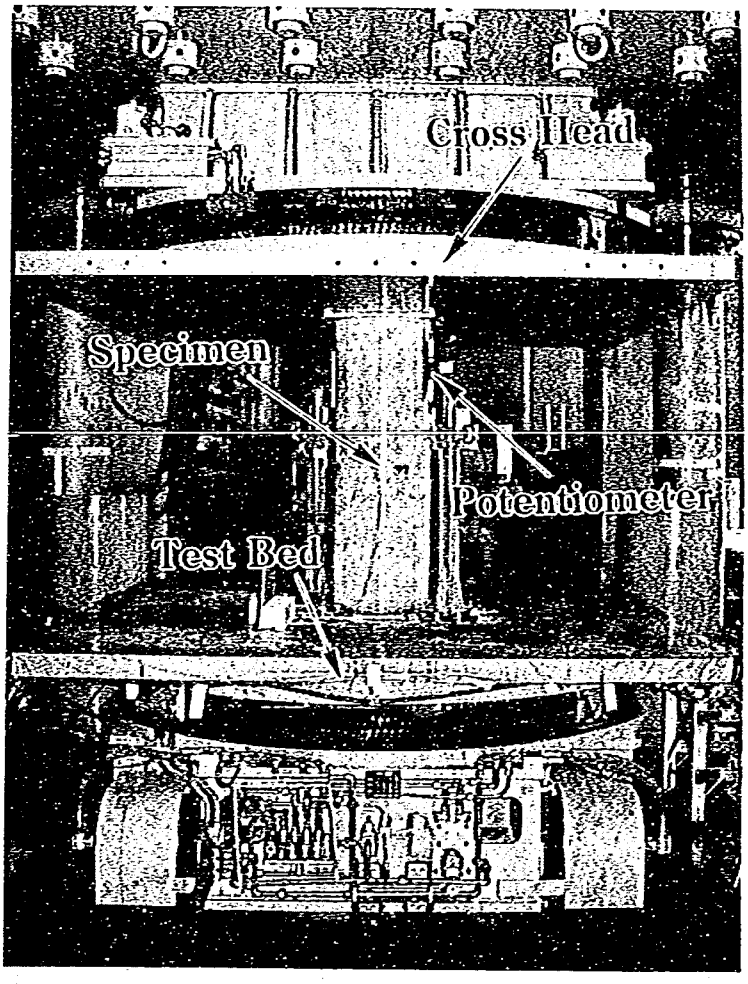
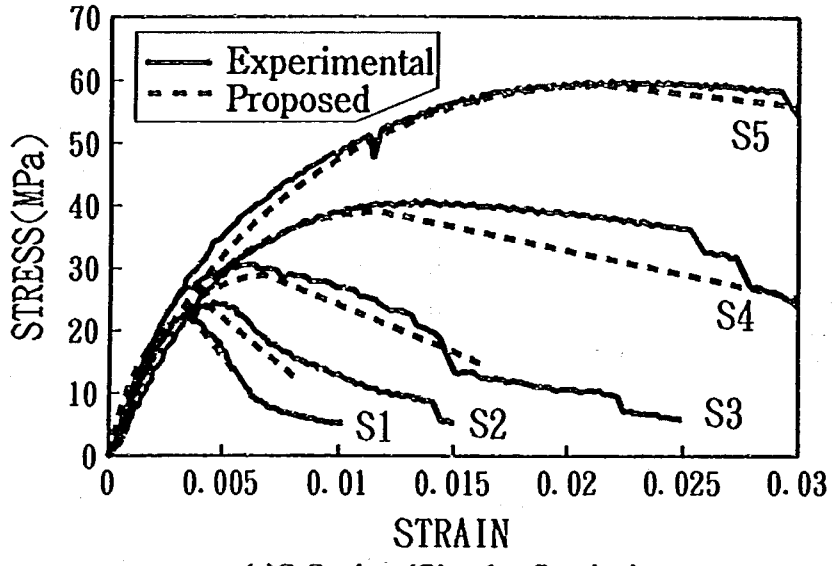
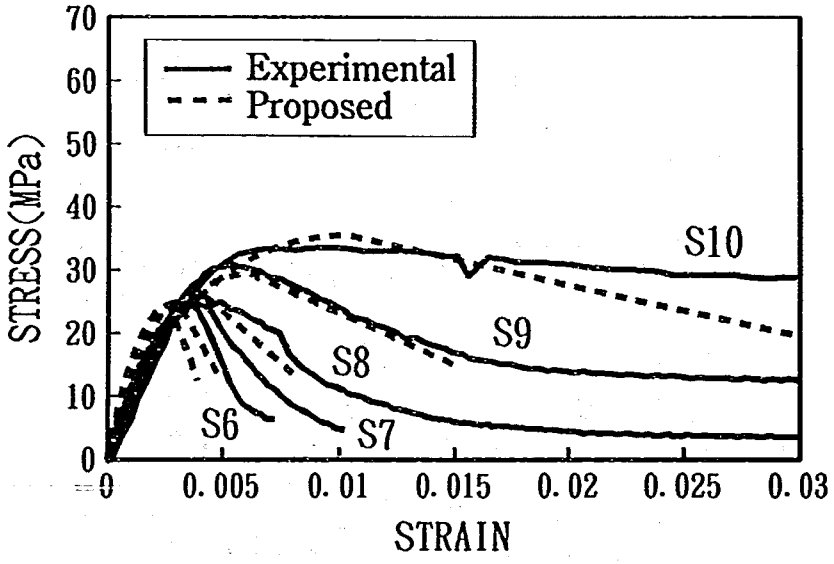


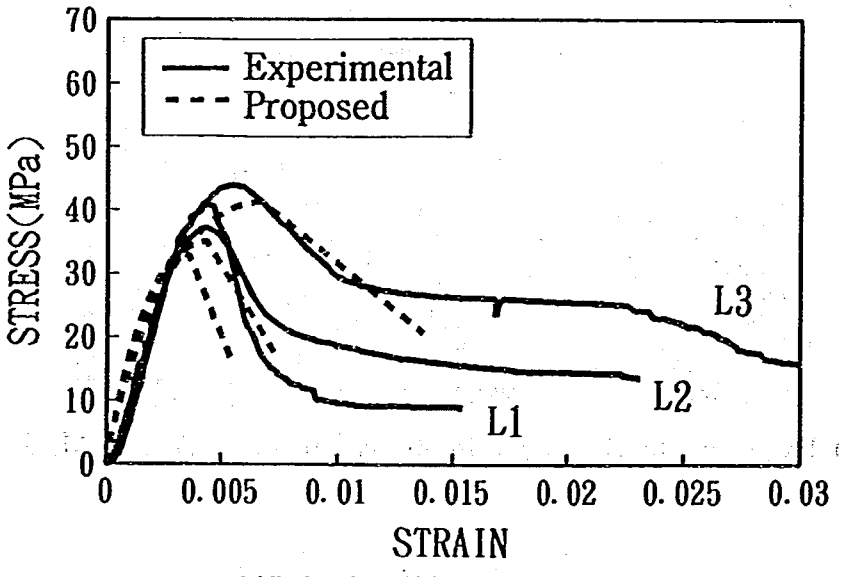
Photo 1 Experimental Set−up with 30MN Universal Testing Machine



(a)S Series (Circular Section)



(b)S Series (Square Section)



(c)L Series (Circular Section)

Fig. 2 Comparison of Stress–Strain Relation between Test Results and Predicted Model by Eq.(7)

prevented as the hoop reinforcement ratio increases. It is noted that the square confinement effectiveness is quite different from the circular. Therefore, the effect of cross sectional shape is significant to evaluate the confinement effect.

The stress–strain curve consists of three parts, i.e., stress ascending part, stress descending part and stress converging part. Severe damage such as spalling–off of core concrete, buckling of longitudinal reinforcement and rupture of hoop reinforcement were developed and progressed at the stress converging part. **Photo 2** shows the failure mode of the test specimens L1 to L5. It is observed that the damage of core concrete becomes less as the hoop reinforcement ratio increases.

Effect of Spacing of Hoop Reinforcement

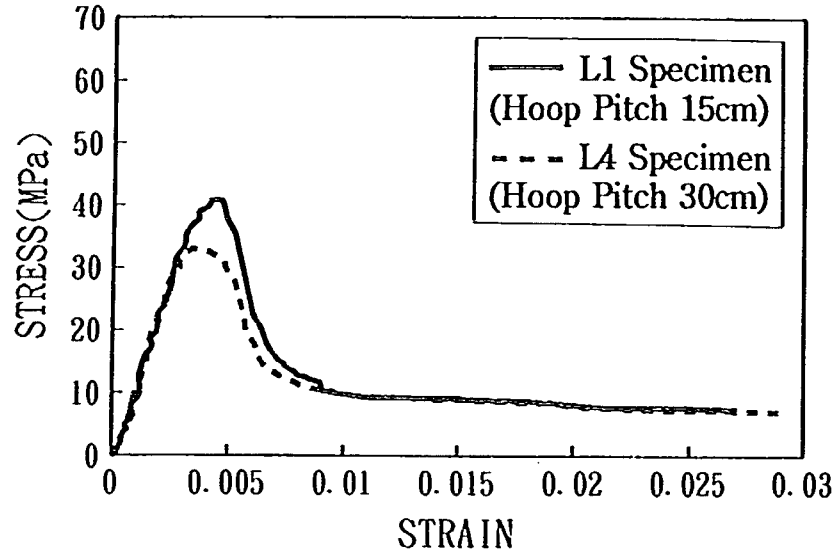
Fig. 3 shows the effect of spacing of hoop reinforcement for the same hoop reinforcement ratio. It is noticed even if the same amount of hoop is provided, deterioration after the peak stress is considerably significant when the spacing of hoop reinforcement increases. According to **Photo 2**, serious outward buckling of longitudinal reinforcement with spalling–off of core concrete was developed in L4 and L5 specimens, which had the spacing of hoop reinforcement of 30cm. Therefore, if the same amount of hoop reinforcement is provided, it is effective in seismic design to place the hoop reinforcement with smaller interval.

Effect of Hook Configuration of Hoop Reinforcement

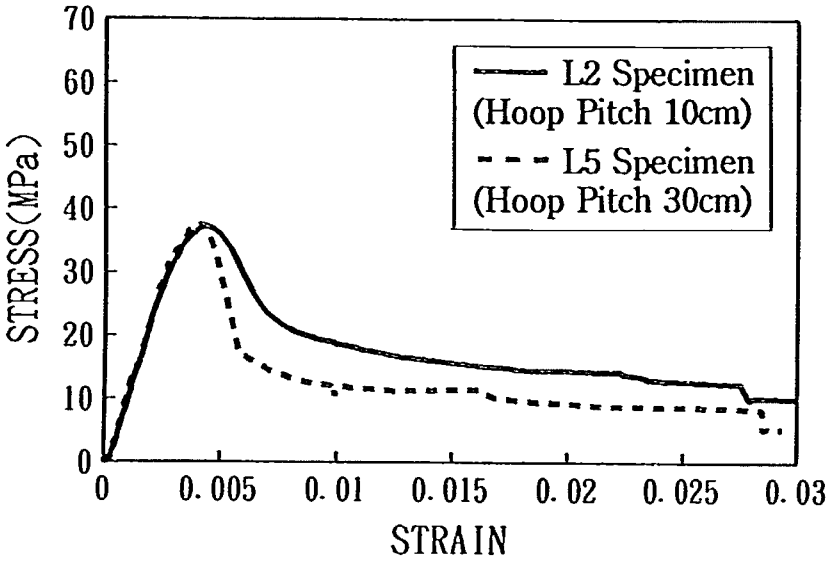
Fig. 4 shows the effect of hook configuration of hoop reinforcement on the stress–strain curve. Although the peak stress is approximately equal, the gradient at the stress descending part for L7 specimen, which used the sharp–angled hook, is slight smaller than the others. A certain reason for this is not sure, however, L6 and L8 specimens, which used smaller and larger angled hook, respectively, show similar stress–strain relation with L2 specimen, which used the welded hoop. It may be, therefore, said that the scatter of the test results is not significant. In all specimens, rupture of hoop reinforcement was developed not at the hook. This mean that the confinement is enough and the effect of hook configuration is not significant, if the hook is designed in accordance with the Specifications.

MODELING OF THE STRESS–STRAIN RELATION

According to the previous stress–strain models, the stress ascending part has been mostly formulated by a second order parabola as shown in **Table 1.** This is because a second order parabola is simple and well represents the stress–strain relation. However, it should be noted that the second order parabola expression can consider three boundary conditions, though the stress–strain model of concrete need to consider the following four boundary conditions.



(a)Hoop Reinforcement Ratio Approximately 0.35%



(b)Hoop Reinforcement Ratio Approximately 0.55%

Fig. 3 Effect of Spacing of Hoop Reinforcement

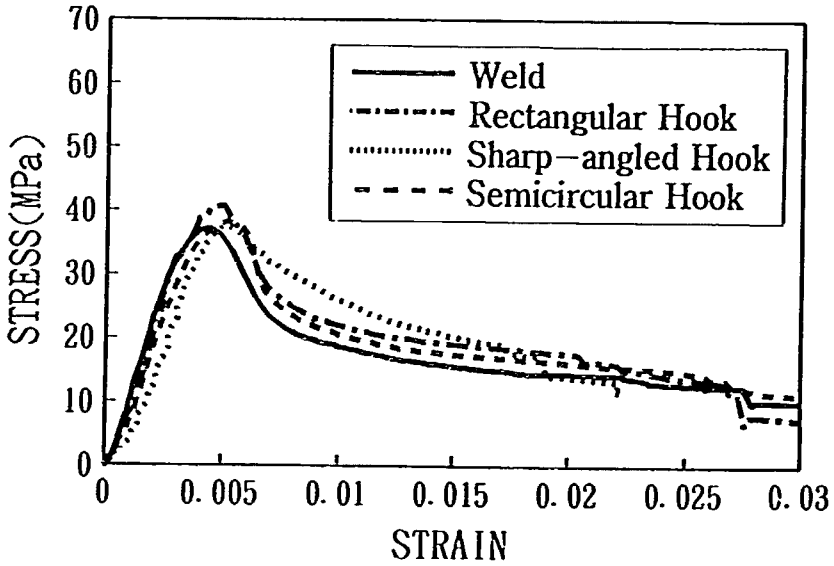
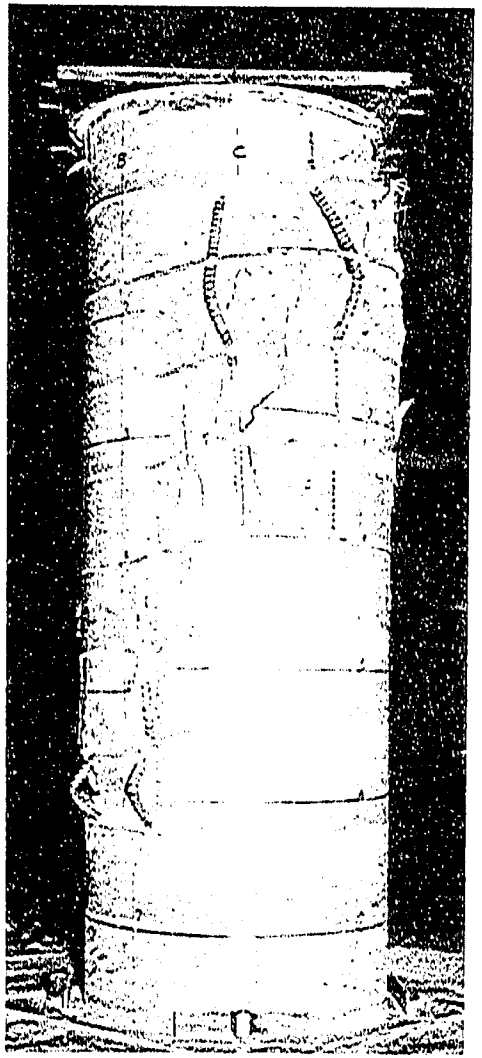
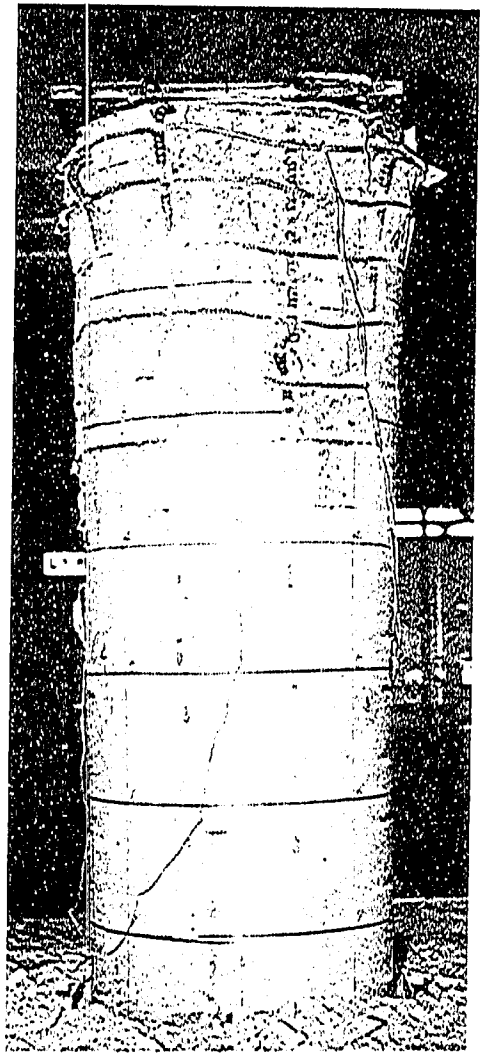


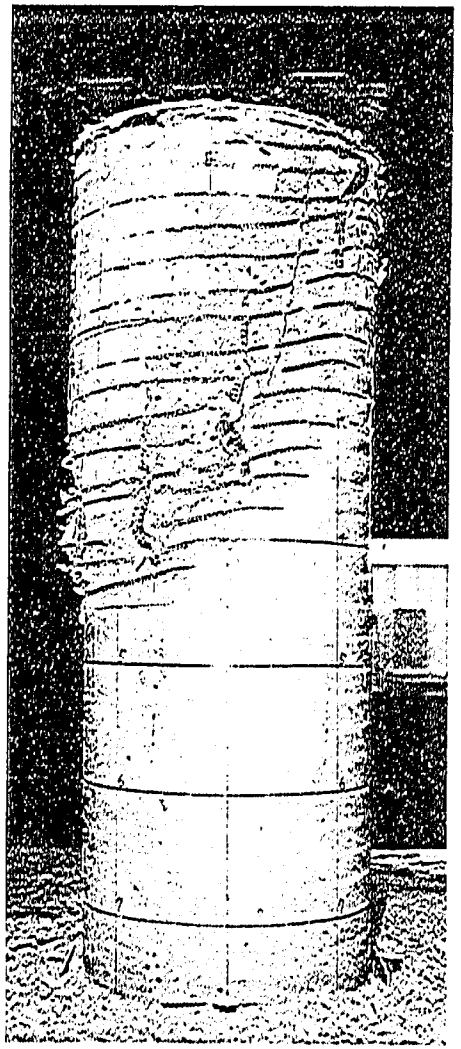
Fig. 4 Effect of Hoop Reinforcement Joint



(a)L1 Specimen

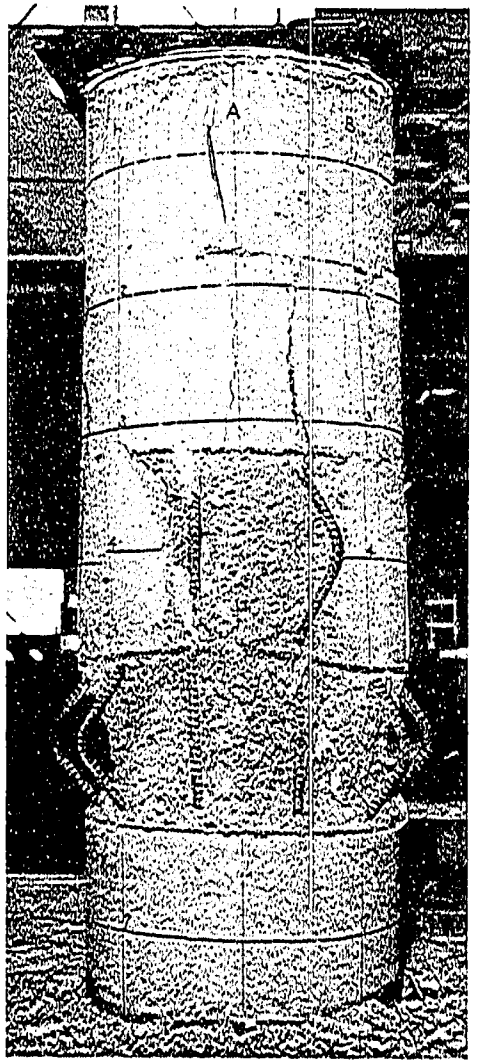


(b)L2 Specimen



(c)L3 Specimen

Photo 2 Failure Mode of Specimens



(d)L4 Specimen



(e)L5 Specimen

Photo 2 Failure Mode of Specimens

a) Initial Condition : $f_c=0$ at $\varepsilon_c=0$ (1)

b) Initial Stiffness Condition : $df_c/d\varepsilon_c=E_c$ at $\varepsilon_c=0$ (2)

c) Final Condition : $f_c=f_{cc}$ at $\varepsilon_c=\varepsilon_{cc}$ (3)

d) Peaked Condition : $df_c/d\varepsilon_c=0$ at $\varepsilon_c=\varepsilon_{cc}$ (4)

By disregarding Eq.(2), most of the previous models adopted the expression as

$$f_c=f_{cc}\left\{\frac{2\varepsilon_c}{\varepsilon_{cc}}-\left(\frac{\varepsilon_c}{\varepsilon_{cc}}\right)^2\right\} \tag{5}$$

However, the initial stiffness $2f_{cc}/\varepsilon_{cc}$ in Eq.(5) depends on the hoop reinforcement ratio, while, as shown in **Fig. 2**, the test results show that the initial stiffness is independent of the hoop reinforcement ratio. For avoiding such unconsistency, Mander adopted a fractional function including the initial stiffness as one of the four boundary conditions. And Muguruma and Fujii proposed to consider Eq.(2) as well as Eqs.(1) and (3) in formulating the second order parabola expression. But Muguruma and Fujii used two equations to represent the stress–strain relation at the ascending part.

To include Eq.(2), and for avoiding to adopt two equations at the ascending part, it is proposed here to assume the stress of concrete as

$$f_c=C_1\varepsilon_c^n+C_2\varepsilon_c+C_3 \tag{6}$$

in which C_1,C_2,C_3 and n are constants to be determined from Eqs.(1) to (4). The exponential function enables to simplify the expression and to satisfy the four boundary conditions. By substituting Eqs.(1) to (4) into Eq.(6), one obtains

$$f_c=E_c\varepsilon_c\left\{1-\frac{1}{n}\left(\frac{\varepsilon_c}{\varepsilon_{cc}}\right)^{n-1}\right\} \tag{7}$$

where

E_c : initial stiffness(MPa) and is defined by the Specifications[10] as shown in Table 5

n : a coefficient and is given as

$$n=\frac{E_c\varepsilon_{cc}}{E_c\varepsilon_{cc}-f_{cc}} \tag{8}$$

Table 5 Initial Stiffness of Concrete (MPa)

Strength of Unconfined Concrete	20.6	23.5	26.5	29.4	39.2	49.0
Initial Stiffness	2.30×10^4	2.45×10^4	2.60×10^4	2.75×10^4	3.04×10^4	3.24×10^4

Because the effect of confinement on the initial stiffness is not significant, the initial stiffness is assumed here by the Specifications.

On the other hand, as shown in **Fig. 5**, the stress descending part is modeled from

the test results by a straight line as

$$f_c = f_{cc} - E_{des}(\varepsilon_c - \varepsilon_{cc}) \quad (9)$$

where

E_{des} : gradient at the descending part(MPa)

It is important in Fig. 5 to define the ultimate strain ε_{cu} so that the gradient E_{des} at the descending part be determined. It is assumed here that the ultimate strain ε_{cu} be taken as the strain corresponding to 50% of the peak stress f_{cc}. When the strain exceeds ε_{cu}, the damage of concrete is substantial and unrepairable. By substituting $f_c = 0.5 f_{cc}$ into Eq.(9), the ultimate strain ε_{cu} is obtained as

$$\varepsilon_{cu} = \varepsilon_{cc} + \frac{f_{cc}}{2E_{des}} \quad (10)$$

Park, Sheikh and Fujii considered the residual stress of 20% or 30% of the peak stress at the stress converging part. In the proposed model, however, special efforts to idealize the stress converging part was not made, because the idealization at such region is not important in seismic design due to excessive and unrepairable damage.

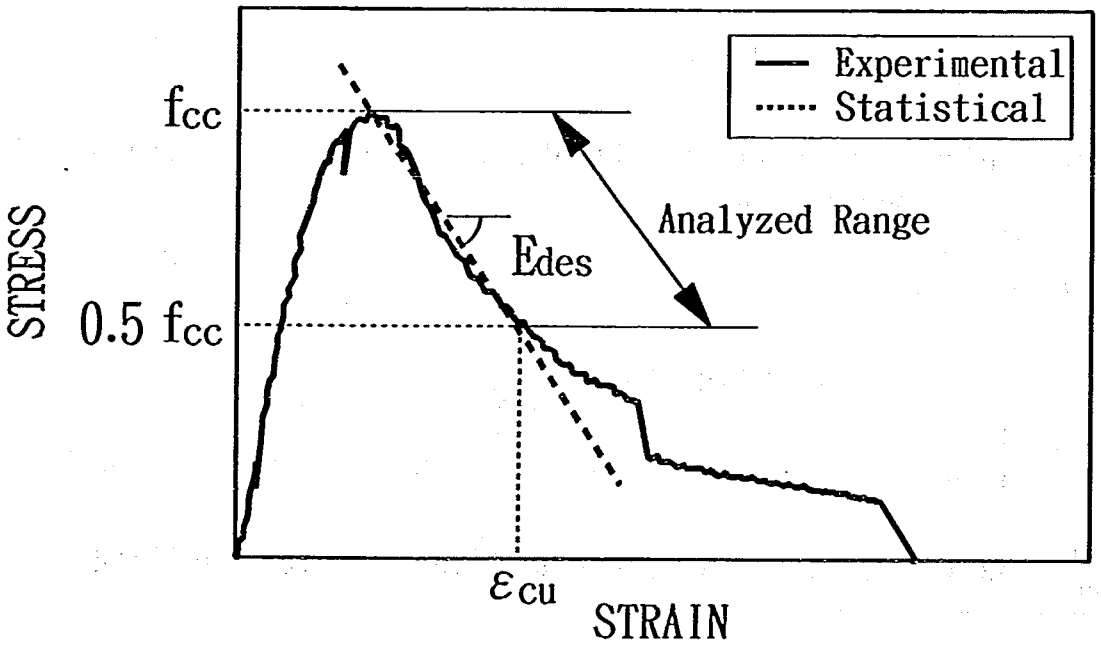


Fig. 5 Definition of Ultimate Strain and Gradient at Stress Descending part

EVALUATION OF CONFINEMENT EFFECTIVENESS

In the proposed model by Eq.(7), factors for controlling the stress–strain relation of confined concrete are the peak stress, the strain corresponding to the peak stress and the gradient at the stress descending part. The effect of confinement on the three parameters was examined based on the test results.

Parameters of confinement effectiveness may be represented as volumetric ratio, confining dimension, confining configuration, yield strength of hoop reinforcement, and strength of unconfined concrete. Because, it makes the expression complicate to incorporate all parameters into the model, volumetric ratio, confining configuration, yield strength of hoop reinforcement and strength of unconfined concrete are considered as the minimum parameters required to formulate a simple model. Other parameters may mostly be regulated by the Specifications.

Fig. 6 shows the confinement effectiveness $\rho_s f_{yh}/f_{co}$ vs. the peak stress f_{cc} thus idealized. The peak stress f_{cc} is proportional to volumetric ratio ρ_s and yield strength f_{yh} of hoop reinforcement, and is inversely proportional to strength of unconfined concrete f_{co}. It is observed that the relation may be approximated by a linear function with different gradient depending on the confining configuration. From a regression analysis for each confining configuration, the relation is written as

$$\frac{f_{cc}}{f_{co}}=1.07+3.70\frac{\rho_s f_{yh}}{f_{co}} \quad \text{: for circular confinement} \qquad (11)$$

$$\frac{f_{cc}}{f_{co}}=1.02+1.01\frac{\rho_s f_{yh}}{f_{co}} \quad \text{: for square confinement} \qquad (12)$$

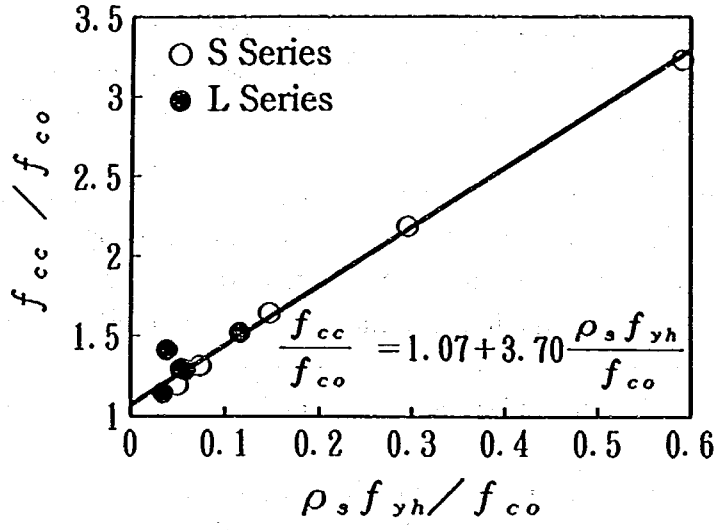
By comparing Eq.(11) and Eq.(12), it is noted that the gradient of the linear approximation for the square confinement is approximately 30% of the gradient for the circular confinement. This clearly shows that the confining configuration has a significant influence on the confinement effect.

Fig. 7 shows the confinement effectiveness $\rho_s f_{yh}/f_{co}$ vs. the strain ε_{cc} corresponding to the peak stress relation. Although some specimens with low hoop reinforcement ratio provide the larger ε_{cc} vs. $\rho_s f_{yh}/f_{co}$ relation may be lineally approximated. From a regression analysis for each confining configuration, the following relation is obtained as

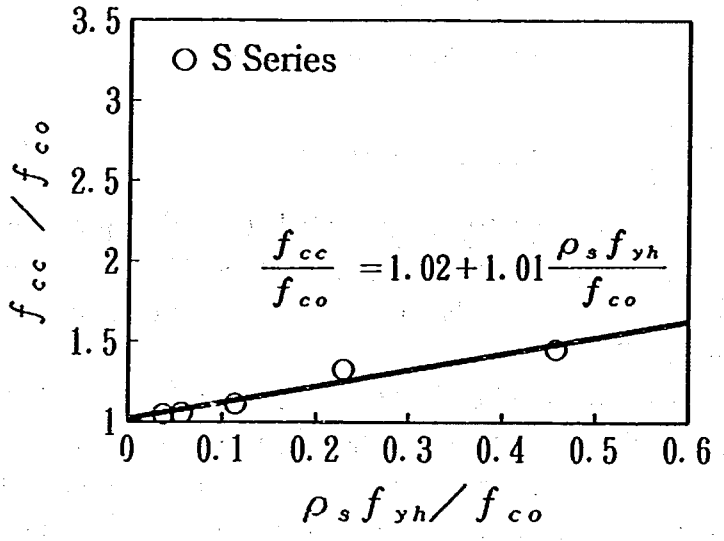
$$\varepsilon_{cc}=0.00216+0.0335\frac{\rho_s f_{yh}}{f_{co}} \quad \text{: for circular confinement} \qquad (13)$$

$$\varepsilon_{cc}=0.00277+0.0126\frac{\rho_s f_{yh}}{f_{co}} \quad \text{: for square confinement} \qquad (14)$$

It is noted that confinement effectiveness to ε_{cc} for the square confinement is approximately 55% of that for the circular confinement.

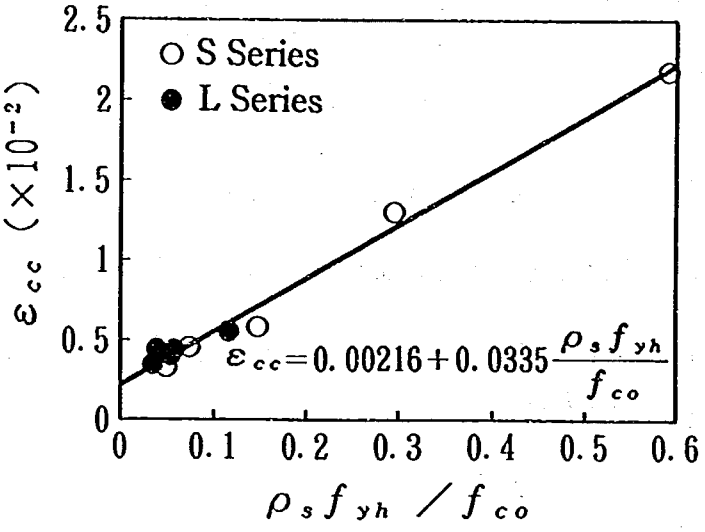


(a)Circular Confinement

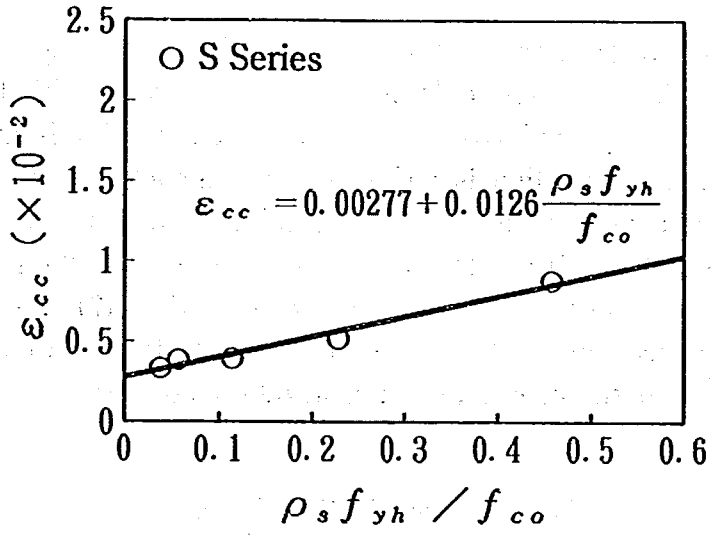


(b)Square Confinement

Fig. 6 Relation between Confinement Effectiveness and Peak Stress



(a)Circular Confinement



(b)Square Confinement

Fig. 7 Relation between Confinement Effectiveness and Strain at Peak Stress

Fig. 8 shows the confinement effectiveness $\rho_s f_{yh}/f_{co}^2$ vs. the gradient at the descending part. It is observed that the gradient E_{des} at the descending part is inversely proportional to $\rho_s f_{yh}/f_{co}^2$. By regressing the test data, it is written as

$$E_{des}=\frac{12.07}{\rho_s f_{yh}/f_{co}^2} \quad : \text{for circular confinement} \tag{15}$$

$$E_{des}=\frac{16.04}{\rho_s f_{yh}/f_{co}^2} \quad : \text{for square confinement} \tag{16}$$

It is noted that E_{des} of square confinement is about 1.33 times larger than E_{des} of circular confinement.

From Eqs.(11) to (16), the effect of confinement may be written as

$$\frac{f_{cc}}{f_{co}}=1+3.70\alpha\frac{\rho_s f_{yh}}{f_{co}} \tag{17}$$

$$\varepsilon_{cc}=0.002+0.033\beta\frac{\rho_s f_{yh}}{f_{co}} \tag{18}$$

$$E_{des}=12\gamma\frac{f_{co}^2}{\rho_s f_{yh}} \tag{19}$$

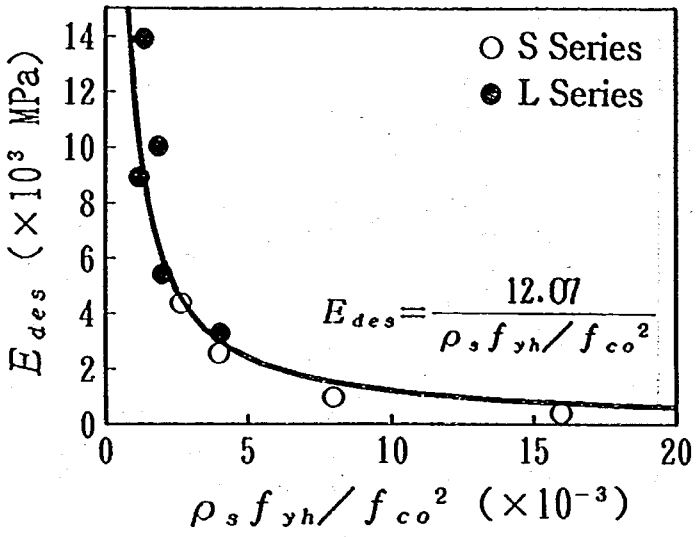
in which α, β, γ are modification factors depending on cross sectional shape and are given in Table 6.

Based on Eqs.(17) to (19), the stress–strain relation was computed for the thirteen specimens in Table 4. This is plotted in Fig. 2 in comparison with the test data. The predicted relations are in very good agreement with the test results. It should be noted that because the initial stiffness condition is included in the model, the gradient at the stress ascending part predicted is independent of the hoop reinforcement ratio.

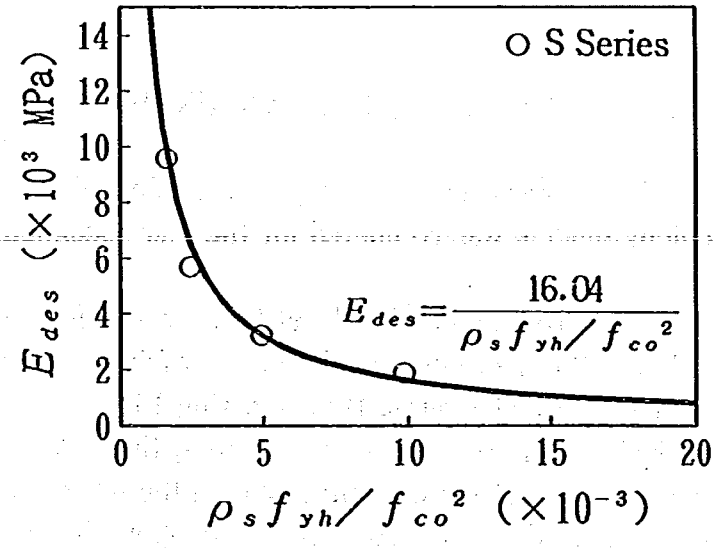
For the reference, if Eq.(5) is adopted, the stress–strain relation becomes as shown in Fig. 9. In Eq.(5), f_{cc} and ε_{cc} were provided by Eqs.(17) and (18). The gradient predicted at the stress ascending part is appreciably smaller than the test result. And also, as expected, it decreases as the hoop reinforcement ratio increases.

Table 6 Modification Factors

Confinement	α	β	γ
Circular	1	1	1
Square	0.3	0.55	4/3



(a) Circular Confinement



(b) Square Confinement

Fig. 8 Relation between Confinement Effectiveness and Gradient at Stress Descending Part

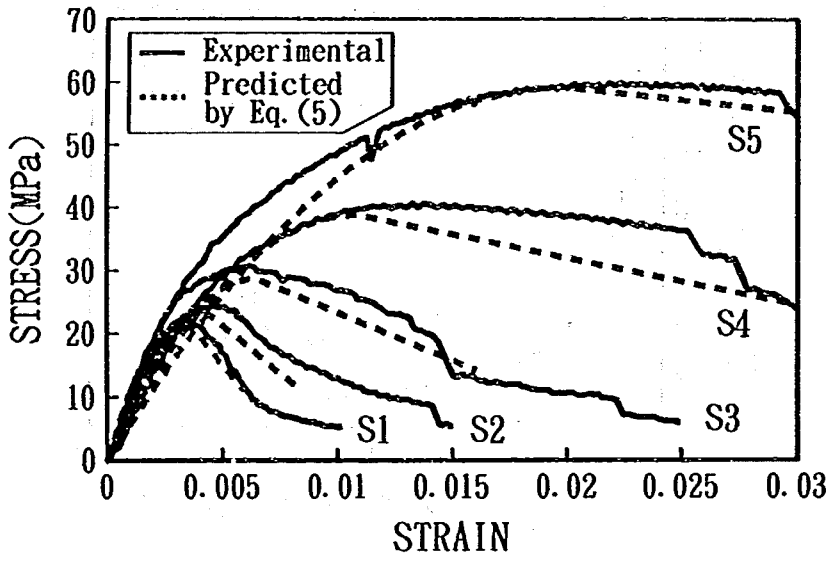


Fig. 9 Stress–Strain Relation by Eq.(5)

COMPARISON WITH PREVIOUS MODELS

To show the effectiveness of the proposed model, the stress–strain relation predicted by the previous models was computed for the test specimens, and compared with the test results.

Figs. 10 to 14 compare the predicted relation by previous models with the test results. It is observed that the previous models mostly evaluate the gradient at the stress ascending part larger than the test results. By comparing Fig. 2 with Figs. 10 to 14, it is obvious that the proposed model predicts the peak stress, the strain at the peak stress and the gradient at the descending part more accurately than the previous models. The gradient at the descending part predicted by the proposed model approximates to test results much better than the previous models, because the effect of low hoop reinforcement ratio is incorporated into the proposed model.

From this comparison, the proposed model provides better agreement than the previous models to the stress–strain relation of confined concrete with low hoop reinforcement ratio.

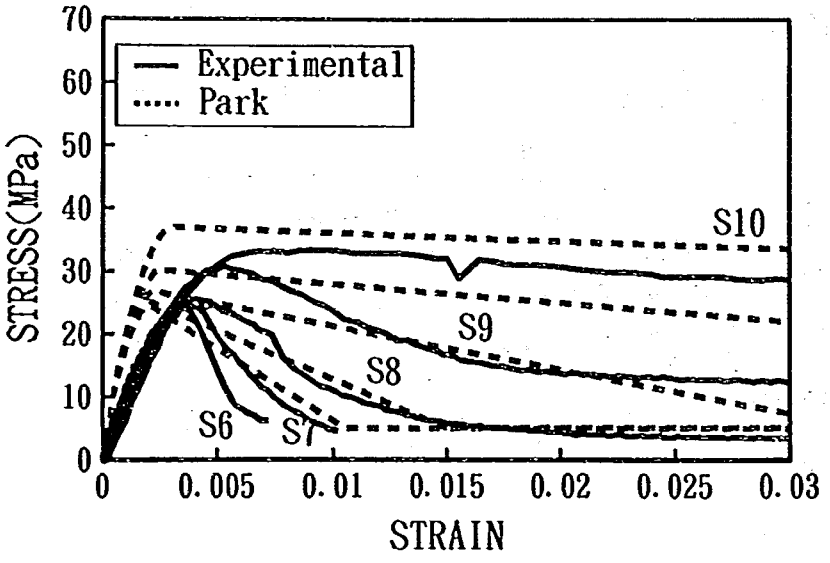


Fig. 10 Stress–Strain Relation by Park

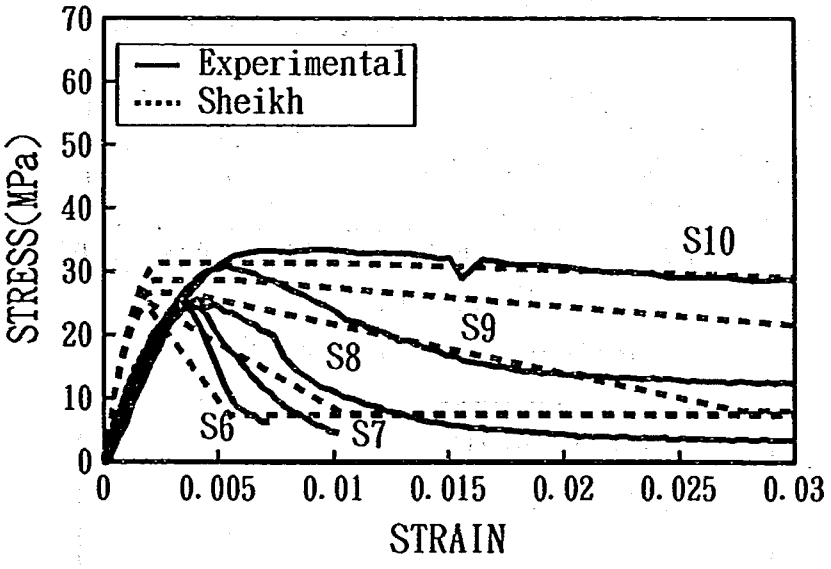
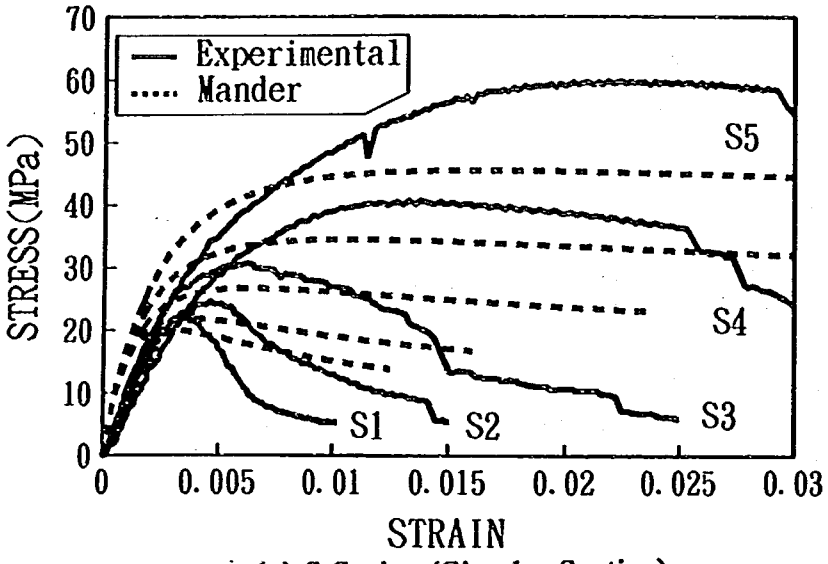
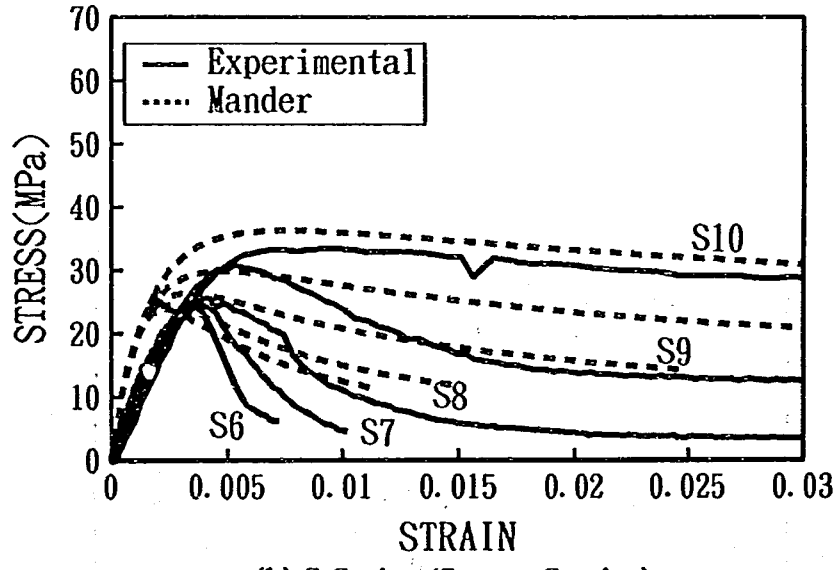


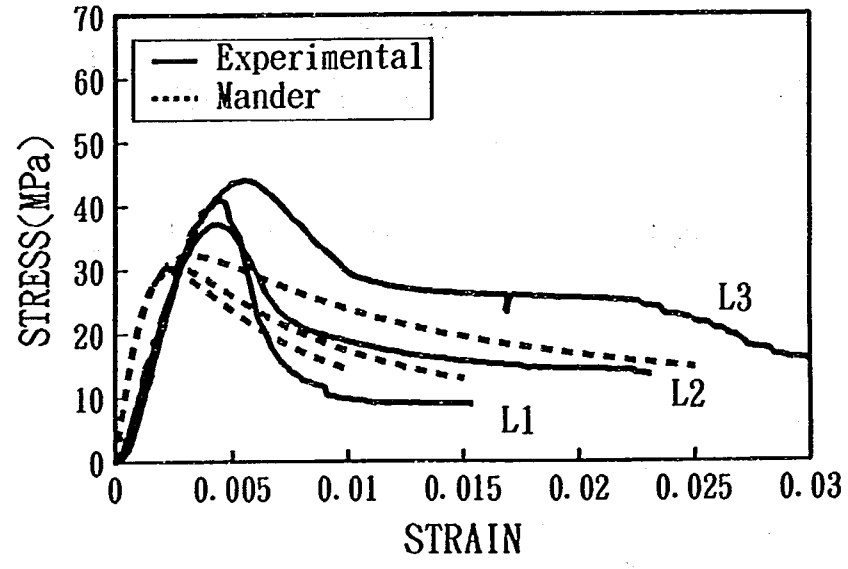
Fig. 11 Stress–Strain Relation by Sheikh



(a) S Series (Circular Section)

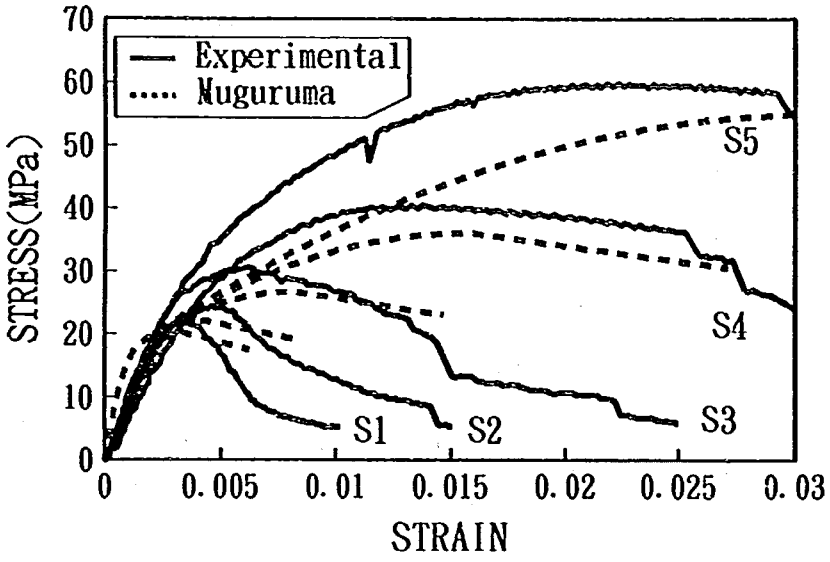


(b) S Series (Square Section)

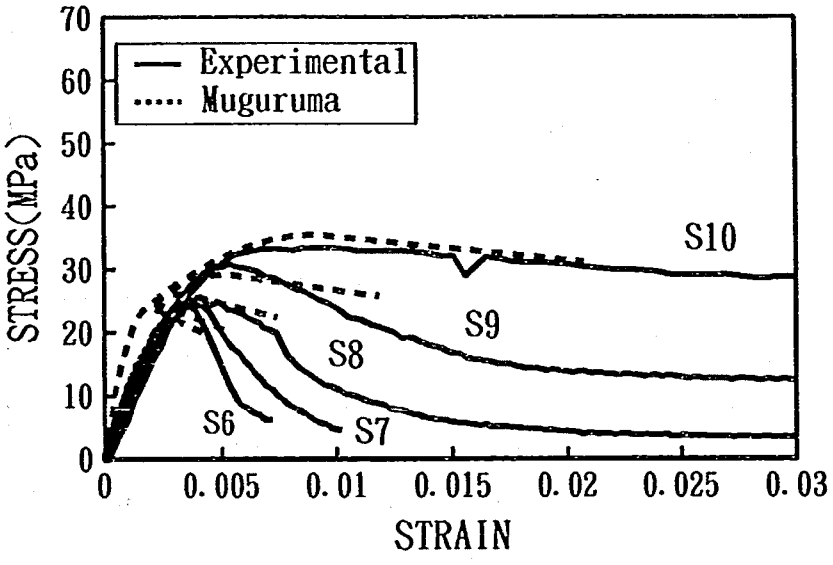


(c) L Series (Circular Section)

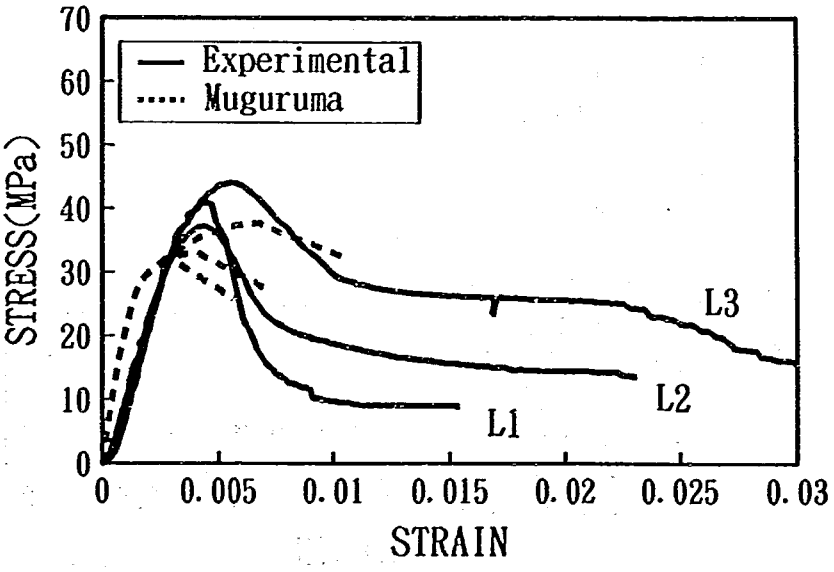
Fig. 12 Stress–Strain Relation by Mander



(a) S Series (Circular Section)

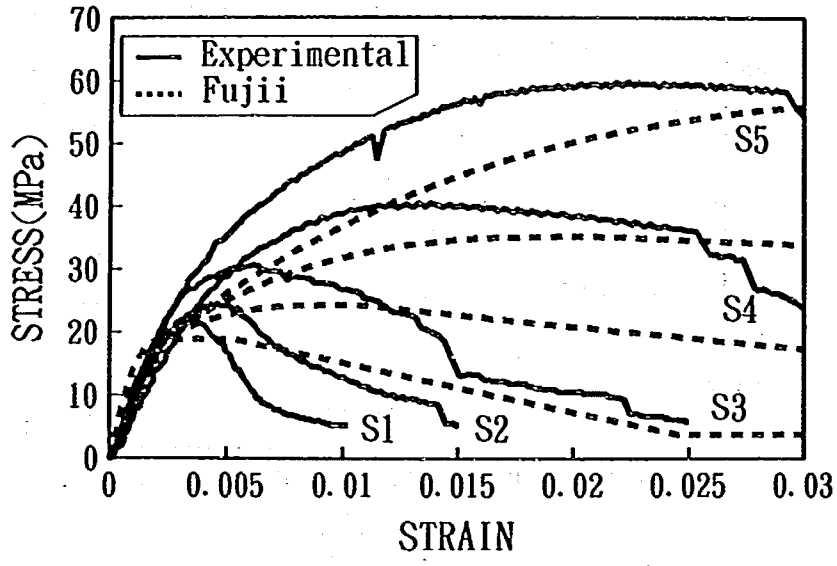


(b) S Series (Square Section)

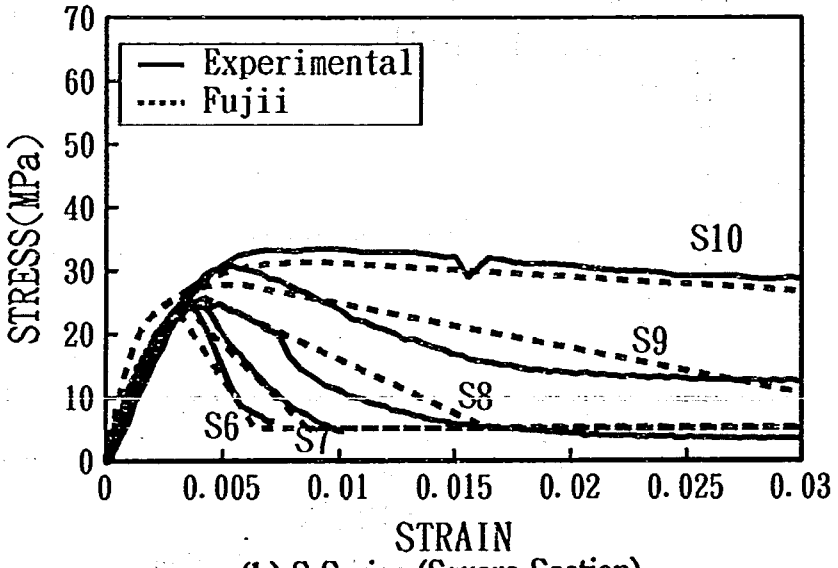


(c) L Series (Circular Section)

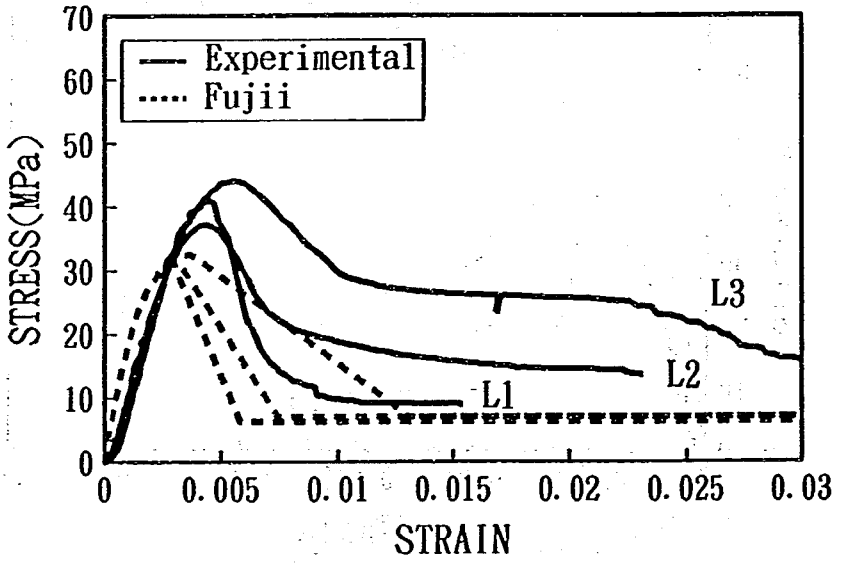
Fig. 13 Stress–Strain Relation by Muguruma



(a) S Series (Circular Section)



(b) S Series (Square Section)



(c) L Series (Circular Section)

Fig. 14 Stress–Strain Relation by Fujii

CONCLUDING REMARKS

To propose an accurate stress–strain model of confined concrete with low hoop reinforcement ratio, a series of loading tests were made for fifteen confined concrete columns. The conclusions from the study presented herein may be deduced as;

1) To consider four boundary conditions by Eqs.(1) to (4) into the stress–strain relation of concrete, the exponential function given by Eq.(7) is proposed.
2) The ultimate strain ε_{cu} is defined as the strain corresponding to 50% of the peak stress, because th idealization of stress–strain relation over the strain ε_{cu} is not important in seismic design due to substantial and unrepairable damage of concrete.
3) The peak stress, the strain at the peak stress and the gradient at the descending part are proposed to be evaluated by Eqs.(17) to (19) based on the loading test results for specimens with a cross sectional dimension of 20 to 50cm and the volumetric ratio of hoop reinforcement of 0.3 to 4.7%.
4) In comparison with the previous models, the proposed model seems to provide better agreement with the test results for the confined concrete with low hoop reinforcement ratio.

REFERENCES

1) Kent, D. C. and Park, R. : Flexural members with confined concrete, Journal of the Structural Division, ASCE, Vol.97, No.ST7, pp.1969–1990, Jul. 1971
2) Park, R. et al : Ductility of square–confined concrete columns, Journal of the Structural Division, ASCE, Vol.108, No.ST4, pp.929–950, Apr. 1982
3) Sheikh, S. A. and Uzumeri, S. M. : Strength and ductility of tied concrete columns, Journal of the Structural Division, ASCE, Vol.106, No.ST5, pp.1079–1102, May 1980
4) Sheikh, S. A. and Uzumeri, S. M. : Analytical model for concrete confinement in tied columns, Journal of the Structural Division, ASCE, Vol.108, No.ST12, pp.2703–2722, Dec. 1982
5) Mander, J. B., Priestley, M. J. N and Park, R. : Theoretical stress–strain model for confined concrete, Journal of the Structural Division, ASCE, Vol.114, No.ST8, pp.1804–1826, Aug. 1988
6) Mander, J. B., Priestley, M. J. N and Park, R. : Observed stress–strain behavior of confined concrete, Journal of the Structural Division, ASCE, Vol.114, No.ST8, pp.1827–1849, Aug. 1988
7) Muguruma, H. et al : A stress–strain model of confined concrete, Annual Report on Cement Engineering, Vol.34, pp.429–432, 1980
8) Muguruma, H. et al : A study on the improvement of bending ultimate strain of concrete, 24th Structural Engineering Symposium, pp.109–116, 1978
9) Fujii, M. et al : A study on the application of a stress–strain relation of confined

concrete, Annual Report on Cement Engineering, Vol.42, pp.311–314, 1988
10) Japan Road Association : Part IV Design of Foundations, Design Specifications of Road Bridges, Feb. 1991

Seismic Response of Reinforced Concrete Bridge Piers Subjected to Eccentric Loading

Kazuhiko KAWASHIMA
Shigeki UNJOH
and
Hidetoshi MUKAI

2nd U.S.–Japan Workshop on
Seismic Retrofit of Bridges
Berkeley, U.S.A.
January, 1994

SEISMIC RESPONSE OF REINFORCED CONCRETE BRIDGE PIERS SUBJECTED TO ECCENTRIC LOADING

Kazuhiko KAWASHIMA[1], Shigeki UNJOH[2] and Hidetoshi MUKAI[3]

1) Head, Earthquake Engineering Division, Public Works Research Institute, Ministry of Construction, Tsukuba Science City, Japan
2) Senior Research Engineer, ditto
3) Assistant Research Engineer, ditto

ABSTRACT

Presented are the seismic response characteristics of C-shaped reinforced concrete bridge piers which is subjected to eccentric loading by the dead weights of superstructure and cantilevered beam. The shaking table test and dynamic loading tests of model piers were made to investigate the seismic response characteristics. It is found that the response of pier increased only in one direction in which the bending moment increased and that the excessive residual displacement was developed. It is also found that the ductility significantly decreased with increase of bending moment by the eccentric loading.

INTRODUCTION

Recently, new types of structures have been constructed in urban areas by land use restriction and other construction conditions. C-shaped reinforced concrete (RC) bridge pier as shown in **Fig. 1** are one of the typical examples. However, the seismic response characteristics of this type of RC piers have not yet been studied. Because the C-Shaped RC piers are subjected to eccentric loading by the dead weights of superstructure and cantilevered beam, it is anticipated that the seismic response of the piers is developed only in one direction during an earthquake. Therefore is an important subject to investigate the strength and ductility characteristics and to develop the seismic design method against large-scale earthquakes.

This paper presents the seismic response characteristics of C-shaped reinforced concrete bridge piers through the shake table test and dynamic loading tests of model piers.

DEFINITION OF ECCENTRIC LOADING

In order to define the amount of the eccentric loading, bending moment ratio is

assumed as

$$r_M = \frac{M_E}{M_0 + M_E} \tag{1}$$

where

r_M : bending moment ratio

M_E : bending moment by design seismic load, and

M_0 : bending moment by eccentric loading of superstructure and cantilevered beam

Eq.(1) shows that when the eccentric loading increases r_M deceases, on the other hand, when the eccentric loading decreases r_M increases. $r_M=1$ means concentric loading.

Fig. 2 shows distribution of the bending moment ratio r_M based on the survey of 45 existing C−shaped RC bridge piers in the Metropolitan area, bending moment ratio r_M is in the range of 0.4 − 0.9. Averaged bending moment ratio r_M is 0.55.

SEISMIC RESPONSE CHARACTERISTICS OF C−SHAPED RC PIER BASED ON SHAKING TABLE TESTS

Bridge Pier Model Studied

In order to investigate the seismic response characteristics of a C−shaped RC pier, shaking table test was made at the Public Works Research Institute. Objective of the shaking table test is to investigate how the C−shaped pier responds and behaves in the transverse direction to a bridge axis during an actual earthquake.

Fig. 3 shows a C−shaped bridge pier model used for the shaking table test. Details of the pier model was determined based on the actual bridge pier. The actual pier with average bending moment ratio, r_M , of 0.55 was selected as a prototype. The height of pier is 10.2m and the height of girder is 1.5m. The similarity ratio of the pier model with the prototype pier was assumed as 1/4.6.

The specimen has an effective height, h, of 2.55m and cross section of 52cm × 42cm (width along bridge axis : 52cm). The shear span ratio h/d, which is defined as the effective height divided by the effective depth, d, of the cross section of 37cm, is 6.9. Longitudinal reinforcing bars are arranged by 5 reinforcing bars with diameter of 16mm (D16) in the initial compression side by the eccentric loading, 5 reinforcing bars with that of 22mm (D22) in the tension side, and 3 reinforcing bars with that of 16mm (D16) in the other sides. The reinforcement ratio is 0.45, 1.06 and 0.27, respectively. Tie reinforcement was arranged by 17.3cm pitch by reinforcing bars with diameter of 10mm (D10). Tie reinforcement ratio is 0.16. Averaged yielding stress of the longitudinal and tie reinforcement was 35.38KN for D16, 34.32KN for D22 and 34.83KN for D10. Averaged compression strength of the concrete was 3.29KN. It should be noted here that since weight of the superstructure supported by the pier model is 393.2KN, seismic coefficient of

the pier model can be regarded as 0.27. Axial stress by the dead weight of superstructure was 90N. Computed yield displacement, δ_y, corresponding to one displacement ductility factor and yield strength of the pier in the direction in which the bending moment increases are 75.5KN and 20.5mm computed from the shifted origin. On the other hand, in the direction in which the bending moment decreases they are 115.7KN and 91.3mm, respectively.

Shaking Table Test

A pier model is fixed at the center of the shaking table and two spans of simply supported girders with total weights of 393.2KN and length of 15m were placed on the pier model. Because two ends of the girder could not be supported by the shaking table, they are supported by the two steel frames placed outside of the table. The pier model and girders were connected by fixed bearings. The steel frames and girder were connected by movable roller bearings so that inertia force developed at the girder during excitation be directly applied to the pier model. It should be noted here that although the direction of the eccentric loading is assumed to be transverse direction, the girder axis was set up in parallel direction with transverse direction of the pier model. However, since the two girders was to load the weight of superstructure and to simulate the inertia force, the direction of the girders is not important.

The shaking table was excited along transverse direction to bridge axis (direction to the girder axis of model bridge). An acceleration record triggered at the Hachirogata during the Nihon-kai-chubu, Japan, Earthquake of 1983 was used as an input motion by reducing the time axis one half so that the predominant frequency of the record matches with the fundamental natural frequency of the pier model. Intensity of the record was assumed as 3.5 times the original.

Extensive instrumentations were made to measure basic parameters including accelerations at the foot of pier and at the girder as well as relative displacement of the girder with reference to shaking table. Inertia force of the superstructure was computed by multiplying the acceleration developed at the girder by the mass of girder.

Seismic Response Characteristics

Fig. 4 shows acceleration of shaking table, response acceleration and displacement of girder. Although measured peak acceleration of shaking table is 812cm/s^2, this is spike-like response and effective seismic intensity to excite the pier model is about 0.35G as assumed. The pier model developed residual lateral displacement with an amount of 16cm at the pier crest in the direction in which eccentric weight is loaded. However, the stopper for preventing falling-off of girders worked at this moment. If the stopper was not installed the larger residual displacement would be developed. Such a permanent displacement is clearly observed in **Fig. 5** from biased inelastic response displacement. The drift of response displacement was developed at time 12sec when the first large excitation,

which exceeded the yielding displacement, loaded. However, after the excitation with larger displacement at time 17sec, the residual displacement reached to about 16cm. Therefore, accumulation of drifting of response displacement after the first large excitation seems to be less significant. It should be noted here that although the residual displacement was developed in the shaking table test of RC pier model subjected to concentric loading, the amount was much smaller than that mentioned above.

Fig. 5 shows the failure mode of the pier model after the excitation by shaking table. Compression failure was found in the compression side by the eccentric loading. Only horizontal tension crack was found in the tension side.

Fig. 6 shows the hysteresis loop of the load–displacement relation obtained through the shaking table test. The biased displacement response was clearly developed after the first significant excitation with larger displacement exceeding the yield displacement. The degradation of the stiffness in accordance with nonlinear response can be clearly observed.

DYNAMIC LOADING TEST OF RC PIER MODELS

Bridge Pier Models Studied

In order to investigate the strength and ductility characteristics of C–shaped RC pier, dynamic loading tests were made. Fig. 7 shows a C–shaped bridge pier model used for the dynamic loading test. The pier models are basically the same as the shaking table test as mentioned in the above. Three pier models in total were tested, in which bending moment ratio, r_M , and loading direction was varied as a parameters to be investigated.

All pier models have a loading effective height, h, of 2.55m and cross section of 52cm ×42cm (width along in bridge axis : 52cm). The shear span ratio, h/d, is 6.9. The bending moment ratio, r_M , was assumed as 0.69 (P–60; small eccentric loading), 0.55 (P–62; medium eccentric loading) and 0.51 (P–64; large eccentric loading), in which the specimen number is the serial number of pier models tested at the Public Works Research Institute. P–62 has the same condition as one used for the shaking table test. The detail of the piers is the same as P–62. Eccentric weight in transverse direction was not loaded for P–65. Axial loading was assumed as 196.1KN which is the same as the shaking table test. Therefore, axial stress by the axial loading is 90.2N. It should be noted here that the axial force to P–60 was assumed as 127.5KN (axial stress is 58.8N) because of limitation of loading apparatus.

Dynamic Loading Test

The pier model was anchored to the reaction wall with bolts. The large–stroke dynamic actuator, which was installed to the reaction wall in such a manner, was fixed to the head of the pier model. Also, axial loading apparatus was fixed to the head of the pier models so that the necessary eccentric loading be applied. At the pier crest the steel–made apparatus was set for the purpose to eccentrically impose the axial force.

Fig. 8 shows the pattern of loading displacement for dynamic loading tests. The yield displacement corresponding to one ductility factor was assumed as an unit loading displacement. However, the pier models subjected to eccentric loading is initially displaced by displacement of δ_0. Therefore, unit loading displacement, δ_1, was assumed with the assumption of that the origin is shifted to the initial point as

$$\delta_1 = \delta_y - \delta_0 \qquad (2)$$

where

δ_1 : unit loading displacement

δ_y : yielding displacement

δ_0 : initial displacement by eccentric loading

The pier models were subjected to a series of step-wise increasing symmetric displacement cycles as shown in Fig. 8. At each step, 10 cycles of loading with the same displacement amplitude was carried out. It should be noted here that the yield displacement was determined by computation with the strain of main reinforcement at the base. The loading velocity was assumed as 1cm/s. The loading direction was assumed as transverse and longitudinal directions depending on the test objectives.

Failure Mode of Pier Models

Fig. 9 shows the failure mode of P-62 (r_M=0.55; medium eccentric loading). Damage of a side parallel to the loading direction is shown. During δ_1 to δ_2 loading cycles, only small horizontal cracks were found on the concrete surface. This is by the loading in the plus side (the loading in which bending moment increases, this side is referred to A-side), no cracks was found at the minus side (the loading in which bending moment decreases, this side is referred to B-side). After δ_3 loading cycles the cracks was initiated to be developed in B-side. During δ_4 loading cycles, diagonal cracks were developed from the bottom of A-side to B-side. With increase of loading cycles, the significant cracks were developed at the bottom of B-side and cover concrete was spalled-off. During δ_6 loading cycles, concrete of the bottom of pier was failed with a triangular wedge shape and 2 reinforcing bars were fractured in the B-side. During δ_7 loading cycles, deformation of pier was significantly extended at the base and the pier was inclined. It should be noted here that comparing of the failure mode with the shaking table test result, the failure mode was significantly different between two tests. Although the diagonal crack was developed in the dynamic loading test, such diagonal crack was not developed during the shaking table test. This is because that although displacement in the minus side was forced to be loaded to the pier in the dynamic loading test, displacement during shaking table test was developed in one direction in which the bending moment increases.

Figs. 10 and 11 show the failure modes of P-60 (r_M=0.69; small eccentric loading) and P-64 (r_M ; large eccentric loading). In case of P-60, from δ_1 loading cycles, crack was developed also in the B-side. Then the crack increased in both A-side

and B–side. During δ_6 loading cycles, cover concrete was spalled–off in the both sides of the bottom. During δ_7 loading cycles, 3 longitudinal reinforcing bars were fractured. The difference in the failure mode between P–62 and P–60 is that the damage was developed in both sides and the progress of the damage of P–60 with loading cycles became slower than that of P–62.

On the other hand, in case of P–64 (r_M=0.51; large eccentric loading), during δ_3 loading cycles the diagonal crack was developed. The cover concrete in the B–side of the bottom was spalled–off during δ_4 loading cycles. During δ_5, concrete at the bottom of B–side was failed by compression and one longitudinal reinforcing bar was fractured. Comparing with the failure mode of P–62, the progress of damage of P–64 became faster than P–62.

Strength and Ductility Characteristics

Fig. 12 shows the effect of bending moment ratio, r_M, on load–displacement relation. In the plus side in which the bending moment increases, the displacement range in which load reaches to peak and the displacement increase stably was shorter as the bending moment ratio is smaller. Therefore, the bending moment ratio is smaller, the ductility becomes smaller.

Table 1 shows the strength and ductility of the tested pier models. The ductility was almost same when r_M is 0.69 and 0.55, but when the r_M is 0.51 the ductility decreases to one of half of those. The ratio of peak strength by yield strength of the P–64 decreases by 10% than P–60 and P–62.

CONCLUDING REMARKS

In order to investigate the seismic response characteristics of C–shaped reinforced concrete bridge piers which is subjected to eccentric loading in the transverse direction to bridge axis by the dead weights of superstructure and lateral beam, the shaking table test and dynamic loading tests of model piers were made to investigate the seismic response characteristics.

According to the above results the following conclusions may be deduced:

1) When the pier model subjected to eccentric loading, the displacement was developed only in one direction in which the bending moment increases. The large amount of residual displacement was finally developed.
2) When the bending moment ratio is 0.51, the ductility decreases to one half that greater than 0.55. Therefore, the bending moment ratio is smaller, ductility becomes smaller.

REFERENCES

1) Kawashima, K., Hasegawa, K., Koyama, T. and Yoshida, T.(1988) "Hysteretic Behavior

of Reinforced Concrete Bridge Piers by Dynamic Loading Tests and Shaking Table Tests," Ninth World Conference on Earthquake Engineering, Tokyo–Kyoto, Japan

2) Kawashima, K., Hasegawa, K., Koyama, K. and Yoshida, T.(1985) "Experimental Investigation on Dynamic Strength and Ductility of Reinforced Concrete Bridge Piers, (Part.1)," Technical Memorandum of PWRI, No.2232

4) Iwasaki, T., Kawashima, K., Hasegawa, K., Koyama, T. and Yoshida, T.(1987) "Effect of Number of Loading Cycles and Loading Velocity of Reinforced Concrete Bridge Piers," 19th Joint Meeting, Wind and Seismic Effects, UJNR, Tsukuba, Japan

5) Iwasaki, T., Kawashima, K., Hasegawa, K. and Yoshida, T.(1988) "Dynamic Strength and Ductility of Reinforced Concrete Bridge Piers," 20th Joint Meeting, Wind and Seismic Effects, UJNR, Gaithersburg, Maryland

6) Iwasaki, T., Ueda, O., Kawashima, K., Hasegawa, K. and Yoshida, T(1989). "Inelastic Behavior of Reinforced Concrete Bridge Pier, –Effect of Bilateral Loading and Circular Hollow Section–," 21st Joint Meeting, Wind and Seismic Effects, UJNR, Tsukuba, Japan

7) Kawashima, K., and Koyama, T.(1988) "Effect of Number of Loading Cycles on Dynamic Characteristics of Reinforced Concrete Bridge Pier Columns," Structural Eng./Earthquake Eng., Proc. JSCE, Vol.5, No.1, pp.183–191

8) Kawashima, K., and Koyama, T.(1988) "Effect of Cyclic Loading Hysteresis on Dynamic Behavior of Reinforced Concrete Bridge Pier," Structural Eng./Earthquake Eng., Proc. JSCE, Vol.5, No.2, pp.343–350

Table 1 Strength and Ductility of Pier Models

	P–60	P–62	P–64
Loading Direction	Trans.	Trans.	Trans.
Bending Moment Ratio r_M (Eccentric Loading)	0.69 Small	0.55 Medium	0.51 Large
Yield Strength P_y (KN)	124.5	147.1	223.6
Peak Strength P_{max} (KN)	145.1	179.5	238.3
P_{max}/P_y	1.17	1.22	1.07
Yield Displacement δ_y (cm)	1.6	1.3	2.0
Ultimate Displacement δ_u (cm)	8.8	7.3	5.4
Ductility Factor δ_y/δ_u	5.5	5.6	2.7

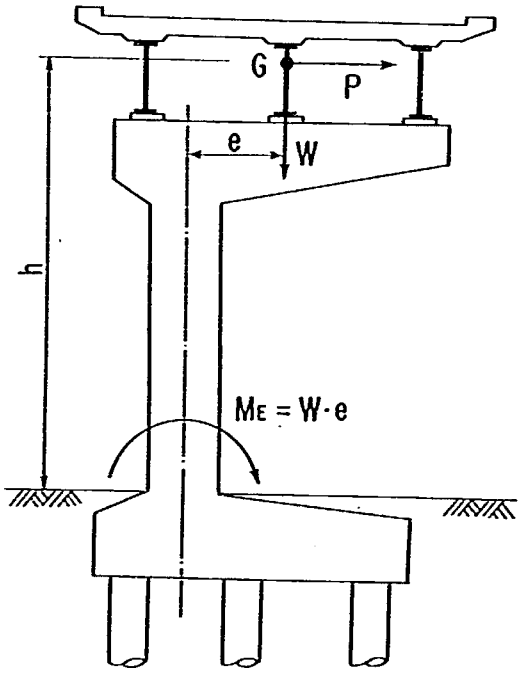


Fig. 1 C–Shaped Reinforced Concrete Bridge Pier Subjected to Eccentric Loading

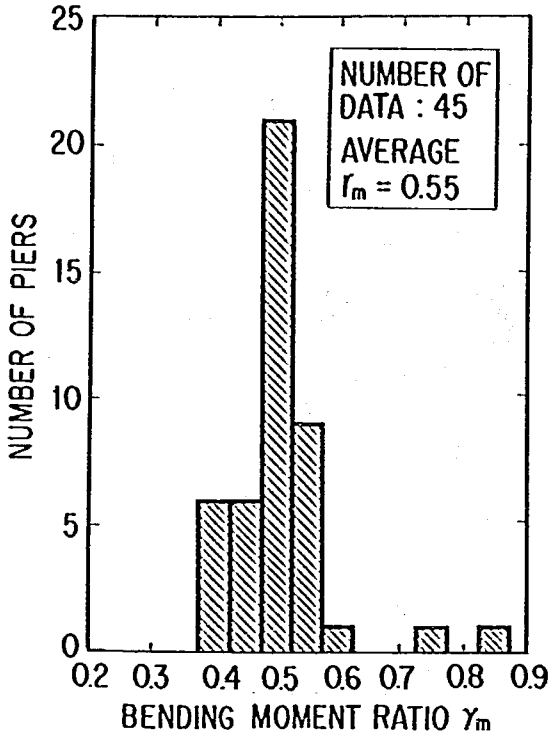


Fig. 2 Distribution of Bending Moment Ratio of Actual Bridge Piers Surveyed

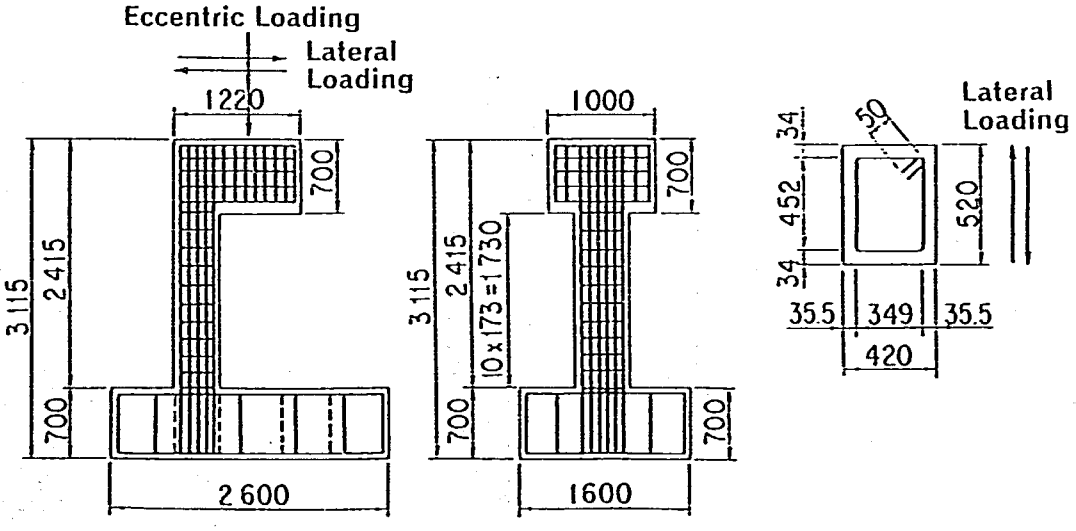


Fig. 3 C–Shaped Bridge Pier Model for Shaking Table Test

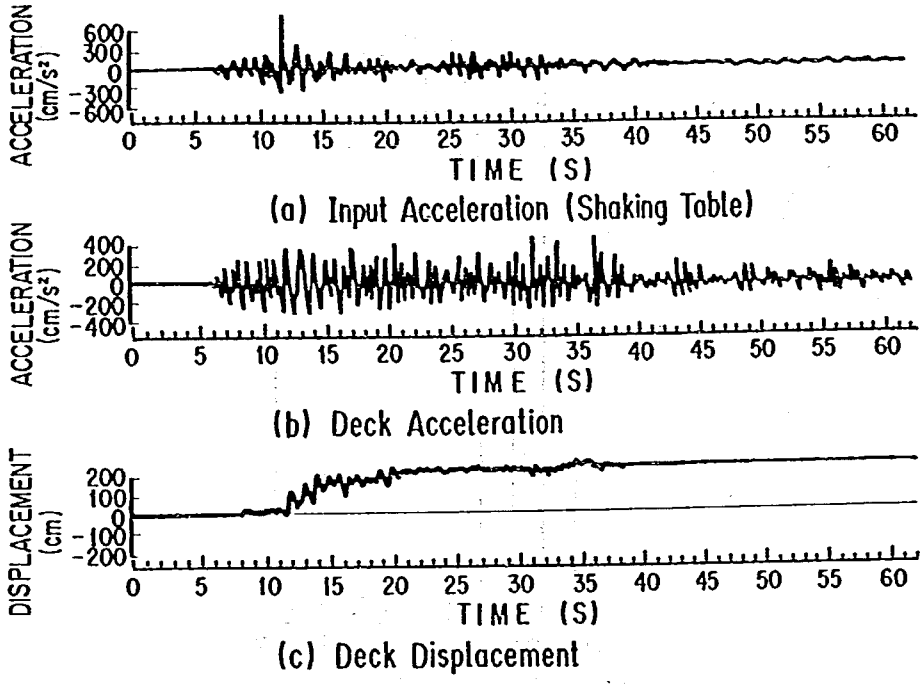


Fig. 4 Response Accelerations and Displacement

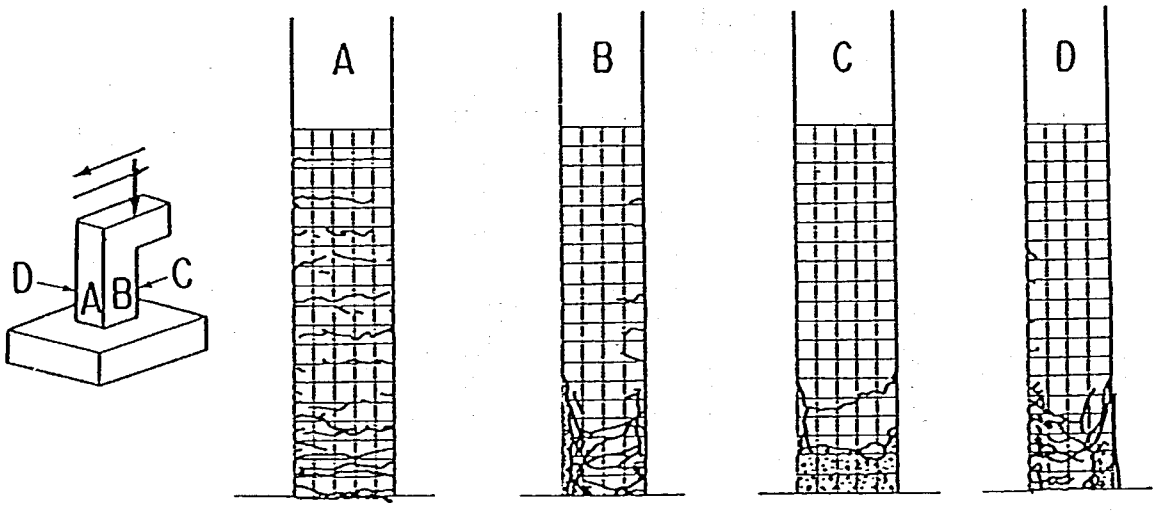


Fig. 5 Failure Mode of the Pier Model after Excitaion by Shaking Table

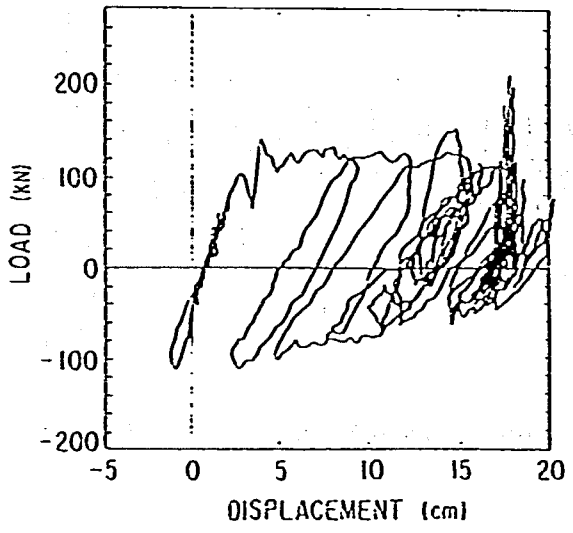


Fig. 6 Hysteresis Loop of load–displacement relation obtained through Shaking Table Test

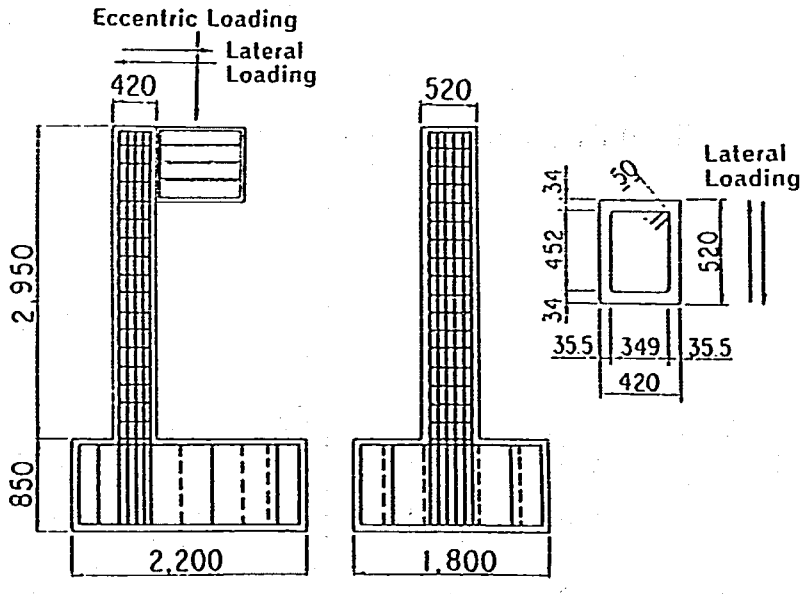


Fig. 7 C–Shaped Bridge Pier Model for Dynamic Loading Tests

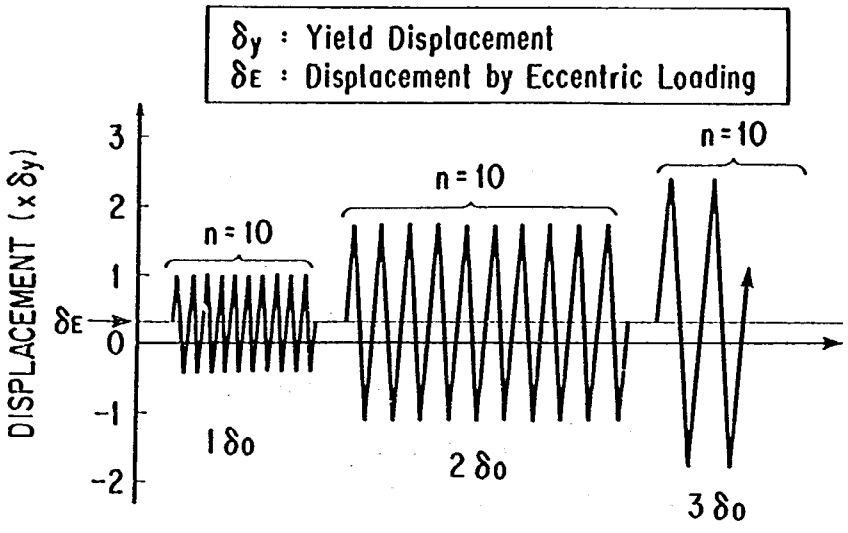


Fig. 8 Loading Pattern of Displacement for Dynamic Loading Tests

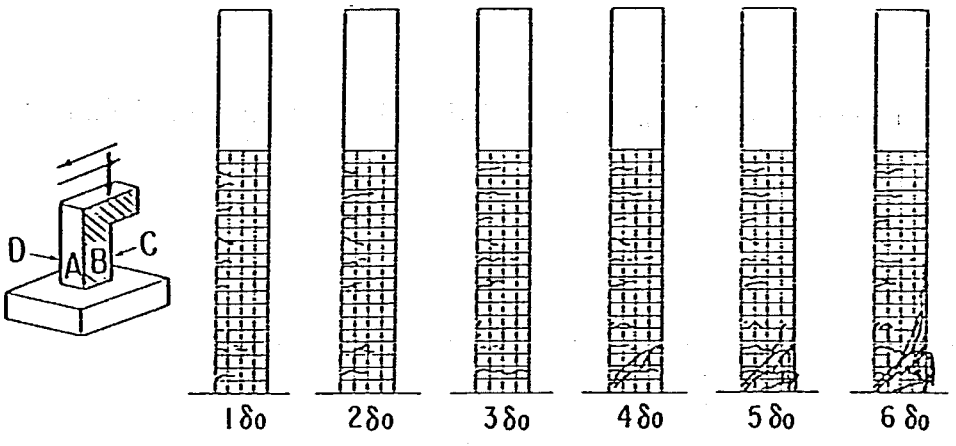


Fig. 9 Failure Mode of P–62 (r_M=0.55)

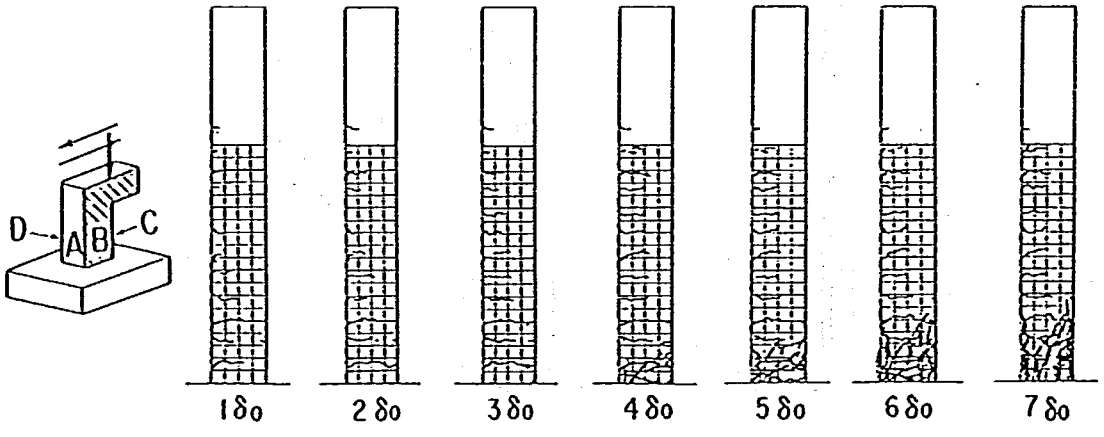


Fig. 10 Failure Mode of P–60 (r_M=0.69)

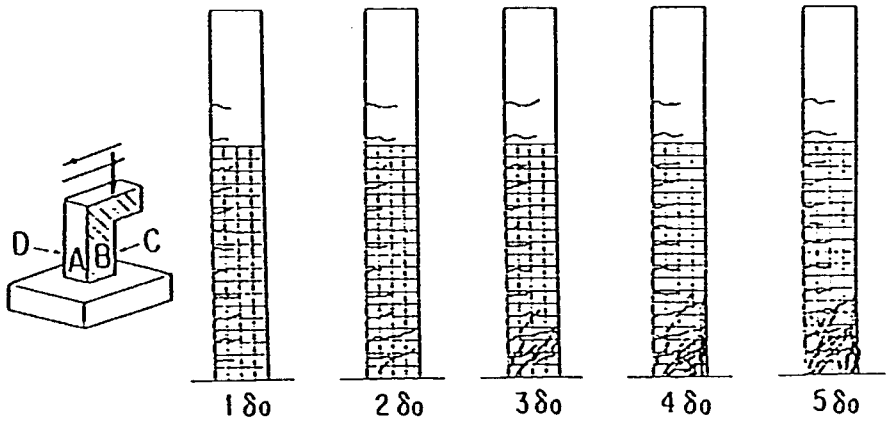


Fig. 11 Failure Mode of P–64 (r_M=0.59)

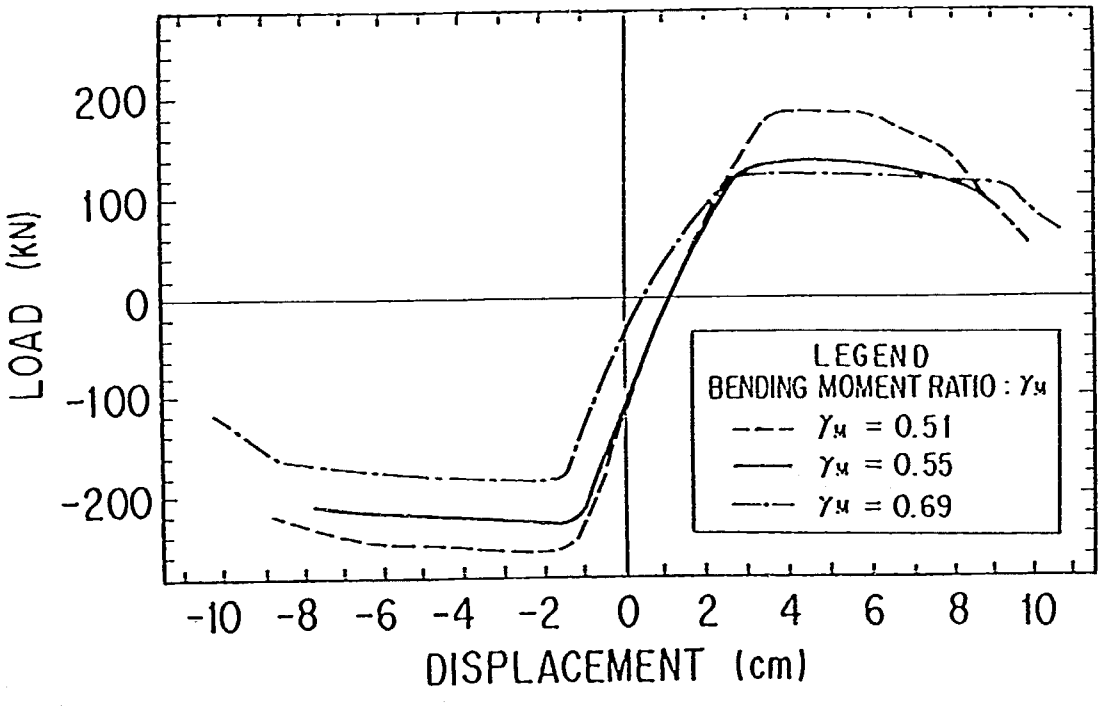


Fig. 12 Effect of Bending Moment Ratio r_M on Load–Displacement Relation

Menshin Design of Highway Bridges in Japan

Kazuhiko KAWASHIMA
and
Shigeki UNJOH

3rd U.S.–Japan Workshop on
Earthquake Protective Systems for Bridges
Berkeley, U.S.A.
January, 1994

MENSHIN DESIGN OF HIGHWAY BRIDGES IN JAPAN

Kazuhiko Kawashima[1] and Shigeki Unjoh[2]

1) Head, Earthquake Engineering Division, Public Works Research Institute, Ministry of Construction, Tsukuba Science City, Japan
2) Senior Research Engineer, ditto

ABSTRACT

This paper presents the back ground of seismic isolation of highway bridges in Japan. The Menshin Design which emphasis to reduce deck response by increasing energy dissipating capability and to distribute seismic lateral force of deck to as many substructures as possible is presented. Design guidelines for the Menshin Design and its implementation are described. A new joint research program on Development of New Materials and Passive and Active Control of Long-span Bridges is introduced.

INTRODUCTION

The technology for reducing bridge response has been adopted for long time in Japan (Ref. 1). It has been used from short and medium size bridges to long span bridges. Viscous damper is one of the most typical examples of such technologies (Refs. 2 and 3). It has been successfully adopted to distribute the lateral force to several substructures. The viscous damper provides a resistive force when subjected to a high-velocity motion such as the one encountered during an earthquake, while it does not offer the resistive force to low-velocity motion such as the deck motion caused by temperature change. Hence, by providing the viscous damper the seismic lateral force can be more evenly carried by many columns without constraining deck elongation and shrinkage due to temperature change.

The SU Damper is also an outcome of technical development for reducing bridge response (Ref. 4). It consists of friction bearing and prestressed strand connecting columns and a deck. By adjusting the prestressing of the strand, natural period of the deck is controlled. The strand also prevents the excessive relative displacement of the deck. The friction bearing dissipates the energy so as to increase the damping of the bridge.

Various dampers have also been developed for long span bridges. A special type of vane-damper was adopted to Higashi Kobe Bridge (Ref. 5) and Tsurumi Fairway Bridge

(cable stayed bridges). A device to control the natural period and to increase energy dissipation was adopted at Hituishi–Iwaguro bridge (cable stayed bridge) of the Honshu–Shikoku Bridge (Ref. 6).

Base isolation (Refs. 7–10) has been highlighted in Japan as a new technology to reduce seismic response of structures. Special interest was due to the fact the energy dissipation is made by bearings and that compact ruminated rubber bearing such as LRB is available. Various high damping rubber bearings (HDR) have also been developed. Although various dampers have been successfully adopted for long time as describe above, it requires to install dampers in addition to bearings. Maintenance of dampers requires some special attention in addition to the usual maintenance. Some space on the pier crest is also occupied by the dampers. It is good from such maintenance and space point of view to adopt the compact type of bearings with energy dissipating capability such as LRB and HDR. Furthermore, it matches with the trend that rubber bearings should be more used. Existing steel bearings cause problem due to corrosion.

One more important motivation to adopt the seismic isolation is that it becomes possible to construct multi–span continuous bridges. The expansion joints cause vibration and noise pollution, and are not comfortable to drivers. They need to be replaced frequently, and this often causes traffic congestion. Therefore although simply supported girder bridges or two and three span continuos girder bridges have been frequently constructed, such trend needs to be changed. Super multi–span continuous bridges with as long continuos deck as possible are required. For such purpose, LRB and HDR are effective. Because the lateral stiffness of LRB and HDR is small, it absorbs the deck elongation and shrinkage due to temperature change.

Based on those considerations, the seismic isolation is considered promising for highway bridges. However, there are various unique environmental and natural conditions that the occurrence of an earthquake with magnitude over 8 is much frequent and the ground is generally much softer in Japan as compared with in New Zealand, U.S.A. and Italy where many seismic isolated bridges have been constructed, specific researches and technical developments are required in Japan. Based on such technical development, the Menshin Design which is slightly different with the seismic isolation was developed, and is being adopted.

This paper describes the history of the technical development in seismic isolation of highway bridges, and the state of the art of the Menshin Design and its implementation.

PAST TECHNICAL DEVELOPMENT FOR SEISMIC ISOLATION

Guidelines for Seismic Isolation Design of Highway Bridges

For studying the application of seismic isolation to highway bridges, a committee chaired by Professor Tsuneo Katayama, University of Tokyo, was formed through 1986 to 1989 at the Technology Research Center for National Land Development, which was the first major activity to study the seismic isolation of highway bridges in Japan. Three programs were studied in the committee, i.e., 1) survey of seismic isolation devices which can be used for highway bridges, 2) study on the key points of the seismic isolation design of highway bridges, and 3) trial designs of seismic isolated highway bridges. As the final accomplishments of the three year study, "Guidelines for Seismic Isolation Design of Highway Bridges" was published in 1989 (Ref. 11).

Pilot Construction Program of Menshin Bridges

Five highway bridges were constructed as a pilot program under the supervision of the Ministry of Construction to verify the effectiveness and performance of the seismic isolation (Ref. 1). A working group was formulated in the Ministry of Construction to supervise the design and construction. Because the Menshin Design was being developed by the Joint Research which will be described later, it was adopted in the design. Miyagawa Bridge in Shizuoka-ken was completed in March 15, 1991 as the first Menshin highway bridge in Japan (Ref. 12).

Joint Research on Menshin Bridges between PWRI and 28 Companies

A three-year joint research program on the Menshin Design of Highway Bridges was made between Public Works Research Institute and twenty eight companies since July 1989. The goal of the program was to develop the Menshin Design method and the new Menshin devices for highway bridges. Table 1 shows the research items and the contribution of each organization.

There were four research topics in the joint program:

1)Development of new Menshin devices

The Menshin devices for highway bridges need to be compact and weather-proof since they are installed at narrow pier crests exposed to weathering condition. Ten new devices in total were developed in the program. Among them, 4 high damping rubber bearings (HDR) (Ref. 13), 2 sliding Menshin devices with HDR (Ref. 14), and a roller Menshin device with HDR (Ref. 15) seem promising for application. All Menshin devices developed were tested with use of the dynamic loading system at PWRI under the same loading conditions developed in the program (Ref. 16).

2)Development of expansion joints and restrainers

A knock–off mechanism at an abutment to reduce the impact force induced by the collision between a deck and an abutment (Ref. 17), and a finger expansion joint which is distinguished from the regular finger joints by the transverse movement (Ref. 18), were developed. A special restrainer which absorbs the energy and allows the deck to move in two lateral directions was developed (Ref. 19).

3)Development of Menshin Design method

Taking into account the high seismic activity and the soft soil condition, the Menshin Design method was developed as will be described later.

4)Application of Menshin design

It was found that the Menshin Design can be effectively used to construct super–multi–span continuous bridges with deck length of 1 km (Ref. 20). Connection of existing simple supported girders to reduce the number of expansion joints, and retrofitting of existing bridges to increase the seismic safety by using Menshin Design were studied (Ref. 21).

The final accomplishment of the program was complied in March 1992 as the " Manual of Menshin Design of Highway Bridges" (Refs. 22 and 23).

MENSHIN DESIGN

Although the elongation of natural period and the increase of energy dissipation capability of a structure are key factors in seismic isolation, the elongation of fundamental natural period is not easily achieved for bridges in Japan from various reasons.

First reason is the soft soil condition. Because most of the populated areas are located on alluvial fan deposits, soils are very weak. Second reason is the high seismicity accompanying earthquakes with magnitude over 8 (Ref. 24). Large earthquakes in magnitude produce a ground motion predominant in long period (Ref. 25). Reflecting these environmental and natural conditions, the conservative lateral force coefficients as shown in Figs. 1 and 2 have been adopted in seismic design of highway bridges (Ref. 26).

Third reason is difficulty to widen the clearance between decks, and between the deck and abutment. The increase of natural period produces a large relative displacement between the deck and the substructures, and requires special expansion joints which absorb large relative displacement. From the demand of driving comfort, maintenance problems and noise and vibration pollution, every efforts are now directed to reduce the clearance at

expansion joints. Because even regular expansion joints currently used cause considerable problem, the increase of gap clearance can not be incorporated.

Fourth reason is the evaluation on collision developed either between abutment and deck or between adjacent decks. When enough clearance is not provided, collision would take place. In fact, collision took place in the past earthquakes (Ref. 27). It is known from these past experiences that collision did not cause critical structural problems although expansion joints were often badly damaged (Ref. 28 and 29). On the contrary, collision dissipates energy. From experiment and analysis, it is effective to constrain the deck response by collision at small deck displacement (Ref. 30). From these reasons, it is superior not to provide a large gap so as to allow the large relative displacement of deck. A little bit larger gap than the normal gap.

Based on these considerations, it seems preferable not to intentionally increase natural period and not to widen the gap clearance at joints. Instead of intentional increase of natural period, combination of increase of energy dissipating capability and distribution of seismic lateral force to as many substructures as possible is preferred in highway bridges. It may be effective to adjust the natural period of bridges so as to avoid the resonance with ground motion. This is an extension of the existing seismic design approach which has been adopted in highway bridge in Japan. The design concept in which bridges are designed taking advantage of the increase of energy dissipating capability and the distribution of seismic lateral force is proposed to be referred as "Menshin Design(免震)" (Refs. 22 and 1).

Followings are the basic principles of Menshin Design for highway bridges with ordinary span length:

1) Seismic lateral force should be distributed to as many substructures as possible. The seismic lateral seismic force should be reduced by increasing the energy dissipating capability with use of Menshin bearings.

2) The natural period of bridges should be not be forcibly elongated, but adjusted so as to avoid the resonance with a ground motion.

3) Gap at expansion joints should not be so widened.

4) The Menshin Design should be adopted only at the site with stable soil behavior. The site vulnerable to soil liquefaction and other type of failure should be avoided.

5) The Menshin Design is encouraged to construct super–multi–span continuous bridges.

MENSHIN DESIGN METHOD

Manual of Menshin Design

The Manual for Menshin Design of Highway Bridges was developed as the final accomplishment of the 3 year joint research program between the Public Works Research Institute and 28 companies (Ref. 22). Although this is not the mandate specifications, it is recommended to consider the basic requirements of the Manual in addition to the Design Specifications of Highway Bridges (Ref. 26). The Manual consists of 9 chapters and 10 appendices. The table of contents is presented in the appendix.

The mandate specification for Menshin Design is being formulated at the Menshin Design Working Group, the Seismic Design Subcommittee of the Bridge Committee, Japan Road Association, based on the Manual of Menshin Design of Highway Bridges. Because seismic performance of Menshin bridges has not yet fully confirmed through seismic experience in the past earthquakes, at the design seismic lateral force is not allowed to reduce from the value specified by the Design Specifications of Highway Bridges. Since various data are being accumulated on the seismic performance of the Menshin bridges, it is expected to reduce the seismic lateral force in the new specifications.

Idealization

In Menshin Design, bridges are designed by following the standard static design method (static frame analysis). Precise evaluation of seismic safety is made by the dynamic response analysis. In such analysis, the Menshin devices are idealized by as a set of equivalent linear springs. Equivalent stiffness and the equivalent damping ratio of the isolator and damper are the major parameters used in the analysis. In the static frame analysis, natural period of the bridge can be computed for each seismic design structural unit as :

$$T = 2.01\sqrt{\delta} \tag{1}$$

$$\delta = \frac{\int w_i \cdot u_i^2}{\int w_i \cdot u_i} \tag{2}$$

where

T : natural period (sec)

w_i : dead weight (tf/m) of the seismic design structural unit (superstructure and substructure above the ground surface assumed in seismic design) at point "i"

u_i : lateral displacement (m) developed in the seismic design structural unit at point "i" when subjected to w_i in the direction considered in design

Damping ratio of the bridge is computed as

$$\left.\begin{aligned} h &= \frac{\sum K_{Bi} \cdot u_{Bi}^2 \cdot c_{hi}}{\sum K_{Bi} \cdot u_{Bi}^2 \cdot c_i} \\ c_{hi} &= h_{Bi} + \frac{h_{Pi}}{K_{Pi}} + \frac{h_{Fui}}{K_{Fui}} + \frac{h_{F\theta i} \cdot H^2}{K_{F\theta i}} \\ c_i &= 1 + \frac{K_{Bi}}{K_{Pi}} + \frac{K_{Bi}}{K_{Fui}} + \frac{K_{Bi} \cdot H^2}{K_{F\theta i}} \end{aligned}\right\} \quad (3)$$

where

h : modal damping ratio of bridge
h_{Bi} : damping ratio of i–th damper
h_{Pi} : damping ratio of i–th pier/abutment
h_{Fui} : damping ratio of i–th foundation associated with translational movement
$h_{F\theta i}$: damping ratio of i–th foundation associated with rotation
K_{Pi} : equivalent stiffness of i–th pier/abutment
h_{Fui} : translational stiffness of i–th foundation
$K_{F\theta i}$: rotational stiffness of i–th foundation
u_{Bi} : design displacement of i–th menshin device
H : height from the bottom of pier to the gravity center of deck

Eq.(3) gives the approximate estimation of the damping ratio of a bridge. When mode shapes are computed, the modal damping ratio may be computed as

$$h = \frac{\sum_{j=1}^{n} \phi_{ij}^T \cdot h_j \cdot k_j \cdot \phi_{ij}}{\phi_i^T \cdot K \cdot \phi_i} \quad (4)$$

where

ϕ_{ij} : mode vector of j–th structural component for i–th mode
h_j : damping ratio of j–th structural component
k_j : stiffness matrix of j–th structural component
ϕ_{iT} : mode vector of bridge for i–th mode
K : stiffness matrix of bridge.

Table 2 shows the damping ratio recommended for structural component Eqs.(3) and (4).

Design Force

Menshin devices are designed by the seismic coefficient method (SCM) and the bearing capacity method (BCM). The allowable stress approach is adopted in the seismic coefficient method, while the bearing capacity approach is adopted in the bearing capacity method. Bridges are designed by the seismic coefficient method, and then the ductility of reinforced concrete piers is checked by the bearing capacity method.

In the seismic coefficient method, the design lateral force coefficient is given as

$$k_h = c_Z \cdot c_G \cdot c_I \cdot c_T \cdot c_E \cdot k_{h0} \geqq 0.1$$
$$c_T \cdot c_E \geqq 0.8 \qquad (5)$$

where

c_Z : modification factor for zone (refer to Fig. 3)
c_G : modification factor for ground condition (refer to Table 3)
c_I : modification factor for importance (refer to Table 4)
c_T : modification factor for structural response (refer to Table 5)
c_E : modification factor for energy dissipation capability (refer to Table 6)
k_{h0} : standard design horizontal seismic coefficient (=0.2)

The modification factors c_Z, c_G, c_I and c_T are specified in the Design Specifications of Highway Bridges (Ref. 26). The modification factor c_E takes a value shown in Table 6 depending on the modal damping ratio of the bridge in the fundamental mode. The design lateral force is reduced as large as 20%.

In the bearing capacity method, the lateral force coefficient khc and the equivalent lateral force coefficient khe are given as

$$k_{he} = \frac{k_{hc}}{\sqrt{2\mu - 1}} \qquad (6)$$

$$k_{hc} = c_Z \cdot c_I \cdot c_R \cdot c_E \cdot k_{hc0} \geqq 0.3 \qquad (7)$$

where

c_Z : modification factor for zone (refer to Fig. 3)
c_I : modification factor for importance (refer to Table 4)
c_R : modification factor for structural response (refer to Table 7)
c_E : modification factor for energy dissipation capability (refer to Table 8)
k_{hc0} : standard lateral force coefficient for bearing capacity method (=1.0)
μ : allowable ductility factor of reinforced concrete piers

The modification factors c_Z, c_I, and c_R are specified in the Seismic Design

Specifications of Highway Bridges. The modification factor c_E depends on the modal damping ratio of the bridge, and takes a value of Table 8. The design force is reduced as large as 30%.

Design of Isolators and Energy Dissipators

In design of isolators and energy dissipators, the design displacement of menshin device u_B, the equivalent stiffness K_B and the equivalent damping ratio h_B of the Menshin device are the key factors.

The design displacement of Menshin device u_B is evaluated as

$$u_B = \frac{k_h \cdot W_u}{K_B} \quad \text{(S.C.Method)} \tag{8}$$

$$u_B = \frac{k_{hc} \cdot W_u}{K_B} \quad \text{(B.C.Method)} \tag{9}$$

where

k_h : lateral force coefficient by Eq.(5)
k_{hc} : lateral force coefficient by Eq.(7)
K_B : equivalent stiffness (tf/m) of Menshin device
W_u : weight of the superstructure (tf) supported by the Menshin device

Requirements for Dynamic and Static Load

Various requirements for the devices against static load and dynamic load are described in the Manual. It is unique that precise loading test procedures for both dynamic and static loads are described in the Manual. Some of the important requirements for dynamic load is as:

1) Menshin devices have to be designed and fabricated so that their equivalent stiffness k_B and equivalent damping ratio h_B be within $\pm 20\%$ of the design values.

2) Menshin devices have to be stable against 50 cycles of harmonic loading with design displacement of u_B given by Eq.(9).

3) Deck should return to the rest position even after it was subjected to a large earthquake. The residual displacement u_{BR} developed in menshin devices after it is smoothly released from the deformed displacement of given by Eq.(9) needs to satisfy.

$$u_{BR} \leqq 0.1 \cdot u_B \qquad (10)$$

4) The equivalent stiffness and the equivalent damping ratio of menshin devices need to be stable against the change of load condition at normal time, change of natural environment such as the temperature change and earthquake-induced cyclic loading. Stability has to be examined for 1) cyclic loading associated with the elongation and shrinkage of deck due to temperature change and traffic load, 2) effect of loading hysteresis, 3) variation of vertical loading, 4) effect of loading rate, 5) effect of pre-deformation due to creep and shrinkage, 6) direction of excitation, and 7) change of the equivalent stiffness and the equivalent damping ratio depending on the temperature change.

On the other hand, major requirements for static load include :

1) Materials and mechanism of the menshin devices need to give credit to long term use. They need to be stable against the daily and annual cyclic elongation and shrinkage of deck due to the temperature change.

2) The menshin devices need to be stable against local shear strain. Check of the local shear strain needs to be made in accordance with the Design Guidelines of Bearings (Ref. 35).

3) In the rubber-type menshin devices, the creep of rubber which would be developed for the life time of bridges in vertical direction due to the dead weight of superstructure needs not to exceed 5% of the total thickness of rubber.

4) The equivalent stiffness of menshin device at −10℃ need not to exceed 1.5 time the equivalent stiffness at 40℃.

IMPLEMENTATION OF MENSHIN DESIGN

Table 9 shows the directory of Menshin bridges which were completed or are under construction. There are over 30 bridges under design and planning stage. It should be noted that as describe above because the seismic lateral force is not allowed at this stage to reduce from the value specified in the Design Specifications of Highway Bridges, some bridges which merely adopted Menshin bearings are included in Table 9. From the same reason, Menshin bearings have been adopted for most of existing bridges as a tool which enables to make simply supported girders continuous. Although the seismic retrofit was not the official reason for adopting the Menshin bearings, the seismic retrofit effect is of course expected in addition to make the deck continuous.

The Road Bureau of the Ministry of Construction compiled in June 1993 a technical development program which is required to challenge toward 21 century (Ref. 34). Seventy four technologies were identified as essential, and the further development of the Menshin Design is included as a technology required to mitigate road environment. Obviously effectiveness of constructing super-multi-span bridges to reduce noise and vibration pollution is highly expected in the Menshin Design. The Ministry of Construction is now intending to effectively use the Menshin Design technology which enables to construct super-multiple-continuous bridges which are advantageous for road environment and enough seismic safety.

Typical implementation of the Menshin Design is as follows. The first Menshin bridge in Japan is Miyagawa Bridge as shown in **Photos 1** and **2**, Shizuoka-ken. It was completed in March 1991. A series of forced excitation tests using an eccentric mass-shaker and quick-release hydraulic jacks were conducted as shown in **Photos 1** and **2** to verify the design. Strong motion observation has been made since the completion, and an analysis of the first data was made (Ref. 31).

Photo 3 shows Yama-age Bridge in Tochigi-ken (Ref.32). This was the first Menshin bridges utilizing high damping rubber bearings. Superstructure is of 6-span post-tensioning prestressed concrete box girder with deck length of 246.3m. Forced excitation tests using an eccentric mass-shaker and quick-release hydraulic jacks were made.

Photo 4 shows On-netoh Bridge on National Highway No.44 in Hokkaido. this bridge experienced a significant shaking during the Kushiro-oki Earthquake in January 1993. The peak acceleration of about 360 cm/sec^2 was induced on the ground surface near the bridge. No damage was developed due to the earthquake. The relative displacement at the bearings in longitudinal direction was only 2 to 2.5 cm. This earthquake provided as important data on the response of a Menshin bridge in cold area. Because temperature dependence of LRB was precisely investigated in laboratory (Ref. 33), a precise analysis is expected.

Photos 5 and **6** show Higashi-ohgi-shima Viaduct with 9-span continuous prestressed concrete girder on Metropolitan Expressway and Matsuno-hama Viaduct with 4-span continuous steel box girder on Hanshin Expressway, respectively. The forced excitation tests were also made for these bridges and the dynamic characteristics of Menshin bridges were investigated.

A unique application of Menshin Design is the O-hito Viaduct which is under construction in Shizuoka-ken as a part of the Izu Crossing Highway. The bridge is of 29-span

continuous prestressed concrete girder with deck length of 725m.

Menshin design has been applied for the jointless system and seismic strengthening of existing simply-supported girder bridges. Photo 7 shows the replacement of existing steel bearings by LRB.

A NEW JOINT RESEARCH FROGRAM ON SEISMIC CONTROL OF LONG-SPAN BRIDGES

A new three-year joint research program on "Development of Seismic Control Systems of Long-Span Bridges" was initiated from October 1993. This research is being made jointly between the Public Works Research Institute, Public Works Research Center and 19 companies. The Public Works Research Center is a foundation belonging to the Public Works Research Institute.

This research is directed to develop a new passive and active control technologies and to use intelligent materials for long-span bridges. As the post Honshu-Shikoku Bridge Project, new bridge construction with center span length over 2 km is being considered. In the technical development program of the Road Bureau of the Ministry of Construction, development of seismic design method for long-span bridge is included as one of the 74 key technologies. Passive and active control technologies for new types of structures are the key issue. The joint research is intended to support this technical development.

The research program includes the following three topics.

1) Development of New Materials and Passive and Active Control
   It is intended to effectively use new materials such as super low-yield strength metals, super plastic rubbers, super high damping rubbers and rheological fluid. They may be used to produce energy dissipators for various purpose. Intelligent dampers, a tuned liquid damper and an intelligent knock-off device are to be developed.

2) Development of New Control Design Method
   Depending on new materials and passive and active control developed in 1), new controlling methods need to be developed. Accurate evaluation method of damping of structure which use new materials and controlling devices, and optimum control points are to be investigated.

3) Application to Bridges
   Various application of the new materials and controlling systems can be considered. Application of the controlling systems to substructures, high piers, suspended slabs,

cable stayed bridges and suspension bridges are studied. Application of active control of bridges during construction stage is promising.

Table 10 shows the research objectives and the contribution of each organization. The 19 companies include material makers, bearing supports fabricators, consulting engineering companies, steel bridge fabricators and general contractors.

CONCLUDING REMARKS

Seismic isolation expanded the freedom of design and construction practice of highway bridges. It has been used as a tool to construct super–multi–span continuous bridges, curved and skewed bridges capable to move in two horizontal directions and seismic strengthening. Data on bridge response through forced excitation tests, shaking table tests, loading tests of energy dissipators and isolators, strong motion observation and seismic excitation are being accumulated. It was very important that On–netoh bridge located close to the fault of Kushiro–oki Earthquake in January 1993 behaved quite well. Through the analysis of those data, the seismic response of Menshin bridges is being verified.

Implementation of the Menshin Design is being made throughout the country. The Menshin Design was applied to 15 new bridges and 8 existing bridges. A number of bridges are being designed and planned.

A new three–year joint research was initiated among PWRI, PWRC and 19 companies to develop new materials and passive and active control systems for long–span bridges. New innovative materials and systems are studied in the program. It is expected to develop new materials, dampers, controlling algorithm and application.

REFERENCES

1) Kawashima, K., Hasegawa, K., and Nagashima, H. : A Perspective of Menshin Design for Highway Bridges in Japan, Proc. 1st U.S.–Japan Workshop, September 1991
2) Oseki, J. : Shear Viscous Damper – Application to Design of Multi–span Continuous Bridges –, Bridges and Foundation, 1980 (in Japanese)
3) Fukuoka, S. : Design of Multi–span Continuous Highway Bridges with Use of Shear Viscous Damper, Bridges and Foundations, 1980 (in Japanese)
4) Okamoto, S. and Uemae, Y. : Aseismic Bridge Structure by Elastic Supports Using Tie Members (SU Damper Method), Proc. Symposium on New Ideas in Structural Design, Japan Society of Civil Engineers and Architectural Institute of Japan, 1963 (in Japanese)
5) Kitazawa, M., Ishizaki, H., Emi, S. and Nishimori, K. : Characteristics of Earthquake Responses and Design of Aseismic Design on the Long–period Cable–stayed Bridge

(Higashi–Kobe Bridge) with All Movable Shoes in Longitudinal Direction, Proc. Japan Society of Civil Engineers, No. 422/I–14, October 1990 (in Japanese)
6) Kanemitsu, H. and Higuchi, K. : Displacement Control of Bridges with Suspended Girder, Technical Report of the Honshu–Shikoku Bridge Authority, 1981 (in Japanese)
7) Buckle, I. G. and Mayes, R. L. : Seismic Isolation:History, Application and Performance –A World View, Earthquake Spectra, Vol. 6, No. 2, May 1990
8) McKay, G. R., Chapman, H.E. and Kirkcaldie, D. K. : Seismic Isolation : New Zealand Application, Earthquake Spectra, Vol. 6, No. 2, May 1990
9) Skinner, R. I., Tyler, R. G., Heine, A. J. and Robinson, W. H. : Hysteresis Dampers for the Protection of Structures from Earthquakes, Proc. New Zealand – Japan Workshop on Base Isolation of Highway Bridges, Wellington, New Zealand, December 1987
10) Billings, I. J. and Kirkcaldie, D. K. : Base Isolation of Bridges in New Zealand, Proc. New Zealand – Japan Workshop on Base Isolation of Highway Bridges, Wellington, New Zealand, December 1987
11) Technology Research Center for National Land Development : Guidelines for Design of Base–isolated Highway Bridges, Final Report of Base Isolation to Seismic Design of Highway Bridges (Chairperson : Professor T. Katayama), March, 1989 (in Japanese)
12) Matsuo, Y., and Hara, K.: Design and Construction of Miyagawa Bridge, 1st U.S.–Japan Workshop, September 1991.
13) Suizu, Y. and Sudoh, C. (Part 1), Kawashima, K., Koshitoge, M., Endo, K., Yamada, C., and Nishimoto, T. (Part 2), and Nishikawa, I., Katoh, M., Itoh, M., and Muramatsu, Y. (Part 3): Development of High Damping Rubber Bearing for Menshin Design, 1st U.S.–Japan Workshop, September 1991
14) Iguchi, T.: Development of a Sliding Friction Damper, 1st U.S.–Japan Workshop, September 1991
15) Takaku, T., Shimada, M., Tsumura, N. and Izuma, S. : Development of Roller Type Bearing for Menshin Bridges, 1st U.S.–Japan Workshop, September 1991
16) Kawashima, K., Makiguchi, K., Suizu Y., and Endo, K. : Approving Test Procedure for Menshin Devices, 2nd U.S.–Japan Workshop, December 1992
17) Goto, Y., Kikuchi, T., Kimishima, T., Matsumoto, F., Ozaki, D., and Tsukamoto, A. : Development of Expansion Joint, Stopper and Knock–off Abutment for Menshin Bridges, 2nd U.S.–Japan Workshop, December 1992
18) Kimishima, T., Harada, H., and Ozaki, D.: Development of Finger Joint Movable in Horizontal Directions for Menshin Bridges, 1st U.S.–Japan Workshop, September 1991
19) Ozaki, D., and Matsumoto, F.: Development of Falling–off Prevention Devices for Menshin Bridges, 1st U.S.–Japan Workshop, September 1991
20) Goto, Y., Tokunaga, M., Yoshimura, T., and Sintaku, M.: Seismic Response of Multi–span Continuous Bridge with Deck Length of 1 km, 1st U.S.–Japan Workshop, September 1991
21) Yamaguchi, M., Makiguchi, Y., Kawasaki, I.: Application of Menshin Design to Seismic

Retrofit of Existing Bridges by Connecting Concrete Slabs of Adjacent Girders, 1st U.S.–Japan Workshop, September 1991
22) Public Works research Institute and 28 Companies: Manual of Menshin Design of Highway Bridges, March 1993, Technical Note, No. 60, Public Works Research Institute (in Japanese)
23) Kawashima, K. : Manual for Menshin Design of Highway Bridges, Proc. 2nd U.S.–Japan Workshop, December 1992
24) Arakawa, T. and Kawashima, K.: Seismicity and Maximum Possible Earthquake around Japan for Application to Seismic Risk Analysis, Technical Memorandum, Vol. 2098, Public Works Research Institute, March 1984 (in Japanese)
25) Kawashima, K., Aizawa, K. and Takahashi, K. : Attenuation of Peak Ground Motions and Absolute Acceleration Response Spectra, Report of PWRI, Vol. 166, Public Works research Institute, September 1985 (in Japanese)
26) Japan Road Associations : Design Specifications for Highway Bridges – Part V Seismic Design –, February 1990 (in Japanese)
27) Public Works Research Institute : Report on the Disaster Caused by the Miyagi–ken–oki Earthquake of 1978, Vol. 159, March 1983 (in Japanese)
28) Williams, D. and Godden, W. G. : Experimental Model Studies on the Seismic Response of High Curved Overcrossings, Report No. EERC 76–18, Earthquake Engineering Research Center University of California, Berkeley, 197
29) Kawashima, K. and Penzien, J. : Correlative Investigation on Theoretical and Experimental Dynamic Behavior of A Model Bridge Structure, Report No. EERC 76–26, Earthquake Engineering Research Center, University of California, Berkeley, 1976
30) Kawashima, K., Hasegawa, K. and Nagashima, H. : Experiment and Analysis on Seismic Response of Menshin Bridges, 1st U.S.–Japan Workshop, September 1991
31) Kawashima, K., Nagashima, H., Masumoto, S. and Hara, K.: Response Analysis of Miyagawa Bridges based on a Measured Acceleration Record, 2nd U.S.–Japan Workshop, December 1992
32) Uzuka, T., Kawakami, K., Kumakura, K. and Tani, H.: Menshin Design and Construction of Multi–span Continuous Prestressed Concrete Bridge, 2nd U.S.–Japan Workshop, December 1992
33) Nakano, O., Nishi, H., Shiroi, T. and Kumagai, K. : Temperature Dependency of Base Isolated Bearings, 2nd U.S.–Japan Workshop, December 1992
34) Road Bureau of Ministry of Construction: Five–year Technical Development Program–Challenge to New Possibility toward 21th Century–, June 1993 (in Japanese)
35) Japan Road Association : Guide–Specification of Design of Bearings, July 1991 (in Japanese)

Note

1) 1st U.S.–Japan Workshop : Proc. 1st U.S.–Japan Workshop on Earthquake Protective Systems of Bridges, Buffalo, New York, U.S.A., September 1991, Technical Report NCEER 92–0004, National Center for Earthquake Engineering Research, State University of New York at Buffalo, February 1992
2) 2nd U.S.–Japan Workshop: Proc. 2nd U.S.–Japan Workshop on Earthquake Protective Systems of Bridges, Tsukuba, Japan, Technical Memorandum, No. 3196, Public Works Research Institute, December 1992

APPENDIX

TABLE OF CONTENTS OF MANUAL FOR MENSHIN DESIGN OF HIGHWAY BRIDGES

1. General
   1.1 Scope of Application
   1.2 Definition of Terms
2. Basic Principle of Menshin Design
3. Menshin Design
   3.1 General
   3.2 Lateral Force Coefficient for Seismic Coefficient Method
   3.3 Lateral Force Coefficient and Equivalent Lateral Force Coefficient for Bearing Capacity Method
   3.4 Characteristics value for Menshin Devices
   3.5 Computation of Natural Period of Bridge
   3.6 Computation of Modal Damping Ratio of Bridges
4. Design of Menshin Devices
   4.1 Basic Principle for Design of Menshin Devices
   4.2 Design of Laminated Rubber Bearings
   4.3 Design of Lead Rubber Bearings
   4.4 Design of High Damping Rubber Bearings
   4.5 Design of Steel Dampers
   4.6 Design of Friction Dampers
   4.7 Design of Viscous Dampers
   4.8 Design of Roller Dampers
5. Dynamic Response Analysis
   5.1 General
   5.2 Dynamic Response Analysis Method
   5.3 Analytical Models
   5.4 Design Seismic Forces
   5.5 Check of Safety

6. Design Details
6.1 General
6.2 Gap between Structures
6.3 Falling–off Prevention Devices
6.4 Knock–off Devices
6.5 Details of Expansion Joints
7. Approving Tests of Menshin Devices
7.1 General
7.2 Approving Tests for Confirming Requirements for Dynamic Loads
7.3 Approving Tests for Confirming Requirements for Static Loads
8. Seismic Retrofit of Existing Bridges with Use of Menshin Design
9. Application of Menshin Design for Making Existing Simply Supported Girder Bridges Continuous

Appendices
1. Procedure of Menshin Design
2. Menshin Devices for Highway Bridges
3. References for Dynamic Response Analysis
4. Expansion Joints and Falling–off Prevention Devices for Highway Bridges
5. Design Example of Prestressed Concrete Bridges
6. Design Examples of Steel Girder Bridges
7. Design Examples of Super–multi–span Continuous Bridges
8. Design Examples for Seismic Retrofit
9. Design Examples for Making Existing Simply Supported Girders Continuous
10. Standard Acceleration Ground Motions Recommended for Dynamic Response Analysis

Table 1 Research Theme and Organizations of Joint Research Program between the Public Works Research Institute and 28 Private Firms for Developing Menshin Design Method of Highway Bridges

Research Theme	P	Ka	Si	Ob	Ku	Tn	H	Ni	Su	M	G	OR	Ti	I	Nk	Ko	Ns	Ol	Y	To	Bs	Bb	Se	Sh	Pc	J	N	Chief	Sub-Chief
1. Development of Device for Isolation																													
1.1 High Energy Absorbing Rubber Bearing								○											○	○	○			○					
1.2 Friction Damper													○									○	○						
1.3 Steel Damper								○							○													Ol	Bs
1.4 Link Bearing Develop of																	○												
1.5 Viscous Damper																		○											
1.6 Test Method	○							○							○		○	◎	○	○	○	○	○	○					
2. Development of Expansion Joint and Falling-off Prevention Device for Isolated Bridge																													
2.1 Expansion Joint				○									○															Tc	—
2.2 Falling-off Prevention Device	○												○					○											
3. Development of Design Method for Isolated Bridge																													
3.1 Design Philosophy	○	○	○	○		○						○	◎					○							○	○	○		
3.2 Dynamic Responce Analysis Method	○		○		○	◎		○			○			○													Ka	Pc
3.3 Design Method of Device for Isolation	○						○	○				◎	○		○		○	○	○	○	○	○	○	○					
3.4 Simplified Design Method	○	○	◎		○	○					○	○																	
3.5 Design Method of Expansion Joint and Falling-off Prevention Device	○			○			○								○			○							◎				
4. Application of Base Isolation to Bridge																													
4.1 Application to Prestressed Concrete Bridge	○	◎							○	○			○														○		
4.2 Application to Steel Bridge	○													○	○	○											◎	Ob	J
4.3 Application to Multiple Super-long Bridge	○			◎					○							○									○	○	○		
4.4 Application to Seismic Retrofit	○									○				○				○								◎			

P: Public Works Research Institute, Ka: Kajima, Si: Shimizu, Ob: Ohbayashi, Ku: Kumagai, Tn: Takenaka Doboku + Takenaka, H: Hazama, Ni: Nishimatsu, Su: Sumitomo, M: Mitsui, G: Goyoh, Ok: Okumura, Ti: Taisei + Tokyo Fablic + Nippon Chuzo, I: Ishikawajima Harima, Nk: NKK + Nippon Chuzo, Ko: Kobe Steel, Ns: Nippon Seiko, Oe: Oiles, Y: Yokohama Rubber, To: Toyo Rubber, Bs: Bridgestone, Bb: BBM, Se: Seibu Polymer, Sh: Showa Densen, Pc: Pacific Consultants, J: Japan Engineering Consultant, N: New Structural Engineering Consultants.

Table 2 Damping Ratio Recommended for Structural Components

Structural Components	Steel	Concrete
Super Structures	0.02～0.03	0.03～0.05
Menshin Device	Damping Ratio	
Pier/Columns	0.03～0.05	0.05～0.1
Footing	0.1～0.3	

Table 3 Modification Factor for Ground Condition c_G

Ground Group	I	II	III
c_G	0.8	1.0	1.2

Table 4 Modification Factor for Importance c_I

Group	c_I	Definition
1st class	1.0	Bridges on expressway (limited access highways), general national road and principal prefectural road. Important bridges on general prefectural road and municipal road.
2nd class	0.8	Other than the above

Table 5 Modification Factor for Structural Response c_T

Ground Group	Structural Response Coefficient c_T		
Group I	$T<0.1$ $c_T=2.69T^{1/3}\geqq 1.00$	$0.1\leqq T<1.1$ $c_T=1.25$	$1.1<T$ $c_T=1.33T^{-2/3}$
Group II	$T<0.2$ $c_T=2.15T^{1/3}\geqq 1.00$	$0.2\leqq T<1.5$ $c_T=1.25$	$1.3<T$ $c_T=1.49T^{-2/3}$
Group III	$T<0.34$ $c_T=1.80T^{1/3}\geqq 1.00$	$0.34\leqq T<1.5$ $c_T=1.25$	$1.5<T$ $c_T=1.64T^{-2/3}$

Table 6 Modification Factor for Modal Damping Ratio of Bridge c_E
(Seismic Coefficient Method)

Damping Ratio h	Modification Factor c_E
$h<0.1$	1.0
$h\geqq 0.1$	0.9

Table 7 Modification Factor for Structural Response c_R

Ground Group	Structural Response Coefficient c_R		
Group I	$T\leqq 1.4$ $c_R=0.7$		$1.4<T$ $c_R=0.876T^{-2/3}$
Group II	$T<0.18$ $c_R=1.15T^{1/3}\geqq 0.7$	$0.18\leqq T\leqq 1.6$ $c_R=0.85$	$1.6<T$ $c_R=1.16T^{-2/3}$
Group III	$T<0.29$ $c_R=1.15T^{1/3}\geqq 0.7$	$0.29\leqq T\leqq 2.0$ $c_R=1.00$	$2.0<T$ $c_R=1.59T^{-2/3}$

Table 8 Modification Factor for Modal damping Ratio of Bridge c_E
(Bearing Capacity Method)

Damping Ratio h	Modification Factor c_E
$h<0.1$	1.0
$0.1\leqq h<0.12$	0.9
$0.12\leqq h<0.15$	0.8
$0.15\leqq h$	0.7

Table 9 Directory of Menshin Bridges in Japan
(a) New Constructions

Bridge	Location	Deck Length	Administrator	Year Constructed	Super–Structure Type	Bearing Type
Onnetoh Bridge	Hokkaido	102.2m	Hokkaido Development Bureau	1993	4–Span Continuous Steel Plate Girder	LRB
Nagakigawa Bridge	Akita	97m	Noshiro Construction Office, MOC	Under Construction (1993)	3–Span Continuous Steel Plate Girder	LRB
Maruki–bashi Bridge	Iwate	92.5m	Iwate–ken	1992	3–Span Continuous Prestressed Concrete Box Girder	LRB
Yama–age Bridge	Tochigi	250m	Tochigi–ken	1993	6–Span Continuous Prestressed Concrete Box Girder	HDR
Miyagawa Bridge	Shizuoka	110m	Shizuoka–ken	1991	3–Span Continuous Steel Plate Girder	LRB
O–hito Viaduct	Shizuoka	725m	Shizuoka–ken	Under Construction	29–Span Continuous Prestressed Concrete Slab	LRB
Hirao Bridge	Yamaguchi	350m	Yamaguchi–ken	Under Construction (1993)	5–Span Continuous Prestressed Concrete Box Girder	HDR
Uehara Bridge	Nagoya	65m	Nagoya City	1991	2–Span Continuous Steel Plate Girder	LRB
Route #12 Interchange Bridge	Tokyo	136.6m	Metropolitan Expressway Public Corp.	1991	6–Span Continuous Prestressed Concrete Slab	LRB
Bay Shore Route	Tokyo	417.6m	Metropolitan Expressway Public Corp.	Under Construction (1994)	9–Span Continuous Prestressed Concrete Box Girder	LRB
Matsunohama Bridge	Osaka	211.5m	Hanshin Expressway Public Corp.	Under Construction	4–Span Continuous Steel Box Girder	LRB
Izumisano Bridge	Osaka	318m	Hanshin Expressway Public Corp.	Under Construction	6–Span Continuous Steel Box Girder	LRB
Trans Tokyo Bay	Tokyo	910m	Trans Tokyo Bay Highway Corp.	Under Construction (1994)	11–Span Continuous Steel Box Girder	HDR
Trans Tokyo Bay	Tokyo	800m	Trans Tokyo Bay Highway Corp.	Under Construction (1994)	10–Span Continuous Steel Box Girder	LRB
Karasaki Bridge	Fukushima	76.95m	Soma Kyodo Power Company Ltd.	1991	2–Span Continuous Prestressed Concrete Box Girder	HDR

Note) LRB: Load Rubber Bearing, HDR: High Damping Rubber Bearing

(b) Existing Bridges

Bridge	Location	Deck Length	Administrator	Year Constructed	Super–Structure Type	Bearing Type
Komatsukawa Route	Tokyo	120m	Metropolitan Expressway Public Corp.	Under Construction	Interconnection of Simply–Supported Girder (3–Spans)	LRB
Komatsukawa Route	Tokyo	120m	Metropolitan Expressway Public Corp.	Under Construction	Interconnection of Simply–Supported Girder (3–Spans)	LRB
Route #6	Tokyo	80m	Metropolitan Expressway Public Corp.	1992	Interconnection of Simply–Supported Girder (4–Spans)	LRB
Route #6	Tokyo	80m	Metropolitan Expressway Public Corp.	1992	Interconnection of Simply–Supported Girder (4–Spans)	LRB
Route #6	Tokyo	80m	Metropolitan Expressway Public Corp.	1992	Interconnection of Simply–Supported Girder (4–Spans)	LRB
Moriguchi Route	Osaka	90m	Hanshin Expressway Public Corp.	1991	Interconnection of Simply–Supported Girder (2and3–Spans)	LRB
Moriguchi Route	Osaka	90m	Hanshin Expressway Public Corp.	1991	Interconnection of Simply–Supported Girder (2and3–Spans)	LRB
Sakai Route	Osaka	89.5m	Hanshin Expressway Public Corp.	1993	Interconnection of Simply–Supported Girder (4–Spans)	LRB

Table 10 Research Theme and Organizations of New Joint Research Program on Seismic Control of Long-Span Bridge

Research Theme		Research Group																				
				Material Makers				Bridge Fabricaters		General Contractors							Consulting Firms					
		P	PC	OI	BS	YG	NJ	IH	KH	OB	OR	KA	KU	SU	TA	PS	OC	KC	KG	NG	PA	YE
Development of New Materials and Passive and Active Control	Application of Super Low Yield Strength Metals	○	○	○			○															
	Development of Super Plastic Rubber Dampers	○	○		○																	
	Development of Super High Damping Rubber Bearings	○	○			○																
	Development of Electro Rheological Fluid Dampers	○	○	○																		
	Development of Intelligent Knock-off Devioces	○	○							○												
	Development of Intelligent Dampers	○	○	○								○	○									
	Application of Tuned Liquid Dampers	○	○									○										
Development of New Control Design Method	Development of Evaluation Method of Damping Characteristics	○	○					○		○		○					○		○		○	○
	Optimal Control Points by Dampers	○	○					○	○						○			○			○	○
Application to Bridges	Seismic Responce Control during Construction	○	○								○											
	Development installed in Damping Materials Pavement, Curb and Handrails	○	○				○					○		○		○						
	Application to Substructures	○	○														○					
	Application to Bridges with High Pier	○	○					○	○											○		○
	Application to Suspended Slab Bridges	○	○											○		○						
	Application to Cable-Stayed Bridges	○	○							○						○		○				
	Application to Suspension Bridges	○	○																○			

P: Public Works Research Institute, PC: Public Works Research Center, OI: Oiles, BS : Bridgestone, YG: Yokohama Rubber, NJ: Shin-Nippon Steel, IH: Ishikawajima Harima, KH: Kawasaki Heavy Industry, OB: Ohbayashi, OR: Oriental, KA: Kajima, KU: Kumagai, SU: Sumitomo, TA: Takenaka, PS: PS, OC: Oriental Consultant, KC: Kaihatsu Consultant, KG: Kensetsu Gijutsu Consultant, NG: Nihon-Gijutsu Kaihatsu Consultant, PA: Pacific Consultant, YE:Yachiyo Engineering Consultant

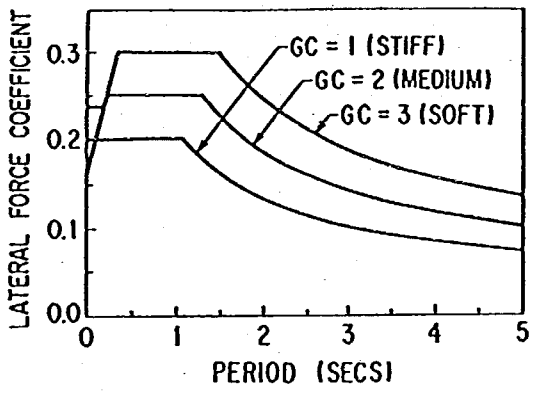


Fig. 1 Lateral Force Coefficient for Seismic Coefficient Method ($c_z = c_I = 1.0$)

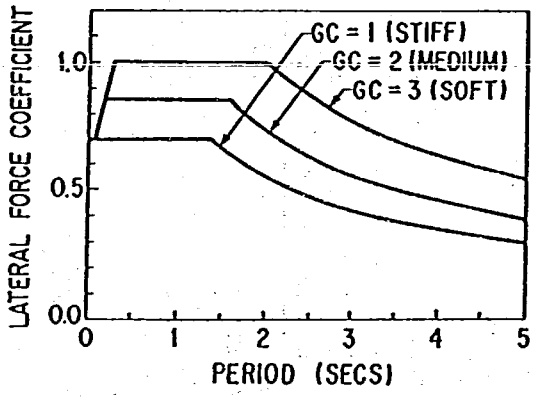


Fig. 2 Lateral Force Coefficient for Bearing Capacity Method ($c_z = c_I = 1.0$)

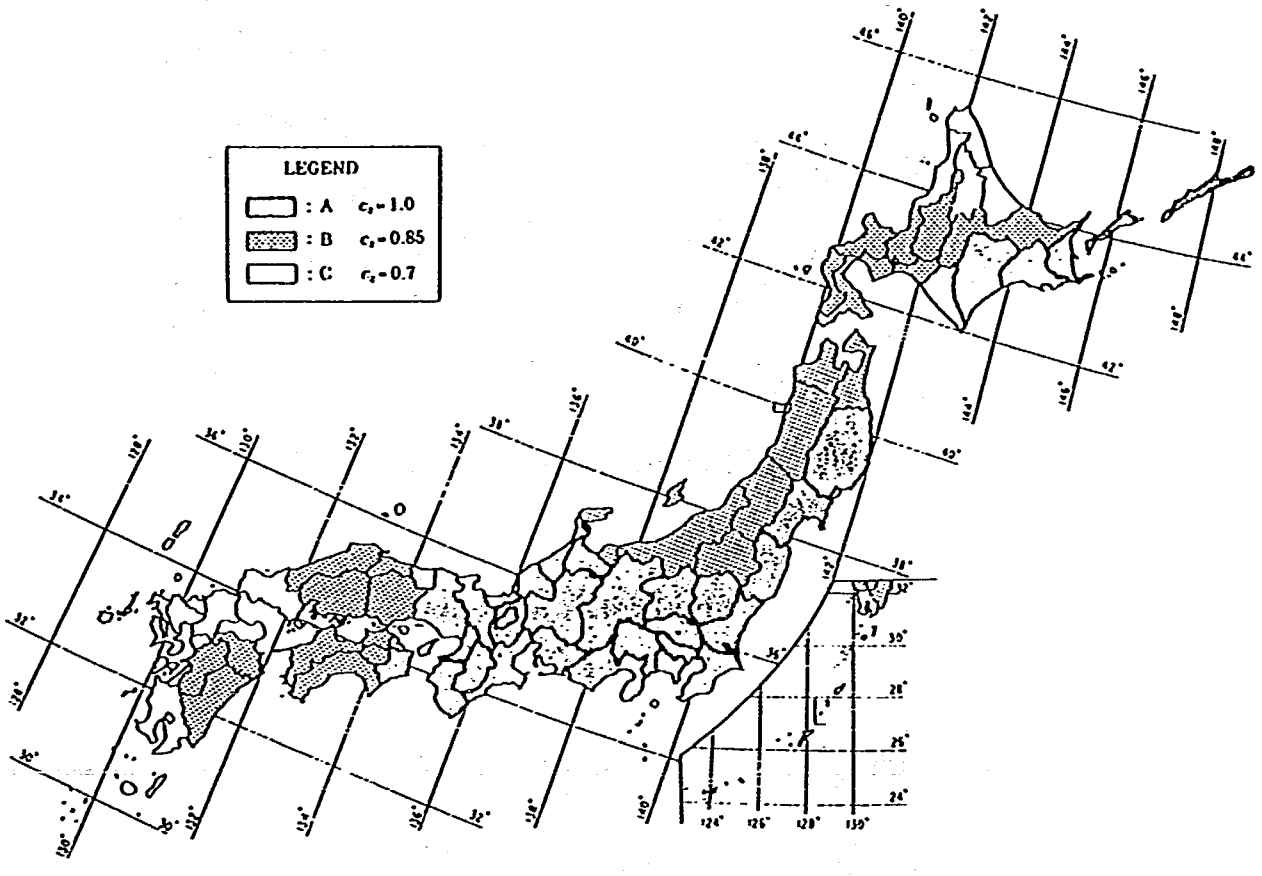


Fig. 3 Modification Factor for Zone c_z

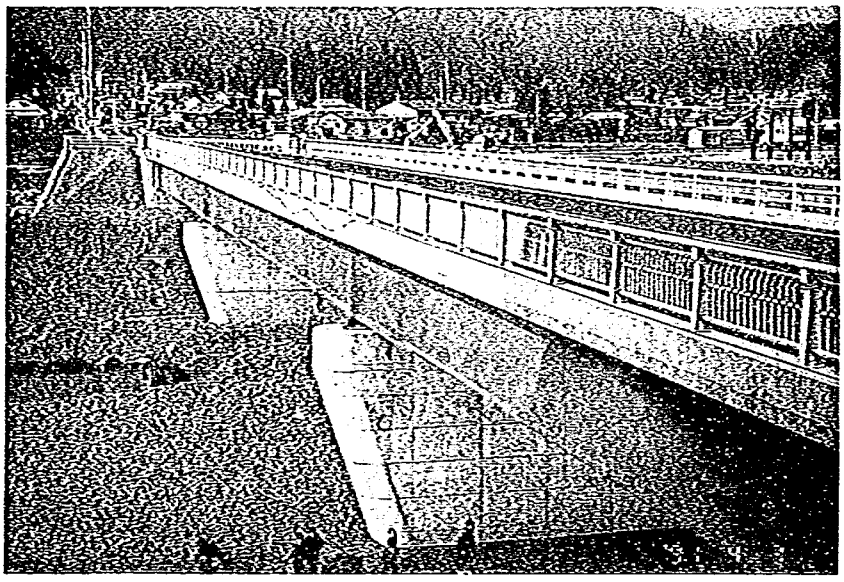


Photo 1 Miyagawa Bridge (Shizuoka−ken)

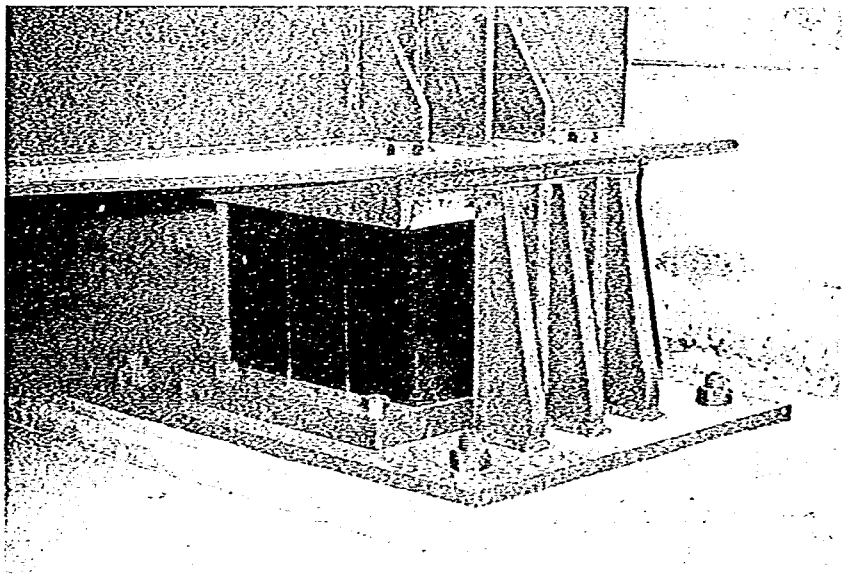


Photo 2 LRB used for Miyagawa Bridge

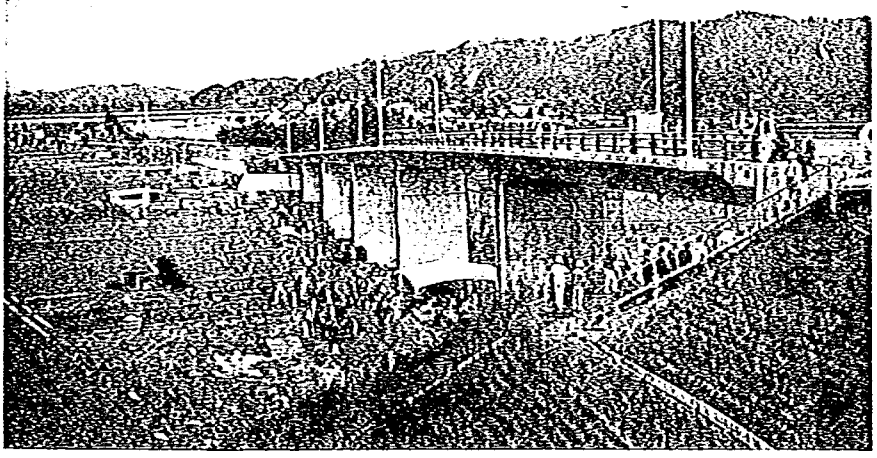


Photo 3 Yama-age Bridge (Tochigi-ken)

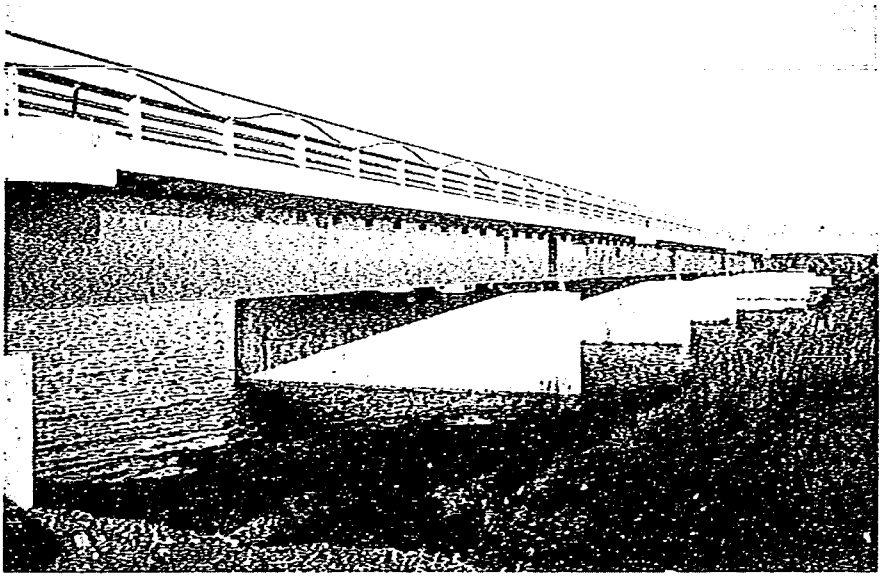


Photo 4 On-netoh Bridge (Hokkaido Development Bureau)

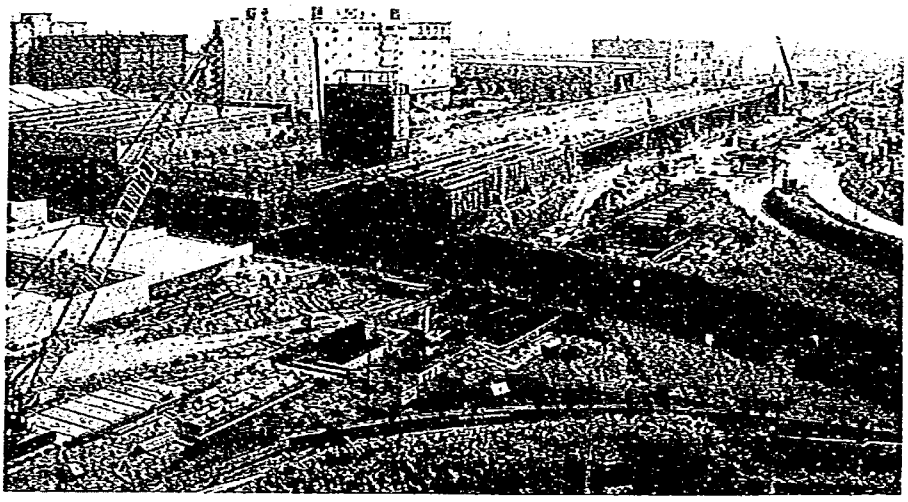


Photo 5 Higashi-ohgi-shima Viaduct (Metropolitan Expressway)

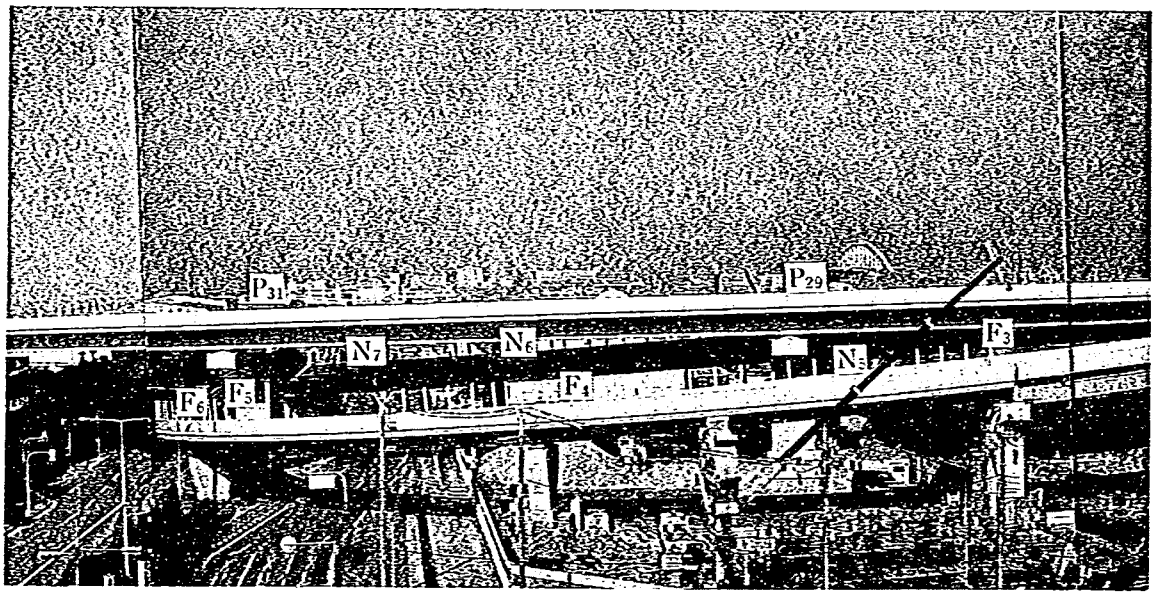
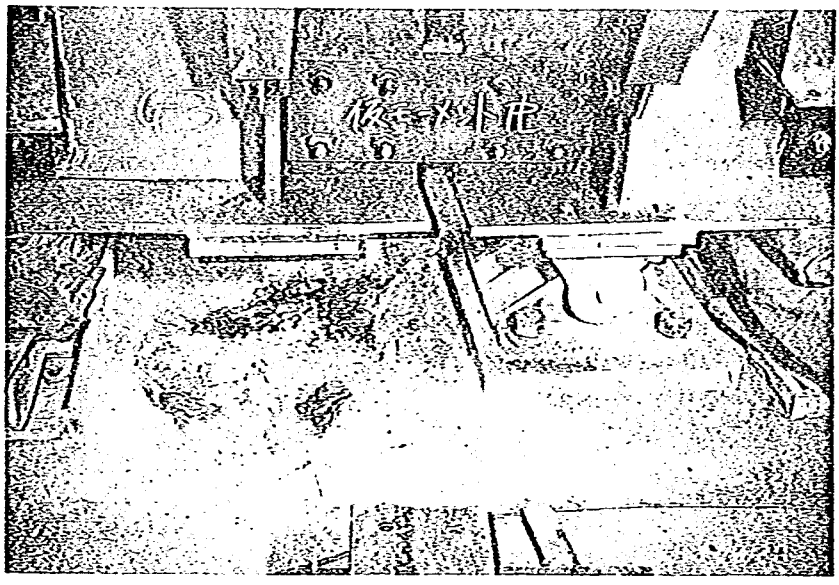
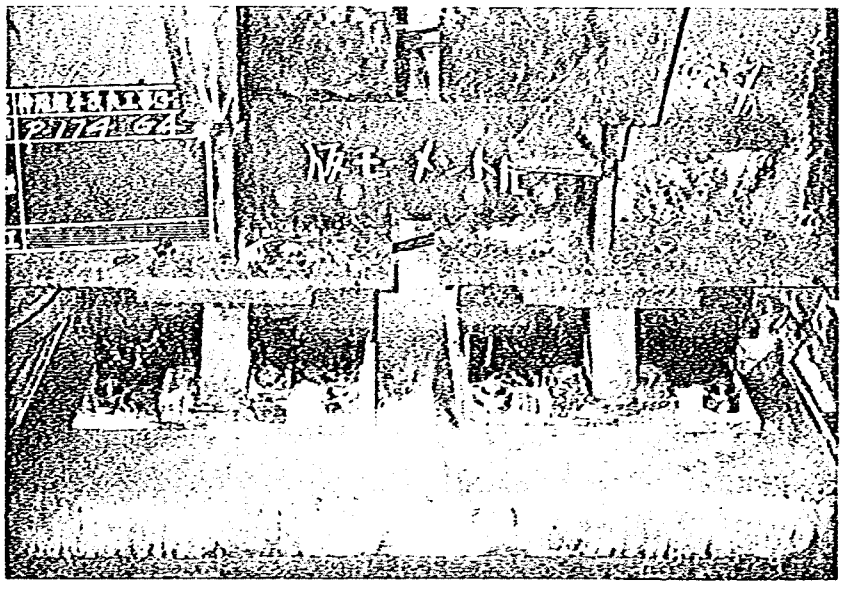


Photo 6 Matsuno-hama Viaduct (Hanshin Expressway)



(a) Removal of Existing Bearings



(b) Set-up of LRB

Photo 7 Jointless System of Existing Bridges (Hanshin Expressway)

Seismic Response Control of Highway Bridges by Variable Stiffness Control

Kazuhiko KAWASHIMA
Shigeki UNJOH
and
Hidetoshi MUKAI

3rd U.S.–Japan Workshop on
Earthquake Protective Systems for Bridges
Berkeley, U.S.A.
January, 1994

SEISMIC RESPONSE CONTROL OF HIGHWAY BRIDGES BY VARIABLE STIFFNESS CONTROL

Kazuhiko KAWASHIMA[1], Shigeki UNJOH[2] and Hidetoshi MUKAI[3]

1) Head, Earthquake Engineering Division, Public Works Research Institute, Ministry of Construction, Tsukuba Science City, Japan
2) Senior Research Engineer, ditto
3) Assistant Research Engineer, ditto

ABSTRACT

Presented is a concept of the variable stiffness control to control bridge response against an earthquake. The proposed concept is to shift the instantaneous natural period of bridges using the variable dampers by avoiding the resonance with ground motions. The effectiveness of the variable stiffness control through the analytical simulation is presented.

INTRODUCTION

The authors proposed variable dampers in which the damping coefficient can be variable dependent on structural response of highway bridges. Various studies including the applicability and practicability have been made at the Public Works Research Institute.[1)-9)]

Variable stiffness control is an another interesting field of extension of the variable damper. If one shifts the natural period of structures, the structural response may be significantly reduced by avoiding the resonance with the ground motion. The variable stiffness control is to shift the instantaneous natural period of bridges using the variable dampers.

This paper proposes the concept of the variable stiffness control using the variable dampers and the effectiveness of the variable stiffness control through the analytical simulation is presented.

CONCEPT OF VARIABLE STIFFNESS CONTROL

Most of bridges with an usual size have the natural period ranging from 0.3 to 1.5 second, and this natural period range corresponds to the predominant period of earthquake-induced ground motions. Thus the resonance of the bridge response with the ground motion tends to be developed during an earthquake. The bridge response can be

reduced if the resonance of bridge response with the ground motion is avoided.

Although it is hard to predict the predominant period of ground motion prior to an earthquake, it can be evaluated time by time during an earthquake. The moving window analysis may be used for evaluating the instantaneous predominant period of ground motion T^* . The resonance of bridge response with the ground motion may be avoided if the instantaneous natural period of bridges T be shifted from the instantaneous predominant period of ground motion T^* during an earthquake.

There are various methods to shift the instantaneous natural period of bridges during an earthquake. Flexibility of bearings may be changed, and active tendons/bracings may be adopted. If one provides the variable dampers for a bridge which is elastically supported by rubber bearings, the natural period of the bridge can be varied by changing the damping coefficient of the variable dampers. If one makes the damping ratio of the variable damper very large, the variable damper would acts as a damper stopper. On the other hand, if one makes the damping ratio small, the natural period of the bridge takes the value computed from the stiffness of the rubber bearings and piers. The variable dampers have various advantage for controlling the instantaneous natural period of bridges because it is more stable for long term use than the active tendons/bracing systems.

Fig. 1 shows the principal of the variable stiffness. The natural period of a bridge T is variable in the range between T_P and T_F . The periods T_P represents that when the damper acts as a damper stopper, it means that the bearing support condition is pinned. On the other hand, the period T_F represents that when the dampers do not work, i.e., the bearing support condition is free. If the instantaneous predominant period of ground motion T^* approaches the natural period of the bridge T , the bridge response becomes larger by the resonance effect. Therefore, if the natural period of the bridge T can be far from the predominant period of ground motion T^* , the bridge response can be significantly reduced.

ALGORITHM OF THE VARIABLE STIFFNESS CONTROL

Fig. 2 shows the algorithm of the variable stiffness control. The instantaneous predominant period of ground motion T^* at time t_i is computed by the moving window Fourier Spectrum. The damping coefficient of variable dampers is varied so that the instantaneous natural period of the bridge T be shifted to prevent the resonance with the ground motion.

Although several algorithm can be considered, the period shift is assumed here as

$$T_{i+1} = \alpha T_i^* \quad (\beta_1 \cdot T_i^* < T_i < \beta_2 \cdot T_i^*) \qquad (1)$$

where,

T_i : instantaneous natural period of a bridge at time t_i

T^* : instantaneous predominant period of ground motion at time t_i

α : control coefficient

β_1 , β_2 : on−off coefficient to control

The coefficient α has to be determined depending on the natural period of the bridge T and the instantaneous predominant period T^* of an ground motion. It is proposed that α is set as

$$\alpha \begin{cases} >1/2 & (T^* \leqq T) \\ <2 & (T^* > T) \end{cases} \tag{2}$$

The coefficient β represents the on−off coefficient of the variable stiffness control. When the instantaneous predominant period of the ground motion T_i^* at time t_i is far from the natural period of the bridge T , the variable stiffness does not need to work. Therefore, a certain period range to prevent the resonance is determined by the coefficient β .

EARTHQUAKE RESPONSE ANALYSIS METHOD

The equations of motion for a linear multi−degree−of−freedom system with the variable stiffness control may be written as

$$\underline{M}\ddot{\underline{x}} + (\underline{C} + \underline{C}_V)\dot{\underline{x}} + \underline{K}\underline{x} = -\underline{M}\ddot{X}_0 \tag{3}$$

in which $\underline{M}$, $\underline{C}$ and $\underline{K}$ represent mass, damping and stiffness matrices of the system, respectively. $\underline{x}$ and x_0 denote displacement vector of the system and an earthquake ground motion, respectively. $\underline{C}_V$ denotes a damping matrix of the variable dampers and is assumed as

$$\underline{C}_V = \sum_{k=1}^{nV} \underline{c}_{ij}^{\,V} \tag{4}$$

where

$$\underline{c}_{ij}^{\,V} = \begin{bmatrix} C & -C \\ -C & C \end{bmatrix} \tag{5}$$

in which $\underline{c}_{ij}^{\,V}$ and n_V represent damping matrix of the variable dampers, which are installed between the i−th node and the j−th node, and a number of the variable dampers installed, respectively. C is the damping coefficient of an each variable damper and is given according to the control algorithm as shown in Fig. 2.

Although there are various methods to prescribe the damping matrix $\underline{C}$ of the structure, it is assumed here to be written as Eq.(6) assuming that the damping matrix $\underline{C}$ can be diagonalized by the modal matrix.

$$C = (\underline{\Phi})^{-1} diag[2h_k w_k](\underline{\Phi}^T)^{-1} \tag{6}$$

in which, Φ denotes a modal matrix of the system and $diag[2h_k w_k]$ denotes a diagonal matrix with elements of $2h_k w_k$ ($k = 1,2,3,\cdots$; mode number).

Since $\underline{C}_V$ is time−varying, Eq.(3) has to be solved by a direct integration method.

According to the above analytical method, a computer program "VSTIFF," which can analyze earthquake response of a multi−degree−of−freedom system with the variable

stiffness, was developed.

EFFECTIVENESS OF VARIABLE STIFFNESS CONTROL

To study the effectiveness of the variable stiffness control, a three–span continuous girder bridge, as shown in Fig. 3, with a span length of 90m is analyzed. The response in longitudinal direction is considered. The superstructure of the model is supported by elastic bearings, and four variable dampers with the same characteristics are installed between the deck and the piers. The weight of the superstructure and spring stiffness of the rubber bearings are assumed as 4,719KN and 6,247KN/m, respectively. The stiffness of piers is assumed so that the fundamental natural period of the bridge be about 0.5 sec when the deck support condition is hinged. The stiffness of rubber bearings is set so that the fundamental natural period of bridge be 1.0 sec. The damping ratio of the bridge without control is assumed as 0.02.

An acceleration ground motion as shown in Fig. 4 is used as an input acceleration. The instantaneous predominant frequency ($1/T^*$) of the input acceleration is also shown in Fig. 4. Because the predominant period of ground motion is about 1 sec, α in Eq.(1) was assumed as 1/2.

Fig. 5 shows the dependence of the natural period/damping ratio of the bridge on the damping coefficient of variable dampers. Fig. 6 shows the corresponding mode shapes of the bridge. When the damping coefficient C of the variable dampers is 0, the 1st mode is a rigid vibration mode of the deck in the longitudinal direction and is the most predominant mode against ground motions. The 2nd mode is the vertical vibration of the deck which does not contribute the bridge response against the horizontal ground motion. The natural periods of these modes are 1.0 sec and 0.23 sec, respectively.

If one increases the damping coefficient of the variable dampers, the natural periods of the 1st and 2nd modes increase. At the damping coefficient C of about 4,200KN·sec/m, the fundamental natural period of bridge take very large value, because this corresponds to the critical damping of the structure. Furthermore if one increases the damping coefficient of the variable dampers, the 1st and 2nd modes become overdamped modes and they do not contribute the response against a ground motion. However, a new mode as shown in Fig. 5 appears as a predominant mode and the natural period decrease with increase of the damping coefficient of the variable dampers. The natural period of the mode gradually approaches 0.45 sec, which is the natural period when the bearing support condition is pinned, as the damping coefficient of the variable dampers increase.

Fig. 7 shows the control relation between the predominant natural period of the bridge and the damping coefficient of the variable dampers. Although the period shift may be made in the damping coefficient range of 0 to over 8,000KN·sec/m, it is assumed here that the period shift be made in the range of damping coefficient C over 4,200KN·sec/m.

Fig. 8 and Table 1 compares the deck acceleration and displacement of the bridge

with and without control. The peak displacement and peak acceleration of deck decreases to 17% and 50% of those without control. The bending moment of pier bottom decreases to 52% of the one without control. The peak damping force required for the four variable dampers is 761KN×4=3,040KN and the peak stroke is 3.1cm.

CONCLUDING REMARKS

The concept of the variable stiffness control to control bridge response against an earthquake was presented. The effectiveness of the variable stiffness control was studied through the analytical simulation. It is demonstrated that the peak displacement and peak acceleration of deck decreases to 17% and 50% of those without control, and that the bending moment of pier bottom decreases to 52% of the one without control. The peak damping force required for the four variable dampers is 761KN×4=3,040KN and peak stroke is 3.1cm. The effectiveness of the variable stiffness control is also being studied through the shaking table tests.

Table 1 Peak Responses

	DECK		PIER BOTTOM
	DISP. (cm)	ACCEL. (gal)	BENDING MOMENT(tfm)
NO CONTROL	33.1	1,301	3,288
WITH CONTROL	5.6	653	1,701
VD	DAMPING FORCE : 77.6 tf STROKE : 3.1 cm		

REFERENCES

1) Kawashima, K. and Unjoh, S. : "Development of Hybrid Control Technology." Civil Engineering Journal, Tokyo, Japan, pp. 2–5, Vol. 32–6, 1989 (in Japanese).
2) Taguchi, J., Iwasaki, T., Adachi, Y., Sasaki, Y. and Kawashima, K. : " U.S.–Japan cooperative research program on hybrid control of seismic response of bridge structures." 22nd Joint Meeting, U.S.–Japan Panel on Wind and Seismic Effects, UJNR, Gaithersburg, Maryland, USA, May, 1990, NIST Special Publication
3) Kawashima, K., Unjoh, S., Nagashima, H. and Shimizu, H. : "Current research efforts in Japan for passive and active control of highway bridges against earthquakes." Proc. 23rd Joint Meeting, U.S.–Japan Panel on Wind and Seismic Effects, UJNR, Tsukuba, Japan, 187–209, 1991
4) Kawashima, K., Unjoh, S. and Shimizu, H. : "Earthquake response control of highway bridges by variable damper." Proc. of Colloquium on Control of Structures, Japan Society

of Civil Engineers, Part. B, pp.221–224, July, 1991 (in Japanese)
5) Kawashima, K., Unjoh, S. and Shimizu, H. : "Seismic response control of highway bridges by variable damper." 24th Joint Meeting, U.S.–Japan Panel on Wind and Seismic Effects, UJNR, Gaithersburg, May, 1992, NIST Special Publication 843
6) Kawashima, K., Unjoh, S., Iida, H. and Mukai, H. : "Effectiveness of the variable damper for reducing seismic response of highway bridges, Proc. of 2nd U.S.–Japan Workshop on Earthquake Protective Systems for Bridges, Tsukuba, Dec. 7–8, 1992, Technical Note of the Public Works Research Institute, No. 3196
7) Kawashima, K., Unjoh, S. and Mukai, H. : "Seismic response control of highway bridges by variable dampers." 25th Joint Meeting, Panel on Wind and Seismic Effects, UJNR, Tsukuba, May, 1993, Technical Note of Public Works Research Institute, No. 3217
8) Kawashima, K., Unjoh, S. and Shimizu, H. : "Earthquake Response Control of Highway Bridges by Variable Damper", Transactions of the Japan National Symposium on Active Structural Response Control, Japan Science Council, pp.311–317, March, 1992 (in Japanese)
9) Kawashima, K., Unjoh, S. and Shimizu, H. : "Experimental Study on Dynamic Characteristics of Variable Damper", Transactions of the Japan National Symposium on Active Structural Response Control, Japan Science Council, pp.311–317, March, 1992 (in Japanese)

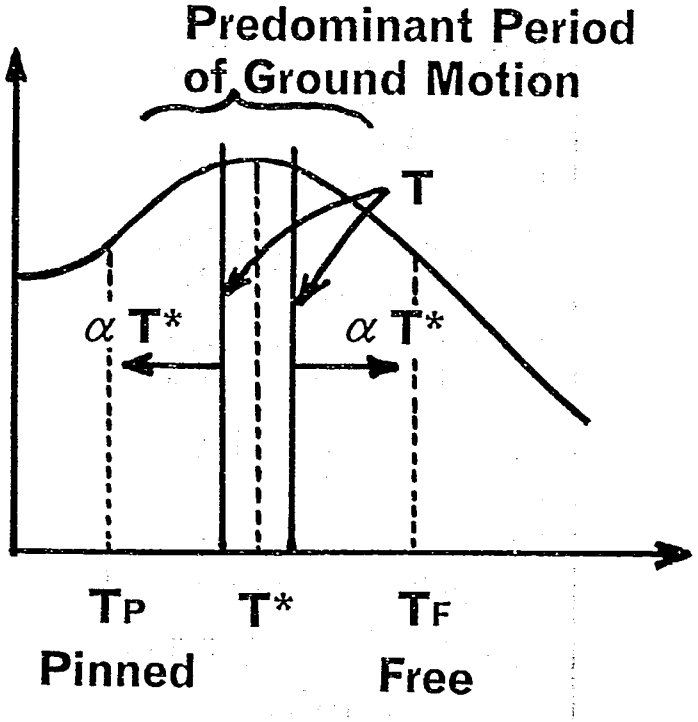


Fig. 1 Concept of Variable Stiffness

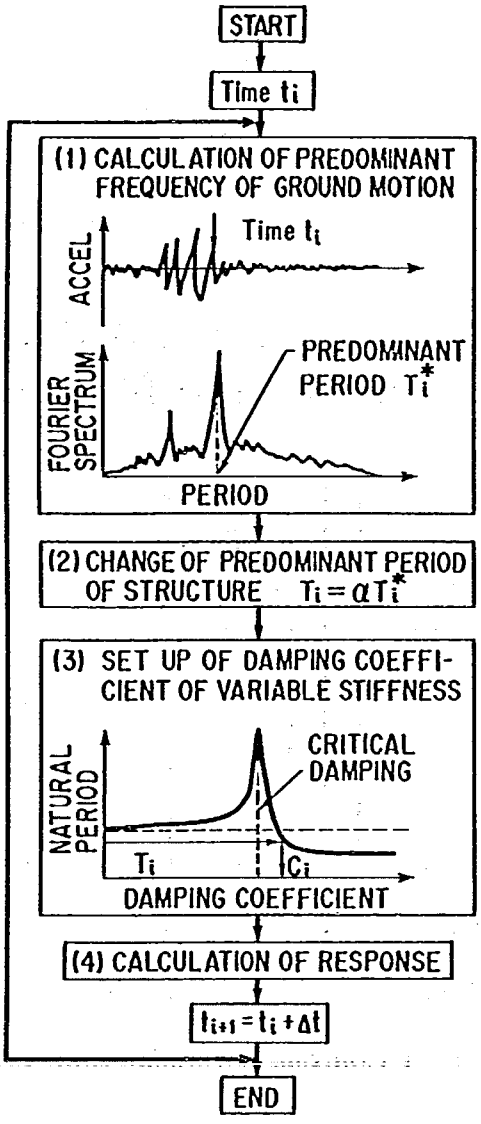


Fig. 2 Control Algorithm of Variable Stiffness

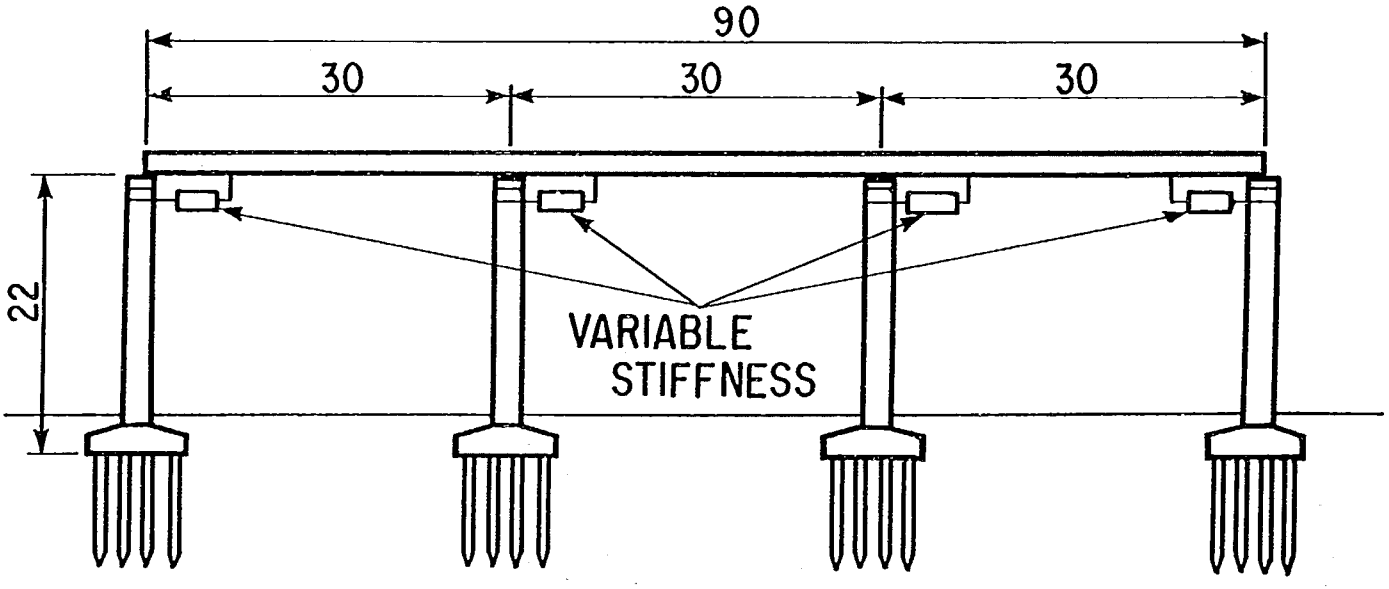


Fig. 3 Model Bridge Analysed

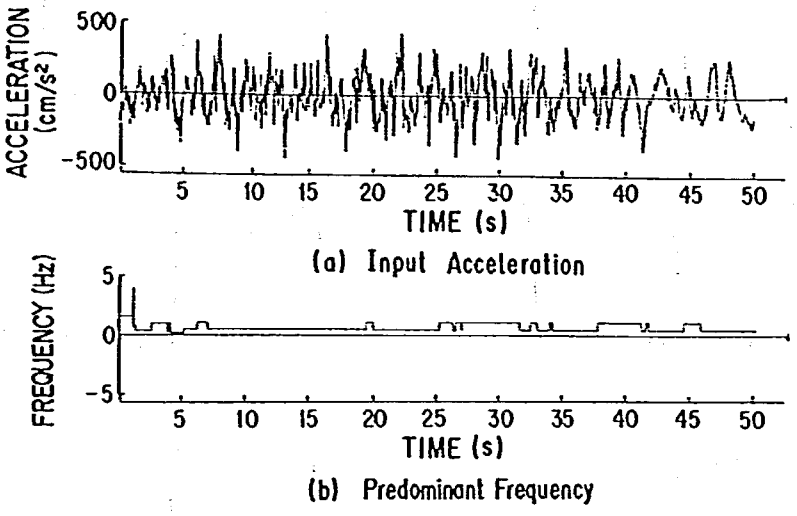


Fig. 4 Input Acceleration and the Predominant Period

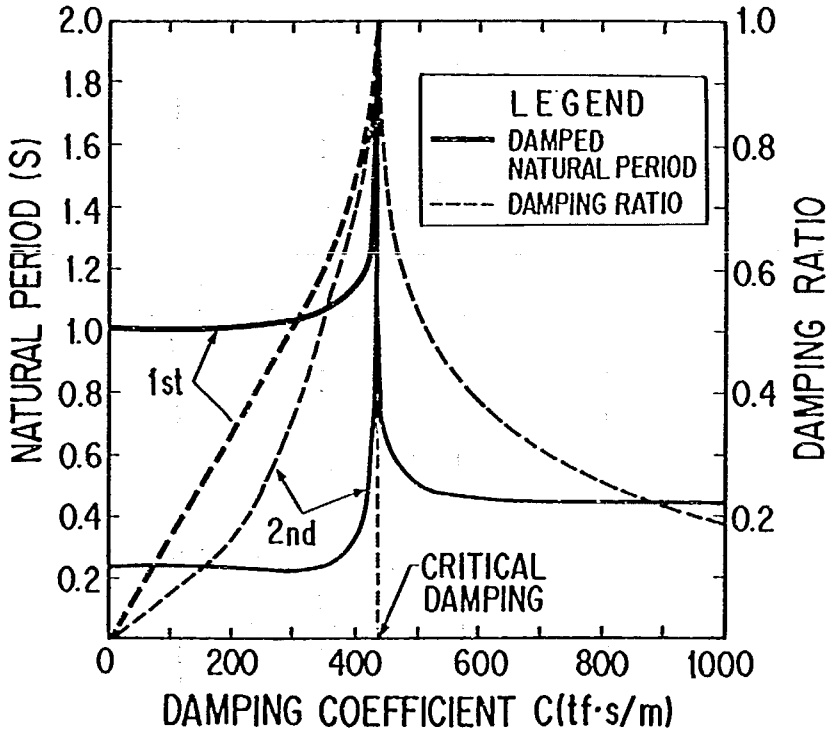


Fig. 5 Dependence of Natural Period/Damping Ratio of the Bridge on Damping Coefficient of Variable Dampers

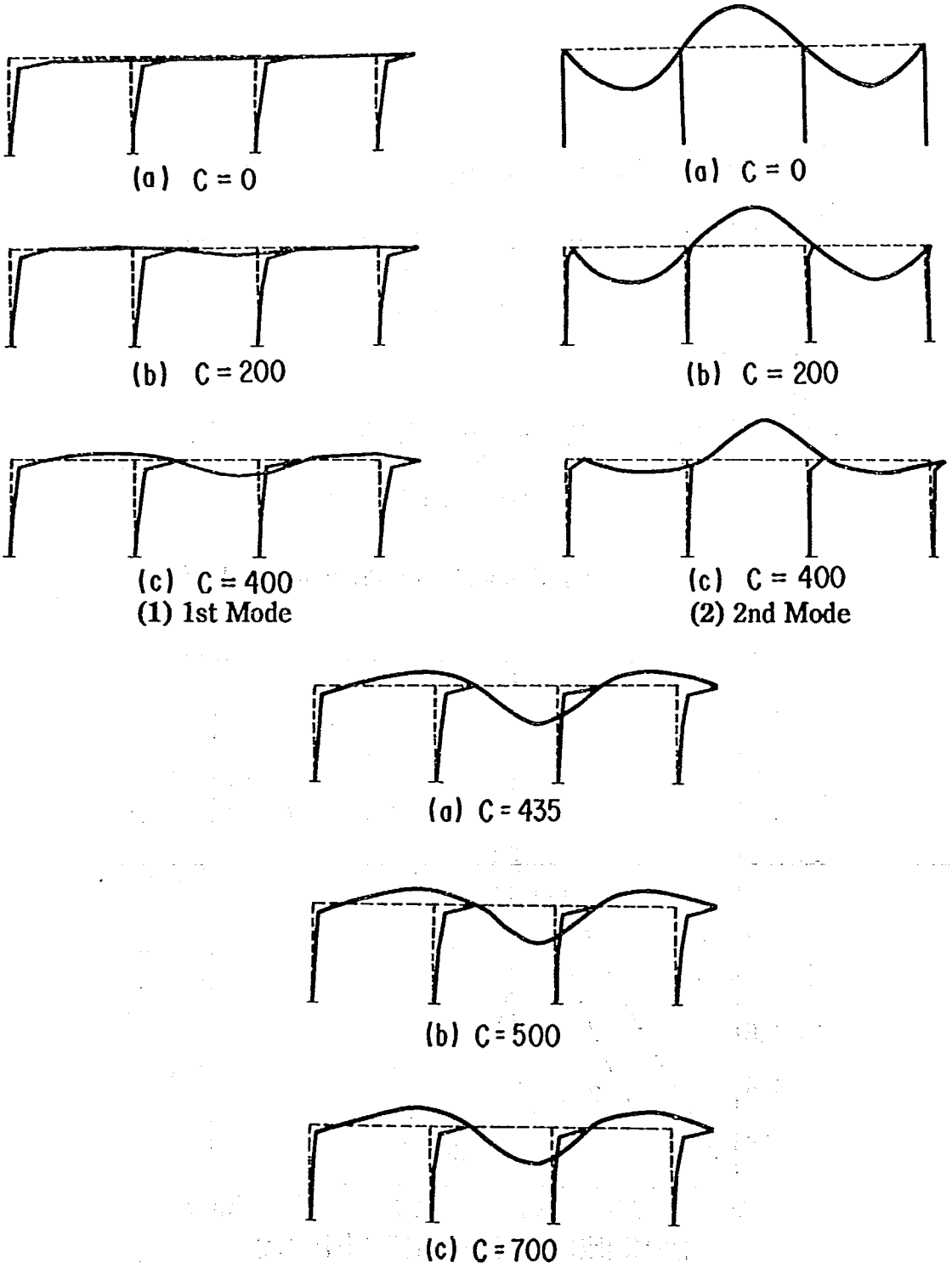


Fig. 6 Dependence of Natural Modes of the Bridge on Damping Coefficient of Variable Dampers

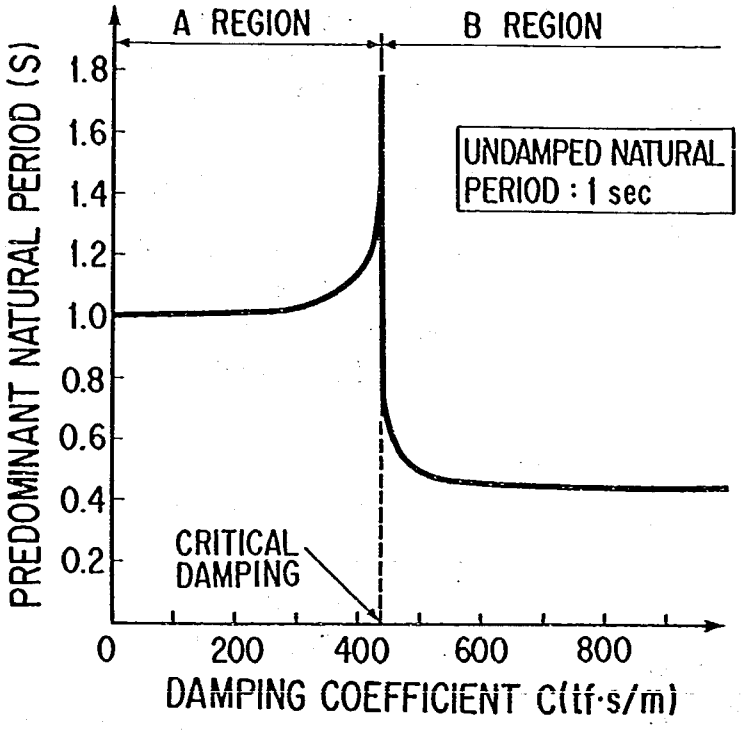


Fig. 7 Dependence of Natural Period of the Bridge on Damping Coefficient of Variable Dampers used for the Control

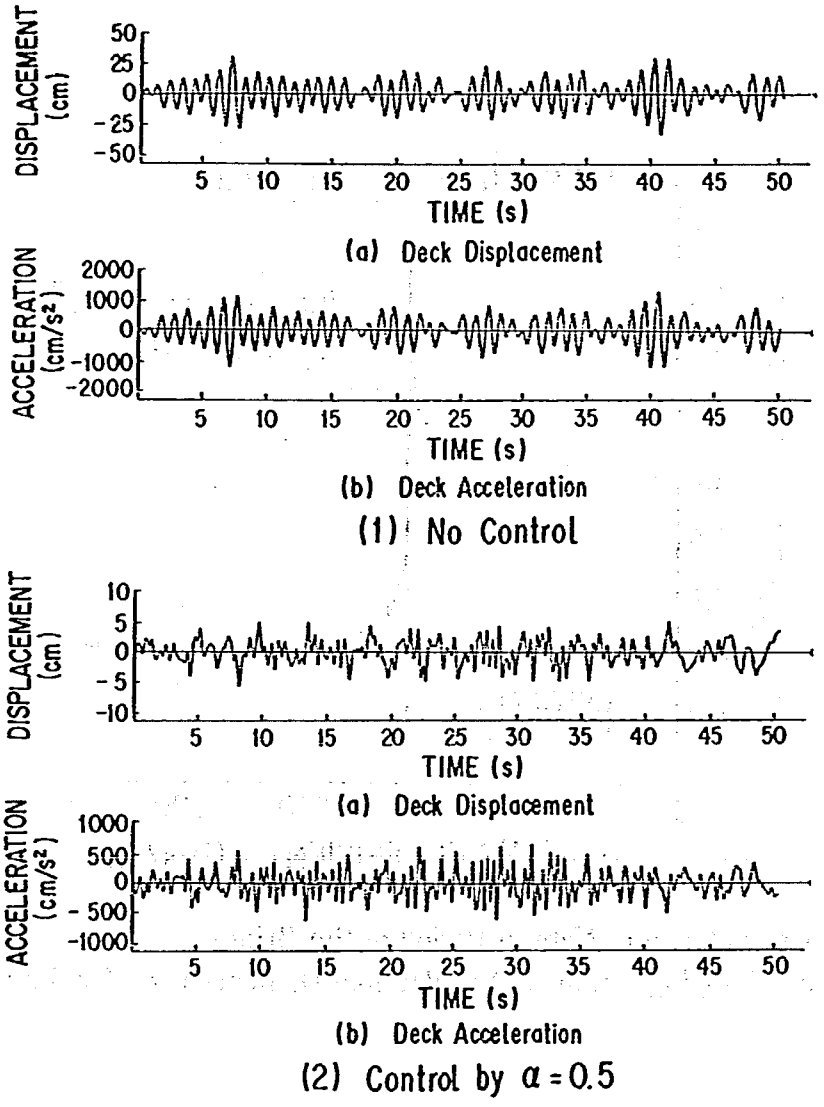


Fig. 8 Effectiveness of Variable Stiffness Control

Application of Electro-Rheological Fluid for Variable Damper

Kazuhiko KAWASHIMA
Shigeki UNJOH
Shigenobu SUZUKI
and
Shigeki ENDOH

3rd U.S.-Japan Workshop on
Earthquake Protective Systems for Bridges
Berkeley, U.S.A.
January, 1994

APPLICATION OF ELECTRO-RHEOLOGICAL FLUID FOR VARIABLE DAMPER

Kazuhiko KAWASHIMA[1], Shigeki UNJOH[2], Shigenobu SUZUKI[3] and Shigeki ENDOH[3]

1) Head, Earthquake Engineering Division, Public Works Research Institute, Ministry of Construction, Tsukuba Science City, Japan
2) Senior Research Engineer, ditto
3) Research and Development Division, Bridgestone Corporation, Ogawahigashi-cho, Kodaira-shi, Tokyo, Japan

ABSTRACT

This paper presents the potential application of electro-rheological (ER) fluid for the seismic response control of structural systems. Variable damper systems using ER fluid and the trial design are presented. The applicability of the ER damper for the seismic response control of structural systems are discussed.

INTRODUCTION

Electro-rheological (ER) fluid is the fluid in which the viscosity is variable depending on the applied electric field. Although the ER fluid has been studied for a long time, reliable ER fluid has not developed. The ER fluid which has high applicability for practical use has recently been developed and the application has begun to be made especially in mechanical structural systems.

The authors have been studied the variable damper using ER fluid (referred to ER damper hereinafter). The ER damper has the advantages that the damping characteristics is variable within a quick response (on the order of milliseconds) to the applied electric field, and that the mechanical system of ER damper can be simple without complicated valve systems. Therefore the reliability for practical use may be higher than an usual active control devices.

To control structural vibration during earthquakes, relatively larger damping force is required for the ER damper. Therefore, it is a critial issue to design the practical ER damper system which can vary a wide range of the damping force. This paper presents the parametric design study of the ER damper, and the applicability for practical use is discussed.

DESIGN OF ER DAMPER

The damping force of the ER damper may be given by the sum of the damping force developed by the fluid viscosity through an orifice and that developed by ER effects as shown in Eq.(1). Supposing a cylinder type damper system with an orifice as shown in Fig. 1, which may be suitable for developing a larger damping force, the damping force developed by the fluid viscosity and the ER effects may be given as Eqs. (2) and (3), respectively.

$$F = F_V + F_E \tag{1}$$

$$FV = \frac{12 \cdot L \cdot A^2 \cdot \eta}{B \cdot H^3} \cdot \upsilon \tag{2}$$

$$FE = \frac{3 \cdot L \cdot A}{H} \cdot \tau_y(E) \tag{3}$$

Where,

F : Total Damping Force developed by ER Damper
F_V : Damping Force developed by Fluid Viscosity through Orifice
F_E : Damping Force developed by ER Effects
A : Pressure Area of Piston
υ : Velocity of Piston
L ,B ,H : Length, Width and Distance of Electrodes
η : Viscosity of ER Fluid
$\tau_y(E)$: Shear Stress developed by ER Effects
E : Applied Electric Field Strength

It should be noted here that $\tau_y(E)$ is controlled by the applied electric field strength between the electrodes. Therefore, when $E=0$, i.e., no control, $\tau_y(0)=0$, on the other hand, when $E=E_{max}$ which is the maximum electric field strength applicable for the ER damper, maximum shear stress, $\tau_y(E_{max})$, is developed.

Based on the above theories, the damping force developed by the ER damper against the steady state loading with a constant displacement may be written in Fig. 2. As well-known, the damping force developed by the fluid viscosity is dependent on the piston velocity and it is not controllable. On the other hand, the damping force developed by the ER effects is not dependent on the loading velocity and is controlled only by the electric filed strength. In order to control a wide range of the damping force it is required to design the damping force developed by the fluid viscosity should be as small as possible than that developed by the ER effects.

APPLICABILITY OF ER DAMPER

Assuming that $D \gg D_s$, $D \gg H$ (see Fig. 1) for the simplicity, the pressure area, A , and the width of the electrodes, B , can be approximated as $A = \pi \cdot D^2/4$ and $B = \pi \cdot D$. Hence, Eqs. (1) to (3) may be rewritten as

$$\frac{F}{L} = \frac{F_V}{L} + \frac{F_E}{L} = \frac{3\pi \cdot D^3 \cdot \eta}{4 \cdot H^3} + \frac{3\pi \cdot D^2}{4 \cdot H} \cdot \tau_y(E) \tag{4}$$

$$0 \leqq \frac{F_E}{L} \leqq \frac{F_{Emax}}{L} = \frac{3\pi \cdot D^2}{4 \cdot H} \cdot \tau_y(E) \tag{5}$$

According to Eqs. (4) and (5), the relation between the size of the ER damper and the maximum damping forces developed by the fluid viscosity and the ER effects can be illustrated as shown in Fig. 3. The damping forces in Fig. 3 are represented as the force per unit length of the electrodes. Fig. 3 shows that the larger damping forces can be developed by increasing the diameter of the piston and length of the electrode, and also by decreasing the distance between the electrodes. Since the damping force developed by the fluid viscosity sensitively varies depending on the piston diameter and the distance of the electrodes, the damping force developed by the fluid viscosity tends to be larger than that developed by the ER effects for a larger size of the damper.

Fig. 4 shows the computed damping forces for various sizes of the damper. The damping forces are computed for the cases of the distance of the electrodes of 1, 2 and 3mm. The viscosity of the ER fluid, η , and the maximum shear stress by ER effects, τ_{ymax} , are assumed as 1.5×10^{-6} kgf·s/cm^2 and 1.5×10^{-2} kgf/cm^2 (E=3 kV/mm), respectively. These values are employed as typical values based on the ER fluid which is now in practical use. Supposing the damper system with piston diameter of 300mm, length of the electrodes of 500mm and distance between the electrodes of 2mm, the maximum damping force controlled by the ER effects may be 20tf, which is applicable to the seismic response control of structures.

Since the damping force developed by the fluid viscosity is dependent on the applied piston velocity, it becomes much larger than that developed by the ER effects in some loading conditions as fast loading velocity. In order to decrease the damping force developed by the fluid viscosity, it is made by decreasing the piston diameter or by increasing the distance of the electrodes, and by increasing length of the electrodes.

DEVELOPMENT OF EXPERIMENTAL ER DAMPER

For the purpose of proving the design method and investigating the effectiveness and applicability of the ER damper, experimental model of the ER damper as shown in Photo 1 is now being developed. This model is designed so that the maximum damping force developed by the ER effects be about 40kgf. The length of the electrode and the distance between the electrodes is designed as 134mm and 3mm, respectively. Anhydrous type ER fluid is used for the model. When the piston velocity is 300mm/sec, the damping force

developed by the fluid viscosity is about half of that developed by the ER effects.

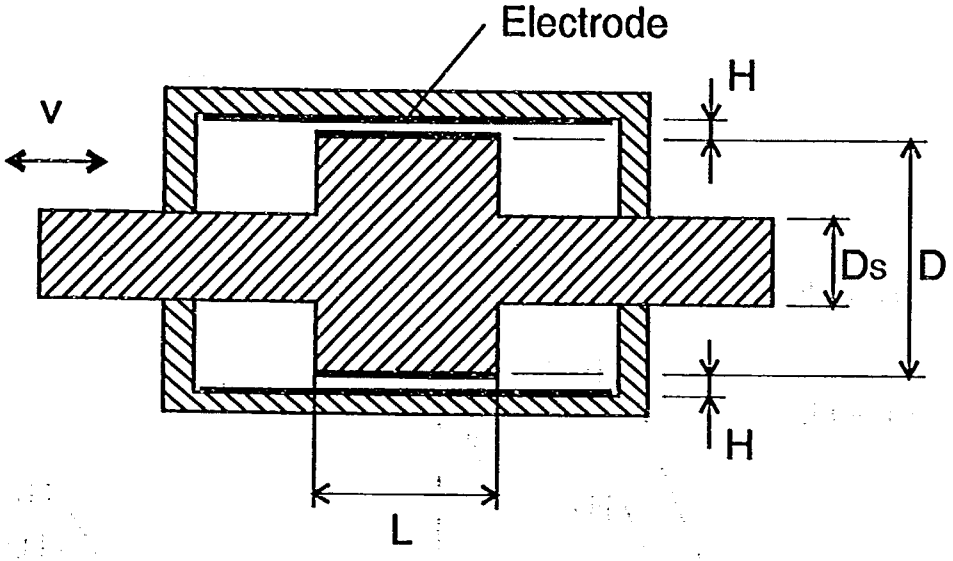
A wide area of experiments using the model, such as load–displacement relation, velocity dependency, displacement dependency, temperature dependency, controllability, etc. is now planning.

CONCLUSIONS

The applicability of the ER damper for the seismic response control of structures is studied through the trial design of the ER damper. It is showed that the cylinder type damper with diameter of 300mm can develop the required damping force to control the seismic response of actual structures. The experimental ER damper model is also being developed and the comprehensive tests will be made in the future.

REFERENCES

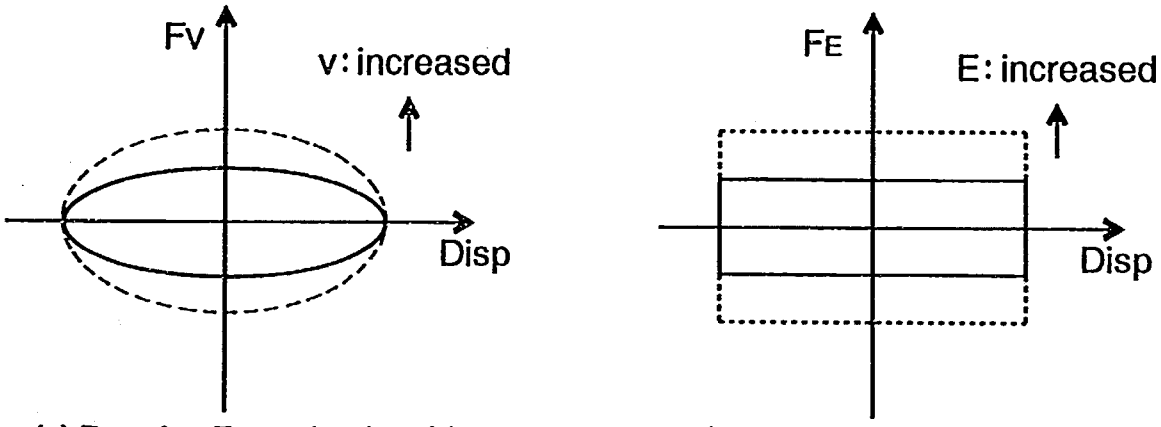
1) Ushijima, T, Takano, K. and Noguchi, T. : Rheological Characteristics of ER Fluids and their Application to Anti–Vibration Devices with Control Mechanism for Automobiles, SAE paper #881787, 1988
2) Duclos, T., G. : Design of Devices Using Electrorheological Fluids, SAE Technical Paper #881134, 1988
3) Ehrgott, R., C. and Masri, S., F. : Modeling the Oscillatory Dynamic Behavior of Electrorheological Materials in Shear, Smart, Mater. Struct. 1, 1992
4) Sasada, T., Kishi, T. and Kamijo, K. : Electro Viscous Effects of Polymer and Solid Particle Solutions, Proceedings of the Japan Society of Mechanical Engineers. Vol.41, No.342, 1975
5) Sasada, T., Kamijo, K. and Kishi, T. : Electro Viscous Effects of Uni–phase Liquid, Proceedings of the Japan Society of Mechanical Engineers. Vol.41, No.343, 1975
6) Edited by Scott, D. and Yamagichi, J. : Solidifying Fluid Transforms Clutches and Flow Valves, Automotive Engineering, Vol.91, No.11, 1983



Pressure Area of Piston : $A = \frac{\pi}{4}(D^2 - Ds^2)$

Width of Electrode : $B = \pi(D + H)$

Fig. 1 Cylinder Type ER Damper



(a) Damping Force developed by the Fluid Viscosity

(b) Damping Force developed by the ER Effects

Fig. 2 Illustration of the Damping Force developed by the ER Damper

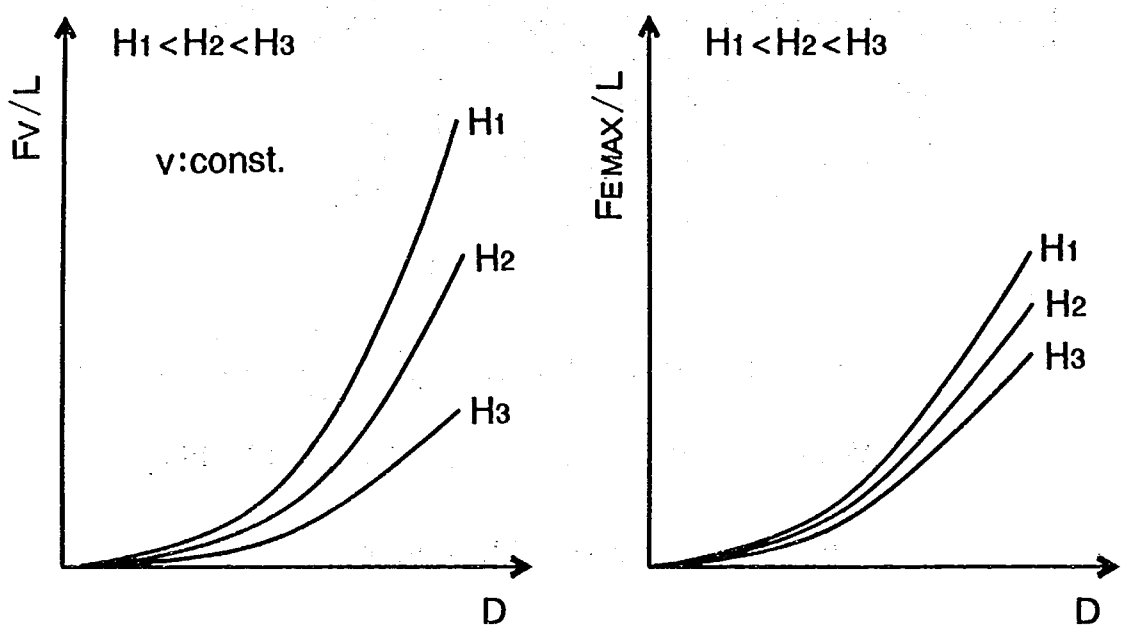


Fig. 3 Variation of the damping Force depending on the Damper Size

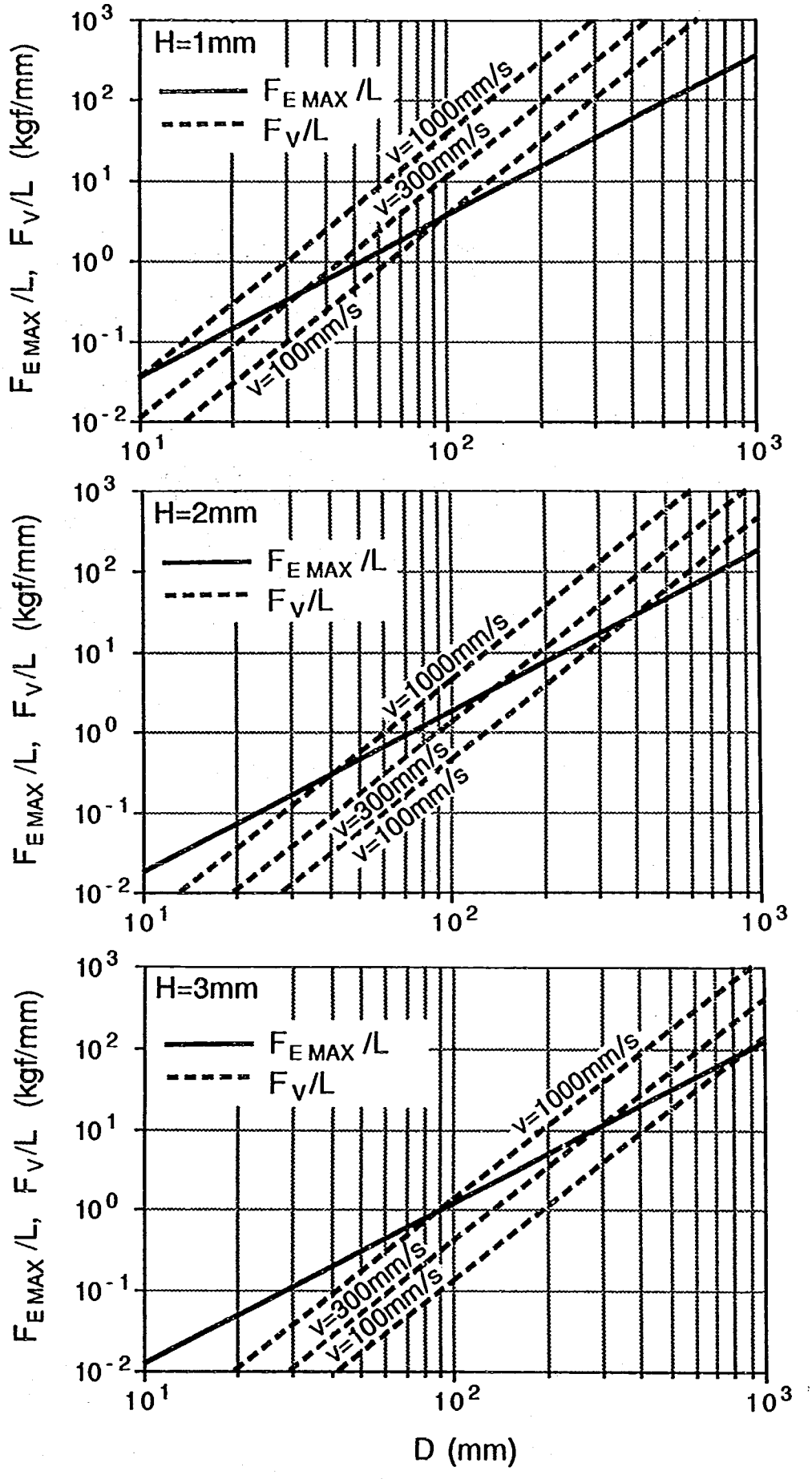


Fig. 4 Computed Damping Force with Various Size of Damper

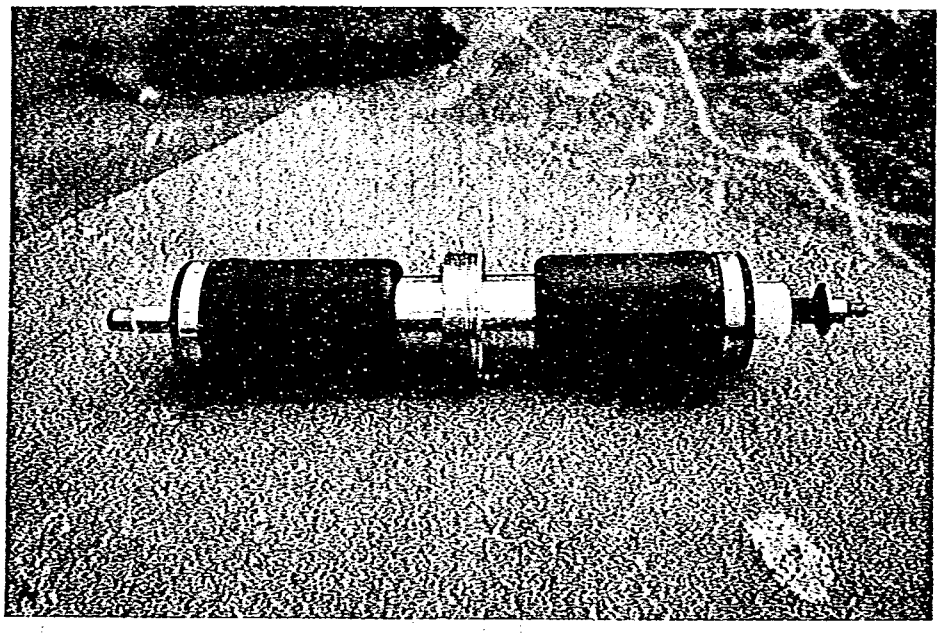


Photo 1 Experimental ER Damper

Response of On-netoh Bridge During Kushiro-oki Earthquake of January 1993

Masashi SATO
Hiroaki NISHI
Kazuhiko KAWASHIMA
and
Shigeki UNJOH

3rd U.S.-Japan Workshop on
Earthquake Protective Systems for Bridges
Berkeley, U.S.A.
January, 1994

RESPONSE OF ON-NETOH BRIDGE DURING KUSHIRO-OKI EARTHQUAKE OF JANUARY 1993

Masashi SATO[1], Hiroaki NISHI[2], Kazuhiko KAWASHIMA[3] and Shigeki UNJOH[4]

1) Head, Structure Division, Structure Department, Civil Engineering Research Institute, Hokkaido Development Bureau, Hiragishi 1-3, Toyohira-ku, Sapporo, Japan
2) Research Engineer, ditto
3) Head, Earthquake Engineering Division, Public Works Research Institute, Ministry of Construction, Tsukuba Science City, Japan
4) Senior Research Engineer, ditto

ABSTRACT

On-netoh bridge is being constructed in the East of Hokkaido for the replacement of the existing bridge. Menshin design using lead rubber bearings is employed for the On-netoh bridge. In January, 1993, the Kushiro-oki Earthquake with magnitude of 7.8 occurred and it was the first time that a Menshin designed bridge experienced a major earthquake. This paper presents earthquake response characteristics of a Menshin designed bridge during the Kushiro-oki Earthquake. The analysis of acceleration records measured close to the On-netoh bridge and the simulation analysis using the measured record are made.

INTRODUCTION

The On-netoh bridge is now under construction on the national highway No.44 at Nemuro City in Hokkaido[1]. The Menshin design was adopted for the side-span of the On-netoh bridge. Since Hokkaido is located in the North of Japan and is in a cold district, one of the authors have been studied the temperature dependency of the horizontal stiffness of laminated rubber bearings through loading tests of full-size models. It was found that the stiffness of the isolation bearings have the relatively strong temperature dependency[2].

In January, 1993, the Kushiro-oki Earthquake with magnitude of 7.8 on the Richiter scale occurred approximately 100km from the On-netoh bridge as shown in Fig. 1. It was the first time that a major earthquake occurred near the Menshin designed bridge and also that it was at a low temperature condition. Although the strong motion observation was not

made for the On−netoh bridge, it was obtained at the existing bridge which is located less than 200m from the On−netoh bridge. Earthquake response characteristics of the On−netoh bridge is studied through the analysis of measured acceleration records and the simulation analysis of the On−netoh bridge.

ON−NETOH BRIDGE

The existing bridge was constructed in 1961 on National Highway No.44 at On−netoh in Nemuro, Hokkaido. **Fig. 2** shows the side view of the existing bridge. The bridge length is 96.95m long which consists of a steel Warren−type truss bridge with span length of 60m and a steel composite girder bridge with that of 35m. Width of the deck is 7.5m. Since the existing bridge becomes too old for use and the On−netoh bridge is now being constructed for the replacement of the existing bridge. **Fig. 3** shows the locations of two bridges.

Fig. 4 shows the On−netoh bridge which is constructed by the Hokkaido Development Bureau. Bridge length is 456m long and the bridge consists of 3 four−span continuous plate girder bridges with bridge length of 102.2m, 104.8m and 104.8m and Nielsen−type Lohse girder bridge with span length of 140m. The construction will be completed in 1995. The Menshin design using lead rubber bearings is employed for the side bridge at the Kushiro side. **Photo 1** shows the general view of the bridge. The site is in a cold region where the mean of the lowest temperature for the last 30 years at the site is −9.1℃. Therefore, it is a distinctive characteristics of the bridge that the Menshin design is adopted for a bridge in a cold district.

Rubber bearings are used for the both ends of the girder of the On−netoh bridge, i.e., at A1 abutment and P4 pier. Lead rubber bearings are used at Piers P1, P2 and P3. The stiffness of the bearings are designed so that the distribution ratio of the inertia force of a superstructure in the longitudinal direction be 5% for A1 and P4, and 30% for P1, P2 and P3. On the other hand, the stoppers to prevent displacement in the transverse direction are installed at all of the bearings. **Fig. 5** shows the bearings used for the bridge.

Fig. 6 shows a cross section of the strata of the construction site of the On−netoh bridge. It consists of sand (AS1), silt (AC), sand (AS2) and loam (Nm) layers. The loam layer which is selected as the supporting layer of the foundations is inclined with angle of about 10% from the Kushiro side to the central span. The supporting layer is located at 10m for A1 to 19m for P1 under the sea level.

The On−netoh bridge is designed according to the Design Specifications of Highway Bridges issued in 1980[3]. The seismic lateral force was not decreased considering the damping effects of the Menshin bearings. **Table 1** shows the natural periods of substructures and the corresponding seismic lateral force coefficients. **Table 2** shows the design conditions for the Menshin bearings. Menshin design was made according to Guidelines for base Isolation of Highway Bridges[4] and Manual for Menshin Design of

Highway Bridges[5].

Table 1 Natural Period and Lateral Force Coefficient

	Ground Condition	Natural Period (sec)	Lateral Force Coefficient (Kh)
A1	Type I	0.964	0.23
P1	Type II	0.970	0.25
P2	Type II	1.044	0.28
P3	Type II	1.062	0.28

Table 2 Design Conditions of Bearings

	RB	LRB
Maximum Vertical Reaction Force R (tf)	50.0	135.0
Dead-Load Reaction Force W (tf)	23.0	92.0
Live-Load Reaction Force W (tf)	27.0	43.0
Design Displacement U_B (cm) (Bearing Capacity Method, Type H Ground)		15.0
Equivalent Stiffness K_B (kgf/cm)	615	2280
Equivalent Damping Ratio h_{eq}		0.21

Note) RB and LRB represent rubber bearing and lead rubber bearing, respectively

EARTHQUAKE RESPONSE OF ON-NETOH BRIDGE DURING KUSHIRO-OKI EARTHQUAKE OF 1993

The Kushiro-oki Earthquake occurred at 8:06 PM, January 15, 1993. The earthquake was located in the center of eastern Hokkaido and affected over a wide area including Tohoku and Kanto regions. The earthquake registered magnitude of 7.8 on the Richiter scale and the epicenter was reported as approximately 30km off the south coast of Kushiro city at lat. 42° 51' N, long. 144° 23' E. Depth was 107km. A number of aftershocks with epicenters of over 90km deep occurred within one day after the main shock and a few occurred after two days.

Three SMAC-Q type strong motion seismographs are installed at the pier crest, abutment crest and ground surface near the abutment of the existing bridge. Strong motions were successively measured at three seismographs. Fig. 7 shows the measured acceleration records. Duration time is over 240 seconds. Table 3 shows the peak

acceleration measured at the ground surface and the abutment. Peak accelerations of the ground surface are 341.5cm/sec^2 in the longitudinal direction and 363.1cm/sec^2 in the transverse direction. The peak acceleration of UD component is 114.4cm/sec^2 which corresponds to about 33% of horizontal peak accelerations. Peak accelerations of the abutment in the longitudinal and transverse directions are about 425cm/sec^2 and 300cm/sec^2, respectively. **Fig. 8** shows acceleration response spectrum of the measured strong motion at the ground surface. The analysis was made for the main shaking of 40 seconds from the time of 90 second to 130 second. The predominant period of the response spectrum of horizontal components was found to be in the range of 0.5 to 4.0 second, which contains relatively long period components and the peak is around 0.8 second. The predominant period of UD component is less than 1 sec.

Table 3 Measured Peak Acceleration (cm/sec^2)

	LG	TR	UD
Ground	342	363	114
Abutment	425	300	–

Photo 2 shows the situation of the bearings of the On–netoh bridge after the earthquake. The rubbing between the sole plate of the bearing and the side stopper occurred and the coming off of the painting was found. According to the marks, peak relative displacement of the bearings is estimated as about 4 to 5cm. Larger displacement was found at Pier P4 than the other piers and abutment. No damage or mark were found at expansion joints or hand rails at A1 abutment side.

RESPONSE ANALYSIS OF THE ON–NETOH BRIDGE

Nonlinear time history response analysis for the On–netoh bridge was made. Direct integration method using Newmark β algorithm was used for the analysis. Reyleigh–type damping was assumed to represent the damping characteristics of the bridge. **Fig. 9** shows the analytical idealization of the On–netoh bridge. It was assumed that the piers be in the elastic range and that nonlinear effect of Menshin bearings be expressed as a bi–linear model.

The foundations of A1, P1~P3, which are the pile foundation, are modelled as a linear spring model. On the other hand, that of P4, which is a direct foundation, is assumed as fixed. The characteristics of the bearings used for the analysis are shown in Table 4. Although the mean and lowest temperature in the Nemuro region at the time of the earthquake were reported as −4.8℃ and −7.9℃, respectively, the stiffness of Menshin bearings at the temperature of 20℃ and −20℃ was assumed in this analysis. Stiffness of

the Menshin bearings at those temperature condition were computed based on the loading tests of bearings. Analysis was made for the longitudinal direction which corresponded to the direction of Menshin design. The strong motion data with duration time of 120 seconds between the time of 50 second to 170 second was used as an input ground motion.

Table 4 Characteristics of Bearings for Analysis

Bearings	Characteristics		20°	−20°
RB	Stiffness	K_{RB} (tf/m)	363.0	472.0
LRB	First Stiffness	K_1 (tf/m)	5188.0	8953.2
	Second Stiffness	K_2 (tf/m)	471.1	645.0
	Ratio of Stiffness	K_2/K_1	0.07212	0.07204
	Yield Displacement	δ (m)	0.01832	0.01244

Note) RB and LRB represent rubber bearing and lead rubber bearing, respectively

Fig. 10 shows the time histories of acceleration and displacement of deck and relative displacement of bearing at pier P2 when the temperature is assumed as −20℃. The responses of the deck were not elongated comparing with the ground motion because the stiffness of the bearings become relatively large in the cold district. Peak deck acceleration is computed as 505cm/sec^2. Amplification of the ground motion is estimated as 1.48. However, the response acceleration of the deck seems to be decreased during the time of 45 to 60 second when the excitation of the strong ground motion. The response of deck displacement and relative displacement of bearings are almost the same and the peak response occurred around the peak of the input ground motion. The residual displacement with about 2mm is found at the bearings.

Table 5 shows the computed peak bending moment at the bottom of piers. Although the peak bending moment at the bottom of pier P1 to P3 is in the range of 1,200 to 1,500tf·m when the temperature is assumed as 20℃, on the other hand, they become twice when the temperature is assumed as −20℃. However, those for Abutment A1 and Pier P4 do not change drastically depending on the temperature, because the variation of the stiffness of rubber bearings with temperature is relatively small. Comparing the bending moment of the piers between computed through the nonlinear analysis and designed, the computed bending moment is about twice the designed bending moment.

Relative displacement of bearings are also shown in Table 5. As mentioned before, the peak relative displacement was estimated as 4 to 5cm from the observation of the bridge after the Earthquake, however, that computed with assumption of temperature of −20℃ is about 8 to 9cm. Therefore, relative displacement of expansion joints is also estimated as 8 to 9cm. Design displacement according to seismic lateral force coefficient

method is 5.5 to 6.6cm. Based on the analysis, it is estimated that the inertia force beyond the design seismic lateral force acted to the piers. However, the actual bridge response is much smaller than the computed one.

Table 5 Computed Peak Response

	Peak Bending Moment at the Base of Pier (tfm)			Peak Relative Displacement of Bearing (cm)
	20°	−20°	design value	−20°
A1	485.7	475.8		
P1	1175.6	2227.5	806.0	9.0
P2	1295.2	2464.8	1053.0	8.6
P3	1528.1	2733.9	1203.0	8.0
P4	58488	60157	19129	

CONCLUSIONS

The On−netoh bridge, which employs the Menshin design in the cold and snowy district at Nemuro, Hokkaido, experienced the Kushiro−oki Earthquake of 1993. The peak acceleration measured on the ground surface is over 350cm/sec^2. The analytical simulation using the measured ground motion shows that the bending moment at the bottom of pier is estimated to be over the designed one. The effect of the earthquake may be small and the seismic isolation may be successively functioned.

REFERENCES

1) Ikeda, H., Matsumoto, N. and Fukuda, K. : Design Plan of On−netoh Bridge − Design of the Bridge with Menshin Devices −, Bridges and Foundations, Vol. 90−5, 1990
2) Nakano, O., Taniguchi, H. and Nishi, H. : Effect of Temperature on the Dynamic Behavior of Base−Isolated Bearings, Proceedings of the 24th Joint Meeting, Wind and Seismic Effects, UJNR, Gaithersburg, May, 1991
3) Japan Road Association : Part V, Seismic Design of Design Specifications of Highway bridges, 1990
4) Technology Research Center for National Land Development : Guidelines for Base Isolation of Highway Bridges, 1989
5) Public Works Research Institute : Development of Menshin Design of Highway Bridges, October 1992, Technical Note of Public Works Research Institute, Vol. 60

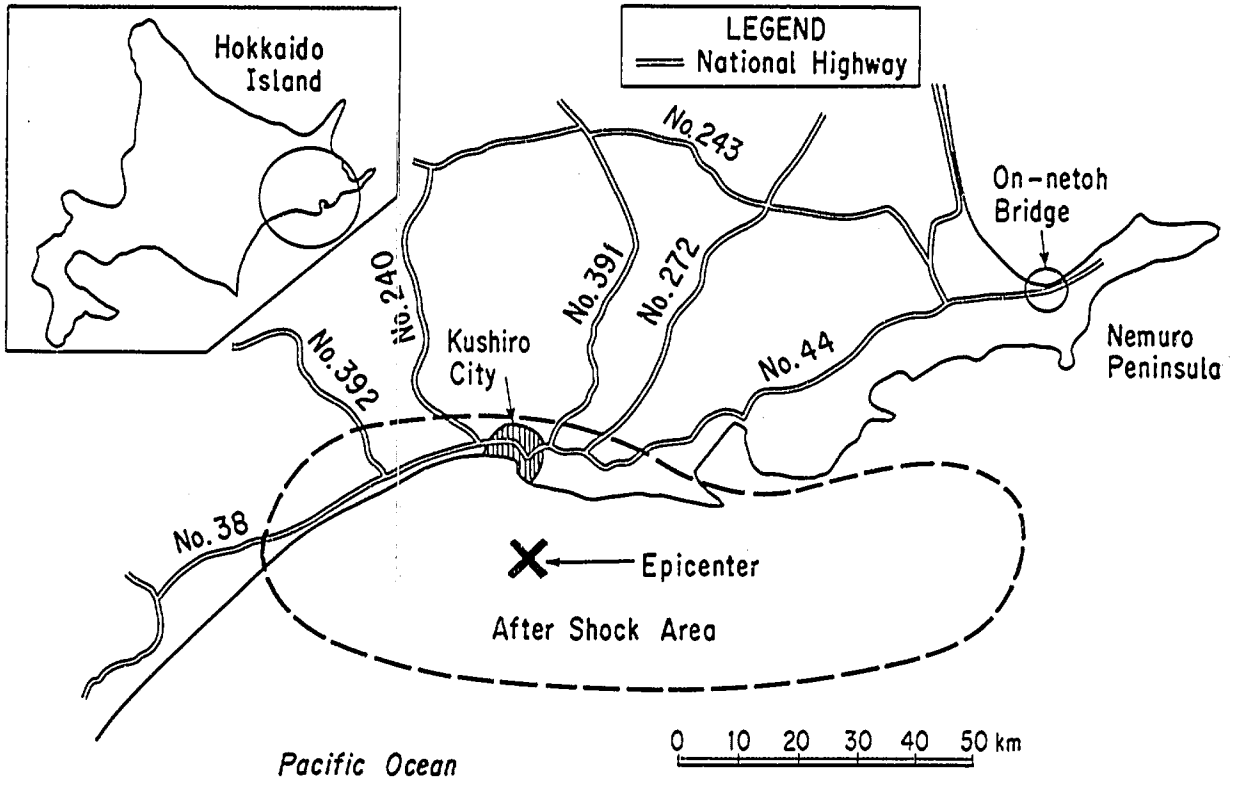


Fig. 1 Locations of the On-netoh Bridge and the Earthquake Epicenter

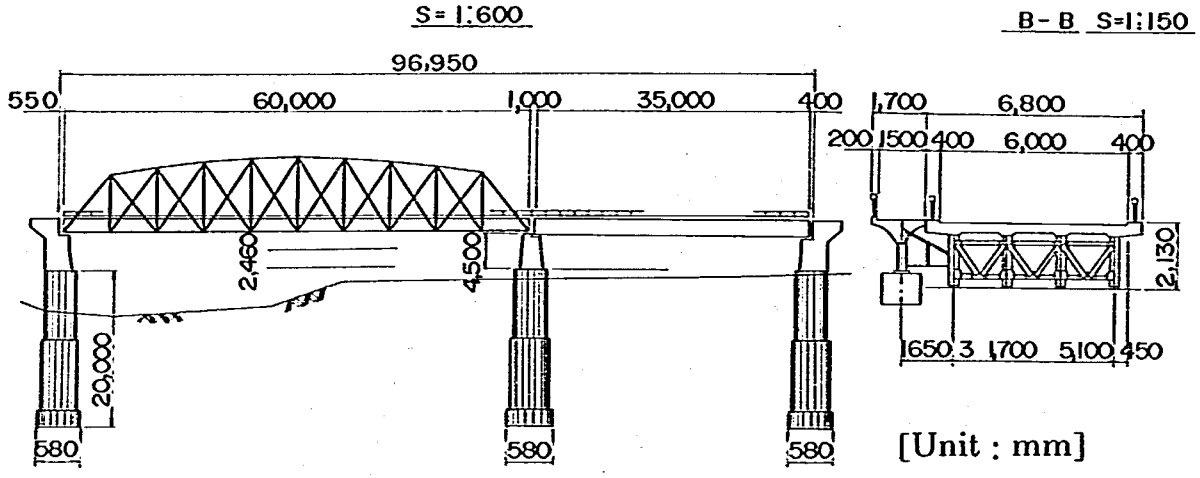


Fig. 2 Side View of the Existing Bridge

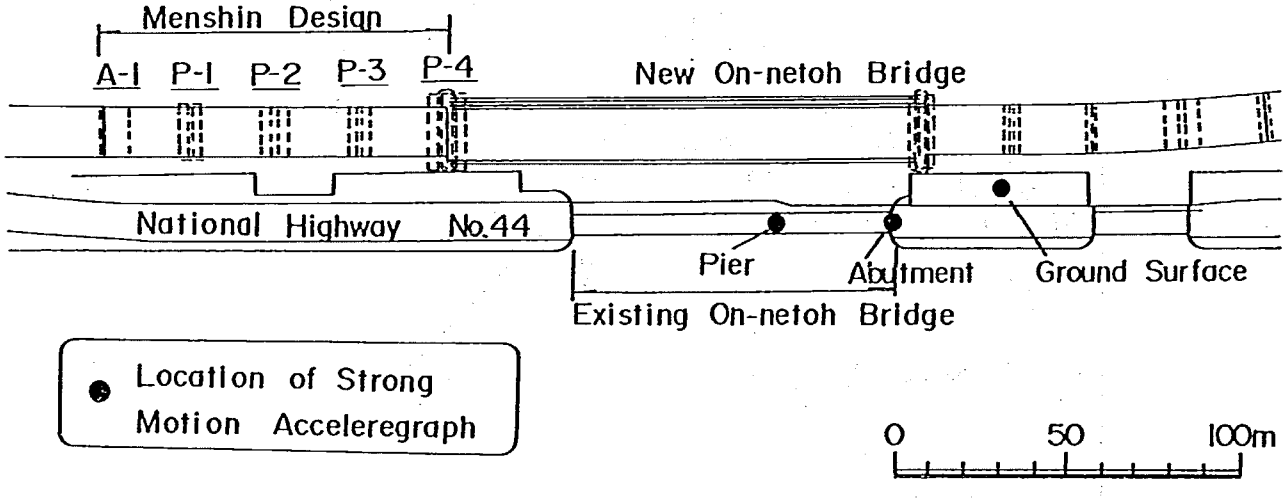


Fig. 3 Locations of two Bridges

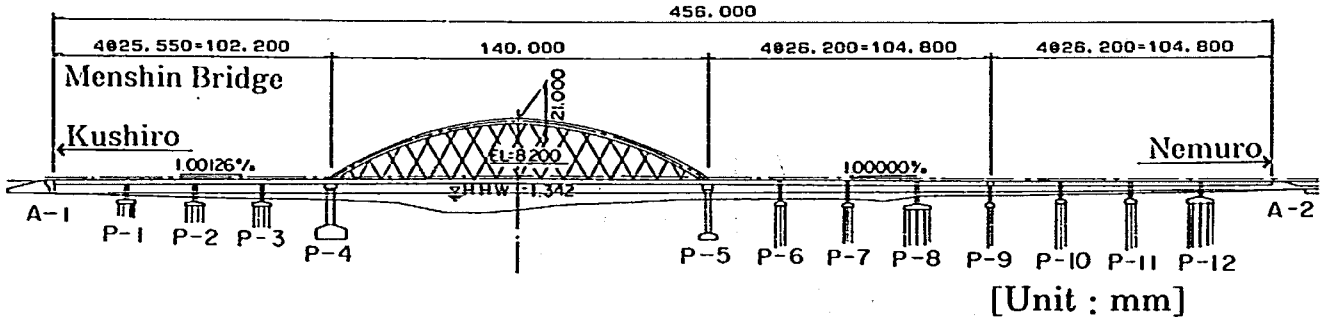


Fig. 4 Side View of the On-netoh Bridge

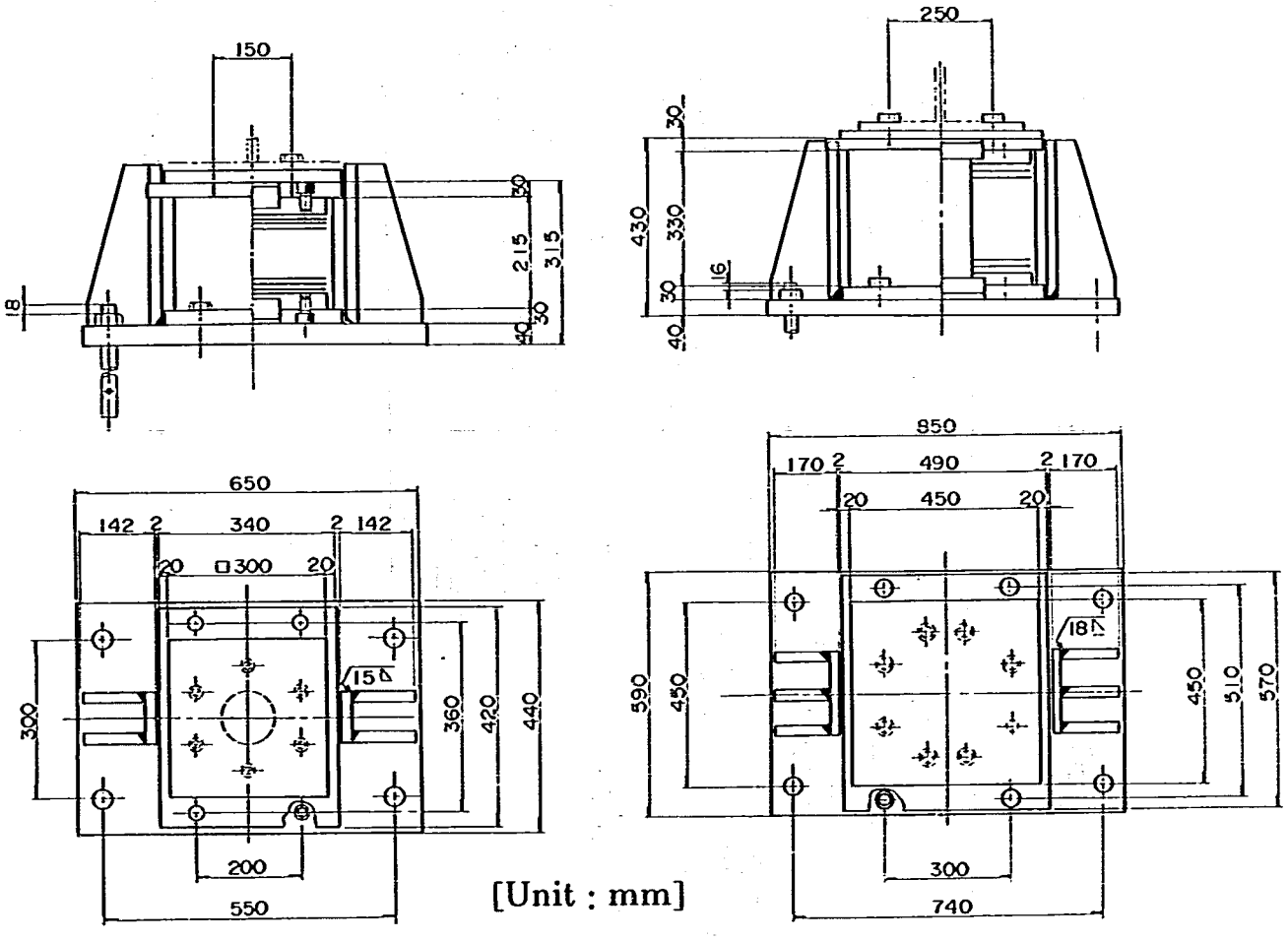


Fig. 5 Bearings used for the On-netoh Bridge

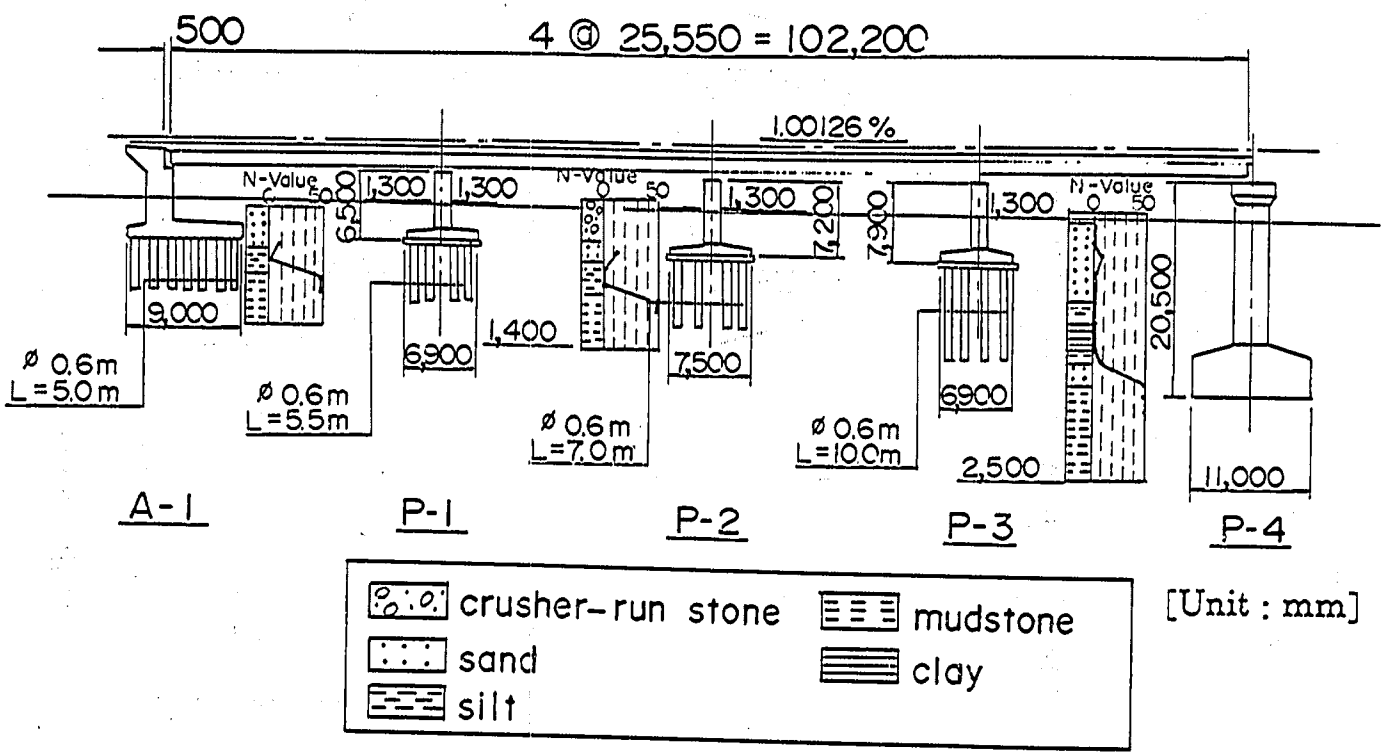


Fig. 6 Ground Condition of the On-netoh Bridge

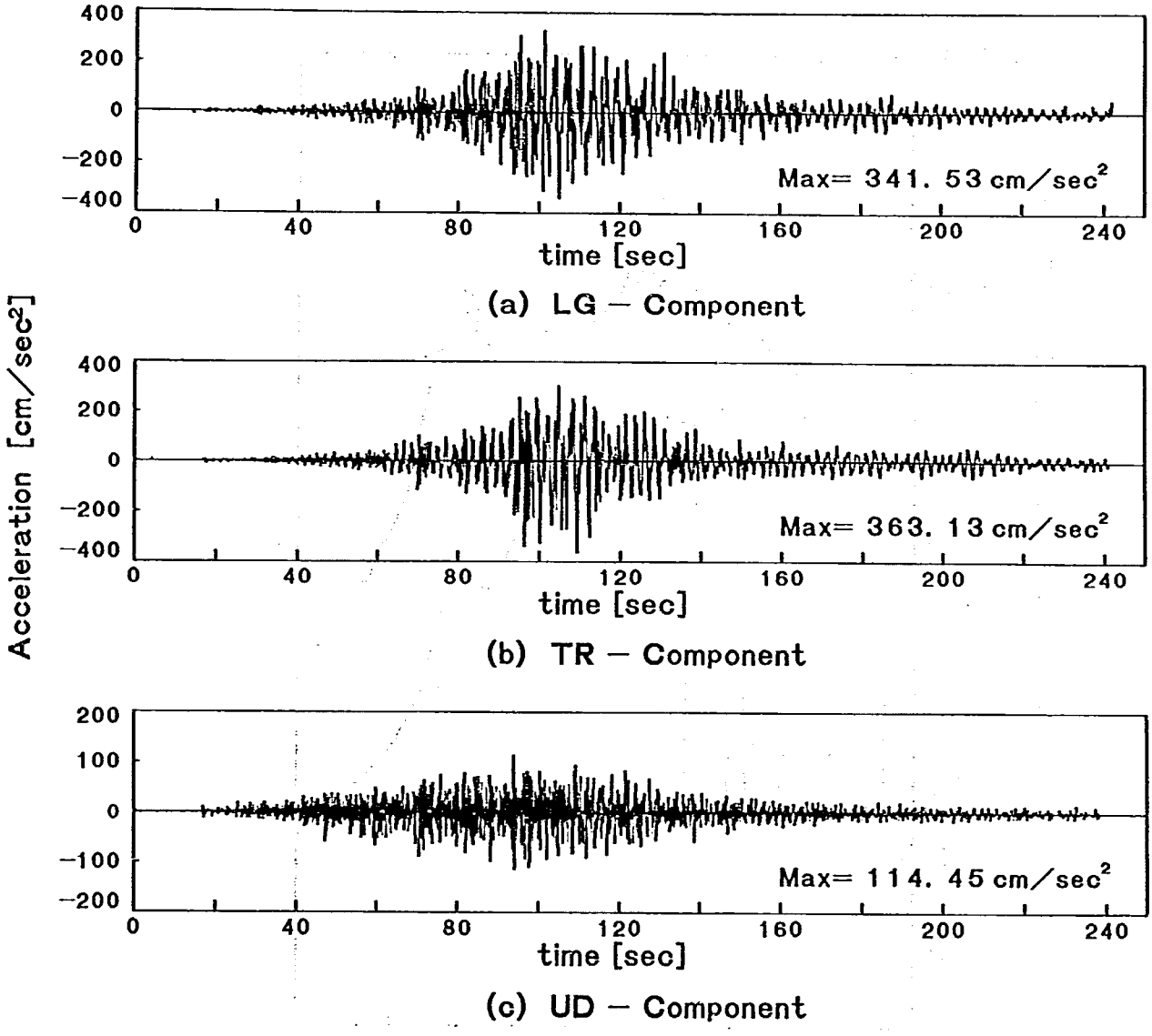


Fig. 7 Strong Motion Record on the Ground Surface

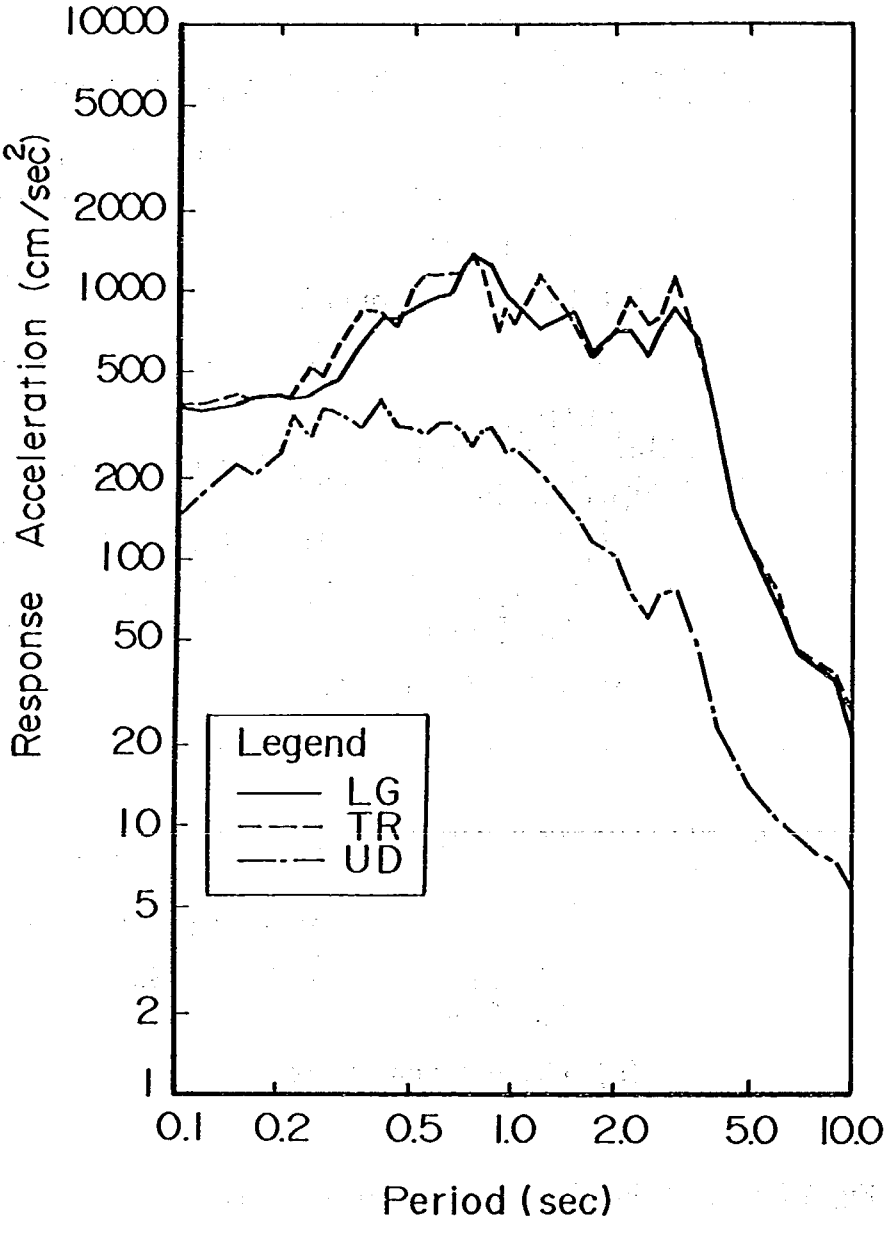


Fig. 8 Acceleration Response Spectrum

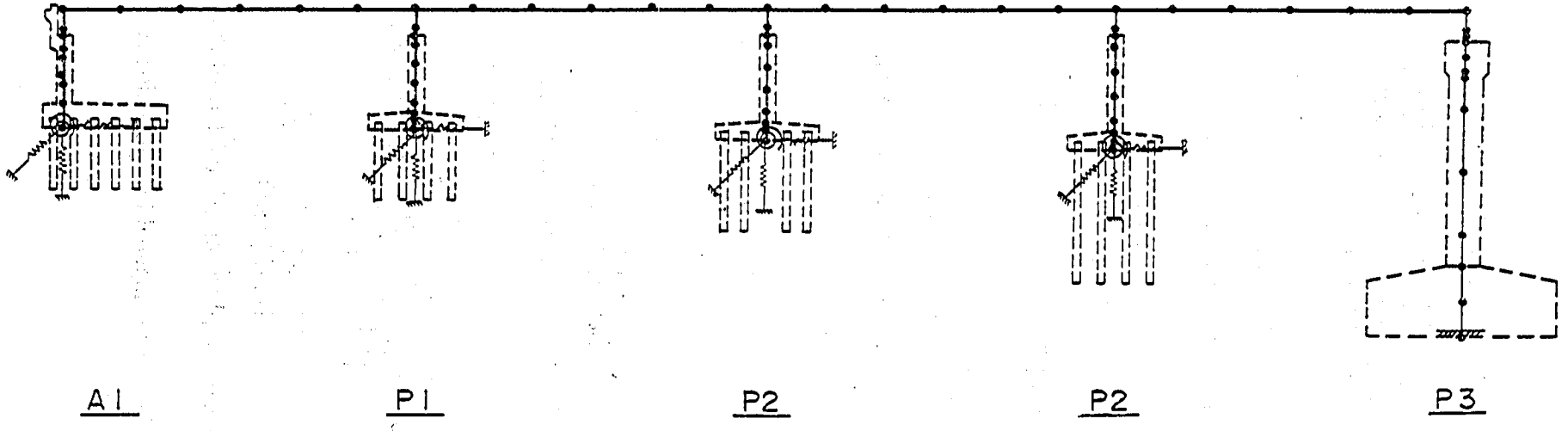
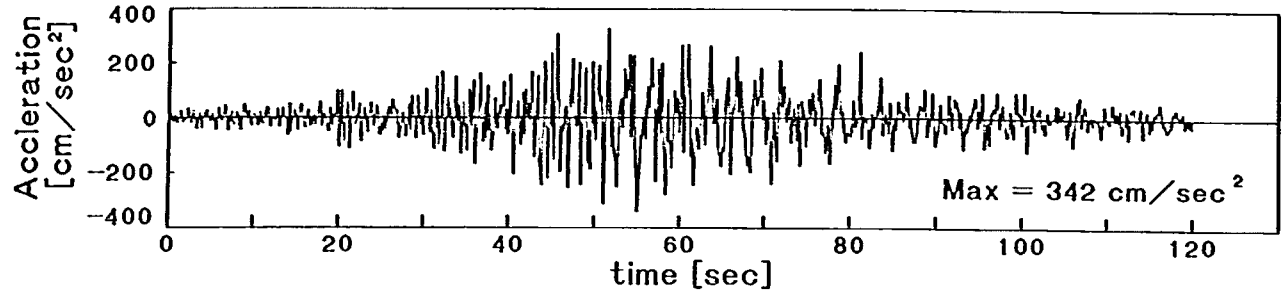
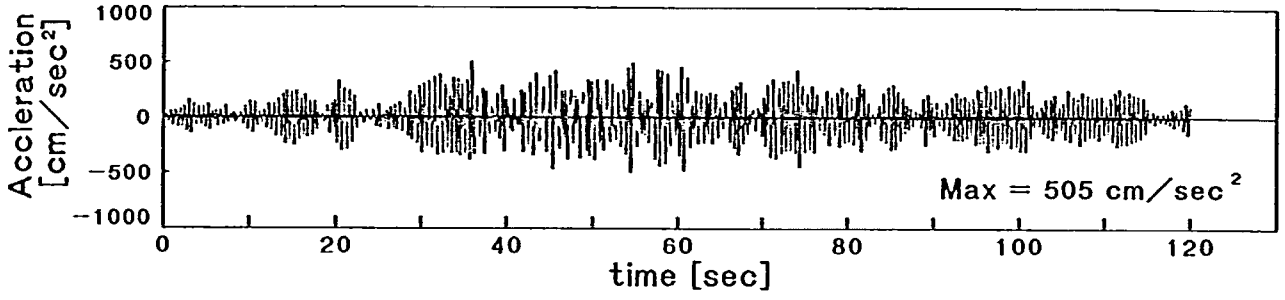


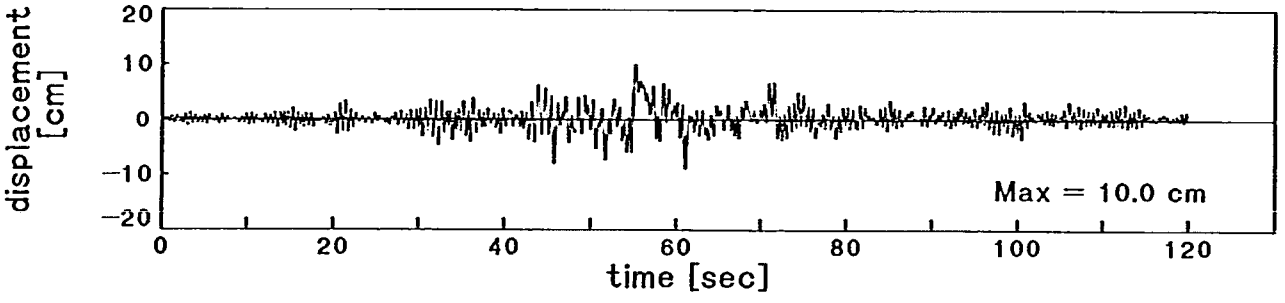
Fig. 9 Analytical Idealization



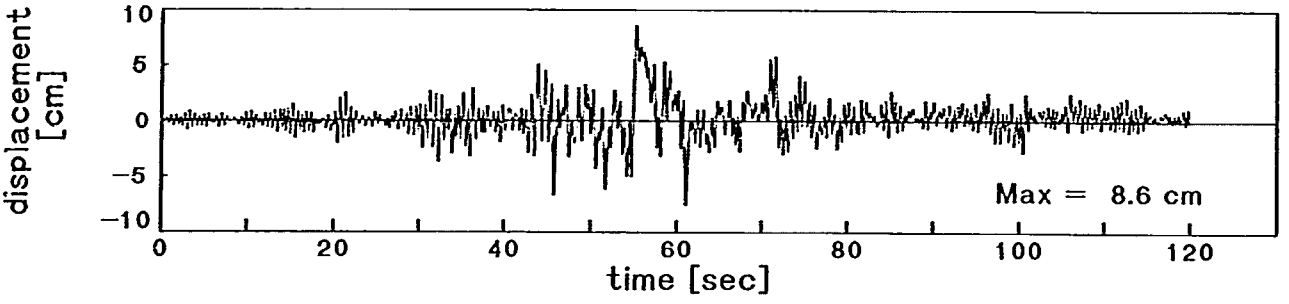
(a) Input Ground Motion



(b) Response Acceleration of Deck



(c) Displacement of Deck



(d) Relative Displacement of Lead Rubber Bearing

Fig. 10 Time Histories computed by Simulation Analysis

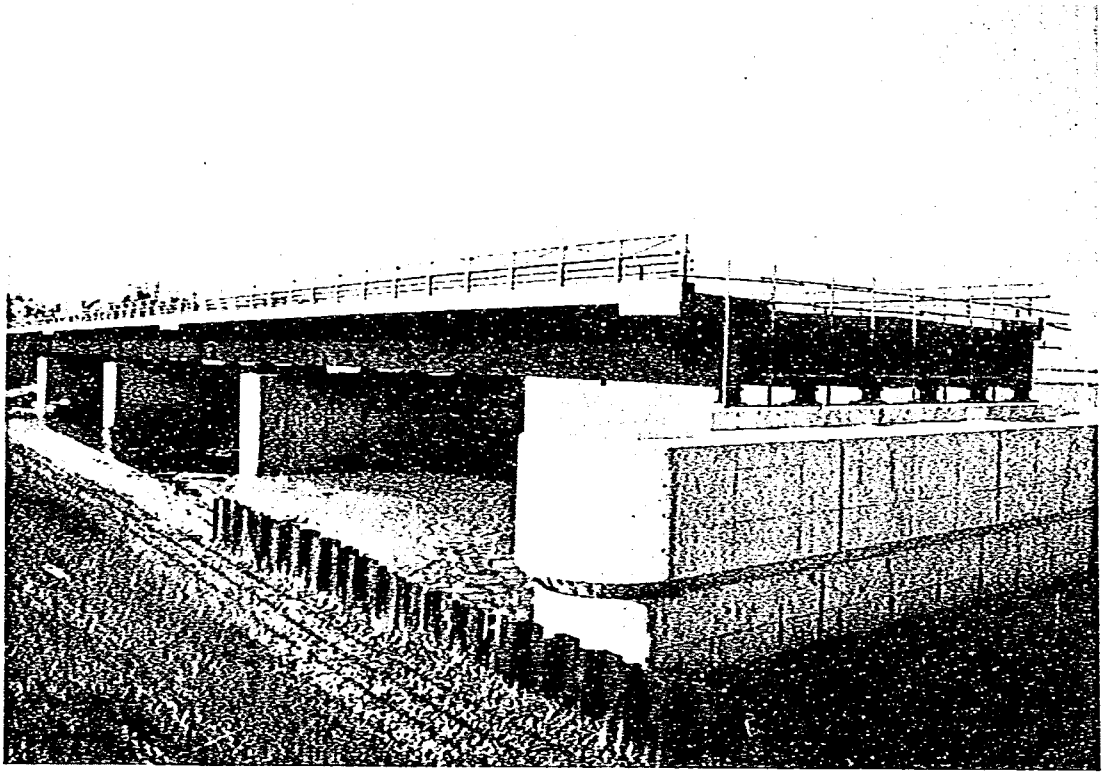
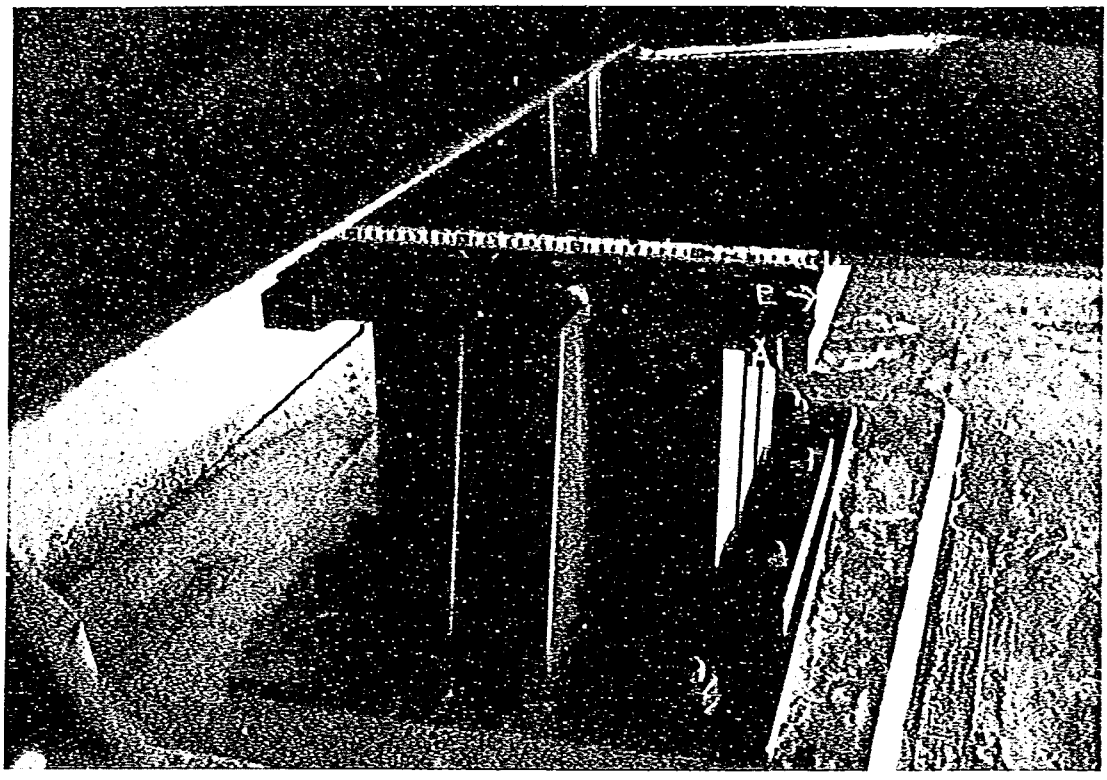
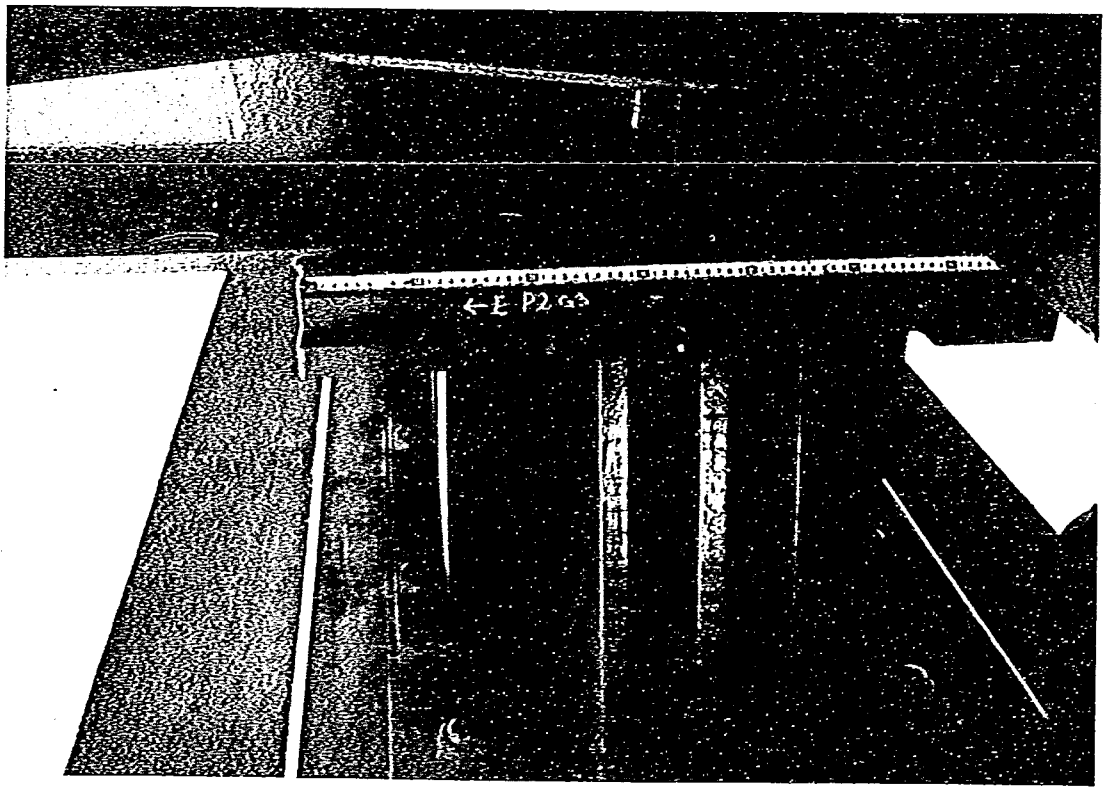


Photo 1 On-netoh Bridge



(a) A1 (RB)



(b) P2 (LRB)

Photo 2 Bearings after the Earthquake

Menshin Design Example of Highway Bridge

Kazuhiko KAWASHIMA
Shigeki UNJOH
Tsuneo UZUKA
Kazuhiko KAWAKAMI
Kazuomi KUMAKURA
and
Hideo TANI

3rd U.S.–Japan Workshop on
Earthquake Protective Systems for Bridges
Berkeley, U.S.A.
January, 1994

MENSHIN DESIGN EXAMPLE OF A HIGHWAY BRIDGE

Kazuhiko KAWASHIMA[1], Shigeki UNJOH[2], Tsuneo UZUKA[3]
Kazuhiko KAWAKAMI[4], Kazuomi KUMAKURA[5] and Hideo TANI[6]

1) Head, Earthquake Engineering Division, Public Works Research Institute, Ministry of Construction, Tsukuba Science City, Japan
2) Senior Research Engineer, ditto
3) Director, Road Construction Division, Department of Public Works, Tochigi Prefectural Government, Utsunomiya, Tochigi-ken, Japan
4) Section Chief, ditto
5) Senior Chief, ditto
6) Technical Staff, ditto

ABSTRACT

This paper presents a Menshin design example of a highway bridge based on the Japanese design specifications. The design of Yama-age Bridge which was completed in May 1993 in Tochigi Prefecture is presented as an example. The Yama-age bridge is of 6-span continuous concrete box girder with length of 246.3m. High damping rubber bearings were adopted as Menshin devices.

YAMA-AGE BRIDGE

Fig. 1 and **Photo 1** show the Yama-age bridge[1)-3)]. **Table 1** summarizes the design outlines of the Yama-age bridge. The superstructure is of 6-span continuous prestressed concrete two-cell box girder with length of 246.3m. The deck width ranging from 6.5m (standard section) to 8.0m (wide section). The abutment is of a inverted T-type reinforced concrete substructure and the piers are of reinforced concrete wall type with rectangular section. The foundations of all substructures are of direct foundation. High damping rubber (HDR) bearing is adopted for the bridge. Since Menshin design is applied only in longitudinal direction, the displacement in transverse direction is restrained by stoppers. Forced excitation test using an eccentric-mass shaker and quick-release jacks was also made for the bridge in December 1992 as shown in **Photo 2**[4)].

The ground condition of the Yama-age bridge consists of sand-gravel layers and slate layer. N-value by the standard penetration test for the sand-gravel layers is ranging from 30 to 50, and that of the slate layer is greater than 50. The ground condition is

classified as Class I.

MENSHIN DESIGN OF YAMA-AGE BRIDGE

Design Specifications

The Yama-age Bridge was designed in accordance with the regulations of the "Design Specifications for Highway Bridges[5]". "Guidelines for Design of Menshin Highway Bridges[6]" and "Manual for Menshin Design of Highway Bridges[7)-8)]" were also referred for the Menshin design issues. It should be noted that since the bridge was designed based on the Design Specifications for Highway Bridges, the design lateral force was not reduced in consideration of the damping effect of Menshin bearings.

Menshin Design

Fig. 2 shows the Menshin design flow used for the Yama-age Bridge. In the Menshin design of highway bridges, the Menshin devices are designed by the "Seismic Coefficient Method" and the "Bearing Capacity Method". In both methods, the lateral force is statically applied to the bridge, and the seismic safety is checked based on the allowable stress design approach in the Seismic Coefficient Method and bearing capacity basis considering ductility in the Bearing Capacity Method. Bridges are designed by the Seismic Coefficient Method, and then the ductility is checked for reinforced concrete piers by the Bearing Capacity Method.

Design of Menshin Bearing

The relation between shear modulus of elasticity $G(\gamma)$ and shear strain γ for HDR bearings adopted is shown in Fig. 3. The stiffness of the bearings shows the nonlinear characteristics depending on the strain of the bearing. The shear modulus of HDR is given by the following experimental equations.

$$\left.\begin{aligned} G(\gamma)&=26.3-46.0\gamma+45.7\gamma^2-21.1\gamma^3+3.88\gamma^4 \quad (0<\gamma\leqq 1.8)\\ G(\gamma)&=0.31+6.89\gamma-1.08\gamma^2 \quad (\gamma>1.8)\end{aligned}\right\} \quad (1)$$

The design of HDR bearings was made according to the following procedure as :

1) Assume the design displacement of bearings for two levels of seismic lateral forces and compute the shear strain of bearings.

$$\gamma=\frac{u_B}{H_R} \quad (2)$$

where,

γ : shear strain

u_B : design displacement of bearing

H_R : thickness of rubber bearing

2) Compute the shear modulus of elasticity and the equivalent stiffness of bearings.

$$K_B = A_0 \times G(\gamma) \tag{3}$$

where,

$G(\gamma)$: shear modulus of elasticity

K_B : equivalent stiffness

A_0 : sectional area of bearing

3) Compute the natural period of the bridge and the horizontal design lateral force coefficient.

$$K_T = \sum K_B \tag{4}$$

$$T = \frac{2\pi \cdot R_d}{\sqrt{g \cdot K_T}} \tag{5}$$

where,

K_T : total stiffness of bearings

T : natural period

R_d : dead load of superstructure

g : gravity acceleration

4) Compute the displacement of bearings, and compare it with the assumed displacement.

$$u_s = \frac{R_d \cdot k_h}{K_B} \tag{6}$$

where,

k_h : lateral force coefficient

Tables 2 to 4 show the design of HDR bearings of the Yama-age bridge.

Design Lateral Force Coefficient

The bridge was designed based on the Seismic Coefficient Method. Since the seismic design structural unit of the Yama-age bridge is defined as the total bridge system, analytical idealization of the bridge is shown in **Fig. 4.** Bearings and foundations were modeled as equivalent linear spring elements. Natural period of the bridge is computed for the seismic design structural unit as :

$$T = 2.01 \cdot \sqrt{\delta} \tag{7}$$

$$\delta = \frac{\int w(s)\, u(s)^2 ds}{\int w(s)\, u(s) ds} \tag{8}$$

where,

T : natural period

$w(s)$: dead weight of the seismic design structural unit at point "s"

$u(s)$: lateral displacement at point "s" when subjected to $w(s)$ in the direction considered in design

Design seismic coefficient is computed as:

[Seismic Coefficient Method]

$$k_h = c_z \cdot c_G \cdot c_I \cdot c_T \cdot k_{h0} \quad (9)$$

$$c_T = 1.33 \cdot T^{-2/3} \text{ (Ground Condition : Class I)} \quad (10)$$

where,

k_h : lateral force coefficient
c_z : modification factor for zone (Fig. 5)
c_G : modification factor for ground condition (Table 5)
c_I : modification factor for importance (Table 6)
c_T : modification factor for structural response (Table 7)
k_{h0} : standard design horizontal seismic coefficient (=0.2)

[Bearing Capacity Method]

$$k_{he} = \frac{k_{hc}}{\sqrt{2 \cdot \mu - 1}} \quad (11)$$

$$k_{hc} = c_z \cdot c_I \cdot c_R \cdot k_{hc0} \quad (12)$$

$$c_R = 0.876 \cdot T^{-2/3} \text{ (Ground Condition : Class I)} \quad (13)$$

where,

k_{he} : equivalent lateral force coefficient for Bearing Capacity Method
k_{hc} : lateral force coefficient for Bearing Capacity Method
c_R : modification factor for structural response (Table 8)
μ : allowable ductility factor of reinforced concrete piers
k_{hc0} : standard design horizontal seismic coefficient (=1.0)

The natural period in longitudinal direction is 1.56sec, and that of the transverse direction is 0.194sec. Therefore, the lateral force coefficients are 0.16 and 0.20 in longitudinal and transverse directions, respectively. Since the natural period in longitudinal direction with usual design is 1.075sec, the lateral force coefficient is 0.20. Hence, by adopting the Menshin design, the lateral force is reduced by 20% than the usual design.

Table 9 shows the relative displacement of bearings by the Seismic Coefficient Method. Table 10 shows the bending moment at the bottom of piers. The bending moment is compared between with and without the Menshin design. Fig. 6 shows the cross section of pier (P1).

Check of Bearing Capacity for Lateral Force

To prevent a brittle failure such as falling-off of superstructure during large earthquakes, the bearing capacity of the reinforced concrete piers designed by the Seismic Coefficient Method was checked by the Bearing Capacity Method.

The natural period of the bridge is computed using the equivalent stiffness of bearings corresponding to the design displacement and equivalent yielding stiffness of substructures. Since it is 1.77 sec, the lateral force coefficient for the Bearing Capacity

Method k_{hc} is 0.60. Tables 11 and 12 shows the check results of the bearing capacity of the reinforced concrete piers.

Dynamic Analysis

Dynamic Analysis was made to check the safety of the Yama-age Bridge. the response spectrum analysis and the time history analysis were made. The response spectrum and time history acceleration data of the earthquake ground motion corresponding to the Seismic Coefficient Method was used as an input acceleration. Table 13 shows the equivalent stiffness and the equivalent damping ratio of HDR bearings.

Since the damping characteristics of the HDR bearings varies depending on the displacement, the following experimental equation on the damping ratio was used.

$$h_B = 0.172 - 0.00693\gamma + 0.00276\gamma^2 - 0.006924\gamma^3 \qquad (14)$$

where,

h_B : effective damping ratio

γ : shear strain of bearing

The damping ratio for the superstructure, substructures, and the foundations were assumed as 3%, 5%, and 10%, respectively. Table 14 shows the natural period and the damping ratio of an each vibration mode. The 1st to 3rd vibration modes are shown in Fig. 7. The 1st mode is a sway mode of the superstructure and this is the most predominant mode in longitudinal direction. The damping ratio of the 1st mode is 14.3%.

Tables 15 and 16 shows the displacement of bearings and sectional forces of the pier bottom computed through the dynamic analyses in comparison with those by the Seismic Coefficient Method. The displacement of bearings and bending moment by the dynamic analyses are less than those by the Seismic Coefficient Method.

Fig. 8 shows the acceleration responses of deck and pier P1 computed through the time history analysis. It is found that the period of the deck response is elongated by adopting the Menshin design and that the deck acceleration is reduced comparing with that of the pier top.

It should be noted here that although the design lateral force was not reduced in consideration of the damping effect by Menshin devices in the design, it is found through the dynamic analyses that the response of the bridge is significantly reduced (by about 35 – 40% than those by the Seismic Coefficient Method) by adopting the Menshin design.

Design Details

According to the design specifications, the falling-off prevention devices are installed for the bridge. Fig. 9 shows the stopper to prevent excessive displacement of the deck.

REFERENCES

1) Ikeda, T., Ozeki, k., Kumakura, K. and Abe, N. : Design of the Karasnyama No.1 Bridge

(Base Isolated Bridge), Bridge and Foundation Engineering, Vol.25, No.6, June 1991 (in Japanese)
2) Ikeda, T., Kumakura, K., Tani, H. and Abe, N. : Plan and Design of the Karasuyama No.1 Bridge, Bridge Engineering, Vol.27, No.6, June 1991 (in Japanese)
3) Uzuka, T., Kawakami, K., Kumakura, K. and Tani, H. : Menshin Design and Construction of Multi-span Continuous Prestressed Concrete Bridge, Proc. the 2nd U.S.-Japan Workshop on Earthquake Protective Systems for Bridges, December, 1992, Technical Memorandum of PWRI, No.3196
4) Kakinuma, T., Kawakami, K., Kumakura, K., Tani, H. and Abe, N. : Vibration Test of A Menshin Designed Multi-span Continuous Prestressed Concrete Bridge, Proc. the 3rd U.S.-Japan Workshop on Earthquake Protective Systems for Bridges, January, 1994, San Francisco
5) Japan Road Association : Design Specifications for Highway Bridges, Part I - V, February 1990 (in Japanese)
6) Technology Research Center for National Land Development : Guidelines for Base Isolation of Highway Bridges (Draft), March 1989 (in Japanese)
7) Public Works Research Institute : Development of Menshin Design of Highway Bridges, October, 1992, Technical Note of PWRI, Vol.60
8) Kawashima, K. : Manual for Menshin Design of Highway Bridges, Proc. the 2nd U.S.-Japan Workshop on Earthquake Protective Systems for Bridges, December, 1992, Technical Memorandum of PWRI, No.3196
9) Kawashima, K., Okado, M. and Horikawa, M. : Design Example of A Highway Bridge Based on The Manual for Menshin Design of Highway Bridges, Proc. the 2nd U.S.-Japan Workshop on Earthquake Protective Systems for Bridges, December, 1992, Technical Memorandum of PWRI, No.3196

Table 1 Design Outline of Yama-age Bridge

Bridge Type	Prestressed Concrete Post Tensioning
Structure	6-Span Continuous Box Girder
Road Class	Design Vehicle Speed : 60km/h
Bridge Length	246.3m
Span Length	$6 \times 40.8 = 244.8$m
Deck Width	Standard Section : 8.0m(roadway)+2.5m(sidewalk)=10.5m Widening section :11.0m(roadway)+2.5m(sidewalk)=13.5m
Live Load	TL-20
Impact Coefficient	$i = 1.0/(20+L)$
Alignment	$R = \infty \sim A = 240$m
Vertical Gradient	1.0% ~ VCL=100m, R=2,500m ~ 5.0%
Cross Slope	1.5%(roadway), 2.0%(sidewalk)
Abutment Skew Angle	90° (A1), 90° 27' 43" (A2)
Ground Condition	Class : I
Design Lateral Force Coefficient	$k_h = 0.16$ (Longitudinal direction) $k_h = 0.20$ (Transverse direction)

Table 2 Dimension of HDR Bearings (unit:mm)

Item	A1	P1	P2	P3	P4	P5	A2
Dimension	700×855	950×1500	1030×1580	950×1500	950×1500	950×2500	700×855
Thickness of Rubber Layers	14.7×14 =205.8	21.0×6 =126.0	34.0×3 =102.0	24.0×5 =120.0	24.0×6 =144.0	18.7×8 =149.6	13.8×19 =262.2
Thickness of Insert Plates	4.2×13 =54.6	4.2×5 =21.0	4.2×2 =8.4	4.2×4 =16.8	4.2×5 =21.0	4.2×7 =29.4	4.2×18 =75.6
Height of bearing	260.4	147.0	110.4	136.8	165.0	179.0	337.8

Note)Dimension A×B represents the widths in longitudinal and transverse directions, respectively.

Table 3 Design of HDR Bearings by Seismic Coefficient Method

Item [ ]:Unit		A1	P1	P2	P3	P4	P5	A2
Assumed Displacement	u_s [cm]	7.784						
Thickness of Rubber Bearing	H_R [cm]	20.58	12.60	10.20	12.00	14.40	14.96	26.22
Shear Strain	γ	0.378	0.618	0.763	0.649	0.541	0.520	0.297
Shear Modulus of Elasticity	$G(\gamma)$ [kgf/cm^2]	14.377	10.914	9.749	10.618	11.787	12.050	16.150
Area of Bearing	A_0 [cm^2]	5,872	14,137	16,161	14,137	14,137	14,137	5,872
Equivalent Stiffness	K_B [kgf/cm^2]	4,102	12,245	15,446	12,509	11,571	11,387	3,617
Number of Bearing on Each Substructure		2						
Sum of K_B	K_T [kgf/cm^2]	141,756						
Natural Period	T [sec]	1.337						
Dead load of Superstructure	R_d [kgf]	6,294,200						
Factor for Structural Response	c_T	1.096						
Design Lateral Force Coefficient	k_h	0.18						
Designed Displacement	u_s [cm]	7.770						

Table 4 Design of HDR Bearings by Bearing Capacity Method

Item	[ ]:Unit	A1	P1	P2	P3	P4	P5	A2
Assumed Displacement	u_s [cm]	32.69						
Thickness of Rubber Bearing	H_R [cm]	20.58	12.60	10.20	12.00	14.40	14.96	26.22
Shear Strain	γ	1.588	2.594	3.205	2.724	2.270	2.185	1.247
Shear Modulus of Elasticity	$G(\gamma)$ [kgf/cm^2]	8.674	10.916	11.299	11.064	10.385	10.208	8.469
Area of Bearing	A_0 [cm^2]	5,872	14,137	16,161	14,137	14,137	14,137	5,872
Equivalent Stiffness	K_B [kgf/cm^2]	2,475	12,247	17,902	13,035	10,195	9,647	1,896
Number of Bearing on Each Substructure		2						
Sum of K_B	K_T [kgf/cm^2]	134,794						
Natural Period	T_s [sec]	1.372						
Dead load of Superstructure	R_d [kgf]	6,294,200						
Factor for Structural Response	c_T	0.700						
Design Lateral Force Coefficient	k_h	0.70						
Designed Displacement	u_s [cm]	32.69						

Table 5 Modification Factor for Ground Condition c_G

Ground Group	I	II	III
c_G	0.8	1.0	1.2

Table 6 Modification Factor for Importance c_I

Group	c_I	Definition
1st class	1.0	Bridges on expressway (limited access highways), general national road and principal prefectural road. Important bridges on general prefectural road and municipal road.
2nd class	0.8	Other than the above

Table 7 Modification Factor for Structural Response c_T

Ground Group	Structural Response Coefficient c_T		
Group I	$T<0.1$ $c_T=2.69T^{1/3}\geqq 1.00$	$0.1\leqq T<1.1$ $c_T=1.25$	$1.1<T$ $c_T=1.33T^{-2/3}$
Group II	$T<0.2$ $c_T=2.15T^{1/3}\geqq 1.00$	$0.2\leqq T<1.5$ $c_T=1.25$	$1.3<T$ $c_T=1.49T^{-2/3}$
Group III	$T<0.34$ $c_T=1.80T^{1/3}\geqq 1.00$	$0.34\leqq T<1.5$ $c_T=1.25$	$1.5<T$ $c_T=1.64T^{-2/3}$

Table 8 Modification Factor for Structural Response c_R

Ground Group	Structural Response Coefficient c_R		
Group I	$T\leqq 1.4$ $c_R=0.7$		$1.4<T$ $c_R=0.876T^{-2/3}$
Group II	$T<0.18$ $c_R=1.15T^{1/3}\geqq 0.7$	$0.18\leqq T\leqq 1.6$ $c_R=0.85$	$1.6<T$ $c_R=1.16T^{-2/3}$
Group III	$T<0.29$ $c_R=1.15T^{1/3}\geqq 0.7$	$0.29\leqq T\leqq 2.0$ $c_R=1.00$	$2.0<T$ $c_R=1.59T^{-2/3}$

Table 9 Relative Displacement of Bearings by Seismic Coefficient Method (unit:cm)

Item	A1	P1	P2	P3	P4	P5	A2
Relative Displacement of Bearings	10.04	8.31	5.65	6.33	6.62	7.22	9.75
Design Displacement of Bearings	7.77						

Table 10 Bending Moment at the Bottom of Piers (unit:tf·m)

Item	P1	P2	P3	P4	P5
Menshin Design	4,704.7	3,677.2	2,824.4	2,345.0	2,017.0
Usual Design	4,793.2	5,062.8	4,760.8	4,601.5	4,578.2

Table 11 Check of Bearing Capacity of Piers

Item		Unit	P1	P2	P3	P4	P5
Width of pier		m	8.0	8.0	6.5	6.5	6.5
Thickness of pier		m	2.5	2.2	2.2	2.0	2.0
Longitudinal Reinforcement	Main Reinforcement	mm cm^2	D32−ctc150 1.5 step 1,270.72	D32−ctc150 1.5 step 1,270.72	D29−ctc150 1.5 step 835.12	D29−ctc150 1.5 step 835.12	D29−ctc150 1.0 step 552.46
	Side Reinforcement	mm cm^2	D19−ctc150 138.03	D19−ctc150 126.57	D19−ctc150 114.42	D19−ctc150 108.69	D19−ctc150 108.69
Allowable Ductility Factor μ			4.739	3.683	5.393	4.991	4.984
Equivalent Horizontal Seismic Coefficient k_{he}			0.21	0.24	0.19	0.21	0.20
Bearing Capacity for Shear Failure P_s		tf	1,385.95	1,209.86	995.81	899.18	951.53
Bearing Capacity for Flexural force P_u		tf	378.60	347.17	285.88	278.04	269.70
Bearing Capacity for Lateral Force P_a		tf	378.60	347.17	285.88	278.04	269.70
Inertia Force $P = k_{he} \times w$		tf	348.20	346.58	239.58	245.54	250.82

Table 12 Relative Displacement of Bearings by Bearing Capacity Method (unit:cm)

	A1	P1	P2	P3	P4	P5	A2
Relative Displacement of Bearing	48.86	30.50	20.08	24.85	28.51	34.06	48.11
Design Displacement of Bearing	32.69						

Table 13 Equivalent Stiffness and Equivalent Damping Ratio of HDR Bearings

Item	[ ]:Unit	A1	P1	P2	P3	P4	P5	A2
Design Displacement	u [cm]	10.04	8.31	5.65	6.33	6.62	7.22	9.75
Area of Bearing	A [cm^2]	5,872	14,137	16,161	14,137	14,137	14,137	5,872
Thickness of Rubber Bearing	H_R [cm]	20.58	12.60	10.20	12.00	14.40	14.96	26.22
Shear Strain	γ	0.488	0.660	0.544	0.528	0.460	0.483	0.372
Shear Modulus of Elasticity	$G(\gamma)$ [kgf/cm^2]	12.505	10.512	11.621	11.955	12.943	12.583	14.503
Equivalent Stiffness	K_B [kgf/cm^2]	3,568	11,805	18,412	14,084	12,698	11,890	3,248
The Effective Damping Ratio	h_B	0.168	0.167	0.168	0.168	0.169	0.169	0.169

Table 14 Natural Period and Damping Ratio

Mode No.	Natural Period (sec)	Damping Ratio
1	1.546	0.143
2	0.451	0.030
3	0.419	0.030
4	0.357	0.030
5	0.302	0.092
6	0.299	0.056
7	0.273	0.115
8	0.259	0.031
9	0.253	0.114
10	0.236	0.031

Table 15 Displacement of Bearing computed by Dynamic Analysis Method (unit:mm)

	Seismic Coefficient Method	Dynamic Analysis	
		Response Spectrum Analysis	Time History Analysis
A1	100.42	65.76	68.72
P1	83.08	55.05	58.70
P2	77.84	36.85	38.82
P3	77.84	41.59	44.74
P4	77.84	43.60	47.14
P5	77.84	47.85	51.32
A2	97.51	63.47	67.77

Table 16 Sectional Forces at Pier Bottom computed by Dynamic Analysis Method

Item		Seismic Coefficient Method	Dynamic analysis	
			Response Spectrum Analysis	Time History Analysis
Bending Moment (tf·m)	A1	3,998.1	828.9	866.4
	P1	4,354.4	2,665.1	2,710.0
	P2	3,652.9	2,325.6	2,665.7
	P3	2,777.8	1,754.7	1,929.7
	P4	2,322.4	1,464.7	1,570.7
	P5	1,992.3	1,234.7	1,272.4
	A2	900.7	514.4	533.4
Shear stress (tf)	A1	426.6	47.3	49.4
	P1	345.1	200.0	186.2
	P2	286.5	165.0	206.9
	P3	238.5	140.8	162.6
	P4	218.3	129.5	146.1
	P5	218.6	128.2	138.2
	A2	146.8	101.6	90.8

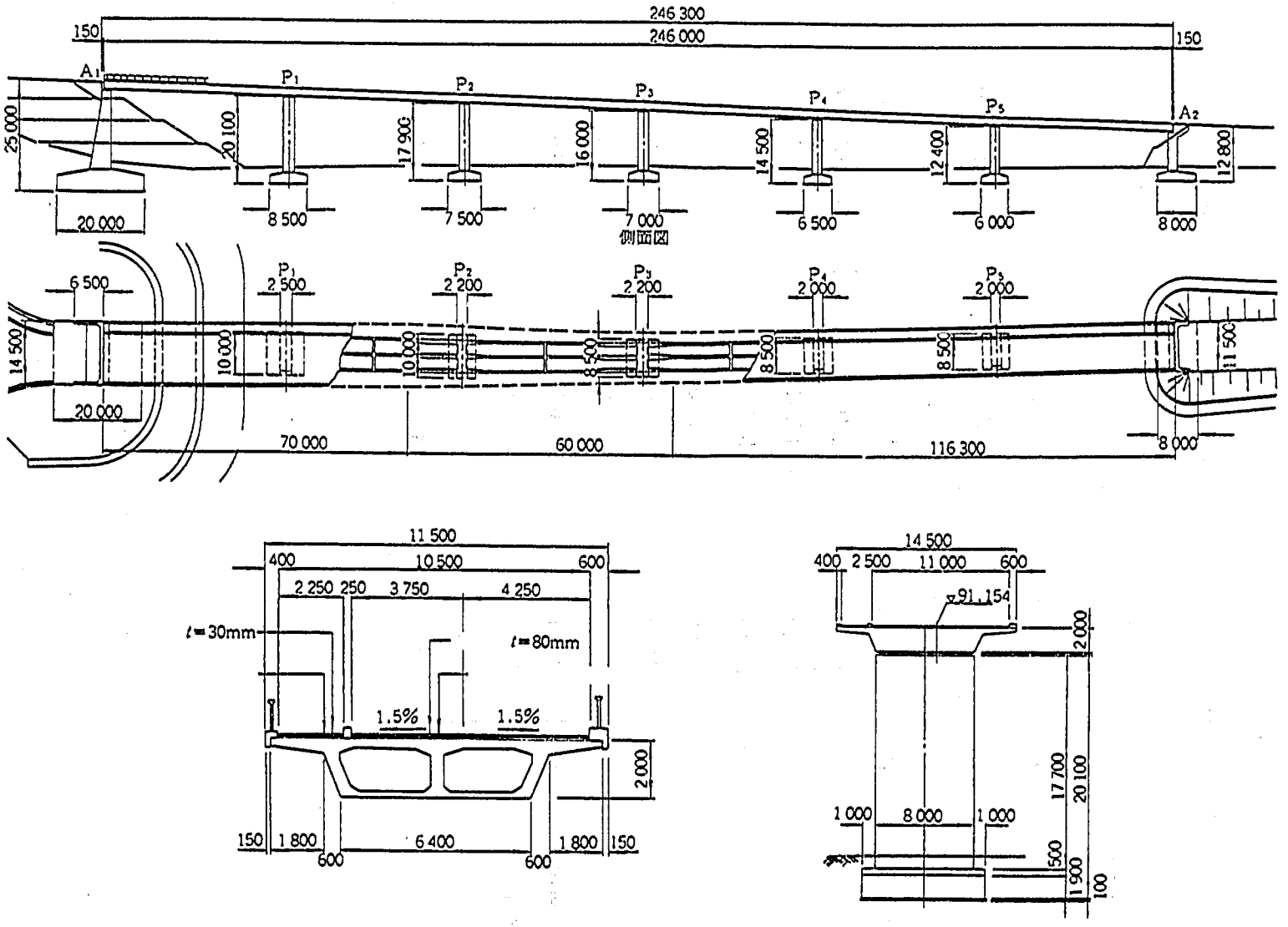


Fig. 1 General View of Yama-age Bridge

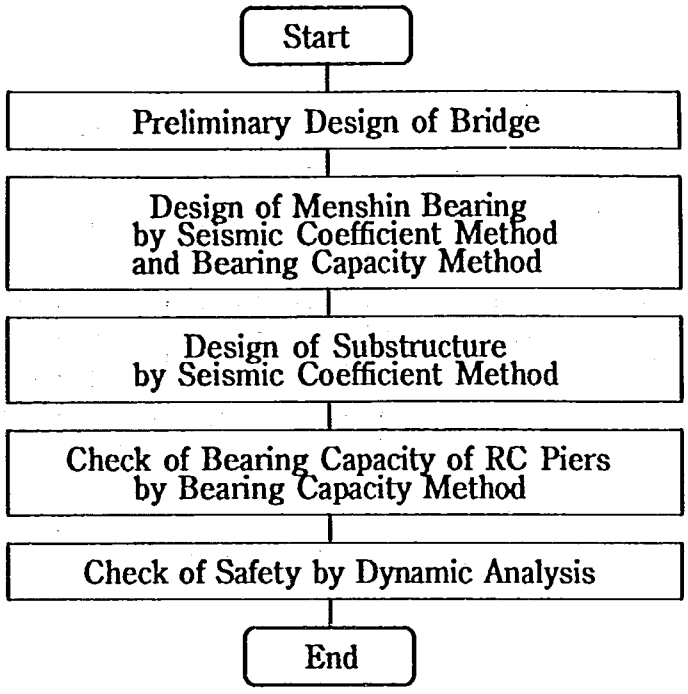


Fig. 2 Menshin Design Flow

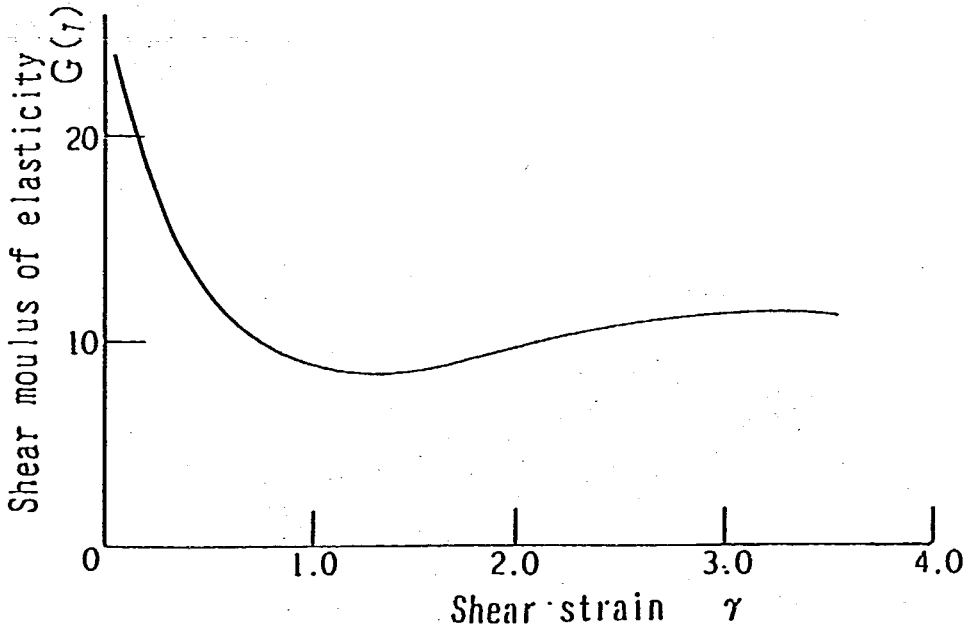


Fig. 3 $G(\gamma) \sim \gamma$ Relation of High Damping Rubber

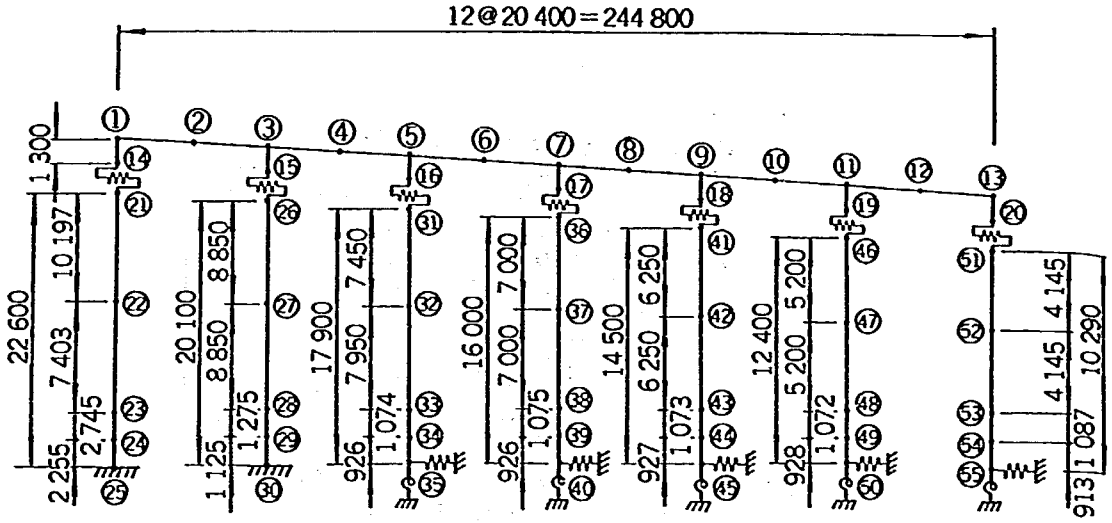


Fig. 4 Analytical Model

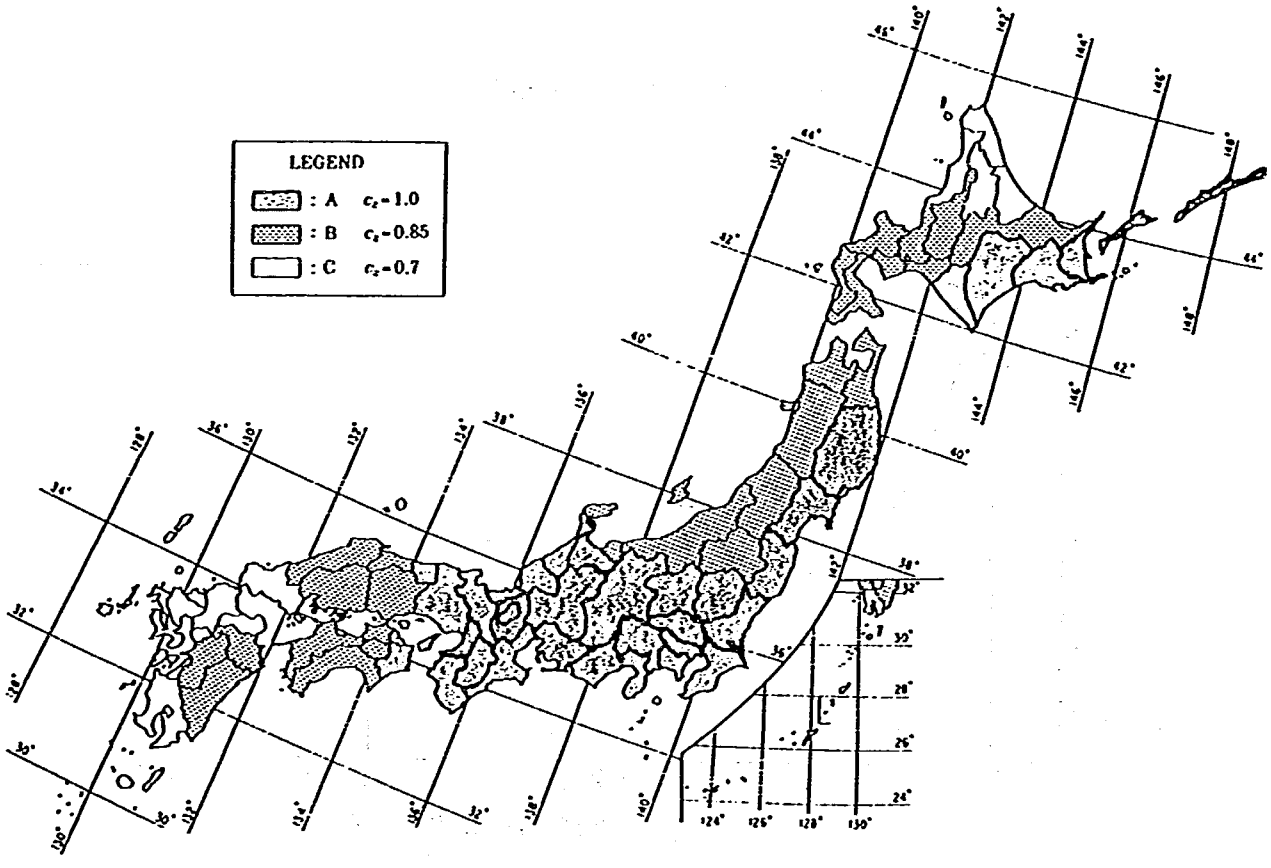


Fig. 5 Modification Factor for Zone c_z

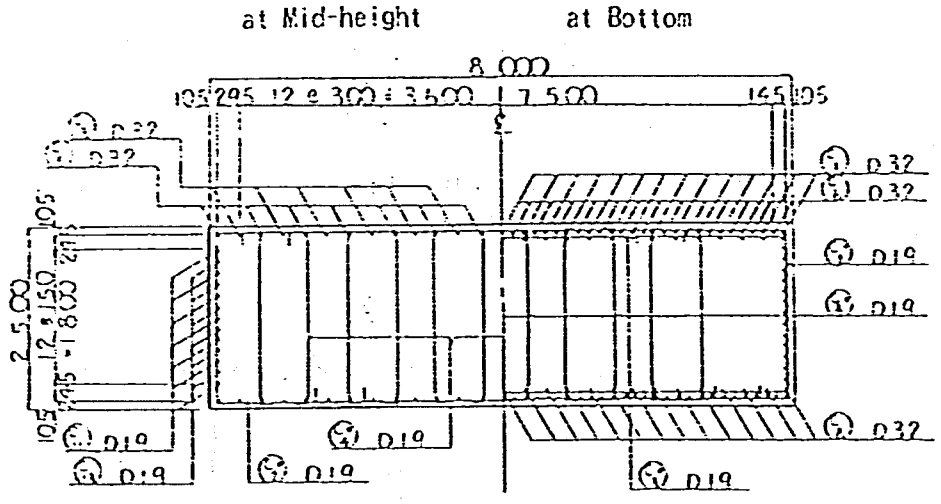


Fig. 6 Cross Section and Reinforcement of Pier (P1)

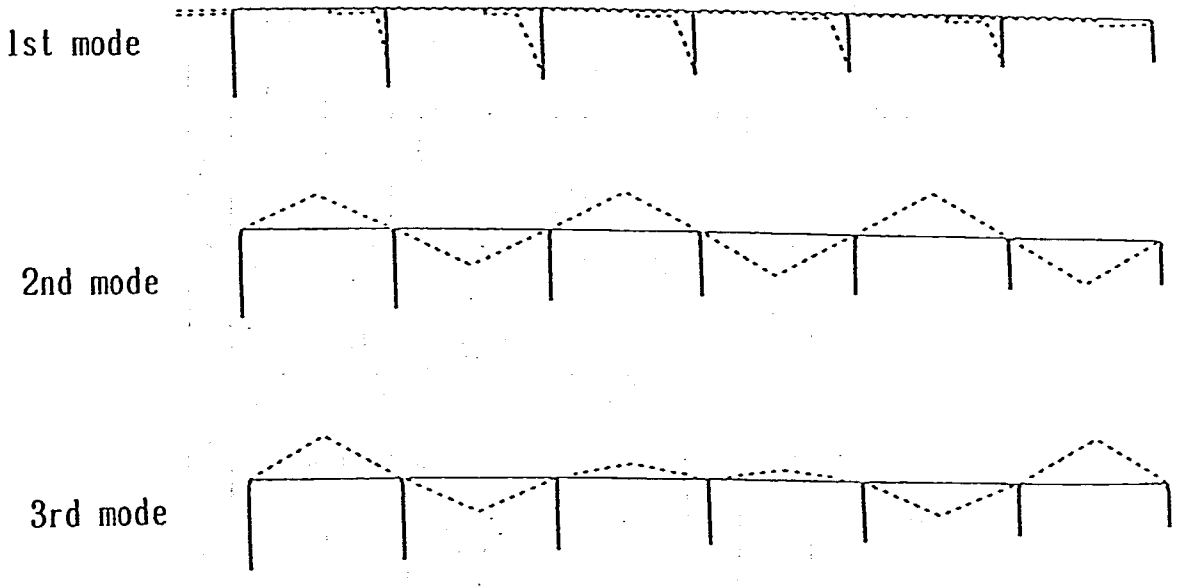


Fig. 7 Vibration Mode Shapes

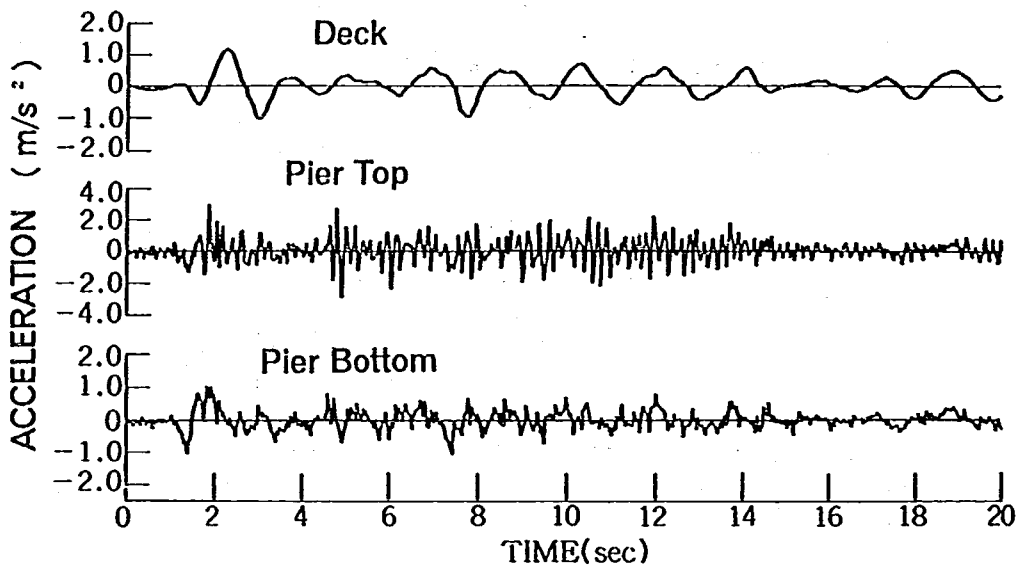


Fig. 8 Acceleration Response of Yama-age Bridge (Pier P1)

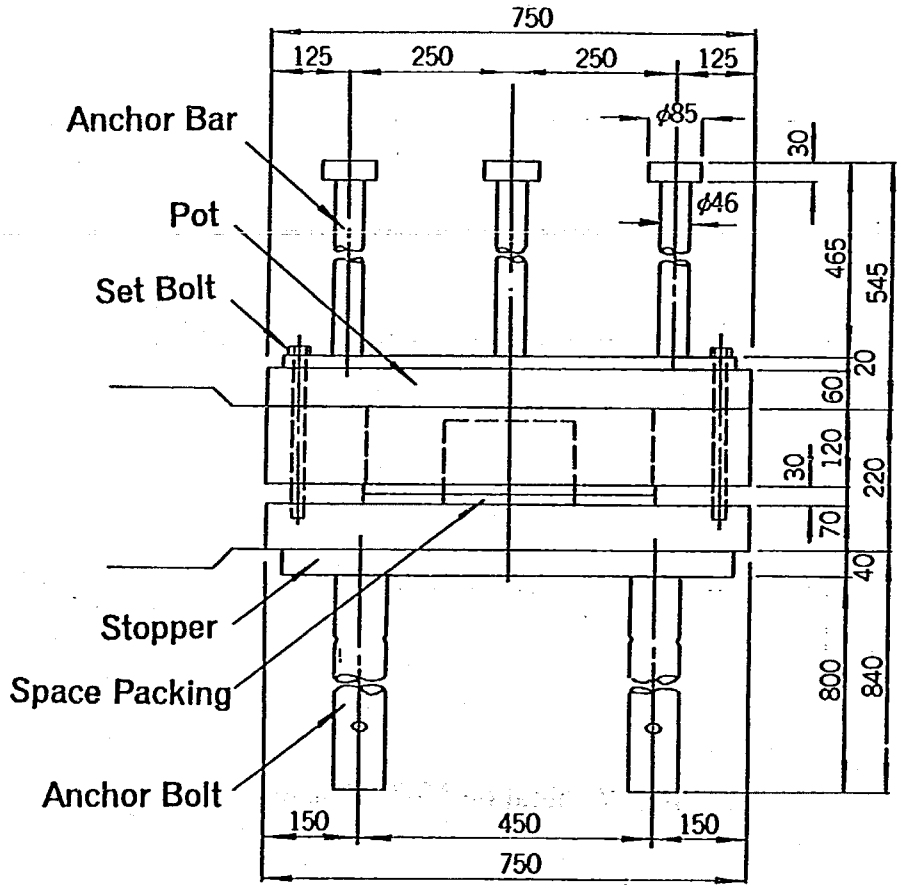


Fig. 9 Stopper

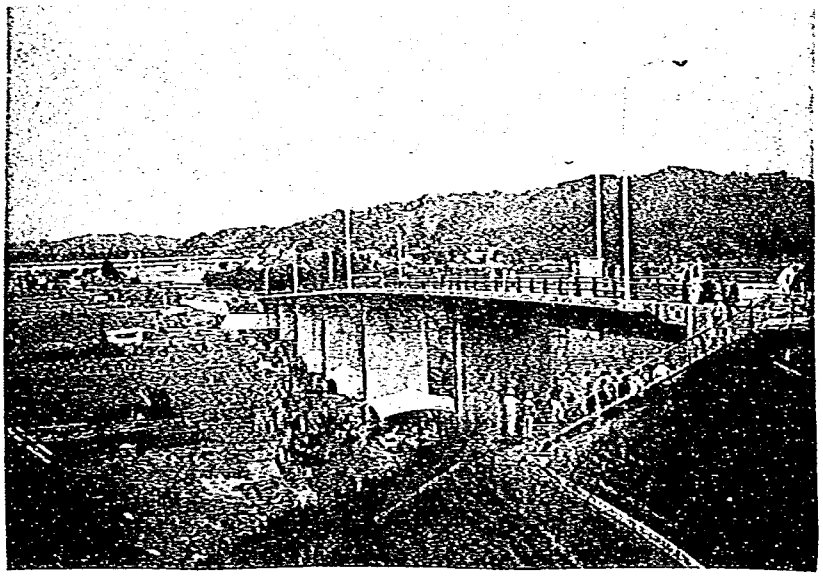


Photo 1 Yama–age Bridge

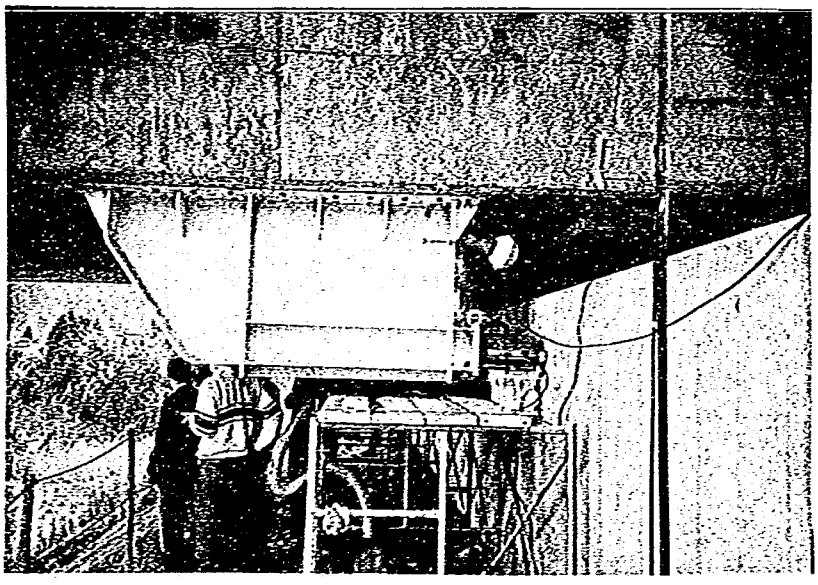


Photo 2 Forced Excitation Test using Quick–Release jacks

Response Analysis of Miyagawa Bridge Based on A Measured Acceleration Record

Kazuhiko KAWASHIMA
Hiroyuki NAGASHIMA
Shinji MASUMOTO
and
Kohji HARA

Journal of Structural Engineering
JSCE, Vol.40A
Tokyo, Japan
March, 1994

JOURNAL OF STRUCTURAL ENGINEERING Vol. 40A (March 1994) JSCE

RESPONSE ANALYSIS OF MIYAGAWA BRIDGE BASED ON A MEASURED ACCELERATION RECORD

Kazuhiko Kawashima *, Hiroyuki Nagashima **, Shuji Masumoto *** and Kohji Hara ****

This paper presents an analysis of a measured acceleration record at Miyagawa Bridge, the first seismically isolated bridge in Japan. Amplification of the peak accelerations is examined between the deck, pier and ground motions. Seismic isolation effect can be clearly observed. Dynamic response analysis using the analytical model adopted for seismic design is made assuming the acceleration recorded at underground as the input ground motion. Response acceleration computed at the deck is quite similar with the measured acceleration although peak acceleration is larger in the analysis.

Key Words: Miyagawa Bridge, strong motion obsarbation, seismically isolated bridge, menshin design

1. INTRODUCTION

Miyagawa Bridge is the first seismically isolated bridge in Japan, and is located on National Highway No. 362 in Shizuoka ken [1) 2)]. It completed in March 1991. Strong motion observation has been made since the completion. Because the first record was obtained by an earthquake with magnitude 4.9, which took place close to the site, an analysis was made for verifying the effectiveness of Menshin Design [3)]. This paper presents the seismic behavior of Miyagawa Bridge based on the analysis of the recorded accelerations.

2. STRONG MOTION OBSERVATION AT MIYAGAWA BRIDGE

As was reported in the previous paper [1) 2)], the Menshin Design (seismic isolation design) of

* Head, Earthquake Engineering Division, Earthquake Disaster Prevention Department, Public Works research Institute, Ministry of Construction, Tsukuba-shi, 305
** Ichihara Construction office, Chiba ken, Ichihara-shi, 290
(Formerly, Research Engineer, Earthquake Engineering Division, ditto)
*** Director, Road Construction Department, Shizuoka ken, Shizuoka-shi, 420
**** Second Design Office, Numazu Construction Office, Shizuoka ken, Numazu-shi, 420

Miyagawa Bridge was made in accordance with the Guidelines of Menshin Design of Highway Bridges [2]. In the Menshin Design, the Menshin devices are designed by both the Seismic Coefficient Method and the Bearing Capacity Method. In both methods, the lateral force is statically applied to the bridge, and the seismic safety is examined based on the allowable stress design approach in the Seismic Coefficient Method and the bearing capacity considering ductility in the Bearing Capacity Method.

The lateral force coefficient was not, however, reduced at the Miyagawa Bridge from the design value specified in the Specifications of Design of Highway Bridges [4], because it was the pilot project for verifying the effectiveness of the Menshin Design. The lateral force coefficient is therefore 0.2 in both longitudinal and transverse directions.

Lead rubber bearings [5] were adopted so that damping ratio of 0.12 can be obtained for the first mode of the bridge. Natural period of the bridge in longitudinal direction was assumed as 0.76 second in the Seismic Coefficient Method and 1.0 second in the Bearing Capacity Method. Because of the deformation dependence of the stiffness of the lead rubber bearings, the natural period is not the same for the Seismic Coefficient and the Bearing Capacity Method.

Soil condition at the site is I–group (stiff) based on the classification of ground condition specified in the Seismic Design Specifications of Highway Bridges [4].

Three 3–components feed–back servo type strong motion accelerometers were placed on the deck and pier crest at pier 1 (P1) and 10 m below the ground surface 10 m apart from the abutment 1 (A1) as shown in Fig. 1. The data are recorded on the analog magnetic type recording system when the ground acceleration larger than the triggering level is developed.

The first record was obtained by an earthquake with magnitude 4.9 which took place about 30 km north east from the site. Seismic Intensity of Japanese Methodological Agency was II.

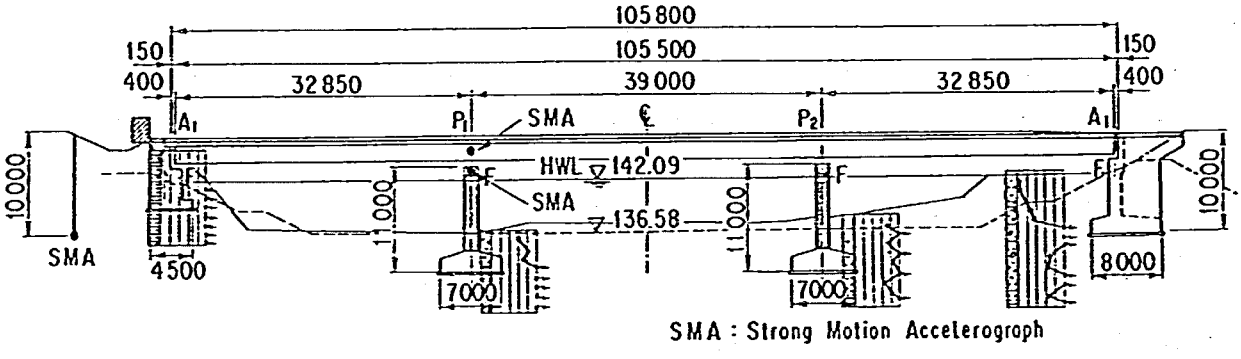


Fig. 1 Miyagawa Bridge and Location of Accelerometers

3. ANALYSIS OF MEASURED RECORDS

Fig. 2 shows the accelerations recorded at the deck, pier crest and 10m below the ground surface. Because intensity was so small, first part of the response could not be recorded. But main part could be successfully recorded.

Table 1 shows the peak acceleration. At 10m below the ground surface, the peak acceleration

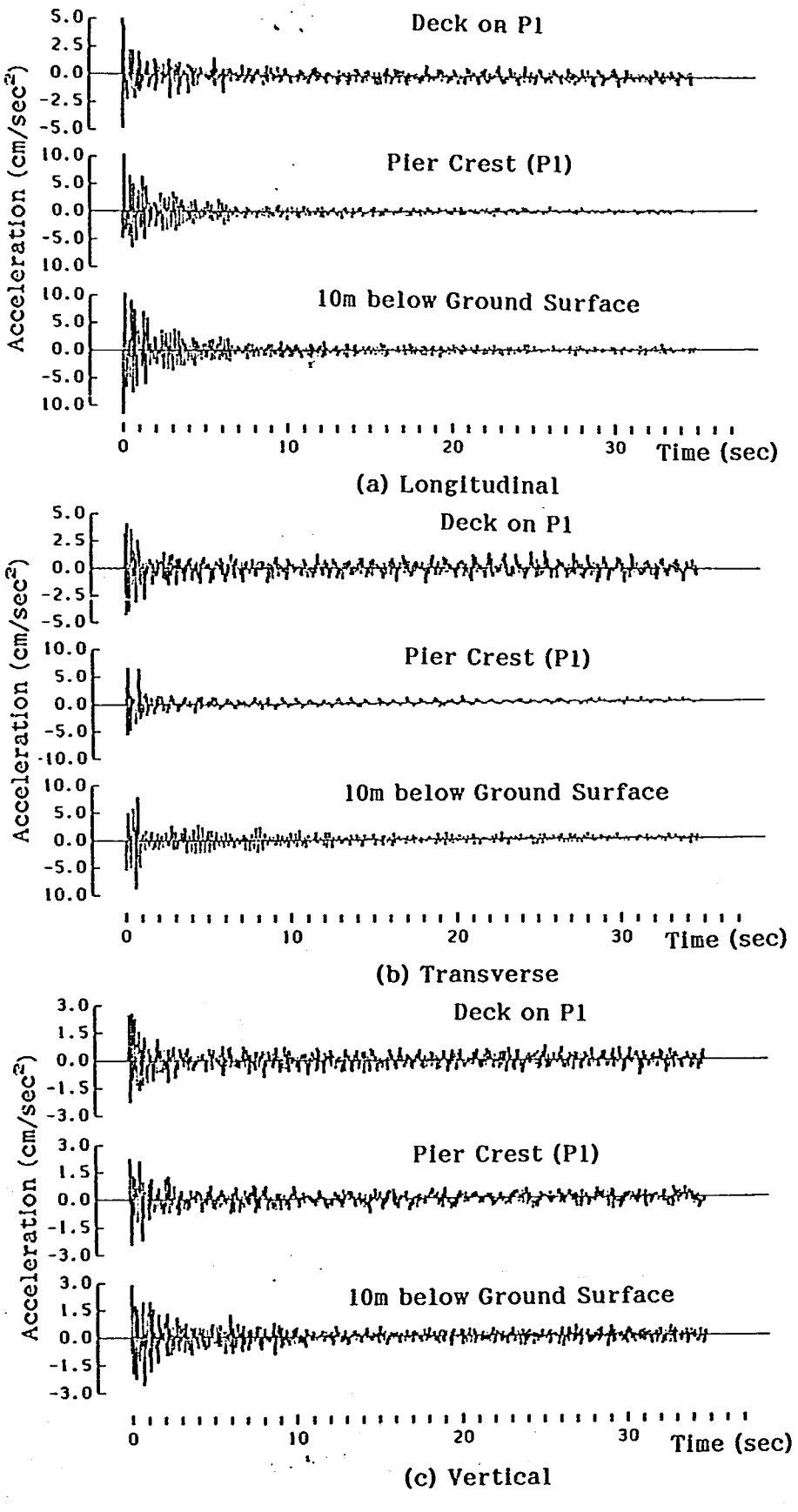


Fig. 2 Measured Accelerations

Table 1 Peak Accelerations Measured

Location	Longitudinal Direction	Transverse Direction	Vertical Direction
Deck on P1	5.0	4.3	2.6
Pier Crest of P1	10.4	6.6	2.5
10 m underground	11.6	8.9	2.9

was 11.6 cm/sec ^{2} in longitudinal direction and 8.9 cm/sec ^{2} in transverse direction. This decreased to 10.4 cm/sec ^{2} in longitudinal direction and 6.6 cm/sec ^{2} in transverse direction on the pier crest. Because the amplification of the peak acceleration from the ground to pier crest is generally about 2.5 for this type of bridges [6], the decrease of pier response in comparison with the ground acceleration at 10 m below the surface is apparent. Furthermore, it decreased to 5.0 cm/sec ^{2} in longitudinal direction and 4.3 cm/sec ^{2} in transverse direction on the deck.

Fig. 3 shows such decrease of amplification in terms of acceleration response spectra with damping ratio of 0.05. It is apparent that although ground motion at 10 m below the surface had the predominant period of 0.2 ~ 0.3 second, it is not predominant in the horizontal deck motion.

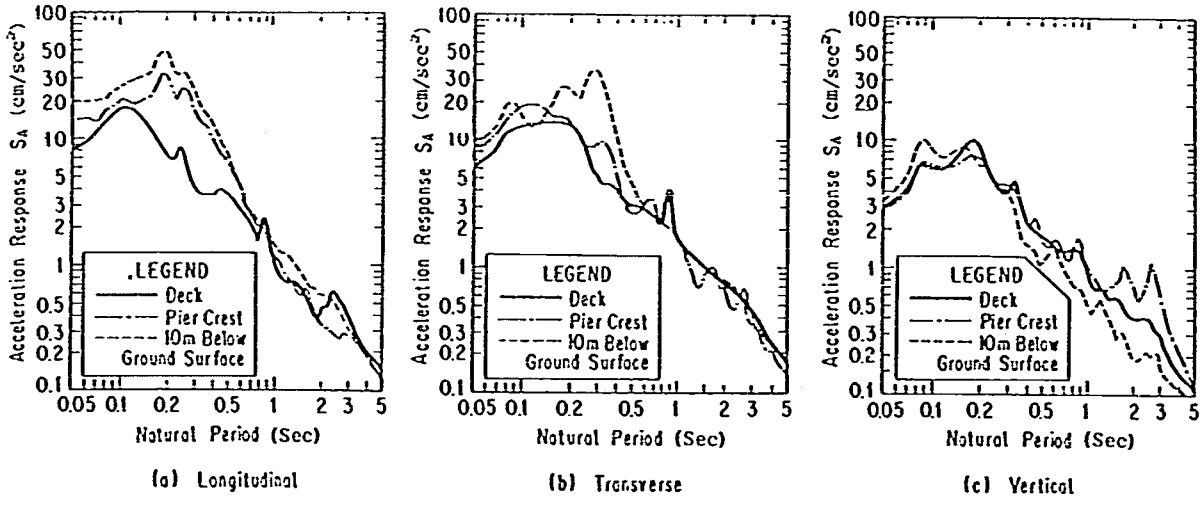


Fig. 3 Acceleration Response Spectra of Measured Acceleration Record (Damping Ratio of 0.05)

For studying the amplification from the 10 m below the ground surface to the pier crest and the deck, ratios of the acceleration response spectra presented in Fig. 3 are shown in Fig. 4. It is seen in Fig. 4 that the acceleration response spectrum ratio R defined as the acceleration response spectrum of the deck motion divided by the acceleration response spectrum of the ground motion measured at 10 m below the ground surface is approximately 0.2 at natural period of 0.2 ~ 0.3 second. The motion at this period is filtered out at the deck due to the effect of seismic isolation.

On the other hand, the ratio R defined as the acceleration response spectrum of the deck motion divided by the acceleration response spectrum of the ground motion measured 10 m below the ground surface increases to 1.4 in longitudinal direction and 2.0 in transverse direction at natural

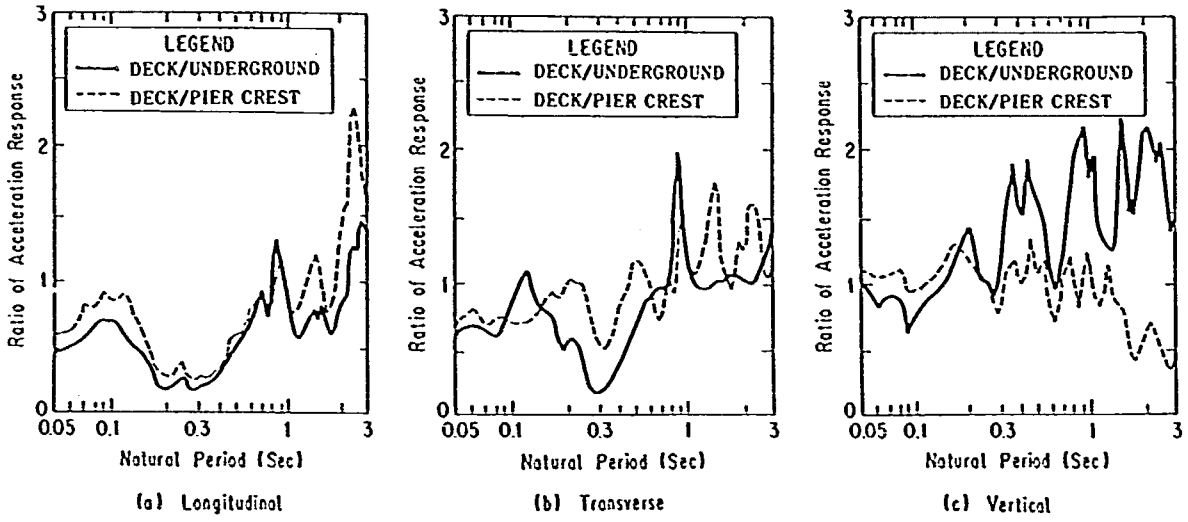


Fig. 4 Ratios of Acceleration Response Spectra

period of about 0.85 second. Reminding the fact that the natural period assumed in the Seismic Coefficient Method was 0.76 second, this represents the amplification of deck response due to resonance of the first mode. Reflecting the fact that the deformation of LRBs developed during the earthquake is much smaller than that assumed in the design by means of the Seismic Coefficient Method, stiffness of LRBs is approximately 25 % higher than that assumed in the design.

The ratio R in vertical component takes about 1.0 for natural period up to 0.3 second. This implies that the amplification from either 10 m below the ground surface or the ground surface to the deck is small. Although the ratio R from 10 m below the ground surface to the deck becomes large for natural period longer than 0.3 second, it requires to clarity the reason after more data are accumulated.

The LRBs were designed so that yielding of the lead plug be developed for the lateral force coefficient over 0.12. Of course, because the response during the earthquake was much smaller that

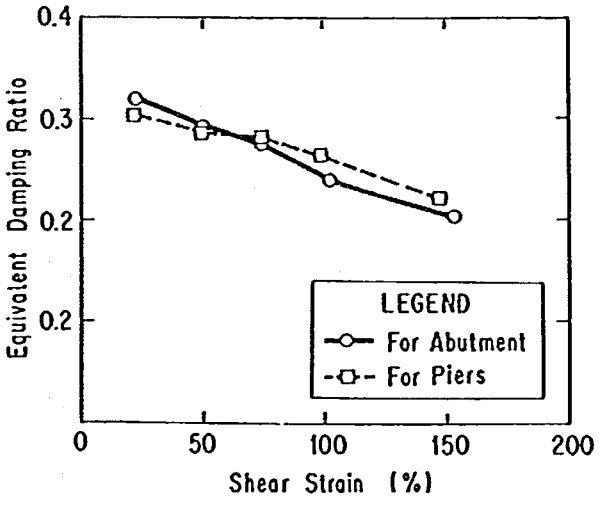


Fig. 5 Equivalent Damping Ratio of Lead Rubber Bearings Based on Full Model Tests

this level, bilinear behavior of LRBs seems not significant. However it should be noted that LRBs show high energy dissipation capability from small displacement. Fig. 5 shows the equivalent damping ratio of the LRBs obtained from the full size test [7] . Although the equivalent damping ratio for shear strain smaller than 20 % is not presented here, it is known that the equivalent damping ratio for smaller shear range can be approximately evaluated by extrapolating the relation presented in Fig. 5. Therefore it may be assumed that the equivalent damping ratio of LRBs was approximately 30 % for the shear strain developed during the earthquake.

4. STUDY OF THE RECORD BY DYNAMIC RESPONSE ANALYSIS

Because dynamic response analysis was made at the design stage for Miyagawa Bridge, it was decided to adopt the same analytical model as shown in Fig. 6 for studying the record. The acceleration recorded at 10 m below the ground surface was regarded as the input ground motion and the response of the deck and substructure were computed and compared with the recorded accelerations. Because the footings of P1 and P2 are almost on the same level with the down-hole accelerometer placed 10 m below the ground surface (refer to Fig. 1), it was considered appropriate to apply the acceleration measured at 10 m below the ground surface to the footings. Although the footing of two abutments, A1 and A2, is slightly higher in level than the down-hole accelerometer, it was disregarded in the analysis because it would cause only minor difference.

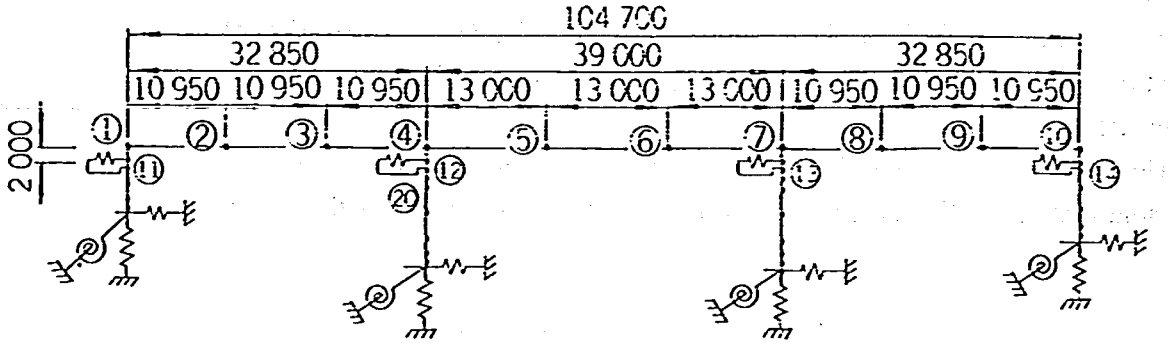


Fig. 6 Dynamic Response Analysis Model of Miyagawa Bridge for Design Purpose

Analysis was made by the equivalent linear analysis. The equivalent linear analysis provides accurate response for the seismic isolated bridges [9] . Because the deformation of the LRBs was quite small during the earthquake, the first stiffness k_1 was assumed as the equivalent stiffness of LRBs as

$$k_1 = 6.5 k_2 \tag{1}$$

$$k_2 = \frac{F - Q_d}{u_B} \tag{2}$$

$$Q_d = A_P \cdot q_0 \tag{3}$$

$$F = A_R \cdot G \cdot \gamma \cdot A_P \cdot q \tag{4}$$

$$q = -283.6\gamma^2 + 183.8\gamma + 85.0 \tag{5}$$

where k_1 : 1st stiffness of LRB (kgf/cm), k_2 : 2nd stiffness of LRB (kgf/cm), Q_d : yielding force of lead (kgf), q_0 : shear stress of yielding of lead plug (= 85.0 kgf/cm^2), G : shear modulus of rubber (kgf/cm^2), F : shear force of LRB (kgf), u_B : design displacement (cm), q : shear stress of lead (kgf/cm^2), γ : shear strain, A_P : sectional area of lead plug (cm^2), and A_R : sectional area of rubber (cm^2).

$$h = \frac{\sum_{j=1}^{n} \underline{\phi}_{ij} h_j \underline{k}_j \underline{\phi}_{ij}}{\underline{\Phi}_i^T \underline{K} \underline{\Phi}_i} \tag{6}$$

where $\underline{\phi}_{ij}$: mode vector of j–th structural component for i–th mode, h_j : damping ratio of j–th structural component , $\underline{k}_j$: stiffness matrix of j–th structural component, $\underline{\Phi}_i$: mode vector of bridge for i–th mode, and $\underline{K}$: stiffness matrix of bridge.

Eq. (6) is effective to evaluate the modal damping ratio of bridges based on an experimental study [8] . Damping ratio of structural components was assumed in design as shown in Table 2. Because the deformation developed in LRBs is small during the design earthquake assumed in the Seismic Coefficient Method, it was assumed in the design that the damping ratio of LRBs is zero in the Seismic Coefficient Method. It may be therefore good to assume zero damping ratio for LRBs for the consistency with the seismic design. However it became apparent that zero damping ratio for LRBs gives appreciably larger bridge response than the measured values. Therefore it was assumed as 0.3 based on the above described full model test results on the damping characteristics of LRB.

Fundamental natural period predicted in longitudinal and transverse direction is 0.50 sec and 0.49 sec, respectively. The translation of only the deck is observed in those mode shapes. Because this corresponds to the natural period of about 0.85 second observed in Fig.4, the stiffness of the bridge assumed in the analysis is appreciably higher than that during the earthquake.

Table 2 Damping Ratio Assumed in Seismic Design of Miyagawa Bridge

Structural Components		For Design		For this Analysis
		Seismic Coefficient Method	Bearing Capacity Method	
Super structure		0.03	0.03	0.03
Piers and Abutments		0.05	0.05	0.05
Foundations		0.1	0.1	0.1
Menshin Bearings	A1	0	0.177	0.3
	P1	0	0.137	0.3
	P2	0	0.139	0.3
	A2	0	0.199	0.3

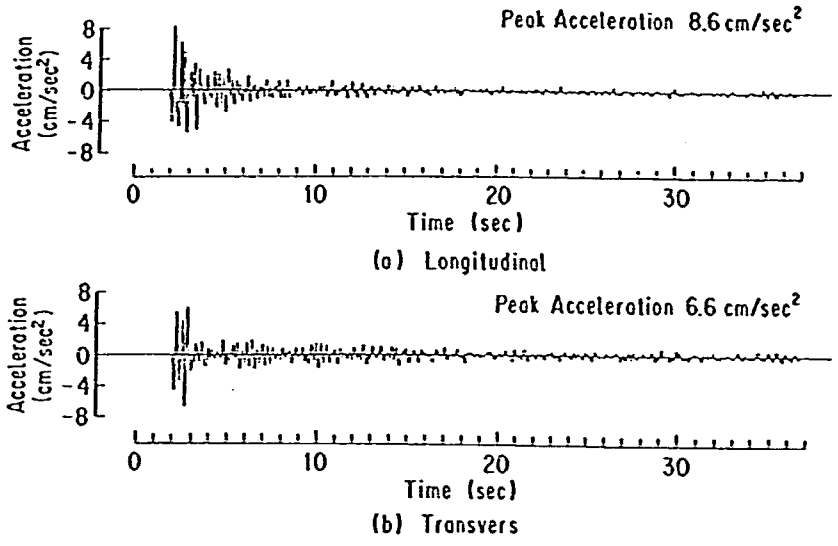


Fig. 7 Computed Deck Acceleration

Fig. 7 shows the response acceleration of the deck thus computed. Although the computed acceleration is 1.5 ~ 1.7 times larger in amplitude than the measured response, overall characteristics of the computed response is similar with the measured acceleration. Overestimation of response acceleration of the deck may be attributed to the fact that the stiffnesse of the model is over estimated and that the damping ratio of the foundation is underestimated in the dynamic analysis. This is for the sake of providing safe-side result for design purpose.

5. CONCLUSION

The first record obtained at the Miyagawa Bridge, the first Menshin bridge in Japan, was analyzed to study the seismic behavior of Menshin bridges. The following conclusions may be deduced based on the analysis presented herein :

1) The deck acceleration is about 50 % in amplitude of the underground acceleration at 10 m below the ground surface. This clearly shows the effectiveness of the seismic isolation.
2) When amplification of the response from the 10 m below the ground surface to the deck is represented in terms of the acceleration response ratio with damping ratio of 0.05, the acceleration response ratio R defined as the response acceleration of the deck motion divided as the response acceleration of ground motion measured at 10 m below the ground surface is only 0.25 at natural period of 0.2 ~ 0.3 second which is the predominant period of the ground motion. However the acceleration response ratio R defined as the response acceleration of the deck motion divided by the response acceleration of ground motion measured at 10 m below the ground surface is 1.4 ~ 2.0 at 0.85 second which is the fundamental natural period of the bridge. Therefore selection of the natural period in consideration with the predominant period of ground motion is very important in the Menshin Design.
3) The dynamic response analysis model which was adopted for the seismic design of Miyagawa Bridge can realistically simulate the response of the deck although the analysis overestimates the measured acceleration.

REFERENCES

1) Matsuo, Oishi, Hara, K. and Yamashita, : Design and Construction of Miyagawa Bridge, Bridges and Foundations, Vol. 91–2, 1991
2) Matsuo, Y. and Hara, K. : Design and Construction of Miyagawa Bridge–First Menshin Bridge in Japan–, 1st U.S.–Japan Workshop on Earthquake Protective Systems of Highway Bridges, National Center for Earthquake Engineering Research Buffalo, N.Y., U.S.A., September 1991
3) Technology Research Center for National Land Development : Guidelines for Base Isolation of Highway Bridges, 1989
4) Japan Road Association : Part V Seismic Design of Design Specifications of Highway Bridges, 1990
5) Robinson, W.H. : Lead Rubber Hysteretic Bearings Suited for Protecting Structures during Earthquakes, Earthquake Engineering and Structural Dynamics, Vol. 10, 1982
6) Kawashima, K. : A State of the Arts of Earthquake Engineering Research for Application to Seismic Design of Bridge Foundations, Technical Report, No. 2385, Public Works Research Institute, July 1986
7) Makiguchi, Y., Matsuo, and Hara, H. : Performance Test of Lead Rubber Bearings for Miyagawa Bridge, Annual Meeting of the Japan Society of Civil Engineers, Part I, 1991
8) Kawashima, K., Nagashima, H. and Iwasaki, H. : Effectiveness of the Energy Proportional Method for Evaluating Modal Damping Ratio of Menshin Bridges, Civil Engineering Journal, 1992
9) Kawashima, K., Nagashima, H., Hasegawa, K., and Iwasaki, H. : Seismic Response Characteristics of Menshin Bridges, Report of PWRI, Vol.188, Public Works Research Institute, March 1993

(Received September 16, 1993)

Evaluation of Modal Damping Ratio Based on Strain Energy Proportional Damping Method

Kazuhiko KAWASHIMA
Hiroyuki NAGASHIMA
and
Hideaki IWASAKI

Journal of Structural Engineering
JSCE, Vol.40A
Tokyo, Japan
March, 1994

JOURNAL OF STRUCTURAL ENGINEERING Vol.40 A (March 1994) JSCE

EVALUATION OF MODAL DAMPING RATIO BASED ON STRAIN ENERGY PROPORTIONAL DAMPING METHOD

Kazuhiko KAWASHIMA*, Hiroyuki NAGASHIMA** and Hideaki IWASAKI***

Presented in this paper are a model free-oscillation test and an analysis for clarifying the strain energy proportional damping method which is widely adopted for evaluating modal damping ratios of structures. Because damping ratios of structural components are sometimes different even in the same structure, it is required in the modal dynamic response analysis to evaluate the damping ratio for each mode. In this paper it is presented from experiments and analyses that the strain energy proportional damping method is quite accurate in evaluating the modal damping ratios of structures for seismic analysis.

Key Words: Seismic Design, Damping Ratio, Energy Dissipation, Bridges

1 INTRODUCTION

The damping ratio is an important parameter for evaluating seismic response of structures. Although the mass and stiffness can be accurately computed from mass and stiffness distribution in structures, the damping ratio can not be evaluated in the similar manner because the prediction of energy dissipation in structures is very complex. Therefore instead of directly evaluating energy dissipation of structures it is generally adopted to evaluate the energy dissipation of structures in terms of damping ratio. The damping ratio is an appropriate parameter for assigning the damping characteristics of structures. It should, however, be kept in mind that the damping ratio can be defined only for a single-degree-of-freedom oscillator. From the analogy of the orthogonal condition of modal matrix with respect to stiffness and

* Head, Earthquake Engineering Division, Earthquake Disaster Prevention Department, Public Works Research Institute, Tsukuba-shi, Ibaraki 305

** Engineer, Planning Department, Kanto Regional Construction Bureau, Ministry of Construction, Chiyoda-ku, Tokyo 100 (Former Research Engineer, ditto)

*** Research Engineer, Ground Vibration Division, Earthquake Disaster Prevention Department, ditto

Note. This paper originally appeared as part of the Civil Engineering Journal, Vol35, No.5, May 1993 (in Japanese). Minor changes have been made.

mass matrices, the damping ratio has been assumed for seismic analysis of structures.

The damping ratios are different depending upon structural components even in the same structure. Therefore it is required to evaluate the modal damping ratio based on the different damping ratio assigned for each structural component. The strain energy proportional damping method has been widely used for such purposes [1) 2)] . Because most of energy dissipation is developed due to the deformation of structures, it has been considered reasonable to employ this method. But experimental verification has not yet fully been made.

This paper attempts to verify the strain energy proportional damping method for the application to the seismic design of structures. Based on model oscillation tests which are carefully designed for evaluating energy dissipation of structural components as well as of the entire structure, accuracy and application of the strain energy proportional damping method is clarified. A bridge is considered for the analysis.

2 ENERGY PROPORTIONAL DAMPING

For a linear discrete structure, the equations of motion may be written as

$$M\ddot{u}+C\dot{u}+Ku=-M\{1,0,0,\cdots 1,0,0\}^{T}\ddot{Z}_{gx} \qquad (1)$$

where

M : mass matrix

C : damping matrix

K : stiffness matrix

u , $\dot{u}$, $\ddot{u}$: displacement, velocity and acceleration vectors

$\ddot{Z}_{gx}$: ground acceleration in x axis

Denoting w_i and ϕ_i as the undamped angular natural frequency and the mode shape for the i-th mode, u , $\dot{u}$, $\ddot{u}$ may be expressed as

$$u=\sum_{i=1}^{k}\phi_i q_i(t)$$

$$\dot{u}=\sum_{i=1}^{k}\phi_i \dot{q}_i(t) \qquad (2)$$

$$\ddot{u}=\sum_{i=1}^{k}\phi_i \ddot{q}_i(t)$$

in which q_i represents the generalized coordinate for the i-th mode and k represents the degree of freedom.

From the orthogonal condition, the stiffness matrix K and mass matrix M become as

$$\begin{aligned}\phi m^{T}K\phi_n&=0\\ \phi m^{T}M\phi_n&=0\end{aligned}\quad (m\neq n) \qquad (3)$$

Assuming that the damping matrix C can also be orthogonalized as

$$\phi m^{T}C\phi_n=0 \qquad (4)$$

one can have k sets of uncoupled equations of motion as

$$\ddot{q}_i+2h_i w_i \dot{q}_i=-\Gamma_{ix}\ddot{Z}_{gx} \qquad (5)$$

in which h_i and Γ_{ix} represent the modal damping ratio and the mode participation factor for the i-th mode, respectively.

It is important to note here that the modal damping ratio h_i which is defined only for a single-degree-of-freedom oscillator has been adopted in a dynamic response analysis of a multi-degree-of-freedom system in the form as in Eq.(5) because there is no other practical definition for energy dissipation for a multi-degree-of-freedom system.

It is then required to evaluate the modal damping ratio in Eq.(5) based on the energy dissipation mechanism of the structure. For such a purpose it is assumed to divide a structure into several structural segments in which energy dissipation has the same mechanism as shown in **Fig. 1** [3) 4)] . The segment is designated hereinafter as a substructure. A substructure may be a deck, a pier or a foundation as shown in **Fig. 2** in the analysis of a bridge.

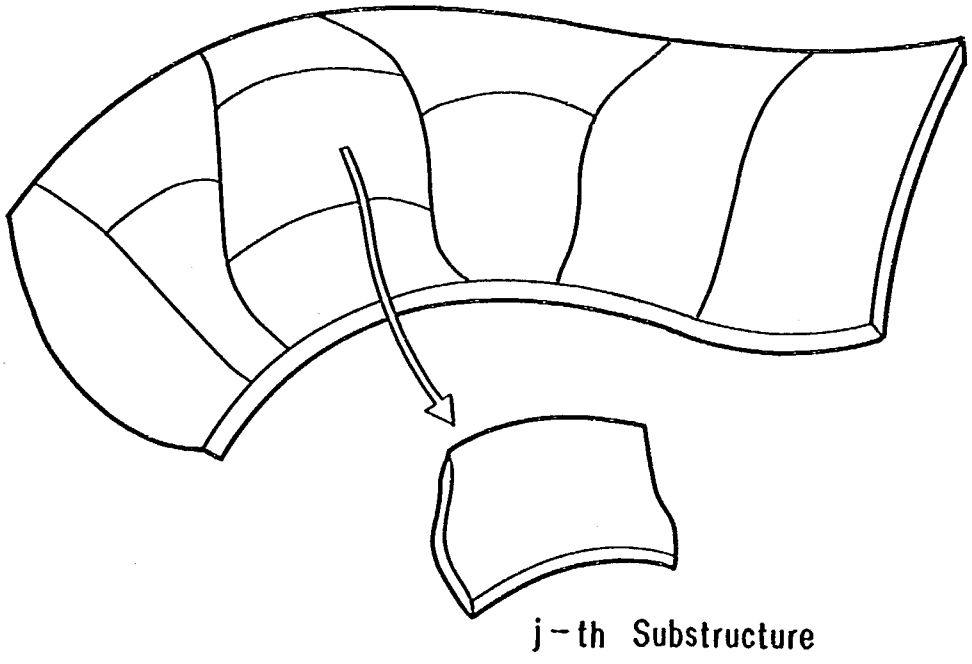


Fig. 1 Substructures

Strain energy in the j-th substructure for the i-th mode may be evaluated as

$$E_{ij}=\phi_{ij}^{T}\cdot k_j\cdot\phi_{ij} \qquad (6)$$

where

E_{ij} : strain energy of j-th substructure for i-th mode

ϕ_{ij} : mode shape of j-th substructure for i-th mode

k_j : stiffness matrix of j-th substructure

Denoting the energy dissipation in the j-th substructure for the i-th mode as ΔE_{ij} , the damping ratio of the j-th substructure may be evaluated as

$$h_{ij}=\frac{1}{4\pi}\cdot\frac{\Delta E_{ij}}{E_{ij}} \qquad (7)$$

Because the damping ratio of a substructure depends on its mode shapes and boundary conditions, it needs to be the one evaluated when the substructure of interest deforms as a part of the entire structure in the i-th mode shape.

Then the strain energy and energy dissipation of the entire structure for the i-th mode can be evaluated as

$$E_i=\sum_{j=1}^{n}E_{ij}$$
$$\Delta E_i=\sum_{j=1}^{n}\Delta E_{ij} \tag{8}$$

in which n represents the number of substructures. The damping ratio of the entire structure (modal damping ratio) for the i-th mode may be written from Eq.(8) as

$$h_i=\frac{1}{4\pi}\cdot\frac{\Delta E_i}{E_i} \tag{9}$$

Substituting Eqs.(7) and (8) into Eq.(9), one obtains an equation for evaluating the modal damping ratio as

$$h_i=\frac{\sum_{j=1}^{n}E_{ij}h_{ij}}{\sum_{j=1}^{n}E_{ij}} \tag{10}$$

Eq.(10) is called as the strain energy proportional damping because the averaged damping ratio over each substructure is taken with the strain energy of the substructure being the weighting function. Substituting Eq.(6) into Eq.(10), Eq.(10) can be modified into a form which is more appropriate for computation

$$h_i=\frac{\sum_{j=1}^{n}\phi_{ij}^{T}\cdot h_{ij}\cdot k_j\cdot\phi_{ij}}{\sum_{j=1}^{n}\phi_{ij}^{T}\cdot k_j\cdot\phi_{ij}} \tag{11}$$

It should be noted that the natural periods of substructures are not necessarily the same as that of the entire structure. Therefore, if the frequency dependence of the damping ratios of substructures is significant, Eq.(11) can not be adopted.

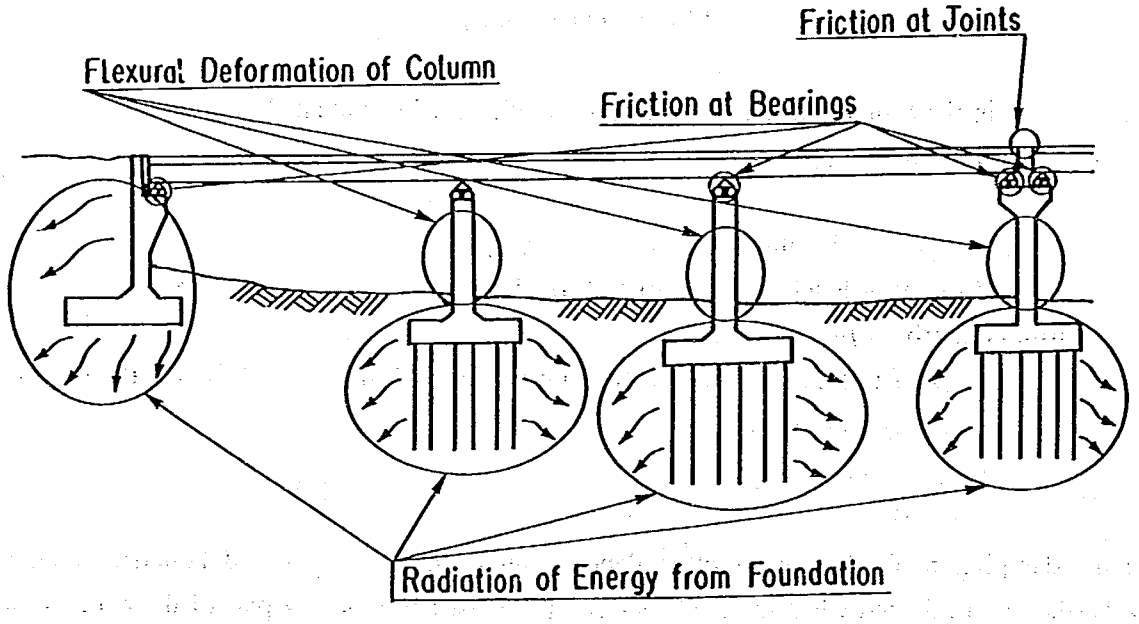


Fig. 2 Substructures of Bridges in View of Energy Dissipation

3 MODEL FREE OSCILLATION TEST

Fig. 3 shows the model bridge studied for verifying the effectiveness of the strain energy proportional damping method. **Photos 1** and **2** show the bridge model and the bearing. The girder is of a rigid steel plate so that energy dissipation during excitation is negligibly small. The girder has a span length of 2.1 m and a weight of 611.7 kgf. Each column with a height of 95 cm consists of four steel plates with the top of each two plates being rigidly connected. The bottom of the columns are rigidly connected to the base frame for preventing energy dissipation at the bottom.

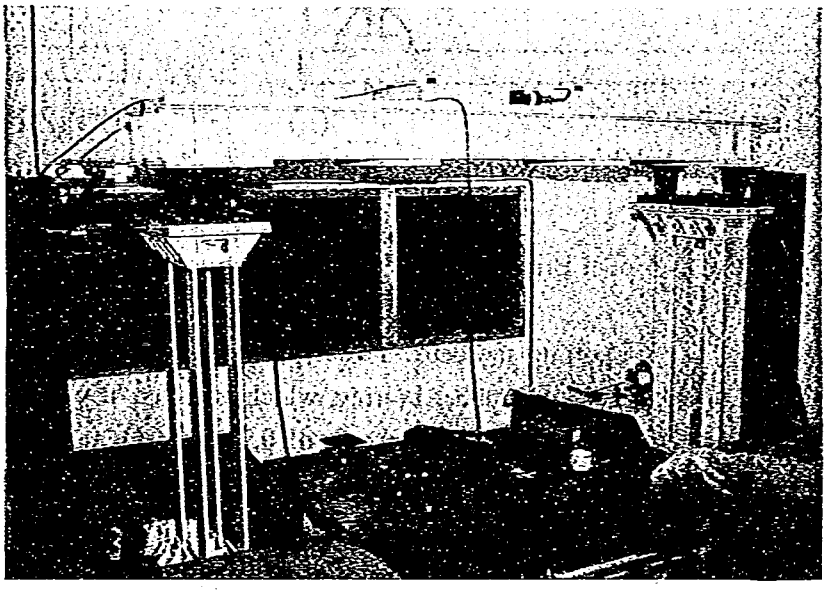


Photo 1 Bridge Model

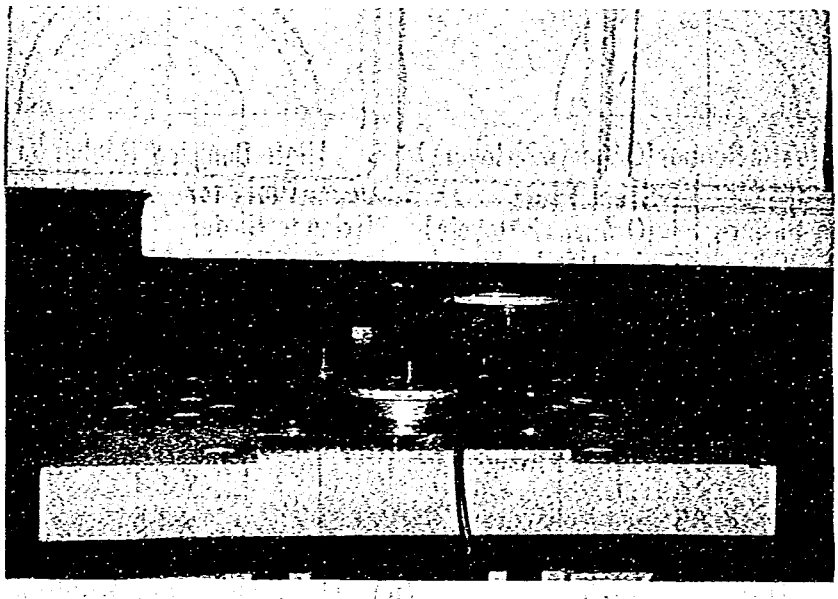


Photo 2 Bearings

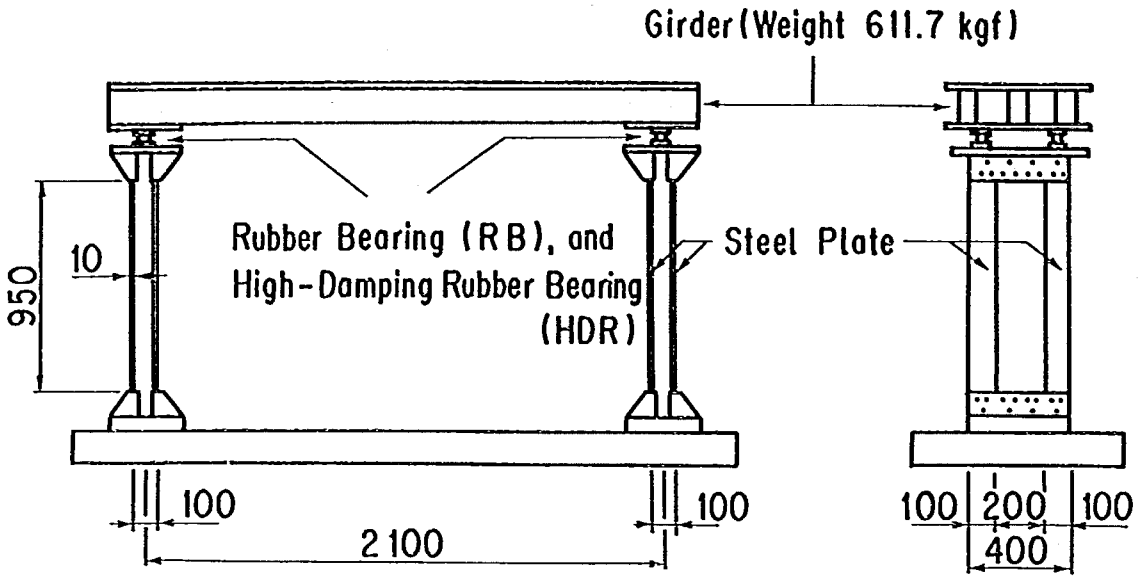


Fig. 3 Model Bridge used for Free Oscillation Test

Four bearings were used for supporting the deck. Two types of bearings as shown in Fig. 4 were used for the test. One is the laminated natural rubber bearing, which is called hereinafter as RB. This was made by laminating 25 natural rubber plates with a thickness of 0.9 mm each and 24 steel plates with a thickness of 0.3 mm each. The total thickness of rubber is 22.5 mm. It has elastic restoring force characteristics. The other is the laminated high damping rubber bearing, which is called as HDR in this paper. This was made by laminating 37 high energy absorbing rubber plates with a thickness of 0.5 mm each and 36 steel plates with a thickness of 0.3 mm each. The total thickness of high energy absorbing rubber is 18.5 mm.

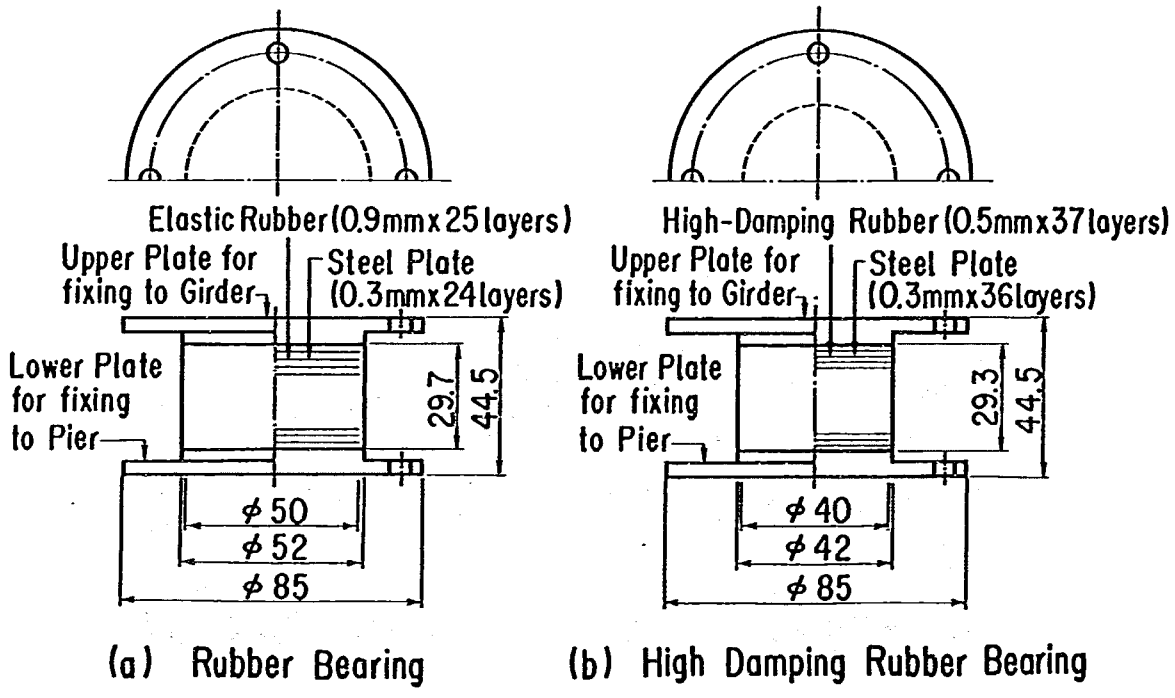


Fig. 4 Model Bearings for Free Oscillation Test

In the model bridge, energy dissipation is developed at bearings and columns. Therefore, bearings and columns are regarded as substructures for evaluating the modal damping ratio of the model bridge by Eq.(11). Because the deck is rigid, no energy dissipation at the deck is considered in the analysis. Only the modal damping ratio for the 1st mode is evaluated in the test in order to make the excitation simple and easy. It should be noted that the frequency dependence of the danping ratios is small for steel, natural rubber and the high damping rubber [5].

For evaluating the damping ratio of each substructure, free oscillation tests were conducted individually for two types of bearings (RB and HDR) and two columns (Column A and B). Free oscillation tests of the model bridge were also conducted for evaluating the modal damping ratio of the entire structure.

In the free oscillation test of the model bridge, the deck was displaced in the longitudinal direction, and by releasing it from the displaced position, free oscillation was developed. The 1st mode shape of the model bridge in the longitudinal direction is of lateral movement of the deck with flexural deformation of cantilevered columns. Similarly the free oscillation test was conducted individually for the columns A and B considering the possible difference in the energy dissipation capabilities of two columns. For the bearings, the free oscillation test was conducted simultaneously for four bearings of a type. This was due to difficulty in conducting the test individually for each bearing. In the free oscillaiton test, four bearings of the same type were directly placed on a rigid steel frame and the deck was placed on the bearings. Then the deck was displaced laterally and released smoothly so that shear deformation was developed in the four bearings. Since the steel frame and deck are rigid, energy dissipation developed in this test represents that developed in the bearings. The tests were made individually for RB and HDR.

Because the stiffness of the bearing depends on temperature, all the tests were conducted in a room with a constant temperature of 20 ℃. Lateral displacements of the deck and columns were measured. Accelerations were measured so that the inertia force of the deck be evaluated. They will be used to evaluate the stiffness of bearings. Each test was made twice to secure the stability of the test results.

4 FREE OSCILLATION OF MODEL BRIDGE

Fig. 5 shows the decay of free oscillation of the bridge model. It is apparent that the free oscillation decays much faster in the model supported by HDR than in the model supported by RB. The logarithmic damping ratio δ can be evaluated from the free oscillation as

$$\delta = log_e\left(\frac{a_m}{a_{m+1}}\right) \tag{12}$$

where

δ : logarithmic damping ratio

a_m : displacement amplitude of m-th peak of free oscillation

The damping ratio h may be evaluated from the logarithmic damping ratio as

$$\delta = \frac{2\pi h}{\sqrt{1-h^2}} \tag{13}$$

Damping ratios have been obtained for both plus and minus displacements in the free oscillation.

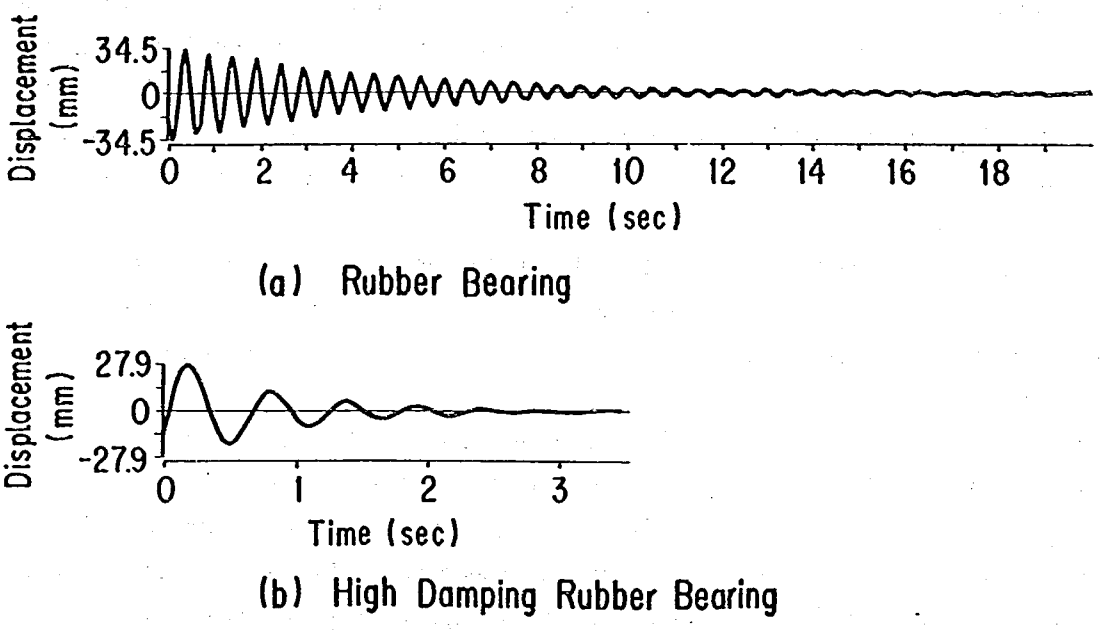


Fig. 5 Decay of Free Oscillation of Bridge Model Deck

Fig. 6 shows the dependence of the thus obtained 1st-mode damping ratio of the entire model bridge on the displacement of the deck. Some scatter is seen at small displacements in the data for the bridge model supported by HDR. Considering that the data with large displacements have more significance for the seismic design, the damping ratio was analyzed for the 1st to 4th cycles of the free oscillation. The displacement ranges of the deck are 6.3 mm – 27.9 mm for the model supported by HDR and 23.8 mm–33.0 mm for the model supported by RB. The averaged damping ratios over the above mentioned ranges are 11.4% for the model supported by HDR and 1.69% for the model supported by RB.

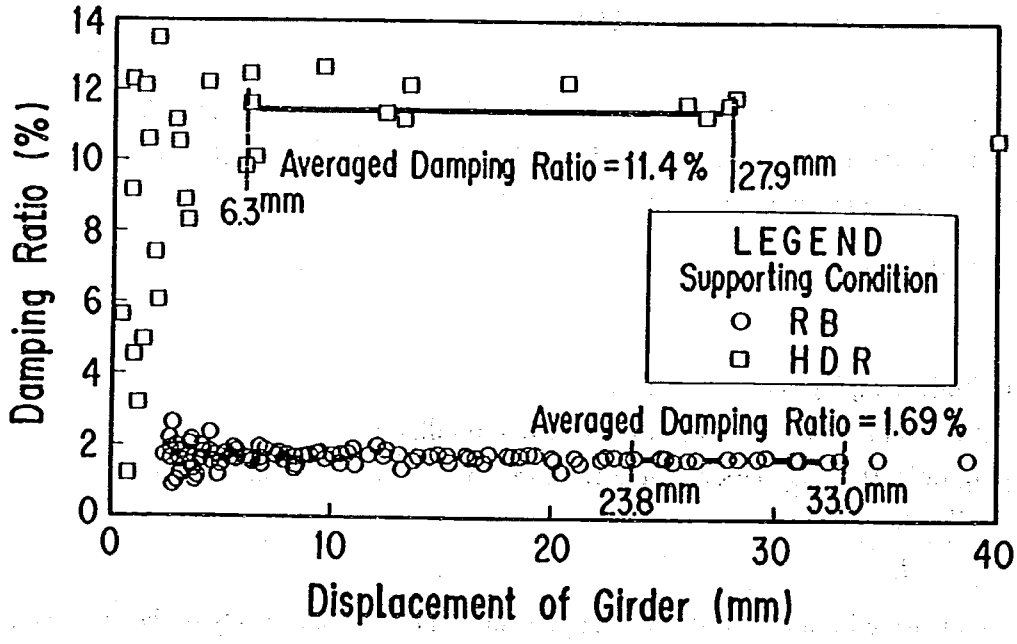


Fig. 6 Damping Ratio of Model Bridge vs. Oscillation Amplitude

Fig. 7 compares the decay of free oscillation of RB and HDR themselves. It is apparent that the oscillation decreases faster in HDR than in RB. Fig. 8 shows the dependence of the bearing's damping ratios on the lateral displacement developed in the bearings. A decrease in the damping ratio at small displacements is observed, especially for HDR. This would be the reason for the decrease of the damping ratio observed for the bridge model supported by HDR, which is shown in Fig. 6. The damping ratios of both RB and HDR have little displacement dependence over the displacement range observed during the above mentioned entire bridge oscillation test. The averaged damping ratios are 3.27% for RB and 25.4% for HDR.

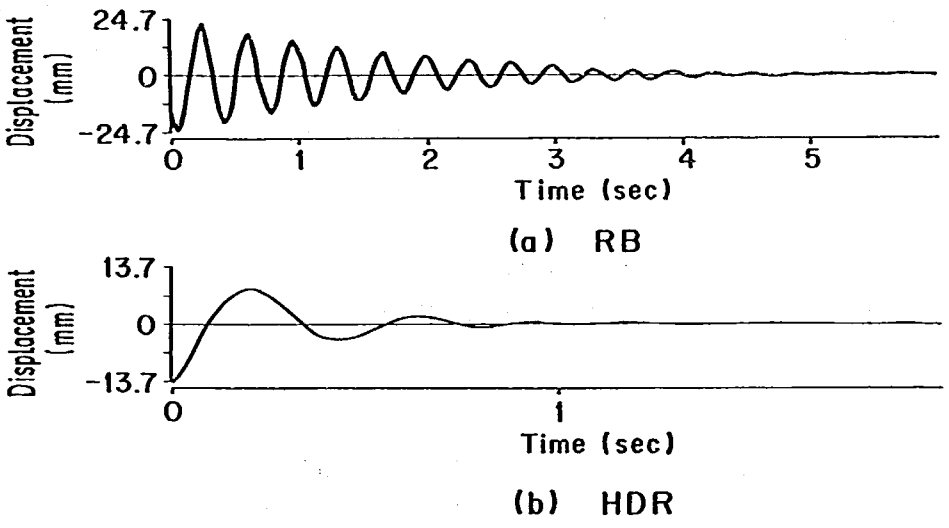


Fig. 7 Decay of Free Oscillation of Bearing Displacement

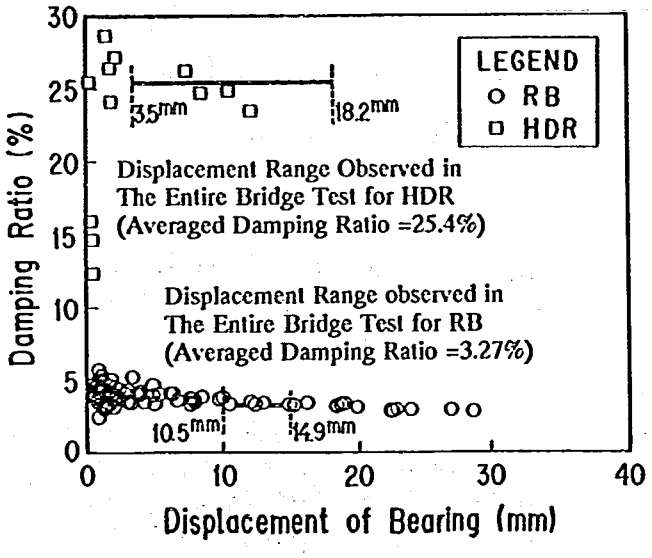


Fig. 8 Damping Ratio of Bearing vs. Shear Displacement

Fig. 9 shows the decay of free oscillation at the top of a column. Fig. 10 shows the displacement dependence of the column's damping ratios. It is interesting to note that the scatter in the damping ratios is larger for Column B than for Column A. This would be due to inevitable difference in the rigidity of the connection between the columns and the steel frame. The displacement observed at the column top

during the free oscillation test of the entire bridge model is 13.4 mm–18.2 mm when the deck is supported by RB and 3.0 mm–10.9 mm when the deck is supported by HDR. For the former displacement range, the damping ratios of the columns A and B are 0.708% and 0.954%, respectively. For the latter, the damping ratios of columns A and B are 0.459% and 0.544%, respectively.

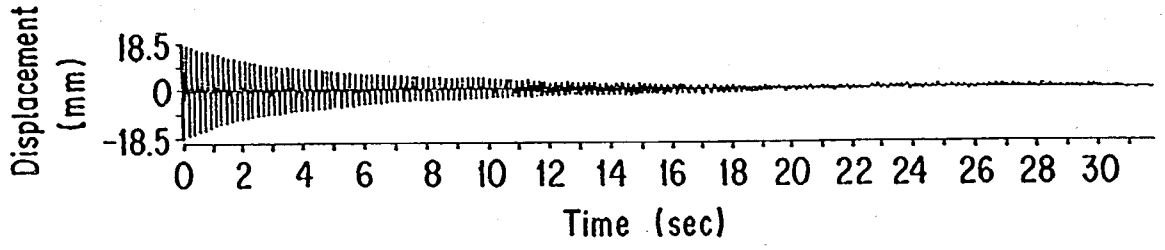
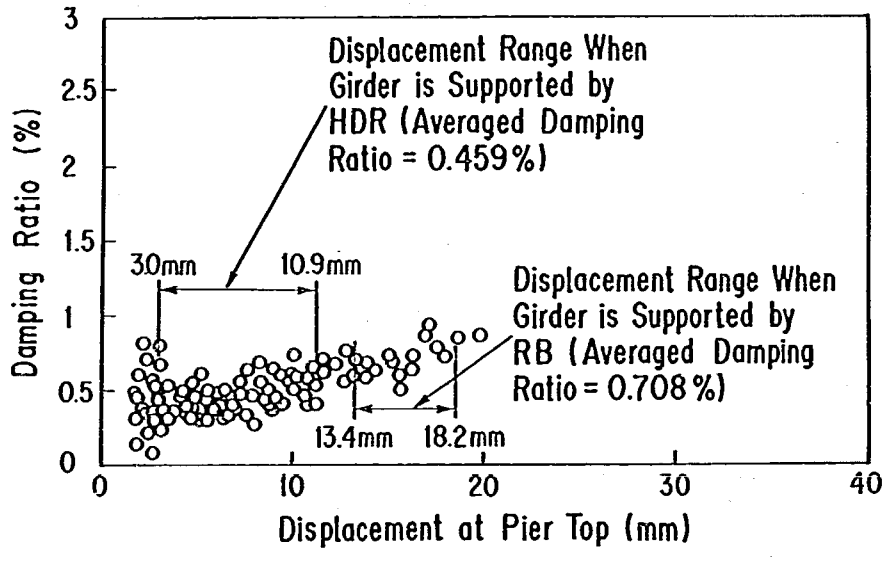
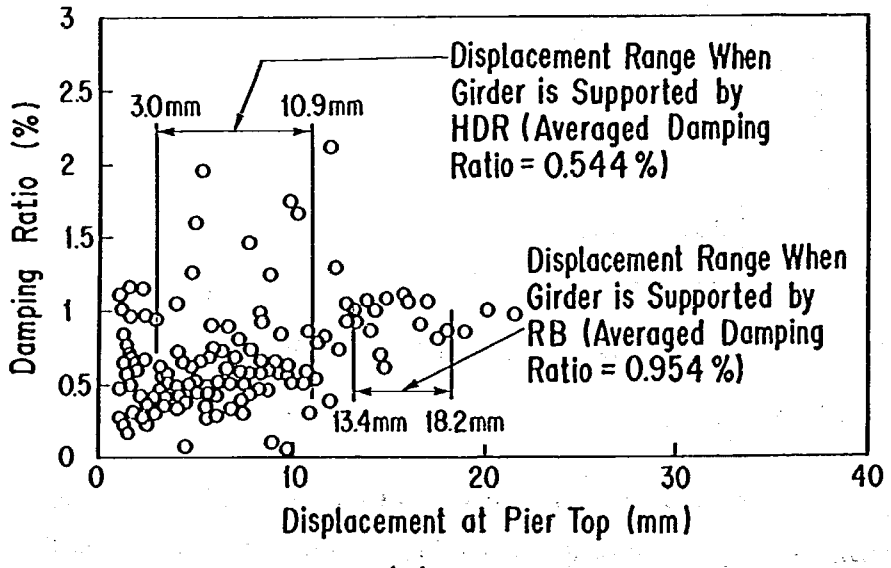


Fig. 9 Decay of Free Oscillation of Column



(a) Column A



(b) Column B

Fig. 10 Damping Ratio of Columns vs. Displacement Amplitude at Column Top

5 ACCURACY OF STRAIN ENERGY PROPORTIONAL DAMPING METHOD

Now that the damping ratio of each substructure has been obtained, the damping ratio h_1 of the entire bridge model for the 1st mode may be evaluated using Eq.(10) as

$$h_1=\frac{w_{1CA}h_{1CA}+W_{1CB}h_{1CB}+W_{1b}h_{1b}}{W_{1CA}+W_{1CB}+W_{1b}} \tag{14}$$

W_{1CA} , W_{1CB} : strain energy of column A and B for 1st mode

W_{1b} : strain energy of bearings for 1st mode

h_{1CA} , h_{1CB} : damping ratio of column A and B

h_{1b} : damping ratio of bearings

Since the damping ratio of the entire bridge model was obtained from the test, accuracy of Eq.(10) can be examined by comparing the damping ratio predicted by Eq.(14) with the one evaluated from the test.

Strain energy of the columns and bearings may be evaluated as

$$W_{1CN}=\frac{1}{2}k_{CN}u_{CN}^2 \quad (N=A,B) \tag{15}$$

$$W_{1b}=\frac{1}{2}k_b u_b^2 \tag{16}$$

where

W_{1CA} ,W_{1CB} : strain energy of column A and B for 1st mode

W_{1b} : strain energy of bearings for 1st mode

k_{CA} , k_{CB} : stiffness of column A and B

k_b : stiffness of bearings

u_{CA} , u_{CB} : lateral displacement at top of column A and B

u_b : shear displacement of bearings

The stiffness of the columns k_{CA} and k_{CB} can be evaluated based on the dimensions of the columns and elastic modulus. The stiffness of the bearings was evaluated as an equivalent stiffness from the hysteresis loop of the force vs. displacement relation. **Fig. 11** shows the relation between the thus evaluated stiffness of the bearings and their shear displacements. As the stiffness of the bearings shows some displacement dependency, it was approximated as

$$\begin{aligned} k_b&=22.7-0.2u_b && \text{for RB} \\ k_b&=8.0-0.2u_b && \text{for HDR} \end{aligned} \tag{17}$$

In the free oscillation test of the entire bridge model, the deck displacement can be evaluated as

$$u_d=u_c+u_b \tag{18}$$

where

u_d : deck displacement

u_c : displacement at column top

u_b : shear displacement of bearings

Since u_d and u_c were measured during the test, u_b can be calculated from Eq.(18). Then the stiffness of the bearings can be estimated by Eq.(17).

Thus the damping ratio of the model bridge was evaluated from Eq.(14) for several peaks of free

oscillations as shown in Table 1. Fig. 12 compares the predicted and measured damping ratios of the bridge model. The predicted values are very close to the measured ones. They are within ± 20% range of the measured damping ratio.

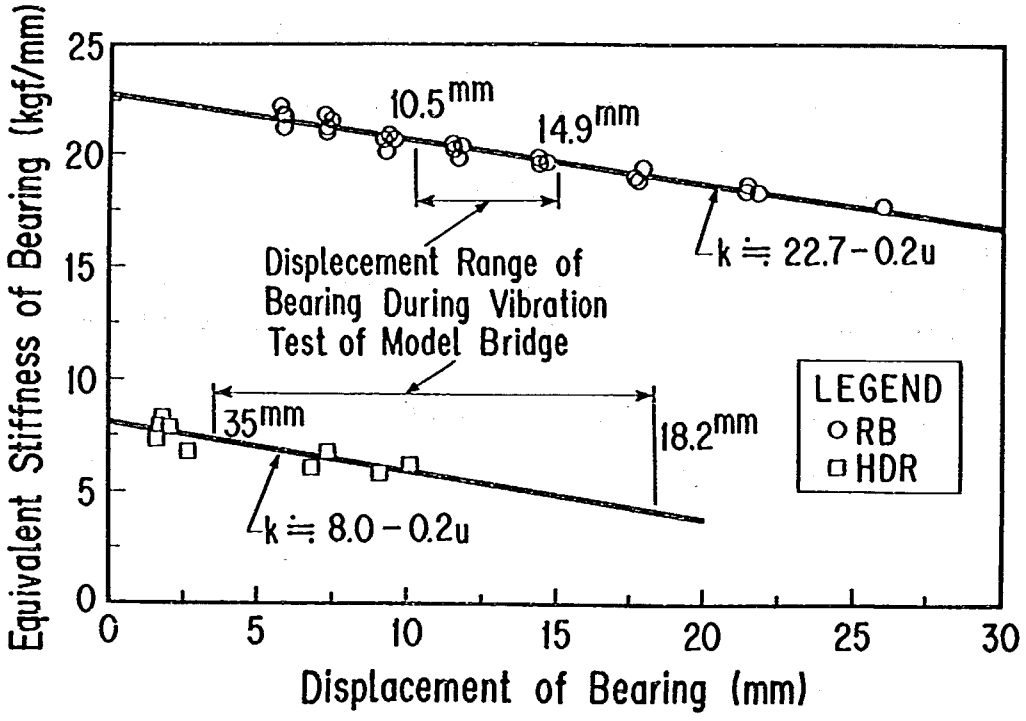


Fig. 11 Displacement Dependence of Stiffness of Bearings

Table 1 Comparison of Predicted and Measured Damping Ratio of Model Bridge

Type of Bearing	Number of Free Oscillation	Displacement of Bridge Model			Damping Ratio and Strain Energy of Structural Members						Modal Damping of Bridge	
		Displacement at Girder d_δ (mm)	Displacement at Pier Top d_p (mm)	Displacement at Bearing d_b (mm)	Pier A		Pier B		Bearing		Estimated by Eq.(11) h_A	Measured h_E
					h_{pA}(%)	W_{pA}	h_{pB}(%)	W_{pB}	h_b (%)	W_b		
Rubber Bearing (RB)	1	33.0	18.2	14.9	0.708	1.437	0.954	1.424	3.273	2.192	1.890	1.690
	2	29.6	16.5	13.3	0.708	1.181	0.954	1.170	3.273	1.775	1.881	1.690
	3	26.5	14.8	11.8	0.708	0.950	0.954	0.944	3.273	1.418	1.877	1.690
	4	23.8	13.4	10.5	0.708	0.779	0.954	0.772	3.273	1.137	1.864	1.690
High-Damping Rubber Bearing (HDR)	1	27.9	10.9	18.2	0.459	0.516	0.544	0.511	25.4	0.710	10.7	11.4
	2	13.4	5.7	8.2	0.459	0.141	0.544	0.140	25.4	0.213	11.2	11.4
	3	6.3	3.0	3.5	0.459	0.039	0.544	0.039	25.4	0.045	9.6	11.4

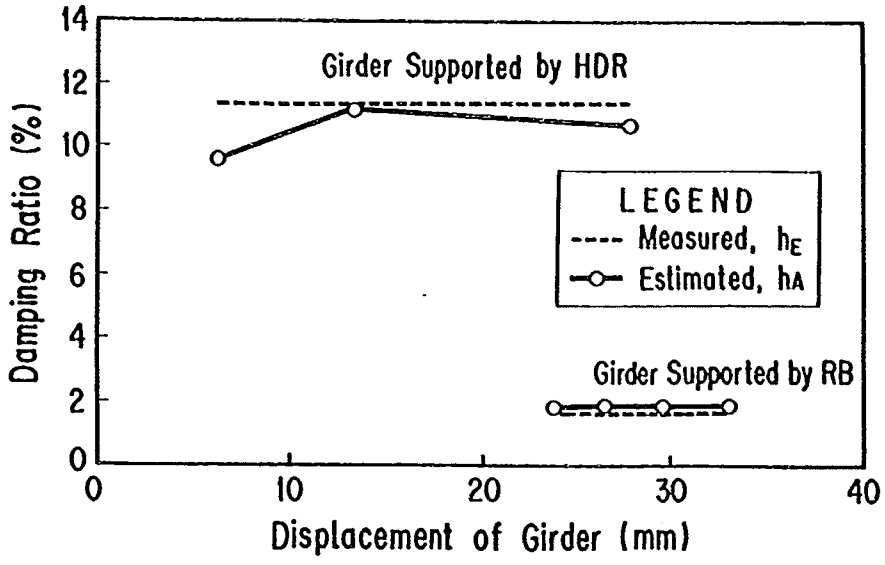


Fig. 12 Accuracy of Predicted Damping Ratio

6 CONCLUSIONS

The effectiveness of the strain energy proportional damping method has been verified through the free oscillation test of a model bridge. Only the damping ratio for the 1st mode was analyzed because of the simplicity of the free oscillation test. It has been made apparent that the damping ratio of the bridge can be predicted with enough accuracy by the strain energy proportional damping method when the damping ratios of substructures are correctly evaluated.

REFERENCES

1) Japan Road Association : Part V Seismic Design, Design Specification of Road Bridges, February 1990
2) Bleich, F. and Teller, L. W. : Structural Damping in Suspension Bridges, Proceedings–Separate No 61, ASCE, March 1951
3) Kawashima, K., Unjoh, S. and Tsunomoto, M. : Damping Characteristics of Cable Stayed Bridges for Seismic Design, Journal of Research, Vol. 27, Public Works research Institute, December 1991
4) Kawashima, K., Unjoh, S. and Tsunomoto, M. : Estimation of Damping Ratio of Cable Stayed Bridges for Seismic Design, Journal of Structural Engineering, Vol. 119, No. 4, ASCE, April 1993
5) Ministry of Construction : Development of Menshin Deisign of Highway Bridges, Technical Note, Vol. 60, Public Works Research Institute, October 1992

(received September 16, 1993)

Development of Variable Damper for Reducing Seismic Response of Highway Bridges

Kazuhiko KAWASHIMA
Shigeki UNJOH
and
Hidetoshi MUKAI

Journal of Structural Engineering
JSCE, Vol.40A
Tokyo, Japan
March, 1994

JOURNAL OF STRUCTURAL ENGINEERING Vol. 40 A (March 1994) JSCE

DEVELOPMENT OF VARIABLE DAMPER FOR REDUCING SEISMIC RESPONSE OF HIGHWAY BRIDGES

Kazuhiko KAWASHIMA *, Shigeki UNJOH **, and Hidetoshi MUKAI ***

Presented are experimental studies on the dynamic characteristics of a variable damper developed at the Public Works Research Institute. A prototype model of the variable damper is developed and the dynamic characteristics obtained through the dynamic loading tests is presented. It is found that the damping force of the variable damper developed is controlled as commanded.

Key Words: seismic control, variable damper, prototype model

1. INTRODUCTION

Because integration of functions of a damper–stopper and a energy dissipator is effective for increasing seismic safety of highway bridges, the applicability and practicability of the variable damper, in which the damping characteristics is variable depending on the response of highway bridges, has been studied at the Public Works Research Institute [1)-2)].

This paper presents experimental studies on the dynamic characteristics of the variable damper. A prototype model of the variable damper is developed and the load–displacement characteristics and the controllability obtained through the dynamic loading tests are presented.

2. FUNCTIONS OF THE VARIABLE DAMPER

The variable damper is a damper in which the damping force is variable depending on the response of highway bridges as shown in Fig. 1. That is:

* Head, Earthquake Engineering Division, Earthquake Disaster Prevention Department, Public Works research Institute, Ministry of Construction, Tsukuba–shi, 305

** Senior Research Engineer, ditto

*** Assistant Research Engineer, ditto

1) The damping coefficient of the variable damper is taken large during a small deck vibration so that the damper have the same function as a fixed bearing support against the braking load of vehicles. It is movable against actions with low–velocity such as an elongation of deck by temperature change.
2) When the amplitude of deck vibration becomes larger up to a certain level during an earthquake, the damping coefficient is decreased so that the inertia force of a superstructure to substructures be decreased appropriately.
3) Furthermore, when the vibration amplitude of the deck becomes excessive, the damping coefficient is gradually increased in order to suppress the excessive amplitude. Therefore, the damper has a function as a stopper with a shock absorber function. This is to prevent the impact response by the sudden operation of the stopper.

Therefore, the variable damper has the advantages of an usual viscous damper–stopper [3)-5)], a passive energy dissipator and a stopper with a shock absorber function.

The concept of the variable damper, in which the damping characteristics can be variable depending on the situation, has been effectively adopted in a field of mechanical engineering, in particular in a suspension system for an aircraft and an automobile. An active suspension to improve driving comfortability and stability of the automobile is one of the examples [6) 7)]. However, it is a new idea to apply the variable damper for highway bridges based on the concept of distributing the inertia force of a superstructure to substructures.

Although various types of the variable damper can be made, the simplest one may be as shown in Fig. 2. The basic component is an cylinder–type viscous damper. A by–pass pipe is installed between the cylinder–cells divided by the piston. The damping characteristics can be controlled by varying the amount of flow of viscous material which passes through the by–pass. Since various technology for controlling such material flow has been developed, the variable damper is most promising and near to the practical use. Furthermore, the external energy required for the operation is significantly smaller in the variable damper than in active control devices.

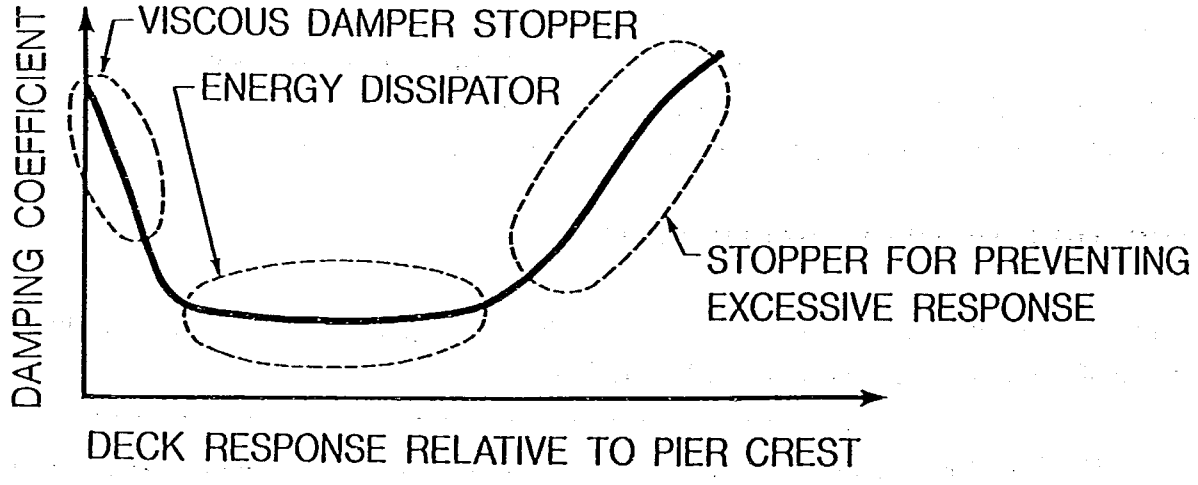


Fig. 1 Basic Concept of Variable Dampers

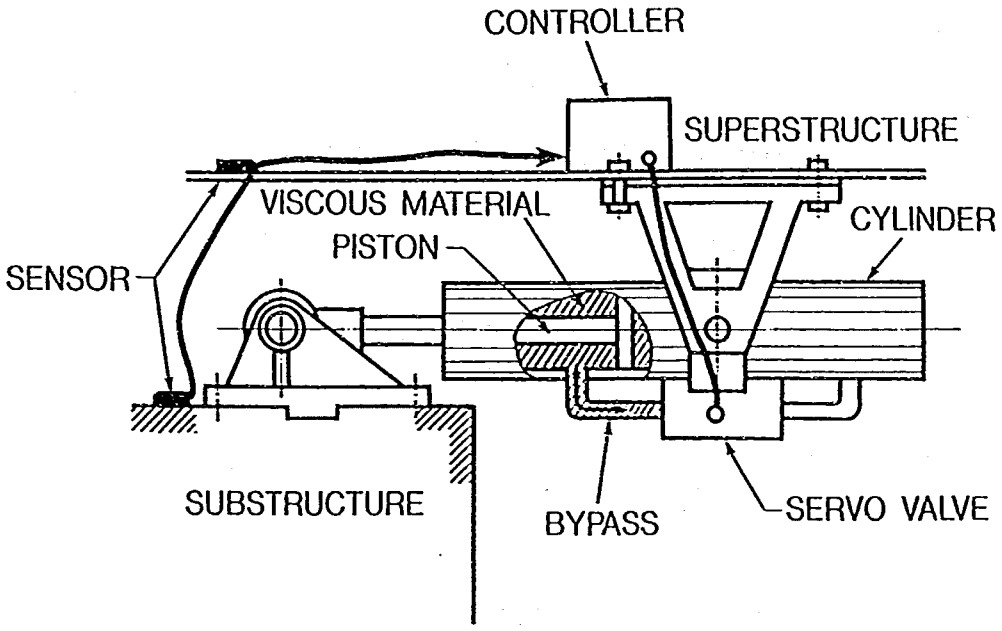


Fig. 2 Variable Damper

3. DEVELOPMENT OF A PROTOTYPE MODEL OF THE VARIABLE DAMPER

3.1 Outline of A Prototype Model of the Variable Damper

Fig. 3 and Photo 1 show a design plan and a view of the variable damper developed. The model is designed so that the maximum damping force is 20tf, maximum relative displacement of damper piston is within ± 10cm. The control of the damping ratio is arbitrarily made by a personal computer depending on relative displacement and velocity developed between deck and substructures.

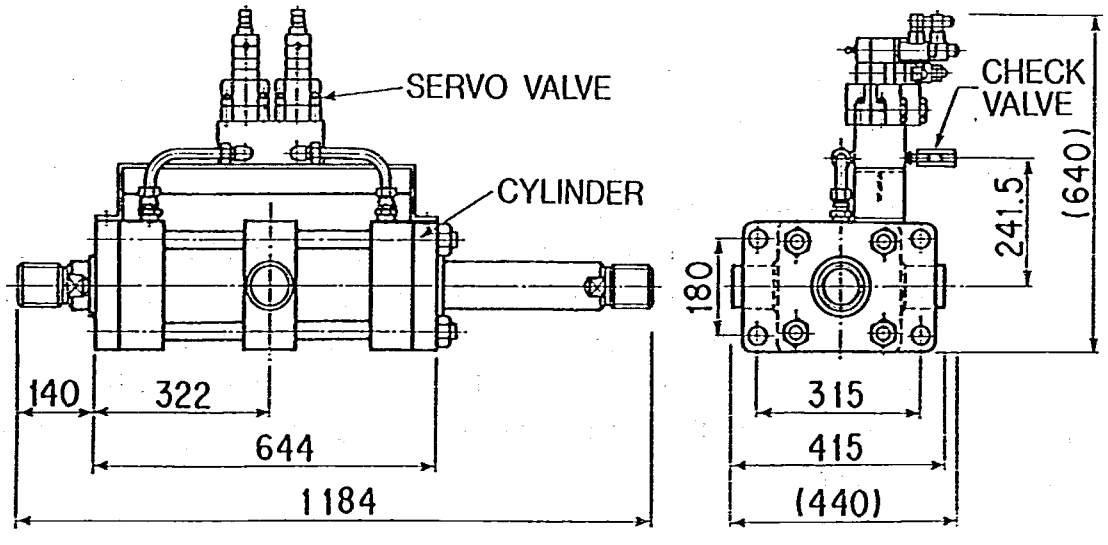


Fig. 3 Prototype Model of Variable Damper

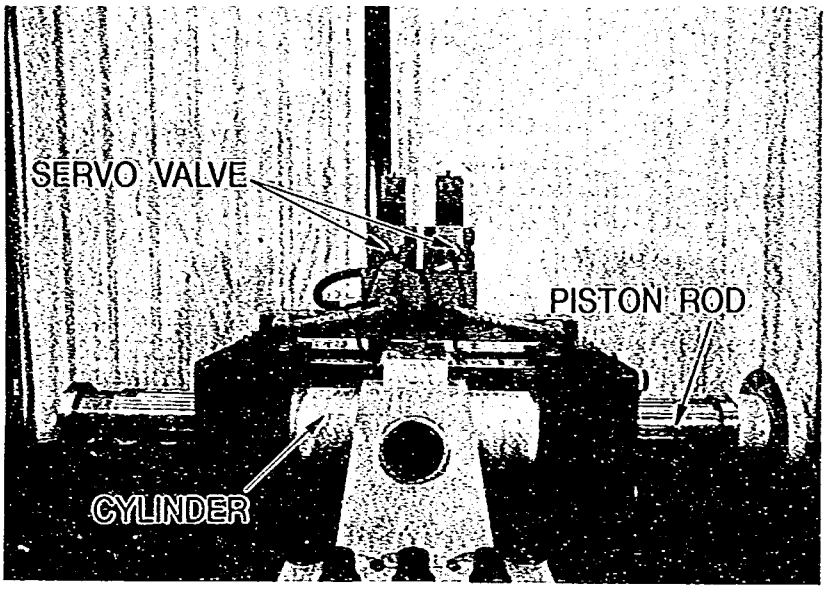


Photo 1 Prototype Model of Variable Damper

The piston–cylinder has the total length of 1,184mm, the pressure area of the piston is 137.4cm ^{2} and the maximum stroke of the piston is $\pm$ 13cm. A steel pipe by–pass with servo valves is installed between the cylinder–cells divided by the piston. The servo valve is a D.C. proportional relief valve. The response time lag of the servo value to the command signal is about 0.05 sec. When the oil pressure through the valve increases to specified one, the pore oil pressure is relieved. This pressure is defined hereafter as control pressure. Therefore, damping force of the piston is developed by the difference of the pressure between two cells in the cylinder. The damping force increases up to when the pressure reaches the specified one, then becomes constant after the pressure exceeds the specified one. Therefore, if the control pressure of the servo valve is assumed to be constant, the damping force is dependent on neither displacement nor velocity of the piston. Therefore, friction type damping force is developed.

The input voltage from a servo amplifier to the servo valve is designed in the range of 0 to 5V. The control pressure is 0 at the input voltage of 0V and increases with increase of the input voltage. The viscous material used for the variable damper is an usual oil for a dynamic loading actuator. The variable damper also has a fail–safe function for an emergency condition such as power failure. The control pressure can be fixed at arbitrary one for such cases.

Fig. 4 shows the flow of the viscous material in the variable damper. The damper piston can move in the left and right directions accompanying with the deck response. When the piston moves in the left side, the viscous material flows from the left cell of the cylinder to the right one through the by–pass and the servo valves. The difference of the pressure in the two cells is adjusted as specified one by servo valves. When the piston moves in the opposite direction, damping force is controlled in the same manner.

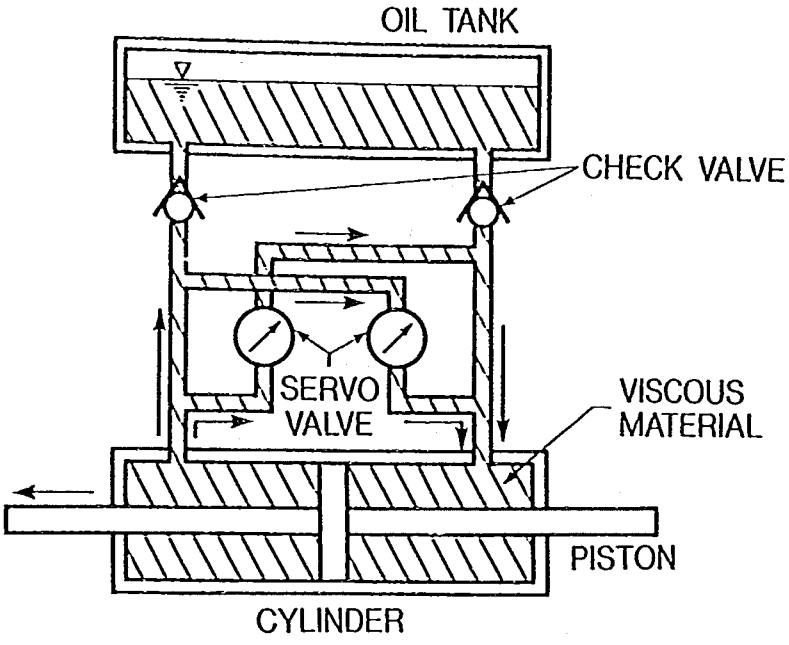


Fig. 4 Flow of Viscous Material

3.2 Dynamic Loading Tests of the Prototype Model of the Variable Damper

The variable damper can vary the damping characteristics depending on the displacement and/or velocity of the structures. Therefore, in order to provide the variable damper with the required damping characteristics it is necessary to know the basic dynamic characteristics. The damping characteristics of the variable damper is controlled by the control pressure of the servo valve and it is controlled only by the input voltage to the servo valve from the servo amplifier. Therefore, in order to arbitrarily control the damping force of the variable damper developed, the relation between the input voltage to the servo valve and damping characteristics of the variable damper is essential.

Fig. 5 shows the set-up of the dynamic loading tests. Under the condition that the control pressure of the servo valve is kept to be constant, the loading was applied to the piston by a dynamic actuator under the displacement control. The input voltage to the servo valve, reaction force and stroke of the piston are measured. The loading is assumed as harmonic and repeated by 10 cycles for each loading amplitude.

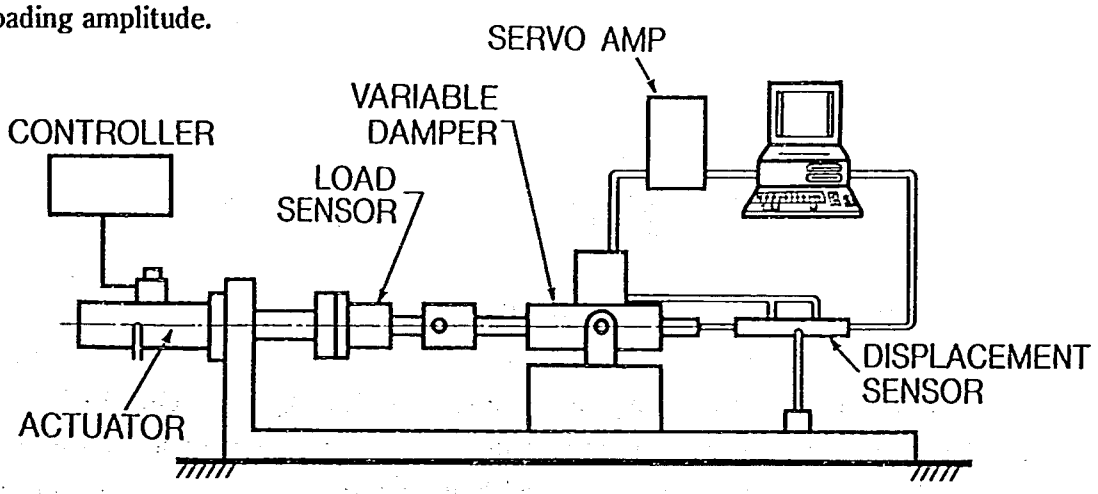


Fig. 5 Set Up of Loading Test

Table 1 shows the experimental cases. Case 1 is to measure the friction force of the damper piston. Static loading was made with loading frequency of 0.05Hz and loading displacement of ±. 100mm. The input voltage of the variable damper is set to be 0V so that the control pressure is 0.Case 2 is to obtain the relation between input voltage to the servo valve and damping force of the variable damper. Loading frequency, loading displacement and input voltage are varied. It should be noted here that the loadings, that exceed 7cm/s in maximum loading velocity were not made because of the capability of a loading apparatus.

Table 1 Experimental Cases

Case	Objective	Loading Frequency (Hz)	Loading Displace-ment (cm)	Input Voltage (Volt)
1	Measurement of Friction Force of Damper-stopper	0.05	±100	0
2	Relation between Damping Force and Input Voltage	0.1~1.0	±2~±100	0~5

3.3 Performance of the Prototype Model of the Variable Damper

(1) Friction force of the damper-piston

Fig. 6 shows hysteresis loops of the load-displacement relation when the damper is loaded with the loading frequency of 0.05Hz and loading displacement of ± 100mm to obtain the friction force of the damper-piston. The load-displacement relation shows almost rectangular shape. It means that the typical friction type load-displacement relation is obtained. The hysteresis is stable for a number of loading cycles. The average friction force is about 1tf.

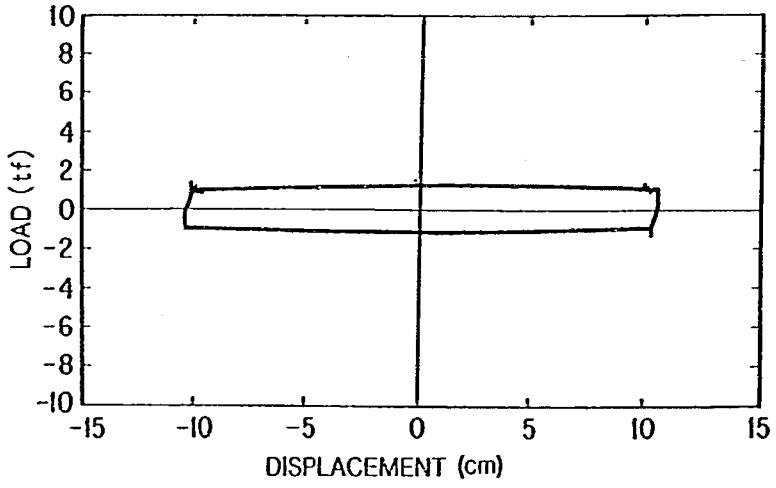
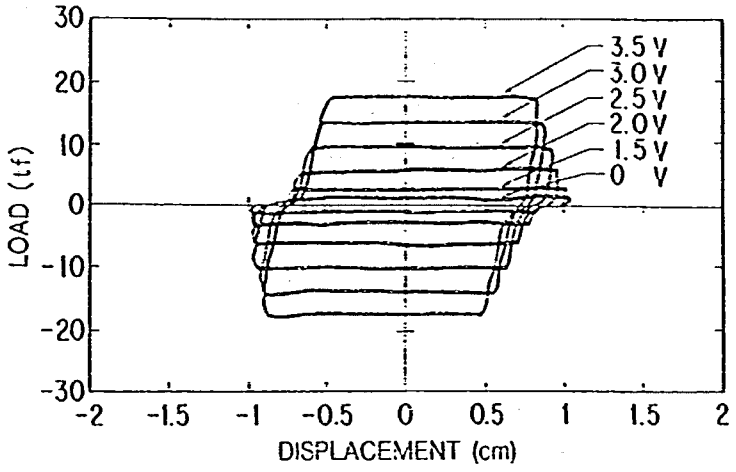


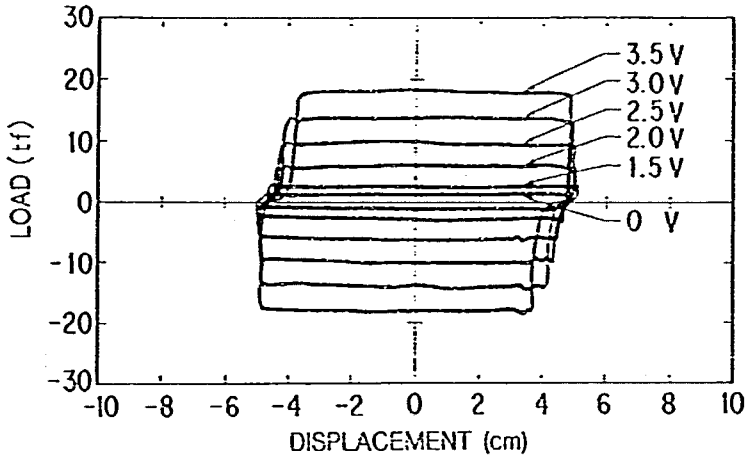
Fig. 6 Hysteresis Loops of Load-Displacement Relation (Displacement = 10cm, Frequency = 0.05Hz)

(2) Hysteresis loops of the load-displacement relation

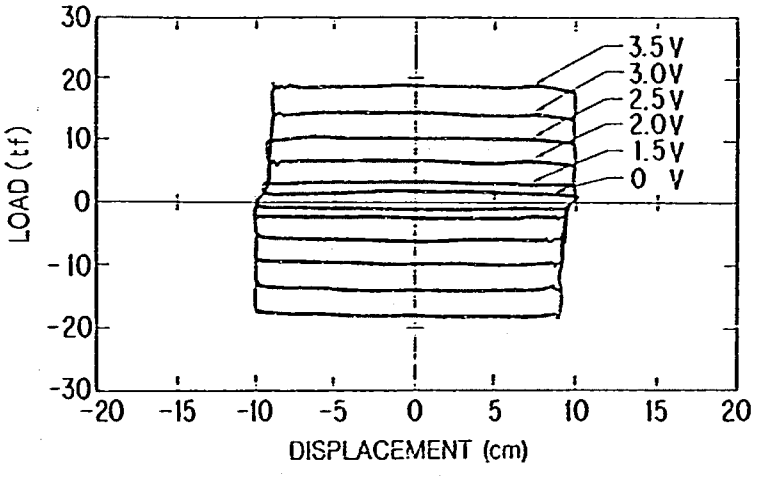
Fig. 7 shows some of hysteresis loops of the load-displacement relation obtained. The hysteresis loops are shown for the loading frequency is 0.1Hz and loading displacement of ± 1cm, ± 5cm and ± 10cm. The variation of hysteresis loops with the input voltage are also shown in Fig. 7. The hysteresis loops have the rectangular shape which means that the variable damper has the typical friction type hysteresis loops as designed. Although the damping force instantaneously



(a) Displacement 1cm



(b) Displacement 5cm



(c) Displacement 10cm

Fig. 7 Hysteresis Loops of Load–Displacement Relation (Frequency = 0.1Hz)

decreases from specified one to 0 at the instance when the direction of movement of the piston changes at maximum displacement, the time-lag is found at the standing of the damping force. This is because increase of the oil pressure from 0 to specified one takes some time. Turbulence is also found at the instance when the damping force reaches specified one. This may be because the pressure wave motion is developed by sudden standing of the pressure. Therefore, the controllability of the damper may be affected by the loading frequency due to the response time lag of the servo valve. Since the response time lag of the servo valve used is about 0.05 sec. It is required to use the servo valve with the faster response capability for more precise control.

(3) The relation between the input voltage and damping force

Fig. 8 shows the relation between the damping force and the input voltage. The empirical equation obtained by a least square method is also shown in Fig. 8. The damping force varies as a power function of the input voltage when the input voltage is lower than 1.8V. When the input voltage is greater than 1.8V the relation becomes almost linear. Therefore, the empirical equation is assumed as

$$F = \begin{cases} 0.42V^{3.7}+1.0 & (0 \leqq V \leqq 1.8) \\ 8.14V-9.95 & (V>1.8) \end{cases} \qquad (1)$$

where, F and V represent damping force (tf) and input voltage (Volt), respectively. In Eq.(1), the constants are determined as averaged values of those obtained in each loading case.

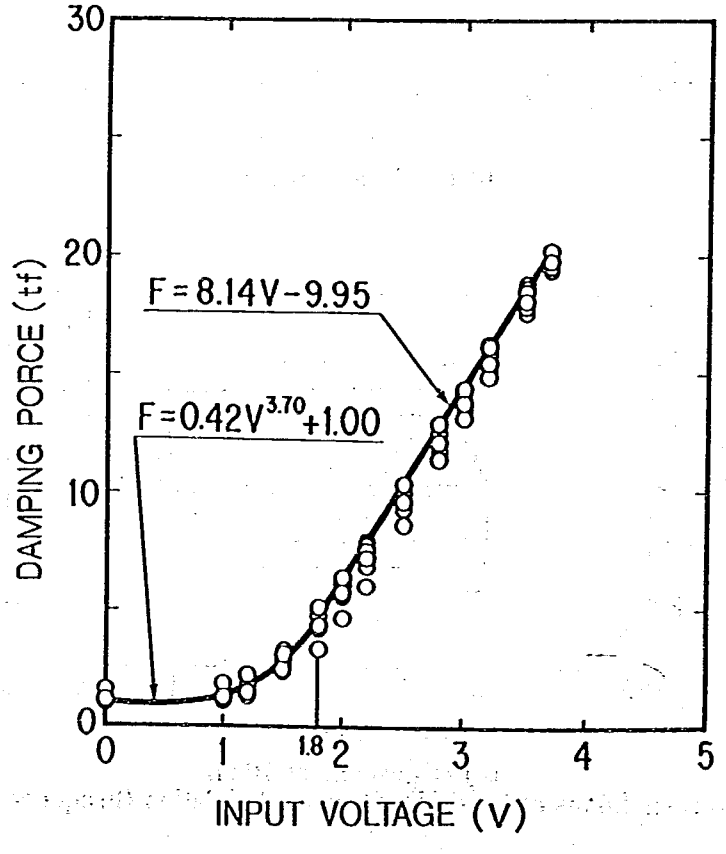
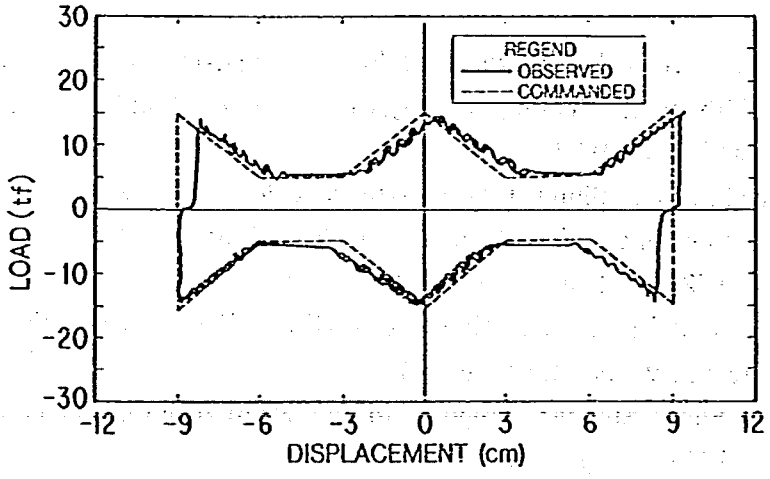


Fig. 8 Damping Force vs. Input Voltage Relation

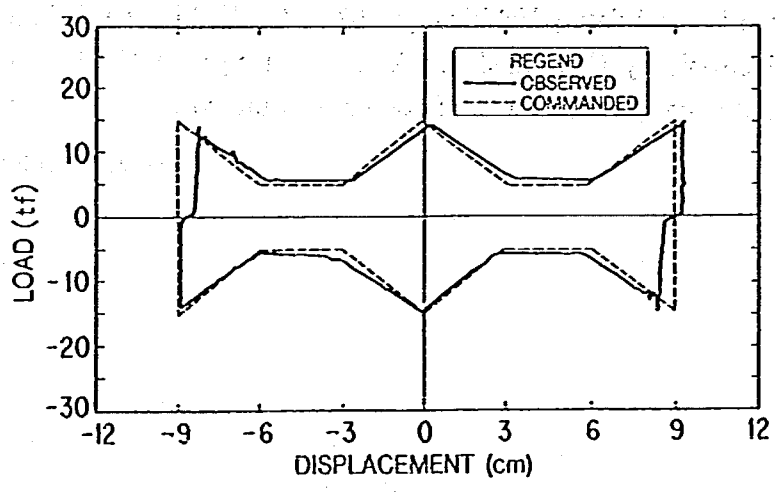
(4) Controllability of the variable damper

Based on the above experimental results, the damping force is controlled by the input voltage using Eq.(1). The controllability of the variable damper so as to control damping force as shown in Fig. 1 is tested. The control of the variable damper can be is made by control signal from a personal computer according to the displacement and/or velocity obtained by sensors.

Fig. 9 shows hysteresis loops of load–displacement relation to show the controllability of the variable damper. The commanded damping force and the measured one are shown in Fig. 9. Fig. 9(a) and (b) show the cases when the sampling time of displacement is assumed as 0.1sec and 0.01sec, respectively. The loading frequency is 0.1 Hz. The damping force is found to be controlled almost as commanded. When the sampling time is 0.1 sec, corrugation is found when the damping force is varied with the displacement. Therefore, it is required to use the appropriate sampling time in order to precisely control in consideration with the loading velocity.



(a) Sampling Time 0.1sec



(b) Sampling Time 0.01sec

Fig. 9 Controllability of the Variable Damper Developed

4. CONCLUDING REMARKS

The applicability and controllability of the variable damper developed for reducing seismic response of highway bridges are experimentally studied. The prototype model of the variable damper was developed and the performance was studied through the dynamic loading tests. According to the above investigations the following conclusions may be deduced. Based on the dynamic loading tests of the prototype model developed, the load–displacement relation is obtained as designed. The damping force of the variable damper is controlled by the input voltage. The relation between the damping force and input voltage is given by the empirical equation. Furthermore, it is found that the damping force of the variable damper developed can be controlled almost as commanded. To implement the variable damper for actual highway bridges, further investigations on the controllability with faster loading frequency as well as the durability for long term use are required.

REFERENCES

1) Kawashima, K., Unjoh, S. and Shimizu, H. : Seismic Response of Highway Bridges by Variable Damper, 24th Joint Meeting, U.S.–Japan Panel on Wind and Seismic Effects,UJNR, Gaithersburg, Maryland, May, 1992
2) Kawashima, K., Unjoh, S. and Shimizu, H. : Earthquake Response Control of Highway Bridges by Variable Damper, Proceedings of Colloquium on Control of Structures, Japan Society of Civil Engineers, Part. B, pp.221–224, July, 1991 (in Japanese)
3) Fukuoka, S. : Design of Multi–span Continuous Girder Bridge using Viscous Shear Stopper, Bridge, pp.22–29, February, 1980 (in Japanese)
4) Izeki, H. : Viscous Shear Stopper, Proposal to the Multi–Continuous Girder Bridge, Bridge, pp.30–33, February, 1980 (in Japanese)
5) Matsumura, S., Fukuoka, S, Mizumoto, Y. and Nakata, T. : Seismic Design of Multi–Span Continuous Girder Bridge using Damper Stopper, Bridge and Foundation, pp.31–37, May, 1982 (in Japanese)
6) Milliken, Jr., W., F. : Lotus Active Suspension System, Proceedings of 11th International Conference on Experimental Safety Vehicles, pp.467–475, Washington D.C., May, 1987
7) Sugawara, F. : Electronically Controlled Shock Absorber System Used as a Road Sensor which Utilizes Super Sonic Waves, Proceedings of Society of Automotive Engineers, pp.6.15–6.25, 1986

(received September 16, 1993)

Seismic Behavior of Buried Pipelines Through Field Observation

Kazuhiko KAWASHIMA
Hideki SUGITA
and
Tomoru NAKAJIMA

Journal of Structural Engineering
JSCE, Vol.40A
Tokyo, Japan
March, 1994

JOURNAL OF STRUCTURAL ENGINEERING Vol. 40 A (March 1994) JSCE

SEISMIC BEHAVIOR OF BURIED PIPELINES THROUGH FIELD OBSERVATION

Kazuhiko KAWASHIMA *, Hideki SUGITA ** and Tomoru NAKAJIMA **

This paper presents seismic response characteristics of embedded pipes based on field measurements. Strains induced in steel pipe and ductile pipes with expansion joints are studied. Special attention is placed for effect of bends on pipe response. Soil springs which are important in seismic design by means of the seismic deformation method is also studied based on the measured data.

Key Words: *seismic deformation method, buried pipe, seismic design, strong motion observation*

1. INTRODUCTION

Seismic design of embedded pipes is generally made by the seismic deformation method [4] in which embedded pipes are assumed to respond in accordance with strain induced in ground during earthquakes. Pipes are considered to be beams elastically supported by soils when the stiffness of the soil is modelled by springs. Although the seismic deformation method has been adopted for seismic design of embedded lifeline facilities, measured data available for evaluation pipe response during earthquakes is very limited. Strong motion observation was initiated for measuring pipe response, because precise evaluating of pipe response in ground is essential for improving seismic design method. Special attention was paid to obtain response data for pipe with bends and expansion joints.

This paper presents an analysis of the measured data of pipe response, and soil spring stiffness to be used in the seismic deformation method is also presented.

* Head, Earthquake Engineering Division, Earthquake Disaster Prevention Department, Public Works research Institute, Ministry of Construction, Tsukuba-shi, 305

** Research Engineer, ditto

2. OBSERVATION SYSTEMS

Fig. 1 shows the observation systems placed at Sodegaura city, about 50 km east of Tokyo, for measuring seismic behavior of embedded pipes. Continuous steel pipe with a diameter of 15 cm and ductile pipes with diameters of 15 cm (right side in Fig.1) and 30 cm (left side in Fig.1) are embedded 1 m below the ground surface As shown in Photos 1 and 2. The length of the continuous steel pipe is 120 m and there is a bend at 20 m from the right end. The length of one element of the ductile pipe is 5 m in the 15 cm diameter pipe and 6 m in the 30 cm diameter pipe. They were jointed together by expansion joints which are capable of absorbing a relative deformation of ± 10 % of pipe

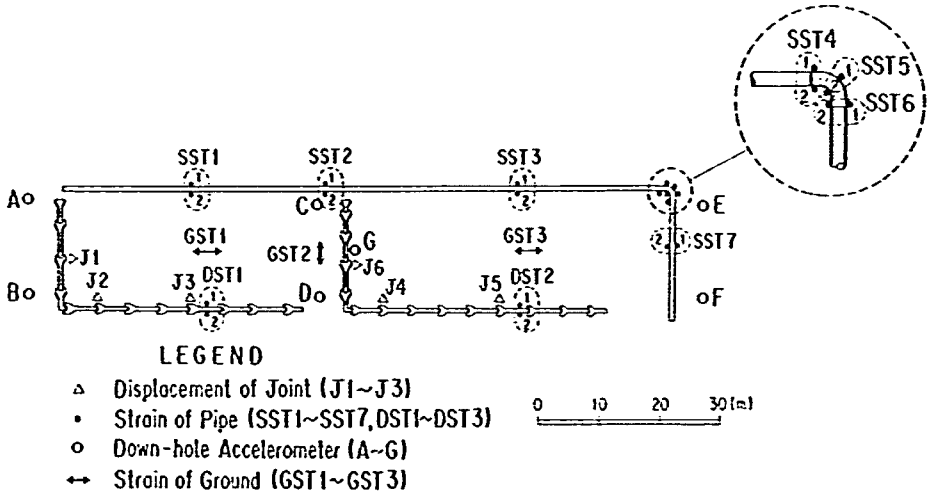


Fig. 1 Observation Systems

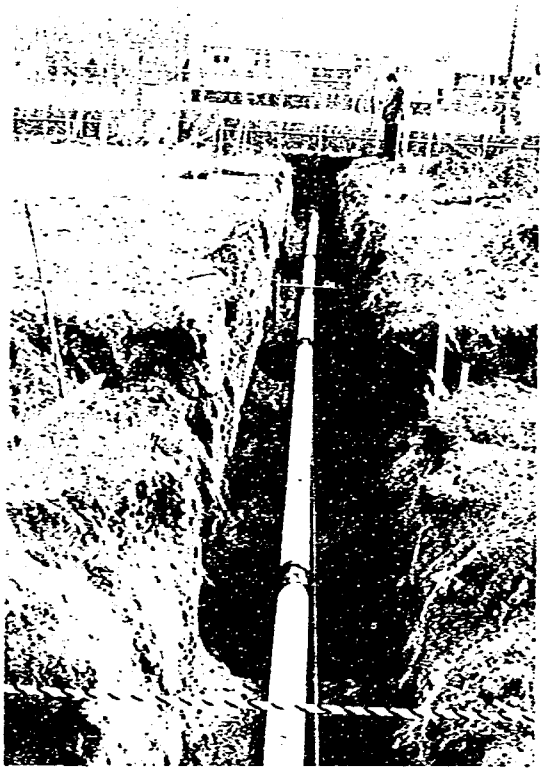


Photo 1 Steel Continuous Pipe (Straight Section)

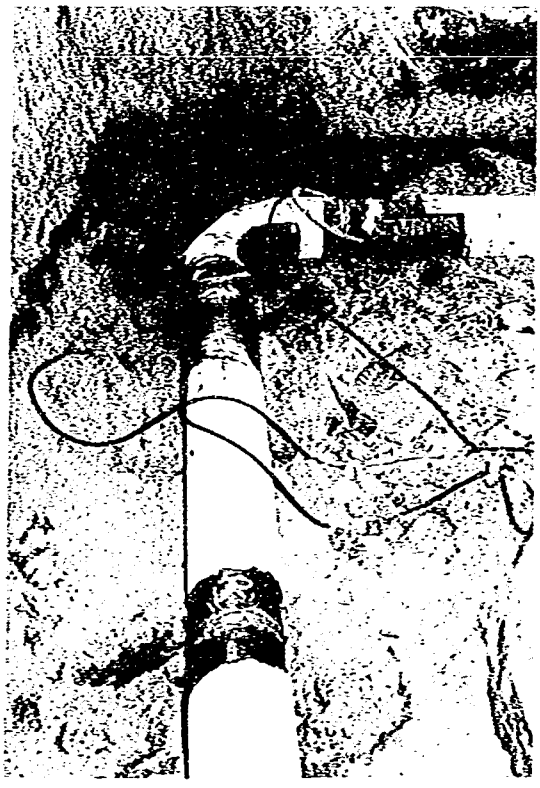


Photo 2 Steel Continuous Pipe (Bend Section)

length in the axial direction and a rotation of ± 6 degrees. Stoppers for preventing excessive pulling-out are provided at the expansion joints.

Dense instrumentation is made to measure the pipe response. The strain induced in the steel and ductile pipes as well as relative displacements developed between two adjacent ductile pipe sections were measured. Strain gauges with coating against water are placed on the both sides of the pipes so that the flexural strain as well as the axial strain could be detected.

The ground acceleration and ground strain were measured. Three-components down-hole accelerometers were installed at seven points to measure ground acceleration. The accelerometers A-F were installed 1 m below the ground surface, and the accelerometer G was installed 30 m below the ground surface. The measured data was used to compute the averaged ground strain induced at the site. Special devices were installed 1 m below the ground surface to directly measure ground strain. The devices consist of two 80 cm diameter circular plates and a 6 cm diameter double tubed steel rod. The circular plates were connected to the double tubed steel rod.

Movement of the circular steel plates in accordance with soils vibration during earthquakes would develop small relative displacements between the two circular plates. Ground strain may be evaluated by dividing the relative displacement by the length of the double tubed steel rod. This device has been successfully used for measuring ground strain at several observation sites [1) 3)].

All the measured signals are digitized with an interval of 1/100 second and recorded with a

Table 1 Major Earthquakes Triggered

NO. OF EQ.	DATE	EPICENTER			MAGNITUDE (M)	FOCAL DEPTH (km)
		EPICENTRAL REGION	LONGITUDE	LATITUDE		
EQ-1	1989. 10. 14	NEAR IZU-OHSHIMA	135° 03′	34° 54′	5.7	25
EQ-2	1990. 6. 1	EAST OF CHIBA-KEN	140° 40′	35° 38′	6.0	70
EQ-3	1990. 6. 5	MIDDLE OF KANAGAWA-KEN	139° 20′	35° 50′	5.3	120
EQ-4	1990. 6. 27	SAGAMI-BAY	139° 07′	35° 00′	5.4	148
EQ-5	1990. 8. 23	MIDDLE OF CHIBA-KEN	140° 24′	35° 21′	5.4	50
EQ-6	1990. 8. 23	MIDDLE OF CHIBA-KEN	140° 24′	35° 21′	5.2	49
EQ-7	1990. 12. 11	MIDDLE OF CHIBA-KEN	140° 19′	35° 19′	4.0	35
EQ-8	1990. 12. 16	MIDDLE OF CHIBA-KEN	140° 13′	35° 37′	4.6	77
EQ-9	1991. 6. 28	TOKYO-BAY	139° 52′	35° 29′	4.6	68
EQ-10	1991. 7. 14	EAST OF NAGANO-KEN	138° 31′	36° 25′	5.4	187
EQ-11	1991. 9. 29	NORTH OF CHIBA-KEN	140° 06′	35° 45′	4.9	80
EQ-12	1991. 11. 19	TOKYO-BAY	140° 02′	35° 36′	4.9	81
EQ-13	1992. 2. 2	TOKYO-BAY	139° 08′	35° 20′	5.7	90

digital acquisition systems. Pre-event memory of about 10 seconds are provided to get full records from their start.

3. MEASURED DATA

Observation was initiated in January 1989 and many records have been already obtained. In this report the pipe response was analyzed based on the measured data obtained after October 1989. Record which are large enough for analysis were measured by thirteen earthquakes as shown in Table 1.

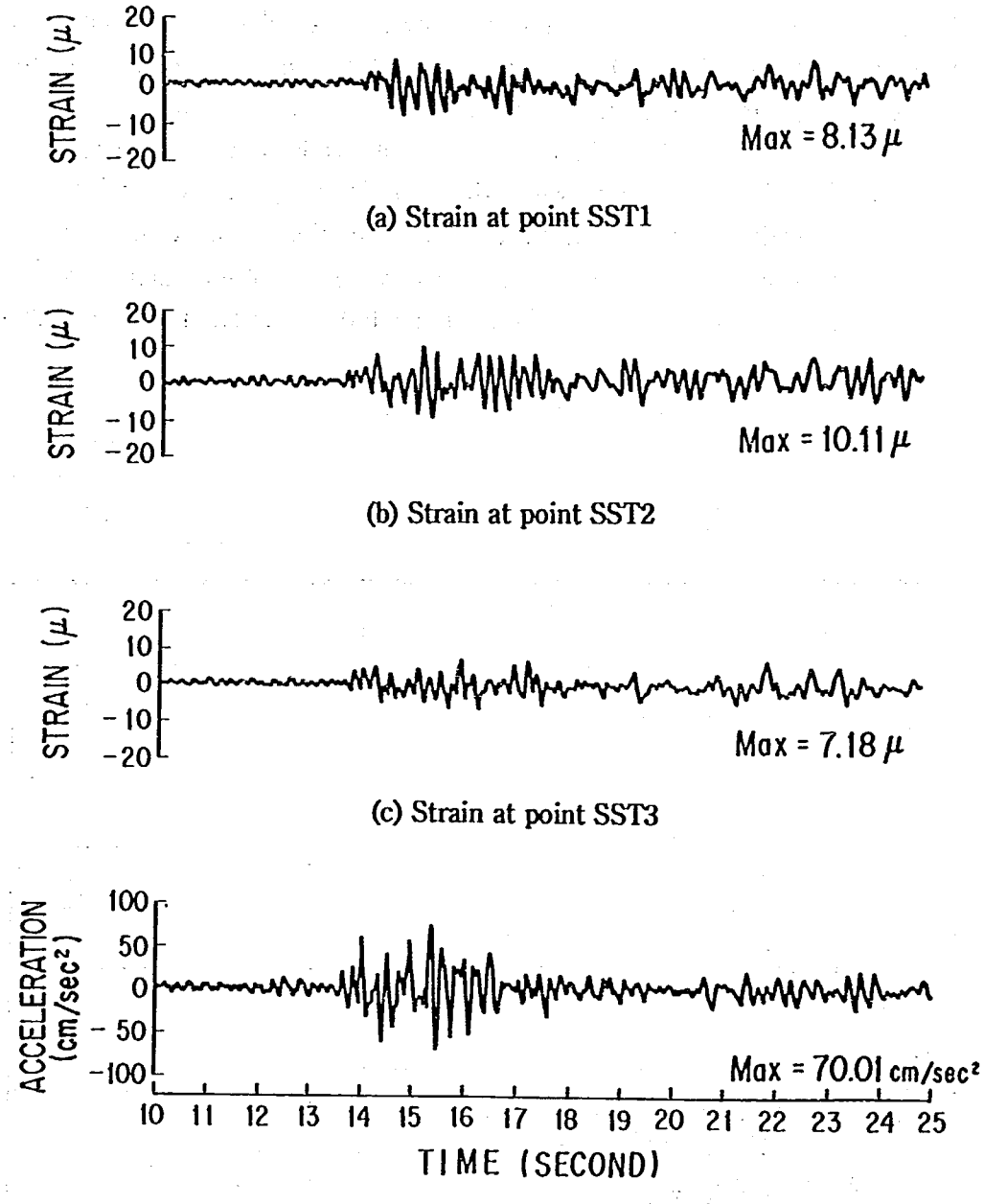
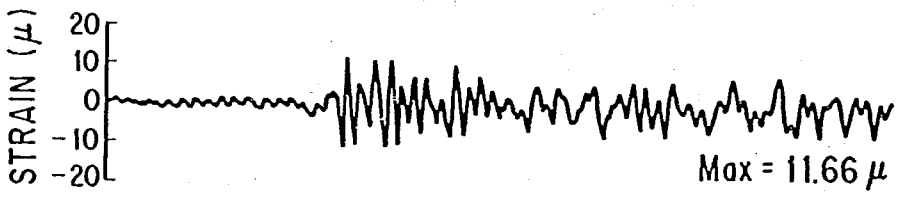


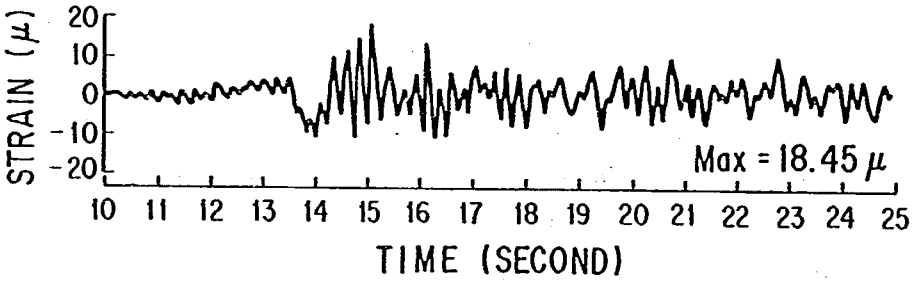
Fig. 2 Measured Axial Strain of Steel Pipe and Ground Acceleration C Point during EQ 13

Fig. 2 shows the measured axial strain induced in the steel pipe and ground accelerations developed by an earthquake with epicentral distance of 75 km and an earthquake magnitude of 5.7. This earthquake is designated hereinafter as EQ 13 earthquake. The peak ground acceleration was about 65 to 70 cm/sec ^{2} and the peak pipe strain was about 7.2 to 10.1 μ . It is interesting to note in Fig. 2 that although there are many similarities of the pipe strains in the wave form between the three locations, they are not identical. This clearly shows that the pipe response in axial direction depends considerably on the response of nearby soil.

Because the ground motion was small, the devices for measuring ground strain did not directly detect ground strain. Fig. 3 shows ground strains computed for the EQ 13 earthquake from measured

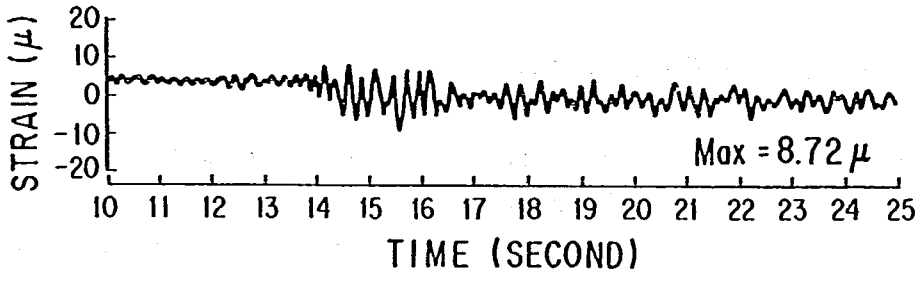


(a) Averaged Strain Between △ ABC

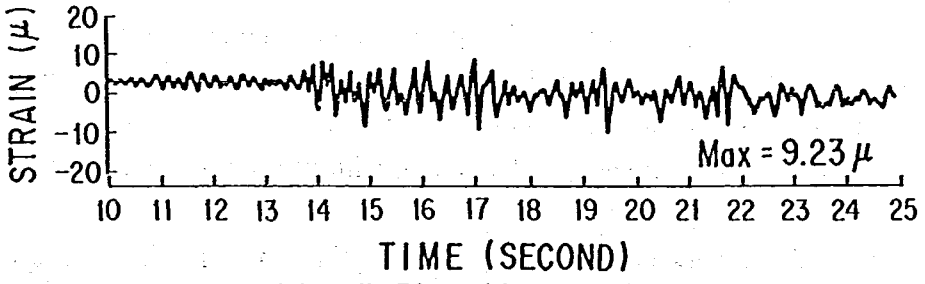


(b) Averaged Strain Between △ BCD

Fig. 3 Ground Strain Computed for EQ 13 from Measured Ground Acceleration



(a) Ductile Pipe with 30cm Diameter



(b) Ductile Pipe with 15cm Diameter

Fig. 4 Measured Axial Strain of Ductile Pipe during EQ 13

ground accelerations. The measured ground accelerations were double integrated to obtain the ground displacements [7] . Assuming triangular elements such as Δ ABC and Δ BCD, the ground strain along pipe axis was computed with use of the standard finite element method [5] . Linear interpolation function for displacements was assumed in each finite element. It should be noted in Fig. 3 that there is some drift of zero strain at 13–14 second. Because the ground accelerations are quite small, there way be some error in computing the ground strain. It should be also noted that the peak strain is 1.6 times larger in Δ BCD than Δ ABC. This way be developed due to special variation of ground. If the ground strain computed for Δ ABC, which is the averaged ground strain between points A and C, is compared with the axial pipe strain at point SST1, in Fig. 2, it is found that the strains obtained are quite similar.

Fig. 4 shows axial strain induced during the EQ 13 earthquake in the ductile pipes. Almost no relative displacement was developed at the joints. It is interesting to note that the strain of the ductile pipe at the point DST–1 is quite similar with the strain of the steel pipe at the point SST–1. The strain of the ductile pipe is not necessarily smaller than the strain of the steel pipe. This implies that reduction of axial force induced in the ductile pipe due to the expansion joints was quite small during the EQ 13. The forces developed at the expansion joints during the EQ 13 were so small that friction at the expansion joints prevented slippage to occur between the adjacent pipe sections.

Fig. 5 shows a distribution of peak strain along the steel pipe for the EQ 13 earthquake. Both axial and flexural strains are presented. It should be noted that although axial strain is predominant in the straight section, flexural strain becomes larger than the axial strain at the bends. Flexural strain has to be therefore taken into account in seismic design of pipes at bend sections.

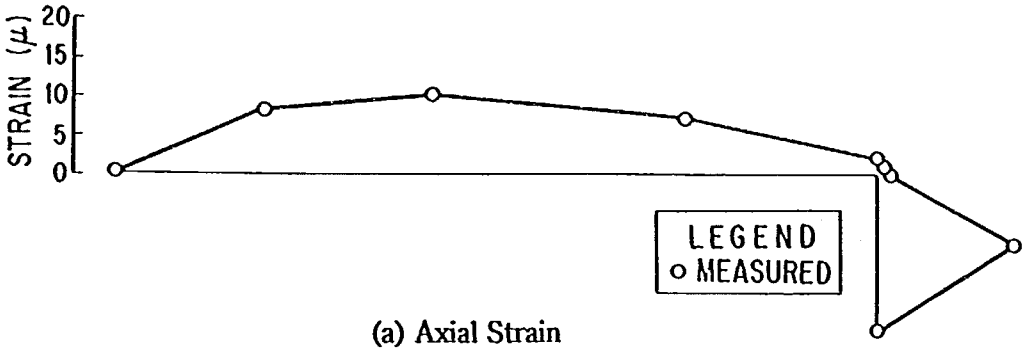
Fig. 6 shows the axial strain of steel pipe vs. peak ground acceleration in pipe axis relation for the data obtained by the thirteen earthquakes presented in Table 1. The strain at SST3 was plotted. Although number of the data obtained is still small, clear correlation between the pipe strain and the peak ground acceleration is observed. By increasing the number of data, this is expected to provide a practical estimation for the pipe strain induced during earthquakes.

4. EVALUATION OF SOIL SPRING STIFFNESS

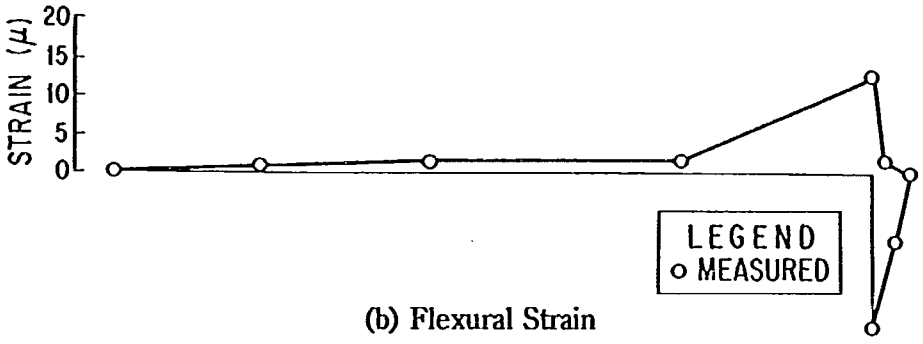
An analytical model presented in Fig. 7 is often adopted to estimate dynamic response analysis of embedded pipes [6] . The pipe is idealized by a beam elastically supported by springs which represent pipe –soil interaction. Soil response is computed by prescribing the input ground motion at the base rock.

In the analytical model presented in Fig. 7, it is essential to determine the stiffness of the soil springs which elastically support correctly the pipe. Various methods have been proposed from analytical and experimental studies to estimate the soil springs. However due to limitation of measured data available for estimating soil springs based on measured seismic response data of pipes, few studies have been made for soil springs. Therefore, with use of the analytical model presented in Fig. 7, the soil springs stiffness were studied.

The response displacements of soils which were estimated from the measured accelerations were used for computing the pipe responses. The steel pipe was idealized by a discrete analytical model with 24 beam elements as shown in Fig. 8. Because the displacements which were computed



(a) Axial Strain



(b) Flexural Strain

Fig. 5 Peak Strain of Steel Pipe during EQ 13

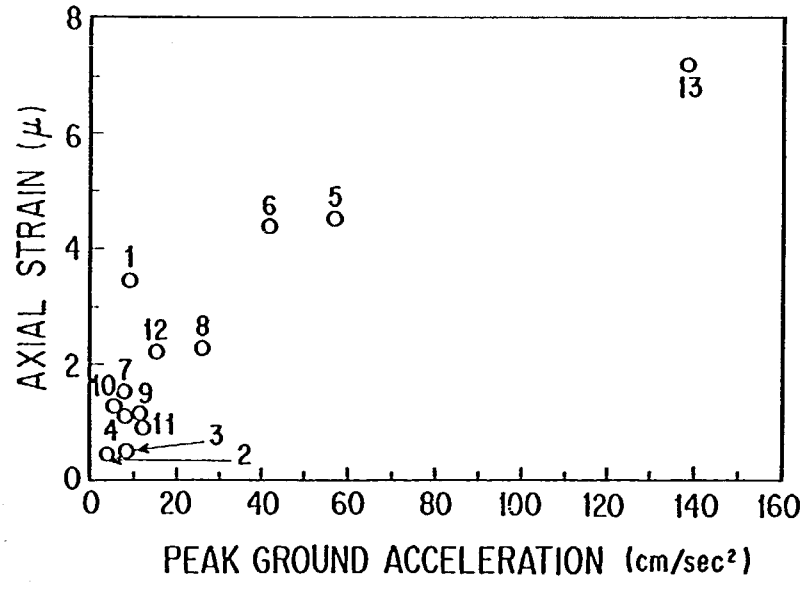


Fig. 6 Axial Strain of Steel Pipe vs. Peak Ground Acceleration Relation

from the measured accelerations were available at only six points, the displacements at each nodal point of the analytical model were computed from either linear interpolation or extrapolation of the displacements from the six points.

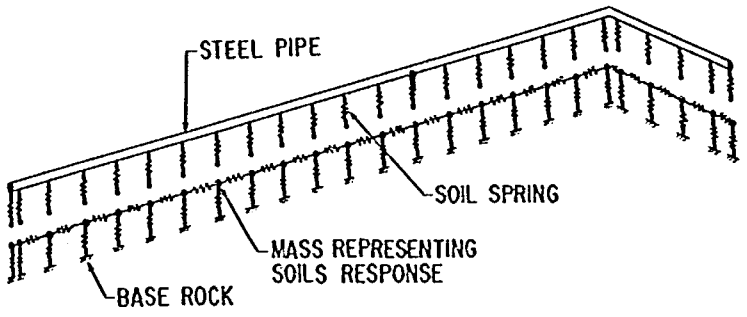


Fig. 7 Analytical Model for Dynamic Response Analysis of Embedded Pipes

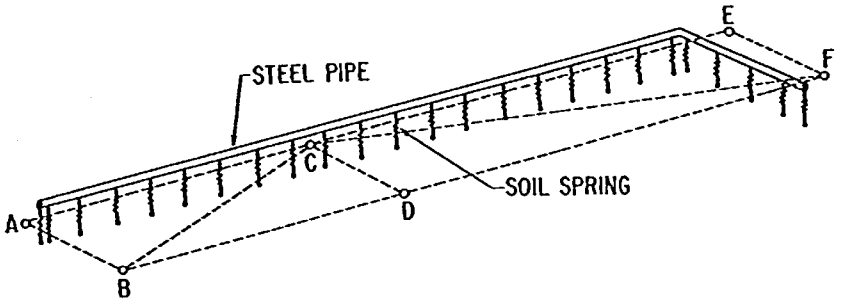


Fig. 8 Analytical Model Used for Pipe Response

In the Design Specifications of Petroleum Pipelines [2], the soil spring stiffness is stipulated to be estimated as

$$K = c \times G_s \qquad (1)$$

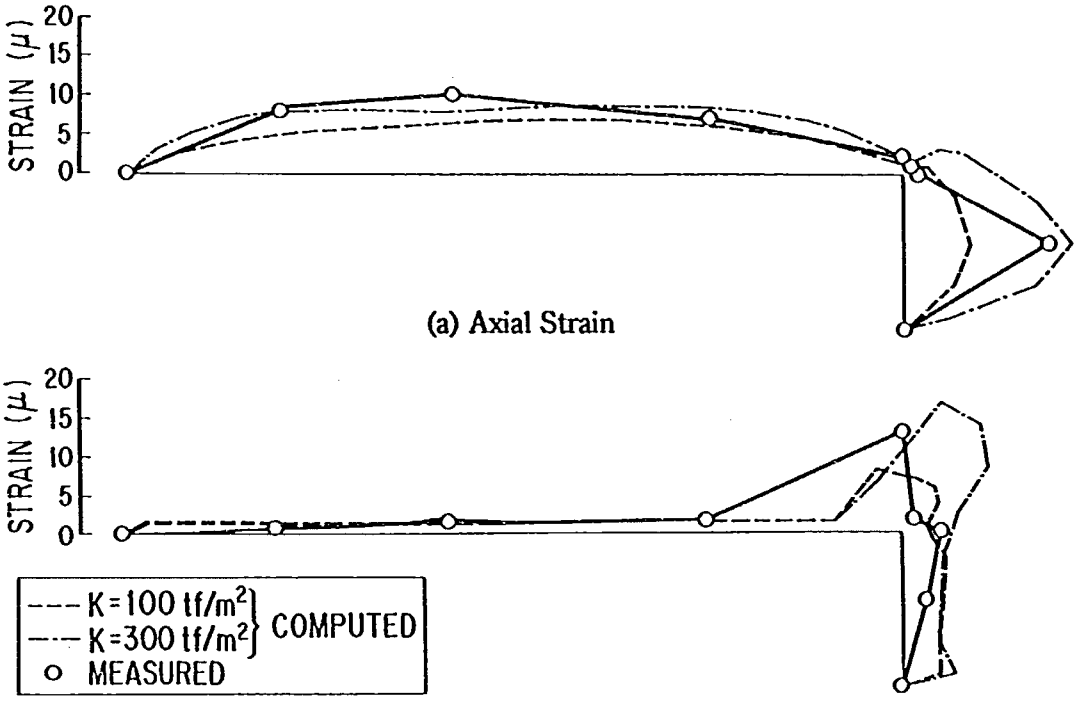
where K : stiffness of soil spring per unit length, c : a coefficient, and G_s : shear moduli of soils. The shear moduli of soils are estimated as

$$G_s = \frac{\gamma_t}{g} \times V_s^2 \qquad (2)$$

where γ_t : unit weight of soils, V_s : shear wave velocity of soils, and g : acceleration of gravity. In the specifications the coefficient c is stipulated to be determined by appropriate tests, and a value of 3.0 is recommended when such test data is not available.

The soil spring which gives realistic estimation for the measured pipe strain was therefore studied. Fig. 9 shows the approximation of the computed pipe strain assuming a soil spring stiffness of 100 tf/m^2 and 300 tf/m^2. The computed axial and flexural strain along the longer straight pipe approximates quite well the measured pipe strain. However the approximation along the shorter straight pipe and bent is rather poor. Approximation at these parts require further clarification by accumulating the measured data. Because shear wave velocity which was measured at three points in the observation site was about 150 m/sec at the depth between the ground surface and 15 meters below the ground surface, the soil spring stiffness of 100tf/m^2 and 300tf/m^2 are predicted by

assuming a coefficient "c" of about 0.05 and 0.16 respectively in Eq.(1). From such evidence it may be said that the recommended value of 3.0 for the coefficient "c" in Eq.(1) is excessively conservative. It is important to precisely study the coefficient "c" which gives a realistic soil spring stiffness.



(a) Axial Strain

(b) Flexural Strain

Fig. 9 Best Correlation of Pipe Strain for EQ 13

5. CONCLUSIONS

For accumulating actual seismic behavior of embedded pipes during earthquakes, seismic observation of two types of pipes was initiated. Based on the analyses of the measured data on the strain of embedded pipes, the following conclusions may be deduced:

1) Although axial strain is predominant in the straight section, flexural strain is more predominant than axial strain at the bend section of the pipe based on the measured data. Flexural strain should be considered in seismic design at bend sections.

2) Considerably good correlation was observed between the measured axial strain of the pipe and the peak ground acceleration. Accumulation of measured data is expected to provide a realistic estimation method for the pipe strain based on the peak ground acceleration.

3) The computed pipe strain assuming Eqs.(1) and (2) was excessively larger than the measured pipe strain. It is thought that the spring stiffness predicted by Eq.(1) assuming the coefficient "c" of 3.0 is too conservative. Coefficient "c" has to be precisely studied by analyzing more measured data.

6. FUTURE DIRECTIONS

Accumulation of measured data is required for providing a realistic estimation method for the pipe strain based on the peak ground acceleration, and for studying the coefficient "c" which gives a realistic soil spring stiffness. Because the observation site is located at one of the highest seismicity area in Japan, it is anticipated to have a number of measured data in a short time.

REFERENCES

1) Iawamoto, T.et.al.: Observation of Dynamic Behavior of Buried Pipelines during Earthquakes, Eighth World Conference on Earthquake Engineering, San Francisco, U.S.A., 1984
2) Japan Road Association : Design Specifications of Petroleum Pipelines, 1974
3) Katayama, T. and Sato, N. : Ground Strain Measurement by a Very Densely Located Seismometer Array, Proc. 6th Japan Earthquake Engineering Symposium, Tokyo, 1982
4) Ministry of Construction : New Seismic Design Methods, Technical Note of PWRI, No. 1185, Public Works Research Institute, 1977
5) Okubo, T., Arakawa, T. and Kawashima, K. : Dense Instrument Array Program of the Public Works Research Institute and Preliminary Analysis of the Records, Eighth World Conference on Earthquake Engineering, San Francisco, U.S.A., 1984
6) Tamura, C., Okamoto, S. and Hamada, M. : Dynamic Behavior of a Submerged Tunnel during Earthquakes, Report of the Institute of Industrial Science, University of Tokyo, Vol.24, No.5, 1975
7) Tamura, K., Kawashima, K., Aizawa, K. and Takahashi, K. : Recording Accuracy of Digital Strong Motion Accelerographs with Independent Triggering and Recording Systems for Analysis of Finite Ground Strains Induced during Earthquakes, Proc. Japan Society of Civil Engineering, Vol. 392/I−9, 1988
8) Kawashima, K., Hasegawa, K. and Nagashima, H.: Seismic Behavior of Buried Pipelines through Field Observation, Proc. of 3rd U.S. National Conference on Lifeline Earthquake Engineering, Los Angeles, CA, August 1991

(Received on 16 September, 1993)

Seismic Response Control of Highway Bridges by Variable Damper

Kazuhiko KAWASHIMA
Shigeki UNJOH
and
Hidetoshi MUKAI

5th U.S. National Conference on
Earthquake Engineering, EERI
Chicago, U.S.A.
July, 1994

SEISMIC RESPONSE CONTROL OF HIGHWAY BRIDGES BY VARIABLE DAMPER

Kazuhiko Kawashima [1], Shigeki Unjoh [2] and Hidetoshi Mukai [3]

ABSTRACT

This paper proposes the variable dampers which vary the damping coefficient depending on structural response, and the variable stiffness control in which the natural period of structures is varied depending on the structural response. Effectiveness of the variable dampers is presented through a numerical analysis and a series of shake table tests. The effectiveness of the variable stiffness control is also presented through a numerical analysis.

INTRODUCTION

Variable damper, in which damping coefficient can be variable dependent on structural response, for structural response control against an earthquake was proposed by the authors in 1989 (Kawashima and Unjoh 1989), and various studies have been made at the Public Works Research Institute. The variable damper has been effectively adopted in a field of mechanical engineering, in particular in a suspension system for an aircraft and an automobile. An active suspension for improving driving comfortableness and stability of automobiles is one of such examples (Sugawara 1986; Millikan 1987). However, it is a new idea to apply the variable

1 Head, Earthquake Engineering Division, Earthquake Disaster Prevention Department, Public Works Research Institute, Ministry of Construction, Tsukuba-shi, 305
2 Senior Research Engineer, ditto
3 Assistant Research Engineer, ditto

damper for structural response control against an earthquake.

Variable stiffness is another interesting field of extension of the variable damper. If one shifts the natural period of structures, the structural response may be significantly reduced by avoiding the resonance with the ground motion.

This paper presents the current studies for the variable dampers and variable stiffness for response control of bridges against an earthquake.

VARIABLE DAMPERS

A unique technic in application of dampers to bridges is distribution of lateral force to as many piers as possible. Although damper is effective for reducing deck response, it is also effective for transmitting lateral force from deck to piers when it is used at over-damper range. Thus the damper stoppers have been successfully implemented in many bridges.

Because few energy dissipation is made in the damper stopper, it is effective to decrease the damping ratio so that energy dissipation can be made when the bridge is subjected to a ground motion caused by a large earthquake. Because the damper stopper is effective for preventing a small deck vibration associated with breaking loads and wind effects, the function as the damper stopper is effective at small deck displacement. On the other hand when the deck response becomes excessive during an earthquake, the stopper is required to present further build up of the deck response.

Thus, the variable dampers with the following requirements may be superior to the existing dampers and damper stoppers:

1) Damping coefficient is very large during a small deck vibration for preventing the deck vibration due to breaking loads of vehicles and wind effects. It is movable against the low rate motions such as the elongation of deck by temperature change.

2) Against the seismic response with the deck response over a certain value, the damping coefficient needs to be set so as to make energy dissipation maximum.

3) Against excessive deck response during an earthquake, high damping coefficient is required to function as a stopper. Smooth and gradual increase of the damping force may be effective for preventing shocks.

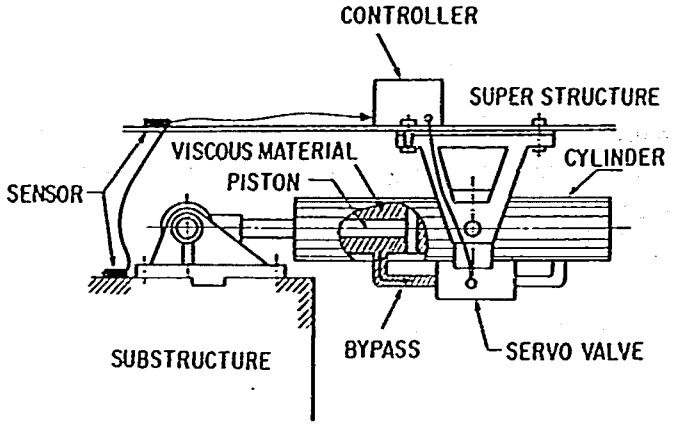


Fig. 1 Variable Damper

Although various types of the variable damper can be made, the simplest structure may be an piston-cylinder viscous damper as shown in Fig. 1. A by-pass is installed between the

cylinder–cells divided by the piston. Damping coefficient of the damper can be controlled by varying an amount of viscous flow of the by–pass. Various technologies for controlling such flow are available. External energy required for such control is generally much smaller than that required for the active control.

EFFECTIVENESS OF VARIABLE DAMPERS

Fig. 2 shows the deck displacement dependent damping ratio of the variable damper proposed for bridges (Kawashima, Unjoh, Nagashima and Shimizu 1991). Various control algorithm may be used such as to vary h_1 , h_2 and h_3 in time depending on bridge response for optimizing the deck response. The damping ratio can be varied depending on both the deck velocity and the deck displacement (Kawashima, Unjoh and Shimizu 1991). Partial control in which the control is made only partially in time can be made (Kawashima, Unjoh and Shimizu 1991). It should be noted that any relation between the damping ratio vs. the relative displacement and/or relative velocity can be incorporated in the analysis. The damping ratios h_1 , h_2 and h_3 are assumed here to be constant during an earthquake.

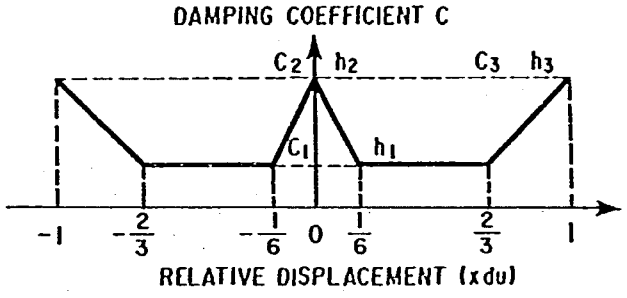


Fig. 2 Analytical Idealization of Damping Force vs. Relative Displacement Relation

For studying the effectiveness of the variable damper, a simple span girder bridge, as shown in Fig. 3, with a span length of 30m was analyzed. The response in longitudinal direction was considered. Although the variable damper has better implementation for multi–span continuous bridges, a simple span bridge was considered for analysis for simplicity. The deck was assumed to be supported by elastic bearings, and two variable dampers were installed between the deck and the piers.

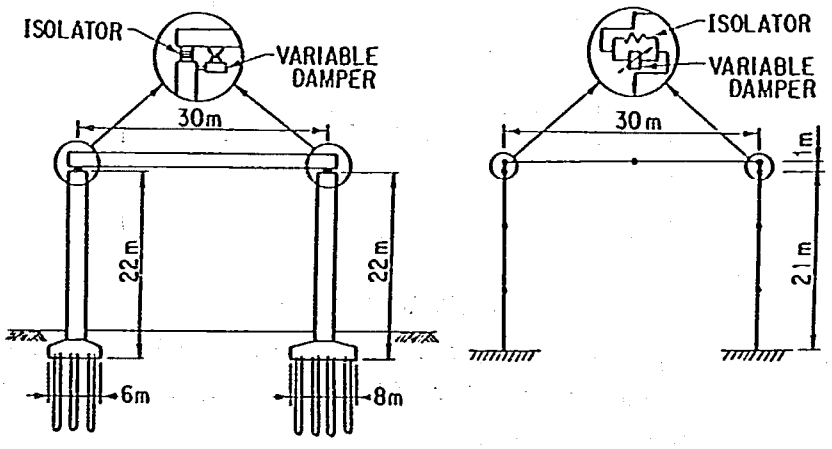


Fig. 3 Bridge Analyzed and Analytical Idealization

The fundamental natural period of the bridge is 0.5second if the both bearings are hinged, and is 1.0second it the bridge supported by the rubber bearings.

The bridge response with and without control by the variable dampers was computed. The damping ratios in Fig. 2 were assumed as $h_1=0.5$ and $h_2=h_3=3$. As shown in Table 1, the peak deck displacement and the peak deck acceleration decrease to 26% and 44% of those without control, respectively.

The damping force and stroke required for the variable dampers are 632 KN × 2 = 1264 KN and 5.78cm, respectively. Because the weight of deck is 2368KN, the damping force is 53% of the deck weight. The variable dampers with this specification can be designed and fabricated within the current scope of dampers technology.

Table 1 Peak Responses

Analytical Cases	Deck			Pier		Variable Damper		
	Displacement (cm)	Velocity (cm/s)	Acceleration (cm/s^2)	Shear Force (KN)	Bending Moment (KN·m)	Damping Force (KN)	Relative Displacement (cm)	Relative Velocity (cm/s)
NO CONTROL	33.00	189.0	1.300	1.637	32.333	———	———	———
WITH CONTROL	8.46	48.4	567	786	15.102	614	5.78	60.7

VERIFICATION OF VARIABLE DAMPER THROUGH SHAKE TABLE TEST

For verifying the feasibility of the variable dampers, a prototype variable damper was developed. It is a piston-cylinder type viscous damper with a by-pass installed between two cylinder-cells divided by the piston. The model was designed so that the maximum damping force is 200KN and the stroke is ± 13cm. Damping force can be controlled by a personal computer depending on a relative displacement and/or a velocity between a deck and a pier. The electricity required for control is only 50W. This is extremely small as compared with the energy required for the active control.

A series of dynamic loading tests was made for the model. Fig. 4 shows a hysteresis loop of the damping force vs. stroke. Both command signal and actual data are presented. The hysteresis loop obtained by the loading test is very close with the command.

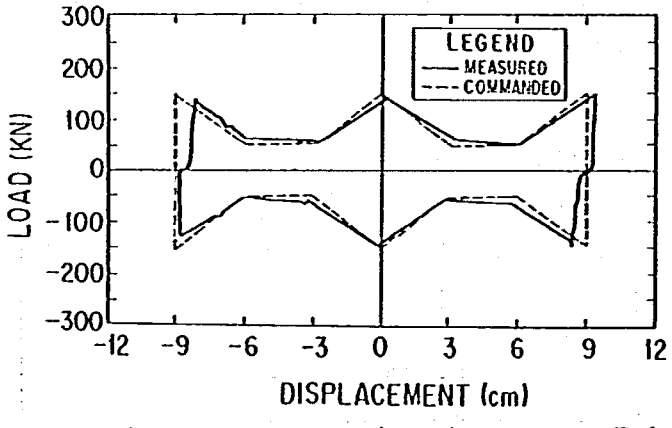


Fig. 4 Damping Force vs. Relative Displacement Relation from Dynamic Loading Test of Variable Damper

For verifying the effectiveness of the variable damper, a series of shake table tests was

made. A simple span bridge model was fabricated on a shake table as shown in Fig. 5. The deck is 7.6m long and 390KN in weight. The piers are 1.6m long. The deck is supported by four rubber bearings, and the prototype variable damper was installed between the deck and the pier.

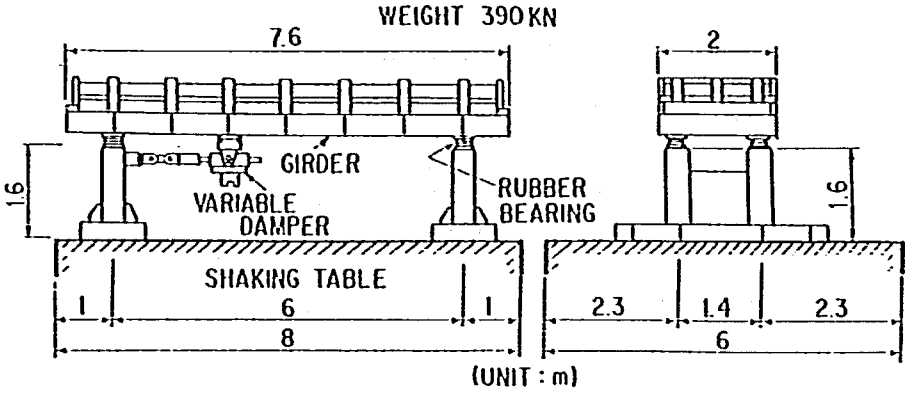


Fig. 5 Shake Table Test of a Model Bridge with a Variable Damper

The model bridge was excited by a ground acceleration. The peak table acceleration was set as about 180cm/sec^2 and 413cm/sec^2. The excitation by the table motion with peak acceleration of 413cm/sec^2 was not made for the model without control, because the deck response became excessive.

Figs. 6 and 7 compares the deck displacement of the model bridge, with and without control by the variable damper, subjected to the table acceleration with peak acceleration of about 180cm/sec^2. Predicted response by the analysis which will be described later is also presented. The deck responses are 376cm/sec^2 and 9.2cm for no control, and they are decreased to 203cm/sec^2 and 1.3cm by the variable damper. The maximum damping force required for this control is 71KN, which corresponds to 18% of the deck weight.

A simulation of the experiments by the analytical method presented in the previous chapter was made. The deck, piers and rubber bearings were idealized by a discrete linear frame. Figs. 6 and 7 compare the deck displacement and the damping force developed in the variable damper between the experiments and analyses. The predicted responses are quite close with the measured responses.

VARIABLE STIFFNESS CONTROL

Most of bridges with usual size have the natural period ranging from 0.3 to 1.5second, and this natural period range corresponds to the predominant period of earthquake-induced ground motions. Thus the resonance of the bridges response with the ground motion tends to be developed during an earthquake. The bridge response could be reduced provided the resonance of bridge response with the ground motion could be avoided.

Although it is hard to predict the predominant period of ground motion prior to an earthquake, it can be evaluated time by time during an earthquake. The moving window analysis may be used for evaluating the instantaneous predominant period of ground motion T^*. The resonance of bridge response with the ground motion may be avoided if the instantaneous natural period of bridges T be shifted from the instantaneous predominant period of ground motion T^* during an earthquake.

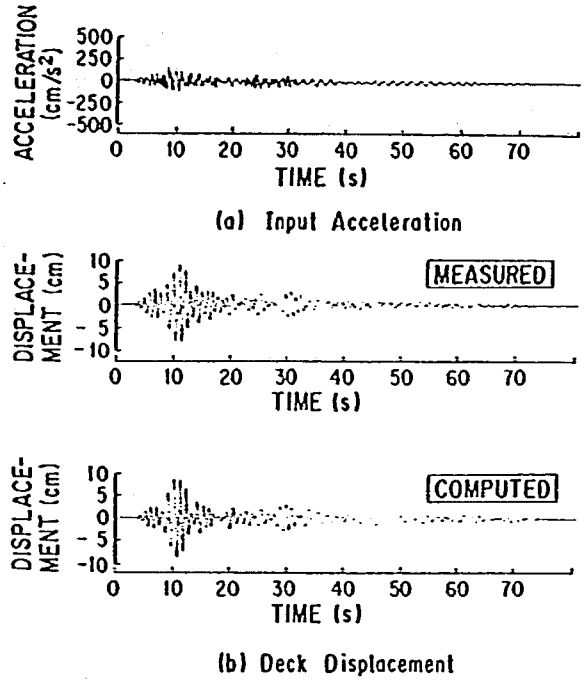


Fig. 6 Measured and Predicted Response of a Model Bridge without Control, subjected to a Table Motion with Peak Acceleration of 172cm/sec ^{2}

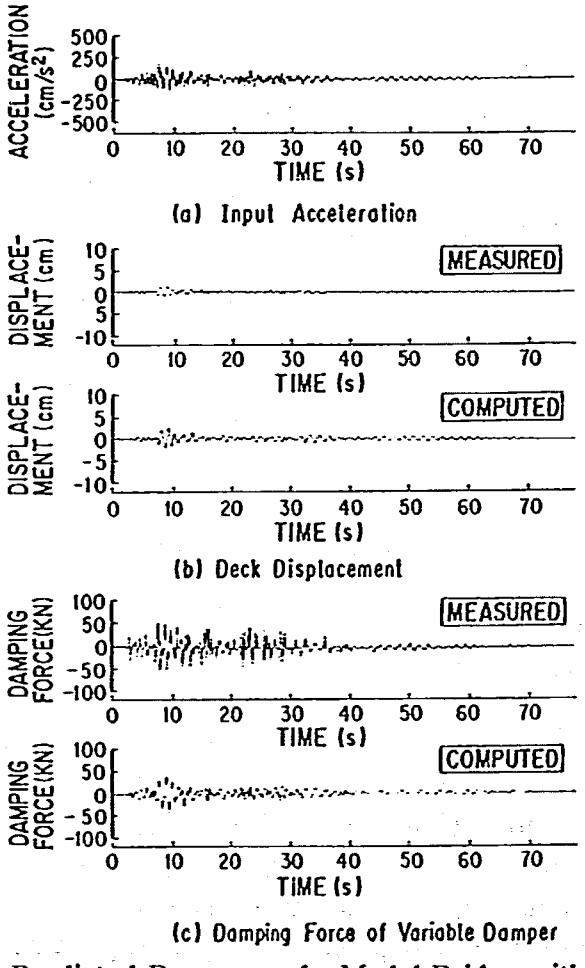


Fig. 7 Measured and Predicted Response of a Model Bridge with Control, subjected to a Table Motion with Peak Acceleration of 185cm/sec ^{2}

There are various methods to shift the instantaneous natural period of bridges during an earthquake. Flexibility of bearings may be changed, and active tendons/bracings may be adopted.

If one provides the variable dampers for a bridge which is elastically supported by rubber bearings, the natural period of the bridge can be varied by changing the damping coefficient of the variable dampers. If one makes the damping ratio of the variable damper very large, the variable damper would acts as the damper stopper. On the other hand, if one makes the damping ratio small, the natural period of the bridge takes the value computed from the stiffness of the rubber bearings and piers. The variable dampers have various advantage for controlling the instantaneous natural period of bridges because it is more stable for long term use than the active tendons/bracing systems.

Fig. 8 shows the algorithm of the variable stiffness control. The instantaneous predominant period of ground motion T^* at time t_i is computed by the moving window Fourier Spectrum. The damping coefficient of variable dampers is varied so that the instantaneous natural period of the bridge T be shifted to prevent the resonance with the ground motion.

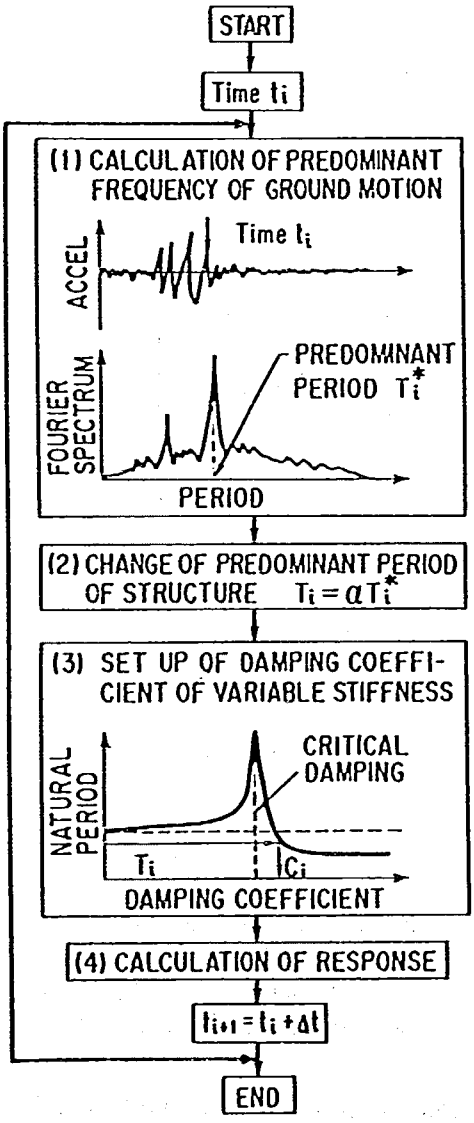


Fig. 8 Control Algorithm of Variable Stiffness

Although several algorithm can be considered, the period shift is assumed here as

$$T = \alpha T^* \qquad (1)$$

in which T instantaneous natural period of a bridge at time t_1, T^* instantaneous predominant period of an earthquake ground motion at time t_1, α control coefficient. The coefficient α has to be determined depending on the undamped natural period of the bridge T_0 and the instantaneous predominant period T^* of an ground motion.

EFFECTIVENESS OF VARIABLE STIFFNESS CONTROL

To study the effectiveness of the variable stiffness control, a three-span continuous girder bridge, as shown in Fig. 9, with a span length of 90m is analyzed. The response in longitudinal direction is considered. The superstructure of the model is supported by elastic bearings, and four variable dampers with the same characteristics are installed between the deck and the piers. The weight of the superstructure and spring stiffness of the rubber bearings are assumed as 4,719KN and 6,247KN/m, respectively. The stiffness of piers is assumed so that the fundamental natural period of the bridge is 0.5sec when the deck is supported by hinges. The stiffness of rubber bearings is set so that the fundamental natural period of bridge is 1 sec when the deck is supported by the elastic bearings. The damping ratio of the bridge without control is assumed as 0.02.

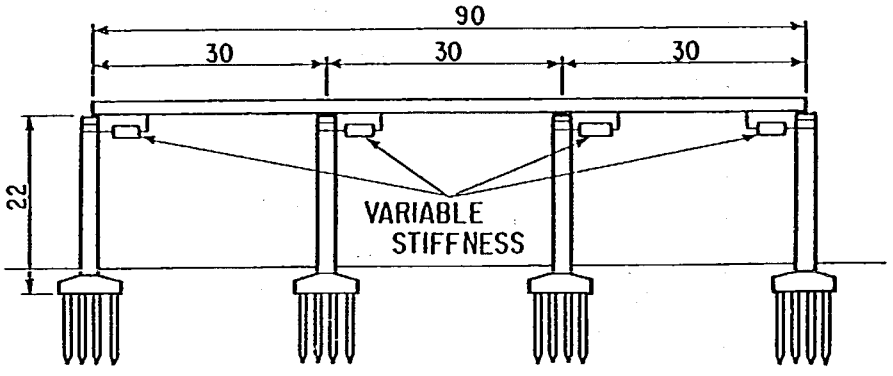


Fig. 9 Model Bridge Analysed

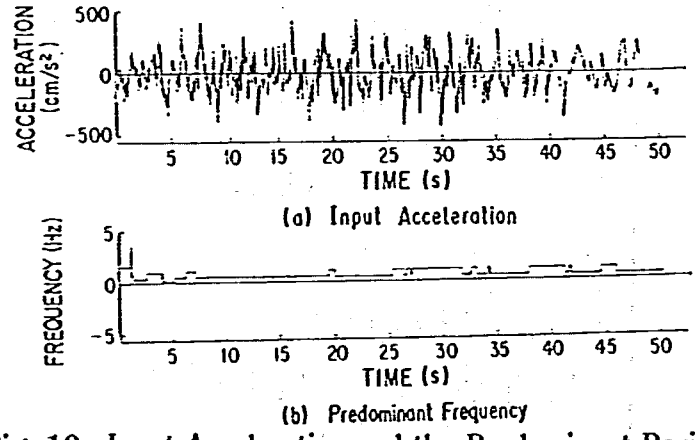


Fig. 10 Input Acceleration and the Predominant Period

An acceleration ground motion as shown in Fig. 10 is used as an input acceleration. The instantaneous predominant frequency $(1/T^*)$ of the input acceleration is also shown in Fig.

10. Because the predominant period of ground motion is about 1sec., α in Eq. (1) was assumed as 1/2.

Fig. 11 shows how the natural period of the bridge change depending on the damping coefficient of the variable dampers. At the damping coefficient C of about 4,200KN·sec/m, the fundamental natural period of bridge take very large value, because this corresponds to the critical damping of the structure. Although the period shift may be made in the damping coefficient range of 0 to over 8,000KN·sec/m, it is assumed here that the period shift be made

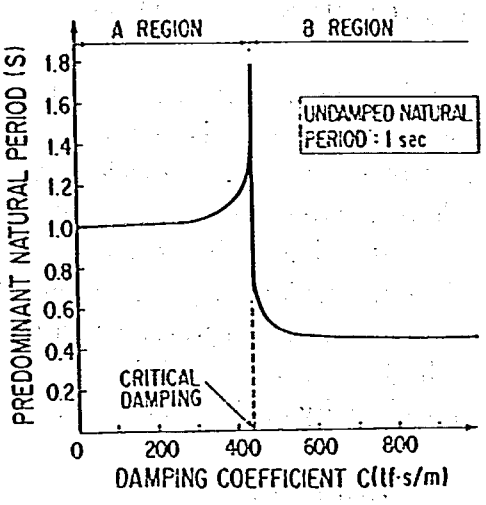


Fig. 11 Dependence of Natural Period of the Bridge on Damping Ratio of Variabl Dampers

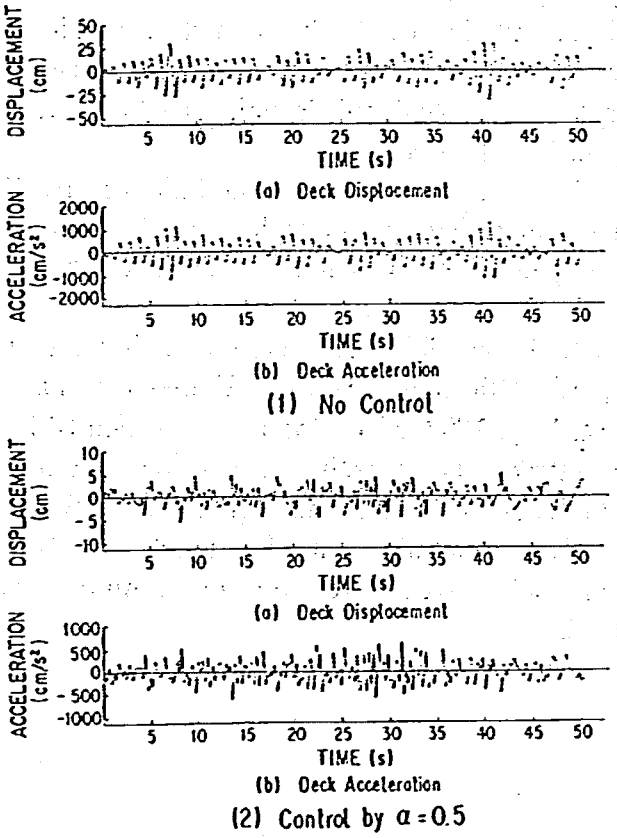


Fig. 12 Effectiveness of Variable Stiffness Control

in the range of damping coefficient C over 4,200KN·sec/m.

Fig. 12 compares the deck acceleration and displacement of the bridge with and without control. The peak displacement and peak acceleration of deck decreases to 17% and 50% of those without control. The bending moment of pier bottom decreases to 52% of the one without control. The peak damping force required for the four variable dampers is 761KN × 4 = 3,040KN and peak stroke is 3.1cm.

CONCLUDING REMARKS

Because the variable damper is a simple extension of the damper stopper technology which has been used in Japan for long time, it is expected that the variable dampers be implemented in near future. Various research on the variable stiffness including development of the prototype model and shake table tests are currently being made.

The research presented herein is being made as a part of the U.S.–Japan Cooperative Research on Hybrid Control of Bridges under auspices of the Panel on Wind and Seismic Effects, UJNR. The authors extend their sincere appreciation to the strong support of Dr. S. C. Liu, NSF, Dr. H. S. Lew, NIST, Mr. J. D. Cooper, FHWA, Professor M. Shinozuka, Princeton University and Professor J. N. Yan, University of California at Irvine.

REFERENCES

1) Kawashima, K. and Unjoh, S. (1989). "Development of Hybrid Control Technology." Civil Engineering Journal, Tokyo, Japan, pp. 2–5, Vol. 32–6 (in Japanese).

2) Taguchi, J., Iwasaki, T., Adachi, Y., Sasaki, Y. and Kawashima, K. (1990). " U.S.–Japan cooperative research program on hybrid control of seismic response of bridge structures." 22nd Joint Meeting, U.S.–Japan Panel on Wind and Seismic Effects, UJNR, Gaithersburg, Maryland, USA, May, 1990, NIST Special Publication.

3) Kawashima, K., Unjoh, S., Nagashima, H. and Shimizu, H. (1991). "Current research efforts in Japan for passive and active control of highway bridges against earthquakes." Proc. 23rd Joint Meeting, U.S.–Japan Panel on Wind and Seismic Effects, UJNR, Tsukuba, Japan, 187–209.

4) Kawashima, K., Unjoh, S. and Shimizu, H.(1992). "Seismic response control of highway bridges by variable damper." 24th Joint Meeting, U.S.–Japan Panel on Wind and Seismic Effects, UJNR, Gaithersburg, May, 1992, NIST Special Publication 843

5) Milliken, Jr., W., F. (1987). "Lotus active suspension system." Proc. 11th International Conference on Experimental Safety Vehicles, Washington D.C., U.S.A., 467–475.

6) Sugawara, F. (1986). "Electronically controlled shock absorber system used as a road sensor which utilizes super sonic waves." Proc. Society of Automotive Engineers, Milwaukee, Wisconsin, U.S.A., 6.15–6.25.

Seismic Response of Reinforced Concrete Bridge Piers Subjected to Eccentric Loading

Kazuhiko KAWASHIMA
Shigeki UNJOH
and
Hidetoshi MUKAI

5th U.S. National Conference on
Earthquake Engineering, EERI
Chicago, U.S.A.
July, 1994

SEISMIC RESPONSE OF REINFORCED CONCRETE BRIDGE PIERS SUBJECTED TO ECCENTRIC LOADING

Kazuhiko KAWASHIMA [1], Shigeki UNJOH [2] and Hidetoshi MUKAI [3]

ABSTRACT

Presented are the seismic response characteristics of C-shaped reinforced concrete bridge piers which are subjected to eccentric loading by the dead weight of superstructure and cantilevered beam. Shaking table test and dynamic loading tests of model piers were made to investigate the seismic response characteristics. It is found that the response of piers is developed only in one direction, in which the eccentric loading is applied, resulting in large residual displacement. It is also found that the ductility of the piers significantly decreases as the eccentric loading increases.

INTRODUCTION

Recently, new types of structures have been constructed in urban areas because of land use restriction and other construction conditions. C-shaped reinforced concrete (RC) bridge piers as shown in Fig. 1 are one of the typical examples. Because the C-Shaped RC piers are subjected to eccentric loading by the dead weight of superstructure and cantilevered beam,it is anticipated that the seismic response of the piers is developed only in one direction during an

1 Head, Earthquake Engineering Division, Earthquake Disaster Prevention Department, Public Works Research Institute, Ministry of Construction, Tsukuba-shi, 305
2 Senior Research Engineer, ditto
3 Assistant Research Engineer, ditto

earthquake. It is therefore important to investigate the strength and ductility characteristics and to develop the seismic design method against large-scale earthquakes.

This paper presents the seismic response characteristics of the C-shaped RC bridge piers through a shaking table test and dynamic loading tests of model piers.

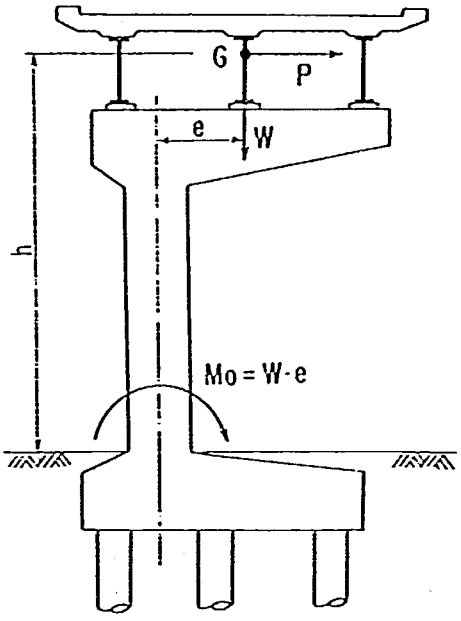


Fig. 1 C-Shaped Reinforced Concrete Bridge Pier Subjected to Eccentric Loading

DEFINITION OF ECCENTRIC LOADING

To define the eccentricity, a bending moment ratio r_M is assumed as

$$r_M = \frac{M_E}{M_0 + M_E} \qquad (1)$$

where

M_E : bending moment due to design seismic lateral force

M_0 : bending moment due to eccentric loading of superstructure and cantilevered beam

Eq.(1) means that as the eccentric loading increases r_M deceases.

Fig. 2 shows the bending moment ratio r_M for 45 existing C-shaped RC bridge piers in the Metropolitan area. The bending moment ratio r_M is in the range of 0.4 – 0.9. Mean value of the bending moment ratio r_M is 0.55.

SEISMIC RESPONSE OF C-SHAPED RC PIERS BASED ON SHAKING TABLE TESTS

Bridge Pier Model

To investigate the seismic response of the C-shaped RC pier, a series of shaking table test was made at the Public Works Research Institute. Fig. 3 shows the model designedwith the scale ratio of the model to the prototype pier of 1/4.6. The bending moment ratio r_M is 0.55.

The specimen has an effective height h of 2.55m and cross section of 52cm × 42cm. The

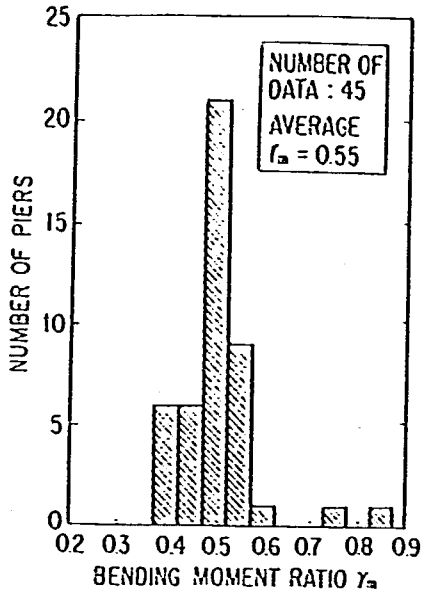


Fig. 2 Bending Moment Ratio r_M for 45 Existing Bridge Piers

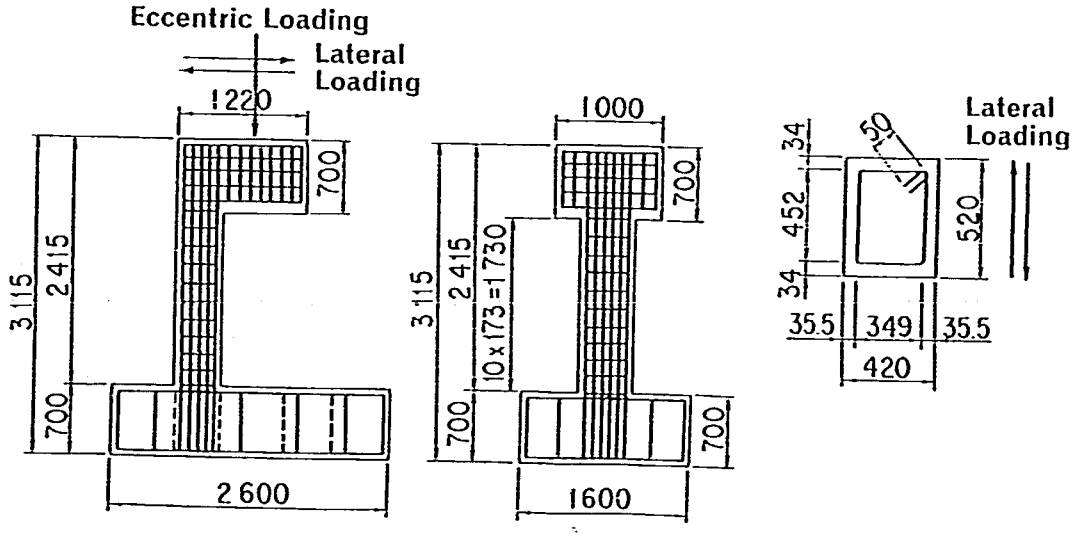


Fig. 3 C-Shaped Bridge Pier Model for Shaking Table Test

shear span ratio h/d , which is defined as the ratio of the effective height to the effective width d of the cross section, is 6.9. Reinforcing bars with a diameter of 16mm (D16) and 22mm (D22) are provided as the longitudinal reinforcement at the side where either compression or tension are developed due to the eccentric loading. Reinforcing bars with a diameter of 16mm (D16) are placed at two other sides. The reinforcement ratio is 1.78%. Reinforcing bars with a diameter of 10mm (D10) are placed as the tie reinforcement with 17.3cm interval. Tie reinforcement ratio is 0.16%. Averaged yielding stresses of the longitudinal and tie reinforcement are 35.38KN for D16, 34.32KN for D22 and 34.83KN for D10, respectively. Averaged compression strength of the concrete is 3.29KN. It should be noted here that since the weight of the superstructure supported by the model is 393.2KN, the model can be considered to be designed assuming the seismic lateral force coefficient of 0.27. Axial stress

induced by the dead weight of superstructure is 90N. Computed yield displacement δ_y corresponding to one displacement ductility factor and yield force of the pier in the direction in which the eccentric loading is applied are 20.5mm and 75.5KN, respectively. On the other hand, they are 91.3mm and 115.7KN, respectively in the opposite direction.

Shaking Table Test

The pier model was fixed at the center of shaking table and two spans of simply supported girders with total weight of 393.2KN and length of 15m were placed on the pier model. Two ends of the girder were supported by the two steel frames placed outside of the table. The girder was supported by the pier model with fixed bearings, and by the steel frames with movable roller bearings. Therefore, the inertia force developed at the girder during excitation is directly applied to the pier model.

The pier model was excited along transverse direction to the bridge axis. An acceleration record measured at the Hachirogata during the Nihon-kai-chubu, Japan, Earthquake of 1983 was used as an input motion by reducing the time axis one half so that the predominant frequency of the record matches with the fundamental natural frequency of the pier model. Peak acceleration of the record was assumed as 0.35G.

Extensive instrumentations were made to measure basic parameters including accelerations at the foot of pier and at the girder as well as relative displacement of the girder with reference to the shaking table. Inertia force of the superstructure was computed by multiplying the acceleration developed at the girder by the mass of girder.

Seismic Response Characteristics

Fig. 4 shows the table acceleration, the response acceleration and displacement of girder. Although the peak acceleration of the shaking table is 812cm/s^2, this is due to a spike-like acceleration and the effective seismic intensity to excite the pier model is about 0.35G. The residual lateral displacement of 16cm is developed at the pier crest in the direction of eccentricity. The stopper provided for preventing falling-off of girders prevented further drifting. Such a permanent displacement is clearly observed in Fig. 5 from biased inelastic response displacement. The drift of the response displacement which exceeded the yield displacement was developed at the time of 12sec when the first strong excitation is loaded. However, after the excitation at the time of 17sec, the residual displacement reached to about 16cm. Increase of the drifting of the response displacement after the first strong excitation seems to be less. It should be noted here that although the residual displacement was also developed in the shaking table test of RC pier model subjected to concentric loading, the amount of residual displacement is much smaller (Kawashima, et al. 1993).

Fig. 5 shows the failure mode of the model after the excitation. Compression failure was developed in the compression side due to the eccentric loading, while only horizontal tension crack was developed in the tension side.

Fig. 6 shows the hysteresis loop of the load-displacement relation obtained through the test. The biased displacement response exceeding the yield displacement was clearly developed after the first significant excitation. The degradation of the stiffness in accordance with nonlinear response can be clearly observed.

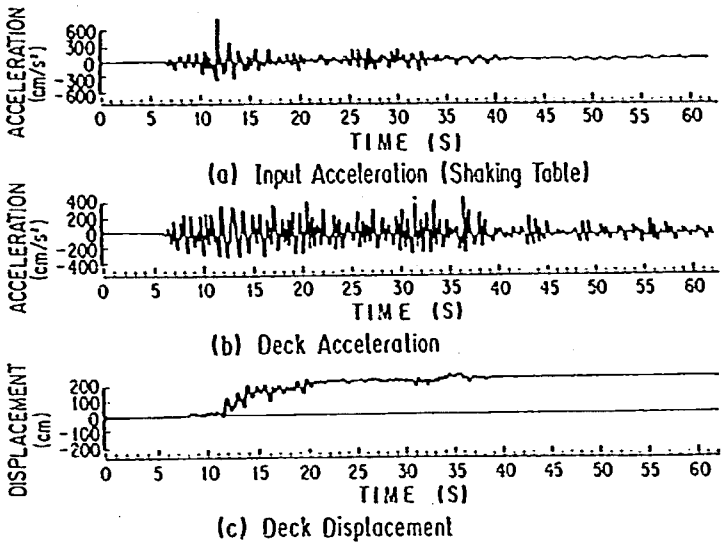


Fig. 4 Response Accelerations and Displacement

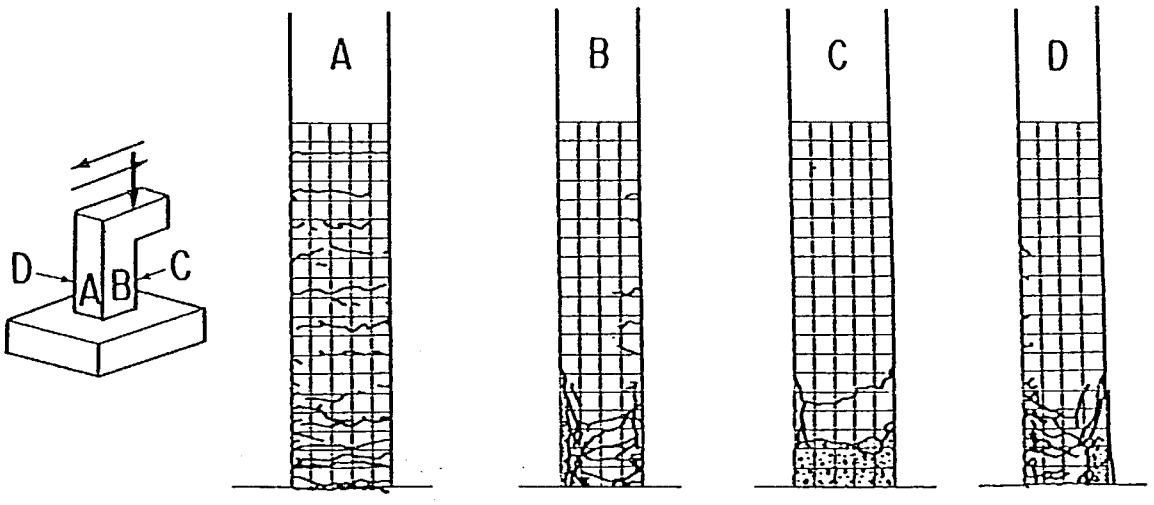


Fig. 5 Failure Mode of the Pier Model after Excitaion by Shaking Table

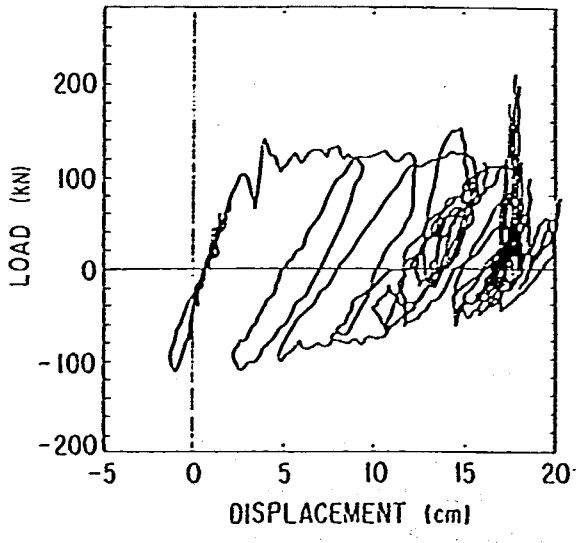


Fig. 6 Hysteresis Loop of load–displacement relation obtained through Shaking Table Test

DYNAMIC LOADING TEST OF RC PIER MODELS

Bridge Pier Models Studied

Dynamic loading with use of an actuator was made for comparing the strength and ductility with those obtained by the shaking table test. Fig. 7 shows three models used for the test. The models are basically the same as the specimens used for the shaking table test, and the bending moment ratio r_M was varied from 0.51 to 0.69 as a parameter to be investigated.

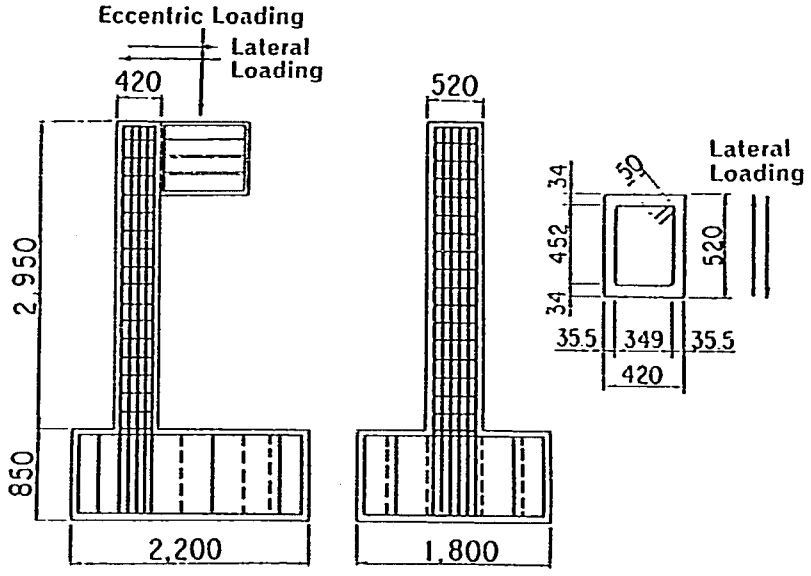


Fig. 7 C-Shaped Bridge Pier Model for Dynamic Loading Tests

The three models have an effective height h of 2.55m and cross section of 52cm × 42cm. The shear span ratio h/d is 6.9. The bending moment ratios r_M were assumed as 0.69 (P-60; small eccentric loading), 0.55 (P-62; medium eccentric loading) and 0.51 (P-64; large eccentric loading), in which the specimen number represents the serial number of models at the Public Works Research Institute. P-62 has the same scale and arrangement of reinforcement with the one used for the shaking table test. Axial force applied to the models was 196.1KN so that it matches with the shaking table test. The axial stress developed in the piers is therefore 90N. It should be noted however that the axial force for P-60 was 127.5KN (axial stress was 58.8N) because of the limitation of loading apparatus.

Dynamic Loading Test

The pier model was anchored to the reaction wall with bolts. A dynamic actuator was fixed to the head of the pier model. Axial loading apparatus was fixed to the head of the pier models so that the eccentric loading be applied. A steel apparatus was set at the pier crest to apply the axial force eccentrically.

Fig. 8 shows the loading scheme for the tests. The pier models were subjected to a series of step-wise increasing symmetric displacement cycles. At each step, 10 cycles of loading with the same displacement amplitude was carried out. The yield displacement corresponding to one ductility factor was assumed as an unit loading displacement. Because the

pier models is deformed due to subjected to the eccentric loading, the unit loading displacement δ_1 is defined as

$$\delta_1 = \delta_y - \delta_0 \qquad (2)$$

where

δ_y : yield displacement

δ_0 : displacement developed due to the eccentric loading

The unit loading displacement was used for controlling the dispalcement in the step-wise loading scheme. The loading velocity was assumed as 1cm/s.

Four sides of the pier are reffered as A, B, C, and D-side as shown in Fig. 5.

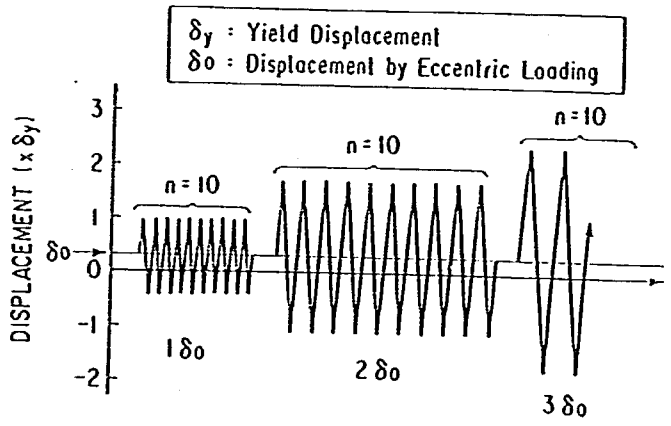


Fig. 8 Loading Scheme for Dynamic Loading Tests

Failure Mode of Pier Models

Fig. 9 shows the failure mode of P-62 (r_M=0.55) at B-side. During δ_1 to δ_2 loading, only small horizontal cracks were found at A-side. No crack was found at C-side. After δ_3 loading the cracks was initiated at C-side. During δ_4 loading, diagonal cracks were developed from the bottom of A-side to C-side. As the loading cycles increase, significant cracks were developed at the bottom of C-side and the cover concrete was spalled-off. During δ_6 loading, triangular wedge of the concrete at the bottom failed and two longitudinal reinforcing bars were ruptured in B-side. During δ_7 loading, the deformation of the pier was significantly extended at the base. It should be noted that the failure mode developed during the shaking table test is significantly different from that developed during the dynamic loading test. Although the diagonal crack was developed by the dynamic loading test, such diagonal crack was not developed by the shaking table test. This is because that although the loading in the direction of A-side was forced to be applied during the dynamic loading test, the reseponse displacement during the shaking table test was developed in only C-side direction.

Figs. 10 and 11 show the failure modes of P-60 (r_M=0.69) and P-64 (r_M=0.51), respectively. In P-60, crack was developed at the C-side from δ_1 loading. Then the crack increased at both A-side and C-side. During δ_6 loading, cover concrete was spalled-off at the both sides at the bottom. During δ_7 loading, three longitudinal reinforcing bars were ruptured. The failue mode of P-60 is different from that of P-62. The damage was developed only at the compression side due to the eccentric loadingin P-62, while the damage was developed at both tension and compression sides in P-60.

On the other hand, in P-64 (r_M=0.51), the diagonal crack was developed during δ_3

loading. The cover concrete at the C−side at the bottom was spalled−off during δ_4 loading. Compression failure of concrete was developed during δ_5 loading at the C−side at the bottom and one longitudinal reinforcing bar was ruptured. The progress of damage of P−64 was faster than P−62.

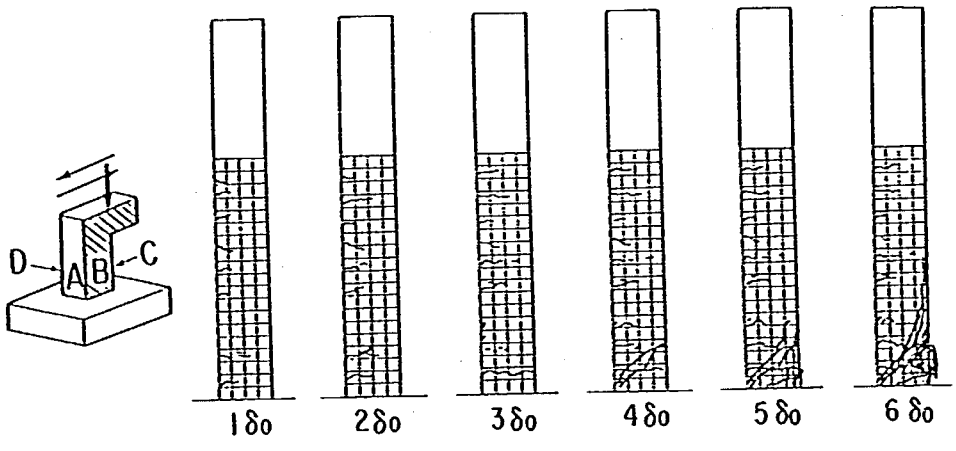


Fig. 9 Failure Mode of P−62 (r_M=0.55)

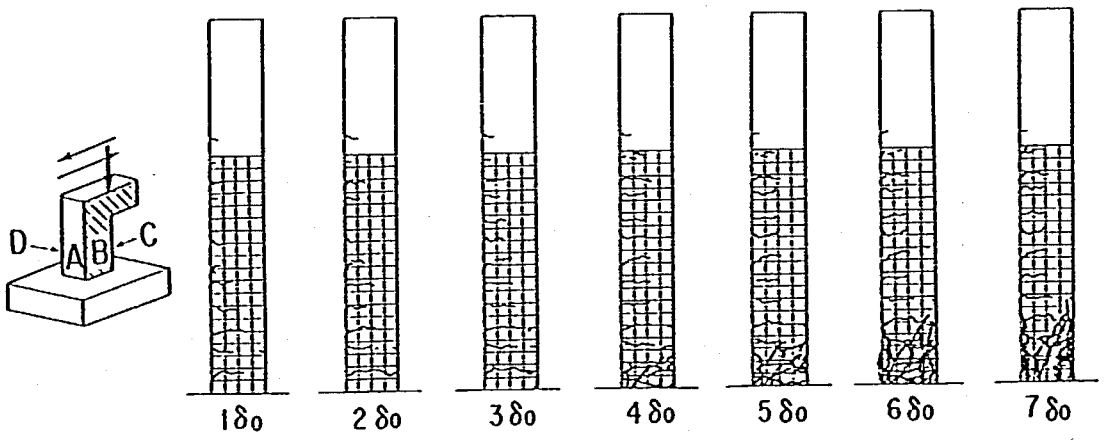


Fig. 10 Failure Mode of P−60 (r_M=0.69)

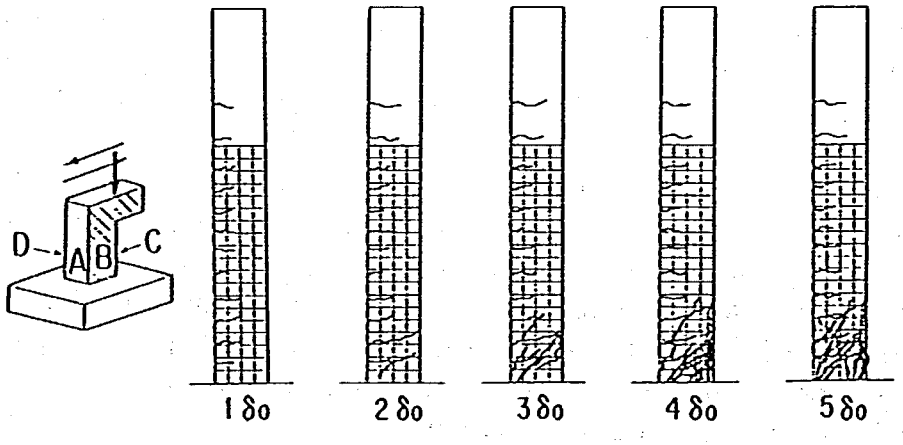


Fig. 11 Failure Mode of P−64 (r_M=0.51)

Strength and Ductility Characteristics

Fig. 12 shows the effect of bending moment ratio r_M on the load–displacement relation. In the side of eccentricity, the peak strength decreases faster as the loading displacement incerases. The ductility becomes smaller as the bending moment ratio decreases.

Table 1 compares the strength and ductility of the models. The ductility is almost the same for r_M of 0.69 (P–60) and 0.55 (P–62), but when the r_M is 0.51 (P–64) the ductility decreases to one half of P–60 and P–62. The ratio of the peak force to the yield force of P–64 decreases by 10% than those of P–60 and P–62.

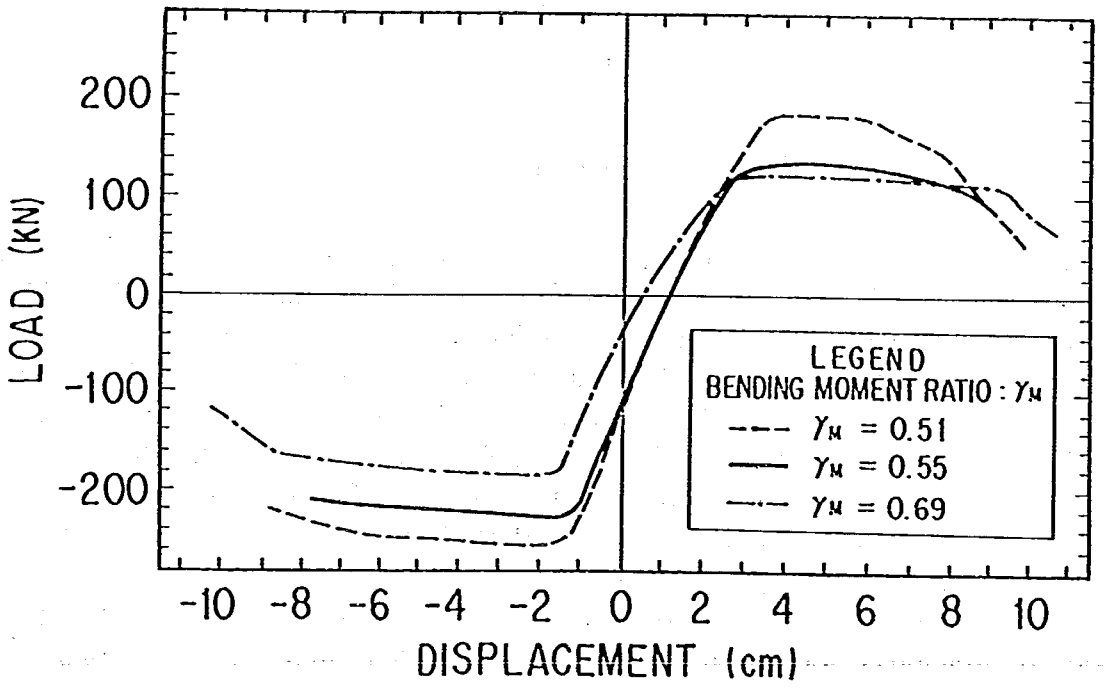


Fig. 12 Effect of Bending Moment Ratio r_M on Hysteretic Behavior

Table 1 Strength and Ductility of Pier Models

	P–60	P–62	P–64
Bending Moment Ratio r_M (Eccentric Loading)	0.69 (Small)	0.55 (Medium)	0.51 (Large)
Yield Force P_y (KN)	124.5	147.1	223.6
Peak Force P_{max} (KN)	145.1	179.5	238.3
P_{max}/P_y	1.17	1.22	1.07
Yield Displacement δ_y (cm)	1.6	1.3	2.0
Ultimate Displacement δ_u (cm)	8.8	7.3	5.4
Ductility Factor δ_y/δ_u	5.5	5.6	2.7

CONCLUDING REMARKS

To investigate the seismic response characteristics of C-shaped reinforced concrete bridge piers subjected to the eccentric deck dead weight, a series of shaking table tests and dynamic loading tests for model piers were made. Based on the above results, the following conclusions may be deduced:

(1) When the pier model are subjected to eccentric loading, the residual displacement is developed only in one direction where the eccentric loading is applied.

(2) The ductility becomes smaller as the bending moment ratio decereses. When the bending moment ratio becomes as small as 0.51, the ductility decreases to one half of the ductility of piers with thebending moment ratio greater than 0.55.

REFERENCES

1) Kawashima, K., Hasegawa, K., Koyama, T. and Yoshida, T. (1988) "Hysteretic Behavior of Reinforced Concrete Bridge Piers by Dynamic Loading Tests and Shaking Table Tests," Ninth World Conference on Earthquake Engineering, Tokyo-Kyoto, Japan
2) Kawashima, K., Hasegawa, K. and Nagashima, H., Koyama, T. and Yohida, T. (1993) "Development of Seismic Design Method of Reinforced Concrete Bridge Piers subjected to Large Ground Motion," Report of PWRI, No.188, Public Works Research Institute
3) Kawashima, K., and Koyama, T.(1988) "Effect of Number of Loading Cycles on Dynamic Characteristics of Reinforced Concrete Bridge Pier Columns," Structural Eng./Earthquake Eng., Proc. JSCE, Vol.5, No.1, pp.183-191
4) Kawashima, K., and Koyama, T.(1988) "Effect of Cyclic Loading Hysteresis on Dynamic Behavior of Reinforced Concrete Bridge Pier," Structural Eng./Earthquake Eng., Proc. JSCE, Vol.5, No.2, pp.343-350

RECENT SELECTED PUBLICATIONS AT EARTHQUAKE ENGINEERING DIVISION, PUBLIC WORKS RESEARCH INSTITUTE (No.3)

ISSN 0386-5878
Technical Memorandum of PWRI No. 3276
March, 1994

Kazuhiko Kawashima, Head,
Earthquake Engineering Division

This reports presents some of the selected publications in the research on earthquake damage investigation, seismic design, seismic evaluation and strengthening of highway bridges, dynamic strength and ductility of structural components, structural response of menshin bridges (seismic isolated bridges), hybrid control, and seismic response of embedded pipes. They were presented at international conferences and workshops held in the last one years.

郵 便 はが き

Postage stamp

3 0 5 - □ □

建設省土木研究所地震防災部耐震研究室
〒305 茨城県つくば市大字旭1番地

Earthquake Engineering Division,
Public Works Research Institute
Tsukuba Science City
Japan 305

No. 053

No. 053

配布先氏名

配布先住所

Receipt of

Technical Memorandum of PWRI No. 3276

Name _____

Address _____

_____

_____